

MOLECULAR ANALYSIS OF ACUTE AND CHRONIC DUCK HEPATITIS B VIRUS (DHBV) INFECTIONS IN DUCKS

Huey Chi LOW

B.Sc. (Biomedical Science), B.Sc. (Hons)

A thesis submitted to the University of Adelaide
in fulfilment of the requirements for the degree of Doctor of Philosophy

Disciple of Microbiology and Immunology
School of Molecular and Biomedical Science
The University of Adelaide
South Australia

April 2012

Dedication

To my loving family

who never gave up on me over all these years

Dad

For your silent encouragement and support (financially and emotionally)

Words just simply could not describe how much you mean to me

Mom

For always sacrificing your all to give me the best in everything

I could never ever repay you for all you have done for me

Elder sis

For always being there for me, cheering me up, and trying to help as best as you can

I could not hope for a better, crazier sister than you

This belongs to you all as much as it belongs to me

To God my Heavenly Father be all the glory in the name of His Son

Even youths grow tired and weary, and young men stumble and fall;
But those who hope in the Lord will renew their strength.
They will soar on wings like eagles;
They will run and not grow weary, they will walk and not be faint.
Isaiah 40:31

Table of Contents

Abstract ..... **i**
Declaration of originality and consent ..... **vii**
Publications and presentations resulting from this thesis ..... **viii**
Acknowledgements ..... **x**
Abbreviations ..... **xiv**
Chapter 1: Introduction **1**
1.1. Epidemiology of hepatitis B virus 1
1.2. Hepadnaviruses 1
1.2.1. The Hepadnaviridae family 1
1.2.2. HBV virion structure 2
1.2.3. HBV genome 3
1.2.3.1. HBV genomic structure 3
1.2.3.2. Open reading frames present on the HBV genome 3
1.2.4. HBV replication 4
1.2.4.1. HBV attachment and entry 4
1.2.4.2. Transcription and replication 5
1.2.4.3. Encapsidation, reverse transcription, budding and release 5
1.3. HBV mode of transmission 7
1.4. HBV infection outcomes 8
1.4.1. Acute HBV infection 9
1.4.1.1. Serological markers during acute HBV infection 9
1.4.1.2. Immune responses during acute HBV infection 9
1.4.1.3. Occult HBV infection 10
1.4.2. Chronic HBV infection 11
1.4.2.1. Serological markers during chronic HBV infection 11
1.4.2.2. Immune responses during chronic HBV infection 12
1.4.2.3. Chronic HBV-induced liver pathology 13
1.5. HBV vaccines and treatments 13
1.5.1. HBV vaccines 13
1.5.2. HBV treatments 14
1.5.2.1. Immuno-modulators 14
1.5.2.2. Nucleoside/nucleotide analogues 15
1.5.2.3. Combination therapies and future potential therapies 16
1.6. Clearance of cccDNA from infected hepatocytes 16
1.6.1. Cytolytic hepatocyte killing 16

1.6.2. Non-cytolytic hepatocyte curing 17
1.7. Clonal proliferation of hepatocytes 19
1.7.1. Clonal proliferation of hepatocytes during acute HBV infection....19
1.7.2. Clonal proliferation of hepatocytes during chronic HBV infection 20
1.8. Integration of HBV DNA into the host genome....21
1.8.1. Detection of integrated virus-cell junctions....22
1.9. Animal models for the study of HBV....24
1.10. Study aims and outline 27
Chapter 2: Materials and Methods 40
2.1. Animals....40
2.2. Virus stock....40
2.3. Procedures involving ducks....40
2.3.1. Inoculation of ducks with DHBV 40
2.3.2. Serum sample collection....41
2.3.2.1. Venipuncture 41
2.3.2.2. Blood serum extraction....41
2.3.3. Liver tissue collection....41
2.3.3.1. Liver biopsy....41
2.3.3.2. Autopsy....42
2.3.4. Tissue sample processing 42
2.3.4.1. Tissue fixation, embedding and sectioning 42
2.3.4.1.1. Ethanol:acetic acid....42
2.3.4.1.2. Formalin 43
2.3.4.1.3. 70% ethanol 43
2.3.4.2. Liver tissue processing 43
2.4. Histology and immunohistochemical analysis of tissue sections....43
2.4.1. Haematoxylin and eosin (H&E) staining....43
2.4.2. Immunohistochemical detection of DHBsAg 44
2.4.3. Periodic acid-Schiff diastase (PAS-D) staining of Kupffer cells 45
2.4.4. Immunohistochemical detection of proliferating cell nuclear antigen (PCNA)..45
2.4.5. Statistical analysis 46
2.5. Serologic assays....46
2.5.1. DHBV DNA extraction from serum....46
2.5.2. Detection of DHBsAg by ELISA 46
2.5.3. Detection of anti-DHBc antibodies by ELISA 47
2.5.4. Detection of anti-DHBs antibodies by ELISA 48

2.6. Liver DNA extraction 48
2.6.1. DNeasy blood and tissue kit 48
2.6.2. ChargeSwitch gDNA mini tissue kit 49
2.6.3. Total DNA extraction 49
2.6.4. Low melting temperature agarose gel electrophoresis and purification of high molecular weight cellular DNA 49
2.6.5. Nuclear DNA extraction 50
2.6.6. High MW DNA extraction 51
2.6.6.1. High MW DNA extraction I 51
2.6.6.2. High MW DNA extraction II 51
2.6.6.3. High MW DNA extraction III 52
2.6.7. cccDNA extraction method 52
2.7. Plasmid DNA extraction 52
2.7.1. Mini prep 52
2.7.2. Maxi prep 52
2.8. DNA analysis 53
2.8.1. Measurement of DNA concentration 53
2.8.2. Restriction enzyme digestion 53
2.8.3. DNA ligation 54
2.8.4. Primer design 54
2.8.5. PCR amplification of DNA 54
2.8.6. PCR purification 55
2.8.7. Agarose gel electrophoresis 55
2.8.8. Agarose gel extraction 55
2.8.9. Quantitation of DNA by quantitative PCR 55
2.8.9.1. Quantitation of serum DHBV DNA by qPCR 56
2.8.9.2. Quantitation of DHBV DNA in the liver by qPCR 56
2.8.9.3. Mathematical calculation of the copy number of DNA 57
2.8.9.3.1. Copy number of plasmid DNA per mass 57
2.8.9.3.2. Copy number of duck DNA per cell 58
2.8.10. DNA sequencing 58
2.8.11. Cleanup of DNA sequencing products 58
2.8.11.1. Isopropanol cleanup 58
2.8.11.2. Magnesium sulphate cleanup 58
2.8.12. DNA sequencing analysis 59
2.9. Cloning 60

2.9.1. Cloning of PCR products into the plasmid vector pCR 2.1-TOPO....60
2.9.2. Analysis of PCR products cloned into the plasmid vector....60
2.9.3. Plasmid glycerol stock....61
2.10. Inverse nested PCR....61
2.10.1. DNA inversion....61
2.10.2. Low melting temperature agarose gel electrophoresis and purification of high MW cellular DNA followed by DNA inversion....62
2.10.3. 96-well nested PCR....62
2.10.4. 96-well agarose gel electrophoresis....63
2.10.5. 96-well agarose gel extraction....64
2.10.6. 96-well DNA sequencing....64
2.10.7. Cleanup of 96-well DNA sequencing products....64
2.11. Southern blot hybridisation....65
2.11.1. Nitrocellulose membrane preparation....65
2.11.2. ^{32}P probe preparation....66
2.11.3. Hybridisation of the ^{32}P-labelled probe to the nitrocellulose membrane....67
2.12. Linker ligation assay....67
2.13. Cell cultures....70
2.13.1. Preparation of cell cultures....70
2.13.2. Harvesting of cell....70
2.13.3. Counting the number of cells....70
2.13.4. DNA extraction from cells....71
2.13.5. Calculation of cells present per 150 ng of DNA....71
2.14. Fluorescence *in situ* hybridisation....71
2.14.1. Preparation of metaphase chromosome spread slides....71
2.14.2. Fluorescent probe preparation....72
2.14.3. Hybridisation of the fluorescent probe....73
Chapter 3: Development of methods - Optimisation of DNA sequencing and qPCR protocols....92
Chapter 3.1: Optimisation of DNA sequencing....92
3.1.1. Aim....92
3.1.2. Introduction....92
3.1.3. Generation of a standard DNA template for sequencing....93
3.1.4. Optimisation of DNA sequencing reaction protocols....94
3.1.4.1. Amount of DNA template per reaction....94
3.1.4.2. Amount of BigDye Terminator mix per reaction....95

3.1.4.3. Amount of sequencing buffer per reaction 96
3.1.4.4. Final volume of the DNA sequencing reaction 97
3.1.4.5. Comparison of methods to cleanup DNA sequencing products 97
3.1.4.6. The effect of GelRed and ethidium bromide staining prior to DNA sequencing 99
3.1.5. Conclusion 101
Chapter 3.2: Optimisation of qPCR assays 106
3.2.1. Aim 106
3.2.2. Introduction 106
3.2.3. Linearisation of plasmid DNA for use in standard curves 108
3.2.3.1. Linearisation of plasmid DNA using various amounts of restriction enzyme .. 108
3.2.3.2. Generation of qPCR standard curves 109
3.2.3.3. Quantitation of DHBV DNA using the generated standard curves 109
3.2.4. Linearisation of plasmid DNA in the qPCR SYBR Green reaction mix for use in standard curves 111
3.2.4.1. Optimisation of linearisation of plasmid DNA in the qPCR SYBR Green reaction mix 111
3.2.4.2. Generation of qPCR standard curves 113
3.2.5. Linearisation of DHBV DNA samples 115
3.2.6. Standardisation of total amounts of DNA in each qPCR reaction 117
3.2.7. Using pBL4.8 plasmid that contains a single copy of DHBV DNA as DNA template to generate qPCR standard curves 118
3.2.7.1. Generation of qPCR standard curves 119
3.2.7.2. Quantitation of DHBV DNA using the generated standard curves 119
3.2.8. Conclusion 120
Chapter 4: Development of Methods - Establishment and optimisation of qPCR assays for the detection of duck DNA 135
4.1. Aim 135
4.2. Introduction 135
4.3. Amplification and sequencing of duck genes 137
4.3.1. Previous work performed to amplify and sequence the duck β actin gene 137
4.3.2. Amplification and sequencing of the duck GAPDH gene 137
4.3.2.1. Amplification and sequencing of a short fragment of the duck GAPDH gene, using known chicken GAPDH primers 137
4.3.2.2. Amplification of a ~1 kbp fragment of the duck GAPDH gene, using primers designed based on the chicken GAPDH sequence 139

4.4. Production and analysis of plasmids containing duck β actin and GAPDH genes 140
4.4.1. Duck β actin gene 140
4.4.1.2. Analysis of the cloned duck β actin gene sequence 141
4.4.2. Duck GAPDH gene 142
4.4.2.1. Production and analysis of pT2.1DgG plasmid containing duck GAPDH gene 142
4.4.2.2. Analysis of the cloned duck GAPDH gene sequence.....143
4.4.3. Establishment of qPCR assays for the detection of duck β actin and GAPDH.145
4.4.3.1. Optimisation of qPCR primers for duck β actin and GAPDH qPCR assays.....145
4.4.3.1.1. Optimisation of qPCR primers for the detection of duck β actin genes using pT2.1DgB plasmid as template 145
4.4.3.1.2. Optimisation of qPCR primers for the detection of duck GAPDH genes using pT2.1DgG plasmid as template 147
4.4.3.2. Calculation of plasmid copy numbers to generate qPCR standard curves 148
4.4.3.3. Establishment of a qPCR standard curve for duck β actin and GAPDH using pT2.1DgB and pT2.1DgG plasmids 148
4.4.4. Determining the copy numbers of duck β actin and GAPDH genes in duck cells 149
4.4.4.1. Determining the copy number of duck β actin and GAPDH genes using qPCR 150
4.4.4.2. Determining the copy numbers of duck β actin and GAPDH genes using FISH 152
4.5. Discussion.....153
4.6. Conclusion 155
Chapter 5: Development of methods for the invPCR assay.....181
Chapter 5.1: Extraction of cellular DNA from liver tissues 181
5.1.1. Aim 181
5.1.2. Introduction 181
5.1.3. Non-selective and selective DNA extraction methods 183
5.1.3.1. DNeasy blood and tissue kit 183
5.1.3.2. ChargeSwitch gDNA mini tissue kit 184
5.1.3.3. Total DNA extraction 185
5.1.3.4. Low melting temperature agarose gel electrophoresis and purification of high MW cellular DNA 186
5.1.3.5. Nuclear DNA extraction 187

5.1.3.5.1. Optimisation of the nuclear DNA extraction method....187
5.1.3.6. High MW DNA extractions....189
5.1.4. Analysis of extracted DNA....190
5.1.4.1. Amount and purity of total extracts....190
5.1.4.2. Quality of extracts....194
5.1.4.3. Inhibition of downstream reactions....195
5.1.4.3.1. Restriction enzyme digestion....195
5.1.4.3.2. PCR....196
5.1.4.4. Quantitation of DHBV DNA and genomic DNA....196
5.1.5. Conclusion....199
Chapter 5.2: The use of locked nucleic acid (LNA) oligonucleotides to increase the specificity of invPCR assays....210
5.2.1. Aim....210
5.2.2. Introduction....210
5.2.3. Designing DHBV-specific LNA oligonucleotides....212
5.2.4. The use of LNA oligonucleotides to block amplification of DHBV DNA from plasmid DNA templates....213
5.2.5. Results and discussion....214
5.2.6. Conclusion....216
Chapter 5.3: Using linker ligation assay to detect integrated virus-cell junctions....219
5.3.1. Aim....219
5.3.2. Introduction....219
5.3.3. Using linker ligation assay to detect integrated virus-cell junctions in WHV-infected woodchuck liver tissues....220
5.3.3.1. Woodchuck liver tissues....220
5.3.3.2. Woodchuck linker ligation assay results....221
5.3.3.3. Discussion....222
5.3.4. Using linker ligation assay to detect integrated virus-cell junctions in DHBV-infected duck liver tissues....223
5.3.4.1. Duck liver tissues....223
5.3.4.2. Duck linker ligation assay results....224
5.3.4.3. Discussion....225
5.3.5. Conclusion....226
Chapter 5.4: Performing invPCR assays on plasmid DNA as a model system....238
5.4.1. Aim....238
5.4.2. Introduction....238

5.4.3. Plasmid DNA as invPCR assay model system 239
5.4.4. Establish invPCR assay – plasmid DNA template inversion step 240
5.4.4.1. Restriction enzyme digestion of plasmid DNA 240
5.4.4.2. Inversion of plasmid DNA 242
5.4.5. Establish invPCR assay – nested PCR step 244
5.4.5.1. Design of nested primer sets for inverted plasmid DNA 244
5.4.5.2. Nested PCR amplifications of inverted plasmid DNA 244
5.4.6. Parameters of invPCR assays assessed 247
5.4.6.1. The sensitivity of detection of the invPCR assay 248
5.4.6.2. The efficiency of the invPCR assay 249
5.4.6.3. Product size preference during the invPCR assay 250
5.4.6.4. The interference of duck cell DNA with the invPCR assay 252
5.4.6.5. Taq polymerases combinations during nested PCR 253
5.4.7. InvPCR assays detecting duck cellular genes as a model system 254
5.4.8. Conclusion 256
Chapter 5.5: Performing invPCR assays on WHV-infected woodchuck and HBV-infected chimpanzee liver tissues 279
5.5.1. Aim 279
5.5.2. Introduction 279
5.5.3. Woodchuck invPCR assay 279
5.5.3.1. Woodchuck liver tissues 279
5.5.3.2. Woodchuck invPCR assay design 280
5.5.3.3. Woodchuck invPCR assay results 280
5.5.3.4. Discussion 281
5.5.3.5. Conclusion 282
5.5.4. Chimpanzee invPCR assay 282
5.5.4.1. Chimpanzee liver tissues 282
5.5.4.2. Chimpanzee invPCR assay design 283
5.5.4.3. Chimpanzee invPCR assay results 284
5.5.4.4. Discussion 285
5.5.4.5. Conclusion 286
Chapter 6: Establishment of invPCR assays to detect integrated virus-cell junctions in DHBV-infected duck liver tissues 307
6.1. Aim 307
6.2. Introduction 307

6.3. Establishment of invPCR assays specific for the detection of integrated virus-cell junctions in DHBV-infected duck liver tissues 308
6.3.1. Duck liver tissues collected in previous studies 308
6.3.2. Determining the sequence of the most probable left and right hand end junctions of the integrated DHBV DNA 308
6.3.3. Design of invPCR assays 310
6.3.4. Extraction of liver cell DNA 311
6.3.5. Performing the invPCR assay 311
6.3.6. Establishing the duck invPCR assay 312
6.4. Perform preliminary invPCR assays to detect integrated virus-cell junctions in DHBV-infected duck liver tissues 317
6.4.1. Detecting integrated virus-cell junctions in livers tissues collected from ducks with acute DHBV infection 317
6.4.1.1. Duck liver tissues collected from previous studies 317
6.4.1.2. Results and discussion 319
6.4.2. Detecting integrated virus-cell junctions in liver tissues collected from ducks with chronic DHBV infection 319
6.4.2.1. Duck liver tissues collected from previous studies 319
6.4.2.2. Results and discussion 321
6.5. Analysis of the integrated virus-cell junctions detected 322
6.6. Discussion on the efficiency of invPCR assay in detecting integrated virus-cell junctions in DHBV-infected duck liver tissues 324
6.7. Conclusion 329
Chapter 7: The use of invPCR assays to explore the mechanisms involved in clearance of DHBV-infected hepatocytes during acute DHBV infection 348
7.1. Aims 348
7.2. Introduction 348
7.3. To establish and monitor acute DHBV infection in ducks 352
7.3.1. To establish acute DHBV infection in ducks 352
7.3.2. Characterisation of histological and serological changes occurring during various stages of acute DHBV infection 354
7.3.2.1. DHBsAg-positive hepatocytes in the liver 354
7.3.2.2. Levels of inflammation in the liver 354
7.3.2.3. Levels of hepatocyte apoptosis in the liver 357
7.3.2.4. Levels of Kupffer cell infiltration and activation in the liver 358
7.3.2.5. Levels of DHBsAg in the serum 360

7.3.2.6. Levels of anti-DHBc antibodies in the serum 360
7.3.2.7. Levels of anti-DHBs antibodies in the serum....361
7.3.2.8. Levels of DHBV DNA in the serum 362
7.3.2.9. Levels of DHBV DNA in the liver....363
7.4. Using invPCR assay to detect integrated virus-cell junctions during various stages of acute DHBV infection 364
7.4.1. Sequence of the DHBV genome present in ducks....364
7.4.2. Detection of integrated virus-cell junctions during various stages of acute DHBV infection using the invPCR assay 365
7.4.3. InvPCR assay results 366
7.5. Discussion....366
7.5.1. Characterisation of histological and serological changes occurring during acute DHBV infection....366
7.5.2. Detection of integrated virus-cell junctions using the invPCR assay....367
7.6. Conclusion....369
Chapter 8: The use of invPCR to assess levels of clonal proliferation of hepatocytes during various stages of chronic DHBV infection 396
8.1. Aims 396
8.2. Introduction 396
8.3. To establish and monitor chronic DHBV infection in ducks 398
8.3.1. To establish chronic DHBV infection in ducks....398
8.3.2. Characterisation of histological and serological changes occurring during various stages of chronic DHBV infection....400
8.3.2.1. DHBsAg-positive hepatocytes in the liver 400
8.3.2.2. Levels of inflammation in the liver 400
8.3.2.3. Levels of hepatocyte apoptosis in the liver 402
8.3.2.4. Levels of Kupffer cell infiltration and activation in the liver....404
8.3.2.5. Levels of DHBsAg in the serum....406
8.3.2.6. Levels of anti-DHBc antibodies in the serum 407
8.3.2.7. Levels of anti-DHBs antibodies in the serum....408
8.3.2.8. Levels of DHBV DNA in the serum 409
8.3.2.9. Levels of DHBV DNA in the liver....409
8.4. Using invPCR assay to detect integrated virus-cell junctions during various stages of DHBV chronic infection....410
8.4.1. Sequence of the DHBV genome present in ducks....410

8.4.2. Detection of integrated virus-cell junctions during various stages of chronic DHBV infection using the invPCR assay....411
8.4.3. InvPCR assay results....411
8.5. Discussion....412
8.5.1. Characterisation of histological and serological changes occurring during chronic DHBV infection....412
8.5.2. Detection of integrated virus-cell junctions using the invPCR assay....413
8.6. Conclusion....417
Chapter 9: Final discussion and concluding remarks....445
9.1. Introduction....445
9.2. Development of methods....446
9.3. Development of the invPCR assay....447
9.4. The use of invPCR assays to explore the mechanisms involved in clearance of DHBV-infected hepatocytes during acute DHBV infection in ducks....451
9.5. The use of invPCR assay to assess levels of clonal proliferation of hepatocytes during various stages of chronic DHBV infection in ducks....455
9.6. Future studies for characterisation of histological and serological changes occurring during acute and chronic DHBV infection....458
9.7. Future directions to detect integrated virus-cell junctions using invPCR assay462
9.8. Concluding remarks....465
References....466

Ph.D. Candidate:	Huey Chi LOW
Student ID:	1102743
Ph.D. thesis title:	Molecular analysis of acute and chronic duck hepatitis B virus (DHBV) infections in ducks
Date:	September 2012

Response to Ph.D. Thesis Examination

Brief statement from the candidate

Based on the Thesis Examination Reports, Examiner 1did not specify any amendments to be made to the thesis, while Examiner 2 made extensive comments that needed to be addressed. This document thus details all the amendments made to the Ph.D. thesis in response to Examiner 2's comments.

Examiner 2's comments have been paraphrased from the Report and are shown below underlined. Each comment has been addressed individually. The page numbers referenced in this document are based on the page numbers of the amended thesis, which may vary from the page numbers mentioned by Examiner 2 in the Report (unless stated as "originally pages XX-XX", which refers to the page numbers in the original submitted thesis).

Detailed list of amendments made to the Ph.D. thesis in response to Examiner 2's comments

Layout of thesis

1.1. Include page numbers for Tables and Figures. Page numbers have been added for all Tables and Figures. The respective page numbers have been listed in a separate Table and Contents for Tables and Figures (refer point 2.1).

1.2. Integrate Tables and Figures into the text. Tables and Figures for each Chapter has not been integrated into the text and are placed at the end of each Chapter. This was to avoid disruption of the text, and for easy referencing as all the results were compiled together. To overcome the issue of difficulties in locating the Tables and Figures, page numbers for every Table and Figure have been included (as mentioned in point 1.1).

1.3. Reduce Figure sizes to include legend on the same page. Whenever possible, corresponding legends for Tables and Figures and were put on the same page.

1.4. Points were being repeated in different Chapters. Repeated information in later Chapters were removed and referred to previous Chapters. Some of the changes made have been listed below for each corresponding Chapter.

1.5. Results that were discussed in the Results section would not require a separate Discussion section, but can be finalised with a short conclusion. In all instances, discussion of results was moved from Results and put in the Discussion of each Chapter.

1.6. Layout of the thesis can be improved, e.g. integrate Chapter 5.2 with Chapter 6, and move Chapter 5.3 near to Chapter 6 to solve duplicated information in 6.3.1 and 5.3.4.1. After many considerations and testing of different Chapter/Section rearrangements, the original order of the thesis was still deemed the best and thus was maintained. The duplicated information issue was addressed in point 1.4.

1.7. Spelling out numbers in full when at the start of a sentence, or change the sentence structure so that it doesn't start with a number. All sentences starting with numbers were modified so that the numbers would not be at the beginning of a sentence. For instance, the sentence in Section 2.8.7 (page 55) "1% agarose gel was prepared" was changed to "To prepare 1% agarose gel". Other sentences that were modified include:

a) Abstract (page iv) 75.5%
b) Section 2.8.9 (page 56) 150 ng
c) Section 2.8.9.1 (page 56) 5 µL
d) Section 2.8.9.2 (page 56) 150 ng
e) Section 2.10.2 (page 62) 600 µL
f) Section 2.10.3 (page 63) 10 µL
g) Section 2.10.5 (page 64) 100 µL

h) Section 2.10.6 (page 64) 4 µL
i) Section 2.10.7 (page 64) 40 µL
j) Section 2.11.1 (page 65) 2 sheets
k) Section 2.11.2 (page 66) 50 µCi
l) Section 2.11.2 (page 66) 150 ng
m) Section 2.11.2 (page 66) 4 µL
n) Section 2.11.3 (page 67) 12 mL
o) Section 2.12 (page 67) 1 unit
p) Section 2.12 (page 68) 10 µL
q) Section 2.14.3 (page 72) 20 µL
r) Figure 3.2.7 (page 133) 2
s) Section 4.3.1 (page 137) 1023 bp
t) Section 4.4.4.1 (page 150) 10-fold
u) Figure 4.6 (page 170) 1122 bp
v) Figure 4.9 (page 176) 1052 bp
w) Figure 5.1.4 (page 207) 200 ng
x) Figure 5.1.4 (page 207) 100 ng
y) Figure 5.1.4 (page 207) 300 ng
z) Figure 5.1.4 (page 207) 100 ng
aa) Section 5.2.4 (page 213) 5 ng
bb) Section 5.3.3.2 (page 221) 5 DNA sequencing reactions
cc) Section 5.3.4.2 (page 224) 32 DNA sequencing reactions
dd) Section 5.4.6 (page 247) 1 µg
ee) Section 5.4.6.3 (page 250) 0.5 µg
ff) Section 5.4.6.4 (page 252) 1 µg
gg) Section 5.4.6.4 (page 252) 1 µg
hh) Table 5.4.1 (page 257) [a]5 µg
ii) Figure 5.4.3 (page 261) 5 µg
jj) Figure 5.4.4 (page 263) 5 µg
kk) Section 5.5.3.3 (page 280) 96-well
ll) Section 5.5.3.3 (page 281) 7 DNA sequencing reactions
mm) Section 5.5.3.3. (page 281) 5 DNA sequencing reactions
nn) Section 5.5.4.3 (page 284) 96-well
oo) Section 6.3.4 (page 312) 1.75 µg
pp) Section 6.3.6 (page 313) 37 DNA sequencing reactions
qq) Section 6.3.6 (page 314) 11 DNA sequencing reactions
rr) Section 6.3.6 (page 315) 6 DNA sequencing reactions
ss) Section 6.3.6 (page 316) 18 DNA sequencing reactions
tt) Section 6.3.6 (page 317) 72 DNA sequencing reactions
uu) Section 6.3.6 (page 317) 3 of the 4
vv) Section 6.4.1 (page 318) 12 liver tissues
ww) Section 6.6 (page 326) 5 DNA sequencing reactions
xx) Section 6.6 (page 326) 6 DNA sequencing reactions
yy) Section 6.6 (page 328) 10 DNA sequencing reactions
zz) Section 6.6 (page 328) 15 DNA sequencing reactions
aaa) Section 7.4.3 (page 367) 62 DNA sequencing reactions
bbb) Section 8.5.2 (page 416) 2 of the integrated virus-cell junctions
ccc) Section 8.6 (page 419) 3 integrated virus-cell junctions

1.8. Spell out the symbol "~" as "approximately" when at the start of a sentence. All sentences starting with symbols "~" and "+" were modified. For instance, the symbol in Section 2.6.4 (page 50) "~2 µg" was changed to "Up to 2 µg". Other sentences that were modified include:
a) Section 2.6.6.1 (page 51) ~25mg
b) Section 2.11.1 (page 65) ~500 ng
c) Section 2.12 (page 67) ~2 µg
d) Figure 2.4 (page 83) "+"

e) Figure 5.4.3 (page 261) ~1 µg
f) Figure 5.4.4 (page 263) ~1 µg
g) Figure 5.4.7 (page 269) ~1 µg
h) Figure 5.4.8 (page 270) ~1 µg
i) Section 6.3.2 (page 310) ~150 ng

2. **Table of Contents**

2.1. Add list of Tables and Figures. A secondary Table of Contents for Tables and Figures has been added after the primary Table of Contents and before the Abstract (page i).

3. **Abstract**

3.1. Incorrect formatting for Yang and Summers, 1999. The citation formatting errors for Yang and Summers on pages i, iv, v have been corrected. Other citation formatting errors that were not pointed out, for example Mason *et al.*, 2005 in page vi, have also been corrected.

3.2. Unexplained abbreviation "dpi" (page iii). The abbreviation "dpi" in page iii had already been previously explained in page i.

4. **Chapter 1**

4.1. Add page numbers for Tables and Figures, integrate Tables and Figures into text, reduce Figure sizes to include legend on the same page. These comments are respectively addressed in points 1.1, 1.2 and 1.3 above.

4.2. Quote original authors where possible, and insert "reviewed by..." when quoting review articles. Several citations were changed to the original authors. These include:
a) Section 1.1 (page 1) Lok, 2000 → Blumberg *et al.*, 1967
b) Section 1.4 (page 8) Seeger and Mason, 2000; Jilbert *et al.*, 2008b → Stevens *et al.*, 1975
c) Section 1.4 (page 8) Andersson and Dienstag, 2008 → Beasley *et al.*, 1982
Whenever original articles were not available, "reviewed by..." were added to the citations. These include:
a) Section 1.2.2 (page 2) Kann, 2008
b) Section 1.2.4.1 (page 5) Jilbert *et al.*, 2008a; Yang *et al.*, 2010
c) Section 1.2.4.1 (page 5) Jilbert *et al.*, 2008a; Kann, 2008; Rabe *et al.*, 2009
d) Section 1.2.4.2 (page 5) Kann, 2008
e) Section 1.2.4.3 (page 6) Jilbert *et al.*, 2008a
f) Section 1.4 (page 8) Andersson and Dienstag, 2008
g) Section 1.4.1.2 (page 9) Lok, 2000; Visvanathan, 2008
h) Section 1.4.1.2 (page 10) Bowden, 2008
i) Section 1.4.2.1 (page 12) Funk *et al.*, 2002; Yim and Lok, 2006; Yuen and Lai, 2008
j) Section 1.4.2.2 (page 13) Bowden, 2008
k) Section 1.9 (page 23) Zoulim *et al.*, 2008

4.3. Citation "Jilbert *et al.*, 2008" should be labelled as either "2008a" or "2008b". This error in citation have been corrected in the whole thesis, to correctly cite either Jilbert *et al.*, 2008a or Jilbert *et al.*, 2008b.

4.4. Length of Introduction was rather short, suggest including DHBV natural life cycle, experimental infection of ducks during acute and chronic DHBV infection, duck immune responses e.g. IFN as cytokine production may affect integration events. The overall length of Chapter 1 "Introduction" was not extended from its current length of 27 pages (1.5 paragraph spacing). An Introduction chapter of 25 – 30 pages (double spacing) has been the standard required length for a Ph.D. thesis in the Hepatitis Research Laboratory. Therefore, descriptions of the DHBV natural life cycle in the duck model were not included in Chapter 1, but are briefly described in Section 1.9 (page 24), and described in Chapters 6, 7 and 8 wherever necessary. The possible effects of cytokine/chemokine production on the rate of hepadnavirus integration have been included as a future study direction in Section 9.6 (page 460).

4.5. The ducks' short lifespan (9-12 years) as a possible reason for ducks not developing HCC do not correlate with findings that woodchucks develop HCC within 4 years after infection. It was further clarified in Section 1.9 (pages 24-25) that woodchucks tend to develop HCC within 4

years after WHV infection due to the frequent activation of *N-myc* oncogenes so far only observed in the woodchucks. It was also clarified in Section 1.9 (pages 24-25) that compared to humans and chimpanzees, ducks have a short lifespan.

4.6. A better review of the relationship between HCC development and hepadnavirus integration is needed. The possible relationship between HCC development and hepadnavirus integration has already been addressed in Section 1.8 (page 22) and Section 9.5 (pages 456-458).

4.7. A better review of Section 1.8.1 "Detection of integrated virus-cell junctions" is needed. Section 1.8.1 had been expanded from 232 words to 840 words to briefly explain methods that had been used to detect integrated virus-cell junctions (pages 22-24). Description of Southern blot hybridisation and linker ligation assay was moved to Section 1.8.1 from Sections 8.2 and 5.3.2 respectively.

5. **Chapter 2**

5.1. Integrate Tables and Figures into text, reduce Figure size to include legend on same page, correct sentences that start with number or symbol. These comments are respectively addressed in points 1.2, 1.3, 1.9 and 1.10 above.

5.2. Figure 2.7 is unnecessary if space is a problem. Space was not a significant problem, thus Figure 2.7 (Figure 2.8 in the amended thesis) was retained.

6. **Chapter 3**

6.1. Integrate Tables and Figures into text, reduce Figure size to include legend on same page, correct sentences that start with number or symbol. These comments are respectively addressed in points 1.2, 1.3, 1.9 and 1.10 above.

6.2. Detailed descriptions of the optimization of existing assays are not required. The whole chapter needs to be rewritten and summarised, perhaps by tabulating the results. For Chapters 3.1 and 3.2, most of the results were already tabulated, or not included and merely described in-text if there were not a lot of data. The level of detail included in these Chapters was felt to be needed to justify the amount of work and level of detail scrutinized during the optimization of the DNA sequencing and subsequent cleanup of DNA sequencing products (Chapter 3.1), or during the optimization of qPCR assays for DHBV total and cccDNA (Chapter 3.2). Nonetheless, Chapter 3.1 was shortened from 11 pages (originally pages 61-70) to 10 pages (pages 92-101), while Chapter 3.2 was shortened from 18 pages (originally pages 72-89) to 15 pages (pages 106-120).

6.3. Figures 3.1.2 and 3.2.4 can be deleted. Figure 3.1.2 was omitted and simply described in-text in Section 3.1.4.6 (page 100). Figure 3.2.4 was kept as it showed evidence of over-digestion or non-specific digestions occurring when plasmid DNA were *Eco*RI-digested in the qPCR assay SYBR Green mastermix, something not previously performed and shown.

7. **Chapter 4**

7.1. Integrate Tables and Figures into text, reduce Figure size to include legend on same page, correct sentences that start with number or symbol. These comments are respectively addressed in points 1.2, 1.3, 1.9 and 1.10 above.

7.2. The sentence that "Clustal W2 alignment program was used" is repetitive and can be stated once at the beginning of the chapter. The repetitive sentences were removed from Sections 4.3.2.1 (pages 137-138), 4.4.1.2 (page 141), 4.4.2.2 (page 143), and simply referred to Section 2.8.12 (page 59) which had described the alignment program used in detail.

7.3. Chapter is verbose. Chapter 4 was shortened from 24 pages (originally pages 91-114) to 22 pages (pages 135-156).

8. **Chapter 5.1**

8.1. Too much discussion of advantages and disadvantages for each kit, some of which were repeated in the Results section. The discussion of the advantages and disadvantages of each DNA extraction method used in Section 5.1.3 were retained in order to give a more complete picture in determining the most suitable method to be used in the invPCR assay. The repeated discussions of the DNA extraction methods in the Results Section 5.1.4 (pages 190-199) were removed.

8.2. Section 5.1.4 Long discussion on accuracy of spectrophotometers is not needed. Comparison of Nanodrop spectrometer and Spectromax spectrophotometer in Section 5.1.4 (pages 190-191) was not to determine the accuracy of the Nanodrop spectrometer, but rather to show that this new equipment gives the same readings as the Spectromax spectrophotometer, which has been used in the Hepatitis Research Laboratory for many years. Thus, the results generated in this thesis could be confidently compared and even combined with previously generated results, without the potential differences of greater sensitivity or accuracy of the results obtained using the newer Nanodrop Spectrometry, as claimed by the manufacturer (Thermo Fisher Scientific, Canada). There is no doubt that the Nanodrop spectrometer is accurate. This Section was shortened, and some descriptions of the Nanodrop spectrometer was moved to Materials and Methods Section 2.8.1 (page 53).

8.3. Section 5.1.4.4 is mostly repetitive and can be deleted/summarised. Section 5.1.4.4 (pages 196-199) was one of the more important results for Chapter 5.1, as it looks to quantitate the levels of DHBV DNA and duck genomic DNA present in each extracted DNA sample. The ability to extract large amounts of duck genomic DNA with the least amounts of DHBV DNA is one of the main criteria for selecting a DNA extraction method to be used in the invPCR assay. Hence this Section was not removed. It was shortened from 1513 words (originally pages 132-135) to 1188 words (pages 196-199).

8.4. Detailed descriptions of the optimization of existing assays are not required and can be summarized in a table of results. Entire Chapter 5.1 was revised to be more succinct, with repeated information removed in subsequent paragraphs. Chapter 5.1 was shortened from 22 pages (originally pages 115-136) to 19 pages (pages 181-199).

9. **Chapter 5.2**

9.1. Some information in introduction has been repeated in discussions and thus can be removed. Entire chapter was revised to be more succinct, with repeated information removed in subsequent paragraphs. Chapter 5.2 was shortened from 8 pages (originally pages 137-144) to 7 pages (pages 210-216).

10. **Chapter 5.3**

10.1. Section 5.3.3.3 direct comparison of the linker ligation assay and the invPCR assay cannot be made as liver used was from different woodchucks. Direct comparison of the methods on the same liver samples was unfortunately not able to be performed due to the limited availability of in liver samples from the woodchucks. Instead, two woodchucks were chosen based on their similar WHV infection outcome and viral load, for as close a comparison as allowed. The discussion in Section 5.3.3.3 (page 222) was modified from a direct comparison of number of actual integrated virus-cell junctions detected, to the trend of the junctions detected. Statements were also included to note that both assays were compared using different liver samples.

10.2. Section 5.3.4.3 Provide details and reference to results of duck tissues mentioned here. Each duck invPCR assay results from Chapter 6 that was discussed in Section 5.3.4.3 was specifically referenced (pages 225-226).

10.3. Comment on the woodchuck and duck BLAST homology of integrated sites that included non target species homology. Statements were included in Section 5.3.3.2 (page 221) and 5.3.4.2 (pages 224) in regards to the BLAST homology to the insert DNA were not from the target species. This was due to the woodchuck and duck genome being not fully sequenced, and thus an insert DNA BLAST homology to other mammalian or avian species respectively would also be accepted. On a similar note, as the human genome has been fully sequenced and made accessible on GenBank, invPCR assay studies in humans would only accept any insert DNA with BLAST homology to humans as a true integration junction. InvPCR assay studies in chimpanzees similarly would also accept any insert DNA BLAST homology to humans as a true integration junction, based on the close evolutionary relationship between chimpanzees and humans (mentioned in Section 5.5.4.3 page 285).

10.4. Introduction Section 5.3.2 was shortened from 3 pages (originally pages 145-147) to 2 pages (pages 219-220), with discussions regarding the linker ligation assay moved to Introduction

Section 1.8.1 (pages 22-24). The entire Chapter was revised to be more succinct, with repeated information removed in subsequent paragraphs. Chapter 5.3 was shortened from 10 pages (originally pages 145-154) to 8 pages (pages 219-226).

11. **Chapter 5.4**

11.1. The entire Chapter was revised to be more succinct, with repeated phrases/sentences removed in subsequent paragraphs. Chapter 5.4 was shortened from 21 pages (originally pages 155-175) to 19 pages (pages 238-256).

12. **Chapter 5.5**

12.1. Section 5.5.4.1 Error in reporting that chimpanzee was 22 years old with history of chronic HBV for 27 years. Chimpanzee 4x222 was corrected to be "44 years old" at the time of biopsy (page 284).

12.2. Insertion of published papers. Hard copies of the two papers arising from contributions of results obtained in this Chapter were included in a pouch attached to the final bound Ph.D. Thesis. Soft copies (PDF files) of the two papers were also included in the CD containing the softcopy of the final Ph.D. Thesis.

12.3. Statement was included in Section 5.5.3.3 (page 281) that due to the woodchuck genome being not fully sequenced yet, for the woodchuck invPCR assay, an insert DNA BLAST homology to other mammalian species would be accepted. Another similar statement was included in Section 5.5.4.3 (page 285) that due to the close evolutionary relationship of chimpanzees and humans, for the chimpanzee invPCR assay, an insert DNA BLAST homology to either chimpanzee or human would be accepted.

12.4. Entire chapter was revised to be more succinct. Repeated information regarding invPCR assay and integration of viral dslDNA in Section 5.5.3.2 (page 280) were removed and referenced to Section 1.8.1 (pages 23-24). Chapter 5.5 was shortened from 10 pages (originally pages 177-186) to 8 pages (pages 279-286).

13. **Chapter 6**

13.1. Section 6.3.1 is a repeat of Section 5.3.4.1. The repeated information was removed (page 309) and reference back to Section 5.3.4.1 (page 223).

13.2. Section 6.3.2 Elaborate on whether the base pair differences of the DHBV sequences detected were near the 5' and 3' end and thus may affect the ability to detect integrated DHBV DNA. As shown in Figure 6.1 and described in Section 6.3.2, most mutations were at the first 35 nucleotide of the sequenced DHBV, one mutation was at nucleotide 502, and the rest were at the last 20 nucleotide of the sequenced DHBV. A statement was added in Section 6.3.2 that restriction enzymes for the duck invPCR assays should not have digestion sites at nucleotide 502, but the duck invPCR assay PCR primers could be designed to amplify across nucleotide 502 (pages 310-311). Based on Figure 6.4, for the chosen duck D3 invPCR assay design, the restriction enzyme digestion sites are at nucleotides 391, 505 and 526, while primer binding sites range from nucleotides 172 – 231 and 465 – 509. Thus, the mutations found in the DHBV sequences should not affect the restriction enzyme digestions, while PCR amplification should not be affected with a single base pair change at the primer binding site of nucleotide 502, and therefore would not affect the invPCR assay to detect integrated DHBV DNA.

13.3. Include headings for Table 6.3 with more information on the duck samples used. Headings with general information of the groups of ducks tested in this Section were added to Table 6.3 (page 337). Detailed explanations of each type of vaccination, antiviral treatment, time-points of liver biopsy, viral load etc. were not included, as the details of each duck were already mentioned in-text and referred to in the table legend, and would clutter and confuse Table 6.3 when included in the table heading.

13.4. Section 6.4.2.2 Query whether the invPCR assay was repeated for ducks FN76, FN77, FN78. A statement has been added to clarify that the invPCR assays had been repeated multiple times, all achieving similar results, which were no detectable invPCR products with only smears as seen by agarose gel electrophoresis (page 323).

13.5. Section 6.4.2.2 Query whether more work should be done in ducks FN1 and FN3 to determine the effect of antiviral therapy on viral integration. No further analysis of FN1 and FN3 liver samples were performed in this thesis, although future work could continue to analyse these liver samples to observe the possible effects of antiviral therapy on viral integration, clonal proliferation of hepatocytes, and formation of hepatocyte clones. A statement was added in Section 6.4.2.2 (pages 322-323) to note that "no further analysis was performed in this thesis although future work could continue to analyse these liver samples to observe the possible effects of antiviral therapy on viral integration, clonal proliferation of hepatocytes, and formation of hepatocyte clones".

13.6. Section 6.6 Commented that invPCR results seemed variable, especially the DNA sequencing failure rates. Query whether Dr. Mason used exactly the same assay and methods, if so it would be the optimised methods. The methods performed in this thesis were initially slightly different from the methods used by Dr. Mason, due to the different availabilities of equipment in each lab (e.g. plate clamp, plate centrifuge), and potential differences in the quality of reagents used in each lab. Many strategies were suggested in Section 6.6 (pages 325-330) to improve the results obtained from the Hepatitis Research Laboratory. But it is true that sometimes some "batch variations" of invPCR assay results do occur at times, e.g. one batch of sequencing with have significantly more failed results compared to normal. In general however, sequencing reactions performed by Dr. Mason do have less failed results compared to sequencing reactions performed in this thesis.

13.7. Compare results using a table. Presentation of the results obtained from this thesis and from international collaborator Dr. William Mason as a table was not added. Although a table would definitely allow for direct comparison of both studies, there was too much information that would need to be included due to the many different samples and conditions of invPCR assays performed, causing the suggested table to be long and confusing.

13.8. Statement was included in Section 6.3.6 (page 313) that due to the duck genome being not fully sequenced yet, an insert DNA BLAST homology to other avian or mammalian species would also be accepted.

13.9. Entire chapter was revised to be more succinct. Chapter 6 was shortened from 27 pages (originally pages 187-213) to 24 pages (pages 308-331).

14. **Chapter 7**

14.1. The phrase "as there were no control ducks in this study..." was repeated numerous times. The control ducks used in this Chapter was described once in Section 7.3.1 (page 353), and removed from subsequent paragraphs, which only referred back to Section 7.3.1. All the other repeated information throughout the Chapter, like Section 7.3.2.9 (originally pages 231-232) that was repeated in Section 2.8.9.2 (page 57), was removed and referenced back to the corresponding previous Sections.

14.2. Table 7.1 The legend is too long. The histological grading system was moved to Section 2.4.1 (page 44), and simply referred to in the legends of Tables 7.1 (page 372).

14.3. Section 7.3.2.2 Query whether the ducks in this study were kept together as a group. If so, all ducks would be exposed to the same environmental toxins. All ducks in this study were kept together in the same housing pen. Explanations were added that the duck 342 with higher levels of liver injury due to environmental toxin was not due to exposure of only that duck in the whole group to the toxins, but rather the potential higher sensitivity and reactivity of that duck towards the toxins, compared to the other ducks (page 356).

14.4. Figure 7.5A DHBsAg levels were above the limit of detection between 25 and 36 dpi, but was referred to in Section 7.3.2.5 that they were below the limit of detection. The cut-off lines in Figures 7.5A, 7.5B and 7.5C (page 388) were misplaced. The positions of the cut-off lines have been corrected, and now correctly showing that the levels of DHBsAg were always below the level of detection throughout the study, as described in Section 7.3.2.5 (page 361)

14.5. Section 7.3.2.8 Comment that Vickery and Cossart (1996) J. Hepatology 25:504 found that peak viraemia could be delayed in older ducks until 15 dpi. Vickery and Cossart's published study (1996) inoculated 26-day-old ducks with DHBV, which were much younger than the 42-day-old ducks used in this study. As the ducks in Vickery and Cossart (1996) were not age

matched, they were therefore not used for comparison in this Chapter. To emphasise that the comparisons made were with published age matched ducks only, the description "previously published age matched ducks" was included (page 363).

14.6. Move Section 7.6 to Chapter 9. The discussions of future directions from Section 7.6 (originally pages 239-243) were merged with Section 8.6 (originally pages 270-275) and moved to Sections 9.6 and 9.7 (pages 456-466), and replaced with a short "Conclusion" (pages 370-371).

14.7. Figure 7.7 (representation of primer binding sites on AusDHBV rcDNA) was moved to Chapter 2 as Figure 2.4 (page 83), as it was deemed more appropriate for this information to be placed in the Materials and Methods Chapter 2, which describes the qPCR methods and primers used for the amplification of the AusDHBV rcDNA.

14.8. Entire chapter was revised to be more succinct. Chapter 7 was shortened from 29 pages (originally pages 215-243) to 23 pages (pages 349-371).

15. **Chapter 8**

15.1. Section 8.2 Correction that male birds are homozygous for the sex chromosome, and not females as in the case for mammals. A statement clarifying that homozygous sex chromosomes are found in mammalian females but in avian males was added (page 398).

15.2. Chapter has repeated points from Chapter 7, e.g. Section 8.2 detection of integrated virus-cell junctions, Section 8.3.2.4 Kupffer cells and their staining, Section 8.4.1 reason for sequencing the DHBV genome, Section 8.5 reason for low detection rate of integrated virus-cell junctions etc. All repeated explanations, like in Sections 8.3.2.1 to 8.3.2.9, Section 8.4.1, Section 8.5.1, and Section 8.5.2 that had been previously mentioned in Chapter 7 were removed, and replaced with corresponding references to Chapter 7.

15.3. The phrase "as there were no control ducks in this study..." was repeated numerous times. The control ducks used in this Chapter was described once in Section 8.3.1 (pages 399-400), and removed from subsequent paragraphs, which only referred back to Section 8.3.1.

15.4. Section 8.4.3 typo that "4 integrated virus-cell junctions" should be "3". Typo was corrected to "3 integrated virus-cell junctions" (page 412).

15.5. Section 8.5.2 Comment that preliminary work was done on neonatal ducks and thus may behave differently from this study. A note was added that the reported rate of DHBV integration published by Yang and Summers (1999) was obtained from a study of young 6-day-old ducks, and thus may be different to the rate of DHBV integration of 6-week-old ducks in this study (page 414).

15.6. Move Section 8.6 to Chapter 9. The discussions of future directions from Section 8.6 (originally pages 270-275) were merged with Section 7.6 (originally pages 239-243) and moved to Sections 9.6 and 9.7 (pages 456-466), and replaced with a short "Conclusion" (pages 418-419).

15.7. Section 8.5.2 Include more explanations addressing the reasons why Dr. Mason detected more integrated virus-cell junctions compared to this study. The reason that the "invPCR assay is not optimised" is not sufficient. Additional discussions regarding the differences of invPCR assays performed in this thesis compared to invPCR assays performed by collaborator Dr. Mason in the USA, that may have affected the low detection of integrated virus-cell junctions in this thesis, were included (page 417).

15.8. Section 8.5.2 Comment that Australian ducks may have differences in genetic makeup due to breeding in isolation for many generations, thus may affect the rate of viral integration compared to ducks from elsewhere in the world. Additional comment on the possible effects of the genetic makeup of ducks in this Australian study due to isolated breeding on the rates of DHBV integration into the genome have been added (page 416).

15.9. Link natural history of hepatitis in the various species to the quantity of integration sites detected. The ducks' short lifespan as the reason for less integration junctions do not correlate with findings that woodchucks seemed to have the most integration sites in the same infection duration with ducks. Additional comments on the differences of the natural history of DHBV infection in ducks compared to other hepadnavirus infections in their natural hosts, in respect

to the different rates of DHBV integration into the genome and of clonal proliferation of hepatocytes have been added (pages 419-420).

15.10. The cut-off lines in Figure 8.5C (page 436) were misplaced. The positions of the cut-off lines have been corrected.

15.11. Entire chapter was revised to be more succinct. Section 8.2 (pages 397-399) was summarised and shortened, with details of the invPCR assay moved to Introduction Section 1.8.1 (pages 22-24). Chapter 8 was shortened from 31 pages (originally pages 245-275) to 23 pages (pages 397-419).

16. **Chapter 9**

16.1. Sections 7.6 and 8.6 "Future directions" were combined and summarised as new Sections 9.6 (pages 459-462) and 9.7 (pages 463-466).

17. **References**

17.1. PNAS should be shortened to Proc. Nat. Acad. Sci. This journal is commonly shortened as Proc. Nat. Acad. Sci. However, the abbreviation PNAS was still preferred in the context of this thesis, and have been defined in Abbreviations page xviii. Other journals, including the European Molecular Biology Organization (EMBO) and Public Library of Science (PLoS), have also been similarly abbreviated and defined in Abbreviations pages xv and xviii respectively.

Other amendments made to the Ph.D. thesis

1. The entire thesis was reviewed several times thoroughly and in greater depths to correct any typos, incorrect cross references, formatting errors, unexplained abbreviations, grammatical errors, and citation formatting errors that were not pointed out by the Examiners. The list of all changes made are not included in this document, as all the changes were minor and did not alter or affect any information or layout of the thesis.
2. The Declaration of originality and consent (page vii) was updated to the new Thesis Declaration as of July 2012 that was released by the Adelaide Graduate Centre, the University of Adelaide.
3. Section 1.3 "Animal models for the study of HBV" was moved to become Section 1.9 (pages 24-26) for a better flow in the Introduction Chapter 1.

Table of Content for Tables and Figures

Table 1.1 29
Figure 1.1 30
Figure 1.2 32
Figure 1.3 34
Figure 1.4 36
Figure 1.5 38

Table 2.1 74
Table 2.2 75
Table 2.3 77
Table 2.4 78
Figure 2.1 79
Figure 2.2 80
Figure 2.3 81
Figure 2.4 83
Figure 2.5 84
Figure 2.6 85
Figure 2.7 87
Figure 2.8 89
Figure 2.9 90

Table 3.1.1 102
Table 3.1.2 103
Figure 3.1.1 104

Table 3.2.1 121
Table 3.2.2 112
Table 3.2.3 122
Table 3.2.4 123
Table 3.2.5 124
Figure 3.2.1 125
Figure 3.2.2 127
Figure 3.2.3 129
Figure 3.2.4 130
Figure 3.2.5 131
Figure 3.2.6 132

Figure 3.2.7 133
Figure 3.2.8 134

Table 4.1 146
Table 4.2 157
Table 4.3 147
Table 4.4 158
Table 4.5 159
Table 4.6 160
Figure 4.1 161
Figure 4.2 163
Figure 4.3 164
Figure 4.4 166
Figure 4.5 168
Figure 4.6 170
Figure 4.7 172
Figure 4.8 174
Figure 4.9 176
Figure 4.10 177
Figure 4.11 179

Table 5.1.1 200
Table 5.1.2 201
Figure 5.1.1 202
Figure 5.1.2 203
Figure 5.1.3 205
Figure 5.1.4 207
Figure 5.1.5 209

Figure 5.2.1 217
Figure 5.2.2 218

Table 5.3.1 227
Table 5.3.2 228
Table 5.3.3 230
Table 5.3.4 232
Table 5.3.5 233

Figure 5.3.1 234
Figure 5.3.2 236

Table 5.4.1 257
Table 5.4.2 258
Figure 5.4.1 259
Figure 5.4.2 260
Figure 5.4.3 261
Figure 5.4.4 263
Figure 5.4.5 265
Figure 5.4.6 267
Figure 5.4.7 269
Figure 5.4.8 270
Figure 5.4.9 272
Figure 5.4.10 273
Figure 5.4.11 275
Figure 5.4.12 276
Figure 5.4.13. 277

Table 5.5.1 287
Table 5.5.2 289
Table 5.5.3 292
Table 5.5.4 293
Figure 5.5.1 296
Figure 5.5.2 297
Figure 5.5.3 298
Figure 5.5.4 300
Figure 5.5.5 301
Figure 5.5.6 303
Figure 5.5.7 304
Figure 5.5.8 306

Table 6.1 332
Table 6.2 333
Table 6.3 336
Table 6.4 337
Table 6.5 339

Figure 6.1 340
Figure 6.2 342
Figure 6.3 344
Figure 6.4 346
Figure 6.5 347

Table 7.1 372
Table 7.2 374
Table 7.3 376
Table 7.4 377
Figure 7.1 378
Figure 7.2 380
Figure 7.3 382
Figure 7.4 384
Figure 7.5 386
Figure 7.6 388
Figure 7.7 390
Figure 7.8 392
Figure 7.9 394

Table 8.1 420
Table 8.2 422
Table 8.3 423
Table 8.4 425
Figure 8.1 426
Figure 8.2 428
Figure 8.3 430
Figure 8.4 432
Figure 8.5 434
Figure 8.6 436
Figure 8.7 438
Figure 8.8 440
Figure 8.9 442
Figure 8.10 444

Abstract

The hepadnavirus family contains two genera, Orthohepadnaviruses that infect mammals and Avihepadnaviruses that infect birds. The most thoroughly studied members of the hepadnavirus family include hepatitis B virus (HBV), which infects humans and chimpanzees, woodchuck hepatitis virus (WHV), which infects woodchucks, and duck hepatitis B virus (DHBV), which infects ducks. All hepadnaviruses have similar genome structure and organisation of the open reading frames on their genome, and also show extensive nucleotide sequence homology within, but not between, genera. All hepadnaviruses primarily infect hepatocytes and have similar infection outcomes in their natural hosts. The outcome of hepadnavirus infection can be divided into either acute, with successful clearance of infection from the host and establishment of immune control, or chronic, where infection is not cleared, resulting in persistent lifelong infection that is linked to various forms of liver disease.

The mechanisms involved in immune clearance of hepadnavirus infections are poorly understood. It has been hypothesised that virus DNA and proteins are, 1) cleared from the liver cytolytically by killing of the infected hepatocytes, or 2) can be destroyed non-cytolytically by cytokines, leaving the infected hepatocyte intact. In this study, the mechanism of immune clearance was explored using molecular approaches to detect integrated virus-cell junctions, formed by the integration of DHBV DNA into the duck liver genome. The rate of DHBV DNA integration is thought to be low (reported to occur at a rate of ~1 in 10^3 – 10^4 cells by 6 day post infection (dpi)) (Yang and Summers, 1999), and the site of viral DNA integration into the host cell genome is random. Hence, each integration event will produce a unique integrated virus-cell junction that can be used as a genetic marker for that cell, which allows the fate of the DHBV-infected hepatocytes to be observed in the liver during various stages of both acute and chronic DHBV infection. Integrated virus-cell junctions can be detected using inverse nested PCR (invPCR), as described by Yang and Summers (Yang and Summers, 1999). Thus, this study aimed to determine whether cytolytic or non-cytolytic clearance of infected hepatocytes occurred, with the ultimate aim of contributing knowledge to assist in the development of new therapies for patients with chronic HBV infection.

Initially, several molecular assays required for the characterisation of DHBV infection and the invPCR assay were established and optimised. These included DNA sequencing reactions and subsequent purification of DNA sequencing products (Chapter 3.1), quantitative PCR (qPCR) assays used for the detection of DHBV total and cccDNA (Chapter 3.2), as well as cloning and sequencing of the duck beta actin (β actin) and glyceraldehyde-3-phosphate

dehydrogenase (GAPDH) genes. The latter were both used as internal controls in the qPCR assays to quantify levels of DHBV total and cccDNA per cell (Chapter 4). Several parameters were tested and compared for each molecular assay to generate final optimised protocols, which were then applied both throughout subsequent Chapters and in other work performed in the laboratory. The duck β actin and GAPDH genes were characterised and the sequences were submitted to GenBank (GenBank Accession GU564232 and GU564233 respectively).

The invPCR protocol was optimised by comparing 8 different liver cell DNA extraction methods, to determine the method that most efficiently extracted high molecular weight (MW) DNA from small quantities of frozen liver (Chapter 5.1). One of the major problems with the invPCR assay was the high level of virus-virus (false positive) sequences generated from replicative forms of virus DNA. Therefore, the use of locked nucleic acids (LNA) oligonucleotides that were specific for the DHBV genome were tested as a potential selective tool to block the amplification of DHBV DNA (Chapter 5.2). LNA oligonucleotides can bind with high affinity to their complementary DNA sequence, forming high melting temperature LNA-DNA complexes which then block amplification of that DNA sequence. Although the LNAs successfully blocked amplification of virus DNA, due to the high cost of LNA, their use in invPCR assays could not be pursued in this thesis. As a possible alternative to the invPCR assay, a linker ligation assay was assessed for its ability to detect integrated virus-cell junctions in samples of WHV-infected woodchuck and DHBV-infected duck liver tissue (Chapter 5.3). However, as the efficiency of detection of integrated virus-cell junctions using linker ligation assay was similar to the efficiency of the invPCR assay, it was not further developed in this thesis, as the linker ligation assay is more complicated and time-consuming than invPCR.

After optimising all the required molecular assays required for the invPCR assay in previous Chapters, the invPCR assay was first performed on plasmid DNA constructs as model systems, in order to determine the sensitivity and efficiency of the assay (Chapter 5.4). It was found that the invPCR assay was able to amplify from a single copy of DNA template. The invPCR assay was also performed on samples of WHV-infected woodchuck and HBV-infected chimpanzee liver tissue in collaboration with Dr. William Mason (Chapter 5.5). The results of the invPCR assay results confirmed that the assays established in this study had comparable efficiency with previously published invPCR assays, and could be confidently applied in this thesis. The integrated virus-cell junctions obtained in this study were included as a subset of the data published by Mason *et al.* 2009a and 2009b.

In order to establish an invPCR assay specifically for the AusDHBV strain (GenBank Accession AJ006350), several DHBV invPCR assays were designed, and preliminary studies were performed on liver tissues collected previously in the laboratory from ducks with acute and chronic DHBV infection (Chapter 6). Up to 38 integrated virus-cell junctions were successfully detected, among which 3 junctions were repeated, suggesting that clonal proliferation of hepatocytes had occurred in the duck liver. Characterisation of the integrated DHBV DNA showed that, consistent to previous studies, the most probable left and right hand end of the integrated DHBV dslDNA was at nucleotide position 2537 nt and ~2485 nt respectively, with no significant patterns or apparent preference of DHBV integration sites in the duck genome. The duck invPCR assay was subsequently extensively used in Chapters 7 and 8.

To achieve the main aim of this thesis, and to explore if cytolytic or non-cytolytic clearance occurs during the resolution of acute hepadnavirus infection, the invPCR assay was used to detect integrated virus-cell junctions during and after resolution of acute DHBV infection. This DHBV model provided an advantage over the WHV-infected woodchuck and the HBV-infected chimpanzee models, where hepadnavirus infection spreads to >95% of the hepatocytes in the liver. Widespread infection requires the division of infected hepatocytes during clearance to replace hepatocytes killed by the host immune response. But in the duck model, DHBV infection can be established in ducks by inoculation with defined doses of DHBV to achieve a maximum DHBV infection of <10% of the hepatocytes prior to immune clearance. Therefore, when the few DHBV-infected hepatocytes were killed, they would be most likely be replaced by division of uninfected hepatocytes. It is thus expected that if cytolytic hepatocyte killing was the predominant response to DHBV infection, the integrated virus-cell junctions would not be detected in the recovered liver, as the infected hepatocytes would be destroyed and replaced by previously uninfected hepatocytes. Conversely, if non-cytolytic hepatocyte curing was predominant, the integrated virus-cell junctions would still be detected after clearance of infection as they would be present in the cellular genome of the "cured" hepatocytes.

Using AusDHBV, acute DHBV infections were established in 3, 6-week-old ducks (Chapter 7). At 4 dpi, active DHBV replication was occurring (159 and 3.6 copies of DHBV total and cccDNA per infected hepatocyte) with ~4.4% of DHBV surface antigen (DHBsAg)-positive hepatocytes in the liver. At 45 dpi, <0.001% of hepatocytes were DHBsAg-positive, with residual DHBV DNA predominantly in the cccDNA form (~0.02 copies and ~0.01 copies of DHBV total and cccDNA per liver cell). Histological characterisation of liver tissues showed

elevated levels of portal and lobular liver inflammation, hepatocyte apoptosis, and Kupffer cell infiltration and activation during clearance of infection (4 and 18 dpi), returning to "basal" levels after clearance (45 dpi). Serological characterisation revealed anti-DHBc antibodies by 4 dpi and anti-DHBs antibodies by 11 dpi. The neutralising anti-DHBs antibodies would have removed DHBV virions from the serum by forming antibody-antigen complexes to reduce the levels of viraemia, as only $2x10^6$ copies of DHBV DNA was detected per mL of serum at 11 and 14 dpi. The anti-DHBs antibodies were also continuously produced at high levels after resolution of infection (45 dpi), providing protection against further DHBV infection.

Using the invPCR assay, up to 24.3 μg of DNA was analysed from liver tissues at 4, 18 and 45 dpi. However, no integrated virus-cell junctions were detected at any stages of acute DHBV infection out of the 286 invPCR products sequenced. Up to 75.5% of the invPCR products sequenced were found to be virus-virus (false positive) sequences. As DHBV DNA integration has been reported to occur at a rate of ~1 in 10^3 – 10^4 cells by 6 dpi (Yang and Summers, 1999), out of the $9.7x10^6$ cells analysed in this study, ~4.4% of which were DHBsAg-positive, it was expected that at least 40 – 400 integrated virus-cell junctions would be detected, assuming that the DHBV-infected hepatocytes were not cytolytically killed during resolution of infection. The failure to detect integrated DHBV-cell junctions in these studies could be due to several factors. Firstly, the high levels of invPCR assay false positives contributed by virus-virus sequences detected in this study (75.5% of total invPCR products) may have greatly reduced the efficiency of detection of the integrated DHBV-cell junctions. This could be improved by further optimisation of the invPCR assay, as well as the development of assays to reduce the detection of virus-virus sequences. Secondly, as the rate of integration was obtained from studies with ongoing high levels of active viral replication at ~6 dpi, the actual rate of integration in this study may be much lower than expected, and as DHBV infection were cleared by 18 dpi, this further shortened the timeframe for integration events to occur.

As an extension to the aims of this thesis, the molecular assays established in Chapters 3 to 6 were applied to study events occurring during chronic DHBV infection in ducks. In particular, the histological and serological changes occurring during different stages of chronic DHBV infection were characterised. In addition, changes in the hepatocyte population were studied by detecting integrated virus-cell junctions using the invPCR assay. As the frequency of the integrated virus-cell junctions would increase upon clonal proliferation of the infected hepatocytes, the size of hepatocytes clones formed and the rate of clonal proliferation of

hepatocytes could be determined by measuring the number of repeats for each integrated virus-cell junction. By establishing chronic DHBV infection in 6-week-old ducks, it was expected that chronic DHBV infection may be associated with increased levels of immune attack resulting in elevated levels of liver inflammation, hepatocyte apoptosis and activated Kupffer cells, as compared to ducks infected, for example, at 1 day of age. With a higher rate of immune attack and liver cell turnover, it was expected that hepatocyte clones would be formed in the liver by clonal proliferation of hepatocytes, as seen previously in studies performed in chronic hepadnavirus infection in humans, chimpanzees, and woodchucks.

Using the same AusDHBV virions, widespread and persistent DHBV infections (termed chronic DHBV infections) were established in 3, 6-week-old ducks (Chapter 8). At 4 dpi, active DHBV replication was occurring (219.5 and 3.7 copies of DHBV total and cccDNA per infected hepatocyte) with ~4.1% of DHBsAg-positive hepatocytes in the liver. At 18 dpi, the DHBV infection spread to >95% of hepatocytes in the liver, and was maintained until 165 dpi (duck 343) or 327 dpi (ducks 338 and 350), with continuous high levels of DHBV replication (181 – 298 copies of total DNA per liver cell) and viraemia (0.6 – 20 μg/mL DHBsAg; $1x10^6$ – $1x10^9$ copies of DHBV DNA per mL of serum), and the establishment of a pool of 5 – 9 copies of DHBV cccDNA per liver cell. Histological characterisation of liver tissues at 4 dpi showed elevated levels of portal and lobular liver inflammation and hepatocyte apoptosis, but with low levels of Kupffer cell infiltration and activation. By 18 dpi, widespread DHBV infection and marked portal and lobular liver inflammation and elevated levels of hepatocyte apoptosis and Kupffer cell infiltration and activation were observed in the liver. From 60 – 327 dpi, the levels of hepatocyte apoptosis and Kupffer cell activation persisted, while levels of liver inflammation and Kupffer cell infiltration decreased. Serological characterisation revealed anti-DHBc antibodies from 4 dpi, and anti-DHBs antibodies from 4 – 11 dpi, at low and varying titres. However, the anti-DHBs antibodies were not sufficient to complex to and remove the DHBV virions from the serum, as “active” viraemia was also detected, indicating that the levels of circulating DHBV virions in the serum were in excess of the anti-DHBs antibodies.

Using the invPCR assay, up to 22.8 μg of DNA were analysed from liver tissues at 4, 18 and 60, 165, 196, 327 dpi. Out of the 685 invPCR products sequenced, 3 integrated virus-cell junctions were detected, but no hepatocyte clones were found. 81% of the invPCR products sequenced were found to be virus-virus (false positive) sequences. As mentioned previously, integration of DHBV DNA has been reported to occur at a rate of ~1 in 10^3 – 10^4 cells by 6 dpi (Yang and Summers, 1999), thus out of the ~$8x10^6$ cells analysed in this study,

with >95% of the hepatocyte population in the liver infected, it is expected that up to 800 – 8000 integrated virus-cell junctions would be detected, with hepatocyte clone sizes of at least 8 cells. Similar to results obtained in Chapter 7, the failure to detect more integrated DHBV-cell junctions in these studies could be due to high levels of virus-virus (false positive) sequences detected using the invPCR assay (81% of total invPCR products). It is of course possible that physiological differences between mammalian and avian liver biology could explain the lack of viral DNA integration and subsequent formation of hepatocyte clones. On top of that, as the timeframe of this study (327 dpi) was much shorter compared to 2.4 years post infection in woodchucks (Mason *et al.*, 2005) and at least 20 years post infection in humans and chimpanzees (Mason *et al.*, 2009a; Mason *et al.*, 2010), such large hepatocyte clones would not be expected to be found in ducks.

Declaration of originality and consent

I certify that this work contains no material which has been accepted for the award of any other degree or diploma in any university or other tertiary institution and, to the best of my knowledge and belief, contains no material previously published or written by another person, except where due reference has been made in the text. In addition, I certify that no part of this work will, in the future, be used in a submission for any other degree or diploma in any university or other tertiary institution without the prior approval of the University of Adelaide and where applicable, any partner institution responsible for the joint-award of this degree.

I give consent to this copy of my thesis, when deposited in the University Library, being made available for loan and photocopying, subject to the provisions of the Copyright Act 1968.

The author acknowledges that copyright of published works contained within this thesis resides with the copyright holder(s) of those works.

I also give permission for the digital version of my thesis to be made available on the web, via the University's digital research repository, the Library catalogue, and also through web search engines, unless permission has been granted by the University to restrict access for a period of time.

Huey Chi LOW 3rd April 2012

Publications and presentations resulting from this thesis

Manuscripts published

Mason, W., **Low, H.**, Xu, C., Aldrich, C., Scougall, C., Grosse, A., Clouston, A., Chavez, D., Litwin, S., Peri, S., Jilbert, A. and Lanford, R. (2009). Detection of clonally expanded hepatocytes in chimpanzees with chronic hepatitis B virus infection. Journal of Virology. 83(17): 8396-8408.

Mason, W., Xu, C., **Low, H.**, Saputelli, J., Aldrich, C., Scougall, C., Grosse, A., Colonno, R., Litwin, S. and Jilbert, A. (2009). The amount of hepatocyte turnover that occurred during resolution of transient hepadnavirus infections was lower when virus replication was inhibited with Entecavir. Journal of Virology. 83(4): 1778-1789.

Manuscript in preparation

Reaiche, G., Thorpe, M., **Low, H.**, Qiao, Q., Scougall, C., Mason, W. and Jilbert, A. Evidence that cccDNA survives mitosis during antiviral therapy for chronic hepadnavirus infections.

GenBank publications

Low, H., Reaiche, G., Jilbert, A. (2010) *Anas platyrhynchos* beta-actin gene, partial cds. GenBank Accession GU564232.

Low, H., Reaiche, G., Jilbert, A. (2010) *Anas platyrhynchos* glyceraldehyde-3-phosphate dehydrogenase-like protein (GAPDH) gene, partial cds. GenBank Accession GU564233.

Oral presentations

Low, H., Beard, M., Jilbert, A. Using integrated hepatitis B virus (HBV) DNA as genetic marker. School of Molecular and Biomedical Science PhD Symposium, Adelaide, July 2009.

Thorpe, M., Reaiche, G., **Low, H.**, Mason, W., Jilbert, A. Evidence that the episomal DNA that serves as the transcriptional template of duck hepatitis B virus is able to survive mitosis in the growing liver. International Hepatitis B Meeting, San Diego, USA, August 2008.

Low, H., Beard, M., Jilbert, A. Using integrated hepatitis B virus DNA as genetic marker for individual infected hepatocytes. The University of Adelaide PhD major review, Adelaide, September 2008.

Low, H., Grosse, A., Scougall, A., Aldrich, C., Xu, C., Hall, P., Clouston, A., Lanford, R., Mason, W., Jilbert, A. Detection of clonally expanded hepatocytes in chimpanzees with chronic hepatitis B virus infection. Australian Centre for HIV & Hepatitis Virology Research (ACH^2) Annual Scientific Meeting, Barossa Valley, South Australia, June 2008.

Low, H., Mason, W., Jilbert, A. Using integrated hepatitis B virus DNA as genetic marker for individual infected hepatocytes. IMVS Infectious Diseases Laboratories (IDL) research seminar, Adelaide, July 2007.

Low, H., Mason, W., Jilbert, A. Using integrated hepatitis B virus DNA as a genetic marker of individual infected hepatocytes. The University of Adelaide Integrated Bridging Program (IBP) talk, Adelaide, June 2007.

Low, H., Mason, W., Jilbert, A. Using integrated duck hepatitis B virus DNA as a genetic marker for individual infected hepatocytes. Australian Centre for Hepatitis Virology (ACHV) Annual Workshop, Melbourne, May 2007.

Poster presentations

Low, H., Stroeher, U., Mason, W., Jilbert, A. Using hepatitis B virus-cell junctions as genetic markers for individual infected hepatocytes. Australia Virology Group (AVG) Meeting, Lorne, Victoria, December 2009.

Low, H., Stroeher, U., Mason, W., Jilbert, A. Using hepatitis B virus-cell junctions as genetic markers for individual infected hepatocytes. The University of Adelaide, School of Molecular & Biomedical Science School Research Symposium, Adelaide, December 2008.

Low, H., Mason, W., Jilbert, A. Using hepatitis B virus DNA as a genetic markers of individual infected hepatocytes. Australian Society for Microbiology (ASM) Annual Scientific Meeting, Adelaide, July 2007.

Award

Student travel award to the 2008 International Hepatitis B Virus meeting in San Diego, USA.

Acknowledgements

I would really like to take this opportunity to thank my principal supervisor, Associate Professor Allison Jilbert, for accepting me into the Hepatitis B Research family, and for all your hard work and constant guidance and advice (in science and even in life!) all these years. Thank you also for your patience and for believing in me. You have been a role model for me, and words just cannot express how much gratitude I have for what you have sacrificed and done for me. I am a better person and scientist today because of you! Thank you so much!

I would also like to thank my co-supervisors Associate Professor Michael Beard for your concern and support; and Dr. Uwe Stroeher for having the patience in dealing with me, editing my thesis, and giving me the "kick-start" I really needed throughout this long torturous journey. Also not forgetting Dr. William Mason, who has been there with me from the very beginning, and have always been the person I can turn to when I need help with my research. Thank you so much for your patience, advice, for reading my thesis so willingly, and even for inviting me to visit your laboratory at the Fox Chase Cancer Center, USA. You truly have played a pivotal part in my research career. I am honoured to have known you.

To my fellow Hepatitis B Research "family members", both past and present, THANK YOU! Dr. Georget Reaiche-Miller, what would I have done without you? To me, you have been my sister, friend, advisor, counsellor, support etc. throughout my entire laboratory years. I'm so grateful to have been given the privilege to study/work along you, and will sorely miss you. A big thank you also to Catherine Scougall, without whom the laboratory will not be running at all! Thank you for always silently and willingly going above and beyond in helping me in everything small and huge, for helping me so much with my duck studies, for your assurances and encouragement, and even for buying me breakfast and Fruchocs! I could not have done it without you. Not forgetting Dr. Behzad Baradaran for lending your expertise in veterinary in making my duck studies progress smoothly, and for your smile and encouragements; Dr. Feng Feng also for all your help with my duck studies, and all your advice and support in science and life, and Dr. Miao Yang for being part of my project. Arend Grosse, thank you so much for all the memorable times you created in your short time with us. You have opened my eyes to a whole new level of "laboratory efficiency", and your photograph still hangs in the laboratory gently reminding us to "get back to work". To my fellow PhD comrades, what can I say? Thomas Tu, I think I have spent too much time with you, that some of your "nerdiness" has unmistakably rubbed off me. Thank you for being a wonderful friend, a sandbag for punching when things get tough, for filling in my huge gaps of knowledge in science, and

really just for being you. If it were up to me, I would have made you my co-supervisor! You really meant a great deal to me. Chee Quin Teoh, thanks also for being a friend and laboratory colleague by helping me with my duck and laboratory work, and being there for me all these years. Although as nice and memorable the experiences were, I think that I will not really miss the long journeys you used to make me undertake just to get lunch or bubble tea. Thank you Dr. Faseeha Noordeen for all your help with my duck studies, for the excellent and informative conversations over tea, and for being a great (and very responsible) companion on our conferences trips! To past Honours students, thank you so much Dr. Micheal Thorpe, for being a tremendous friend both in and out of the laboratory; Cui Xia (Tricia) Wang for providing me with some samples for my work and for your prayers; Hugh Trahair for being uniquely you and for all the once-in-a-lifetime moments I manage to experience with you around; Qiao (Eric) Qiao for inspiring me to be more hardworking and showing me what it takes to be a good scientist; Wen Ying (Layla) Zhu for being an irreplaceable friend both in and out of the laboratory, I really do not deserve the kindness you have shown me; and last but not least Sophie Trevorrow for your optimism, never-failing smile, and your ever memorable hilarious random comments. My time spent in the laboratory is truly irreplaceable.

I have also been very blessed to have the support from various people from the Molecular Life Sciences Building and the IMVS/SA Pathology. Thank you to all past and present members of the Hepatitis C Research laboratory for being such understanding and friendly neighbours all these years, and for never failing to extend your help when I so needed it. To the academic staffs, especially in the department of Microbiology and Immunology, thank you for your support, guidance and counsel. It has been a memorable journey all the way from undergraduate level until today with you all. Dr. Jamie Botten, I will miss you so much! Thank you for being so encouraging, so patient with me and entertaining my ranting about Star Wars and LEGO, for spoiling me with gifts, and most importantly being my role model as a Christian and a scientist. A huge thank you also to Dr. Christopher Wong for helping me so much both in and out of the laboratory, for the printing of figures in this thesis, for sharing your knowledge with me, and for all the opportunities you have provided for me to teach. My gratitude also goes out to all the general staff of the Molecular Life Sciences Building, in administration, at the store or at Central Services Unit, for all your help and support to make everything run smoothly around the school. Not forgetting Garry Penney for being like a “handyman”, helping me out with all sorts of random favours throughout all these years, and for always smiling and being the friendliest person around. To fellow PhD comrades both past and present: Elizabeth Tran, Sophia Tan, Damien Chong, Magdalene Papadopulos, Min Yan Teh, Shu Ly Lim, May Huey Tan, Donald Jiang, Mabel Lum and many others, thank you for

being such wonderful friends and for all your support, food-fixes (CHOCOLATE!!), and wonderful, memorable times we have had together! Last but not least, my gratitude goes out to all the staff members at the Animal Facility of the IMVS/SA Pathology for all your assistance, providence and patience; to the team at the Tissue Pathology Laboratories of the IMVS/SA Pathology, especially Sophie Kogoj for helping me tirelessly with the tissue cutting and staining, Dr. Tuck Weng Kok for your friendly advice and counsel, Dr. Robert Ratcliff and the team at the Sequencing Facilities for your help with DNA sequencing.

I would also like to take this opportunity to thank the people outside of the university boundaries that have been pivotal to me throughout my journey. To my parents, thank you so much for allowing me to pursue my studies and for supporting me unceasingly. I really appreciate everything that you have sacrificed for me, and I love you both so, so much. To my elder sister, thank you for doing what siblings do best – always being there for me, encouraging and making me laugh, and even for trying to help although you do not understand "science". I am so thankful to have a sister like you. Yee Ming (Isaac) Lam, thank you so much for your undeserving love, patience, support, encouragement, delicious Neslo drinks, pampering, sacrifice to let me complete my PhD, prayers, for understanding my needs in this long journey, and the list goes on and on. I really thank God for you, and cannot wait to go on greater adventures with you! To my grandmother, aunties, uncles and cousins, thank you so much for your support and love. Also not forgetting Amber the cat, for keeping me company and warm all those long, lonely nights, and for having the gift of taking all my troubles away by just a meow, a pat, a stare, or a hug. Ah Ann the cat, I miss you a lot too. You both truly are the little angels in my life.

My gratitude also goes out to my housemates both past and present. Thank you Ruby and Samuel (Miguel-)Lai for bringing order into my chaotic life, for your prayers and sacrificial help all these years. Jezamine Chan, man, I will not be "alive" today if it were not for you! You really mean a lot to me, and living with you is one of the best things that have ever happened to me. To fellow IDKA household members who keep me young: thank you Katrina Ng for being like a big sister to me, for feeding me with all those yummy food, for your patience, and for your randomness that never fails to amuse me; and Wen Chian Chen for caring for me so much, selflessly lending me your things, and tolerating with my crazy antics around the house. I also cannot forget my "pseudo-housemates" – fellow members of the AJIN household. Thank you James Lam, Norman Seah, James Quah, Erwin Lee and Caleb Mamman for bearing with me and allowing me into your house so often. Thank you for looking after and spoiling Amber the cat, and for all those irreplaceable times we had together.

I also could not have done it if it were not for my brothers and sisters in Christ. To Ailyn, Wally, Natalie and Jeremy Hanin, thank you so much for being like a second family to me! Thank you for feeding me, looking after me, and supporting me in every ways big and small throughout my entire stay in Adelaide. I will really miss you all a lot. Thank you to the Pastors who have been praying for me and supporting me all these time, especially Phyllis Lines, Ernest and Bee Bee Lee and their household, (Aunty) Merrilyn Teague, Tim Wallis and his household, Michael and Chew Har Raj and their household. Thank you so much everyone at Influencers Church (formally Paradise Community Church) and Living Water Baptist Church! Lastly to everyone from Overseas Christian Fellowship, current or former, from the three South Australia centres and every centre throughout Australia, and especially to my EXCO comrades who are exceptionally dear to me, thank you so much for being like a family to me, and playing a huge part in my life! I am sorry that I cannot name you all personally, but I treasure you all no less than others. It has been an amazing and honour being on this journey with you all, and I have grown so much because of you all. I will sorely miss the support, your prayers, the crazy times we had, our sharings, and the amazing fellowship.

Last but not least, I would like to give all the glory to God my Father. Thank You for letting me be part of Your family through Your Son, and for sending the Counsellor to guide me and to give me wisdom. Thank You for Your unchanging, undeserving love, and for being my comforter who wipes away all those tears, my strength when I cannot take another step, my provider till overflowing, my support and my shelter from anxiety, my all in all, and being with me so that I did not have to go through it alone. Thank You also for reminding me that this thesis is a gift from You, and that it was not done by my strength or my might, that I may boast in my abilities. *When I said, "My foot is slipping," your love, O LORD, supported me. When anxiety was great within me, your consolation brought joy to my soul. Psalm 94:18-19*.

Abbreviations

µ	micro
<	less than
~	approximately
^{o}C	degree Celsius
%	percent
1H.1	mouse anti-DHBV preS antibodies, IgG2a subtype
2’ CDG	2’ carbodeoxyguanosine
A	adenine
A	Ampere
AB	Applied Biosystems, now part of Life Technologies
AEC	Animal Ethics Committee
AGRF	Australian Genome Research Facility
ALT	alanine aminotransferase
AR	analytical reagent
AST	aspartate-aminotransferase
AU	Anson unit
AusDHBV	Australian strain of DHBV, Genbank Accession AJ006350
b	base(s)
BD	Becton Dickinson
BLAST	Basic Local Alignment Search Tool
bp	base pair(s)
BrdU	Bromodeoxyuridine
BSA	bovine serum albumin
c	centi
C	cytosine
C	core
$CaCl_2$	calcium chloride
cccDNA	covalently closed circular DNA
CDC	Centers for Disease Control and Prevention
cDNA	complementary DNA
Ci	curie
CMI	cell mediated immunity
CPM	counts per minute
CSU	Central Services Unit, the University of Adelaide, SA

CTL	cytotoxic T-lymphocyte
DAB	diaminobenzidine tetrahydrochloride
DAPI	4',6-diamidino-2-phenylindole
ddNTP	dideoxy nucleotide tri-phosphate
DHBcAg	duck hepatitis B core antigen
DHBsAg	duck hepatitis B surface antigen
DHBV	duck hepatitis B virus
DMSO	dimethyl sulfoxide
DNA	deoxyribo nucleic acid
dNTP	deoxy nucleotide tri-phosphate
DOP PCR	semi-degenerate oligonucleotide-primed PCR
dpi	day(s) post infection
DR	direct repeat
dslDNA	double stranded linear DNA
dUTP	deoxyuridine tri-phosphate
EAA	ethanol:acetic acid (3:1 v/v)
EB	elution buffer
EDTA	ethylenediaminetetraacetic acid
ELISA	Enzyme-Linked ImmunoSorbent Assay
EMBO	European Molecular Biology Organization
E. coli	*Esterichia coli*
ER	endoplasmic reticulum
ETV	entecavir
FCCC	Fox Chase Cancer Center, Philadelphia, USA
FCS	foetal calf serum
FTC	emtricitabine
g	gram(s)
g OR x g	x gravitational force, or known as RCF
G	guanine
GAPDH	glyceraldehyde 3-phosphate dehydrogenase
GE	genome equivalents
GE	General Electric Company, Sweden
GSHV	ground squirrel hepatitis virus
H&E	haematoxylin and eosin
H_2O	water
H_2O_2	hydrogen peroxide

H_2SO_4	sulphuric acid
HAART	highly active antiretroviral therapy
HBcAg	HBV core antigen
HBeAg	hepatitis B e surface antigen
HBsAg	HBV surface antigen
HBV	hepatitis B virus
HBxAg	heptatitis B X protein
HCC	hepatocellular carcinoma
HCl	hydrochloric acid
HCV	hepatitis C virus
HI	digested at high concentrations
HIV	human immunodeficiency virus
HNF	hepatocyte nuclear factor
HPRT1	hypoxanthine-guanine phosphoribosyl transferase I
hr	hour(s)
HRP	horseradish peroxidase
IFN	interferon
IgY	immunoglobulin Y
IL	interleukin
IMVS	Institute of Medical and Veterinary Science, SA Pathology
invPCR	inverse nested PCR
IU	International Unit
k	kilo
kb	kilo base pairs
KCl	potassium chloride
L	litre(s)
LB	Luria broth
LHB	large hepatitis B surface proteins
LNA	locked nucleic acid
LO	digested at low concentrations
m	metre(s)
m	mili
M	molar(s)
M	mega
MCS	multiple cloning site

$MgCl_2$	magnesium chloride
$MgSO_4$	magnesium sulphite
MHB	middle hepatitis B surface protein
MHC	major histocompatibility complex
mIU	mili International Unit(s)
min	minute(s)
mol	mole
mRNA	messenger RNA
MW	molecular weight
n	nano
N/A	not available
NA	nucleoside/nucleotide analogue(s)
Na_3Citrate	trisodium citrate
NaCl	sodium chloride
Na_2HPO_4	disodium hydrogen phosphate
NaH_2PO_4	monosodium phosphate
NaN_3	sodium azide
NaOAc	sodium acetate
NaOH	sodium hydroxide
NCBI	National Center for Biotechnology Information
ND	not detected
NDS	normal duck serum
NEB	New England Biolabs, USA
NHMRC	National Health and Medical Research Council, Australia
NK	natural killer
no.	number
NP40	nonyl phenoxylpolyethoxylethanol Tergitol-type NP-40
NSS	normal sheep serum
NSW	New South Wales, Australia
nt	nucleotide(s)
OD	optical density
OH&S	Occupational Health and Safety
OPD	o-phenylenedianine dihydrochloride
ORF	open reading frames
p	pica
P	polymerase

PAMPs	pathogen-associated molecular patterns
PAS-D	periodic acid-Schiff diastase
PBMC	peripheral blood mononuclear cells
PBS	phosphate buffered saline
PBS-T	phosphate buffered saline- tween
pBsSK	pBluescript SK II - plasmid
PCNA	proliferating cell nuclear antigen
PCR	polymerase chain reaction
pfu	plaque forming units
PLoS	Public Library of Science
PNAS	Proceedings of the National Academy of Sciences of USA
PVP	polyvinylpyrrolidone
qPCR	quantitative PCR
rcDNA	relaxed circular DNA
RCF	Relative Centrifugal Force
RI	replicative intermediates
RNA	ribonucleic acid
RNase	ribonuclease
rpm	revolutions per minute
RT	reverse transcription
RT	room temperature
S	surface
SA	South Australia, Australia
SAP	shrimp alkaline phosphatase
SDS	sodium dodecyl sulphate
sec	second(s)
SHB	small hepatitis B surface protein
SOX5	Or1 sex determining region Y-box 5
T	thymine
TAE	tris acetate EDTA
TBP	TATA-binding protein
TE	tris EDTA
TFV	tenofovir
Th1	type 1 T helper cells
Th2	type 2 T helper cells
TLR	Toll-like receptors

Tm	melting temperature
TNF	tumour necrosis factor
TNV	tenofovir
Tris HCl	tris(hydroxymethyl)aminomethane
TUNEL	terminal deoxynucleotidyl transferase dUTP nick end labelling
U	unit(s)
ULN	upper limit of the normal range
USA	the United States of America
UV	ultraviolet
V	Volt(s)
vge	virus genome equivalent
WHO	World Health Organization
WHV	woodchuck hepatitis virus
x	time(s)
YY1	Yin and Yang 1

Chapter 1: Introduction

1.1. Epidemiology of hepatitis B virus

The discovery of hepatitis B virus (HBV) was an interesting journey with a long history. HBV-related outbreaks had been reported as early as 1883, with the term "hepatitis B virus" subsequently introduced by MacCallum in 1947 to describe the second known virus (after hepatitis A virus) that causes hepatitis, or inflammation of the liver. It was not until 1965 that Professor Baruch Blumberg and his team successfully characterised the "Australian leukaemia antigen", now known as HBV antigen, that was found in the serum of patients with Down's syndrome or leukaemia, who were suffering from hepatitis (Blumberg *et al.*, 1967).

Today, HBV infection is classified by the World Health Organization (WHO) as a "major global health problem and the most serious type of viral hepatitis" (WHO, 2008). It is noteworthy that up to three quarters of the world's population is currently living in areas with high levels of HBV endemicity (WHO, 2011). Statistics show that up to 2 billion people have been infected with HBV at some stage in their life, with over 4 million clinical cases of acute HBV infection annually (WHO, 2010). Currently, ~360 million individuals are living with chronic HBV infection, and ~1 million people each year are at risk of serious illness or death from chronic active hepatitis, liver cirrhosis, or primary liver cancer, which is also known as hepatocellular carcinoma (HCC). Worldwide, ~80% of all cases of HCC are linked to HBV infection (WHO, 2011). In addition, despite the availability since 1982 of a HBV vaccine, it is estimated by the Centre for Disease Control and Prevention (CDC) that in the United States of America (USA) alone, an estimated 739,000 new cases of HBV infection occurred between 1998 – 2008 (CDC, 2010). The situation in Australia appears to be slightly better based on per capita, however, ~3417 new cases of HBV infection still occurred between 2000 – 2010 (Commonwealth of Australia, 2011).

1.2. Hepadnaviruses

1.2.1. The Hepadnaviridae family

HBV belongs to the *Hepadnaviridae* family, which contains two genera: Orthohepadnaviruses that infect mammals, and Avihepadnaviruses that infect birds (Table 1.1). Although having similar virion structure, life cycle, sequence homology, genome organisation and infection outcomes, members of the hepadnavirus family have a restricted host range with little or no cross infection among species (reviewed in Zoulim *et al.*, 2008). For example the host range of human HBV is restricted to humans and other primates like

chimpanzees (Desmyter *et al.*, 1973). For this reason some of the other hepadnaviruses and their animal hosts have been used as models to study the pathogenesis of HBV infection, as discussed in detail in Section 1.9.

For HBV, there are currently 8 classified genotypes and at least 6 subgroups with different geographical distribution and some varying viral properties. The genotypes include HBV A, B, C, D, E, F, G and H, with subgroups such as B_j (Japan), B_a (Asia,), A_{africa}, C_{aus}, F1 and F2 (South America). Although the genotypes differ in homology by more than 8% at the nucleotide level, all HBV genotypes show similar morphology, infection routes, and genomic structure (Chu and Lok, 2002; Kidd-Ljunggren *et al.*, 2002). The HBV genotypes appear to have much in common, but there is growing evidence for correlations between HBV genotype and the severity of infection outcome. For example, HBV genotype C patients tend to develop more severe liver disease, and have higher rates of HCC compared to other genotypes (Bartholomeusz and Schaefer, 2004; Schaefer, 2005). In addition, HBV genotypes have been reported to respond differently to antiviral therapies. For example, published evidence indicates a better response to interferon-alpha (IFN-α) in patients infected with HBV genotype B than genotype C (Kao *et al.*, 2000; Wai *et al.*, 2002).

1.2.2. HBV virion structure

HBV is a small enveloped virus, 42 – 47 nm in diameter. Its genome is contained within an icosahedral nucleocapsid. The lipid layer of the outer viral envelope is host-derived, acquired during viral budding from the endoplasmic reticulum (ER). Embedded in the lipid layer are three forms of HBV surface antigen (HBsAg): large hepatitis B surface protein (LHB), medium hepatitis B surface protein (MHB) and small hepatitis B surface protein (SHB). They are present in different amounts, with SHB being the most abundant (constituting up to 85% of the total envelope proteins), followed by LHB (10 – 30%), and MHB (10% – 20%) (reviewed in Kann, 2008).

Contained within the viral envelope is the icosahedral nucleocapsid, comprised of 180 or 240 individual HBV core protein (HBcAg) molecules. Nucleocapsid assembly is spontaneous, starting with rapid dimerisation of HBcAg, followed by a slower formation of hexamers, to generate 'building blocks' for the assembly of the nucleocapsid (reviewed in Kann, 2008). The HBV genome and covalently bound HBV polymerase are found in the nucleocapsid. The HBV genome is discussed in detail in Section 1.2.3. A schematic representation of the HBV virion is shown in Figure 1.1A.

1.2.3. HBV genome

1.2.3.1. HBV genomic structure

HBV has a small DNA genome, ~3200 base pairs (bp) in size. In the viral nucleocapsid, the genome is found in a partially double-stranded relaxed circular form (rcDNA) form, with the HBV polymerase covalently attached to the 5' end of the negative-strand of rcDNA (refer Figure 1.1A for schematic representation of the rcDNA found in the HBV virion). In the rcDNA form, the viral genome has a greater than full-length negative-strand DNA, with a 7 – 9 bp terminal redundancy at the 5' end, and a partially complete positive-strand DNA. The positive-strand DNA has an 18 nucleotide (nt) RNA primer at the 5' end and a variable 3' end, leaving a single-stranded, 600 – 2100 bp gap in the genome. Complementary base pairing between an overlap of 245 bp at the 5' end of the positive- and negative-strands maintains the DNA genome in the rcDNA conformation. There are also direct repeat (DR) sequences, DR1 and DR2, found at the ends of the cohesive overlap, which play an essential role during the replication of HBV genome (Section 1.2.4.2) (Jilbert *et al.*, 2008b; Kann, 2008).

After the HBV rcDNA enters into in the host nucleus, it is converted to covalently closed circular DNA (cccDNA). This conversion includes removing the negative-strand terminal redundancy, the viral polymerase and the RNA primer, as well as completing the positive-strand, and ligating the ends of the strands to form a complete double-stranded circular DNA form (Jilbert *et al.*, 2008b). The cccDNA is then supercoiled by DNA gyrase and DNA topoisomerases, allowing it to exist in the host nucleus in a stable, mini-chromosome, bound by both host histone and non-histone proteins (Newbold *et al.*, 1995; Bock *et al.*, 2001). cccDNA plays a significant role as the template for transcription of HBV pregenomic RNA and messenger RNA (mRNA) for the production of HBV proteins (Summers and Mason, 1982; Tuttleman *et al.*, 1986).

1.2.3.2. Open reading frames present on the HBV genome

There are four partially overlapping open reading frames (ORF) in the HBV genome, namely the P, C, S and X ORF (shown in Figure 1.1B). The P ORF encodes the viral polymerase, which is a reverse transcriptase protein packaged in the mature virion. The HBV polymerase reverse transcribes HBV pregenomic RNA to produce the rcDNA genome. The C ORF encodes HBcAg that forms the HBV icosahedral nucleocapsid. The S ORF encodes HBsAg and contains 3 in-frame start codons that define the start of the preS1, preS2 and S regions of the HBsAg ORF. HBsAg mRNA species of different regions/lengths are transcribed and translated to produce the LHB, MHB and SHB proteins: LHB is the product of the preS1,

preS2 and S regions, MHB is the product of the preS2 and S regions, and SHB is the product of the S region alone.

On the other hand, the X ORF encodes for HBxAg, whose exact function is poorly understood (Kann, 2008). Recent studies suggest that HBxAg plays an essential role in initiating and maintaining transcription from cccDNA by controlling histone acetylation (Belloni *et al.*, 2009; Lucifora *et al.*, 2011). HBxAg also appears to be a transactivator of both viral and cellular promoters and enhancers that may contribute to the formation of HCC by transactivation of oncogenes (Feitelson and Lee, 2007; Park *et al.*, 2007; Kew, 2008; Kew, 2011). Lastly, HBeAg, the secreted form of the HBcAg, is produced from the C ORF by translation of an additional 33 nt, the preC region, at the 5' end of the C ORF. Interestingly, the function of HBeAg and correlations between HBeAg expression and infection outcome are still relatively unknown. It has been reported that HBeAg-positive HBV chronically-infected individuals have a higher chance of viral clearance compared with HBeAg-negative individuals, who tend to develop life-long HBV infection with high levels of the liver enzyme alanine transaminase (ALT) (Pan and Zhang, 2005). This may be due to HBeAg interference and modulation of the host immune responses by depleting type 1 T helper cells (Th1), and suppressing cytotoxic T-lymphocyte (CTL) activation to produce weak cell mediated immunity (CMI) (Milich *et al.*, 1998).

1.2.4. HBV replication

A schematic representation of the HBV replication cycle and description of the steps involved is shown in Figure 1.3.

1.2.4.1. HBV attachment and entry

HBV mainly infects hepatocytes, which are long-lived (6 months – 2 years) and self-renewing cells that constitute ~70% of the total liver cells (~10^{12} cells) (Seeger and Mason, 2000; Mason *et al.*, 2009a). In studies conducted with the duck model, DHBV particles have also been found to be present in low amounts in lymphocytes, renal glomeruli, tubular epithelium and pancreatic cells (Tagawa *et al.*, 1985), and DHBV replication and antigen expression has been demonstrated to occur in the pancreas, spleen and kidneys (Jilbert *et al.*, 1987; Freiman *et al.*, 1988; Cullen *et al.*, 1989).

The entry of HBV into host cells occur via receptor mediated endocytosis (Treichel *et al.*, 1997) triggered and mediated by the binding of HBV protein receptor(s) (possibly preS1 domain of the LHB) to as yet unknown cellular receptor(s) (Blanchet and Sureau, 2007).

Current potential cellular receptor(s) include the immunoglobulin A (IgA) receptor, membrane-bound interleukin 6 (IL-6), fibronectin receptor, and asialoglycoprotein receptor (reviwed in Jilbert *et al.*, 2008a; Yang *et al.*, 2010). Following receptor binding and entry, the nucleocapsid is released into the cytoplasm and transported to the nucleus, where it dissociates to release the rcDNA genome (reviewed in Jilbert *et al.*, 2008a; Kann, 2008; Rabe *et al.*, 2009). The rcDNA is then converted to the stable cccDNA form as previously described in Section 1.2.3.1.

1.2.4.2. Transcription and replication

HBV replication occurs using the cccDNA present in the nucleus as the transcriptional template to produce HBV pregenomic RNA and other mRNAs (Summers and Mason, 1982; Tuttleman *et al.*, 1986). HBV relies on the host RNA polymerase II for transcription, which is regulated by 4 promoters and 2 enhancers on the HBV genome. Subsequent to activation of transcription by the acetylation of the H3 and H4 histones bound to the cccDNA, various longer than genomic length and sub-genomic RNA molecules are produced using the negative-strand of cccDNA as template (Pollicino *et al.*, 2006; Belloni *et al.*, 2009). These include the pregenomic RNA, which is ~150 bp longer than the HBV genome (~3500 bp), and can be packaged and reverse transcribed to form the rcDNA in nucleocapsids. mRNAs that will be translated into viral proteins include the ~3500 base pregenome for translation of the ~845 amino acid viral polymerase and the 183 or 185 amino acid HBcAg; a slightly longer mRNA for translation of the ~214 amino acid HBeAg; a ~2500 base mRNA for the translation of the ~400 amino acid LHB; ~2100 base mRNAs for the translation of both the ~281 amino acid MHB and the ~225 amino acid SHB; and ~900 base mRNA for the translation of ~154 amino acid HBxAg (reviewed in Kann, 2008). All of the HBV mRNA forms are positive sense with a 5' cap and 3' poly-A tail.

1.2.4.3. Encapsidation, reverse transcription, budding and release

Pregenomic RNA contains several unique structures, as shown in Figure 1.4A. Longer than the HBV genome (~3500 bp), it has a ~150 bp terminal redundancy, resulting in a second DR1 (referred to as DR1*) downstream of the DR2 near the 3' end. It also contains 2 encapsidation signals (ε) near the 5' and 3' ends, each could fold into an RNA stem-loop structure with two main stems joined by a bulge at one side, and a conserved loop at the top of the fold. Binding of the HBV polymerase to the 5' stem-loop would initiate the encapsidation of the RNA pregenome and reverse transcription of the pregenomic RNA to produce rcDNA (Summers and Mason, 1982), or the double stranded linear DNA (dslDNA), a by-product of reverse transcription (Staprans *et al.*, 1991).

The reverse transcription process involves many steps, in which the unique characteristics of the pregenomic RNA, like the stem-loop structure, ε, and DR regions (refer Figure 1.4A), play a major role. Firstly, the HBV polymerase is recruited to the stem-loop at the 5' end of the pregenomic RNA, where the tyrosine residue 96 in the polymerase primes reverse transcription of the 5' UUC 3' motif in the bulge region of ε, as the first three bases of the HBV negative-strand (5' GAA 3') (Figure 1.4B). Subsequently, the polymerase-oligonucleotide complex is translocated to DR1* at the 3' end of the pregenomic RNA, where the GAA oligonucleotide acts as a primer to allow the further synthesis and extension of the negative-strand in a 5' to 3' direction towards the 5' end of the pregenomic RNA template (Figure 1.4C). At the same time, the RNase H activity of the polymerase degrades the pregenomic RNA template (Figure 1.4D); however, it stops near the 5' end of the capped pregenomic RNA, leaving behind a 18 bp oligonucleotide that contains 6 bp of nucleotides followed by 11 bp of DR1. Due to the covalent attachment of the polymerase to the 5' end of the negative-strand, the newly synthesised negative-strand DNA is formed in a "looped" structure (Figure 1.4E). After the synthesis of the negative-strand, the 18 bp RNA oligonucleotide translocates to the complementary DR2 about 200 bp away from the 5' end of the negative-strand, made possible by its close proximity to the 5' end of the negative-strand DNA synthesised as a "loop", and to the 8 bp "r" sequence at the 3' end of the negative-strand. There, the oligonucleotide serves as the primer to allow the synthesis of the positive-strand DNA, thus forming a partially double-stranded rcDNA, with the viral polymerase still covalently attached to the 5' end of the negative-strand (Figure 1.4F) (reviewed in Jilbert *et al.*, 2008a). However, sometimes instead of being translocated, the RNA oligonucleotide remains at DR1 at the 3' end of the negative-strand, where it will serve as an *in situ* primer to allow extension of the positive-strand (Figure 1.4G), effectively forming the dslDNA (Figure 1.4H) (Staprans *et al.*, 1991). This dslDNA by-product is produced at ~5% frequency during reverse transcription (Staprans *et al.*, 1991), and could hypothetically exist in at least three different forms due to *in situ* priming of positive-strand DNA synthesis, non-homologous inter- or intra-molecular recombination, denaturation of the cohesive rcDNA ends, or illegitimate replication of dslDNA generated by monomeric cccDNA with deletions and insertions around the site of joining (Yang and Summers, 1995; Yang and Summers, 1999).

After reverse transcription, the now mature nucleocapsid is enveloped by budding into the ER, gaining a bi-layer lipid envelope in which the transmembrane HBsAg proteins are embedded. Progeny virions subsequently leave the cell by exocytosis via the Golgi bodies. Virions

containing dslDNA are also produced and released, but they are non-infectious as they could not readily form wild-type cccDNA in the nucleus of a newly infected cell (Yang *et al.*, 1996).

Alternatively if levels of HBsAg in the ER membrane are low, mature nucleocapsids may be transported to the nucleus to release the newly synthesised rcDNA or dslDNA into the nucleus. As before, rcDNA can be converted to cccDNA, consequently generating a pool of cccDNA. This pool of cccDNA is a natural occurrence observed during various stages of HBV infection, whereby 5 – 50 copies of cccDNA can be found in the nucleus of a single infected hepatocyte (Summers *et al.*, 1990; Zhang *et al.*, 2003). On the other hand, dslDNA will either be converted to form defective cccDNA by non-homologous recombination of the ends of the dslDNA (Yang and Summers, 1995), or it can integrate non-specifically into the cellular genome, again by non-homologous end joining or recombination (Yang and Summers, 1999; Bill and Summers, 2004). These integration events are rare and the cellular integration sites are random, therefore producing unique virus-cell integration junctions during each integration event (Tokino and Matsubara, 1991; Yang and Summers, 1999). The unique virus-cell junctions created by the integration of HBV DNA are a main focus of this study, and will be further discussed in Section 1.8.

Alternatively, if there is over-expression of HBsAg in the ER membrane, ~20 nm filamentous and spherical sub-viral "surface antigen" particles can be secreted (Seeger and Mason, 2000). These particles which predominantly contain SHB and MHB proteins do not contain a nucleocapsid or viral DNA nor RNA, can be secreted in 10^3 – 10^6 fold excess over the infectious virions (Jilbert *et al.*, 2008b), and may be present at up to 10^{14} particles/mL in the serum of an infected individual (Kann, 2008). Although non-infectious, the abundance of these HBsAg particles may play a role by forming complexes with anti-HBs antibodies and by interfering with the efficiency of the immune response during clearance of HBV (Seeger and Mason, 2000).

1.3. HBV mode of transmission

HBV is transmitted parenterally via direct contact with blood or other body fluids (like semen, vaginal fluids and saliva) of a HBV-positive individual. Some common modes of transmission include sexual contact, organ transplantation, blood transfusion, blood contact due to contaminated instruments or contact with open sores of an infected individual, or via perinatal transfer. Increasing the spread is the fact that HBV virions can also survive up to seven days outside the host whilst retaining infectivity (WHO, 2008; CDC, 2011). However, HBV is not spread by ingestion of virion-contaminated food or water (oral transmission), or

by breastfeeding. HBV also cannot cross the skin or mucous membrane barrier without breaks, nor can it cross the blood/placenta barrier (Andersson and Dienstag, 2008; WHO, 2011).

Despite that, HBV is a highly infectious virus, 50 – 100 times more infectious than human immunodeficiency virus (HIV) (WHO, 2008). Both HBV and DHBV have been shown to establish infections by inoculation of only a single virion (Jilbert *et al.*, 1996; Meier *et al.*, 2003; Asabe *et al.*, 2009). Thus, it is not surprising that HBV has been classified as a high risk virus, and is one of the major infectious occupational hazards for health care workers (Andersson and Dienstag, 2008; WHO, 2008).

1.4. HBV infection outcomes

There are two possible outcomes of HBV infection: acute infection, where the infected individual clears the HBV infection within 6 months, and chronic infection, where the infected individual is unable to clear the HBV infection within 6 months. These outcomes are dependent on several factors, related indirectly or directly to the host immune response against the infection (discussed in Sections 1.4.1.2 and 1.4.2.2), which is influenced by age, dose of infection, and pre-disposing medical conditions. A distinct age and dose relationship of the development of acute or chronic infection has been observed in DHBV-infected ducks (Jilbert *et al.*, 1998), WHV-infected woodchucks (Cote *et al.*, 2000), HBV-infected chimpanzees (Asabe *et al.*, 2009), and HBV-infected humans (WHO, 2008), where the risk of developing chronic infection increases with younger age and higher virus dose at the time of infection. This age-related outcome may be due to the inability of immature immune systems in younger individuals to generate sufficient and effective immune responses against the virus (Jilbert *et al.*, 1998), while higher doses and viral loads may overwhelm the immune system and lead to less effective immune responses (Boni *et al.*, 2003). Therefore, it has been observed that 25% – 50% of children less than 5 years old and 90% – 95% of adults successfully clear HBV infection (Stevens *et al.*, 1975); while 90% of infants (infected during or shortly after birth), 25% – 50% of children and <5% of adults fail to clear HBV and develop chronic HBV infection (Beasley *et al.*, 1982; reviewed in Andersson and Dienstag, 2008). Lastly, there are several predisposing medical conditions that may also increase the chances of an infected individual developing chronic HBV infection. The conditions include immunodeficiency or immune-suppression, plus lepromatous leprosy, leukaemia, neoplastic disease, or chronic renal failure (Andersson and Dienstag, 2008).

1.4.1. Acute HBV infection

1.4.1.1. Serological markers during acute HBV infection

An individual is defined to have had an acute HBV infection when serum HBsAg and HBV DNA levels are no longer detectable within 6 months after infection (Andersson and Dienstag, 2008). Upon infection, an asymptomatic incubation period occurs in the first few weeks when the immune system is not activated, or is unable to be activated, hence allowing HBV virions to replicate in high numbers (Wieland *et al.*, 2004). In WHV-infected woodchucks and HBV-infected chimpanzees >95% of hepatocytes are infected by 4 – 10 weeks post infection. This is coupled with high levels of viraemia that may last for several weeks (up to 10^{10} virions per mL) (Kajino *et al.*, 1994; Asabe *et al.*, 2009). The immune response is then activated and rapid clearance of the virus from the serum occurs along with viral clearance from the liver (Seeger and Mason, 2000). It is during this active clearance period that the infected individual may be symptomatic and show clinical signs including jaundice, dark urine, pale stool, extreme fatigue, mild fever, or abdominal pain possibly due to hepatomegaly and splenomegaly (WHO, 2008).

1.4.1.2. Immune responses during acute HBV infection

Though the reasons for the delayed immune response to HBV are not understood, individuals who are ultimately able to mount a strong immune response against HBV are likely to successfully clear the virus within 6 months after infection (Rehermann *et al.*, 1996).

During acute HBV infection, individuals are able to mount vigorous polyclonal and multi-specific CD8+ CTL, and Th1 and Th2 CD4+ T cells against multiple HBV antigens, including HBsAg, HBcAg and polymerase epitopes (reviewed in Lok, 2000; Visvanathan, 2008). The CTL response is rapid and is able to recognise viral protein epitopes presented via MHC class I molecules on the hepatocyte surface. Thus, even before progeny virions are produced, CTL are able to kill the infected hepatocytes via direct cytolytic mechanisms (Menne and Tennant, 1999). Alternatively, the immune response can induce cytokine secretion, like IFN-γ (Penna *et al.*, 1997; Narayan *et al.*, 2006), that can prevent the formation (Wieland *et al.*, 2005) and induce the dissociation of viral nucleocapsids (Xu *et al.*, 2010). On the other hand, activated Th2 CD4+ T cells also secrete antiviral cytokines that provide local protection of susceptible cells against infection, in addition to rapidly stimulating the adaptive immune responses for the production of a range of specific anti-viral antibodies including non-neutralising anti-HBc antibodies and neutralising anti-HBs antibodies (Zhang and Summers, 2004; Bowden, 2008). Anti-HBs antibodies can bind to HBV and interrupt the spread of HBV to the rest of the liver (Vickery *et al.*, 1989; Pugh *et al.*, 1995). In addition, it

has been reported that natural killer (NK) cells are also activated during acute HBV infection (Chemello *et al.*, 1986; Li *et al.*, 2011). NK cells could either be directly cytolytic to the HBV-infected cells, or secrete a range of cytokines and chemokines for the activation and maintenance of adaptive immune responses (Andoniou *et al.*, 2006).

As a summary, serological changes and clinical observations that occur during acute HBV infection are shown in Figure 1.5A. As shown, acute HBV infection is often accompanied by significant elevation of liver enzymes including ALT, presumably released by hepatocytes targeted by host immune responses, and individuals may also exhibit clinical symptoms. HBV DNA, HBsAg and HBeAg can be detected in the serum, and antibody responses also occur first with the production of anti-HBc antibody, a commonly used marker of current or past HBV infections as it is produced during both acute and chronic HBV infections. Finally, clearance of HBV DNA and antigens, and normalisation of ALT levels is accompanied by the production of anti-HBs and anti-HBe antibodies (reviewed in Bowden, 2008).

1.4.1.3. Occult HBV infection

Despite the apparent resolution of acute HBV infection, trace amounts of HBsAg (usually not detectable by standard diagnostic assays), HBV DNA and RNA may still persist for decades in the liver (Rehermann *et al.*, 1996; Michalak *et al.*, 1999; Le Mire *et al.*, 2005). This situation is referred to as residual or occult HBV infection (Raimondo *et al.*, 2007). The DNA that persists in the liver is predominantly in the cccDNA form (Le Mire *et al.*, 2005). It was found in recent studies in the DHBV model, that the persistence of cccDNA did not appear to require ongoing viral replication (Reaiche *et al.*, 2010). Low levels of HBV DNA have also been detected in peripheral blood mononuclear cells (PBMC) of patients following acute HBV infection (Michalak *et al.*, 1994). Furthermore, trace amounts of HBV antigens may also persist in the individual, as anti-HBc antibodies have been detected in individuals up to 13 years after clinical onset of acute HBV infection, suggesting an ongoing antigenic stimulation of the host immune responses by residual HBcAg (Penna *et al.*, 1996; Michalak *et al.*, 1999). In addition, HBV-specific CTL have been shown to persist in the serum in their activated phenotype several decades after clinical and serological recovery from acute HBV infection, suggesting continuous priming by residual HBV antigens (Rehermann *et al.*, 1996). However, it is unclear whether these residual HBV antigens are being expressed on hepatocytes, or are presented by dendritic cells.

In most clinical cases of residual or occult HBV infection, patients were anti-HBc antibody and anti-HBs antibody positive, with no HBsAg detected in the serum, and only trace

amounts of HBV DNA present in the liver prior to treatments or liver transplantation (Savas *et al.*, 2007; Kusumoto *et al.*, 2011). Normally, the low levels of HBV DNA and antigens are controlled by host immune responses in a "carrier state". However, these individuals face the risk of HBV reactivation when, for instance, they become immune-suppressed either by illness or after organ transplantation (Savas *et al.*, 2007), and by cytotoxic chemotherapy (Grewal *et al.*, 2007) or corticosteroid treatment (Kusumoto *et al.*, 2011). Individuals with HIV co-infection are at particular risk of HBV reactivation due to the impairment of the immune system caused by HIV (Fabris *et al.*, 2003), and especially after cessation of the highly active anti-retroviral therapy (HAART) in the immune-impaired individuals (Bloquel *et al.*, 2010).

In cases of therapy-induced HBV reactivation, HBV reactivation has been reported within 27 days – 8.5 months post-treatment (or up to 15 years after organ transplantation), and is associated with a marked increase in HBV DNA levels (up to ~$2x10^5$-fold increase from basal levels), high viral loads (>$9.4x10^5$ virus genome equivalent (vge)/mL), and elevated aspartate-aminotransferase (AST) and ALT levels (>3 upper limit of normal; ULN), even in the presence of anti-HBs antibodies (Lan *et al.*, 2011; Marinone and Mestriner, 2011). Liver biopsies often showed mild active hepatitis and immune-staining showed high levels of HBsAg (up to >95%) present in hepatocytes (Savas *et al.*, 2007). Unfortunately, many of the cases of HBV reactivation are severe, or even fatal, often due to the development of fulminant hepatitis (Grewal *et al.*, 2007; Kusumoto *et al.*, 2011).

1.4.2. Chronic HBV infection

1.4.2.1. Serological markers during chronic HBV infection

An individual is defined to have chronic HBV infection when serum HBsAg and HBV DNA levels are still detectable 6 months after infection, potentially leading to life-long infection (Andersson and Dienstag, 2008). During chronic HBV infection, >95% of the hepatocytes in the liver could be infected by HBV, but over time only 5% – 40% of hepatocytes remain HBV-positive (Nowak *et al.*, 1996; Mason *et al.*, 2008), generating HBV-positive and HBV-negative hepatocyte foci in the liver (Burrell *et al.*, 1984; Gowans *et al.*, 1985).

The general course of chronic HBV infection consists of four phases. The first phase is immune tolerance, characterised by high levels of serum HBV DNA (10^7 – 10^{11} copies/mL), the presence of HBeAg, and normal ALT levels. The immune tolerance phase commonly occurs in individuals infected during childhood and can last up to 20 – 30 years post infection, or may be absent in adults infected with HBV. The second phase is immune clearance or

HBeAg-positive chronic hepatitis which can occur 20 – 50 years post infection, and is characterised by fluctuating serum HBV DNA and ALT levels, and persistence of HBeAg. A significant outcome during this phase is the possible seroconversion from HBeAg to anti-HBe antibodies. The third phase is the inactive HBsAg carrier state or immune control phase that can occur from 30 – 40 years post infection and beyond, and is characterised by persistent low levels of serum HBV DNA (10^3 – 10^5 copies/mL), and normal ALT levels with possible mild to moderate fluctuations. This carrier state may be life-long, with a few cases of spontaneous resolution of HBV, which are characterised by undetectable HBsAg and HBV DNA in the serum and seroconversion from HBsAg to anti-HBs antibodies. The fourth phase that occurs in ~30% of individuals is known as the reactivation phase or HBeAg-negative chronic hepatitis. This phase is characterised by an absence of serum HBeAg, the presence of anti-HBe antibodies, detectable serum HBV DNA and high ALT levels. Occasionally, during this phase individuals may revert back to HBeAg-positive status (reviewed in Funk *et al.*, 2002; Yim and Lok, 2006; Yuen and Lai, 2008).

1.4.2.2. Immune responses during chronic HBV infection

Individuals who mount weak or moderate immune responses against HBV infections are likely to be unsuccessful in clearing the virus, resulting in chronic HBV infection. In these individuals, the immune responses are generally weak, have restricted HBV antigen specificity, and would mostly be clinically undetectable (Visvanathan, 2008). For instance, only low levels of CTL activation may occur, generating "weak" CTL that are limited to a few HBV epitopes, leading to inefficient elimination of HBV-infected hepatocytes (Menne and Tennant, 1999). There is also no detectable seroconversion to anti-HBs antibody (Lok, 2000) which is essential for removing HBV from the circulation and preventing further spread of virus (Vickery *et al.*, 1989; Pugh *et al.*, 1995). Hence, although anti-HBc antibodies are produced, they are unable to bind to HBV virions, and offer no significant protection against further HBV infections (Bowden, 2008). It is likely that in individuals with chronic HBV, immune responses are overwhelmed by the large quantities of HBV particles, especially by the secreted sub-viral HBsAg particles or HBeAg. These antigens may skew the immune response towards preferential production of Th2 cells, depleting Th1 cells (Visvanathan, 2008), which in turn may fail to stimulate the maturation of CTL (Carotenuto *et al.*, 2011).

As a summary, serological changes and clinical observations that occur during chronic HBV infection are shown in Figure 1.5B. As shown, like acute HBV infection, chronic HBV infection is often accompanied by significant elevation of liver enzymes including ALT, presumably released by hepatocytes targeted by the host immune response, and individuals

may also exhibit clinical symptoms. HBV DNA, HBsAg and HBeAg can be detected in the serum, along with anti-HBc antibody response. During the immune clearance phase, anti-HBe antibody seroconversion occurs accompanied by flares of ALT levels and possible clinical symptoms. However, no anti-HBs seroconversion is detected, while HBV DNA, HBsAg and HBeAg potentially persist life-long at low – moderate levels (reviewed in Bowden, 2008).

1.4.2.3. Chronic HBV-induced liver pathology

Throughout chronic HBV infection, ongoing HBV replication and viraemia may continuously stimulate and activate immune responses against the virus. This may result in a range of host-mediated liver pathology that can be observed histologically, as various inflammatory cells, especially T lymphocytes, will accumulate in the liver (Lok, 2000). These inflammatory cells can cause the apoptosis of surrounding hepatocytes, resulting in liver damage that can be observed as elevated serum ALT levels (Goodman, 2008). Constant inflammation and necrosis in the liver may then contribute to the development of liver fibrosis, which is observed as the scarring and distortion of liver architecture by collagen fibre deposition (Seeger and Mason, 2000). Significantly, when these fibrous septa connect to form isolated liver nodules, cirrhosis develops. It is estimated that 15% – 40% of individuals with chronic HBV infection may develop cirrhosis, along with increased risks of portal hypertension or liver failure (Lavanchy, 2004). Lastly, due to the continuous cycles of inflammation-necrosis-liver regeneration, liver cells may undergo neoplastic transformation and progress to form tumours or HCC (Lok, 2000; Goodman, 2008). HCC is thought to develop in ~25% of individuals chronically infected with HBV, usually at late stages or after decades of chronic HBV infection (Mason *et al.*, 2009a). HBV infection is the most common cause of primary liver tumours, and liver cancer is reported as the third highest death-causing cancer in the world (Kew, 2008; WHO, 2011).

1.5. HBV vaccines and treatments

1.5.1. HBV vaccines

The first commercial vaccine against HBV has been available since 1982. It is a plasma-derived vaccine, which contains HBsAg particles purified from the serum of chronically HBV-infected patients, inactivated and administered as 3 doses with aluminium phosphate or aluminium hydroxide adjuvants. More recently, recombinant HBsAg vaccines have been produced by expression of HBsAg in yeast, purification of the HBsAg particles and administration with aluminium hydroxide or thiomersal adjuvants, and a preservative (Lemon and Thomas, 1997; Andersson and Dienstag, 2008). Both vaccines induce anti-HBs antibodies and provide long-term protection against HBV, with booster doses generally

unnecessary (WHO, 2008). The current HBV vaccines are ~95% effective in decreasing the risk of perinatal transmission from HBV-positive mothers to their infants (Lee *et al.*, 2006) and in preventing chronic HBV infection in vaccinated children (WHO, 2011). Although HBV vaccines are unable to treat established chronic HBV infections, their widespread use has significantly reduced the number of new cases of HBV infection reported annually (Pan and Zhang, 2005; WHO, 2008), the number of cases of chronic HBV infection and rates of development of HCC in children (Chang *et al.*, 1997).

1.5.2. HBV treatments

Currently, there are two main types of treatment for chronic HBV infection, namely immune-modulators and nucleoside/nucleotide analogues (NA) (Lai *et al.*, 2002). Treatments are recommended for HBeAg-positive and anti-HBe antibody-positive individuals with HBV DNA levels $>10^5$ copies/mL (~20,000 IU/mL) and ALT levels twice ULN. The endpoint of treatment on the other hand is not definite, with anti-HBe antibody seroconversion, normalised ALT levels, $<10^5$ copies/mL of HBV DNA or even undetectable serum HBV DNA level guidelines being recommended (Lai and Yuen, 2008).

1.5.2.1. Immuno-modulators

Immuno-modulators, as the name suggests, act by modulating and activating the host immune response to recognise HBV antigen-positive hepatocytes. This then allows for the infected hepatocytes to be killed, for viral replication to be inhibited by cytokines, and for neutralising anti-HBs antibodies to be produced that protect against re-infection and assist in the removal of circulating HBV particles (Lai and Yuen, 2008).

The immuno-modulator IFN-α is the first treatment for chronic HBV, and has been used since the mid 1970s (Lok, 2000; Lai *et al.*, 2002). Currently, the most commonly used immuno-modulator is pegylated IFN-α, a long-lived and pharmacokinetically-improved form of IFN-α.. IFN-α functions by suppressing viral replication through the degradation of viral mRNA (Seeger and Mason, 2000), and may stimulate ongoing host immune responses such as the activation of macrophages, NK cells, CTL, and increase the production of various antiviral antibodies, especially during the immune clearance phase, for more effective viral clearance (Lavanchy, 2004).

However, IFN-α therapy has adverse side effects, such as influenza-like syndromes, depression, muscle pain, balding, and moderate suppression of the immune system (Lai *et al.*, 2002; Lai and Yuen, 2008). The response to IFN-α also varies, with some individuals

achieving HBsAg and/or HBeAg seroconversion, and normalisation of ALT levels; while in most individuals, only relatively small reduction of serum HBV DNA levels could be achieved. In particular, the response to IFN-α therapy in HBeAg-negative individuals that have HBV with preC mutations are significantly poorer compared to wild-type HBV infections. However, patients with elevated ALT at the start of IFN-α therapy have been found to have higher rates of HBeAg seroconversion and loss of HBeAg and HBV DNA, suggesting that cell death had been essential for the clearance of HBV (Bowden, 2008; Lai and Yuen, 2008).

1.5.2.2. Nucleoside/nucleotide analogues

NA act by suppressing HBV replication at the reverse transcription stage, thus preventing the production of replicative intermetidates (RI), rcDNA and dslDNA, and decreasing the release of infectious virions. Unlike immune-modulators, NA do not directly influence the host immune response, and do not directly destroy viral DNA or antigens (Zhu *et al.*, 2001; Lai and Yuen, 2008). They can however prevent the accumulation of the cccDNA pool in the nucleus, reduce viral replication and loads, and thus increase the chance of immune-medicated clearance of infection (Lai and Yuen, 2008).

Some of the most commonly used NA include lamivudine, adefovir, entecavir (ETV), and tenofovir (TFV). Most of these NA, including lamivudine, adefovir and TFV, were originally developed to treat HIV. The response to treatment is generally good, with significant reduction in serum HBV DNA levels, normalised ALT levels, and some anti-HBe antibody seroconversion (Lai and Yuen, 2008). Interestingly, increased host immune responses can also be observed, such as the transient stimulation of CD4+ and CD8+ T cells after treatment with lamivudine (Boni *et al.*, 2003), and cytokine production from both Th1 and Th2 cells after treatment with adefovir (Jiang *et al.*, 2010).

However, the major drawback for NA treatment is the emergence of resistant strains of HBV. This occurs due to the selective pressure of the NA on a natural pool of HBV quasispecies that may contain HBV mutants naturally confering resistance to the NA. For instance, when treated with lamivudine, 15% – 32% of individuals showed NA resistance after one year of therapy, which increased to 76% after five years of treatment. The emergence of resistance against ETV on the other hand is much lower at 1.2% after five years of treatment (Lai and Yuen, 2008; Yuen and Lai, 2011). In some cases, liver histology or disease progression even worsened after the emergence of NA resistant HBV strains (Lai and Yuen, 2008; Zoulim,

2011). Therefore, NA monotherapy is not recommended as long-term treatment option for chronic HBV.

1.5.2.3. Combination therapies and future potential therapies

In order to overcome the disadvantages of NA monotherapy, combination therapy with immune-modulators and NA therapy, or therapy with two or more NA, has been used. Briefly, combination therapy with pegylated IFN-α and lamivudine lead to enhanced reductions in serum HBV DNA levels compared to NA monotherapy (Lai and Yuen, 2008). Combination therapy of two or more NA has been found to delay the emergence of NA resistant HBV strains as well as reducing serum HBV DNA levels to below levels of detection. For example during combination therapy with adefovir and lamivudine, up to 42 months post-treatment, emergence of NA resistance was observed in ~2% of patients, while ~89% patients achieved undetectable serum HBV DNA levels (Lampertico *et al.*, 2007; Yatsuji *et al.*, 2008).

Despite these treatment regimes, there is still no efficient treatment for the complete resolution of chronic HBV infection. Current treatments costs are also high (thousands of US dollars per year), and are generally not easily available or affordable in developing nations with endemic HBV infection who would need them most (WHO, 2008; Zoulim, 2011). New therapies are being developed, including prime-boost vaccination using DNA vaccines expressing viral proteins in combination with NA (Miller *et al.*, 2008), or inhibition of HBV entry by amphipathic DNA polymers (Noordeen, 2009). However, the key element for new treatments should target the HBV cccDNA present in the nuclei of infected hepatocytes, as without achieving complete clearance of cccDNA or sufficient immune control of infection, patients will always face the risk of HBV reactivation.

1.6. Clearance of cccDNA from infected hepatocytes

1.6.1. Cytolytic hepatocyte killing

It is suggested that cccDNA, along with all viral DNA, RNA and proteins, could only be cleared from infected hepatocytes cytolytically when the cell is killed or lysed by apoptosis or necrosis. Hepatocyte killing is mediated by cytolytic host immune responses, which include NK cells and CTL, as described in Section 1.4.1.2.

CTL play a major role during HBV clearance by either direct lysis of infected hepatocytes or by cytokine secretion to inhibit HBV replication (further discussed in Section 1.6.2) (Guidotti *et al.*, 1996). In CD8-depleted chimpanzees, clearance of HBV infection was markedly

delayed until CTL were restored. Clearance was also accompanied by a spike in serum ALT levels, suggesting that clearance of HBV DNA was linked to hepatocyte cell death (Thimme *et al.*, 2003). HBV-specific CTL responses are also observed in individuals who can successfully control HBV replication, this is often accompanied by liver inflammation or liver damage (Maini *et al.*, 2000), and subsequent mitosis of nearby hepatocytes to regenerate the liver and to restore the hepatocyte population. This process of liver regeneration can result in clonal proliferation of hepatocytes as described in Section 1.7.

As described above, it is known from studies of HBV, WHV and DHBV infection that cccDNA is not completely removed by treatment with NA, which only inhibit the virus polymerase and prevent reverse transcription (Dandri *et al.*, 2000; Zhu *et al.*, 2001; Foster *et al.*, 2003; Werle-Lapostolle *et al.*, 2004; Reaiche *et al.*, 2010). On top of that, it remains unclear whether cccDNA can be directly removed by cytokines like IFN-β and IFN-γ that inhibit HBV replication by disrupting the assembly of HBV nucleocapsids (Wieland *et al.*, 2005). Thus, it is believed that complete resolution of HBV infection is only possible when cccDNA is cleared by the killing of all infected hepatocytes (Lok, 2000; Summers *et al.*, 2003; Dandri and Petersen, 2005).

Further indirect evidence for cytolytic hepatocyte killing is provided by the extensive liver turnover (cell death and proliferation) that has been reported to occur during clearance of HBV infection. For instance, in WHV-infected woodchucks, inverse nested PCR (invPCR) assays (described further in Section 1.8.1) suggest that a minimum of 0.7 – 1 turnovers of the entire hepatocyte population occurred during clearance of acute WHV infection, with apoptosis, activation of macrophages and hepatocyte regeneration observed at a rate parallel to the reduction of WHV DNA and antigens (Summers *et al.*, 2003). Similar observations of correlations between hepatocyte death and loss of cccDNA have also been found in studies of NA therapy of chronic WHV infection in woodchucks (Zhu *et al.*, 2001) and DHBV infection in ducks (Fourel *et al.*, 1994b). In addition, patients with elevated ALT levels have also been found to have higher clearance of HBeAg and HBV DNA compared to patients with normal ALT levels, hence further emphasising the importance of hepatocyte death during HBV clearance (Liaw *et al.*, 1994; Lai and Yuen, 2008).

1.6.2. Non-cytolytic hepatocyte curing

As an alternative to cytolytic hepatocyte killing, it has been suggested that cccDNA and all other viral DNA, RNA and protiens could be non-cytolytically cleared from infected hepatocytes. Hepatocyte curing is proposed to be mediated by a range of inflammatory

cytokines secreted by host immune responses as described in Section 1.4.1.2, either by having a direct effect on HBV, or through the activation of a range of other immune cell types, for example, liver macrophages or Kupffer cells (Sitia *et al.*, 2011).

Several cytokines have been found to directly inhibit HBV replication. For example, IFN-β and IFN-γ can disrupt the assembly of HBV nucleocapsids (Wieland *et al.*, 2005), which results in the destruction of HBV RI DNA, and subsequently prevents the formation of rcDNA and new cccDNA in the liver. IFN-α can also inhibit the translation and production of viral antigens (Park *et al.*, 2011), as well as accelerate the decay of mature (HBV replication-competent) nucleocapsids via proteosomic activities (Xu *et al.*, 2010). Although cccDNA levels can be reduced 2-fold by IFN-α and IFN-β in HNF1α-null HBV transgenic mice models (Anderson *et al.*, 2005), and cccDNA may subsequently be lost during mitosis (Mason *et al.*, 2009b), it remains unclear whether cccDNA can be directly destroyed by cytokines.

CTL also play a non-cytolytic role during HBV resolution. In HBV transgenic mice models, HBV RI DNA, RNA and proteins can be successfully cleared by perforin-knockout CTL (which have lost their cytolytic abilities) via the secretion of cytokines like IFN-γ and TNF-α that inhibit HBV replication as previously described (Guidotti *et al.*, 1996). However, extension of the mouse studies to natural infections is problematic because HBV transgenic mice (except those that are HNF1α-null) do not contain cccDNA, and virus transcription comes entirely from the HBV transgene. It has also been suggested that it would not be plausible for CTL alone to resolve HBV infection via hepatocyte killing, as there would be neither sufficient activated CTL nor CTL infiltration to the liver to kill all the infected hepatocytes, knowing that direct contact with the target cell is required by CTL for lysis to occur (Chisari and Ferrari, 1995). However, as the exact ratios of infiltrating CTL to infected hepatocytes could not be measured, it remains undetermined whether the cytolytic or non-cytolytic role of CTL plays a more significant role during the resolution of HBV infection.

Furthermore, the resolution of HBV infection was observed without histological evidence of massive liver turnover during the clearance of HBV infection in various animal models, including DHBV-infected ducks (Jilbert *et al.*, 1992), WHV-infected woodchucks (Kajino *et al.*, 1994), and HBV-infected chimpanzees (Guidotti *et al.*, 1999). HBV DNA levels in the liver and serum also decrease before the loss of HBcAg-positive hepatocytes (Guidotti *et al.*, 1999). In addition, by comparing observed and mathematical modelling-generated stimulations of cytolytic and non-cytolytic T cells effector functions in chimpanzees (Murray *et al.*, 2005), and by comparing observed and mathematical modelling-predicted liver

turnover required for WHV clearance in woodchucks (Mason *et al.*, 2009b), both studies observed that the cytolytic hepatocyte killing may not be sufficient for the clearance of infection in each animal model. On a separate note, activated Kupffer cells are shown to promote the infiltration of inflammatory cells (especially neutrophils) into the liver with no apparent increase in hepatocyte death, further emphasizing the importance of non-cytolytic hepatocyte curing during resolution of HBV infection (Sitia *et al.*, 2011).

Lastly, it is possible that both cytolytic hepatocyte killing and non-cytolytic hepatocyte curing play important roles in the clearance of cccDNA from infected hepatocytes during the resolution of HBV infection. It is concluded in most studies that although each tends to favour either cytolytic or non-cytolytic mechanisms, all agree that the immunopathogenesis of HBV is complex and that both mechanisms are likely to be involved (Jilbert *et al.*, 1992; Thimme *et al.*, 2003; Murray *et al.*, 2005; Yang *et al.*, 2010). Thus in summary, cytokines will inhibit HBV replication and production (non-cytolytic hepatocyte curing), while CTL are able to lyse infected hepatocytes to remove traces of HBV DNA and proteins (cytolytic hepatocyte killing).

To further explore the mechanisms involved during the clearance of virus-infected hepatocytes, Chapters 6 and 7 describe studies performed in ducks with acute DHBV-infection that had <10% of DHBV-infected hepatocyte populations in the liver during early stages of infection. By detecting the integrated virus-cell junctions present in the hepatocytes (described in Section 1.8), we hypothesise that the absence or presence of the junctions after the resolution of infection will enable us to determine whether DHBV-infected hepatocytes are cytolytically killed or non-cytolytically cured.

1.7. Clonal proliferation of hepatocytes

Clonal proliferation, or clonal expansion of hepatocytes, is defined as "a single hepatocyte undergoing multiple rounds of mitosis, to form a cluster or clone of that hepatocyte". Clonal proliferation of hepatocytes is important for the regeneration and restoration of liver mass, and is mediated mainly through the proliferation of mature hepatocytes (Summers *et al.*, 2003; Michalopoulos, 2007; Marongiu *et al.*, 2008).

1.7.1. Clonal proliferation of hepatocytes during acute HBV infection

During the clearance phase of an acute HBV infection, large populations of the HBV-infected hepatocytes are killed by the host-mediated immune responses as discussed in Section 1.6.1. During this process, the liver regenerates to restore liver mass by stimulating and elevating the

proliferation of neighbouring mature hepatocytes. Hepatocyte proliferation was observed in WHV-infected woodchucks, where 28% – 82% of Bromodeoxyuridine (BrdU)-positive hepatocytes were found as proliferating pairs (Kajino *et al.*, 1994), forming an initial clustering of progeny cells which could form hepatocyte clones up to 21 cells in size in acute WHV-infected woodchucks by 16 weeks post infection (Mason *et al.*, 2009b).

1.7.2. Clonal proliferation of hepatocytes during chronic HBV infection

During chronic HBV infection, as infected hepatocytes are killed by immune-mediated attack, clonal proliferation of hepatocytes occurs to restore liver mass (Mason *et al.*, 1998), forming hepatocyte clones over time. Hepatocyte clones have been observed using invPCR assays in the liver of chronically WHV-infected woodchucks (clone size of up to 26,000 cells) (Mason *et al.*, 2005), HBV-infected chimpanzees (clone size of up to 10,000 cells) (Mason *et al.*, 2009a), and HBV-infected humans (clone size of up to 58,000 cells) (Mason *et al.*, 2010). Histological analysis of these liver tissues did not show any distinct foci of histologically altered hepatocytes, suggesting that the hepatocytes clones are not liver tumours or carcinogenic hepatocytes, but are normal hepatocytes that underwent clonal proliferation to replace neighbouring hepatocytes that are killed (Mason *et al.*, 2010).

However, although all hepatocytes in theory have the potential to clonally proliferate, hepatocyte clones are likely to be formed by hepatocytes that possess a survival advantage (Wada *et al.*, 1990). An example of survival advantage include hepatocytes that contain pre-neoplastic mutations that allow the cells to be sustained and stimulated to proliferate (Marongiu *et al.*, 2008). This is supported by the finding that 59% of regenerative nodules of hepatocytes were clonal and that clonal expansion may precede hepato-carcinogenesis (Ochiai *et al.*, 2000). Cirrhotic nodules and large dysplastic foci of hepatocytes of at least 10^5 cells have also been commonly observed to be hepatocyte clones (Yasui *et al.*, 1992). As the formation of cirrhotic nodules has been strongly associated with the development of HCC (Fattovich *et al.*, 2004), and since most HCC are thought to be derived from hepatocytes and not other cell types like ductular or oval cells (Farber, 1991; Ochiai *et al.*, 2000), high levels of clonal proliferation of hepatocytes could thus contribute to the development of HCC.

On the other hand, hepatocytes that lose the ability to express HBV antigens, or express mutated strains of HBV that can evade the immune response would also have a survival advantage and clonally proliferate in the liver. As mentioned above, during chronic HBV infection, >95% of hepatocytes can be initially infected, but it has been reported that only 5% – 40% of hepatocytes remain HBV-positive (Burrell *et al.*, 1984; Gowans *et al.*, 1985; Nowak

et al., 1996). Viral antigen- and DNA-positive and -negative hepatocyte foci have also been observed in the liver of WHV-infected woodchucks (Mason *et al.*, 2005) and HBV-infected chimpanzees (Mason *et al.*, 2009a). It is thus likely that these virus-negative foci are hepatocyte clones, formed by the clonal proliferation of hepatocytes that gained their survival advantage after losing viral expression and as such are no longer targeted by the host immune response (Mason *et al.*, 2009b).

Although clonal proliferation of hepatocytes has been detected by various studies in WHV-infected woodchucks (Mason *et al.*, 2005), HBV-infected chimpanzees (Mason *et al.*, 2009b), and HBV-infected humans (Mason *et al.*, 2010; Tu, unpublished), no known work has been published regarding clonal proliferation of hepatocytes in DHBV-infected ducks. As further understanding of clonal proliferation of hepatocytes may shed light on steps in hepatocarcinogenesis, Chapters 6 and 8 describe studies performed in ducks with chronic DHBV-infection to detect of the clonal proliferation of hepatocytes in the liver.

1.8. Integration of HBV DNA into the host genome

As mentioned in Section 1.2.4.3, during reverse transcription of HBV and production of new HBV genomes, dslDNA may be formed instead of rcDNA (Yang and Summers, 1995). Up to 3 forms of dslDNA may be generated with varying 5' and 3' ends (Yang and Summers, 1999), which when transported to the nucleus, may integrate randomly into the cellular genome (Gong *et al.*, 1995; Gong *et al.*, 1999).

Integration occurs via non-homologous end-joining (Yang and Summers, 1999) or illegitimate recombination with the host genome (Gong *et al.*, 1995), and has been proposed to occur mainly into sites of DNA double-stranded breaks during repair and regeneration of the damaged DNA induced by inflammatory responses against infection (Bill and Summers, 2004). The end joining involves the YY1 transcription factor binding site that is part of the DR1 present at both 5' and 3' ends of the dslDNA form (Hayashi *et al.*, 2000), and may result in a range of genetic rearrangements and deletions of both HBV and host genomic DNA at the integration sites (Takada *et al.*, 1990). However, there are no apparent preferences and patterns of HBV integration sites in the host genome, suggesting that each integration event occurs at a random site in the host genome, forming unique integrated virus-cell junctions during each integration event (Tokino and Matsubara, 1991; Mason *et al.*, 2009a). It should also be noted that the 5' and 3' ends of the integrated HBV DNA on the other hand, are generally within ~250 bp of the expected 5' and 3' ends of the dslDNA (Yang and Summers, 1999; Mason *et al.*, 2009a; Mason *et al.*, 2009b). This allows for the prediction of a most

probable 5' and 3' end of the integrated viral DNA, which is crucial for the design of the invPCR assay used widely in this study, as described in Section 1.8.1 and in Chapters 5 and 6.

It is estimated that integration of DHBV DNA occurs once every $10^3 - 10^4$ cells as early as 6 days post infection (dpi) (Yang and Summers, 1999), with low integration rates in the entire liver of ~0.1% during acute WHV infections (Summers *et al.*, 2003) and 1% – 10% during chronic WHV infections (Summers and Mason, 2004). Interestingly, integrated HBV DNA is found in most cirrhotic nodules and HCC (Kew, 2008), but it is not known whether integrations of HBV DNA into the liver cell DNA are directly responsible for their development and formation. Histologically, there are no significant morphological differences between the HBV integration-positive and -negative cirrhotic nodules, as well as no increased neoplastic-appearing focal growths in HBV integration-positive cirrhotic nodules (Yasui *et al.*, 1992), suggesting no direct link between HBV integration and the formation of HCC. On the other hand, in the WHV model, integration of WHV DNA in or near a *myc* gene, especially *N-myc*2, is apparently responsible for HCC, probably via activation of a *myc* oncogene (Bruni *et al.*, 1999). In HBV-infected humans, rare cases of integration of HBV DNA has led to disruption of the cyclin A gene that is involved in cell cycle regulation (Wang *et al.*, 1990), apparently leading to HCC. Although rare HBV integrations may, by chance, enhance or disrupt essential gene regulators to result in the development of tumours (Paterlini-Brechot *et al.*, 2003), it is highly likely that other non-integration factors are also involved (Murakami *et al.*, 2005; Bruni *et al.*, 2006). These factors may include the oncogenic function of HBxAg, the effects of chronic necroinflammatory hepatic diseases due to ongoing liver damage, and the selective clonal proliferation of pre-existing premalignant hepatocytes (Kew, 2008).

1.8.1. Detection of integrated virus-cell junctions

Integrated virus-cell junctions can be detected by several methods, such as Southern blot hybridisation (Hino *et al.*, 1985), *in situ* hybridisation using biotinylated probes (Negro *et al.*, 1985), *Alu*-PCR (Kawai *et al.*, 2001), linker ligation assay (Summers *et al.*, 2003), and last but not least the invPCR assay (Yang and Summers, 1999) which was chosen for this study.

Briefly, Southern blot hybridisation involves extraction of DNA from liver tissues, digestion of the DNA with restriction enzymes, followed by agarose gel electrophoresis, transfer of the electrophoresed DNA onto nitrocellulose membranes, and lastly hybridisation with a radioactive ^{32}P-labelled HBV DNA probe in order to detect integrated HBV DNA present in the liver genome (Hino *et al.*, 1985). The i*n situ* hybridisation method conversely detects HBV DNA on frozen or paraffin-embedded liver tissue sections. Frozen sections were first

fixed on microscope slides in Carnoy's fixative, before adding labelled HBV DNA probes to the slides; while paraffin-embedded sections were firsxt deparaffined in xylene, endogeneous peroxidises inactivated by hydrogen peroxide (H_2O_2), pronase-treated, and post-fixed in paraformaldehyde before hybridising with labelled HBV DNA probes. The commonly used biotin- or digoxygenin dUTP- probes could then be visualised by their repective substrates for colour development, to detect the presence of HBV DNA in the liver cells (Kajino *et al.*, 1994; Jilbert 2000). To increase the hybridisation specificity to nucleic acids, sections could also be preincubated with either DNase and/or RNase (Negro *et al.*, 1985).

Alu-PCR is a PCR-based method that takes advantage of the human *Alu* gene sequence, which is about 281 bp long and reported to be present in every 3 – 6 kbp of the human genome. Thus, using an *Alu*-specific primer and a HBV-specific primer, this method would be able to amplify a population of integrated virus-cell junctions present in the genome that had occurred close to the *Alu* sequences (Kawai *et al.*, 2001). On the other hand, linker ligation assay detects integrated virus-cell junctions by initially excising a fragment of DNA from the genome that spans the entire integrated virus sequence. Linkers were then hybridised to the ends of the DNA fragments, before the integrated virus-cell junctions are amplified using the linker and a virus-specific region as primer binding sites. After removing the linkers, the DNA fragments containing the integrated virus-cell junction are self-ligated or circularised, before being linearised by restriction enzyme digestion to form an inverted DNA fragment containing the liver cell DNA (insert DNA) flanked by viral DNA. Using PCR primers that bind to the flanking virus sequence, the insert DNA could then be amplified and sequenced to determine the integrated virus-cell junction sequence (Summers *et al.*, 2003).

Lastly, the invPCR assay is a sensitive assay designed to able to detect even a single copy of integrated virus-cell junction present in a liver sample (Yang and Summers, 1999). Briefly, the invPCR assay involves three steps: the extraction of genomic high molecular weight DNA from liver tissues, the inversion of genomic DNA by restriction enzyme digestions and DNA ligation to produce inverted DNA fragments that contain the integrated virus-cell junction, and the amplification and sequencing of the inverted DNA fragments. The restriction enzymes and PCR primers to be used in the invPCR assays were chosen and designed based on the likely sequence of the integrated virus DNA. Although the integration of HBV DNA occurs at random sites in the host genome, the 5' and 3' ends of the integrated HBV DNA are generally within ~250 bp of the most probable 5' (left hand) and 3' (right hand) ends of the dslDNA, the form of DNA which is the most common precursor for integration. Hence, the most probable left and right hand ends of the dslDNA sequences of the integrated HBV DNA are

generally used to choose restriction enzymes and to design primers for use in the invPCR assay to specifically amplify and detect the integrated virus-cell junctions. It is also due to the use of sequence-specific restriction enzymes and PCR primers that the invPCR assay is a highly specific assay in detecting a subset of integrated virus-cell junctions in the liver. Methods used during invPCR are described in detail in Section 2.10, and schematic representations of the invPCR assay are shown in Figures 2.6 and 2.7.

However, this high specificity may also limit the range of detectable integrated virus-cell junctions, as the successful detection of integrated virus-cell junctions relies heavily on the first cut restriction enzyme digestion site in the cellular DNA being close (less than 1 kbp) from the ends of the integrated virus sequence. The longer the insert DNA fragment is, the less efficient the self-ligation step, the nested PCR and the DNA sequencing reactions would be. Therefore, only a fraction of the integrated virus-cell junctions present in the liver genome would be detectable by the invPCR assay. In addition, as the invPCR assay uses viral DNA-specific primer sets during nested PCR, "non-integrated" virus sequences, including the viral rcDNA, RI DNA and cccDNA, would also be amplified, contributing to the detection of high levels of virus-virus false positives by the invPCR assays.

1.9. Animal models for the study of HBV

As mentioned in Section 1.2.1, the *Hepadnaviridae* family consists of a number of HBV-like viruses that naturally infect a specific animal host. For example, HBV can infect primates, WHV infects woodchucks, while DHBV infects ducks. All hepadnaviruses have similar virion structures, life cycles, genome sequence homology and organisation, and infection outcomes (reviewed in Zoulim *et al.*, 2008). Therefore, the study of hepadnaviruses in their natural animal hosts, either *in vivo* or *in vitro*, are essential models for understanding the pathogenesis of HBV infection in humans.

There are four commonly used animal models for the study of HBV, namely chimpanzees (Desmyter *et al.*, 1973), woodchucks (Menne and Cote, 2007), transgenic mice (Chisari *et al.*, 1985), and ducks (Mason *et al.*, 1980). Chimpanzees (*Pan troglodytes*), the closest available animal model to humans, can be infected with HBV (Desmyter *et al.*, 1973) resulting in similar natural history and host immune responses to HBV infection of humans. However, unlike humans, HBV-infected chimpanzees do not develop severe cirrhosis or HCC (Mason *et al.*, 2009a). Furthermore, chimpanzee studies are expensive and limited numbers of animals are available, as chimpanzees are an endangered species (Zoulim *et al.*, 2008). Woodchucks (*Marmota monax*) on the other hand are an excellent mammalian model, as WHV shares 70%

sequence homology to HBV (Galibert *et al.*, 1982). As WHV infection uniquely leads to HCC in 100% of woodchucks within 4 years, contributed partly to long-range oncogenic activation of the woodchuck N-*myc*2 gene (Fourel *et al.*, 1994a), this provides an excellent model for the further understanding of HBV-induced carcinogenesis (Zoulim *et al.*, 2008). However, woodchucks are not well defined immunologically (Menne and Cote, 2007), and being native to the USA, are unavailable for studies performed in Australia. Another mammalian animal model commonly used is the mouse (*Mus musculus*). Mice are unable to be infected with human HBV, but transgenic mouse lines have been established, making transgenic mice one of the cheapest and easiest animal models to handle. Genetically defined mouse lines are also available, allowing for knockout/functional studies to be performed (Zoulim *et al.*, 2008). However, cccDNA is not normally produced during HBV infection in most mouse models (Chisari *et al.*, 1985), with the exception of HNF1α-null HBV transgenic mice (Anderson *et al.*, 2005).

Lastly, Pekin ducks are a natural host for DHBV (Mason *et al.*, 1980) and DHBV infection is naturally endemic in Australia (Frieman and Cossart, 1986). DHBV virions have a similar size (40 – 45 nm in diameter), virion structure (Mason *et al.*, 1980), and genome length (~3030 bp) (Triyatni, 1998), structure and ORF organisation to HBV (Funk *et al.*, 2007). However, DHBV shares 40% sequence homology with HBV (Zoulim *et al.*, 2008) and encodes only 2 forms of DHBV surface antigen (DHBsAg), namely the LHB and SHB (Funk *et al.*, 2007) (refer Figure 1.2 for schematic representation of the DHBV virion and ORFs). As DHBV-infected ducks have a similar replication strategy (Funk *et al.*, 2007), infection outcomes, and immune responses to HBV (Jilbert *et al.*, 1998; Jilbert and Kotlarski, 2000), the duck model has been fundamental to the understanding of the lifecycle of HBV and the mechanisms of clearance of HBV infection. However, DHBV-infected ducks do not develop cirrhosis or HCC (Zoulim *et al.*, 2008), possibly due to the shorter lifespan of ducks (9 – 12 years) compared to humans and chimapzees, and that DHBV infection do not cause activation of oncognes like in WHV-infected woodchucks (Fourel *et al.*, 1990; Fourel *et al.*, 1994a). Therefore, with a shorter timeframe of chronic DHBV infection and no increase in clonal proliferation of hepatocytes due to oncogenic mutations, the lower rate of clonal proliferation of duck hepatocytes may have prevented the formation of large hepatocyte clones which may develop into tumours. In addition, as most ducks with chronic DHBV infection had been infected congenitally, the extended period of immune tolerance in young ducks would have also reduced the rate of clonal proliferation of hepatocytes. This is further complicated by the fact that Pekin ducks are also susceptible to the development of amyloidosis after 7 months of

age. Amyloidosis has been reported to occur in both DHBV-infected and uninfected ducks (Guo *et al.*, 1996), and often precludes long-term studies of DHBV infection in ducks.

The study presented in this thesis will be performed using the Pekin duck animal model, along with some samples from the HBV-infected chimpanzees and WHV-infected woodchucks obtained from our collaborators, Dr. Robert Lanford from the Regional Primate Center in San Antonio, Texas, USA, and Dr. William Mason from the Fox Chase Cancer Center (FCCC), Philadelphia, USA.

1.10. Study aims and outline

The two main aims in this study are to explore the mechanisms involved in the clearance of DHBV-infected hepatocytes during acute DHBV infection, and to assess levels of clonal proliferation of hepatocytes that is occurring during various stages of chronic DHBV infection. The studies, which will be performed in DHBV-infected ducks, use the invPCR assay to detect integrated virus-cell junctions as genetic markers for individual infected hepatocytes.

The outline and specific aims for each Chapter are as follows:

Chapter 3: To optimise and establish molecular assays used throughout this study, including:

- DNA sequencing reactions and subsequent purification of DNA sequencing products.
- Quantitative PCR (qPCR) assays using standard curves.

Chapter 4: To establish qPCR assays for the detection of duck DNA. Sub-aims include:

- To identify, sequence and clone into plasmid vectors single copy genes present in duck DNA.
- To use plasmids containing the single copy genes to establish standard curves for qPCR assays.

Chapter 5: To optimise and establish molecular assays required to establish the invPCR assay in the Hepatitis Research Laboratory. Sub-aims include:

- To compare methods for extraction of high MW DNA from small quantities of liver.
- To test the ability of locked nucleic acid (LNA) oligonucleotides to reduce false positives during the invPCR assay.
- To perform linker ligation assays to detect integrated virus-cell junctions in woodchuck and duck liver tissues, as an alternative to the invPCR assay.
- To use plasmid DNA constructs as model systems to determine the sensitivity and efficiency of the established invPCR assays.
- To perform invPCR assays to detect integrated virus-cell junctions in woodchuck and chimpanzee liver tissues.

Chapter 6: To perform preliminary invPCR assay studies on duck liver tissues. Sub-aims include:

- To design and establish invPCR assays specific for the Australian strain of DHBV, AusDHBV (GenBank Accession AJ006350).
- To perform invPCR assays to detect integrated virus-cell junctions in ducks with acute and chronic DHBV infection.

Chapter 7: To explore the mechanisms involved during the clearance of DHBV-infected hepatocytes during acute DHBV infection in ducks. Sub-aims include:

- To establish and characterise acute DHBV infection in ducks.
- To use invPCR assays to detect integrated DHBV-cell junctions, to determine if DHBV-infected hepatocytes are cleared from the liver by cytolytic or non-cytolytic mechanisms.

Chapter 8: To characterise clonal proliferation of hepatocytes during chronic DHBV infection in ducks. Sub-aims include:

- To establish and characterise chronic DHBV infection in ducks.
- To use invPCR assays to detect integrated DHBV-cell junctions during all stages of chronic DHBV infection, to characterise clonal proliferation of hepatocytes.

Chapter 9: Final discussion and concluding remarks.

Table 1.1: The *Hepadnaviridae* family.

Orthohepadnavirus	Avihepadnavirus
HBV[a]	Duck hepatitis B virus (DHBV)[a, b]
Woodchuck hepatitis virus (WHV)[a]	Heron hepatitis B virus[c]
Ground squirrel hepatitis virus[d]	Ross' goose hepatitis B virus[e]
Arctic squirrel hepatitis virus[f]	Snow goose hepatitis B virus[e]
Woolly monkey hepatitis B virus[g]	White stork hepatitis B virus[h]
	Crowned crane hepatitis B virus[i]

References

[a](Mason *et al.*, 1980)
[b](Triyatni *et al.*, 2001)
[c](Sprengel *et al.*, 1988)
[d](Marion *et al.*, 1980)
[e](Chang *et al.*, 1999)
[f](Testut *et al.*, 1996)
[g](Lanford *et al.*, 1998)
[h](Pult *et al.*, 2001)
[i](Prassolov *et al.*, 2003)

Figure 1.1: Schematic representation of the HBV virion (Figure 1.1A) and the ORFs found on the HBV genome (Figure 1.1B) (adapted with permission from Jilbert and Kotlarski, 2000; Kann, 2008).

HBV is an enveloped virus with 3 forms of HBsAg (LHB, MHB, SHB) embedded in a lipid bi-layer. It has an icosahedral nucleocapsid comprised of HBcAg, encapsidating the viral genome in a partially double-stranded rcDNA form. rcDNA has a full-length negative-strand DNA with the viral polymerase covalently attached to its 5' end. Its positive-strand has a RNA primer at the 5' end, and is partially complete at the 3' end (represented by the dotted lines).

HBV has 4 partially overlapping ORFs:

a) P ORF encodes the viral polymerase.
b) C ORF encodes HBcAg. Translation of the preC domain and C ORF produces HBeAg.
c) S ORF encodes HBsAg. Translation of preS1, preS2 and S domains produces LHB, translation of preS2 and S domain produces MHB, and translation of the S domain produces SHB.
d) X ORF encodes HBxAg.

ORFs are represented as arrows with corresponding start and termination sites, positioned relative to the rcDNA genome. The numbering of the HBV genome is based on the 3221 bp HBV isolate 991 genotype A, HBs subtype *adw2* (GenBank Accession X51970) genome starting at the *Eco*RI restriction site as nucleotide 1.

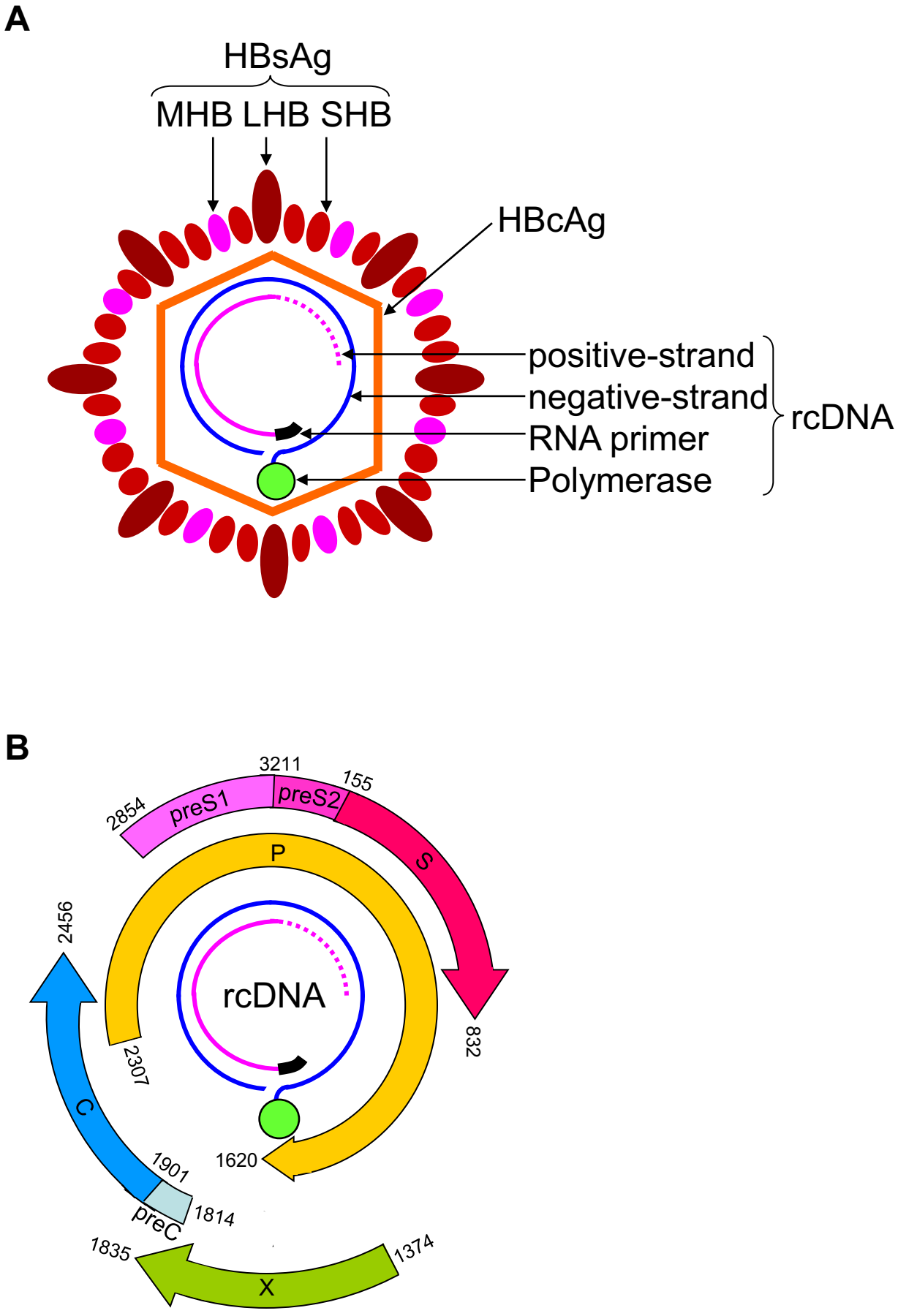

A
HBsAg
MHB LHB SHB
HBcAg
positive-strand
negative-strand
RNA primer
Polymerase
rcDNA
B
3211
155
2854
preS1
preS2
S
P
2456
rcDNA
832
2307
C
1620
1901
1814
preC
1835
1374
X

Figure 1.1

Figure 1.2: Schematic representation of the DHBV virion (Figure 1.2A) and the ORFs found on the DHBV genome (Figure 1.2B) (adapted with permission from Jilbert and Kotlarski, 2000; Funk *et al.*, 2007).

DHBV is an enveloped virus with 2 forms of DHBsAg (LHB, SHB) embedded in a lipid bi-layer. DHBV has an icosahedral nucleocapsid comprised of DHBcAg, and a partially double-stranded rcDNA DNA genome. rcDNA has a full-length negative-strand DNA with the viral polymerase covalently attached to its 5' end. Its positive-strand has a RNA primer at the 5' end, and is partially complete at the 3' end (represented by the dotted lines).

DHBV has 4 partially overlapping ORFs:

a) P ORF encodes the viral polymerase.
b) C ORF encodes DHBcAg.
c) S ORF encodes DHBsAg. Translation of the preS and S domains produces LHB, while translation of the S domain produces SHB.
d) X ORF encodes the hypothetical DHBxAg.

ORFs are represented as arrows with corresponding start and termination sites, positioned relative to the rcDNA genome. The numbering of the DHBV genome is based on the 3027 bp AusDHBV (GenBank Accession AJ006350) genome starting at the *Eco*RI restriction site as nucleotide 1.

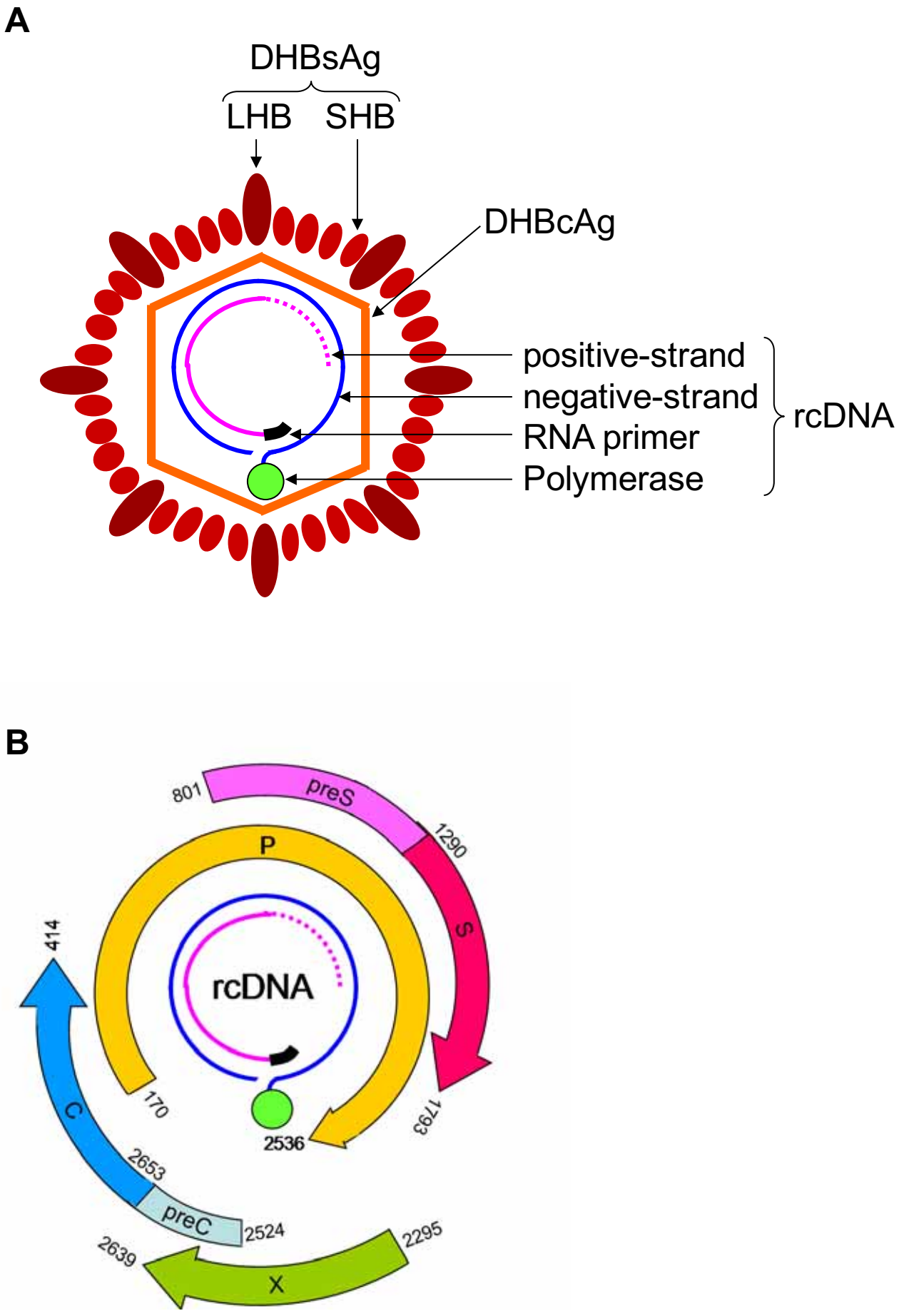

A
DHBsAg
LHB
SHB
DHBcAg
positive-strand
negative-strand
RNA primer
Polymerase
rcDNA
B
801
preS
1290
S
1793
P
rcDNA
2536
170
414
C
2653
preC
2524
2639
X
2295

Figure 1.2

Figure 1.3: Schematic representation of the replication cycle of HBV (adapted with permission from Jilbert and Kotlarski, 2000; Jilbert *et al.*, 2008a).

- HBV mainly infects hepatocytes, and enters the cell via receptor mediated endocytosis.
- HBV dissociates in the cytoplasm, and the nucleocapsid is transported to the nucleus.
- rcDNA is released and converted to cccDNA in the nucleus.
- cccDNA serves as the HBV transcriptional template for all HBV pregenomic and mRNA forms.
- Transcribed mRNAs are translated to produce viral proteins in the ER.
- A complex of the viral polymerase and pregenomic RNA is encapsidated by HBcAg to form immature nucleocapsid.
- Pregenomic RNA is mainly reverse transcribed (95%) to rcDNA to form mature nucleocapsid.
- Mature nucleocapsids can bud from the ER to produce progeny virions, or can be transported to the nucleus.
- rcDNA transported to the nucleus is converted to cccDNA, generating a pool of 5 – 50 copies of cccDNA per infected cell.
- 5% of pregenomic RNA is reverse transcribed to dslDNA, which can bud out of the cell as non-infectious progeny viruses, or can be transported to the nucleus and integrate into the host genomic DNA at random sites, generating unique integrated virus-cell junctions.

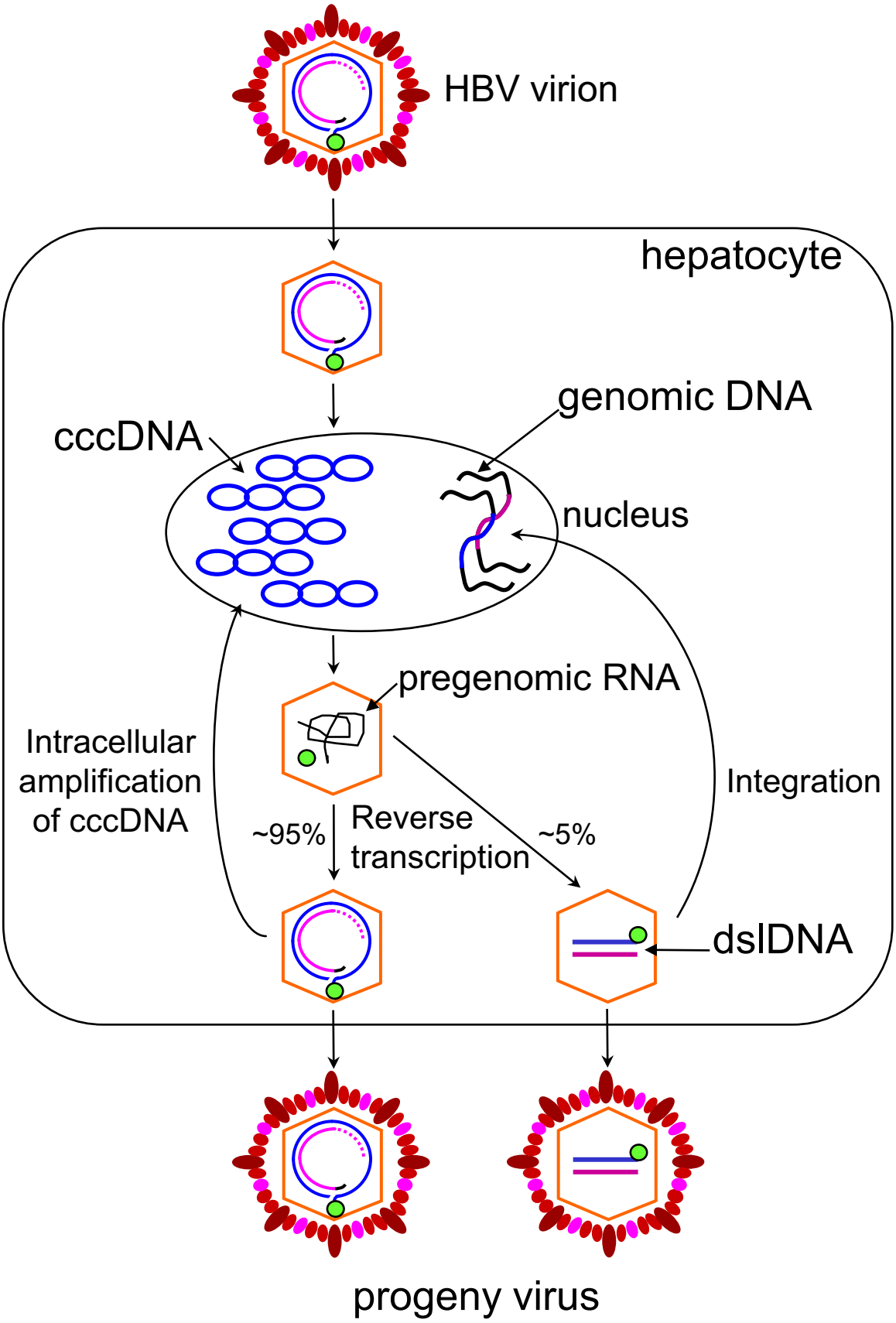

HBV virion
hepatocyte
genomic DNA
cccDNA
nucleus
pregenomic RNA
Intracellular
amplification
of cccDNA
Integration
~95%
Reverse
transcription
~5%
dslDNA
progeny virus

Figure 1.3

Figure 1.4: Schematic representation of events occurring during reverse transcription of the HBV genome (adapted with permission from Jilbert *et al.*, 2008a).

(A) Schematic representation of the pregenomic RNA, showing the characteristic stem-loop structures with the ε bulge region, and the direct repeat (DR) regions.
(B) Recruitment and priming of HBV polymerase (POL).
(C) Translocation of the HBV polymerase to DR1* and initiation of 5' – 3' RNA-dependent DNA synthesis of the negative-strand of DNA.
(D) Concurrent degradation of the RNA template by RNase H, but leaving behind a 18 nt RNA oligonucleotide.
(E) Translocation of the RNA oligonucleotide to DR2 and initiation of 5' – 3' DNA-dependent DNA synthesis of the positive-strand of DNA.
(F) Generation of rcDNA with a gap at the 3' end of the positive-strand of DNA.
(G) Approximately 5% of the time the RNA oligonucleotide does not translocate to DR2, but causes *in situ* priming from DR1 and initiates 5' – 3' DNA-dependent DNA synthesis of the positive-strand of DNA.
(H) Generation of dslDNA.

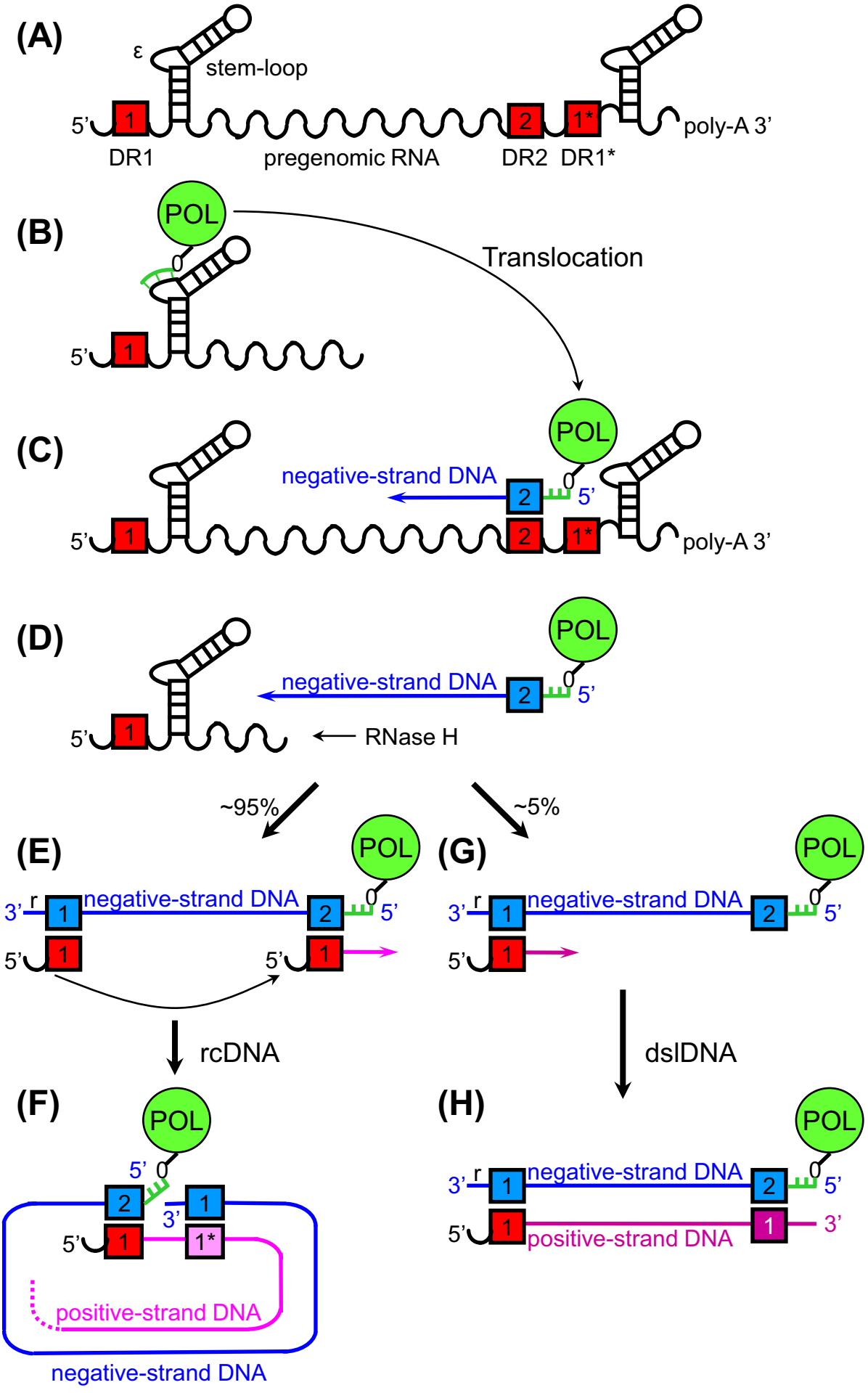

(A)
ε
stem-loop
5'
1
2
1*
poly-A 3'
DR1
pregenomic RNA
DR2
DR1*
(B)
POL
Translocation
5'
1
(C)
POL
negative-strand DNA
2
5'
5'
1
2
1*
poly-A 3'
(D)
POL
negative-strand DNA
2
5'
5'
1
RNase H
~95%
~5%
(E)
POL
3'
r
1
negative-strand DNA
2
5'
5'
1
5'
1
(G)
POL
3'
r
1
negative-strand DNA
2
5'
5'
1
rcDNA
dslDNA
(F)
POL
5'
2
1
3'
5'
1
1*
positive-strand DNA
negative-strand DNA
(H)
POL
3'
r
1
negative-strand DNA
2
5'
5'
1
positive-strand DNA
1
3'

Figure 1.4

Figure 1.5: Serological changes and clinical patterns during acute (A) and chronic (B) HBV infection. Figures are obtained with permission from Bowden (Bowden, 2008).

During acute HBV infection (Figure 1.5A), HBsAg, HBeAg and HBV DNA could be detected 1 – 2 months post-infection, followed by elevated ALT levels by 2 months post-infection. After that, clinical symptoms may develop between 2 – 4 months post-infection, and anti-HBc antibodies could then be detected while ALT levels begin to reduce to normal levels. HBsAg, HBeAg and HBV DNA levels also begin to reduce. Within 6 months post-infection, anti-HBc antibodies, anti-HBe antibodies and anti-HBs antibodies could be detected, with no more HBsAg, HBeAg and HBV DNA detectable in the serum.

During chronic HBV infection (Figure 1.5B), HBsAg, HBeAg and HBV DNA can be detected 1 – 2 months post-infection, followed by elevated ALT levels and detection of anti-HBc antibodies by 2 months post-infection. Although ALT levels gradually reduce, HBsAg, HBeAg and HBV DNA levels remain persistent, clinical symptoms may develop between 2 – 7 months post-infection, but with no detectable anti-HBe antibodies or anti-HBs antibodies. Years after infection, an immune clearance phase may occur when seroconversion to anti-HBe antibodies occurs accompanied by flares of ALT levels, possible clinical symptoms developing, and the reduction but not clearance of HBsAg and HBV DNA.

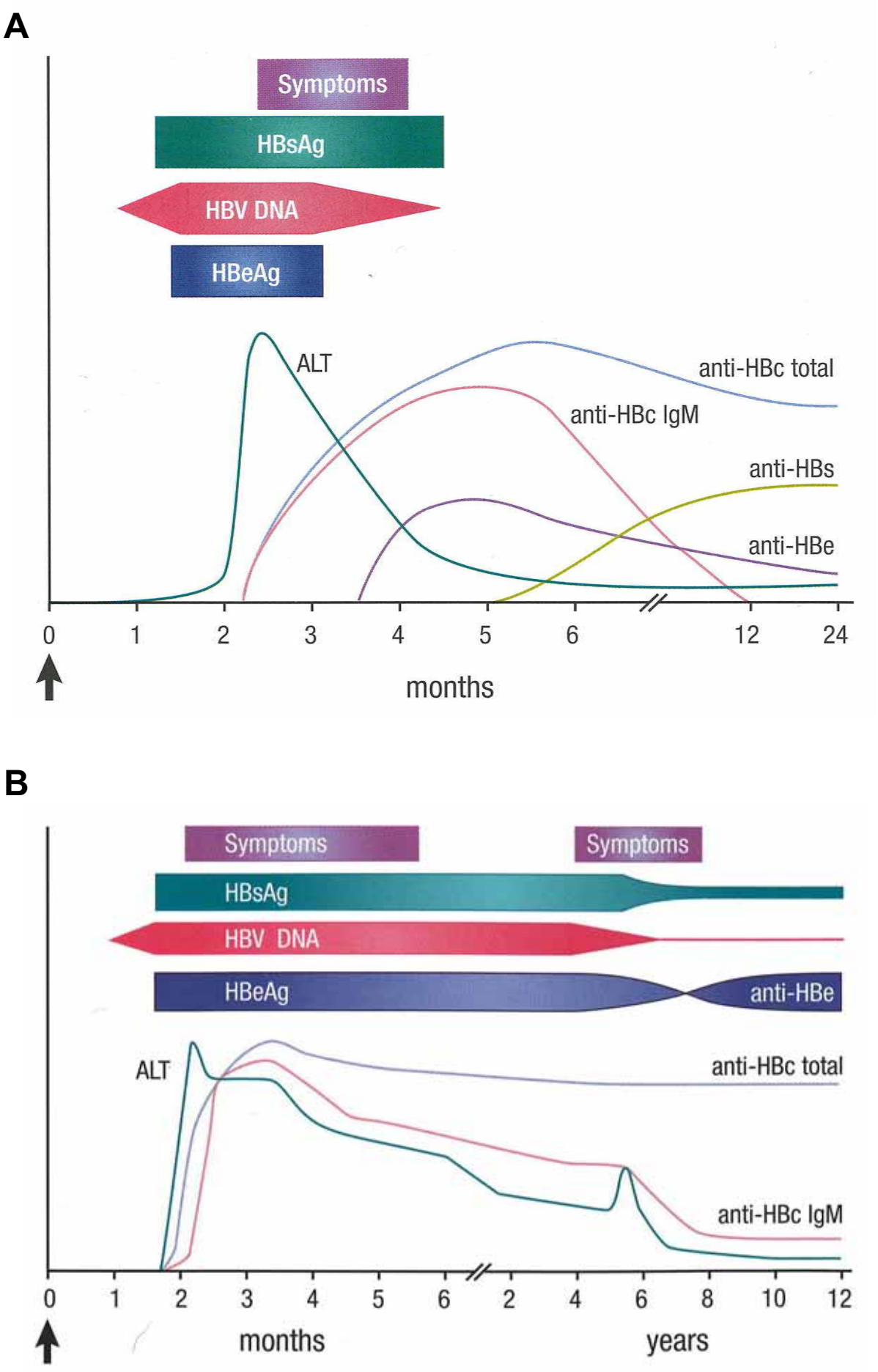

A
Symptoms
HBsAg
HBV DNA
HBeAg
ALT
anti-HBc total
anti-HBc IgM
anti-HBs
anti-HBe
0
1
2
3
4
5
6
12
24
months
B
Symptoms
Symptoms
HBsAg
HBV DNA
HBeAg
anti-HBe
ALT
anti-HBc total
anti-HBc IgM
0
1
2
3
4
5
6
2
4
6
8
10
12
months
years

Figure 1.5

Chapter 2: Materials and Methods

To reduce the risk of contamination of PCR reactions, all stock solutions, primer stocks, restriction enzymes, and PCR reagents, were stored in a clean, DNA-free room separate from the main laboratory. The clean room was only accessible after thorough hand washing, and putting on clean gowns, gloves and booties not previously worn in the main laboratory. All equipment used in the clean room was cleaned with 1.25% hypochlorite to ensure that it was DNA-free. Mastermixes or aliquots were prepared in the clean room and then brought out to the main laboratory. Once in the main laboratory, no equipment or reagents were returned to the clean room.

2.1. Animals

Pekin Aylesbury ducks (*Anas domesticus platyrhynchos*) were obtained as one-day-old ducklings from a commercial hatchery (Pepe's Ducks, New South Wales, Australia). Ducks were housed in the Veterinary Services Division of the Institute of Medical and Veterinary Science (IMVS), part of South Australian (SA) Pathology, and cared for in accordance with the Australian Code of Practice for the Care and Use of Animals for Scientific Purposes, as prescribed by the National Health and Medical Research Council (NHMRC) of Australia. All animal use and handling was approved by the Animal Ethics Committees (AEC) of the IMVS and the University of Adelaide under AEC approval numbers 144/06 and S-010-2007 respectively.

2.2. Virus stock

The DHBV virus stock (Pool 8) used in all experiments was serum pooled from ducks congenitally-infected with the Australian strain of DHBV (AusDHBV, GenBank Accession AJ006350) (Triyatni *et al.*, 2001). Pool 8 has been previously shown to contain $5x10^9$ vge/mL, and 50 μg/mL of DHBsAg (Jilbert *et al.*, 1996). All DHBV virus stocks were maintained at -80^{o}C, and thawed on ice prior to use.

2.3. Procedures involving ducks

2.3.1. Inoculation of ducks with DHBV

The procedure is essentially the same as described below for venipuncture. The area overlying the jugular vein was first disinfected with 70% ethanol (Merck, Australia), and 3 mL of Pool 8 (as described in Section 2.2) containing 1.5×10^{10} vge or 150 μg DHBsAg were administered using 23 gauge needles and 5 mL syringe (Becton Dickinson (BD), NSW).

2.3.2. Serum sample collection

2.3.2.1. Venipuncture

Blood samples were collected from ducks via venipuncture of either the jugular vein or the leg vein. In brief, the area overlying the vein was disinfected with 70% ethanol, before blood was drawn using 21 – 26 gauge needles (BD, NSW) depending on the size of the ducks, and subsequently pressure was applied to the puncture site with sterile swabs until the bleeding subsided. The collected blood samples were then transferred into clean 1.5 mL collection tubes. The collected blood was subsequently treated as described in Section 2.3.2.2 in order to obtain serum.

2.3.2.2. Blood serum extraction

Blood collected into tubes as described in Section 2.3.2.1 was incubated at 37^{o}C for 1 hr, followed by overnight incubation at 4^{o}C to allow for clotting to occur. Subsequently the serum was separated from the clotted blood fraction by centrifugation at 4200 g for 10 minutes (min) at 4^{o}C. Serum (supernatant) was carefully removed and stored at -20^{o}C. Serum was re-centrifuged and re-extracted if found to be contaminated with blood cells after extraction.

2.3.3. Liver tissue collection

2.3.3.1. Liver biopsy

Prior to biopsies, ducks were fasted from solid foods overnight. Liver biopsies were performed under sterile conditions by Dr. Behzad Baradaran (Doctor of Veterinary Medicine) with assistance from Huey Chi Low. Sterile surgical gowns and drapes, and individually-packed sterile disposable materials (gloves, sutures, scalpel blades, swabs) were prepared by the Veterinary Services, IMVS/SA Pathology, and all surgical instruments were sterilised by autoclaving. Ducks were placed under general anaesthesia with 5% isofluorane (Veterinary Companies, Australia) and 5%:400 mL/min oxygen using a rubber balloon placed directly over the head. Throughout the biopsy, anaesthesia was maintained using 3% isofluorane via a size 3 endotracheal tube (ContourTM Mallinckrodt Medical, Ireland). The procedure is outlined below: ducks were laid on their backs on a heated pad, and the feathers on the lower thorax area were trimmed, and the skin was disinfected with Betadine (providone iodine) and 70% ethanol. 300 μL of the local anaesthetic 0.5% Bupivacaine hydrochloride (General Electrics (GE) Healthcare, Sweden), was then injected intradermally along the incision site. A small vertical incision was made in the skin using a scalpel blade through to the peritoneal cavity, and the liver was located. A tissue clamp (DeBakey-Derra vascular clamp, 15.9 cm, Germany) was then used to isolate a 600 – 800 mg portion of liver from the lower section of

the right lobe. The liver fragment was then excised using a scalpel blade with minimal blood loss from the cut liver surface. The incisions in the tissue and skin layers were subsequently closed using 4-0 Vicryl sutures (Ethicon, USA). Finally, Ketoprofen (5 mg/kg body weight, Troy Laboratories, Australia), an antipyretic and analgesic drug was injected intramuscularly to the thigh muscle. Anaesthetic was removed, and the ducks were kept in a separate recovery tub and monitored for ~30 min before being transferred back to their pens. The ducks were able to stand and were fully alert on average within 10 min of the end of surgery.

2.3.3.2. Autopsy

Autopsies were performed by Catherine Scougall, and assisted by Huey Chi Low. The area overlying the jugular vein was disinfected with 70% ethanol before an overdose of the barbiturate anaesthetic Lethabarb (Virbac, Australia) (50 – 150 mg/kg body weight) diluted 1:5 using normal saline, was injected into the jugular vein using a 21 gauge needle. Blood was immediately collected via cardiac puncture using a 19 gauge needle and a 50 mL syringe. 1 mL of the collected blood was placed in 1.5 mL collection tubes and the remaining blood was discarded. Autopsy was performed whereby the abdomen was sterilised using 70% ethanol before a large incision was made using surgical scissors to access the peritoneum. Samples of liver, spleen, pancreas and kidney were then collected.

2.3.4. Tissue sample processing

2.3.4.1. Tissue fixation, embedding and sectioning

All tissue samples collected by biopsy (Section 2.3.3.1) and autopsy (Section 2.3.3.2) were cut into ~8 mm x 8 mm x 5 mm pieces, placed in foam-lined embedding cassettes (Techno-Plas, Australia), and fixed using one of the 3 methods described in Sections 2.3.4.1.1 to 2.3.4.1.3. Fixed materials were then sent to Tissue Pathology Laboratories, IMVS/SA Pathology and Hanson Institute Centre for Neurological Diseases, to be embedded in paraffin wax using the automated processing machines. The paraffin wax embedded tissues were sectioned at 5 – 6 μm and placed onto glass microscope slides.

2.3.4.1.1. Ethanol:acetic acid

Cassettes containing the tissue pieces were submerged in a mixture of ethanol:acetic acid (EAA) (Merck, Australia) 3:1 at room temperature (RT) for 30 min, and subsequently transferred to 70% ethanol at 4^{o}C overnight.

EAA fixation is one of the oldest fixatives used for general histology as it preserves nucleic acids and micro-anatomical structures of the tissue (Kiernan, 2008). In this project, sections of

EAA-fixed liver tissues were used for immuno-staining of DHBV surface antigens (DHBsAg) (Section 2.4.2).

2.3.4.1.2. Formalin

Cassettes containing the tissue pieces were submerged in 10% formalin (BDH-Analar, Dubai) in 1X phosphate buffered saline (PBS) at RT overnight.

Formalin fixation causes high cross-linking of proteins, which preserves the structural stabilisation of tissues (Kiernan, 2008). In this project, sections of formalin-fixed liver tissue were used for haematoxylin and eosin (H&E) staining (Section 2.4.1), immuno-staining of periodic acid-Schiff diastase (PAS-D) staining (Section 2.4.3) and proliferating cell nuclear antigen (PCNA) (Section 2.4.4).

2.3.4.1.3. 70% ethanol

Cassettes containing the tissue pieces were submerged in 70% ethanol at 4^{o}C overnight, and subsequently submerged in 100% ethanol.

Ethanol fixation displaces water from the tissue and disturbs the tertiary structure of proteins. This causes denaturation of soluble proteins, and precipitation of most insoluble proteins. DNA is not denatured and can be extracted for subsequent analyses (Kiernan, 2008). Sections of ethanol-fixed liver tissue were not used in studies in this thesis, but could be used for various downstream DNA analysis like microarrays and PCR amplifications in future works.

2.3.4.2. Liver tissue processing

For the rest of the liver tissue collected by biopsy (Section 2.3.3.1) and autopsy (Section 2.3.3.2): (1) ~75 mg was placed in 500 µL RNAlater (Ambion, Australia) and stored at -80^{o}C; (2) 4 pieces of ~5 mg were each placed in 400 µL of digestion solution for total DNA extraction as described in Section 2.6.3; (3) Any remaining pieces of liver tissue were snap frozen in liquid nitrogen in 1.5 mL screw-capped sterile tubes and stored at -80^{o}C.

2.4. Histology and immunohistochemical analysis of tissue sections

2.4.1. Haematoxylin and eosin (H&E) staining

H&E staining was performed by the Tissue Pathology Laboratories, IMVS/SA Pathology and Hanson Institute Centre for Neurological Diseases on formalin-fixed (Section 2.3.4.1.2) tissue sections on glass slides. It is expected that the nuclei will be stained blue, while other eosinophilic structures like proteins will be stained as various shades of red – pink. Slides

were examined at 100X magnification using an eyepiece graticule and a 1.2 mM x 1.2 mM grid to determine the percentage of the liver that contained inflammatory cells, or were examined at 400X magnification using an eyepiece graticule and a 300 μM x 300 μM grid to determine the number of apoptotic hepatocytes per total hepatocytes present.

Inflammation could be observed as infiltration of mainly small and dense mononuclear lymphocytes (Theise *et al.*, 2007; Goodman, 2008), forming aggregates around the portal tract (portal inflammation) or within the liver parenchyma (lobular inflammation) (Cullen *et al.*, 1989). The inflammation grading system used in this study was adapted from Bedossa and Poynard (Bedossa and Poynard, 1996) and Mason *et al.* (Mason *et al.*, 1994) and are described as follows:

For the grading of portal inflammation, "1" refers to the absence of portal inflammation (normal levels), "2" refers to the presence of mononuclear aggregates in some portal tracts, "3" refers to the presence of some large and dense mononuclear aggregates in some portal tracts, "4" refers to the presence of some large and dense mononuclear aggregates in all portal tracts, "5" refers to the presence of large and dense mononuclear aggregates in all portal tracts.

For the grading of lobular inflammation, "1" refers to the absence of lobular inflammation (normal levels), "2" refers to the scarce presence of some small lobular mononuclear aggregates, "3" refers to the frequent presence of some small lobular mononuclear aggregates, "4" refers to the frequent present of large and dense lobular mononuclear aggregates.

2.4.2. Immunohistochemical detection of DHBsAg

In order to detect DHBsAg expression in the liver, EAA-fixed (Section 2.3.4.1.1) tissue sections on glass slides were stained with anti-DHBV pre-S monoclonal antibody, 1H.1 (Pugh *et al.*, 1995). The precise method used is outlined below. Slides were first dried at 37^{o}C overnight, and then dewaxed by immersion in Analytical Reagent (AR) grade xylene (Chem-Supply, Australia) 2 times for 10 min. Xylene was removed by washing the slides in AR grade 100% ethanol 2 times for 5 min, and in 1X PBS 2 times for 5 min. Endogenous tissue peroxidases were inactivated by immersion of the slides in 0.5% hydrogen peroxide (H_2O_2) (Merck, Australia) in 1X PBS at RT for 15 min with stirring. After washing in 1X PBS 2 times for 5 min, non-specific 1H.1 binding sites were blocked with 200 μL of 3.3% normal sheep serum (NSS) in 1X PBS spread evenly over the tissue sections, and incubated at RT for 30 min in a humid box. NSS was then removed and tissue sections were covered with 100 μL of a 1/500 dilution of 1H.1 in 10% foetal calf serum (FCS) in 1X PBS. Slides were covered

using glass cover slips, and incubated at 37^{o}C for 1 hour (hr) in a humid box, followed by incubation at 4^{o}C overnight. After removing the cover slips by dip washing in 1X PBS, slides were washed in 1X PBS 2 times for 5 min, and covered with 100 µL of horseradish-peroxidase (HRP) conjugated sheep anti-mouse antibody (Amersham Biosciences, Australia, Lot no. 387605), diluted 1/250 in 10% normal duck serum (NDS) in 1X PBS. Slides were covered with glass cover slips, and incubated at 37^{o}C for 1 hr in a humid box. Cover slips were removed by dip washing in 1X PBS and washed in 1X PBS 2 times for 5 min. Subsequently, slides were flooded with ~400 µL of HRP substrate, which consist of 0.04% diaminobenzidine tetrahydrochloride (DAB) (Sigma, USA) in 0.5% H_2O_2 in 1X PBS, and incubated in the dark at RT for 9 min. Slides were then immediately dip washed in 1X PBS and washed in 1X PBS 2 times for 5 min, before being counterstained by immersion in Mayer's haematoxylin for 1 min. Slides were then washed in 1X PBS 3 times for 1 min to differentiate the haematoxylin dye from red to blue, and then dehydrated in AR grade 100% ethanol 2 times for 2 min and AR grade xylene for 2 times for 5 min. Slides were then mounted with cover slips using Entellan (Merck, Australia) and dried in a fume hood overnight. It is expected that any DHBsAg present in the cytoplasm of hepatocytes will be stained dark brown, while the nucleus will be stained blue/purple. Slides were examined at 200X magnification using an eyepiece graticule and a 600 µM x 600 µM grid, with at least $1x10^5$ hepatocytes counted per liver tissue section, to determine the percentage of DHBsAg-positive hepatocytes per $1x10^5$ hepatocytes present in each liver tissue section.

2.4.3. Periodic acid-Schiff diastase (PAS-D) staining of Kupffer cells

PAS-D staining was performed by the Tissue Pathology Laboratories, IMVS/SA Pathology and Hanson Institute Centre for Neurological Diseases on formalin-fixed (Section 2.3.4.1.2) tissue sections on glass slides. It is expected that the nuclei will be stained blue, while Kupffer cells present in the liver will be stained bright pink. Kupffer cells are the phagocytic cells of the liver and they become more prominent and enlarged after phagocytosing cellular debris (Roskams *et al.*, 2007). Slides were examined at magnification using an eyepiece graticule and a 300 µM x 300 µM grid to determine the number of total, unactivated (do not contain PAS-D positive phagocytosed material), and activated (contain PAS-D positive phagocytosed material) Kupffer cells per total liver cells present.

2.4.4. Immunohistochemical detection of proliferating cell nuclear antigen (PCNA)

Formalin-fixed (Section 2.3.4.1.2) tissue sections on glass slides were dried, dewaxed, rehydrated, and washed as described in Section 2.4.2. Antigen retrieval was then performed by microwave (Panasonic, catalogue no. NN-S696WA, Japan) treatment of slides in 10 mM

sodium citrate (pH 6) in a plastic slide box, first at a high setting for 4 min 15 seconds (sec) until the solution started to boil, then at a low setting for 10 min. To prevent over-heating, another plastic pot filled only with water was also heated in the same microwave. After the solution cooled to <50^{o}C, slides were washed in 1X PBS 2 times for 5 min, followed by inactivation of tissue peroxidases and blocking with NSS as described in Section 2.4.2. NSS was then removed and tissue sections were covered with 100 µL of PCNA mouse monoclonal antibodies, PC-10 (1 µg/µL) (Roche, Australia) diluted 1/250 in 10% FCS in 1X PBS. Slides were covered with glass cover slips, and incubated at 37^{o}C for 1 hr in a humid box, followed by overnight incubation at 4^{o}C. After removing the cover slips by dip washing in 1X PBS, slides were washed in 1X PBS 2 times for 5 min, and covered with 100 µL HRP conjugated sheep anti-mouse antibody (Lot no. 387605) diluted 1/250 in 10% NDS in 1X PBS. Slides were covered with glass cover slips, and incubated at 37^{o}C for 1 hr in a humid box. Cover slips were then removed by dip washing in 1X PBS and washed in 1X PBS 2 times for 5 min. Subsequently, slides were stained with DAB and Mayer's haematoxylin, and mounted as described in Section 2.4.2. It is expected that PCNA present in the nucleus of hepatocytes will be stained dark brown, while the nucleus will be stained blue/purple. Sides were examined at 200X magnification using an eyepiece graticule and a 600 µM x 600 µM grid, and the percentage of PCNA-positive hepatocytes per ~1x10^{5} hepatocytes were counted.

2.4.5. Statistical analysis

To determine the statistical significance of the difference in data obtained from different groups of ducks, the p-value was calculated using the Student's unpaired *t*-test, set to two-tailed distribution and two-sample unequal variance (heteroscedastic), using the Microsoft Excel software. The p-value of <0.05 is considered statistically significant.

2.5. Serologic assays

2.5.1. DHBV DNA extraction from serum

DHBV DNA was extracted from 200 µL serum samples using the ChargeSwitch gDNA 1 mL serum kit (Invitrogen, USA) according to the instructions provided by the manufacturer. Proteinase K was made up to 20 mg/mL by dissolving 100 mg of proteinase K (Roche, Australia) in 40% glycerol, 0.1 mM Tris-HCl pH 8.5, and 0.1 mM calcium chloride ($CaCl_2$), according to the recommendations of the manufacturer.

2.5.2. Detection of DHBsAg by ELISA

Serum DHBsAg levels were measured using an Enzyme-Linked ImmunoSorbent Assay (ELISA) described by Miller *et al.*, 2004. 96-well flat bottom microtitre plates (Costar, USA,

catalogue no. 3590) were coated with duplicates of 100 µL of a 1/500 dilution of each serum sample in 1X PBS containing 0.2% NDS, and incubated at 37°C overnight. Plates were sealed with cling wrap during all incubations to prevent evaporation. Plates were washed 3 times with a BIOTEC Plate Washer (Millenium Science, Australia) using 1X PBS-T (1X PBS with 0.05% Tween 20 (Sigma, USA)), and blocked using 200 µL of 5% skim milk with 0.2% NDS in 1X PBS-T at 37°C for 1 hr. Plates were then washed 3 times using 1X PBS-T, and incubated with 100 µL of 1H.1 at a 1/10,000 dilution in 5% skim milk with 0.2% NDS in 1X PBS-T at 37°C for 1 hr. Plates were subsequently washed three times using 1X PBS-T, and incubated with 100 µL of HRP conjugated sheep anti-mouse antibody (Lot no. 387605) at a 1/5000 dilution in 5% skim milk with 0.2% NDS in 1X PBS-T at 37°C for 1 hr. Plates were washed 3 times using 1X PBS, and incubated with 100 µL freshly prepared HRP substrate o-phenylenedianine dihydrochloride (OPD) (Sigma, Australia) in the dark for 15 min. The OPD substrate was prepared by fully dissolving 1 tablet of OPD and 1 tablet of urea buffer (Sigma, Australia) in 20 mL H_2O. The reaction was stopped using 50 µL of 2.5 N sulphuric acid (H_2SO_4), before the absorbance at 490 nm was determined using a SpectraMax M2 automated microplate reader (Molecular Devices, USA).

For each plate, a standard curve was generated using eight, 2-fold dilutions of Pool 8 serum (1/500 to 1/128,000) in 1X PBS. The NDS wells and blank wells were also included to determine the background absorbance (± [mean + (2 x standard deviation)]).

2.5.3. Detection of anti-DHBc antibodies by ELISA

Levels of serum anti-DHBc antibodies were measured using an ELISA described by Miller *et al.*, 2004. 96-well flat bottom microtitre plates were coated with 100 µL of 1 µg/mL of recombinant DHBV core antigen (rDHBcAg) (Jilbert *et al.*, 1992) in ELISA coating buffer (5.3 g Na_2CO_3, 4.2 g $NaHCO_3$, 1 g NaN_3, maintained at pH 9.6), and incubated at 37°C for 1 hr, followed by overnight incubation at 4°C. Plates were sealed with cling wrap during all incubations to prevent evaporation. Plates were washed 3 times using 1X PBS-T, then blocked using 200 µL of 5% skim milk with 0.2% NDS in 1X PBS-T at 37°C for 1 hr. Plates were subsequently washed 3 times using 1X PBS-T, and incubated with duplicates of 100 µL of each individual serum samples serially diluted from 1/500 to 1/15,625,000 in 1X PBS, at 37°C for 1 hr. Plates were washed 3 times using 1X PBS-T, and incubated with 100 µL of rabbit anti-duck immunoglobulin Y (IgY) (Bertram, 1997) at a 1/10,000 dilution of in 5% skim milk with 0.2% NDS in 1X PBS-T at 37°C for 1 hr. Plates were again washed 3 times using 1X PBS-T, and incubated with 100 µL of HRP conjugated goat anti-rabbit antibody at a 1/5000 dilution in 5% skim milk with 0.2% NDS in 1X PBS-T at 37°C for 1 hr. Plates were

washed 3 times using 1X PBS, developed with OPD substrate, stopped, and absorbance read at 490 nm as described in Section 2.5.2.

2.5.4. Detection of anti-DHBs antibodies by ELISA

Levels of serum anti-DHBs antibodies were measured using an ELISA described by Miller *et al.*, 2004. 96-well flat bottom microtitre plates were coated with 100 µL of 1H.1 at a 1/5000 dilution in ELISA coating buffer, and incubated at 37°C for 1 hr, followed by overnight incubation at 4°C. Plates were sealed with cling wrap during all incubations to prevent evaporation. Plates were then washed 3 times using 1X PBS-T, and blocked using 200 µL of 5% skim milk with 0.2% NDS in 1X PBS-T at 37°C for 1 hr. Plates were washed 3 times using 1X PBS-T, and incubated with 100 µL of 10 ng/mL of sucrose (20% – 50%) gradient-purified DHBsAg (prepared by Chee Quin Teoh) diluted in 1X PBS-T, at 37°C for 1 hr. Plates were subsequently washed 3 times using 1X PBS-T, and incubated with duplicates of 100 µL of each individual serum sample serially diluted from 1/100 to 1/12,500 in 1X PBS at 37°C for 1 hr. Plates were washed 3 times using 1X PBS-T, and incubated with 100 µL of rabbit anti-duck IgY (Bertram, 1997) at a 1/10,000 dilution of in 5% skim milk with 0.2% NDS in 1X PBS-T at 37°C for 1 hr. Plates were again washed 3 times using 1X PBS-T, and incubated with 100 µL of HRP conjugated goat anti-rabbit antibody, washed, developed with OPD substrate, stopped, and absorbance read at 490 nm as described in Section 2.5.2.

2.6. Liver DNA extraction

All liver tissue was stored at -80°C and kept on dry ice until use. This prevents repeated thawing, which could cause degradation of DNA. To extract a piece of liver tissue, the frozen liver tissues were placed on a clean, cool surface (for instance a plastic petri dish (Techno-Plas, Australia) chilled on dry ice), and the required pieces of liver tissue were dissected out using sterile scalpel blades.

2.6.1. DNeasy blood and tissue kit

Total DNA was extracted from ~25 mg liver pieces using the DNeasy blood and tissue kit (Qiagen, Germany) according to the instructions provided by the manufacturer. Essentially, liver cells were lysed in 1.2 mAU/mL (Anson unit) of proteinase K solution at 55°C overnight with shaking in a Thermomixer Comfort (Eppendorf, Germany) at 400 revolutions per min (rpm). Subsequently 4 µL of 20 mg/mL RNase (Roche, Australia) was added to the mixture and incubated at RT for 10 min, before purification via spin-columns. To elute DNA, 100 µL of elution buffer (EB) (Qiagen, Germany) was added to the column and incubated at RT for 1 min before centrifugation at 18,000 g (g-force, representing Relative Centrifugal Force

(RCF)) for 1 min. Elution from the column was repeated with 100 µL of EB, and collected in the same collection tube, to obtain a total of ~200 µL of DNA solution. The extracted DNA solution was stored at -20°C.

2.6.2. ChargeSwitch gDNA mini tissue kit

Total DNA was extracted from ~25 mg pieces of liver using the ChargeSwitch gDNA mini tissue kit (Invitrogen, USA) according to the instructions provided by the manufacturer. As some residual magnetic beads were found in the final 200 µL elute, the tube was placed back in the magnetic rack for a further ~15 min before re-extracting the supernatant into a clean 1.5 mL tube.

2.6.3. Total DNA extraction

Total DNA was extracted from ~5 mg liver tissues based on the methods described by Mason *et al.* (Mason *et al.*, 2009b), and represented as a flowchart in Figure 2.1. Liver tissue was lysed in 400 µL of digestion solution (0.1 mM NaCl, 0.5% SDS, 5 mM Tris HCl pH 7.4, 1 mM EDTA pH 8, 1 mg/mL proteinase K) at 55°C for 2 hr with periodic vortexing until no tissue fragments were visible. After cooling to RT, DNA was extracted using an equal volume of buffered AR grade phenol:chloroform (1:1) (Gibco Life Technologies, USA). Phenol:chloroform extraction included mixing the sample by vortexing before separating the organic and aqueous layers by centrifugation at 9,200 g for 5 min. The aqueous layer containing the DNA was carefully removed into a clean collection tube. The DNA was then precipitated using two volumes of 100% ethanol and 1 µL of 20 mg/mL dextran (Sigma, USA) as a carrier. The sample was mixed by gentle inversion, and incubated at -20°C overnight. The DNA was pelleted by centrifugation at 18,000 g for 10 min and the supernatant was discarded. The DNA pellet was washed by brief vortexing with 100% ethanol, and was subsequently pelleted by centrifugation at 18,000 g for 10 min. The DNA pellet was vacumm dried at RT for 30 min, and the DNA was then dissolved in 30 µL EB and stored at -20°C.

2.6.4. Low melting temperature agarose gel electrophoresis and purification of high molecular weight cellular DNA

DNA extracted using the total DNA extraction method described in Section 2.6.3 was separated by gel electrophoresis on 1% low melting temperature agarose gel. The 1% low melting temperature agarose gel was prepared by adding low melting temperature agarose powder (Bio-Rad, USA) to the appropriate volume of 1X Tris Acetate EDTA (TAE) buffer (40 mM Tris Acetate, 1 mM EDTA, made as 50X stock solution and adjusted to pH 7.5 – 7.8 with glacial acetic acid). The agarose in the TAE buffer was then dissolved by boiling in a

microwave oven. The mixture was allowed to cool, then poured into a gel mould with gel comb(s) inserted. After the gel was set, it was placed at 4°C for 30 min to ensure that it was fully set, and then placed into horizontal gel tank half flooded with 1X TAE buffer. Up to 2 µg of extracted total DNA was loaded into each gel well with 1/10 volume of 10X TAE loading buffer (60% sucrose, 1% sarkosyl, 0.1% bromophenol blue, 0.1% xylene cyanol in 1X TAE solution). Samples were electrophoresed "dry" at 50 V until both loading buffer markers had left the well, before flooding the gel tank with 1X TAE buffer. The gel was then electrophoresed until the bromophenol blue and xylene cyanol markers of the loading buffer had sufficiently separated. The gel was then removed from the gel tank and post-stained with 30X GelRed (Biotium, USA) for 15 – 30 min, and visualised under 302 nm ultraviolet (UV) light using the GelDoc XR imaging system (Bio-Rad, USA). The GelRed solution was made up of 30 µL of the 10,000X GelRed stock and 2.5 mL of 4 M $NaCl_2$ in 100 mL of H_2O. A UV converter plate (DKSH, Australia) was used to convert the 302 nm UVB light from the GelDoc XR system to a longer wavelength of 365 nm UVA light, in order to prevent/reduce UV induced DNA damage. Agarose gel slices containing high molecular weight (MW) DNA (10 – 20 kbp or larger) were excised and placed in a clean 1.5 mL tube, followed by DNA extraction using QIAquick gel extraction kit (Qiagen, Germany) as described in Section 2.8.8, The high MW DNA was eluted in a final volume of 30 µL of EB.

2.6.5. Nuclear DNA extraction

Nuclear DNA was extracted from small pieces of liver tissue using a method adapted from Zhang *et al.* (Zhang *et al.*, 2003), and represented as a flowchart in Figure 2.2. Essentially, ~5 mg of liver was homogenised in 1 mL of homogenisation solution (10 mM Tris pH 7.5, 3 mM $MgCl_2$, 0.01% Triton X-100, 0.25 M 85% sucrose) until no tissue fragments were visible, and centrifuged at 400 g for 5 min. The supernatant was then discarded, and the pellet was washed with 1 mL of homogenisation solution with gentle inversion of the tube to resuspend the pellet, and centrifuged at 400 g for 5 min. The pellet was subsequently resuspended in 500 µL of digestion solution (10 mM Tris pH 7.5, 10 mM EDTA pH 7, 200 µg/µL proteinase K, 0.1% Triton X-100) and incubated at 50°C for 1 hr, followed by proteinase K heat inactivation at 72°C for 15 min. After cooling to RT, DNA was extracted using equal volume of phenol:chloroform (1:1) as described in Section 2.6.3. The DNA was precipitated by the addition of 2 volumes of 100% ethanol, and 1/10 volume 3 M sodium acetate (NaOAc) as well as 1 µL of 20 mg/mL dextran as carrier. The DNA solution was mixed and placed at -80°C for 30 min, and the DNA was subsequently pelleted by centrifugation at 18,000 g for 10 min. The DNA pellet was washed with 100% ethanol by vortexing, and pelleted again by

centrifugation at 18,000 g for 10 min. The DNA pellet was vacuum dried at RT for 30 min and subsequently dissolved in 40 µL of EB.

2.6.6. High MW DNA extraction

Three high MW DNA extraction methods were adapted from methods developed by Dr. Jesse Summers of the University of New Mexico, New Mexico, USA (personal communication), to selectively extract the genomic DNA (high MW DNA) whilst removing most of the viral DNA (low MW DNA). All three methods are represented as a flowchart in Figure 2.3.

2.6.6.1. High MW DNA extraction I

Up to 25 mg of liver tissue was homogenised in 500 µL extraction solution (5 mM Tris HCl pH 7.4, 0.5 mM EDTA pH 8, 0.2% NP40, 0.15 M NaCl) until no tissue fragments were visible. This was followed by addition of 300 µL of 3% SDS and 200 µL 2.5 M KCl, with through mixing by vortexing. This allows for high MW protein-bound DNA to complex with the anionic SDS detergent, forming K-SDS-protein-DNA complexes. The mixture was incubated at RT for 15 min to allow the complexes to precipitate, followed by centrifugation at 18,000 g for 5 min. The cccDNA-rich supernatant was removed, and the pellet was redissolved in 500 µL of TE (10:1) (10 mM Tris HCl pH 7.4, 1 mM EDTA pH 8) with heating at 55^{o}C. To digest proteins, 500 µg/mL of Pronase (Boehringer Ingelheim, Germany) was added to the redissolved pellet and incubated at 55^{o}C for at least 1 hr. After cooling to RT, 50 mM NaCl was added to improve the efficiency of DNA extraction using an equal volume of phenol:chloroform (1:1) and ethanol precipitated as described in Section 2.6.3. The final vacuum-dried DNA pellet was dissolved in 20 µL of EB.

2.6.6.2. High MW DNA extraction II

The high MW DNA extraction method II was similar to the high MW DNA extraction method I described in Section 2.6.6.1 with the exception of 2 steps. Firstly, the Pronase protein digestion step was omitted to reduce the extraction of DHBV DNA covalently bound to the viral polymerase protein. Secondly, after the DNA was extracted using phenol:chloroform, the DNA was extracted again using an equal volume of phenol (Gibco Life Technologies, USA) for more complete removal of any DHBV DNA covalently bound to the viral polymerase protein (Summers, personal communication). The final vaccum-dried DNA pellet was dissolved in 20 µL of EB.

2.6.6.3. High MW DNA extraction III

The high MW DNA extraction method III was similar to the high MW DNA extraction method II described in Section 2.6.6.2 but with additional steps after the DNA was extracted using phenol. To completely remove any remaining proteins, 5 μg/mL Pronase was added to the mixture along with 5 mM Tris HCl pH 8 and 5 mM EDTA pH 8. The mixture was incubated at 55^{o}C for 1 hr, and after cooling to RT, was extracted using an equal volume of phenol, and was ethanol precipitated as described in Section 2.6.3. The final vacuum-dried DNA pellet was dissolved in 20 μL of EB.

2.6.7. cccDNA extraction method

cccDNA could be extracted from the cccDNA-rich supernatant collected during high MW DNA extractions described in Section 2.6.6, as shown in the flowchart Figure 2.3. After transferring the cccDNA-rich supernatant to a clean 1.5 mL tube, DNA was extracted using an equal volume of phenol twice, followed by an equal volume of phenol:chloroform (1:1), and ethanol precipitated as described in Section 2.6.3. The final vacuum-dried DNA pellet was dissolved in 200 μL of EB.

2.7. Plasmid DNA extraction

2.7.1. Mini prep

Plasmid DNA was extracted from bacterial colonies in a small scale using Qiagen Mini Prep kit (Qiagen, Germany) according to the instructions provided by the manufacturer, and stored at -20^{o}C until use.

2.7.2. Maxi prep

Plasmid DNA was extracted from bacterial broth cultures in a large scale using the Jetstar Plasmid Purification Maxi kit (Astral Scientific, Australia). Transformed *Escherichia coli* DH5α (*E. coli*) was cultured in 10 mL of Luria broth (LB) with 60 μg/mL of ampicillin (Sigma, USA) at 37^{o}C with shaking for ~8 hr, then subcultured in 500 mL of LB with 60 μg/mL of ampicillin at 37^{o}C with shaking overnight. *E. coli* were pelleted by centrifugation at 6000 g at 4^{o}C for 10 min and the supernatant was discarded. The bacterial pellet was resuspended in 10 mL of Solution E1 and lysed in 10 mL of Solution E2 with ~20 gentle agitations until the solution became viscous. Not more than 4 min later, 10 mL of Solution E3 was added, and mixed well with gentle inversions until homogenous. The mixture was centrifuged at 18,000 g at 18^{o}C for 30 min, and the supernatant was loaded onto columns pre-equilibrated with 30 mL of Solution E4. The lysate was allowed to run by gravity flow until the column was almost dry, before 60 mL of Solution E5 was loaded and allowed to run by

gravity flow to wash the DNA. When the column ran dry, the DNA was eluted into Oakridge tubes with 15 mL of Solution E6, and precipitated using 10.5 mL AR grade 100% isopropanol. The DNA was pelleted by centrifugation at 37,000 g at 4^{o}C for 30 min, the supernatant was discarded, and the pellet was washed by vortexing with 5 mL 70% AR grade ethanol. DNA was pelleted again by centrifugation at 37,000 g at 6^{o}C for 15 min, the supernatant was discarded, and the DNA was air-dried before redissolving in 200 µL of H_2O by vortexing. The DNA was left at 4^{o}C overnight to ensure that it was completely dissolved before storing at -20^{o}C until use.

2.8. DNA analysis

2.8.1. Measurement of DNA concentration

The concentration of DNA was measured using the Nanodrop 1000 spectrophotometer (Thermo Fisher Scientific, Canada) with a measurement scale of 2 – 3700 ng/µL ± 2 ng/µL, based on the absorbance of light at 260 nm wavelength. The Beer-Lambert equation is then used to correlate the absorbance to concentration using the formula:

$$\mathbf{c} = (\mathbf{A} \times \mathbf{e})/\mathbf{b}$$

where **c** refers to the DNA concentration (ng/µL), **A** refers to the absorbance at 260 nm, **e** refers to the wavelength-dependent extinction coefficient for DNA (50 ng-cm/µL), and **b** refers to the path length of the spectrometer used (0.1 cm) (Thermo Fisher Scientific, 2008). The concentration of DNA (ng/µL) was then calculated using the formula:

DNA concentration (ng/µL) = absorbance at 260 nm x dilution factor x 50

2.8.2. Restriction enzyme digestion

All restriction enzyme digests were performed in clean 1.5 mL tubes. Samples were digested with suitable units (U) of restriction enzyme(s) in 1X recommended New England Biolabs (NEB, USA) buffer, 1X bovine serum albumin (BSA) if required, and made up to 30 – 50 µL final volume using H_2O. One restriction enzyme U is defined by the manufacturer NEB as the amount of enzyme required to digest 1 µg of λ DNA in 1 hour at 37°C in a total reaction volume of 50 µL. The digestion mixture was mixed well, and incubated for at least 1 hr at the optimum reaction temperature for each restriction enzyme. For heat inactivation of the restriction enzyme, the digestion mixture was incubated at the recommended inactivation temperature. The complete information of the manufacturer's recommended restriction enzyme digestion and inactivation conditions are compiled in Table 2.1.

2.8.3. DNA ligation

To ligate DNA, 400 U of T4 DNA ligase (NEB, USA) and 1X T4 DNA ligase reaction buffer (NEB, USA) was added to a maximum of 2 μg of DNA sample, followed by at least 1 hr incubation at RT. To heat inactivate T4 DNA ligase, the reaction mixture was incubated at 65^{o}C for 10 min.

2.8.4. Primer design

Primers were designed using the free online primer design tool, Primer3 (http://biotools.umassmed.edu/bioapps/primer3_www.cgi). Specific primer selection criteria were applied including optimum primer size of 20 nt and primer melting temperature of 57^{o}C, adjusting the primer guanine and cytosine (GC) content to 40% – 60%. All primers were synthesised by GeneWorks (Adelaide, Australia) at 40 nmole scale and at the sequencing/PCR grade purity, which according to the manufacturer GeneWorks, are the highest yield and most stable oligonucleotides, as they do not contain salts that would potentially inhibit sequencing or PCR reactions, but only contain trace non-inhibitory salts that help stabilise the oligonucleotides for longer storage. The list of primers used in this study is summarised in Table 2.2.

2.8.5. PCR amplification of DNA

All PCR work was performed in a clean PCR hood, sterilised by UV irradiation for 15 min after each use.

PCR amplification was performed using either AmpliTaq Gold (AB, USA) or GoTaq Flexi polymerase (Promega, Australia). Each standard PCR mastermix contained 1X PCR reaction buffer, 16.5 mM $MgCl_2$, 0.2 mM deoxy nucleotide tri-phosphate (dNTP), 0.5 mM of each forward and reverse primer, and 0.25 U Taq polymerase (either AmpliTaq Gold or GoTaq Flexi), made up to at least 10 μL final volume using H_2O. The PCR reaction buffer used for the AmpliTaq Gold polymerase was 10X GeneAmp PCR buffer II, while 5X GoTaq Flexi PCR buffer was used for GoTaq polymerase.

The PCR reactions were performed in 200 μL PCR tubes in a 96-well MyCycler thermal cycler (Bio-Rad, USA). The PCR protocol consisted of polymerase heat activation at 95^{o}C for 10 min for AmpliTaq Gold, or for 2 min for GoTaq Flexi. This was followed by 35 cycles of a DNA denaturing step at 95^{o}C for 15 sec, a primer annealing step at 54^{o}C for 15 sec and an extension step at 72^{o}C with variable extension time based on the expected PCR product size. The extension time was estimated by allowing at least 1 min of extension time for each 1 kbp

of expected PCR product, with preferably longer extension time than the estimation to allow for the complete extension and synthesis of the PCR products. At the end of the 35 cycles, a final extension step at 72^{o}C for 7 min step was included to fully extend all the PCR products, before holding the reaction at 15^{o}C or 4^{o}C.

2.8.6. PCR purification

PCR products were purified using the QIAquick PCR purification kit (Qiagen, Germany) according to the instructions provided by the manufacturer.

2.8.7. Agarose gel electrophoresis

To prepare 1% agarose gel, DNA grade agarose powder (Quantum Scientific, Australia) was added to the appropriate volume of 1X TAE buffer. The agarose in the TAE buffer was then dissolved by boiling in a microwave oven. The mixture was allowed to cool before being poured into a gel mould with gel comb(s) inserted. After the gel was fully set, it was placed into a horizontal gel tank and flooded with 1X TAE buffer. Samples were loaded into the wells with 1/10 volume of 10X TAE loading buffer, and electrophoresed at 70 – 120 V until the bromophenol blue and xylene cyanol markers of the loading buffer had sufficiently separated. The gel was then removed from the gel tank, post-stained with 30X GelRed, and visualised under 302 nm UV light using the GelDoc XR imaging system.

2.8.8. Agarose gel extraction

Specific DNA bands were extracted from agarose gels using the QIAquick gel extraction kit (Qiagen), QIAEX II gel extraction kit (Qiagen, Germany), or the Invitrogen gel extraction kit (Invitrogen, USA) according to the instructions provided by the manufacturer.

2.8.9. Quantitation of DNA by quantitative PCR

Quantitative PCR (qPCR) reactions were performed in duplicates in MicroAmp Optical 8-tube strips (Applied Biosystems (AB), USA, catalogue no. 4316567 or 4358293) capped with optical caps (AB, USA), using either the ABI Prism 7000 (AB, USA), or the ABI StepOne Plus (AB, USA) qPCR instrument. Each qPCR mastermix consisted of 150 ng of the DNA template, 1X SYBR Green PCR Master Mix (AB, USA, catalogue no. 4309155), and 6 μM of each forward and reverse primers. The volume was subsequently made up to 20 μL using H_2O. The qPCR protocol consisted of initial polymerase activation at 95^{o}C for 10 min. This was followed by 40 cycles of a DNA denaturation step at 95^{o}C for 15 sec and a primer annealing and extension step at 60^{o}C for 1 min. The PCR cycle at which the fluorescence value of each sample passed the threshold was determined as the threshold cycle C_T value in the log-linear

amplification phase. An additional 40 cycles of 60°C to 95°C were performed to determine the dissociation temperature and melt curve for each PCR product. The dissociation temperature and melting curve data were used to determine whether non-specific amplification or more than one PCR product was present in the reaction.

To construct a standard curve for qPCR, at least 2 µg of plasmid DNA which contains the target DNA was digested using 20 U of *Eco*RI (NEB, USA) overnight as described in Section 2.8.2. The concentration of digested DNA was determined using a Nanodrop spectrophotometer as described in Section 2.8.1, and serial dilutions of 10^8 to 10^1 copies of plasmid DNA were then used to generate the standard curve. The mathematical calculation of the copy number of each plasmid is shown in Section 2.8.9.3.1. To standardise the total amount of DNA present in each qPCR reaction, 150 ng of normal duck liver (NDL) DNA extracted from NDL samples using the DNeasy blood and tissue kit as described in Section 2.6.1, were also added to each qPCR reaction.

All data was analysed using either ABI Prism or StepOne Plus software supplied by AB depending on which instrument was used. The C_T value of each standard (10^8 to 10^1 copies of target DNA) was plotted against the log concentration of the standard, generating a standard curve that can be subsequently used to calculate the concentration of target DNA in each sample. The limit of sensitivity of this assay was 10^1 copies of target DNA.

2.8.9.1. Quantitation of serum DHBV DNA by qPCR

The level of DHBV DNA in the serum was quantitated by qPCR using the primer set 423 – 576c (Table 2.2). The DNA template used was DNA extracted from the serum fraction using the Invitrogen ChargeSwitch gDNA 1 mL serum kit as described in Section 2.5.1, and diluted 1/5 in H_2O. The qPCR mastermix was prepared as described in Section 2.8.9, with 5 µL of the diluted serum DNA added to each qPCR mastermix as template, and qPCR performed as described in Section 2.8.9.

2.8.9.2. Quantitation of DHBV DNA in the liver by qPCR

The levels of DHBV cccDNA and total DNA in the liver were quantitated by qPCR using the primer sets CC2 – MG1 and 423 – 576c respectively (Table 2.2). The DNA template used was DNA extracted from the liver using the Invitrogen ChargeSwitch gDNA mini tissue kit as described in Section 2.6.2, and digested using 20 U of the restriction enzyme *Eco*RI overnight as described in Section 2.8.2. The concentration of digested DNA was determined using the Nanodrop spectrophotometer as described in Section 2.8.1. The qPCR mastermix was

prepared as described in Section 2.8.9, with 150 ng of the digested liver DNA added to each qPCR mastermix as template, and qPCR performed as described in Section 2.8.9.

The different forms of DHBV DNA can be distinguished by these two primer sets, as the cccDNA primer set (CC2 – MG1) binds specifically to the cohesive overlap region of the DHBV rcDNA (as shown in Figure 2.4). Therefore, when the DHBV cccDNA (completely double stranded) is denatured during PCR amplification, the 2 complete circular strands formed and could be subsequently amplified by the CC2 – MG1 primer set. In contrast, when the DHBV rcDNA (incomplete 3' positive strand DNA and gap in the negative strand DNA) is denatured during PCR amplification, 2 linear strands of DNA are formed which would not be amplified by the CC2 – MG1 primer set (Reaiche, 2008). On the other hand, to detect DHBV total DNA, the primer set (423 – 576c) was designed to bind sequences of the polymerase ORF of the DHBV genome. As this region is complete in all the forms of DHBV DNA, all DHBV rcDNA, RI and cccDNA can be amplified by the 423 – 576c primer set, thus detecting the DHBV total DNA present in the DNA samples (Reaiche *et al.*, 2010).

2.8.9.3. Mathematical calculation of the copy number of DNA

2.8.9.3.1. Copy number of plasmid DNA per mass

To calculate the copy number of plasmid DNA per plasmid mass, the following formula provided by AB was used (AB, 2003).

No. of moles (mole) = mass of plasmid (g) / MW (Da or g/mole)
MW (Da or g/mole) = no. base pairs x average MW of dsDNA (Da or g/mole)
Copy number = no. of moles (mole) x Avogadro's number (molecules/mole)

Where: Average MW of 1 base pair (bp) of dsDNA = 660 Da or g/mole
Avogadro's number = 6.023e23 molecules/mole

Therefore, the mass (g) of plasmid required:
= copy number needed x no. base pair x (average MW of dsDNA / Avogadro's number)
= copy number needed x no. base pair x 1.096e-21

In summary, based on the formula, it was calculated that to obtain 10^{10} copies of DHBV, 65.6 ng of pBL4.8 plasmid (5988 bp) was required, while 49.4 ng of pBL4.8x2 plasmid (9015 bp) was required (as each plasmid contains 2 copies of DHBV). To obtain 10^{10} copies of duck β actin, 55.4 ng of pT2.1DgB (5053 bp) was required; while 54.6 ng of pT2.1DgG (4983 bp)

was required to obtain 10^{10} copies of duck GAPDH. To obtain 10^{10} copies of pBsSK plasmid, 32.5 ng of pBsSK (2961 bp) was required.

2.8.9.3.2. Copy number of duck DNA per cell

Each gram (g) of duck liver was reported to contain ~6.8 x 10^8 cells (Jilbert *et al.*, 1992), and each duck cell was reported to contain ~2.5 pg of DNA (Tiersch and Wachtel, 1991; Krishan *et al.*, 2005).

Therefore, it is expected that 1 mg of duck liver would contain ~1.75 µg DNA, while 150 ng of DNA, which was the amount of DNA used as template in each qPCR reaction, would contain ~53,571 cells equivalent of DNA.

2.8.10. DNA sequencing

Each DNA sequencing mastermix contained 80 – 200 ng DNA template, 160 nm of either forward or reverse PCR primer, 0.25X BigDye Terminator mix (AB, USA), 1X BigDye Terminator buffer (AB, USA) and was made up to 20 µL using H_2O. Sequencing reactions were performed in 200 µL PCR tubes in a 96-well MyCycler thermal cycler. The sequencing protocol consisted of 30 cycles of a DNA denaturing step at 96^oC for 10 sec, primer annealing step at 50^oC for 10 sec, and an extension step at 60^oC for 4 min, before holding at 4^oC. Cleanup of DNA sequencing products were then performed as described in Section 2.8.11.

2.8.11. Cleanup of DNA sequencing products

2.8.11.1. Isopropanol cleanup

Sequencing products were cleaned by the addition of 80 µL 75% AR grade isopropanol, vortexed, and incubated at RT for 15 min. The mixture was centrifuged at 18,000 g for 20 min, and the supernatant was removed immediately. The pelleted DNA was washed with 250 µL of 75% AR grade isopropanol by vortexing, the DNA was repelleted by centrifugation at 18,000 g for 5 min, and the supernatant was immediately removed. The pelleted DNA was vacuum dried and sent to Division of Molecular Pathology, IMVS/SA Pathology for sequence analysis using the AB3730 DNA Sequencer (AB, USA).

2.8.11.2. Magnesium sulphate cleanup

Sequencing products were cleaned by the addition of 75 µL 0.2 mM magnesium sulphate ($MgSO_4$) mixture (60 µL H_2O, 140 µL 100% ethanol, 4 µL 0.01M $MgSO_4$), vortexed, and incubated at RT for 15 min. The mixture was centrifuged at 18,000 g for 15 min, the supernatant tipped off, and blot-dried for ~2 min to remove any excess supernatant. The

pelleted DNA was air dried and sent to the Australian Genome Research Facility (AGRF) for sequence analysis using the AB3730xl 96-capillary Sequencer (AB, USA).

2.8.12. DNA sequencing analysis

The results of the DNA sequences that were produced by the DNA sequencing facilities were compiled as *.ab1* formatted files. These *.ab1* DNA sequence result files were accessed using the Chromas Lite application provided by Technelysium (available for free at http://www.technelysium.com.au/chromas.html), to view the DNA sequencing electropherogram and its corresponding DNA sequence. Each obtained DNA sequence was then scanned through and edited manually. This is because sometimes, the computer-generated DNA sequence may not correspond to its actual sequence determined by the highest DNA sequencing electropherogram peaks, or may report a nucleotide as "N" for unknown. These errors commonly occur in regions of high repeats of the same nucleotides, or when more than one nucleotide was present in the DNA sequence due to random mutations or the presence of virus quasispecies. These nucleotides were corrected manually using the Chromas Lite application. In addition, the beginning and end of each DNA sequence was also trimmed to remove nucleotides that have low intensity DNA sequencing electropherogram peaks or have high background noise.

The final DNA sequences were further analysed by comparing the final DNA sequence against sequences found in the online nucleotide databank GenBank, or by aligning the DNA sequence with a known sequence. These analyses could be performed using the online BLAST program by the National Center for Biotechnology Information (NCBI) (accessible at http://www.ncbi.nlm.nih.gov/BLAST/Blast.cgi?), using the MEGABLAST nucleotide search function (general search for similar DNA nucleotide sequences available in the GenBank databank), or using the Align 2 Sequences nucleotide search function (specific search for similar DNA nucleotide sequences in one known DNA sequence). Both program functions would compare and align the DNA sequences according to regions of similar DNA sequences. In addition, using the Align 2 Sequences search function, the alignment scores of the finalised DNA sequence and the known sequence used for alignment could be determined by the BLAST program, and expressed as % of coverage and % of sequence similarity. The finalised DNA sequence could also be aligned with multiple known DNA sequences using the online ClustalW2 multiple sequence alignment program provided by the European Bioinformatics Institute (EBI) (accessible at https://www.ebi.ac.uk/Tools/msa/clustalw2/), from which the multiple sequence alignment output file could be viewed and arranged using the online

Jalview multiple alignment editor provided by the University of Dundee (accessible at http://www.jalview.org).

2.9. Cloning

2.9.1. Cloning of PCR products into the plasmid vector pCR 2.1-TOPO

PCR products purified as described in Section 2.8.6 were cloned into the pCR 2.1-TOPO plasmid using a TOPO TA cloning kit (Invitrogen, USA) according to the instructions provided by the manufacturer. The pCR 2.1-TOPO plasmid map is shown as Figure 2.5.

2.9.2. Analysis of PCR products cloned into the plasmid vector

To determine the size of the PCR product that was cloned into the plasmid vector, the extracted plasmid DNA (Section 2.7) was digested with *Eco*RI as described in Section 2.8.2. This *Eco*RI digestion would excise the cloned PCR product, as the cloning sites in the pCR 2.1-TOPO plasmid vector are flanked by two *Eco*RI digestion sites 11 and 6 nt away from the cloned DNA fragment. The digested plasmid was then visualised by agarose gel electrophoresis as described in Section 2.8.7 to determine the size of the cloned PCR product. A successfully cloned plasmid is expected to produce 2 bands: a high MW band which corresponds to the plasmid vector (3.9 kb), and a band which corresponds to the cloned PCR product, allowing the size of the cloned PCR product to be determined.

To determine the orientation of the inserted PCR product in relation to the pCR 2.1-TOPO *lacZ* gene promoter, the plasmid DNA was extracted as described in Section 2.7 and amplified as described in Section 2.8.5, using a forward primer specific for the PCR product, with either T7 forward primer or M13 reverse primer. If the PCR product was inserted in a "forward" direction in relation to the pCR 2.1-TOPO *lacZ* gene promoter, a PCR product will only be obtained with the specific forward primer – M13 reverse primer set; on the other hand if the PCR product was inserted in a "reverse" direction in relation to the pCR2.1-TOPO *lacZ* gene promoter, a PCR product will only be with the specific forward primer – T7 forward primer set. Alternatively, the T7 forward primer was used with either the specific forward or reverse primer. If the insert was in a "forward" direction in relation to the pCR 2.1-TOPO *lacZ* gene promoter, a PCR product will only be obtained with the T7 forward primer – specific forward primer set; while if the insert was in a "reverse" direction in relation to the pCR 2.1-TOPO *lacZ* gene promoter, a PCR product will only be obtained with the T7 forward primer – specific reverse primer set. Lastly, all PCR products were visualised by agarose gel electrophoresis as described in Section 2.8.7.

To confirm the sequence of the insert, plasmid DNA was amplified as described in Section 2.8.5 using T7 forward primer and M13 reverse primer, and purified as described in Section 2.8.6, and subsequently sequenced as described in Sections 2.8.10 and 2.8.11.

2.9.3. Plasmid glycerol stock

To generate glycerol stocks of successfully cloned plasmid, the colony of the transformed *E. coli* DH5α was picked and grown in 10 mL of LB with 60 μg/mL of ampicillin, incubated at 37^{o}C shaking overnight. In a screw-cap 1.5 mL tube, 400 μL of 80% glycerol was added to 500 μL of bacterial culture, mixed well by inversion, snap frozen dry ice for 3 – 4 min, and stored at -80^{o}C.

2.10. Inverse nested PCR

2.10.1. DNA inversion

The various inverse nested PCR (invPCR) designs used are described in Table 2.3. Schematic representations of DNA inversion for the detection of the integrated virus-cell left hand end junction and the integrated virus-cell right hand end junction are shown as Figures 2.6 and 2.7 respectively.

Essentially, ~1.75 μg of DNA (calculated amount of DNA in 1 mg of liver as shown in Section 2.8.9.3.2) was extracted as described in Section 2.6.3. To invert the DNA for invPCR, DNA was digested with a restriction enzyme (designated as first cut restriction enzyme) in a final volume of 30 μL, the restriction enzyme was subsequently heat inactivated as described in Section 2.8.2. This was followed by circularisation of DNA fragments using 500 U of concentrated T4 DNA ligase (NEB, USA, catalogue no. M0202T), 1X T4 DNA ligase buffer made up to 360 μL final volume with H_2O at RT for 2 hr. T4 DNA ligase was heat inactivated at 72^{o}C for 20 min, followed by DNA precipitation by the addition of 10 μL of 50 μM NaCl, 1 μL of 20 mg/μL dextran, and 2X volume of AR grade 100% ethanol and placed at -20^{o}C overnight. DNA was pelleted by centrifugation at 18,000 g for 15 min, the supernatant was discarded, and the pellet was washed with 1 mL of 100% AR grade ethanol with vortexing. DNA was pelleted again by centrifugation at 18,000 g for 15 min, the supernatant was discarded, and the pellet was vacuum dried at RT for 30 min. DNA pellet was dissolved and digested with a restriction enzyme (designated as second cut restriction enzyme), and another restriction enzyme to destroy cccDNA (designated as cccDNA destroying enzyme) in a final volume of 50 μL as described in Section 2.8.2. DNA was then stored at -20^{o}C until use.

2.10.2. Low melting temperature agarose gel electrophoresis and purification of high MW cellular DNA followed by DNA inversion

To remove virus RI DNA and other contaminating viral DNA, high MW DNA was extracted from total DNA after separation by low melting temperature agarose gel electrophoresis as described in Section 2.6.4. After the high MW DNA was extracted from the low melt gel and place in clean 1.5 mL tube, 1 mL of 1X NEB buffer required for the first cut restriction enzyme and 1 µL of 10% Triton X-100 was added, and gel was incubated at 4^{o}C overnight with shaking. The supernatant was removed, and the gel was placed at 72^{o}C for 15 min to allow the low melt agarose to melt. The sample was then cooled to the incubation temperature of the first cut restriction enzyme (without allowing the gel to re-set), before adding the first cut restriction enzyme to the sample and incubating for 1 hr. The sample was subsequently heat inactivated as described in Section 2.8.2. DNA was then purified using the QIAquick PCR Purification Kit. Specifically, 600 µL of PB was added to the mixture and transferred into a purification column. DNA was bound to the column by centrifugation at 18,000 g for 1 min, and the column was washed using 500 µL of PB followed by two 750 µL of PE washes, each with centrifugation at 18,000 g for 1 min. The column was subsequently spun dry to remove all traces of PE at 18,000 g for 1 min and the column basket was transferred to a clean 1.5 mL tube, and vacuum dried at RT for 30 min. The DNA was eluted using 100 µL of EB by incubating at RT for 1 min, prior to centrifugation at 18,000 g for 1 min. Eluted DNA was subsequently ligated, purified, and cut with second cut restriction enzyme and the cccDNA destroying enzyme to digest the cccDNA as described in Section 2.10.1.

2.10.3. 96-well nested PCR

DNA was inverted as described in Section 2.10.1 or Section 2.10.2 and was amplified using a nested PCR in a 96-well PCR tray (Integrated Sciences, Australia, catalogue no. AB0600). The first round PCR mastermix contained 1X AmpliTaq PCR II buffer, 2.5 mM $MgCl_2$, 0.2 mM dNTP, 0.25 µM of each forward and reverse PCR primers of the invPCR outer primer set, 0.25 U of AmpliTaq Gold polymerase, and was made up to 1 mL with H_2O. Inverted DNA was either added directly into the mastermix or distributed evenly to all wells on the PCR tray, or alternatively was serially diluted on the PCR tray. For example, 1/3 serial dilution of inverted DNA was performed by first placing mastermix in column 1 of the PCR tray (120 µL in wells B1-G1, and in well A1 a final volume of 180 µL of mastermix and inverted DNA). Serial dilution of the inverted DNA was then performed by transferring 60 µL of the mastermix-inverted DNA mix from well A1 to well B1 and mixing well by pipetting up and down, followed by subsequent dilutions down to well G1, where 60 µL of solution was discarded. Pipette tips were changed between each dilution to ensure no carry-over of DNA

during serial dilution. Subsequently, 10 µL of the mastermix-inverted DNA mix was distributed evenly from column 1 to all columns corresponding to the same serial dilution row. Lane H was commonly used as for PCR negative controls, and contained 10 µL of the PCR mastermix only. A schematic representation of the serial dilution is shown in Figure 2.8. The PCR tray was covered with RNase/DNase-free silicon sealing pad (DSKH, Australia, catalogue no. 6555), and a first round PCR reaction was then performed in a 96-well MyCycler thermal cycler. The PCR protocol consisted of polymerase heat activation at 95^{o}C for 10 min, followed by 35 cycles of DNA denaturing step at 95^{o}C for 15 sec, primer annealing step at 54^{o}C for 15 sec and extension step at 72^{o}C for 3 min, followed by a 72^{o}C for 7 min step to fully extend all PCR products, before holding the reaction at 4^{o}C.

The second round PCR mastermix consisted of 0.5X clear GoTaq Flexi PCR buffer, 0.5X green GoTaq Flexi PCR buffer, 2.5 mM $MgCl_2$, 0.2 mM dNTP, 0.25 µM of each forward and reverse PCR primers of the invPCR inner primer set, 0.25 U of GoTaq Flexi polymerase, and was made up to 1 mL with H_2O. Subsequently, 10 µL of the mastermix was distributed equally to all wells of the PCR tray. Transfer of the first round PCR product to the second round PCR mastermix was performed in a sterile PCR hood using a sterilised 96-pin device. The second round PCR reaction was then performed in a 96-well MyCycler thermal cycler. The PCR protocol consisted of a polymerase heat activation at 95^{o}C for 2 min, followed by 35 cycles of a DNA denaturing step at 95^{o}C for 15 sec, a primer annealing step at 54^{o}C for 15 sec and an extension step at 72^{o}C for 3 min, followed by a 72^{o}C for 7 min step to fully extend all PCR products, before holding the reaction at 4^{o}C. InvPCR products were stored at -20^{o}C until further use.

2.10.4. 96-well agarose gel electrophoresis

At least 100 mL of 1.3% agarose gel was prepared by adding molecular grade agarose powder (Bio-Rad, USA) to the appropriate volume of 1X TAE buffer. The agarose in the TAE buffer was then dissolved by boiling in a microwave oven. The mixture was allowed to cool before being poured into a gel mould (Rapid Load Tray, catalogue no. B2-RL-UVT, Thermo Scientific, Canada) with 4 gel combs (25 teeth, catalogue no. B2-RL-25D, Thermo Scientific, Canada) inserted, and set in a horizontal gel tank (EasyCast B2 Mini Gel, Thermo Scientific, Canada). After the gel was fully set, the gel tank was flooded with 1X TAE buffer. All 96 PCR products were then loaded into the wells with 10X TAE loading buffer, and electrophoresed at 180 V until the bromophenol blue and xylene cyanol markers of the loading buffer had sufficiently separated. The gel was then removed from the gel tank and

post-stained with 30X GelRed, and visualised under 302 nm UV light using the GelDoc XR imaging system and the UV converter plate as described in Section 2.6.4.

2.10.5. 96-well agarose gel extraction

Single bands were extracted from the agarose gel into a 96-well tray (DKSH, Australia, catalogue no. CP6551) which was then covered with a silicon sealing mat, and the DNA was extracted using QIAEX II beads (Qiagen, Germany). First, 100 µL of 5 µL QIAEX II beads in 100 µL QX1 buffer (Qiagen, Germany) and 1 µL 10% Trixon X-100 was added to each well, and incubated at 55^{o}C for 15 min to dissolve the gel. To resuspend the beads, the tray was firmly clamped and shaken vigorously. The tray was again incubated at 55^{o}C 15 min. Beads were pelleted by centrifugation at 700 g for 3 min, the supernatant was flung out of the tray, and the beads were washed twice with 50 µL of QX1 buffer containing 1 µL of 10% Triton X-100 and washed 3 times with 100 µL of PE buffer (Qiagen, Germany). For each wash, beads were resuspended by vigorous shaking, pelleted by centrifugation at 700 g for 3 min and the supernatant was flung out of the tray. Beads were air dried, and the DNA was eluted with 30 µL of EB. The beads were resuspended by vigorous shaking, incubated at RT for 5 min, and pelleted by centrifugation at 700 g for 3 min. The supernatant contained the eluted DNA.

2.10.6. 96-well DNA sequencing

DNA sequencing reactions were performed in a 96-well PCR tray, each well contained the sequencing mastermix of 1X BigDye Terminator mix, 0.5X BigDye Terminator buffer and 1.5 µM PCR primers of the invPCR inner primer set (refer Table 2.3) made up to 10 µL using H_2O. As DNA template, 4 µL of invPCR products extracted as described in Section 2.10.5 was added. Sequencing reactions were performed in the 96-well MyCycler thermal cycler, with the sequencing protocol which consisted of 95^{o}C for 2 min to activate polymerase, followed by 25 cycles of a DNA denaturing step at 95^{o}C for 10 sec, a primer annealing step at 55^{o}C for 10 sec, and an extension step at 60^{o}C for 4 min, before holding the reaction at 4^{o}C.

2.10.7. Cleanup of 96-well DNA sequencing products

The DNA sequencing products in the 96-well PCR tray were cleaned using CleanSeq magnetic beads (Agencourt Bioscience, USA). In brief, 10 µL of magnetic beads and 42 µL of 85% AR grade ethanol were added to each well, the tray was briefly vortexed, and was incubated on a magnetic base at RT for 10 min. Keeping the tray on the magnetic base, the supernatant was flung out, and beads were washed twice with 100 µL of 85% AR grade ethanol with incubation at RT for 10 min between washes. Tray was then removed from the magnetic base and air dried. Returning the tray onto the magnetic base, DNA was eluted from

the beads with 80 µL of 0.02 mM EDTA pH 8 with incubation at RT for 5 min. From the eluted DNA, 40 µL was transferred to a clean 96-well PCR tray, sealed with ThermalSeal film (Sigma, USA, catalogue no. Z723304-100EA) and sent to AGRF for sequence analysis using the AB3730xl 96-capillary Sequencer.

2.11. Southern blot hybridisation

2.11.1. Nitrocellulose membrane preparation

A 1.5% agarose gel was prepared as described in Section 2.8.7, and was placed into horizontal gel tank half flooded with 1X TAE buffer. Up to 500 ng of DNA extracted from liver as described in Section 2.6, or 50 – 100 pg plasmid DNA extracted as described in Section 2.7, were mixed with 3.5 µL of 10X TAE loading buffer, and 31.5 µL of TE (10:1, pH 8), and were loaded into each gel well. Samples were electrophoresed "dry" at 80 mA until both loading buffer markers had left the well, before flooding the gel tank with 1X TAE buffer. The gel was then electrophoresed at a constant 20 mA overnight. The gel was carefully removed from the gel tank and held in 0.05 M NaOAc pH 4.6 with shaking at RT for 1 hr, followed by 0.05 M NaOAc pH 4.6 pre-warmed to 55^{o}C, with shaking at 55^{o}C for 1 hr. After that, gel was treated with Blot I (1.5 M NaCl, 0.5 M NaOH) shaking at RT for ~30 min, and subsequently treated with Blot II (1 M ammonium acetate, 0.02 M NaOH, pH 8) with shaking at RT for >1 hr.

DNA was transferred from the gel onto a Schleicher and Schuell BA85 nitrocellulose membrane (Sigma, USA) via capillary action. First, 3 sheets of 25 x 25 cm Whatmann 3MM paper (Crown Scientific, Australia) were placed on a clean metal tray on a clean flat surface and saturated with Blot II. Air bubbles were excluded from the papers using a clean 10 mL pipette as a rolling pin. The treated gel was placed face down on the centre of the Whatmann paper, and overlaid with nitrocellulose membrane cut to the same size as the gel that had been pre-soaked in Blot II for 3 min. The nitrocellulose membrane was then covered by 3 sheets of Whatmann paper cut to the same size as the gel that had been pre-soaked in Blot II. Again, air bubbles were excluded from the nitrocellulose membrane and Whatmann papers using a clean 10 mL pipette as a rolling pin. An additional 2 sheets of dry Whatmann paper were then put on the stack, followed by 7 – 8 cm of absorbent towels and a glass plate. The entire structure was covered with glad wrap, and a 100 g weight was placed on the top. Extra Blot II was added to ensure that the structure was kept wet for the transfer to occur. The DNA was allowed to transfer to the membrane overnight at RT after which the stack of paper was carefully dismantled and the nitrocellulose membrane was removed. The nitrocellulose membrane was washed in 2X SSC (3 M NaCl, 3 M Na_3Citrate, pH 7.0) twice, shaking at RT

for 5 min, blotted dry on Whatmann paper, and then baked at 80^{o}C in a vacuum oven for 2 hr between 2 sheets of Whatmann paper, sandwiched between 2 glass plates. The nitrocellulose membrane was stored between 2 sheets of Whatmann paper pressed between 2 glass plates at RT until use.

2.11.2. ^{32}P probe preparation

Radioactive DNA probes were generated by random-priming with ^{32}P dATP or dCTP (Perkin Elmer, Australia) using the Megaprime DNA Labelling System kit (Amersham Biosciences, Australia). First, 50 μCi of ^{32}P dCTP (Perkin Elmer, Australia) was kept behind Perspex, and defrosted at RT for 30 min before use. Up to 150 ng of the plasmid DNA to be used as a probe, and 5 μL of Megaprime DNA Labelling Systems primers were added into a screw-cap Eppendorf tube and made up to 25 μL using H_2O. The mixture was vortexed and spun briefly, before heating for 2 min at 100^{o}C, then placed immediately into ice for 2 min. From the Megaprime DNA Labelling System kit, 4 μL of dATP, dCTP, dGTP and dTTP (excluding the nucleotide that was ^{32}P-labelled) and 5 μL of reaction buffer were added, and the mixture was vortexed and spun briefly before adding 5 μL of ^{32}P-labelled nucleotide and 2 μL of Klenow enzyme from the Megaprime kit. The mixture was flicked and spun briefly before incubation at 37^{o}C for 30 min to allow synthesis of the radioactive probe. To stop the reaction, 50 μL of H_2O plus 20 μL of 0.5 M EDTA (pH 8) was added to the mixture, followed by 12 μL of 3 M NaOAc pH 4.6, and lastly the probe was precipitated by 2 volumes of 100% AR grade ethanol to remove any unincorporated nucleotides, mixed well, and stored at -20^{o}C overnight. The mixture was thawed at RT for 30 min, centrifuged for 10 min at 10,000 g, and supernatant was removed to a 1.5 mL flip top tube labelled wash 1. The pelleted DNA was then washed twice with 200 μL of 70% AR grade ethanol and centrifuged for 2 min at 10,000 g. The supernatant was removed to 1.5 mL flip top tubes labelled washes 2 and 3 respectively. The radioactivity of each wash was measured using a β counter (Beckman Coulter, Australia, catalogue no. LS 6000 TA), to check whether the unincorporated ^{32}P-labelled nucleotides had been removed by the washes. The pelleted DNA was redissolved in 50 μL H_2O, boiled for 3 min, and put immediately on ice for 5 min. To check the radioactivity of the probe, 1 μL of the probe was spotted onto 1 cm^2 Whatmann paper. When dried, the paper was put into a scintillation vial, 1 mL of OptiPhase HiSafe 2 scintillation fluid (Perkin Elmer, USA) was added, and the probe was read by a Wallac 1214 Betarack scintillation β counter (LKB Instruments, Australia) to obtain counts per min (CPM). A final concentration of 3 – 6 x 10^6 CPM/mL of probe was added into 12 mL of hybridisation solution pre-warmed to 42^{o}C before use for the hybridisation of the nitrocellulose membrane described in Section 2.11.3. The hybridisation solution was made up of 50% deionised formamide, 100 μg/mL salmon sperm

as carrier DNA, 0.02% PVP, 0.02% Ficoll 400, 25 mM Na_2HPO_4, NaH_2PO_4, pH 6.5, 0.2 mg/mL BSA, 5X SSC, 10% dextran sulphate, and was stored at -20°C until use.

2.11.3. Hybridisation of the ^{32}P-labelled probe to the nitrocellulose membrane

The prepared nitrocellulose membrane (Section 2.11.1) was placed into a siliconised hybridisation bottle with the DNA-bound side facing inwards, and 12 mL of pre-hybridisation solution pre-warmed to 42°C was added into the bottle and incubated for at least 1 hr at 42°C in a rotating hybridisation oven. The pre-hybridisation solution was made up of 50% deionised formamide, 500 μg/mL denatured salmon sperm DNA as carrier, 0.1% filtered PVP, 0.1% Ficoll 400, 1% glycine, 50 mM Na_2HPO_4, NaH_2PO_4, pH 6.5, 0.2 mg/mL BSA, 5X SSC, and was stored at -20°C until use. The pre-hybridisation fluid was then removed, and replaced with 12 mL of hybridisation solution containing 3 – 6 x 10^6 CPM/mL of the ^{32}P-labelled DNA probe (Section 2.11.2), and incubated at 42°C overnight in a rotating hybridisation oven. The hybridisation solution was then removed, and the nitrocellulose membrane was washed twice with 2X SSC for 5 min at RT, twice with 2X SSC, 0.1% SDS for 30 min at 55°C, and twice with 0.1X SSC, 0.1% SDS for 30 min at 55°C, all in a rotating hybridisation oven. The nitrocellulose membrane was removed from the bottle, blotted dry on Whatmann paper, and wrapped in glad wrap. The nitrocellulose membrane was then exposed to Kodak Biomax XAR film (Sigma, USA) in an X-ray cassette for different lengths of time at -80°C, and lastly the film was developed using an automatic X-ray film developer (Ilford, Switzerland).

2.12. Linker ligation assay

The various linker ligation assay designs used are described in Table 2.4. A schematic representation of the steps involved during linker ligation assay is shown in Figure 2.9.

Up to 2 μg of DNA extracted using the total extraction method as described in Section 2.6.3, was placed in a 200 μL PCR tube. To dephosphorylate the terminal phosphate groups in the DNA, 1 unit of shrimp alkaline phosphatase (SAP) (GE Healthcare, Sweden) and 1X NEB4 buffer was then added to the DNA. The mixture was made up to 20 μL final volume using H_2O, incubated at 37°C for 1 hr, followed by heat inactivation of SAP at 80°C for 20 min. DNA was then digested with 10 U of *Pvu*II restriction enzyme with incubation at 37°C for 1 hr. *Pvu*II was chosen as it does not have a digestion site in all the HBV, WHV and DHBV genomes, therefore preventing the detection of viral cccDNA by linker ligation assay. As the DNA was previously dephosphorylated, the only phosphorylated 5' ends present in the DNA (needed for ligation of the non-phosphorylated linkers) would be those generated by the *Pvu*II digestion. The DNA was then purified using the QIAquick PCR purification kit as described

in Section 2.8.6 to remove the *Pvu*II. Specifically, 1 mL of PB was added to the mixture and transferred into a purification column. DNA was bound to the column by centrifugation at 18,000 g for 1 min, and the column was washed using 500 µL of PB followed by two 750 µL of PE washes, each with centrifugation at 18,000 g for 1 min. The column was subsequently spun dry to remove all traces of PE at 18,000 g for 1 min and the column basket was transferred to a clean 1.5 mL tube. The DNA was eluted using 100 µL of EB by incubating at RT for 1 min, prior to centrifugation at 18,000 g for 1 min.

Linkers were then added to 50 µL the purified DNA by adding 2 µL of linkers, 100 U of concentrated T4 DNA ligase, 1X T4 DNA ligase buffer made up to a 200 µL final volume with H_2O at RT overnight. The linkers were made up of 0.25 µM of each of the LL 1415 and LL 1337 oligonucleotides (refer Table 2.2) in 100 µL of EB, and were annealed together by heating at 80^oC for 10 min to first dissociate the oligonucleotide strands, then cooled to RT to allow complementary base pairing of the oligonucleotide strands. As the linkers do not have 5' phosphorylated ends, only the 3' end of the longer LL1415 strand will be ligated to the phosphorylated 5' ends of the DNA created by *Pvu*II digestion.

To terminate all the 3' ends of the linkers, 8 µL of 2.5 mM dideoxy nucleotide tri-phosphate (ddNTP) and 0.2 U of *Taq* DNA polymerse (NEB, USA) was added to the mixture, and incubated at 72^oC for 2 hours. The use of ddNTPs instead of dNTPs would prevent the amplification of linkers from the shorter LL1337 oligonucleotides in subsequent steps. The DNA was then purified using the QIAquick PCR purification kit as described in Section 2.8.6. Specifically, 1 mL of PB was added to the mixture and transferred into a purification column. DNA was bound to the column by centrifugation at 18,000 g for 1 min, and the column was washed using 500 µL of PB followed by two 750 µL of PE washes, each with centrifugation at 18,000 g for 1 min. The column was subsequently spun dry to remove all traces of PE at 18,000 g for 1 min and the column basket was transferred to a clean 1.5 mL tube, and vacuum dried at RT for 30 min. The DNA was eluted using 100 µL of EB by incubating at RT for 1 min, prior to centrifugation at 18,000 g for 1 min.

For better separation of the long DNA fragments (>3000 bp), 75 µL of dimethyl sulfoxide (DMSO) was added to the DNA, made up to 500 µL by H_2O, and incubated at 95^oC for 2 min. PCR mastermix which consisted of 1X AmpliTaq PCR II buffer, 2.5 mM $MgCl_2$, 0.2 mM dNTP, 0.25 µM each of LL1415 and the virus linker primers (refer Table 2.4) and 0.25 U of AmpliTaq Gold polymerase, was then added to the DNA and made up to 1 mL with H_2O, from which 10 µL of the PCR mix was distributed evenly to each of the 96 wells in the 96-

well PCR tray, the PCR tray was covered with RNase/DNase-free silicon sealing pad, and the linker ligation assay PCR was performed in a 96-well MyCycler thermal cycler. The PCR protocol consisted of polymerase heat activation at 95^{o}C for 10 min, followed by 35 cycles of DNA denaturing step at 95^{o}C for 20 sec, primer annealing step at 54^{o}C for 20 sec and extension step at 72^{o}C for 3 min, followed by a 72^{o}C for 10 min step to fully extend all PCR products, before holding the linker ligation assay PCR products at 15^{o}C.

Next, 4.5 µL of the ligation mastermix (50 µL of 10X T4 DNA ligase buffer, 10,000 U of concentrated T4 DNA ligase, 20 U of *Pvu*II, 5 U of Exonuclease I (NEB, USA), 400 µL of H_2O) was distributed evenly to each of the 96 wells of a 96-well PCR tray. The linker ligation assay PCR products were transferred to the ligation mix in a sterile PCR hood using a sterilised 96-well pin 5 times to increase the amount of transferred linker ligation assay PCR products. The ligation reaction was then performed in a 96-well MyCycler thermal cycler, with incubation at 37^{o}C for 30 min for P*vu*II and Exonuclease I digestions, 25^{o}C for 2 hr for ligations, and 80^{o}C for 20 min for heat inactivation of the ligase, before holding the circularised DNA at 15^{o}C. *Pvu*II was used to remove the linkers from the DNA fragments, while Exonuclease I was used to remove any DNA overhangs that may interfere with the subsequent blunt end self-ligation of the DNA fragments.

The 96-well nested PCR was then performed as described in Section 2.10.3 with the addition of restriction enzyme digestion to linearise the circularised DNA. Briefly, the ligated DNA was transferred to 10 µL of the first round nested PCR mastermix (1X AmpliTaq PCR II buffer, 2.5 mM $MgCl_2$, 0.2 mM dNTP, 0.25 µM of each forward and reverse PCR primers of the invPCR outer primer set, 0.25 U of AmpliTaq Gold polymerase, 5 µL of linearisation restriction enzyme, made up to 1 mL with H_2O) in a sterile PCR hood using a sterilised 96-well pin. PCR was then performed in a 96-well MyCycler thermal cycler using the PCR protocol of the restriction enzyme reaction temperature for 1 hr, polymerase heat activation at 95^{o}C for 10 min, followed by 35 cycles of DNA denaturing step at 95^{o}C for 15 sec, primer annealing step at 54^{o}C for 15 sec and extension step at 72^{o}C for 3 min, followed by a 72^{o}C for 7 min step to fully extend all PCR products, before holding the reaction at 15^{o}C. This was followed by transferring of the first round PCR products to 10 µL of the second round nested PCR mastermix (0.5X clear GoTaq Flexi PCR buffer, 0.5X green GoTaq Flexi PCR buffer, 2.5 mM $MgCl_2$, 0.2 mM dNTP, 0.25 µM of each forward and reverse PCR primers of the invPCR inner primer set, 0.25 U of GoTaq Flexi polymerase, made up to 1 mL with H_2O) in a sterile PCR hood using a sterilised 96-well pin. PCR was then performed in a 96-well MyCycler thermal cycler using the PCR protocol of polymerase heat activation at 95^{o}C for 2

min, followed by 35 cycles of a DNA denaturing step at 95°C for 15 sec, a primer annealing step at 54°C for 15 sec and an extension step at 72°C for 3 min, followed by a 72°C for 7 min step to fully extend all PCR products, before holding the reaction at 15°C, and storing at -20°C. The linearisation restriction enzyme and PCR primer sets used are listed in Table 2.4.

The linker ligation assay products were subsequently visualised using 96-well agarose gel electrophoresis as described in Section 2.10.4, extracted using the 96-well agarose gel extraction as described in Section 2.10.5, sequenced using the R2 inner primer using the 96-well DNA sequencing as described in 2.10.6, and the DNA sequencing products were purified as described in Section 2.10.7. The DNA sequences obtained were lastly analysed as described in Section 2.8.12.

2.13. Cell cultures

2.13.1. Preparation of cell cultures

The chicken hepatocellular carcinoma cell lines, LMH, and dstet5 were prepared and maintained by Miss Cuixia Wang as described in Wang, 2008. The primary duck hepatocyte (PDH) cultures were prepared and maintained by Miss Catherine Scougall and Mr. Qiao Qiao as described in Qiao, 2009.

2.13.2. Harvesting of cell

Cells were harvested by adding 1 mL of 0.1% trypsin (IMVS/SA Pathology, Australia) and incubating at RT for 5 min, with gentle hitting the cell culture flasks to dislodge the cells. When cells had been dislodged, 5 mL of 1X PBS was added to the culture and all the culture containing the cells were collected.

2.13.3. Counting the number of cells

To count the cells present in the collected culture, an aliquot of the culture (Section 2.13.2) was transferred to a clean 1.5 mL tube. After adding an equal volume of trypan blue (Sigma, USA) to the cells, the mixture was put on a haemocytometer (Crown Scientific, Australia) and visualised under light microscopy. Live viable cells would be observed as translucent round cells, while dead non-viable cells would be observed as dark blue cells generally with a shrunk or collapsed morphology. The amount of cells per 10 mL of extracted supernatant could then be calculated using the formula:

$$\text{Amount of cells (per 10 mL)} = \text{dilution factor of trypan blue} \times 10^4 \times \text{average number of cells counted from both haemocytometer chambers}$$

2.13.4. DNA extraction from cells

DNA were extracted from the cells in the collected culture (Section 2.13.2) using the DNeasy blood and tissue kit (Qiagen, Germany) according to the instructions provided by the manufacturer. Briefly, the supernatant was first centrifuged at 300 g for 5 min to pellet the cells. The supernatant was removed, and the pellet was resuspended in 200 µL 1X PBS. The cells were subsequently lysed with 20 µL of proteinase K, and the RNA was removed by digestion with 4 µL of 100 mg/mL RNase. After that, the DNA was precipitated, purified via spin-columns, and eluted twice from the column with 100 µL of AE (Qiagen, Germany), collected in the same collection tube. The extracted DNA was stored at -20^{o}C.

2.13.5. Calculation of cells present per 150 ng of DNA

Using the haemocytometer (Section 2.13.3), it was estimated that a total number of 3.8 x 10^5 viable cells was present in the LMH culture, 5.6 x 10^5 viable cells were present in the dstet5 culture, and 8.3 x 10^5 viable cells were present in the PDH culture. After DNA extraction as described in Section 2.13.4, the concentration of DNA determined by spectrophotometry as described in Section 2.8.1. It was found that 407.34 ng/µL of LMH DNA were extracted, 120.6 ng/µL of dstet5 DNA were extracted, and 90 ng/µL of PDH DNA were extracted.

Based on that, it could be estimated that in 150 ng of DNA, there would be 700 LMH cells, 3,500 dstet5 cells, and 7,000 PDH cells.

However, these values would be rough estimations, as the expected losses of DNA during the DNA extraction process were not taken into account. In addition, as some DNA would also be extracted from the dead non-viable cells present in the cell culture, these values would thus under-estimate the actual number of cells per 150 ng of DNA.

2.14. Fluorescence *in situ* hybridisation

2.14.1. Preparation of metaphase chromosome spread slides

To inhibit cells at the metaphase, cells in the cell cultures (Section 2.13.1) were treated with 0.5 µg/mL colchicine (Sigma, USA) for 14 – 16 hrs. Cells were then harvested using 1 mL of 0.1% trypsin (Section 2.13.2), and centrifuged at 300 g for 5 min to pellet the cells. The supernatant was removed, and the pellet was resuspended in 8 mL of 75 mM KCl and incubated at 37^{o}C for 20 min. After that, 1 mL of methanol (Merck, Australia):acetic acid (3:1) was added to the mixture, and centrifuged at 300 g for 5 min. The supernatant was removed, and the pellet was washed twice using 1 mL of methanol:acetic acid, before resuspending the

pellet in 500 µL of methanol:acetic acid. A few drops of the resuspended cells were then dropped onto glass microscope slides from a height of 5 – 10 cm to spread out the chromosomes of the cells. The microscope slides were then heat-fixed at 60^{o}C for 10 min, and stored at -20^{o}C.

Before use, the slides were incubated at 37^{o}C overnight. After cooling to RT, slides were washed with 2X SSC for 5 min, and 400 µL of 40 µg RNase A (Sigma, USA) in 2X SCC were added to each slide. Slides were covered using glass cover slips, and incubated at 37^{o}C for 30 min in a humid box. After removing the cover slips by dip washing in 1X PBS, the slides were washed in 1X PBS 2 times for 5 min, and treated in 0.005% pepsin (Sigma, USA) in 0.01M HCl (Merck, Australia) at 37^{o}C for no longer than 10 min. Slides were then washed in 1X PBS 2 times for 5 min, and treated in 50 mL of post-fixation buffer (50 mM $MgCl_2$, 1X PBS) at RT for 5 min, followed by treatment in 50 mL of paraformaldehyde mix (50 mM $MgCl_2$, 4% paraformaldehyde (Sigma, USA), 1X PBS) at RT for 5 min. Slides were washed in 1X PBS 2 times for 5 min, and then placed in 70%, 90% and 100% AR grade ethanol for 5 min each. Slides could be left in 100% AR grade ethanol until use, and air dried right before hybridisation with the probe (Section 2.14.2).

2.14.2. Fluorescent probe preparation

To generate fluorescent probes for fluorescence *in situ* hybridisation (FISH), 300 ng of plasmid to be used as probe and 5 µL of 0.9 ng random primer (GeneWorks, Australia), were made up to a final volume of 19.1 µL using H_2O. The mixture was mixed well by vortex, and incubated at 95^{o}C for 15 min, followed by 5 min on ice. In a separate reaction, 4.6 µL of 5X dNTP solution mix (100 µM of dATP, dCTP, dGTP; 20 µM of dTTP) (NEB, USA), 0.3 µL of 1 nmole Spectrum Orange-dUTP fluorescent dye (Vysis, USA), and 1 µL of DNA polymerase I Klenow enzyme (5U) (NEB, USA) were mixed well, before adding into the previous 19.1 µL of mixture. The mixture was then mixed well by vortex, wrapped in aluminium foil, and incubated at 37^{o}C overnight. After that, 5 µL of 20 mg/mL salmon sperm DNA (Sigma, USA), 0.1X volume of 3 M NaOAc, and 3X volume of 100% AR grade ethanol were added into the mixture. The mixture was then incubated at -80^{o}C for 30 – 60 min, and centrifuged at 18,000 g for 20 min. The supernatant was discarded, and the pellet could be stored at -20^{o}C, or resuspended in 20 µL FISH hybridisation mix (10% dextran sulphate, 2X SSC in deionised formamide) to be hybridised to the slides (prepared in Section 2.14.1).

2.14.3. Hybridisation of the fluorescent probe

The metaphase chromosome spreads on the prepared microscope slides (Section 2.14.1) were sealed with Frame-Seal incubation chambers (Bio-Rad, USA), and 20 μL of the prepared fluorescent probe (Section 2.14.2) was added to each chamber. The chambers were then sealed with the provided flexible plastic cover slip (Bio-Rad, USA). Using the OmniSlide Thermal Cycler (Thermo Fisher, Canada), the slides were incubated at 80^{o}C for 5 min to denature the probe, and at 37^{o}C overnight to hybridise the probe. After that, the slides were washed in 0.1X SCC at 57^{o}C, 3 times for 5 min, and then 1 – 2 drops of ProLong Gold antifade reagent with 4',6-diamidino-2-phenylindole (DAPI) (Invitrogen, USA) were added to each slide. Slides were covered using glass cover slips, and then the sides of the cover slip were sealed with clear nail polish. Slides were viewed under immunefluorescence microscopy at 358 – 461 nm which would show dark blue/purple-stained chromosomes (DAPI dye), and at 559 – 588 nm which would show orange/red-stained regions of the chromosome that were bound by the probe.

Table 2.1: List of restriction enzymes used for digestion of double stranded DNA in this study.

Restriction enzyme	Concentration (units/mL)[a]	Digestion site (5' – 3')[b]	Buffer[c]	BSA[d]	Reaction temperature (^{o}C)	Heat inactivation[e]	
						Temperature (^{o}C)	Time (min)
*Afl*III	5,000	A\CRYG/T	3	Yes	37	80	20
*Bgl*II	10,000	A\GATC/T	3	No	37	-	-
*Bsa*BI	10,000	GATNN|NNATC	2	No	60	80	20
*Bsa*WI	5,000	W\CCGG/W	2	Yes	60	80	20
*Bsr*I	5,000	ACTG/GN\	3	No	65	80	20
*Dde*I	10,000	C\TNA/G	3	No	37	65	20
*Eco*RI	20,000	G\AATT/C	*Eco*RI	No	37	65	20
*Hind*III	20,000	A\AGCT/T	2	No	37	65	20
*Kpn*I	10,000	G/GTAC\C	1	Yes	37	-	-
*Pvu*II	20,000	CAG|CTG	4	No	37	-	-
*Nde*I	20,000	CA\TA/TG	4	No	37	65	20
*Nsi*I	10,000	A/TGCA\T	3	No	37	80	20
SacI	20,000	G/AGCT\C	1	Yes	37	65	20
*Sau*3AI	4,000	\GATC/	1, 4	No	37	65	20
*Sfc*I	10,000	C\TRYA/G	4	No	37	65	20
*Tsp*45I	4,000	\GTSAC/	1	Yes	65	-	-

Restriction enzymes digestions are performed as described in Section 2.8.2.

[a]Concentrations of the restriction enzymes produced by manufacturer NEB. A unit (U) is defined as the amount needed to digest 1 μg of λ DNA in 1 hour at 37°C in a reaction volume of 50 μL.

[b]Specific DNA sequences that are recognised by the restriction enzymes for digestion, shown in a 5' – 3' direction. The symbol \ represents digestion site on the 5' – 3' positive DNA strand, the symbol / represents digestion site on the 3' – 5' negative DNA strand, the symbol | represents blunt end restriction enzyme digestion site. "A" represents the nucleotide adenine, "C" represents the nucleotide cytosine, "G" represents the nucleotide guanine, "T" represents the nucleotide thymine. "S" means that both C or G nucleotide would be recognised, "R" means that both A or G nucleotide would be recognised, "Y" means that both C or T nucleotide would be recognised.

[c]Optimum restriction enzyme digestion buffers (NEB, USA) for each restriction enzyme as recommended by manufacturer NEB which would allow for 100% activity of the restriction enzyme when used in a 1X concentration in the restriction enzyme digestion mixture.

[d]Shows whether 1X bovine serum albumin (BSA) is required in the digestion mixture. For some restriction enzymes, 100% activity is only achieved when 100 μg/mL BSA was added to the digestion mixture. As NEB supplies 10 mg/mL BSA (100X), 1X BSA was added into the digestion mixture to allow for 100% of the restriction enzyme during digestion.

[e]Restriction enzymes that could not be heat inactivated were shown as "-".

Table 2.2: List of primers used in this study, with its specific DNA targets, primer binding positions, and primer sequence.

Primer name	Target	GenBank Accession	Primer position (5' – 3')	Primer sequence (5' – 3')
423[a]	DHBV	AJ006350	423-442	ctaagcatcacttggggaaa
576c[a]	DHBV	AJ006350	576-556	gctggagtcaaatatttccaa
BD16 F1	DHBV	AF047045	2981-3000	tagtaagtttccaacccgac
BD16 F2	DHBV	AF047045	3001-3020	tatccgattacggctagaat
BD16 R1	DHBV	AF047045	2760-2741	ccaataaggctctaaagcgt
BD16 R2	DHBV	AF047045	2734-2715	catctctaacaagatcatct
BL R1	DHBV	AJ006350	2750-2729	gcgtctttagcatcccttacaa
BL R2	DHBV	AJ006350	2712-2691	aaagaaatcatcaggcagatca
BLE F1	DHBV	AJ006350	2984-3006	gaatagtaagtttccagcctgac
BLE F2	DHBV	AJ006350	3011-1	cgattacggcaagaattc
BLN F1	DHBV	AJ006350	2801-2825	caactcactttgtggatcttattga
BLN F2	DHBV	AJ006350	2836-2856	cagaccactcagggtatgcat
CC2[b]	DHBV	AJ006350	2462-2481	cctgattggacggctcttac
DHBV C R	DHBV	AJ006350	424-443	atttccccaagtgatgctta
DHBV preC F	DHBV	AJ006350	2480-2499	acatacacccctctctcgaa
DLK F1	DHBV	AJ006350	2798-2817	ttgcaactcactttgtggat
DLK F2	DHBV	AJ006350	2841-2860	cactcagggtatgcatgaaa
DLK R1	DHBV	AJ006350	2751-2732	agcgtctttagcatccctta
DLK R2	DHBV	AJ006350	2694-2713	gaaagaaatcatcaggcaga
DRS F1	DHBV	AJ006350	2163-2182	tagccacagatgctactcca
DRS F2	DHBV	AJ006350	2349-2368	agacgttaccatggcatttt
DRS R1	DHBV	AJ006350	1979-1960	gcccgacaaatctttgaata
DRS R2	DHBV	AJ006350	1902-1883	ttccatctgctttcttcgat
MG1[c]	DHBV	AJ006350	2618-2599	aaaggtacagtcaaggctga
R2[b]	DHBV	AJ006350	52-32	cccgatccaatgattcctcat
LL 1329	DHBV	AJ006350	12-3015	taggtgtgcatgaattcttgccgta
pBS F1	pBsSK plasmid	X52330	1861-1880	aagggattttggtcatgaga
pBS R1	pBsSK plasmid	X52330	1137-1118	cccctgattctgtggataac
pBS R2	pBsSK plasmid	X52330	826-807	ggaaacagctatgaccatga
pBS F2	pBsSK plasmid	X52330	2004-2023	tcagcgatctgtctatttcg
β actin F[d]	Duck β actin	GU564232	1-20	aaactaccttcaactccatc
β actin R[d]	Duck β actin	GU564232	1122-1103	ccttcattcacatctatcac
β actin RT F[e]	Duck β actin	GU564232	577-596	ggatcagcaagcaggagtat
β actin RT R[e]	Duck β actin	GU564232	775-756	ccttcaccattccagttttt
Duck β actin RT F	Duck β actin	GU564232	510-529	gagcgcaagtactctgtctg
Duck β actin RT R	Duck β actin	GU564232	679-660	tcattttgtcacaagggtgt
Duck β actin RT R2	Duck β actin	GU564232	662-643	tgtgggtgttggtaacagtc
Duck G β actin 2F	Duck β actin	GU564232	227-246	gccctgagctaaactcctac
Duck G β actin F	Duck β actin	GU564232	318-337	ccctgtgaataatggcattt
Duck G β actin R	Duck β actin	GU564232	490-471	gggagggaagaggtgctcag
chicken GAPDH F[f]	Duck GAPDH	NC006088	1696-1714	aagggtggtgctaagcgtg
chicken GAPDH R[f]	Duck GAPDH	NC006088	2746-2728	gccaggcagttggtggtgc
GAPDH F[e]	Duck GAPDH	NC006088	897-916	ctctctggcaaagtccaagt
GAPDH R[e]	Duck GAPDH	NC006088	2967-2986	gctgtcaccattgaagtcac

Table 2.2 continued

GAPDH RT F[e]	Duck GAPDH	GU564233	452-471	tgctaagcgtgtcatcatct
GAPDH RT R[e]	Duck GAPDH	K01458	581-562	agtggtcataagaccctcca
duck GAPDH gF	Duck GAPDH	NC006088	1254-1273	ctctactcatggccacttcc
duck GAPDH gR	Duck GAPDH	NC006088	2280-2299	gttgagctcagggatgactt
Duck GAPDH R	Duck GAPDH	GU564233	549-530	tgacaattttcagggacttg
Duck GAPDH RT F	Duck GAPDH	GU564233	319-338	ggtcacattgagaaccctgt
Duck GAPDH RT R	Duck GAPDH	GU564233	470-451	gatgatgacacgcttagcac
chSOX5 F1	Chicken SOX5	FJ548633.1	2921-2940	tggatcctgatcagtttgtg
chSOX5 F2	Chicken SOX5	FJ548633.1	3383-3402	gtgagccctccagtacaact
chSOX5 R1	Chicken SOX5	FJ548633.1	1975-1956	ggtaaaagaaggggagaagg
chSOX5 R2	Chicken SOX5	FJ548633.1	1562-1543	ctgaacagcaaacaccagtt
chSOX5 F	Chicken SOX5	FJ548633.1	1440-1459	cccacctttgcaagttaat
chSOX5 R	Chicken SOX5	FJ548633.1	4143-4124	ctgacgcaaagcaacttcta
WHV P3[g]	WHV	M18752	2165-2145	agcaatgtccctacctgtta
WHV P4[g]	WHV	M18752	2195-2267	ttagtatgctgggatgaattaa
WHV P5[g]	WHV	M18752	2185-2167	aatagctgtatggtgcgga
WHV P6[g]	WHV	M18752	2217-2237	ctaaattgatagcttggatga
BM 1246	WHV	M18752	2250-2224	gttatgttagagctcatccaagctatc
ch TL66 cF[h]	HBV	AF222323	1744-1763	gggggaggagattaggttaa
ch TL67 cR[h]	HBV	AF222323	2472-2453	ttatgagtccaaggaatact
HBV F1[h]	HBV	AF222323	2390-2410	ctcgcagacgaaggtcttcaat
HBV F2[h]	HBV	AF222323	2413-2430	ccgcgtcgcagaagatct
HBV R1b[h]	HBV	AF222323	1991-1969	agatcacggaccgacggaaagaa
HBV R2b[h]	HBV	AF222323	1967-1944	tcagaaggcaaaaaagagagtaac
LL 1415[i]				tgccctcgtccctaatgcag
LL 1337[i]				ctgcattagggacg

All primers are single stranded DNA oligonucleotides synthesised by GeneWorks (Australia). The primers were dissolved in H_2O at 100 μM concentration, and stored at -20^{o}C.

Primers were used during PCR reactions (Sections 2.8.5, 2.10.3), qPCR reactions (Section 2.8.9), and sequencing reactions (Sections 2.8.10, 2.10.6).

References
[a](Reaiche *et al.*, 2010)
[b](Le Mire *et al.*, 2005)
[c](Reaiche, 2008; Thorpe, 2007)
[d](Bishop *et al.*, 2000)
[e](Reaiche, 2003)
[f](Seigneres *et al.*, 2003)
[g](Mason *et al.*, 2009b)
[h](Mason *et al.*, 2009a)
[i](Summers *et al.*, 2003)

Table 2.3: List of restriction enzymes and primers used in each invPCR assay designs performed in this study.

No	invPCR design	Target organism	First cut restriction enzyme	Second cut restriction enzyme	cccDNA destroying enzyme
	Plasmid DNA (model)				
P1	pBL4.8	Plasmid	*Tsp*45I	*Afl*III	-
P1	pBluescript SK II -	Plasmid	*Tsp*45I	*Afl*III	-
	Integrated virus-cell junction				
D1	AusDHBV- right hand end junction	Duck	*Sau*3AI	*Dde*I	*Bsr*I
D2	AusDHBV- left hand end junction	Duck	*Kpn*I	*Afl*III	*Sfc*I
D3	AusDHBV- left hand end junction	Duck	*Eco*RI	*Bsa*WI	*Nde*I
D4	AusDHBV- left hand end junction	Duck	*Nsi*I	*Afl*III	*Kpn*I
D5	AusDHBV- left hand end junction	Duck	*Eco*RI	*Afl*III	*Hind*III
W1[a]	WHV- left hand end junction	Woodchuck	*Sac*I	*Hind*III	*Afl*III
C1[b]	HBV- left hand end junction	Chimpanzee	*Bgl*II	*Bsa*WI	*Bsa*BI

No	invPCR design	Outer primer set		Inner primer set	
		Forward F1	Reverse R1	Forward F2	Reverse R2
	Plasmid DNA (model)				
P1	pBL4.8	pBS F1	pBS R1	pBS F2	pBS R2
P1	pBlueScript SK II (-)	pBS F1	pBS R1	pBS F2	pBS R2
	Integrated virus-cell junction				
D1	AusDHBV- right hand end junction	DRS F1	DRS R1	**DRS F2**	DRS R2
D2	AusDHBV- left hand end junction	DLK F1	DLK R1	DLK F2	**DLK R2**
D3	AusDHBV- left hand end junction	BLE F1	BL R1	BLE F2	**BL R2**
D4	AusDHBV- left hand end junction	BLN F1	BL R1	BLN F2	**BL R2**
D5	AusDHBV- left hand end junction	BD16 F1	BD16 R1	BD16 F2	**BD16 R2**
W1[a]	WHV- left hand end junction	WHV P4	WHV P5	**WHV P3**	WHV P6
C1[b]	HBV- left hand end junction	HBV F1	HBV R1b	HBV F2	**HBV R2b**

The invPCR assays were performed as described in Section 2.10 to detect integrated virus-cell junctions. Briefly, the integrated virus-cell junctions were inverted using the first restriction enzyme and second restriction enzyme to form inverted DNA fragments (refer Figures 2.6 and 2.7 for a schematic representation), while the cccDNA destroying restriction enzyme were used to reduce the detection of virus-virus false positive sequences. The outer primer sets were used during the first round 96-well nested PCR, while the inner primer sets were used during the second round 96-well nested PCR. The primers in bold fonts were used for DNA sequencing.

[a](Mason *et al.*, 2009b)
[b](Mason *et al.*, 2009a)

Table 2.4: List of primers used in each linker ligation assay designs performed in this study.

Target organism	Virus linker primer	Linearisation restriction enzyme	Outer primer set		Inner primer set	
			Forward F1	Reverse R1	Forward F2	Reverse R2
Woodchuck[a]	BM 1246	*Hind*III	WHV P4	WHV P5	WHV P6	WHV P3
Duck	LL 1329	*Bsa*WI	BLE F1	BL R1	BLE F2	BL R2

Linker ligation assay were performed as described in Section 2.12 to detect integrated virus-cell junctions. A schematic representation of the steps involved during the linker ligation assay is shown as Figure 2.9.

[a](Summers *et al.*, 2003)

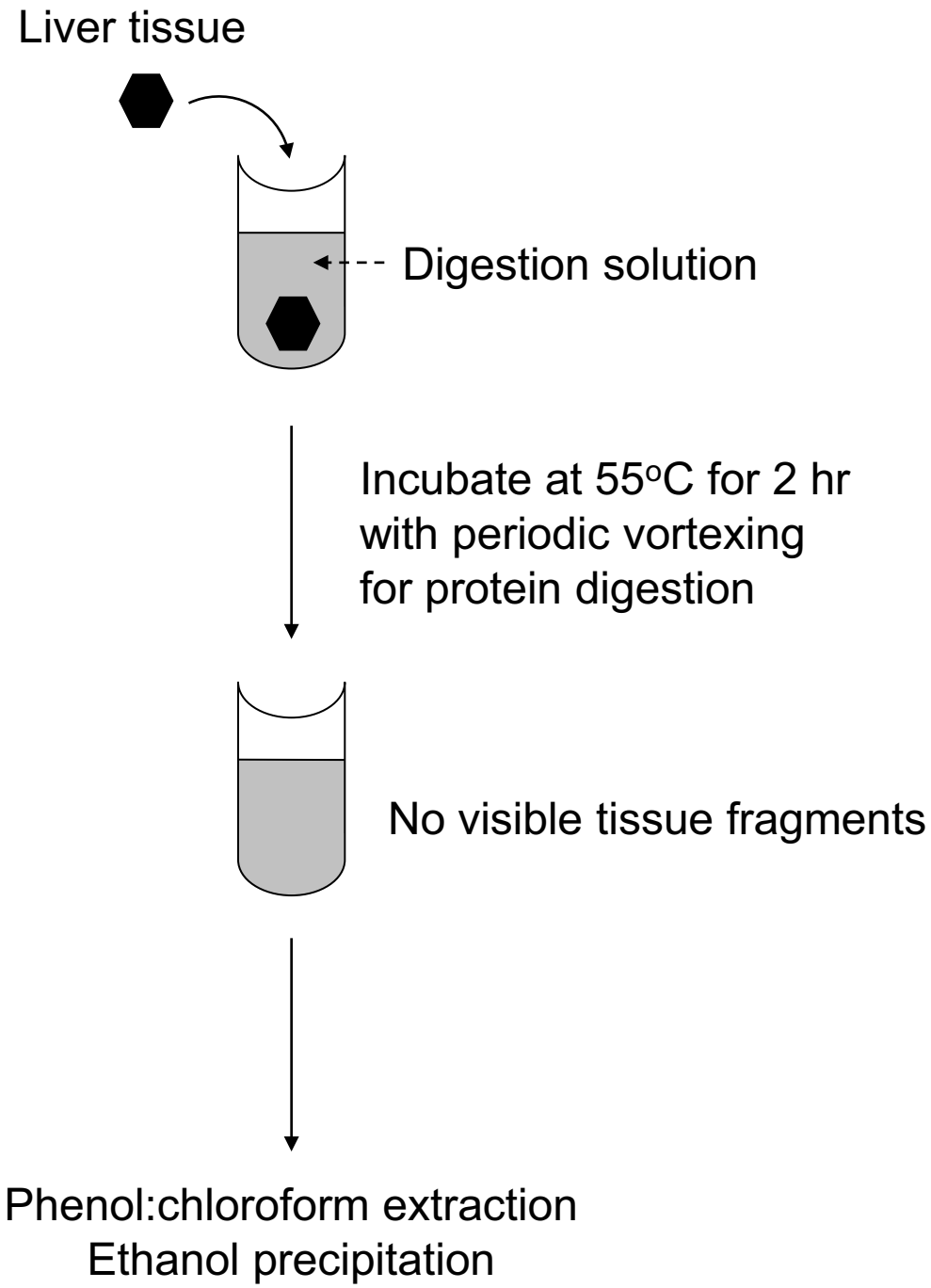


Figure 2.1: Flowchart of the steps involved in the total DNA extraction method described in Section 2.6.3.

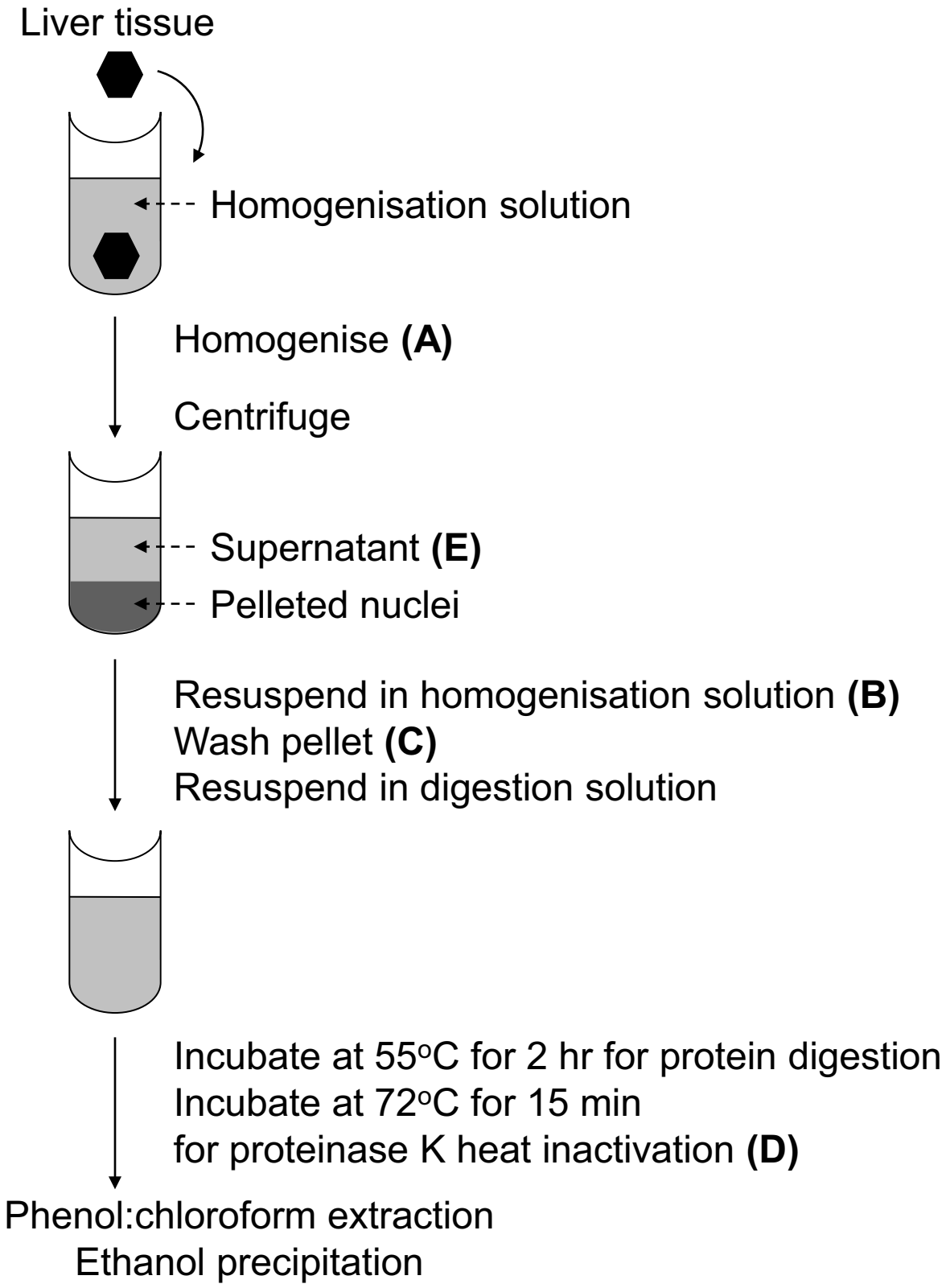


Figure 2.2: Flowchart of the steps involved in the nuclear DNA extraction method described in Section 2.6.5.

Letters **(A)** to **(E)** correspond to the steps in which DNA was visualised using DAPI fluorescent staining during the optimisation of nuclear DNA extraction method, which was performed later in Section 5.1.3.5.1.

Figure 2.3: Flowchart of the steps involved in the high MW DNA extraction methods I, II and III described in Section 2.6.6.

All methods have the same initial steps until the redissolving of DNA pellet in TE, before deviating as represented in the flowchart above.

The cccDNA-rich supernatant that was normally discarded during the high MW DNA extraction methods could be used for the extraction of cccDNA using the cccDNA extraction method as described in Section 2.6.7.

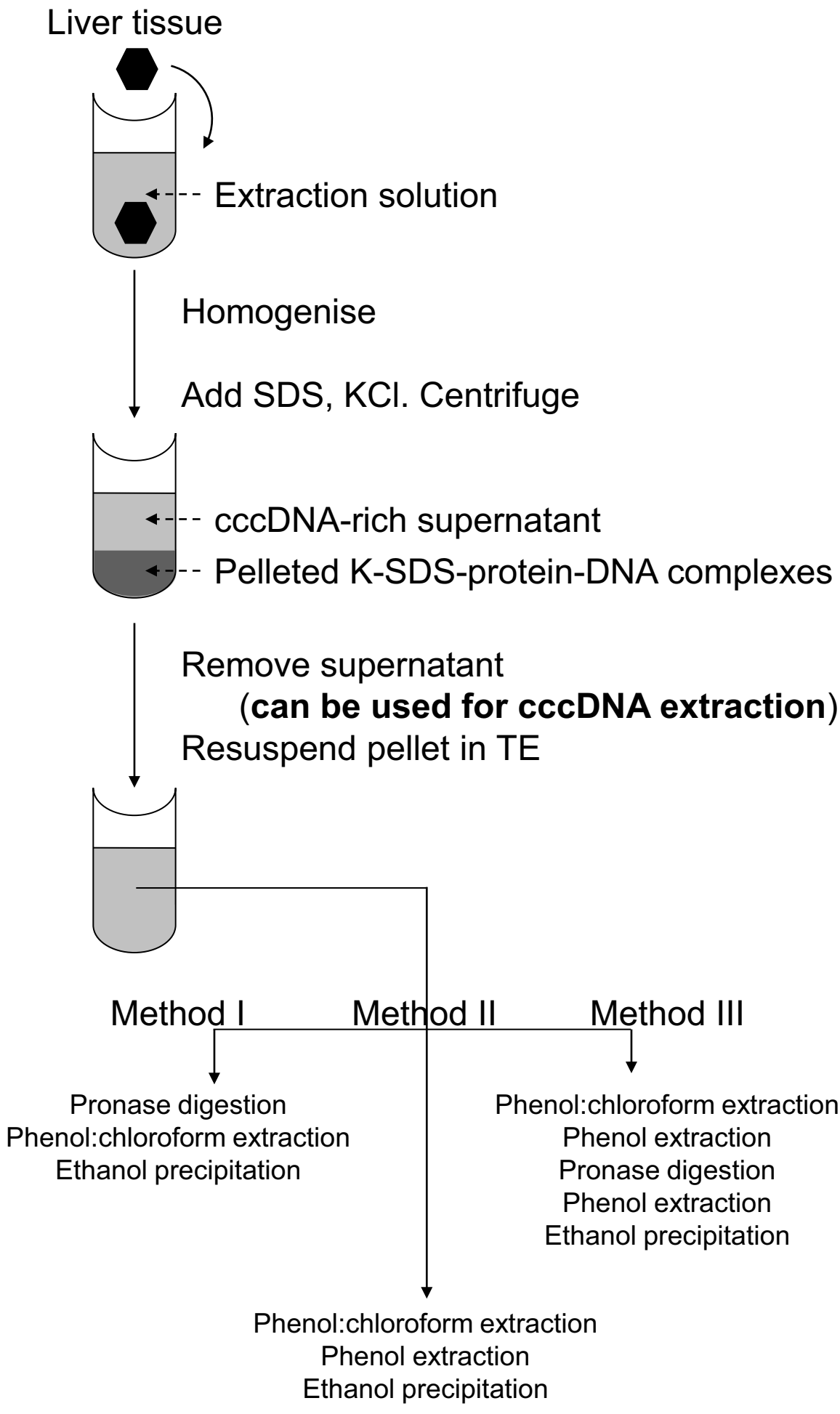

Liver tissue
Extraction solution
Homogenise
Add SDS, KCl. Centrifuge
cccDNA-rich supernatant
Pelleted K-SDS-protein-DNA complexes
Remove supernatant
(can be used for cccDNA extraction)
Resuspend pellet in TE
Method I
Method II
Method III
Pronase digestion
Phenol:chloroform extraction
Ethanol precipitation
Phenol:chloroform extraction
Phenol extraction
Pronase digestion
Phenol extraction
Ethanol precipitation
Phenol:chloroform extraction
Phenol extraction
Ethanol precipitation

Figure 2.3

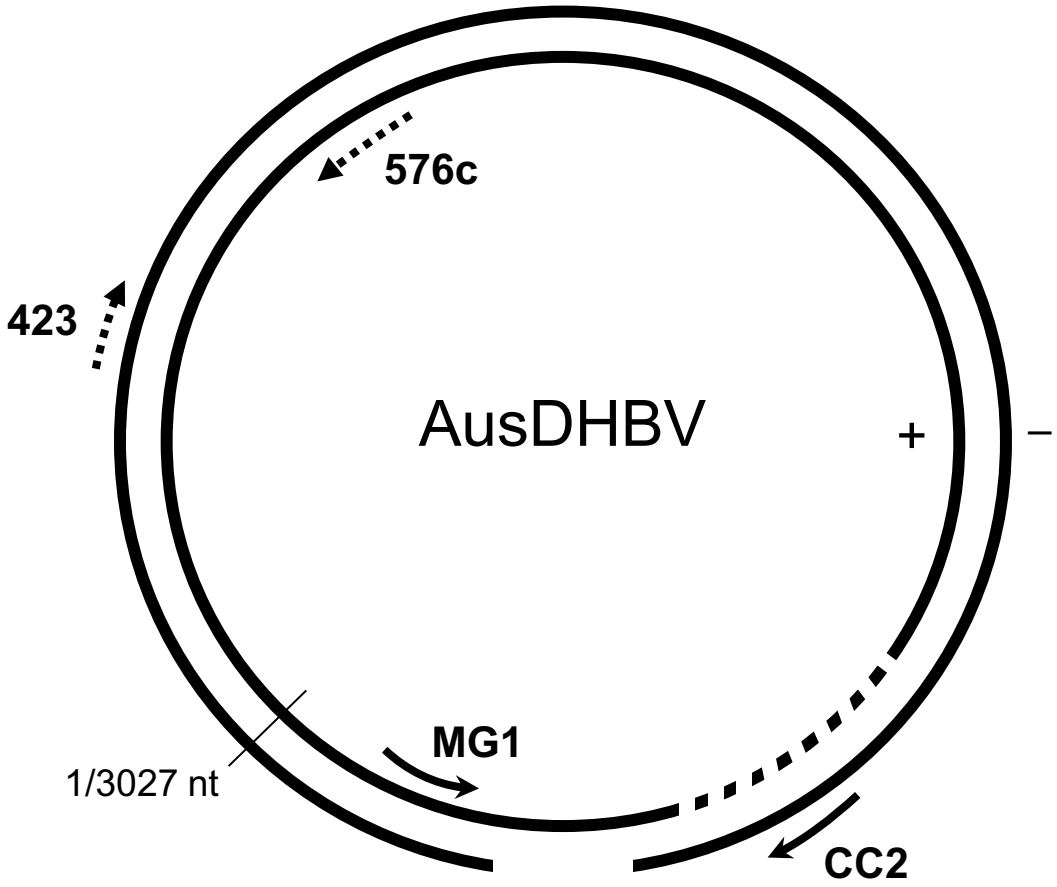
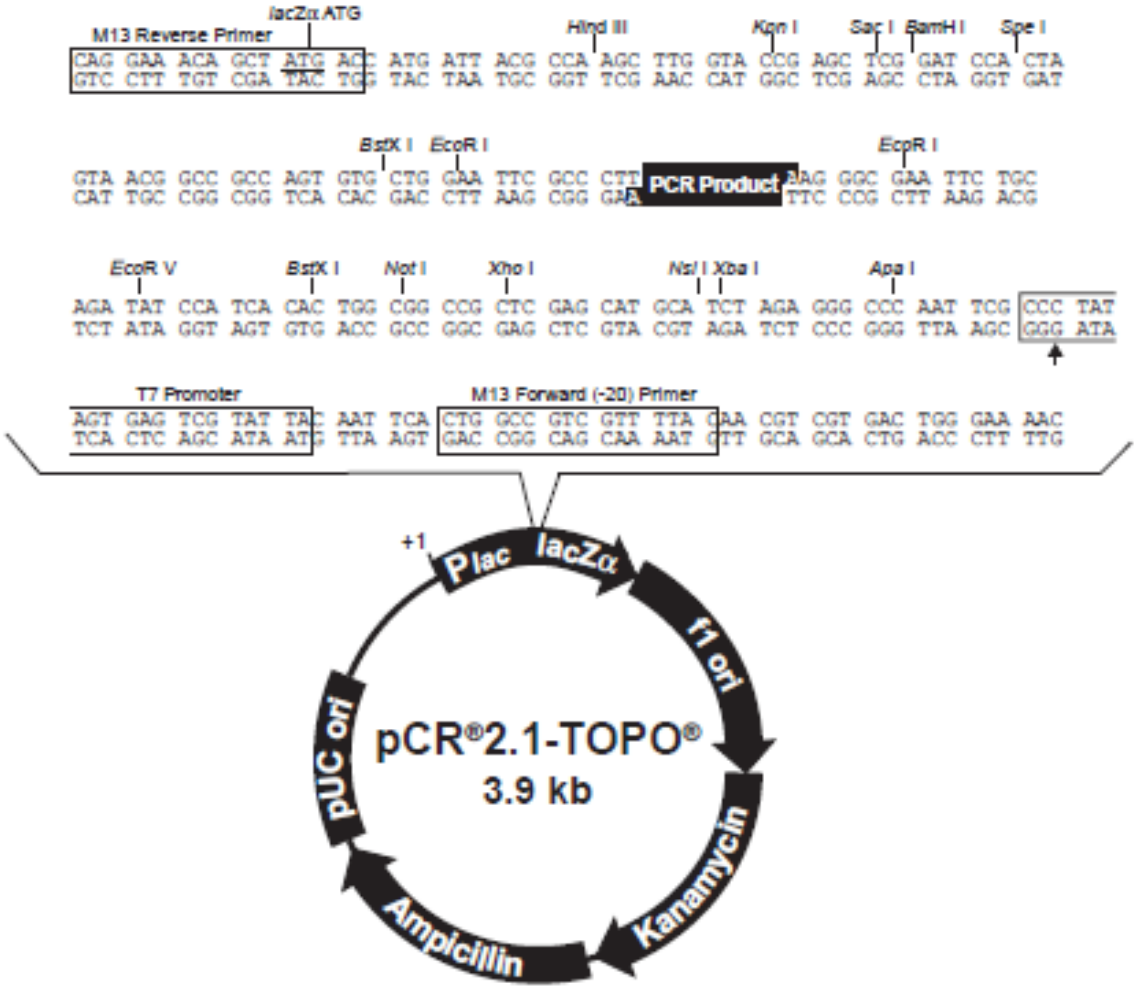


Figure 2.4: Schematic representation of the AusDHBV genome (Genbank Accession AJ006350) in its rcDNA form, and the approximate binding sites of PCR primer sets to amplify DHBV total (423 – 576c) and cccDNA (MG1 – CC2).

Symbols "+ "and "–" represent the DHBV rcDNA positive and negative DNA strands respectively. The PCR primer sequences and binding sites on the AusDHBV genome are shown in Table 2.2.



Comments for pCR®2.1-TOPO®
3931 nucleotides

LacZα fragment: bases 1-547
M13 reverse priming site: bases 205-221
Multiple cloning site: bases 234-357
T7 promoter/priming site: bases 364-383
M13 Forward (-20) priming site: bases 391-406
f1 origin: bases 548-985
Kanamycin resistance ORF: bases 1319-2113
Ampicillin resistance ORF: bases 2131-2991
pUC origin: bases 3136-3809

Figure 2.5: Map of the pCR 2.1-TOPO plasmid provided by the manufacturer, Invitrogen.

The plasmid was used as a vector for cloning of PCR products using the TOPO TA cloning kit (Invitrogen, USA), as described in Section 2.9.1. PCR products would be cloned into the exposed sticky ends in the multiple cloning site as shown by the black highlighted "PCR Product" above. The restriction enzyme digestion sites in the plasmid's multiple cloning site were also shown in the DNA sequences above.

Figure 2.6: Flowchart of the steps involved in the DNA inversion (Section 2.10.1) and nested PCR (2.10.3) of an invPCR assay for the detection of integrated virus-cell left hand end junctions.

Figure 2.6A shows an example of the integrated virus-cell left hand end junction (represented by the red box) formed by the most probable left hand end junction of the integrated virus DNA and a random site in the liver cellular DNA. The digestion sites for the first cut restriction enzyme, second cut restriction enzyme, and the cccDNA destroying enzyme are also shown.

Figure 2.6B shows an example of the DNA fragment that would be formed after digestion with first cut restriction enzyme. The DNA fragment would contain the integrated virus-cell left hand end junction.

Figure 2.6C shows the circularised DNA fragment that would be formed after DNA ligation.

Figure 2.6D shows the linearised inverted DNA fragment that would be formed after digestion with second cut restriction enzyme. The inverted DNA fragment consists of the virus DNA flanking the liver cellular DNA (also known as the insert DNA), and contains the integrated virus-cell left hand end junction. The nested PCR primer binding sites are also shown, which include the outer primer set for the first round PCR reaction (F1 – R1) and the inner primer set for the second round PCR reaction (F2 – R2).

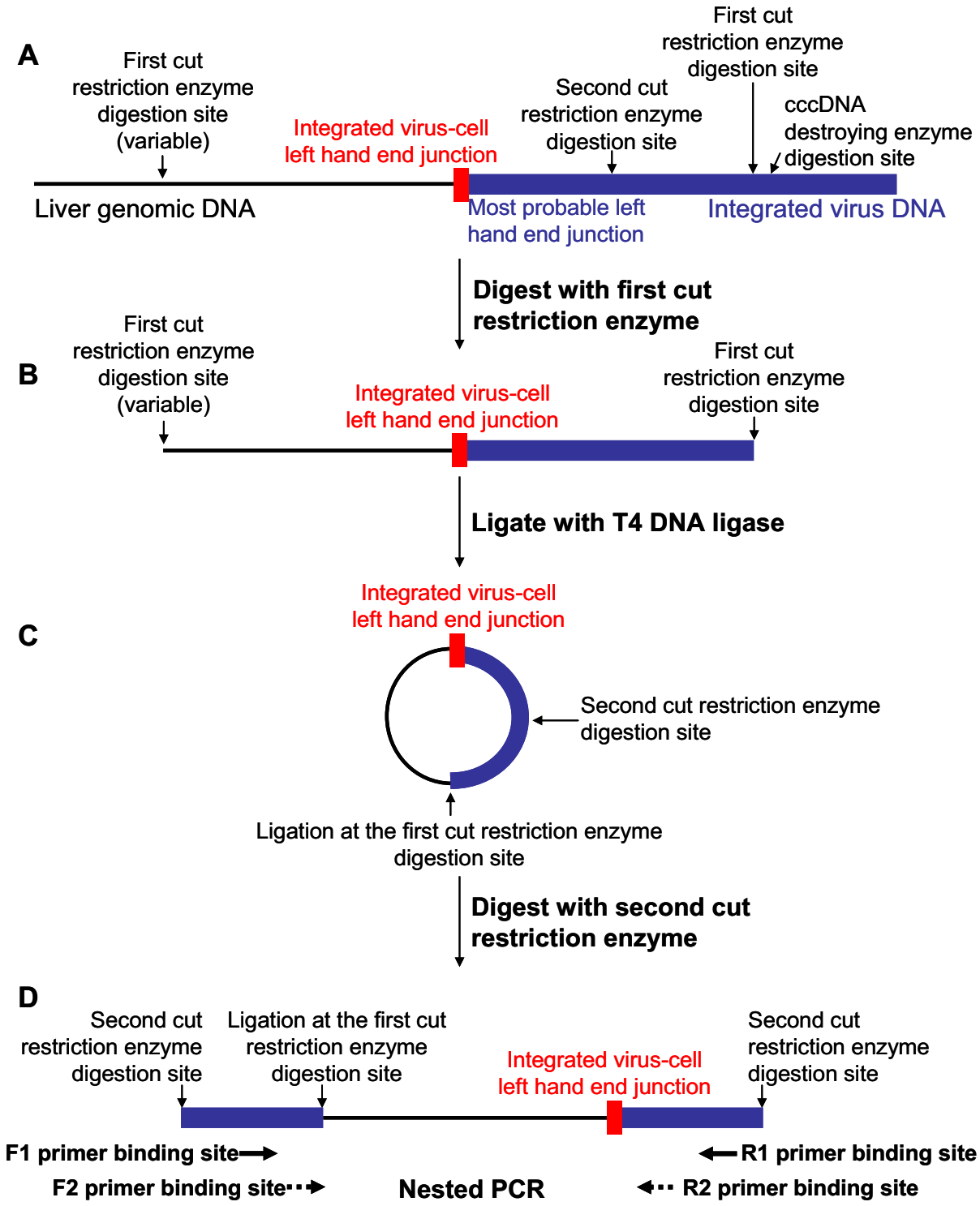

A
First cut restriction enzyme digestion site (variable)
Integrated virus-cell left hand end junction
Second cut restriction enzyme digestion site
First cut restriction enzyme digestion site
cccDNA destroying enzyme digestion site
Liver genomic DNA
Most probable left hand end junction
Integrated virus DNA
Digest with first cut restriction enzyme
B
First cut restriction enzyme digestion site (variable)
Integrated virus-cell left hand end junction
First cut restriction enzyme digestion site
Ligate with T4 DNA ligase
C
Integrated virus-cell left hand end junction
Second cut restriction enzyme digestion site
Ligation at the first cut restriction enzyme digestion site
Digest with second cut restriction enzyme
D
Second cut restriction enzyme digestion site
Ligation at the first cut restriction enzyme digestion site
Integrated virus-cell left hand end junction
Second cut restriction enzyme digestion site
F1 primer binding site
R1 primer binding site
F2 primer binding site
Nested PCR
R2 primer binding site

Figure 2.6

Figure 2.7: Flowchart of the steps involved in the DNA inversion (Section 2.10.1) and nested PCR (2.10.3) of an invPCR assay for the detection of integrated virus-cell right hand end junctions.

Figure 2.7A shows an example of the integrated virus-cell right hand end junction (represented by the red box) formed by the most probable right hand end junction of the integrated virus DNA and a random site in the liver cellular DNA. The digestion sites for the first cut restriction enzyme, second cut restriction enzyme, and the cccDNA destroying enzyme are also shown.

Figure 2.7B shows an example of the DNA fragment that would be formed after digestion with first cut restriction enzyme. The DNA fragment would contain the integrated virus-cell right hand end junction.

Figure 2.7C shows the circularised DNA fragment that would be formed after DNA ligation.

Figure 2.7D shows the linearised inverted DNA fragment that would be formed after digestion with second cut restriction enzyme. The inverted DNA fragment consists of the virus DNA flanking the liver cellular DNA (also known as the insert DNA), and contains the integrated virus-cell right hand end junction. The nested PCR primer binding sites are also shown, which include the outer primer set for the first round PCR reaction (F1 – R1) and the inner primer set for the second round PCR reaction (F2 – R2).

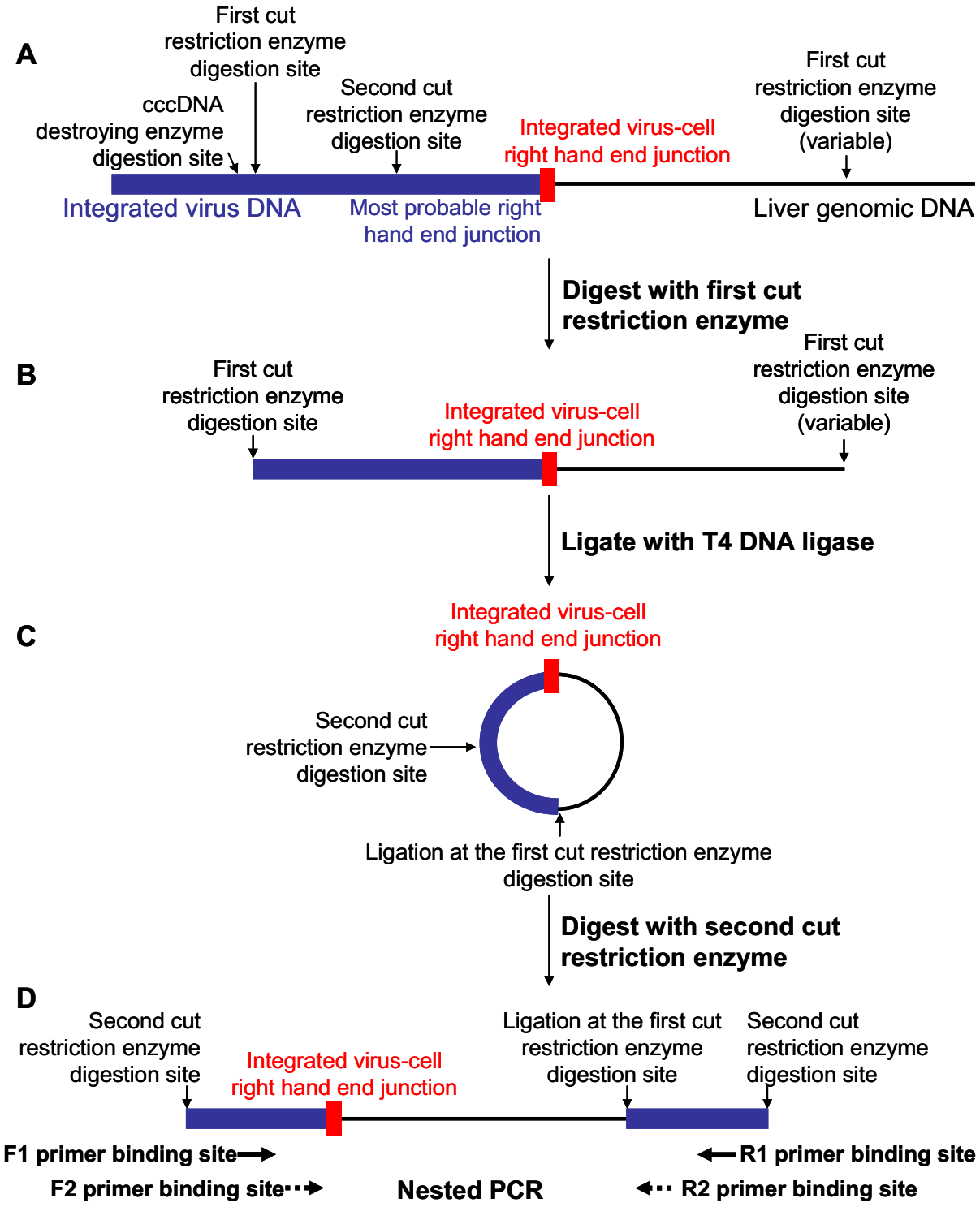

A
First cut restriction enzyme digestion site
cccDNA destroying enzyme digestion site
Second cut restriction enzyme digestion site
Integrated virus-cell right hand end junction
First cut restriction enzyme digestion site (variable)
Integrated virus DNA
Most probable right hand end junction
Liver genomic DNA
Digest with first cut restriction enzyme
B
First cut restriction enzyme digestion site
Integrated virus-cell right hand end junction
First cut restriction enzyme digestion site (variable)
Ligate with T4 DNA ligase
C
Integrated virus-cell right hand end junction
Second cut restriction enzyme digestion site
Ligation at the first cut restriction enzyme digestion site
Digest with second cut restriction enzyme
D
Second cut restriction enzyme digestion site
Integrated virus-cell right hand end junction
Ligation at the first cut restriction enzyme digestion site
Second cut restriction enzyme digestion site
F1 primer binding site
R1 primer binding site
F2 primer binding site
Nested PCR
R2 primer binding site

Figure 2.7

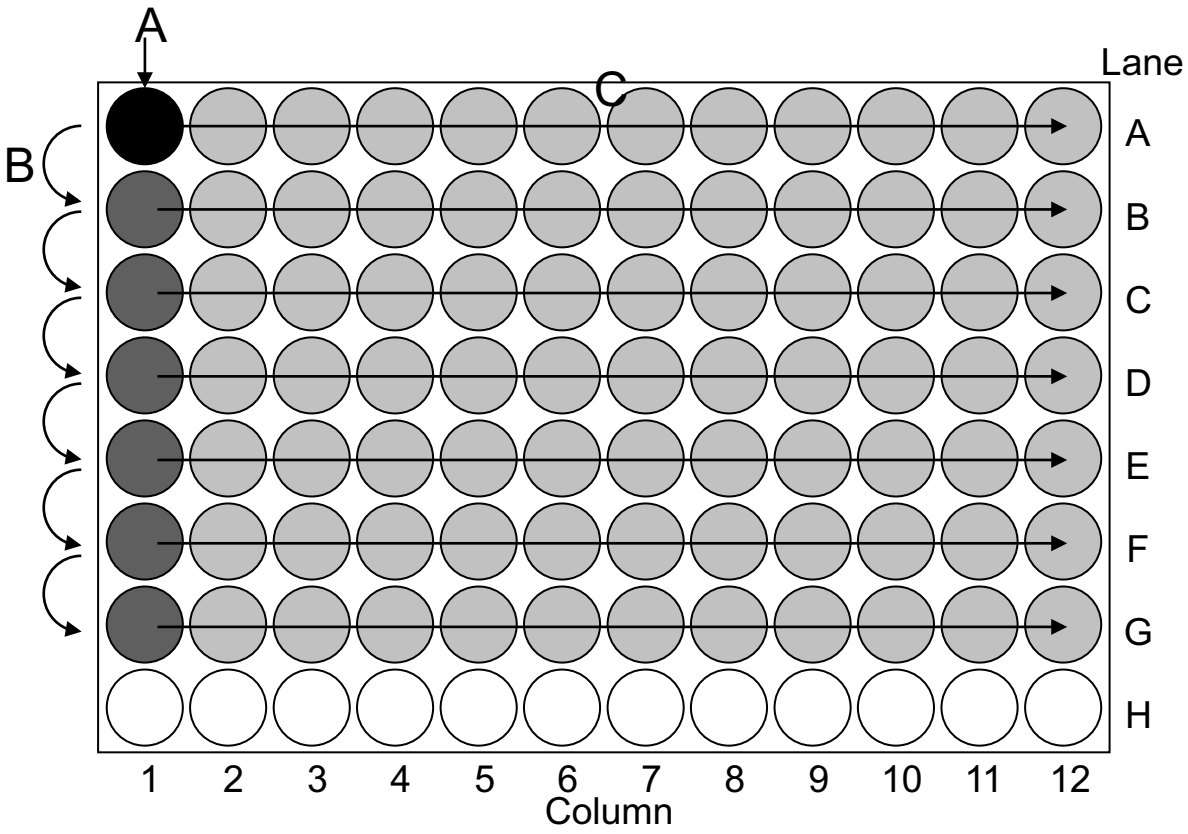


Figure 2.8: Schematic representation of the serial dilution of inverted DNA during 96-well nested PCR.

Figure shows the layout of a 96-well tray with 8 lanes (A – H) and 12 columns (numbered 1 – 12).

As described in Section 2.10.3, first round PCR mastermix and inverted DNA template was placed into well A1 (step A). Serial dilutions of the inverted DNA were then performed from well A1 to wells B1 to G1 using the first round PCR mastermix as diluent (step B), leaving 120 µL of the PCR mastermix-inverted DNA mix in wells A1 to G1. Then, 10 µL of the PCR mastermix-inverted DNA mix were distributed evenly to columns 2 to 12 (step C). Lane H was used for PCR negative (water) controls, and contained 10 µL of the first round PCR mastermix only.

Figure 2.9: Flowchart of steps involved during linker ligation assay (Section 2.12) for the detection of integrated virus-cell left hand end junctions.

Figure 2.9A shows an example of the integrated virus-cell left hand end junction (represented by the red box) formed by the most probable left hand end junction of the integrated virus DNA and a random site in the liver cellular DNA. The digestion sites for *Pvu*II restriction enzyme and the linerisation restriction enzyme digestion site are also shown. *Pvu*II does not have any digestion sites in the whole virus DNA sequence.

Figure 2.9B shows an example of the DNA fragment that would be formed after dephosphorylation of DNA with SAP and digestion with *Pvu*II. The DNA fragment would contain the entire integrated virus DNA.

Figure 2.9C shows the ligation of linkers to the blunt ends of the DNA fragment. The 3' ends of the linkers were subsequently terminated using ddNTPs. After separation of the DNA strands using DMSO, linker ligation assay PCR was performed using the LL1415 – virus specific primer set, which primer binding sites on the DNA fragment as shown.

Figure 2.9D shows the linker ligation assay PCR product. The linker was removed by *Pvu*II digestion, and any DNA overhangs remaining were removed by Exonuclease I.

Figure 2.9E shows the circularised DNA fragment that would be formed after DNA ligation at the blunt ends.

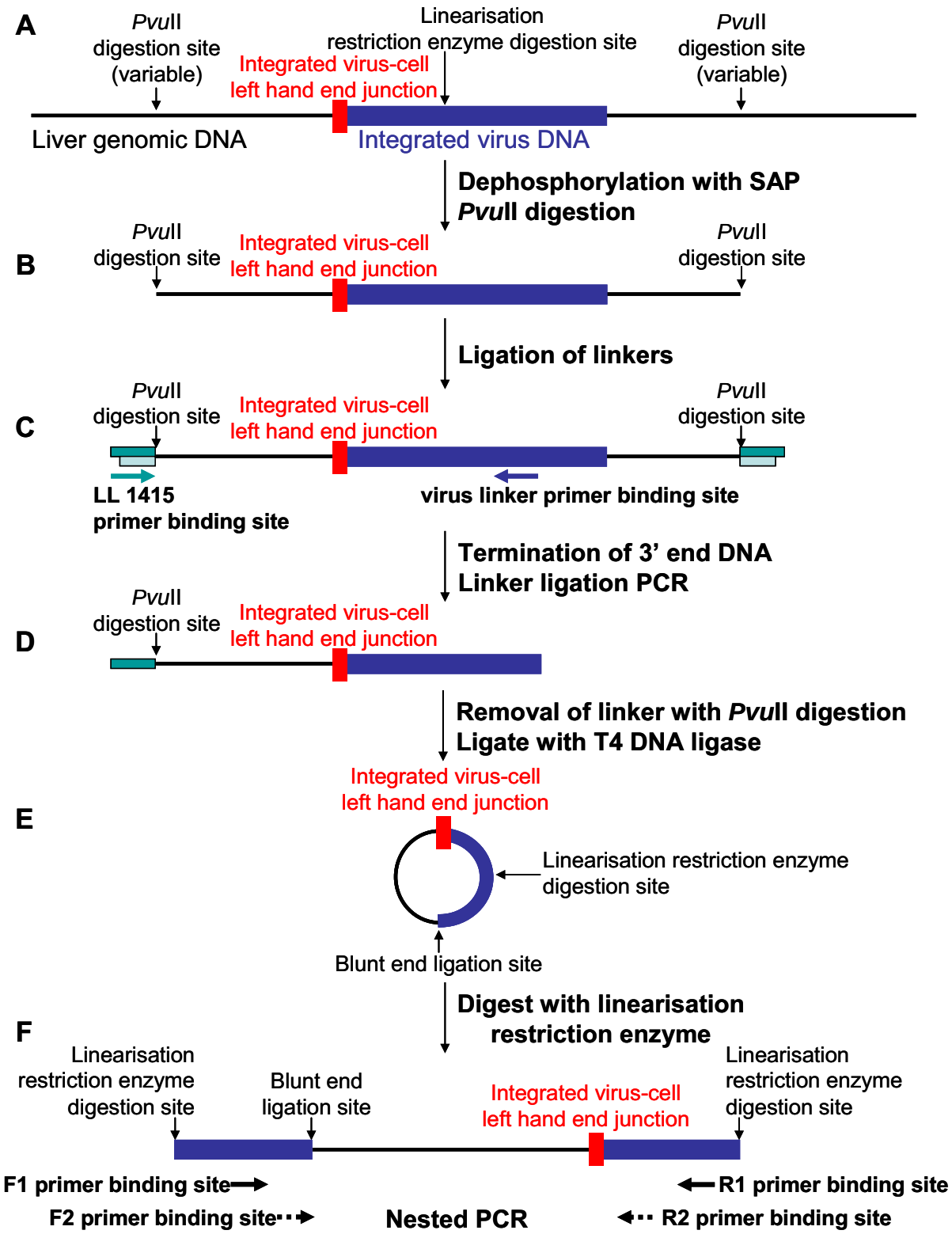

A
PvuII digestion site (variable)
Linearisation restriction enzyme digestion site
PvuII digestion site (variable)
Integrated virus-cell left hand end junction
Liver genomic DNA
Integrated virus DNA
Dephosphorylation with SAP
PvuII digestion
B
PvuII digestion site
Integrated virus-cell left hand end junction
PvuII digestion site
Ligation of linkers
C
PvuII digestion site
Integrated virus-cell left hand end junction
PvuII digestion site
LL 1415 primer binding site
virus linker primer binding site
Termination of 3' end DNA
Linker ligation PCR
D
PvuII digestion site
Integrated virus-cell left hand end junction
Removal of linker with PvuII digestion
Ligate with T4 DNA ligase
E
Integrated virus-cell left hand end junction
Linearisation restriction enzyme digestion site
Blunt end ligation site
Digest with linearisation restriction enzyme
F
Linearisation restriction enzyme digestion site
Blunt end ligation site
Integrated virus-cell left hand end junction
Linearisation restriction enzyme digestion site
F1 primer binding site
R1 primer binding site
F2 primer binding site
Nested PCR
R2 primer binding site

Figure 2.9

Chapter 3: Development of methods - Optimisation of DNA sequencing and qPCR protocols

Chapter 3.1: Optimisation of DNA sequencing

3.1.1. Aim

a) To optimise and establish standard protocols for DNA sequencing reactions and subsequent cleanup of DNA sequencing products for:
   i) Single tube and 96-well sequencing formats.
   ii) Analysis using the AB3730 DNA Sequencer and the AB3730xl 96-capillary Sequencer.

3.1.2. Introduction

In the Hepatitis Research Laboratory, protocols for DNA sequencing reactions and cleanup of DNA sequencing products in single tubes have been established and routinely used to produce DNA sequencing products that are analysed using the ABI 377 DNA Sequencer (AB, USA) by the DNA Sequencing Facility, Division of Molecular Pathology, IMVS/SA Pathology (Le Mire *et al.*, 2005; Reaiche, 2008). However, as recommended by the DNA Sequencing Facility, a new DNA sequencing protocol had to be optimised and established for the new AB3730 DNA Sequencer (AB, USA) which replaced the older ABI 377 DNA Sequencer. Furthermore, since a significant number of DNA sequencing reactions were also carried out at the sequencing facility operated by the Australian Genome Research Facility (AGRF), the DNA sequencing products produced using the new DNA sequencing protocols also had to be optimised for analysis using the AB3730xl 96-capillary Sequencer (AB, USA) at AGRF. In addition, protocols for the 96-well sequencing format, which was used extensively for invPCR assays in this study, had to be developed and established, as the 96-well sequencing format had not been previously used in the Hepatitis Research Laboratory.

In this chapter, various parameters were tested using a standard DNA template to determine the optimal protocols for DNA sequencing reactions. These parameters include the amount of DNA template, BigDye Terminator mix, and sequencing buffer used per reaction, and the final volume of the DNA sequencing reaction. Five methods to cleanup DNA sequencing products were also tested and compared. Lastly, we assessed the quality of DNA sequencing

products generated using DNA templates extracted from GelRed- and ethidium bromide-stained gels.

The quality of DNA sequencing was determined empirically based on a number of characteristics of the DNA sequencing electropherogram, including the length of readable sequence, and the general quality of the DNA sequencing peaks, which include the height of the DNA sequencing peaks, which reflects the intensity of the fluorescence signal strength, and the presence of background noise. A good sequence would be defined by at least 600 bp of readable sequence, with distinctive high DNA sequencing peaks and low background noise.

Figure 3.1.1A shows an example of an ideal DNA sequencing electropherogram, with a long readable sequence (up to ~950 bp), high DNA sequencing peaks, and low background noise. Figure 3.1.1B shows an example of a DNA sequencing electropherogram with prematurely shortened readable sequence (~400 bp), declining heights of DNA sequencing peaks, and low background noise. This could be due to an exhaustion of DNA sequencing dyes in the reaction, or the presence of excess dNTPs that have affected the ratio of dNTPs and the DNA sequencing dye-labelled dideoxy nucleotide tri-phosphate (ddNTPs), or an improper ratio of primer to template in the DNA sequencing reaction. Figure 3.1.1C shows an example of a failed DNA sequencing electropherogram, with no readable DNA sequence, multiple peaks of various heights, and high background noise. This could be due to the presence of multiple DNA templates, or the presence of carryover contaminants that interfered with the DNA sequencing reaction. Contaminants could be introduced from the DNA template (for example: proteins, organic chemicals and salts), or could be residual contaminants from the PCR reactions (for example: excess PCR primers, PCR primer-dimer artefacts or secondary PCR products) (AB, 2002).

Individual DNA sequencing electropherogram outputs from each DNA sequencing reaction in this Chapter were not individually shown, but have been analysed based on the example electropherograms in Figure 3.1.1, and summarised to show the length of readable sequence, and general quality of DNA sequencing peaks including the height of DNA sequencing peaks and presence of any background noise.

3.1.3. Generation of a standard DNA template for sequencing

The standard DNA template used in every sequencing reaction in this Chapter were PCR products amplified from the pBL4.8x2 plasmid, using the DHBV preC F – DHBV C R primer

set (Table 2.2). The pBL4.8x2 plasmid contains two full-length AusDHBV genomes (GenBank Accession AJ006350) that were cloned in a head-to-tail direction into the *Eco*RI digestion site in the pBlueScript KS II (+) plasmid vector (Triyatni, 1998, plasmid map shown in Figure 3.2.1A). As the DHBV preC F primer binds to 2480 – 2499 nt of the DHBV genome, while DHBV CR primer binds to 443 – 424 nt of the DHBV genome, it is expected that two 991 bp PCR products would be amplified from each pBL4.8x2 plasmid template.

PCR amplification was performed as described in Section 2.8.5, and the 991 bp PCR product was verified by agarose gel electrophoresis as described in Section 2.8.7 (data not shown). The PCR product was then purified using the QIAquick PCR purification kit as described in Section 2.8.6, and the DNA concentration was determined by spectophotometry as described in Section 2.8.1.

3.1.4. Optimisation of DNA sequencing reaction protocols

Based on the DNA sequencing reaction protocol previously established in the Hepatitis Research Laboratory, each DNA sequencing reaction contained up to 200 ng of DNA template, 3 pM of PCR primer, 4X BigDye Terminator mix (AB, USA), 1X BigDye Terminator buffer (AB, USA), and was made up to a final volume of 20 μL using H_2O. DNA sequencing reactions were performed in a 200 μL PCR tube in the 96-well MyCycler thermal cycler (Bio-Rad, USA), using the standard sequencing conditions as described in Section 2.8.10. All DNA sequencing reactions in this section had been performed exactly according to the conditions of this established protocol and had used the same batch of reagents, unless otherwise mentioned. For each DNA sequencing reaction, the DNA template used was from the same stock of PCR product produced in Section 3.1.3, while the PCR primer used was the DHBV preC F primer (Table 2.2).

Four DNA sequencing reaction protocol parameters were optimised as followed:

3.1.4.1. Amount of DNA template per reaction

The optimal amount of DNA template used per DNA sequencing reaction was determined. The previous protocol for the ABI 377 DNA Sequencer required at least 200 ng per kbp of DNA template per reaction. However, the new AB3730 Sequencer was reported by the IMVS/SA Pathology DNA sequencing facility to be at least 4-fold more sensitive and as such required only ~50 ng per kbp of DNA template per DNA sequencing reaction for the same sized product. To confirm this, DNA sequencing reactions were performed in duplicate as

described in Section 3.1.4, using 200 ng, 150 ng, 100 ng, 50 ng, or 20 ng of the 991 bp DNA template (Section 3.1.3) per reaction.

The DNA sequencing results were summarised in Table 3.1.1. All electropherograms showed good quality DNA sequencing results, with similar high DNA sequencing peaks and low background noise. Overall, there were no significant differences observed between using 200 ng, 150 ng, or 100 ng of DNA template per DNA sequencing reaction, with the exception that 100 ng gave a slightly longer (but not significant) length of readable sequence. However, when 50 ng of DNA template was used, the height of the DNA sequencing peaks were markedly lower, but this did not affect the overall length of readable sequence. When 20 ng of DNA template was used, only the first ~500 bp of sequence was readable.

Therefore, these results suggest that 100 ng per kbp of DNA was the optimal amount of DNA template to be used per DNA sequencing reaction, with a maximum of 200 ng and a minimum of 50 ng of DNA template per DNA sequencing reaction.

3.1.4.2. Amount of BigDye Terminator mix per reaction

The optimal amount of BigDye Terminator mix used per DNA sequencing reaction was determined. The previous protocol for the ABI 377 DNA Sequencer required up to 4X final concentration of BigDye Terminator mix per reaction. However, the new AB3730 Sequencer was reported by the IMVS/SA Pathology DNA sequencing facility to be at least 4-fold more sensitive, and as such required only 0.25X final concentration of BigDye Terminator mix per DNA sequencing reaction for the same sized product. To confirm this, DNA sequencing reactions were performed as described in Section 3.1.4, using 0.25X or 0.5X final concentration of BigDye Terminator mix per reaction.

The DNA sequencing results (data not shown) showed that both amounts of BigDye Terminator mix protocols produced equally good quality DNA sequencing results, with high DNA sequencing peaks and low background noise. However, when 0.25X final concentration of BigDye Terminator mix was used, up to ~750 bp of sequence was readable, while when 0.5X BigDye Terminator mix was used, 850 – 900 bp of sequence was readable.

Therefore, these results suggest that 0.25X final concentration of BigDye Terminator mix per reaction would be sufficient for short DNA templates <500 bp in length, while at least 0.5X final concentration of BigDye Terminator mix per reaction was needed for DNA templates >500 bp in length.

On a separate note, when older stocks of 10X final concentration of BigDye Terminator mix that had been thawed and frozen at -20^{o}C repeatedly (more than 5 times), were compared to the use of fresh stocks of 10X final concentration of BigDye Terminator mix, the DNA sequencing results (data not shown) showed no significant differences. Hence, it can be concluded that the activity of the BigDye Terminator mix does not decline significantly from repeated thawing. However, in order to ensure the longevity of the BigDye Terminator mix, the mix should be thawed and kept on ice at all times, and stored at -20^{o}C when not in use.

3.1.4.3. Amount of sequencing buffer per reaction

The optimal amount of sequencing buffer, which was the BigDye Terminator buffer, used per DNA sequencing reaction was determined. The previous protocol for the ABI 377 DNA Sequencer used 1X final concentration of sequencing buffer per reaction. However, the new AB3730 Sequencer was reported by the IMVS/SA Pathology DNA sequencing facility to be at least 4-fold more sensitive, and as such required only 0.75X final concentration of sequencing buffer per DNA sequencing reaction for the same sized product. To confirm this, DNA sequencing reactions were performed as described in Section 3.1.4, using 0.7X, 0.75X and 1X final concentration of sequencing buffer per reaction.

The DNA sequencing results (data not shown) showed that when 1X final concentration of sequencing buffer was used, ~900 bp of sequence was readable with good quality, high DNA sequencing peaks and low background noise. However when 0.7X or 0.75X final concentration of sequencing buffer were used, only ~750 bp of sequence was readable with lower DNA sequencing peaks. This reduction in output quality may be due to less than optimal buffer concentration for the BigDye Terminator mix, possibly due to lower salt content when 0.7X or 0.75X final concentration of sequencing buffer were used.

The amount of sequencing buffer used, whether at 0.7X, 0.75X or 1X final concentration per reaction, would not be significantly different when DNA sequencing reactions were performed in single tubes. However, the difference in amount of reagents required for 96-well DNA sequencing reactions would be notable. Hence, lower concentrations of sequencing buffer could be used in 96-well DNA sequencing reactions, as it would be more cost effective without significantly affecting the DNA sequencing results.

In summary, these results suggest that 1X final concentration of sequencing buffer was the optimal amount of sequencing buffer to be used per DNA sequencing reaction.

3.1.4.4. Final volume of the DNA sequencing reaction

The differences in performing DNA sequencing reactions in 10 µL or 20 µL final volume were compared. Although a 20 µL final volume had been previously optimised in the Hepatitis Research Laboratory and routinely used for all DNA sequencing reactions, a lower final volume was tested as multiple 96-well DNA sequencing reactions would be performed during the invPCR assay. If the efficiency and quality of DNA sequencing were not compromised at a lower final volume, this could significantly reduce the amount of reagents and costs required in this study. In addition, by using the same volume of BigDye Terminator mix in a lower final volume of the DNA sequencing reaction, this would allow the BigDye Terminator mix to be used at a higher concentration per reaction, thus potentially improving the DNA sequencing results as shown in Section 3.1.4.2.

The DNA sequencing results (data not shown) showed that DNA sequencing reactions performed at either 10 µL or 20 µL final volume produced equally good quality DNA results, with up to ~900 bp of readable sequence and high DNA sequencing peaks with low background noise.

Therefore, these results suggest that the DNA sequencing reactions could be performed in either 10 µL or 20 µL final volume. However, since a low final volume (10 µL) DNA sequencing reaction performed in a 200 µL PCR tube would have a large void volume (up to 190 µL), this may increase the amount of evaporation during the sequencing reactions. Hence, it would be recommended that single tube DNA sequencing reactions would still be performed in 20 µL final volume, while final volume of 10 µL were only used during 96-well DNA sequencing reactions to be more cost effective.

3.1.4.5. Comparison of methods to cleanup DNA sequencing products

Various methods could be used to cleanup DNA sequencing products before being sent for analysis. Cleanup of DNA sequencing products is important to remove post-cycle DNA sequencing reaction contaminants like unincorporated BigDye DNA sequencing terminators, salts, dNTPs, primers, enzymes, or other charged molecules that may be present. These contaminants can interfere with the detectors and electrokinetic sample injection of the DNA sequencing instruments, resulting in poor quality DNA sequencing results. For instance, problems with sample injection may lead to shorter lengths of readable sequence and reduced height of the DNA sequencing peaks, while any unincorporated dye would appear as dye

blobs on the DNA sequencing electropherogram and interfere with the actual sequence read (AB, 2006; NorDiag, 2010).

Five methods to cleanup DNA sequencing products were tested, which included: the isopropanol wash either by drying the DNA pellet using vacuum drying as described in Section 2.8.11.1, or by 90^{o}C heat drying of the DNA pellet for ~1 min or until the DNA pellet was dried as described in Section 2.8.11.1, the $MgSO_4$ wash as described in Section 2.8.11.2, and the commercially available purification reagents Agencourt magnetic beads (Agencourt, catalogue no. A29154) described in Section 2.10.7 (but in the single tube format), and the XTerminator beads (AB, catalogue no. 4376486). The XTerminator cleanup method was performed according to the instructions provided by the manufacturer, which first involves adding 20 µL of XTerminator beads and 90 µL of the XTerminator buffer, SAM solution (AB, USA), to each DNA sequencing product. The mixture was then mixed in a thermomixer at 14,000 rpm at RT for 30 min, and centrifuged at 18,000 g for 4 min. The supernatant was then extracted and was ready for DNA sequencing analysis. All five cleanup methods were performed on the DNA sequencing products produced from the sequencing of the standard DNA template (Section 3.1.3) according to the optimised method described in Section 3.1.4.

The DNA sequencing results are summarised in Table 3.1.2. All electropherograms showed good quality DNA sequencing results, with long readable sequence lengths, similar high DNA sequencing peaks and low background noise. However, the XTerminator and Agencourt magnetic beads cleanup methods had initial lower DNA sequencing peaks for the first ~160 or ~25 bp respectively. Despite that, results suggest that all five methods were almost equally efficient and effective for the cleanup of DNA sequencing products.

Next, the reproducibility of results, ease of performing the protocols, and cost of each method were compared. For single tube DNA sequencing, the isopropanol and $MgSO_4$ cleanup methods were preferred as both produced consistently good DNA sequencing results, were simple to perform, and cost efficient. For the isopropanol cleanup method, the DNA pellets were preferably vacuum dried, as drying at 90^{o}C could potentially lead to DNA degradation (Setlow and Setlow, 1995). On the other hand, for 96-well DNA sequencing, the isopropanol and $MgSO_4$ cleanup methods could not be performed in a 96-well tray format, and there was only limited access to the plate thermomixer required for the XTerminator cleanup method. Therefore, the Agencourt magnetic beads cleanup method will be performed, as it could produce good DNA sequencing results, and was simple and quick to perform in a 96-well

format. However, the disadvantage of using the Agencourt magnetic beads included the high cost and short shelf life (6 months) of the reagents.

In summary, all five of the methods to cleanup DNA sequencing products were equally efficient and produced good quality DNA sequencing results. In this study, for single tube DNA sequencing reactions, the isopropanol purification method with vacuum drying was performed when samples were sent to the IMVS/SA Pathology for analysis, while the $MgSO_4$ cleanup method was performed when samples were sent to AGRF for analysis. For 96-well DNA sequencing reactions, the Agencourt magnetic beads method was performed.

3.1.4.6. The effect of GelRed and ethidium bromide staining prior to DNA sequencing

GelRed and ethidium bromide are dyes that bind to DNA and RNA, allowing for fluorescent visualisation of DNA under UV light. As the commonly-used ethidium bromide is a potential mutagen due to its intercalating properties (Ioannau *et al.*, 2010), its long-term use was not recommended by the Occupational Health and Safety Committee of the School of Molecular and Biomedical Science (MBS) of the University of Adelaide. To date, no known studies have been published regarding the biochemical properties of the replacement dye, GelRed.

According to the manufacturer of GelRed, Biotium, GelRed-staining of gels/DNA does not have any effect on the migration of DNA during agarose gel electrophoresis, or on downstream reactions. However, studies performed in the Hepatitis Research Laboratory by Dr. Feng Feng had suggested that the efficiency of cloning using DNA extracted from GelRed post-stained gels was lower compared to using DNA that was either not extracted from gels, or was extracted from ethidium bromide-stained gels (data not shown). In addition, as pre-staining of gels with GelRed had been found to sometimes affect the migration of DNA during gel electrophoresis (data not shown), GelRed had only been used for post-staining.

In this Section, the possible effect of DNA template extracted from either GelRed- or ethidium bromide-stained gels on the quality of DNA sequencing was explored. Although cleanup of PCR products using the QIAquick PCR purification kit (Section 3.1.3) was sufficient to prepare DNA sequencing templates, when multiple PCR products were produced in a single PCR reaction, the desired PCR product to be sequenced had to be extracted from an agarose gel to ensure that the DNA sequencing template only contained a single PCR product, and thus would not produce multiple DNA sequences. Additionally, extracting the PCR products from agarose gels would also cleanup the product for DNA sequencing.

The PCR products (Section 3.1.3) were subjected to agarose gel electrophoresis as described in Section 2.8.7 prior to QIAquick PCR purification. The gel was then cut into two, and post-stained with either GelRed or ethidium bromide. GelRed post-staining was performed as described in Section 2.8.7, while for ethidium bromide post-staining, the gel was stained in 0.5 μg/mL ethidium bromide solution (dissolved using H_2O) for ~10 min, followed by soaking in H_2O for at least 10 min to remove excess dye.

Agarose gel electrophoresis results (data not shown) confirmed that both GelRed and ethidium bromide could efficiently allow the visualisation of DNA under UV light, as both gels visualised the expected PCR products with similar intensity. Subsequently, after both bands were extracted from the gels using QIAEX II beads (Section 2.8.8) and visualised again by agarose gel electrophoresis (Section 2.8.7), results (data not shown) estimated that DNA recovered after agarose gel extraction were ~3 – 4 times lower compared to DNA recovered from purification using the QIAquick PCR purification (Section 2.8.6).

The concentration of DNA extracted from GelRed- and ethidium bromide-stained gels were determined by spectrophotometry as described in Section 2.8.1, and were used as DNA templates for DNA sequencing reactions. As comparison, DNA purified using the QIAquick PCR purification kit (Section 3.1.3) was also used as DNA template. All DNA sequencing reactions were performed as described in Section 3.1.4, using 100 ng of DNA template.

The DNA sequencing results (data not shown) showed that both the purified DNA and DNA extracted from ethidium bromide-stained gel produced good DNA sequencing results, with ~950 bp of readable sequence, high DNA sequencing peaks and low background noise. On the other hand, the DNA extracted from GelRed-stained gel produced DNA sequencing peaks that gradually became lower from ~500 bp onwards, but up to ~900 bp of sequence was still readable. Similar observations were also seen when the experiment was repeated using a different DNA sequencing primer, DHBV C R (Table 2.2) (data not shown).

These results suggest that purifying PCR products using either the QIAquick PCR purification kit or extraction of PCR products from agarose gels could equally be used efficiently as DNA sequencing templates. However, as the DNA extracted from GelRed-stained agarose gels produced lower quality DNA sequencing results, this suggests that through undefined mechanisms, GelRed could have interfered with the DNA sequencing reactions. Possible ways of interference include permanent alteration of the DNA sequence structure during binding, or incomplete removal of GelRed dye during agarose gel extraction resulting in

chemical interference during DNA sequencing. Unfortunately, although DNA extracted from ethidium bromide-stained gels produced better results, due to its potential harmful effects and disposal issues, it is no longer used in MBS to visualise DNA.

In conclusion, DNA sequencing reactions performed using DNA templates extracted from GelRed-stained gels produced poorer quality DNA sequencing results compared with using DNA templates extracted from ethidium bromide-stained gels or purified with the QIAquick PCR purification kit. PCR products were thus preferably purified using the QIAquick PCR purification kit, unless present as multiple PCR products per PCR reaction.

3.1.5. Conclusion

In summary, a standard DNA sequencing reaction protocol for single tube and 96-well format has been optimised and established (methods were summarised in Sections 2.8.10 and 2.10.6 respectively). Each DNA sequencing reaction would contain 100 ng of DNA template, 0.25X or 0.5X final concentration of BigDye Terminator mix (for DNA templates <500 bp or >500 bp in length respectively) and 1X final concentration of sequencing buffer in a final volume of 20 µL when performed in single tubes, or 10 µL when performed in 96-well formats. To cleanup the DNA sequencing products, the isopropanol purification method with vacuum drying and $MgSO_4$ purification method would be performed for DNA sequencing reactions performed in single tube (summarised in Section 2.8.11), while the Agencourt magnetic beads method would be performed for 96-well DNA sequencing reactions (summarised in Section 2.10.7). On a separate note, as it was suspected that GelRed-staining of DNA may interfere slightly with the DNA sequencing reactions, PCR products were preferably purification with the QIAquick PCR purification kit and used as DNA templates for DNA sequencing reactions.

Table 3.1.1: DNA sequencing results obtained during the optimisation of the amount of template DNA used per DNA sequencing reaction.

Amount of DNA template per reaction (ng)	Length of readable sequence (bp)[a]	Quality of DNA sequencing electopherogram[a]
200	750-850	High DNA sequencing peaks, low background noise
150	750-900	High DNA sequencing peaks, low background noise
100	800-930	High DNA sequencing peaks, low background noise
50	800-900	Lower DNA sequencing peaks, low background noise
20	~500	Lower DNA sequencing peaks, background noise increased after ~500 bp

DNA sequencing reactions were performed using the same DNA template (Section 3.1.3) as described in Section 3.1.4.1. The DNA sequencing electropherograms obtained from each sequencing reaction were analysed based on Section 3.1.2.

[a]The results shown were averages obtained from duplicate DNA sequencing reactions.

Table 3.1.2: DNA sequencing results obtained from using various methods to cleanup DNA sequencing products.

Methods for the cleanup of DNA sequencing products	Length of readable sequence (bp)	Quality of DNA sequencing electopherogram
Isopropanol wash (vacuum-dried pellet)[a]	850-900	High DNA sequencing peaks, low background noise
Isopropanol wash (90^{o}C-dried pellet)[b]	850	High DNA sequencing peaks, low background noise
$MgSO_4$ wash[c]	800	High DNA sequencing peaks, low background noise
Agencourt magnetic beads[d]	700	Low signal strength for first ~25 bp followed by high DNA sequencing peaks, low background noise
XTerminator[e]	650	Low signal strength for first ~160 bp followed by high DNA sequencing peaks, low background noise

DNA sequencing reactions were performed using the same amount of the same DNA template (Section 3.1.3) as described in Section 3.1.4. The DNA sequencing electropherograms obtained from each sequencing reaction were analysed based on Section 3.1.2.

[a]The isopropanol cleanup method with vacuum drying of the DNA pellet was performed as described in Section 2.8.11.1.

[b]The isopropanol cleanup method with 90^{o}C heat drying of the DNA pellet was performed as described in Section 3.1.4.5.

[c]The $MgSO_4$ cleanup method was performed as described in Section 2.8.11.2.

[d]The magnetic beads (Agencourt Bioscience, catalogue no. A29154) cleanup method was performed as described in Section 2.10.7, but in the single tube format.

[e]The BigDye XTerminator (Applied Biosystems, catalogue no. 4376486) cleanup method was performed as described in Section 3.1.4.5.

Figure 3.1.1: DNA sequencing electropherograms generated using the ChromasLite software to show a graphical output of the DNA sequencing results. Each peak represents a nucleotide of the DNA template, with its nucleotide base (A, C, G, T) colour-coded and listed above the individual peaks.

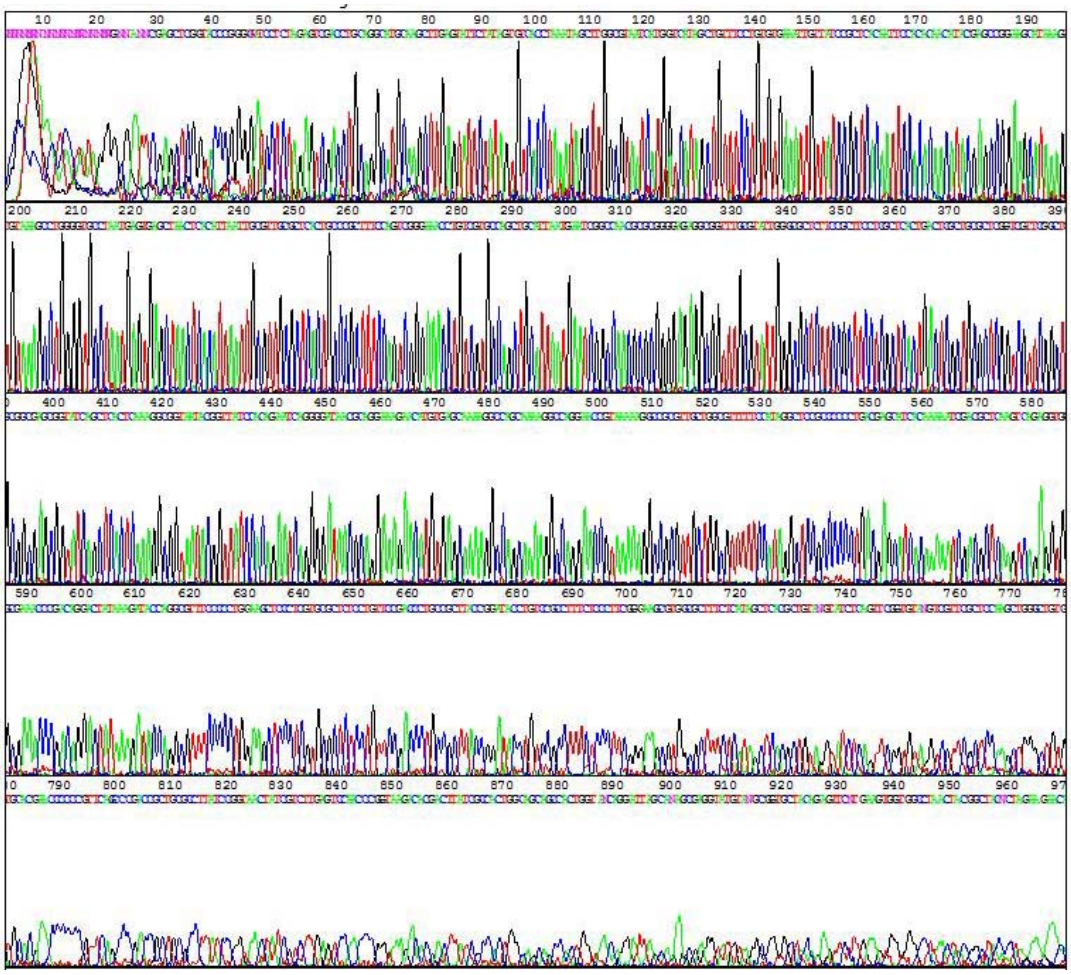
DNA sequencing reactions were performed as described in Sections 2.8.10 and 2.10.6, with subsequent cleanup of sequencing products as described in Sections 2.8.11 and 2.10.7. The DNA sequencing results, including the DNA sequencing electropherograms, were analysed as described in Section 2.8.12.

Figure 3.1.1A shows an example of an ideal DNA sequencing result, with long readable sequence (up to ~950 bp), high DNA sequencing peaks, and low background noise.

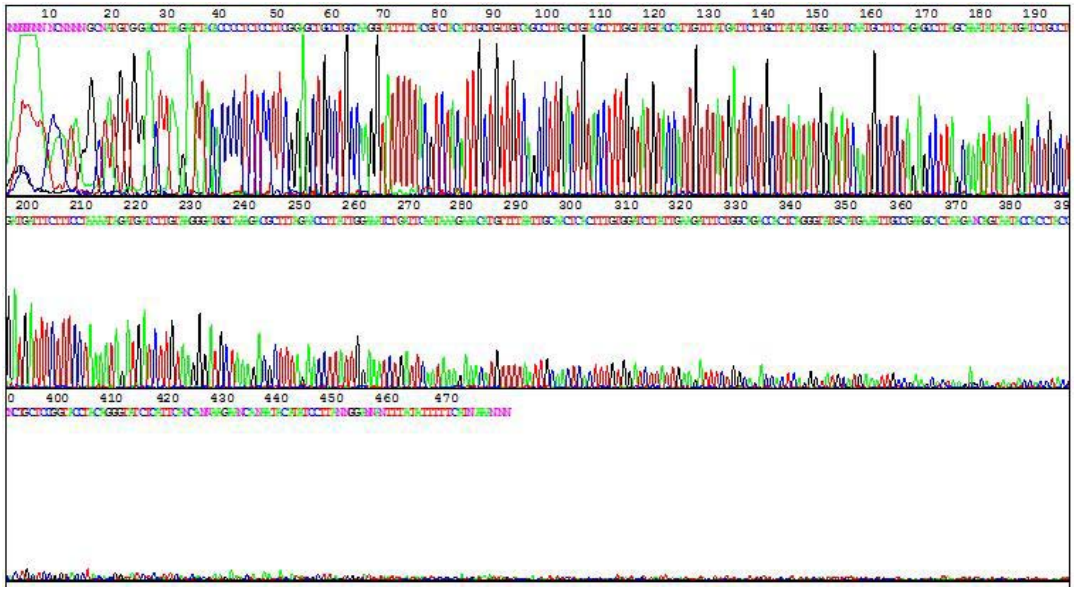
Figure 3.1.1B shows an example of a DNA sequencing result that had a prematurely shortened DNA sequence, as seen by the declining heights of the DNA sequencing peaks.

Figure 3.1.1C shows an example of a failed DNA sequencing result, with no readable distinct sequences, multiple peaks of various heights per base pair, and high background noise.

A



B



C

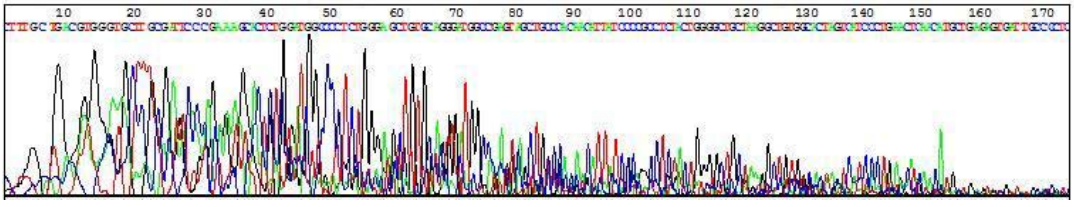


Figure 3.1.1

Chapter 3.2: Optimisation of qPCR assays

3.2.1. Aim

a) To optimise and establish standard protocols for qPCR assays for the detection of as few as 10 copies of DHBV total and cccDNA.

3.2.2. Introduction

In the Hepatitis Research Laboratory, protocols for qPCR assays described in Section 2.8.9 was established by Dr. Marc Le Mire (2003, 2005), and routinely used to detect and quantitate DHBV total and cccDNA. Specifically, the qPCR assays used serial dilutions of the pBL4.8x2 plasmid that contained 2 copies of the full-length AusDHBV genome (GenBank Accession AJ006350) cloned in a head-to-tail direction in the pBluescript KS II (+) plasmid vector (Triyatni, 1998, plasmid map shown in Figure 3.2.1A), as standard curves for the quantitation of DHBV DNA. To detect total DHBV DNA, the 423 – 576c primer set (Reaiche *et al.*, 2010) was used, while to detect DHBV cccDNA, the MG1 – CC2 primer set (Thorpe, 2007; Reaiche, 2008) was used (primer sequences are listed in Table 2.2). The primer binding sites on the pBL4.8x2 plasmid are shown in Figure 3.2.1A. To date, these established qPCR assays have a reported minimum sensitivity or limit of detection of 10 copies of DHBV DNA per 52,000 cells, equivalent to 0.0002 copies of DHBV DNA per cell (Miller *et al.*, 2008).

However, a few concerns had arisen to prompt the need for improved and more accurate qPCR assays to be established. Firstly, it was unknown whether the efficiency of amplification from circular DNA templates, like plasmids or DHBV cccDNA, would be lower than the efficiency of amplification from linearised DNA templates, due to supercoiling of the circular DNA forms (Chen *et al.*, 2007; Hou *et al.*, 2010; Lin *et al.*, 2011). If the qPCR efficiency differs, these may result in the under-quantitation of circular DNA, as well as generation of inaccurate qPCR standard curves from the plasmids. On a separate note, secondary forms of plasmids may also affect UV absorbances during Nanodrop spectrometry to result in inaccurate measurements of plasmid concentrations (Lin *et al.*, 2011).

Secondly, it was also unknown whether the sensitivity of amplification would be affected by the presence of higher total amounts of DNA in a qPCR reaction (Ellison *et al.*, 2011), as in the current qPCR protocol, at least 250X the amount of duck cell DNA were loaded into each qPCR reaction compared to plasmid DNA. Lastly, during the amplification of the pBL4.8x2 plasmid, which was used to generate standard curves, an alternative by-product may be produced that may result in over-quantitation of the plasmids (as illustrated in Figure 3.2.7).

Therefore, new plasmids that would not produce amplification by-products may be more suitable to be used for the generation of standard curves for DHBV DNA qPCR assays.

Based on the three concerns mentioned above, studies reported in this Chapter 3.2 involve optimisation and establishment of new qPCR assays for the detection of DHBV DNA, specifically the linearisation of DNA templates using restriction enzymes, the standardisation of total amounts of DNA in each qPCR reaction, and the use of the pBL4.8 plasmid that contained 1 copy of the full-length AusDHBV genome (GenBank Accession AJ006350) cloned in the pBluescript KS II (+) plasmid vector (Triyatni, 1998, plasmid map shown in Figure 3.2.1B), to generate standard curves for DHBV DNA qPCR assays.

The specificity of qPCR assays were determined by the amplification of only a single PCR product per reaction. This could be observed from the qPCR melt curves that show the melting temperature (Tm) of each PCR product, whereby the number of Tm peaks represents the number of PCR products amplified per reaction. Figure 3.2.2A shows an example of the expected melt curves generated from the specific amplification of DHBV total DNA as a Tm peak at 75.82^{o}C, while Figure 3.2.2B shows an example of the expected melt curves generated from the specific amplification of DHBV cccDNA as a Tm peak at 79.24^{o}C. The expected Tm for a qPCR product could be calculated using the online program BioMath Calculators for Oligos, accessible by http://www.promega.com/biomath/calc11.htm.

On the other hand, the quality of generated qPCR standard curves was determined by 4 parameters of the standard curves, including: the slope, the Y-intercept, the R^2 value, and the range of plasmid serial dilution copy numbers (from 10^8 – 10^1 copies) detectable during qPCR. Briefly, the slope of the standard curve reflects the efficiency of the PCR, of which a good PCR efficiency corresponds to a slope value between -3.58 and -3.10. The Y-intercept of the standard curve is the C_T value/threshold cycle that shows the relative concentration of a single copy of the DNA template, of which a good PCR sensitivity corresponds to a Y-intercept C_T value of ~40. The R^2 value or coefficient of correlation of the standard curve, is a statistical evaluation that could be used to evaluate the efficiency of the qPCR primer set, of which an efficient standard curve should have a R^2 value >0.99. Lastly, all the plasmid serial dilution copy numbers (10^8 – 10^1 copies) should be detected in each qPCR assay (information provided by the manufacturer of the qPCR reagent SYBR Green, Life Technologies, USA).

3.2.3. Linearisation of plasmid DNA for use in standard curves

3.2.3.1. Linearisation of plasmid DNA using various amounts of restriction enzyme

The qPCR amplification from circular and linearised plasmid DNA templates were compared to ensure that the efficiency and accuracy of qPCR amplification from circular plasmid templates were not affected by their various secondary forms in solution.

To linearise the pBL4.8x2 plasmid (used to generate standard curves for qPCR assays), the *Eco*RI restriction enzyme was used, as *Eco*RI digestion site was used to clone the full-length AusDHBV DNA into the pBluescript KS II (+) plasmid vector (Triyatni, 1998). Hence, it is expected that *Eco*RI digestion of pBL4.8x2 plasmid would produce a 2961 bp plasmid vector, and two copies of 3027 bp full-length DHBV DNA (refer Figure 3.2.1A for plasmid map). In addition, *Eco*RI is an efficient restriction enzyme whose activity is not methylation sensitive, has low level star activity if used at manufacturer (NEB) recommended conditions, and thus would be suitable to be used for overnight digestion reactions.

In addition, to observe whether the restriction enzyme mix (*Eco*RI protein, salt present in the *Eco*RI buffer, or the glycerol present with the *Eco*RI) could potentially inhibit or interfere with the qPCR polymerase activities, this Section would also perform restriction enzyme digestions using two different amounts of DNA. By digesting DNA in higher amounts, DNA has to be diluted before being used as qPCR template, therefore this would introduce less amounts of restriction enzyme mix into each qPCR wells. Comparatively, by digesting DNA in lower amounts that could be used as qPCR template directly without further dilutions, although this may ensure more complete digestion of the DNA, this would introduce higher amounts of restriction enzyme mix into each qPCR wells.

All *Eco*RI digestions were performed as described in Section 2.8.2, in 1.5 mL tubes using 20 U of *Eco*RI in 1X final concentration of *Eco*RI buffer made up to 30 µL of final volume, and incubated at 37^{o}C overnight to ensure complete digestion of the DNA. To perform digestion of higher amounts of DNA (designated in this study as A1), 2 µg of pBL4.8x2 plasmid would be used; while to perform digestion of lower amounts of DNA (designated in this study as A2), 45 ng of pBL4.8x2 plasmid would be used (as the final concentration of pBL4.8x2 in the 30 µL of final volume of the restriction digestion mixture would correspond to 10^{10} copies of DHBV DNA (refer Section 2.8.9.3.1 for mathematical calculations). Thus, it is expected that there would be ~4.4X less restriction enzyme digestion mix introduced into the qPCR reaction mix using the A1-digested DNA, compared to the A2-digested DNA. To ensure complete digestion of the pBL4.8x2 plasmid, digested plasmids were visualised using agarose gel

electrophoresis as described in Section 2.8.7. Results (data not shown) showed that both A1 and A2 samples showed successful digestion of the pBL4.8x2 plasmid to produce the expected 2961 bp and 3027 bp bands. Therefore, the A1- and A2-digested pBL4.8x2 were subsequently used as DNA templates to generate qPCR standard curves.

3.2.3.2. Generation of qPCR standard curves

A1- and A2-digested pBL4.8x2 plasmid DNA were used as DNA templates to generate DHBV total and cccDNA qPCR standard curves. As comparison, undigested pBL4.8x2 plasmid DNA was also used as DNA template.

Firstly, the DNA concentration of the undigested, A1- and A2-digested plasmid DNA was measured using Nanodrop spectrometry as described in Section 2.8.1, and $10^8 – 10^1$ copies of pBL4.8x2 (refer Section 2.8.9.3.1 for mathematical calculations) were used to produce qPCR standard curves. Both qPCR assays to detect DHBV total and cccDNA were performed using the 423 – 576c or MG1 – CC2 primer sets respectively as described in Section 2.8.9.

Results (data not shown) showed that the melt curves for all qPCR using the undigested, A1- and A2-digested pBL4.8x2 as DNA template only had a single peak at ~76^{o}C or ~79^{o}C for the detection of DHBV total or cccDNA respectively. These confirmed that only a single qPCR product was produced, and that qPCR amplification using all 3 DNA templates produced the same, expected qPCR product.

The quality of both DHBV total and cccDNA standard curves generated using all 3 DNA templates are summarised in Table 3.2.1. For both DHBV total and cccDNA qPCR assays, it was found that that the efficiency (based on the slope) of the A1-digested DNA template was the highest, while the amplification sensitivity (based on the Y-intercept) and the efficiency of primer amplification (based on the R^2 value) were similar for all DNA templates. However, while the range of detectable copy numbers of DHBV total DNA were similar for all DNA templates ($10^7 – 10^1$), the undigested DNA template had greater range of detectable copy numbers of DHBV cccDNA ($10^8 – 10^2$) followed by A1- and A2-digested DNA templates.

3.2.3.3. Quantitation of DHBV DNA using the generated standard curves

The standard curves generated in Section 3.2.3.2 were then used to quantify the levels of DHBV total and cccDNA in 5 DHBV-infected duck liver tissues (designated as Sample 1 to Sample 5) with previously undetermined levels of DHBV DNA. DNA were extracted from each duck liver tissue using the DNeasy blood and tissue kit as described in Section 2.6.1.

After measuring the concentration of DNA using Nanodrop spectrometry as described in Section 2.8.1, 150 ng of DNA were used as template for each qPCR reaction performed as described in Section 2.8.9, using the 423 – 576c or MG1 – CC2 primer sets to detect DHBV total or cccDNA respectively.

Results of the DHBV total DNA qPCR assays shown in Figure 3.2.3A indicated that the levels of DHBV total DNA in all 5 samples were similar when based on the standard curves generated using the undigested and A1-digested DNA. For Samples 1 to 4, the levels of DHBV total DNA were ~5.8X higher based on the standard curves generated using the undigested and A1-digested DNA as compared to using the A2-digested DNA; while for Sample 5, the levels of DHBV total DNA were 1.7X higher based on the standard curve generated using the A2-digested DNA as compared to the other 2 standard curves. In contrast, results of the DHBV cccDNA qPCR assay shown in Figure 3.2.3B indicated that the levels of DHBV cccDNA in all 5 samples were ~1.7X higher based on the standard curves generated using the undigested DNA compared to the other 2 standard curves. Comparing both qPCR assays, the trends of DHBV total and cccDNA levels obtained from all standard curves were similar, with DHBV total DNA levels on average ~2.4X higher than DHBV cccDNA levels.

Based on all these results in Sections 3.2.3.2 and 3.2.3.3, it was likely that the presence of ~4.4X higher amounts of restriction digestion mix, introduced by the A2-digested DNA template, may have slightly altered the salt concentrations in the qPCR mix, which could reduce the efficiency of the qPCR polymerase (Lin *et al.*, 2011). Thus, this may result in the poor quality of the qPCR standard curves generated using the A2-digested DNA, as well as the lower levels of DHBV DNA quantitated based on those qPCR standard curves.

Interestingly, the quality of the qPCR standard curves as well as the levels of DHBV total DNA quantitated based on the standard curves generated using the undigested and A1-digested DNA were similar. This suggests that PCR amplifications from a circular or linear plasmid DNA template were equally efficient, and that the standard curves generated from either DNA templates were able to efficiently quantitate DHBV total DNA.

However, the levels of DHBV cccDNA quantitated based on the standard curves generated using A1-digested DNA were lower compared with the levels based on the standard curves generated using the undigested DNA. This may be due to less efficient PCR amplifications of circular forms of plasmid DNA template (undigested) compared to linear forms of plasmid DNA tempalte (A1-digested), resulting in the actual copy number of PCR products amplified

from the undigested DNA templates to be less than the expected copy number. Therefore, higher levels of DHBV DNA would be obtained when based on the standard curves generated using the undigested DNA which had overestimated the copy numbers in the standard curves.

It was unclear why only the DHBV cccDNA qPCR assay, and not the DHBV total DNA qPCR assay, was affected by the circular plasmid DNA template. It may be due to the DHBV cccDNA primer binding sites that were less accessible than the DHBV total DNA primer binding sites in the circular plasmid forms, resulting in difference in amplification effiencies.

In summary, the plasmid DNA used as DNA template for standard curves in qPCR assays should be linearised by restriction enzymes, as qPCR amplifications from the circular plasmid DNA forms may not be efficient, and may result in over-quantitation of DNA samples when based on the generated standard curves. As the introduction of restriction enzyme digestion mix into the qPCR reaction mix may reduce the efficiency of qPCR amplifications, the A1-digestion of plasmid DNA that would carry over smaller amounts of restriction enzyme digestion mix into the qPCR reaction mix, would be used as DNA templates to generate standard curves for the DHBV total and cccDNA qPCR assays.

3.2.4. Linearisation of plasmid DNA in the qPCR SYBR Green reaction mix for use in standard curves

3.2.4.1. Optimisation of linearisation of plasmid DNA in the qPCR SYBR Green reaction mix

It was suggested in Section 3.2.3 that the introduction of restriction enzyme digestion mix into the qPCR reaction mix may reduce the efficiency of the qPCR polymerase amplification. Therefore, to further reduce the carry over of restriction enzyme digestion mix from the plasmid DNA, restriction enzyme digestion of plasmid DNA directly in the qPCR SYBR Green reaction mix were tested. If the plasmid DNA was found to be efficiently and completely digested in the qPCR reaction mix, this would omit the restriction enzyme digestion step for plasmid DNA, and to prevent the introduction of restriction enzyme buffers into the qPCR reaction mix. Linearisation of plasmid DNA templates could then be carried out by adding *Eco*RI into each qPCR reaction mix, and adding an initial 37^{o}C for 1 hr incubation step to the qPCR amplification cycle. The qPCR polymerase, AmpliTaq Gold, would not be affected at this temperature as the polymerase is a hot-start protein, and would require heating at 95^{o}C for 10 min to be activated. In addition, as *Eco*RI would be heat-inactivated during the polymerase activation incubation, this could prevent any further DNA digestion or interference with the qPCR polymerase activities during qPCR amplification.

The various controls and restriction enzyme digestion conditions tested are listed in Table 3.2.2, with incubations at 37°C for 1 hr, 3 hr or overnight. The plasmid used was the same pBL4.8x2 plasmid that was used in Section 3.2.3.1. As 1 µL of *Eco*RI (20 units) is reported by the manufacturer NEB to be sufficient to digest 20 µg of λ DNA within 1 hr, the amount of *Eco*RI used in each reaction was in excess, and thus should have led to complete digestion of the pBL4.8x2. Again, it is expected that *Eco*RI digestion of pBL4.8x2 would produce 3 fragments of 2961, 3027 and 3027 bp (refer Figure 3.2.2A). All digested DNA products were visualised using gel electrophoresis as described in Section 2.8.7. As shown in Table 3.2.2, Test 5 was the actual test sample, while Test 6 was a control to compare the efficiency of digestion in optimal conditions. To determine whether the use of higher amounts of *Eco*RI than required may lead to over-digestion or star digestion, and to observe any effects of different digestion reaction final volumes, Tests 1 to 4 were also performed.

Table 3.2.2: The various controls and restriction digest conditions tested in this section.

Test no.	pBL4.8x2		*Eco*RI[a] (µL)	Buffer (µL)[b]		H_2O[c] (µL)	Final volume (µL)
	Amount (ng)	Final concentration (ng/µL)		*Eco*RI buffer	SYBR Green mastermix		
1	4657	233	2	2	-	14.0	20
2	4657	233	1	2	-	15.0	20
3	4657	93	2	5	-	41.0	50
4	4657	93	1	5	-	42.0	50
5	1863	93	1	-	10	8.2	20
6	1863	93	1	2	-	16.2	20

All samples were incubated at 37°C for 1 hr, 3 hr or overnight.

[a]1 µL of *Eco*RI contains 20 U, which is reported by manufacturer NEB to be sufficient to digest 20 µg of λ DNA within 1 hr.

[b]Amount of buffer required to have 1X final concentration of buffer.

[c]Amount of water required to make up the final volume.

The gel electrophoresis results (Figure 3.2.4) showed that in the Test control (Tests 1, 2, 3, 4, 6), two ~3000 bp bands were seen in close proximity as expected, and thus showed that pBL4.8x2 had been completely digested by *Eco*RI in all the controls. Some star activity, as seen by the presence of multiple smaller-sized bands than the expected ~3000 bp bands, was observed Test 3 and 4. These suggest that *Eco*RI star activity may occur during longer incubations of *Eco*RI (overnight incubation), when lower concentrations of DNA were present in the mixture, as no star activity were observed in Tests 1 and 2 (overnight incubation with higher concentrations of DNA). Therefore, this showed that only higher final concentrations of DNA should be used during overnight digestion incubations.

Results (Figure 3.2.4) also showed that in the actual Test sample (Test 5), pBL4.8x2 was able to be specifically and completely digested by *Eco*RI in the SYBR Green mastermix after 1 hr incubation. However, by 3 hr of incubation, multiple smaller bands were observed while the expected ~3000 bp bands became fainter. After overnight incubation, only multiple smaller bands were observed while the expected ~3000 bp bands were no longer present. These showed that over-digestion or non-specific digestions would occur during *Eco*RI digestion of DNA in the SYBR Green mastermix with incubation time of more than 1 hr.

Based on the results obtained above, to prevent over-digestion or non-specific digestions of pBL4.8x2 in the SYBR Green mastermix, Test 5 (Table 3.2.2) was repeated with lower amounts of *Eco*RI (0.25 µL and 0.5 µL compared to 1 µL), and with shorter incubation periods (30 min compared to 1 hr). In addition, lower amounts of pBL4.8x2 DNA (450 ng or final concentration 22.5 ng/µL) were digested, to further mimic the amount of pBL4.8x2 (150 ng) that would be present during actual experimental qPCR reactions.

The gel electrophoresis results (Figure 3.2.5) showed that 450 ng of pBL4.8x2 was able to be completely digested by 0.25 µL (5 U) of *Eco*RI in the SYBR Green mastermix after 30 min incubation, as only the expected ~3000 bp bands were observed. However, as previously observed in Figure 3.2.4, during longer incubation times (1 hr) or when higher amounts of *Eco*RI and lower concentrations of DNA were present in the mixture (0.5 µL and 1 µL), over-digestion or non-specific digestions occurred, as observed by the multiple smaller bands and the absence of the expected ~3000 bp bands.

In summary, *Eco*RI digestions of pBL4.8x2 could be performed directly in the SYBR Green mastermix. However, the incubation time should be kept to a maximum of 30 min, and minimal amounts of *Eco*RI should be added into each reaction.

3.2.4.2. Generation of qPCR standard curves

After optimising the *Eco*RI digestion of pBL4.8x2 in SYBR Green mastermix, qPCR assays were performed using the SYBR Green mastermix-digested pBL4.8x2 as DNA templates to generate DHBV total and cccDNA qPCR standard curves. As comparison, undigested and A1-digested pBL4.8x2 (previously performed in Section 3.2.3) were also used as DNA templates. The qPCR reactions were performed as described in Section 3.2.3.2, with an additional *Eco*RI-digestion incubation of 37^{o}C for 30 min was performed prior to starting the standard qPCR reactions for the SYBR Green mastermix-digested pBL4.8x2.

Results (data not shown) showed that the melt curves for all qPCR assays using the undigested, A1- and SYBR Green mastermix-digested pBL4.8x2 as DNA template only had a single peak at ~76^{o}C or ~79^{o}C for the detection of DHBV total or cccDNA respectively. These confirmed that only a single qPCR product was produced in each qPCR reaction, and qPCR amplification using all 3 DNA templates produced the same, expected qPCR product.

The quality of both DHBV total and cccDNA standard curves generated using all 3 DNA templates is summarised in Table 3.2.3. It was found that for the DHBV total DNA qPCR assay, the efficiency (based on the slope), amplification sensitivity (based on the Y-intercept), and efficiency of primer amplification (based on the R^2 value) of the A1- and SYBR Green mastermix-digested DNA templates were similar and were higher than the undigested DNA template, with all 3 DNA templates showing similar range of detectable copy numbers of DHBV total DNA for (10^8 – 10^1). Interestingly, for the DHBV cccDNA qPCR assay, the efficiency, amplification sensitivity, and efficiency of primer amplification of the A1-digested DNA template was the highest compared to the undigested and SYBR Green mastermix-digested DNA template that generated similar results. The range of detectable copy numbers of DHBV cccDNA however was higher for the undigested and A1-digested DNA templates (10^8 – 10^1) when compared to SYBR Green mastermix-digested DNA template (10^8 – 10^2).

These results showed that the DHBV total and cccDNA qPCR standard curves generated by the A1-digested DNA template were of a higher quality compared to the undigested DNA template, confirming the results obtained in Section 3.2.3.2. For the SYBR Green mastermix-digested DNA template, as the quality of DHBV cccDNA qPCR standard curves was lower than the A1-digested DNA template, but the quality of DHBV total DNA qPCR standard curves was comparable, these suggest that the digestion of plasmid DNA in the qPCR SYBR Green mastermix could successfully linearise the plasmid DNA, and would not interfere with subsequent qPCR amplifications. It is unclear why the quality of DHBV total DNA qPCR standard curves were higher compared to the DHBV cccDNA qPCR standard curves, but this may be due to the different efficiencies of the DHBV total and cccDNA qPCR primer sets.

In summary, to further prevent the carry-over of restriction enzyme mix into the qPCR reaction mix that may interfere with qPCR amplification, plasmid DNA could be directly digested in the SYBR Green mastermix before performing the qPCR assays. However, as the quality of DHBV total and cccDNA qPCR standard curves generated by the A1-digested DNA template were slightly higher than the SYBR Green mastermix-digested DNA template, A1-digestion of plasmid would be performed for all subsequent qPCR assays in this thesis.

3.2.5. Linearisation of DHBV DNA samples

Results from Sections 3.2.3 and 3.2.4 suggested that the efficiency of qPCR amplification after linearisation of the circular plasmid DNA templates was higher compared to undigested circular plasmid DNA templates. Therefore similarly, DNA extracted from DHBV-infected duck liver tissues were also linearised by restriction enzyme digestion. As DHBV DNA could be present in the supercoiled cccDNA form, it is expected that the efficiency of qPCR amplification would be increased after linearisation of the extracted liver DNA.

The liver tissues used were 5 DHBV-infected duck liver tissues (designated as Sample 1 to Sample 5) previously used in Section 3.2.3.3. DNA was extracted from liver tissues using the DNeasy blood and tissue kit as described in Section 2.6.1, and DNA concentrations were measured using Nanodrop spectrometry as described in Section 2.8.1. DNA were then *Eco*RI-digested as described in Section 2.8.2, in 1.5 mL tubes using 20 U of *Eco*RI in 1X final concentration of *Eco*RI buffer made up to 30 µL of final volume, and incubated at 37^{o}C overnight to ensure complete digestion of the DNA. As AusDHBV (GenBank Accession AJ006350) contains one *Eco*RI digestion site at 3027/1 nt, it is expected that the DHBV DNA would be linearised to form a 3027 bp DNA fragment after complete *Eco*RI digestion.

Similar to Section 3.2.3.1, different amounts of DNA template were digested and tested to further determine whether the introduction of restriction enzyme mix into the qPCR reaction mix inhibited or interfered with the qPCR polymerase activities. To perform digestion of higher amounts of DNA (designated in this study as A1), 2 µg of DHBV DNA would be used (final concentration 66.7 ng/µL); while to perform digestion of lower amounts of DNA (designated in this study as A2), 900 ng of DHBV DNA would be used (final concentration 30 ng/µL). Thus, it is expected that there would be ~2.2X less restriction enzyme digestion mix introduced into the qPCR reaction mix using A1-digested DNA, compared to the A2-digested DNA. DHBV total and cccDNA qPCR assays were subsequently performed using the 423 – 576c or MG1 – CC2 primer sets respectively as described in Section 2.8.9, using 150 ng of the undigested, A1- and A2-digested DHBV DNA as DNA template. As standard curves, 10^{8} – 10^{1} copies of A1-digested pBL4.8x2 plasmid were used (Section 3.2.3).

DHBV total DNA (Figure 3.2.6A) and DHBV cccDNA (Figure 3.2.6B) qPCR quantitation results showed that the A2-digested DNA had the lowest quantitated levels of DHBV total and cccDNA compared to undigested and A1-digested DNA. However, qPCR amplification of A2-digested Sample 5 was not successful. There was no identifiable trend between the quantitated levels of DHBV total and cccDNA from undigested and A1-digested DNA, with

higher levels of DNA quantitated for A1-digested Samples 1 and 5, and undigested Samples 2, 3, and 4. Comparing both qPCR assays, the trends of DHBV total and cccDNA levels obtained from all standard curves were similar, with DHBV total DNA levels on average ~4.3X higher than DHBV cccDNA levels, similar to results obtained in Section 3.2.3.3.

Based on these results, it was likely that the presence of ~2.2X higher amounts of restriction digestion mix, introduced by the A2-digested DNA template, may have altered the salt concentrations in the qPCR mix, which could reduce the efficiency of the qPCR polymerase activity. Thus, this may result in the lower levels of DHBV total and cccDNA quantitated in these qPCR assays. However, it was unclear why variable results with no identifiable trends were observed between the undigested and A1-digested DNA templates. One possible reason could be due to the inaccurate quantification of DNA template by Nanodrop spectrometry, as secondary forms of plasmids may affect the UV absorbances during Nanodrop spectrometry (Lin *et al.*, 2011), or that particles present in the restriction enzyme mix may absorb light at 260 nm, resulting in false quantification of DNA and the addition of variable amounts of undigested and digested DNA template for each qPCR reaction.

To observe the potential effect of the restriction enzyme mix on the quantification of DNA using Nanodrop spectrometry, Nanodrop spectrometry absorbance readings of the restriction enzyme mix (containing 10 U of *Eco*RI and 1X *Eco*RI buffer) were obtained as described in Section 2.8.1. Results (data not shown) showed that in comparison to the absorbance readings of H_2O, the absorbance at 260 nm was similar, while the absorbance at 280 nm was ~6X higher in the restriction enzyme mix. These results confirmed that the presence of "impurities" (*Eco*RI, glycerol, Tris, salt...) in the restriction enzyme mix does absorb light at 280 nm. However, as the absorbance at 260 nm was similar, the quantitation of DNA should not be affected. To confirm this, Nanodrop spectrometry absorbance readings of pBL4.8x2 plasmid DNA in restriction enzyme mix was obtained. Results (data not shown) showed that in comparison to the absorbance readings of the same amounts of pBL4.8x2 in H_2O, the absorbance at 260 nm and 280 nm was ~7% and ~26% higher. Therefore, although the effect of the restriction enzyme mix on Nanodrop spectrometry absorbance readings were subtle, results suggest that it could account for some inaccuracies of amounts of DNA quantitated, and thus different amounts of DNA template may be added for each qPCR reaction, explaining some (but not all) of the qPCR quantifications variations observed in Figure 3.2.6.

In summary, introduction of restriction enzyme digestion mix into the qPCR reaction mix may reduce the efficiency of qPCR amplification, resulting in lower levels of quantitated

DNA. Hence, it was decided that A2-digested DNA would not be used as DNA template for all future qPCR assays. No clear conclusions could be drawn in this Section whether the linearisation of DHBV DNA templates could improve the efficiency of qPCR amplification. However, as Section 3.2.3.3 showed that linearisation of plasmid DNA templates could be more efficiently amplified during qPCR assays, it was decided that DHBV DNA templates for subsequent qPCR assays would also be A1-digested before use.

3.2.6. Standardisation of total amounts of DNA in each qPCR reaction

To determine whether the presence of higher total amounts of DNA in a qPCR reaction may affect the efficiency of qPCR amplification, the total amounts of DNA added to each qPCR reaction were standardised. This was because in the current qPCR protocol, the amount of plasmid DNA that were loaded to generate the qPCR standard curves (0.5 ng) was ~250X less than the amount of duck liver DNA loaded into each qPCR reaction (150 ng). Therefore, if the efficiency of qPCR amplification had indeed been reduced in the presence of higher total amounts of DNA, DHBV DNA levels present in duck liver tissues may be under-estimated.

To standardise the total amounts of DNA in each qPCR reaction, normal duck liver (NDL) DNA was used. NDL DNA was extracted from NDL using the DNeasy blood and tissue kit as described in Section 2.6.1, and A1-digested by *Eco*RI as optimised in Section 3.2.5. As comparison, undigested NDL would also be used. DHBV total and cccDNA qPCR assays were performed using the 423 – 576c or MG1 – CC2 primer sets respectively as described in Section 2.8.9, using 10^8 – 10^1 copies of A1-digested pBL4.8x2 plasmid to generate qPCR standard curves. Undigested or digested NDL DNA were added to each qPCR reaction to standardise the total amount of DNA present in each qPCR reaction to 150 ng. As a control, standard curves were also generated using pBL4.8x2 DNA only without NDL DNA.

Results (data not shown) showed that the melt curves for all qPCR assays with digested or undigested NDL DNA, or without added NDL DNA, only had a single peak at ~76^{o}C or ~79^{o}C for the detection of DHBV total or cccDNA respectively. These confirmed that only a single qPCR product was produced in each qPCR reaction, and that qPCR amplification using all 3 DNA templates produced the same, expected qPCR product.

The quality of both DHBV total and cccDNA standard curves generated using all 3 DNA templates were summarised in Table 3.2.4. For the DHBV total DNA, the efficiency (based on the slope) and the amplification sensitivity (based on the Y-intercept), and range of detectable copy numbers of DHBV total DNA of for added undigested NDL DNA were the

highest, while the efficiency of primer amplification (based on the R^2 value) was the lowest. On the other hand, for the DHBV cccDNA qPCR assay, it was found that the efficiency, amplification sensitivity, and the efficiency of primer amplification for no added NDL DNA was the highest followed by added undigested and digested NDL DNA, with the range of detectable copies of DHBV cccDNA similar for all 3 DNA templates. As the the quality of standard curves were similar, this suggests that there was no significant difference in the standard curves generated using all 3 DNA templates.

In summary, the standardisation of total amounts of DNA in each qPCR reaction did not seem to significantly affect the efficiency of qPCR amplification. Nevertheless, to ensure that the efficiency of qPCR assays would not be affected by the difference in total amounts of DNA present in each qPCR reaction, undigested NDL DNA would be used in future qPCR assays to standardise the total amounts of DNA in each qPCR reaction. A1-digested NDL DNA would not be used in order to prevent further introduction of restriction enzyme mix into the qPCR reaction mix that may reduce the efficiency of qPCR amplification.

3.2.7. Using pBL4.8 plasmid that contains a single copy of DHBV DNA as DNA template to generate qPCR standard curves

There were concerns that alternative by-products may be produced during the amplification of DHBV total and cccDNA from the (circular) pBL4.8x2 plasmid. This was because as the pBL4.8x2 plasmid contains 2 copies of the full-length AusDHBV genome (Triyatni, 1998), the qPCR primer sets 423 – 576c and MG1 – CC2 for the amplification of DHBV total and cccDNA respectively, could each bind to 2 sites on the pBL4.8x2 as shown in Figure 3.2.1A, to produce 2 copies of qPCR products from each pBL4.8x2. However, as illustrated in Figure 3.2.7, a ~3180 bp full-length DHBV PCR by-product could also be amplified, potentially resulting in over-quantitation of pBL4.8x2 copy numbers during qPCR assays.

Therefore, the pBL4.8 plasmid was tested to replace the pBL4.8x2 plasmid and to generate qPCR standard curves. The pBL4.8 plasmid was chosen, as it contains only a single copy of the same full-length AusDHBV genome cloned in the same pBluescript KS II (+) vector as pBL4.8x2 plasmid (Triyatni, 1998). Therefore, the qPCR primer sets, 423 – 576c and MG1 – CC2 for the amplification of DHBV total and cccDNA respectively, will bind once to the pBL4.8 and only generate 1 copy of qPCR product from each pBL4.8 template. The pBL4.8 plasmid map and the primer binding sites are shown in Figure 3.2.1B.

3.2.7.1. Generation of qPCR standard curves

The pBL4.8 plasmid was used as DNA template to produce qPCR standard curves for DHBV total and cccDNA. As comparison, qPCR standard curves were also produced using the pBL4.8x2 plasmid. All plasmids were A1-digested as previously described in Section 3.2.3, and 10^8 – 10^1 copies of plasmid (refer Section 2.8.9.3.1 for mathematical calculations) were used to produce qPCR standard curves. NDL DNA extracted from NDL using the DNeasy blood and tissue kit (Section 2.6.1) were also to standardise the total amounts of DNA present in each qPCR reaction. Both qPCR assays to detect DHBV total and cccDNA were performed using the 423 – 576c or MG1 – CC2 primer sets respectively as described in Section 2.8.9.

Results (data not shown) showed that the melt curves for both qPCR assays using the pBL4.8x2 and pBL4.8 plasmid as DNA templates only had a single peak at ~76^{o}C or ~79^{o}C for the detection of DHBV total or cccDNA respectively. These confirmed that only a single qPCR product was produced in each qPCR reaction, and that qPCR amplification using both DNA templates produced the same, expected qPCR product.

The quality of both DHBV total and cccDNA standard curves generated are summarised in Table 3.2.5. It was found that for both DHBV total and cccDNA qPCR assays, the efficiency (based on the slope), amplification sensitivity (based on the Y-intercept), efficiency of primer amplification (based on the R^2 value), and range of detectable copy numbers of DHBV DNA were similar for both the pBL4.8x2 and pBL4.8 DNA templates.

In summary, as no significant differences were observed, these suggest that both pBL4.8x2 and pBL4.8 plasmid DNA could be equally used to as DNA templates to produce good quality qPCR standard curves for thedetection of DHBV total and cccDNA.

3.2.7.2. Quantitation of DHBV DNA using the generated standard curves

To further compare the use of pBL4.8x2 or pBL4.8 plasmid DNA to generate qPCR standard curves, the standard curves generated in Section 3.2.7.1 were used to quantify the levels of DHBV total and cccDNA in 5 DHBV-infected duck liver tissues (designated as Sample 1 to Sample 5) previously used in Sections 3.2.3.3 and 3.2.5.

DNA was extracted from duck liver tissues using the DNeasy blood and tissue kit (Section 2.6.1). DNA was then A1-digested as described in Section 3.2.5, and 150 ng of DNA were used as DNA template for each qPCR reaction performed as described in Section 2.8.9, using the 423 – 576c or MG1 – CC2 primer sets to detect DHBV total and cccDNA respectively.

Surprisingly, results (Figure 3.2.8) showed that for the same amount of liver DNA template from 5 duck liver samples, both the DHBV total and cccDNA levels were consistently ~7.5X lower based on the standard curves generated by pBL4.8x2, as compared to the DHBV DNA levels based on the standard curves generated by pBL4.8.

These results suggest that some qPCR by-products may indeed have still been produced from the amplification of pBL4.8x2, although after *Eco*RI-digestion, it is expected that the by-products shown in Figure 3.2.7 would not have been amplified. It might be possible that the *Eco*RI-digestion of pBL4.8x2 was not 100% complete, resulting in the amplification of qPCR by-products from the undigested circular pBL4.8x2, to generate higher copies of qPCR products than expected. Subsequently, the qPCR standard curves generated would reflect an over-estimation of DHBV DNA levels, and thus result in the under-estimation of the actual levels of DHBV DNA present in the liver DNA samples.

In summary, as the amplification of pBL4.8x2 plasmid potentially produces alternative qPCR by-products, the pBL4.8 plasmid would be used as DNA templates for all subsequent qPCR assays to generate standard curves for DHBV total and cccDNA.

On a separate note, it was observed that ABI StepOne Plus (AB, USA) qPCR instrument was slightly more sensitive than the ABI Prism 7000 (AB, USA) qPCR instrument, as the previous was able to consistently detects as low as 10^1 copies of standard curves DNA templates, compared to the ABI Prism 7000 qPCR instrument that mainly detects as low as 10^2 copies of standard curves DNA templates only (data not shown). Therefore, the ABI StepOne Plus qPCR instrument would be preferably used for all subsequent qPCR assays.

3.2.8. Conclusion

In conclusion, standard qPCR assays for the detection of DHBV total and cccDNA have been optimised and established. Briefly, qPCR were to be performed using the ABI StepOne Plus qPCR instrument, using 10^8 – 10^1 copies of pBL4.8 plasmid (replacing the pBL4.8x2 plasmid) to generate qPCR standard curves. To ensure that the secondary forms of circular DNA template, presence of carry over restriction enzyme mix, and different total amounts of DNA templates in each qPCR reaction would not interfere with the efficiency of qPCR amplifications, all DNA samples were to be linearised using *Eco*RI at high amounts (2 μg) to allow or dilution of the DNA samples and the restriction enzyme mix before use, and with added undigested NDL DNA to standardise the total amounts of DNA templates added in each qPCR reaction. The established qPCR methods are described in detail in Section 2.8.9.

Table 3.2.1: Summary of the slope, Y-intercept, R^2 value, and range of detectable copy numbers of plasmid DNA serial dilution obtained from the DHBV total and cccDNA qPCR standard curves.

DHBV total DNA qPCR				
pBL4.8x2	**Slope**	**Y-intercept**	**R^2 value**	**Detectable plasmid DNA copy numbers**
Undigested	-3.077	36.178	0.996	$10^7 – 10^1$
A1-digested	-3.115	36.344	0.991	$10^7 – 10^1$
A2-digested	-2.422	32.303	0.964	$10^7 – 10^1$

DHBV cccDNA qPCR				
pBL4.8x2	**Slope**	**Y-intercept**	**R^2 value**	**Detectable plasmid DNA copy numbers**
Undigested	-2.752	35.285	0.973	$10^8 – 10^2$
A1-digested	-3.059	35.937	0.987	$10^7 – 10^2$
A2-digested	-2.980	35.336	0.992	$10^7 – 10^3$

qPCR standard curves were generated using undigested, A1- and A2-digested pBL4.8x2 DNA as DNA templates as described in Section 3.2.3.2. DHBV total and cccDNA qPCR assays were performed using the 423 – 576c or MG1 – CC2 primer sets respectively as described in Section 2.8.9. The qPCR standard curves and the corresponding data (slope, Y-intercept, R^2 value, the range of detectable copy numbers of plasmid DNA serial dilution) were generated using the ABI Prism 7000 software (AB, USA).

Table 3.2.3: Summary of the slope, Y-intercept, R^2 value, and range of detectable copy numbers of plasmid DNA serial dilution obtained from the DHBV total and cccDNA qPCR standard curves.

DHBV total DNA qPCR				
pBL4.8x2	**Slope**	**Y-intercept**	**R^2 value**	**Detectable plasmid DNA copy numbers**
Undigested	-3.417	38.96	0.994	$10^8 – 10^1$
A1-digested	-3.596	39.817	0.995	$10^8 – 10^1$
SYBR Green mastermix-digested	-3.610	39.503	0.998	$10^8 – 10^1$

DHBV cccDNA qPCR				
pBL4.8x2	**Slope**	**Y-intercept**	**R^2 value**	**Detectable plasmid DNA copy numbers**
Undigested	-3.256	37.288	0.998	$10^8 – 10^1$
A1-digested	-3.495	38.552	0.999	$10^8 – 10^1$
SYBR Green mastermix-digested	-3.257	37.193	0.997	$10^8 – 10^2$

qPCR standard curves were generated using undigested, A1- and SYBR Green mastermix-digested pBL4.8x2 DNA as DNA templates as described in Section 3.2.4.2. DHBV total and cccDNA qPCR assays were performed using the 423 – 576c or MG1 – CC2 primer sets respectively as described in Section 2.8.9. The qPCR standard curves and the corresponding data (slope, Y-intercept, R^2 value, the range of detectable copy numbers of plasmid DNA serial dilution) were generated using the StepOne Plus software (AB, USA).

Table 3.2.4: Summary of the slope, Y-intercept, R^2 value, and range of detectable copy numbers of plasmid DNA serial dilution obtained from the DHBV total and cccDNA qPCR standard curves.

DHBV total DNA qPCR				
NDL added	**Slope**	**Y-intercept**	**R^2 value**	**Detectable plasmid DNA copy numbers**
None	-3.287	38.603	0.999	$10^7 – 10^2$
Undigested	-3.298	39.165	0.996	$10^8 – 10^2$
Digested	-3.250	38.766	0.999	$10^7 – 10^2$

DHBV cccDNA qPCR				
NDL added	**Slope**	**Y-intercept**	**R^2 value**	**Detectable plasmid DNA copy numbers**
None	-3.188	38.017	0.998	$10^7 – 10^1$
Undigested	-3.137	37.961	0.998	$10^7 – 10^2$
Digested	-2.959	37.109	0.998	$10^7 – 10^1$

qPCR standard curves were generated using A1-digested pBL4.8x2 DNA as DNA templates without, and with added undigested or *Eco*RI-digested NDL DNA to standardise the total amounts of DNA template present in each qPCR reaction to 150 ng. NDL DNA was extracted from NDL samples using the DNeasy blood and tissue kit as described in Section 2.6.1. For the *Eco*RI-digested NDL DNA, A1-digestions were performed as described in Section 3.2.6.

DHBV total and cccDNA qPCR assays were performed using the 423 – 576c or MG1 – CC2 primer sets respectively as described in Section 2.8.9. The qPCR standard curves and the corresponding data (slope, Y-intercept, R^2 value, the range of detectable copy numbers of plasmid DNA serial dilution) were generated using the StepOne Plus software.

Table 3.2.5: Summary of the slope, Y-intercept, R^2 value, and range of detectable copy numbers of plasmid DNA serial dilution obtained from the DHBV total and cccDNA qPCR standard curves.

DHBV total DNA qPCR				
Plasmid	**Slope**	**Y-intercept**	**R^2 value**	**Detectable plasmid DNA copy numbers**
pBL4.8x2	-3.542	39.526	0.998	$10^8 – 10^1$
pBL4.8	-3.618	43.212	0.999	$10^8 – 10^2$

DHBV cccDNA qPCR				
Plasmid	**Slope**	**Y-intercept**	**R^2 value**	**Detectable plasmid DNA copy numbers**
pBL4.8x2	-3.388	38.880	0.996	$10^8 – 10^1$
pBL4.8	-3.492	42.656	0.999	$10^8 – 10^3$

qPCR standard curves were generated using A1-digested pBL4.8x2 or pBL4.8 plasmid DNA templates as described in Section 3.2.7.1. DHBV total and cccDNA qPCR assays were performed using the 423 – 576c or MG1 – CC2 primer sets respectively as described in Section 2.8.9. The qPCR standard curves and the corresponding data (slope, Y-intercept, R^2 value, the range of detectable copy numbers of plasmid DNA serial dilution) were generated using the StepOne Plus software.

Figure 3.2.1: Map of (A) pBL4.8x2 plasmid and (B) pBL4.8 plasmid.

Both plasmids were created by Triyatni (Triyatni, 1998), by cloning full-length AusDHBV DNA (3027 bp, GenBank Accession AJ006350) into the pBluescript KS II (+) plasmid vector (2961 bp) at the *Eco*RI site at 3027/1 nt.

Arrow heads of the AusDHBV genome represent the 5' – 3' direction of the AusDHBV, which were numbered (1 nt) from the *Eco*RI site at the 5' end of the AusDHBV.

The approximate binding sites of qPCR primer sets, 423 – 576c and MG1 – CC2 (refer Table 2.2), for the amplification of DHBV total and cccDNA respectively, are also shown.

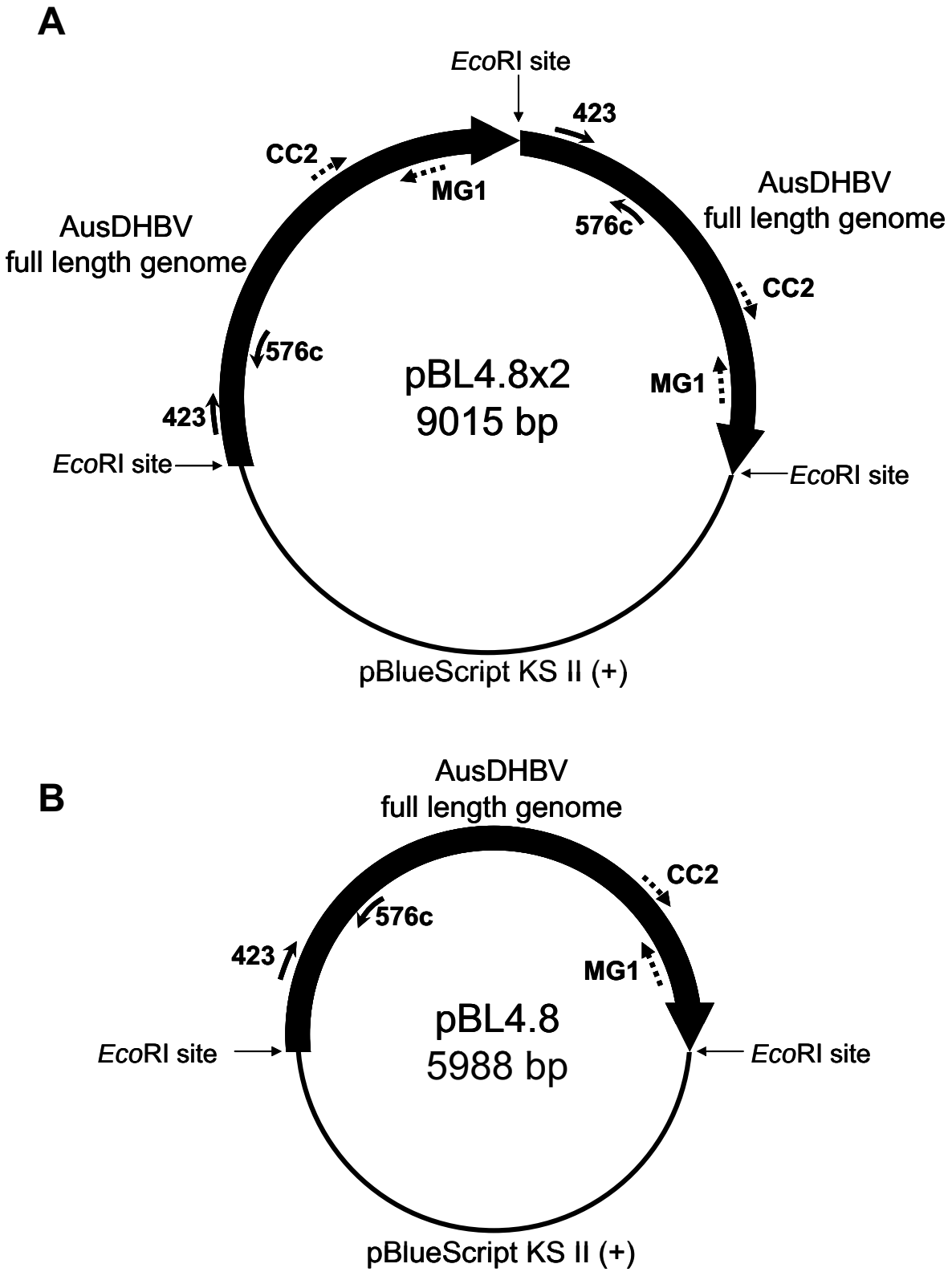

A
EcoRI site
423
CC2
MG1
AusDHBV
full length genome
576c
AusDHBV
full length genome
CC2
576c
pBL4.8x2
9015 bp
MG1
423
EcoRI site
EcoRI site
pBlueScript KS II (+)
B
AusDHBV
full length genome
CC2
576c
423
MG1
pBL4.8
5988 bp
EcoRI site
EcoRI site
pBlueScript KS II (+)

Figure 3.2.1

Figure 3.2.2: Examples of qPCR melt curves from qPCR assays to detect (A) DHBV total DNA or (B) DHBV cccDNA, showing the expected Tm peaks of 79.24^{o}C and 75.82^{o}C respectively.

qPCR reactions were performed as described in Section 2.8.9, using pBL4.8x2 plasmid as DNA template. The 423 – 576c primer set was used to amplify DHBV total DNA, while the MG1 – CC2 primer set was used to amplify DHBV cccDNA. The qPCR melt curves were generated using the StepOne Plus software (AB, USA).

Each qPCR product amplified would have a specific Tm peak in the qPCR melt curve. The expected Tm for each DHBV total and cccDNA PCR products were calculated using the online program BioMath Calculators for Oligos, accessible at http://www.promega.com/biomath/calc11.htm.

The single Tm peak observed in Figures 3.2.2.A and 3.2.2B represent that only a single qPCR product was amplified in the qPCR assay. Figure 3.2.2C is a merged qPCR melt curve as an example of how the different Tm peaks produced by the DHBV total and cccDNA qPCR products could be used to identify the respective qPCR products.

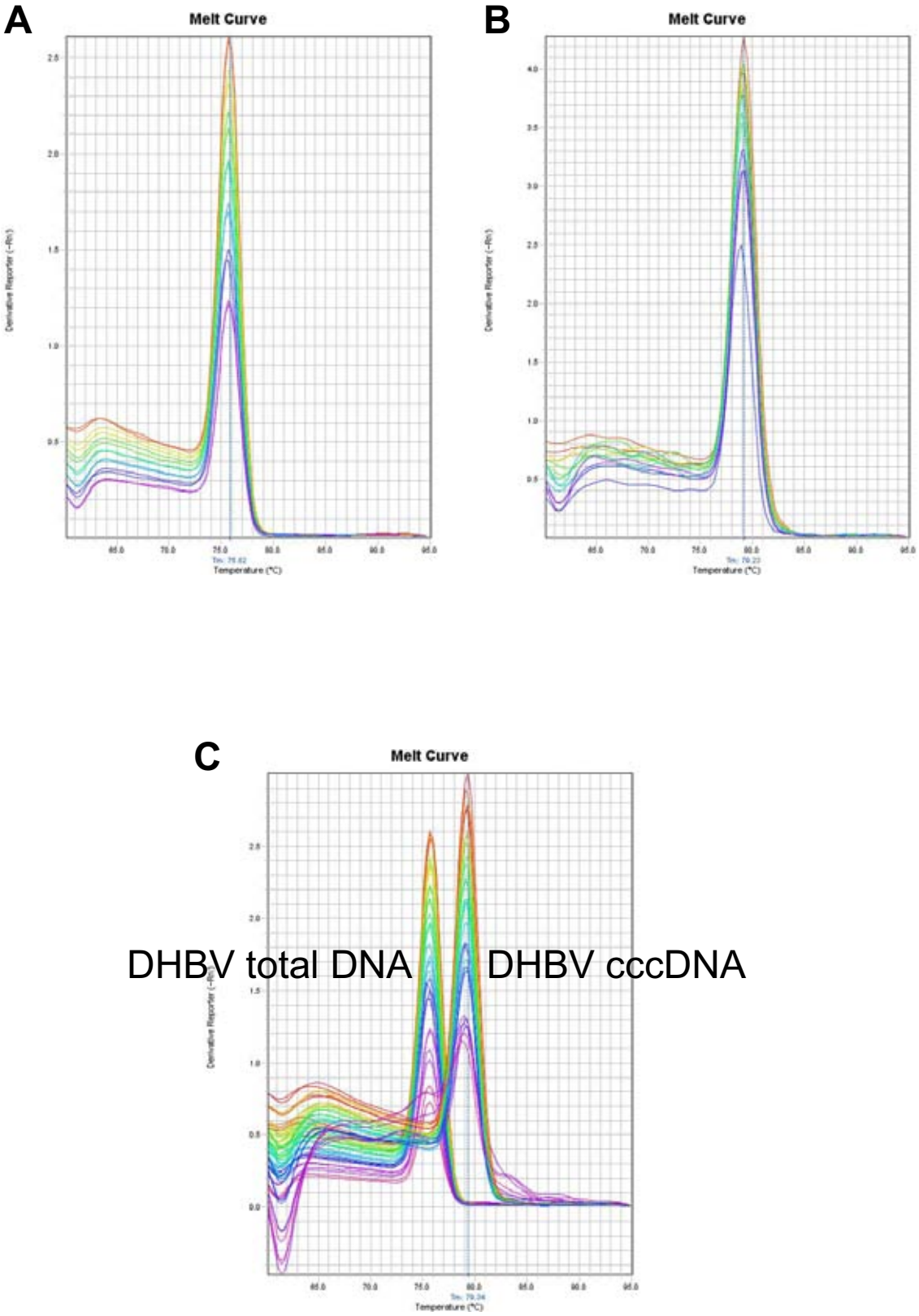

A
Melt Curve
Temperature (°C)
B
Melt Curve
Temperature (°C)
C
Melt Curve
DHBV total DNA
DHBV cccDNA
Temperature (°C)

Figure 3.2.2

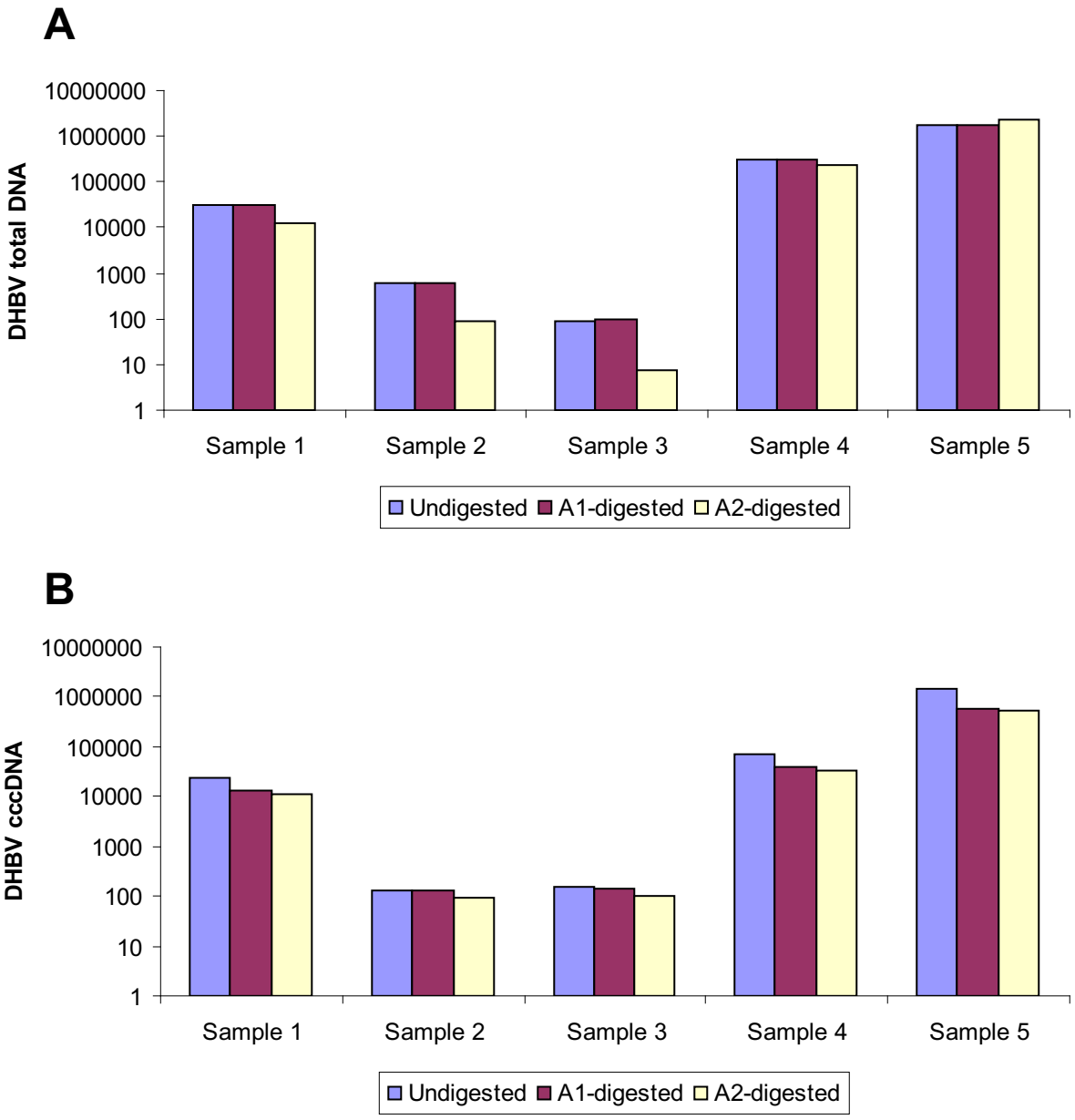


Figure 3.2.3: Levels of (A) DHBV total DNA and (B) DHBV cccDNA in duck liver Samples 1 to 5 quantitated based on qPCR standard curves generated using undigested, A1- and A2-digested pBL4.8x2 plasmid DNA templates.

qPCR standard curves were generated using undigested, A1- and A2-digested pBL4.8x2 DNA as DNA templates as described in Section 3.2.3.2. Samples 1 to 5 DNA were extracted from 5 DHBV-infected duck liver tissues using the DNeasy blood and tissue kit as described in Section 2.6.1. DHBV total and cccDNA qPCR assays were performed using the 423 – 576c or MG1 – CC2 primer sets respectively as described in Section 2.8.9.

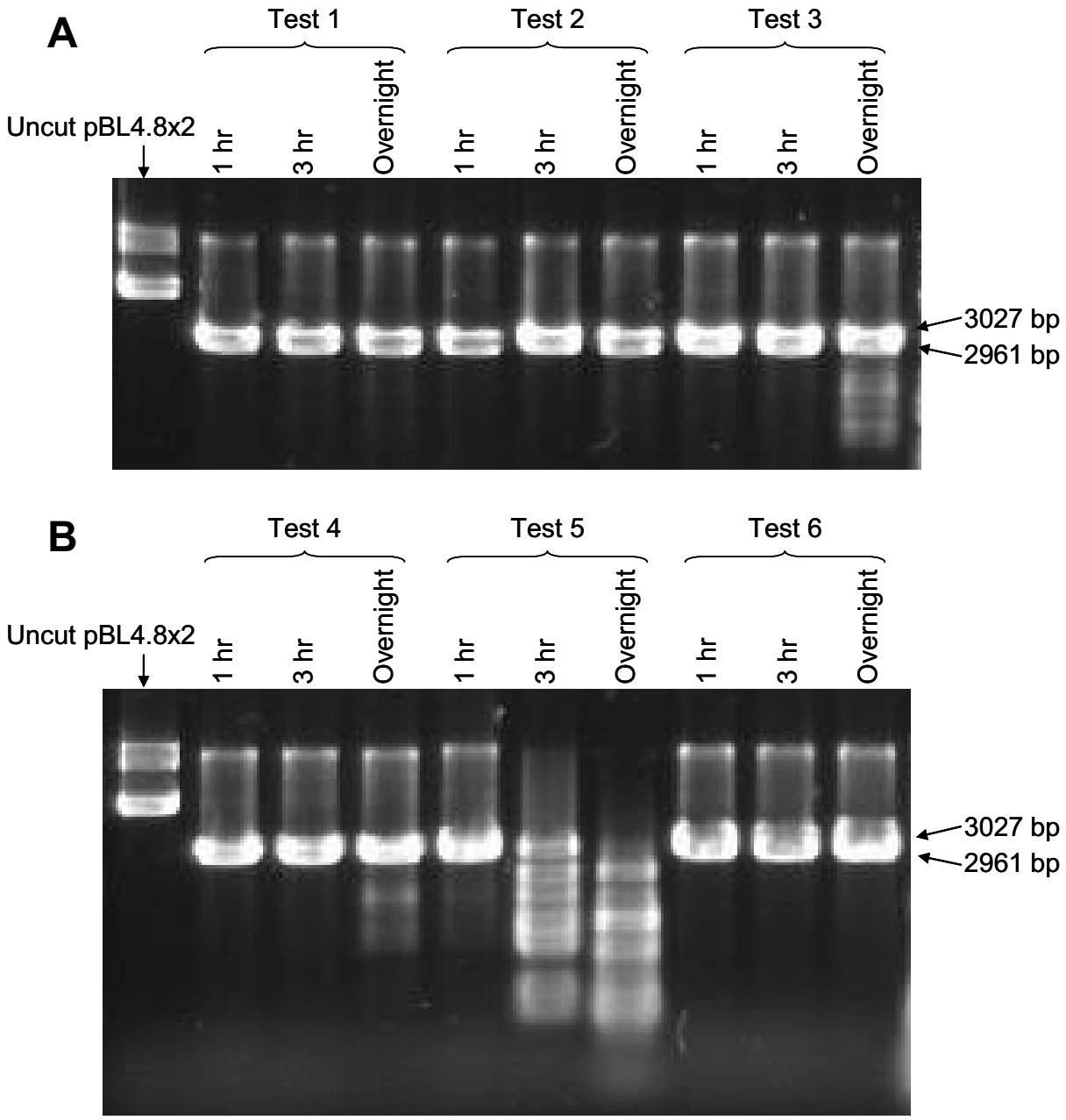


Figure 3.2.4: *Eco*RI-digested pBL4.8x2 plasmid visualised using agarose gel electrophoresis under 302 nm UV light.

pBL4.8x2 plasmid was digested using 6 different conditions (Tests 1 to 6) as described in Section 3.2.4.1. All digested plasmid DNA were visualised by GelRed-stained agarose gel electrophoresis as described in Section 2.8.7. It is expected that *Eco*RI digestion of pBL4.8x2 would produce 3 fragments of 2961, 3027 and 3027 bp in size.

Some star activity was observed in overnight incubations of Test 3 and 4 as seen by the multiple smaller-sized bands, while significant over-digestions or maybe non-specific digestions have occurred in 3 hr and overnight incubations of Test 5 as seen by the multiple smaller-sized bands..

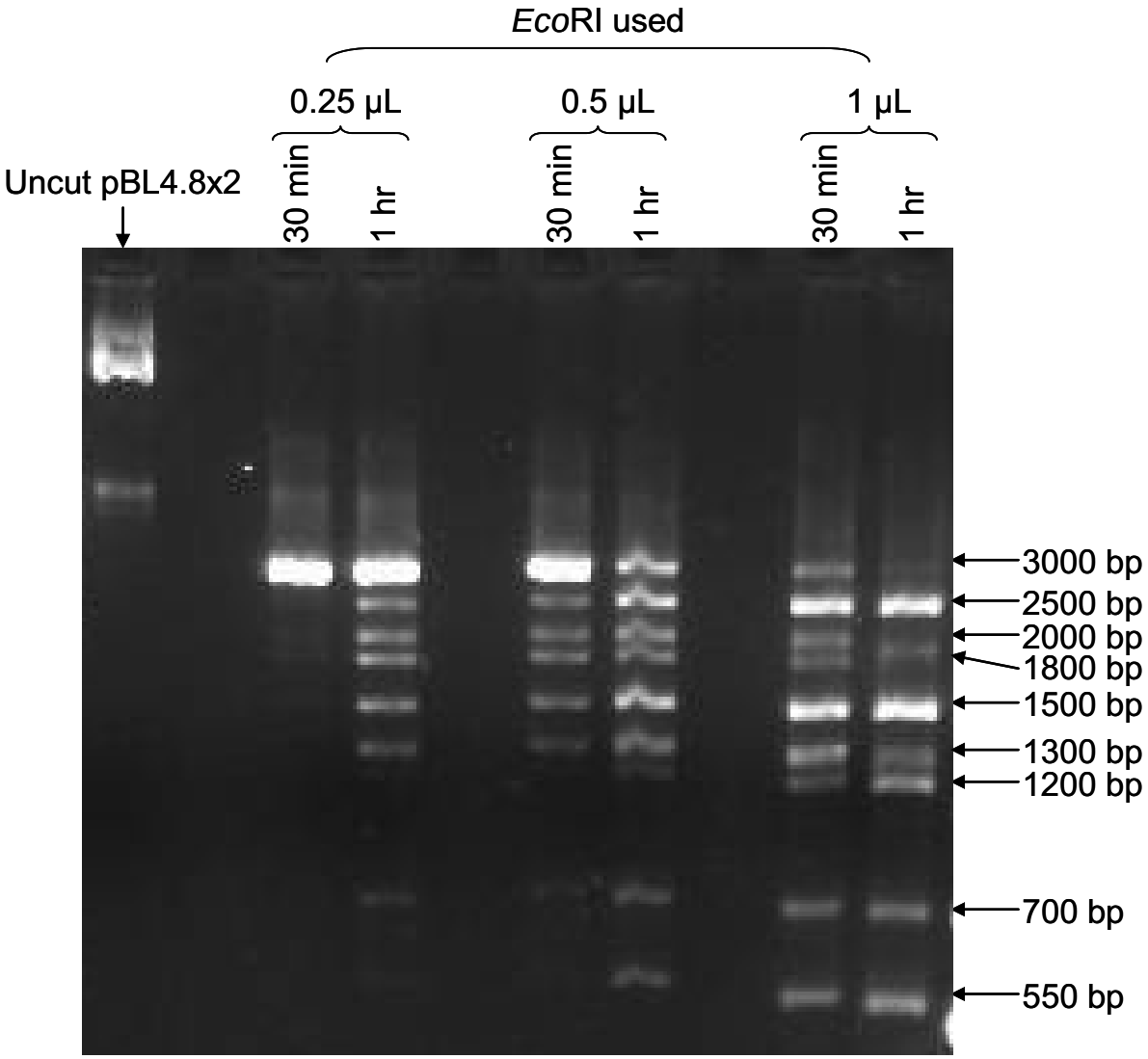


Figure 3.2.5: *Eco*RI-digested pBL4.8x2 plasmid visualised using agarose gel electrophoresis under 302 nm UV light.

pBL4.8x2 plasmid was digested in 1X qPCR SYBR Green mastermix using various amounts of *Eco*RI, at 30 min or 1 hr incubation as described in Section 3.2.4.1. All digested plasmid DNA were visualised by GelRed-stained agarose gel electrophoresis as described in Section 2.8.7. It is expected that *Eco*RI digestion of pBL4.8x2 would produce 3 fragments of 2961, 3027 and 3027 bp in size.

Other than pBL4.8x2 digestion using 0.25 µL (5 U) of *Eco*RI for 30 min, some over-digestions or maybe even non-specific digestions may have occurred as seen by the multiple smaller-sized bands.

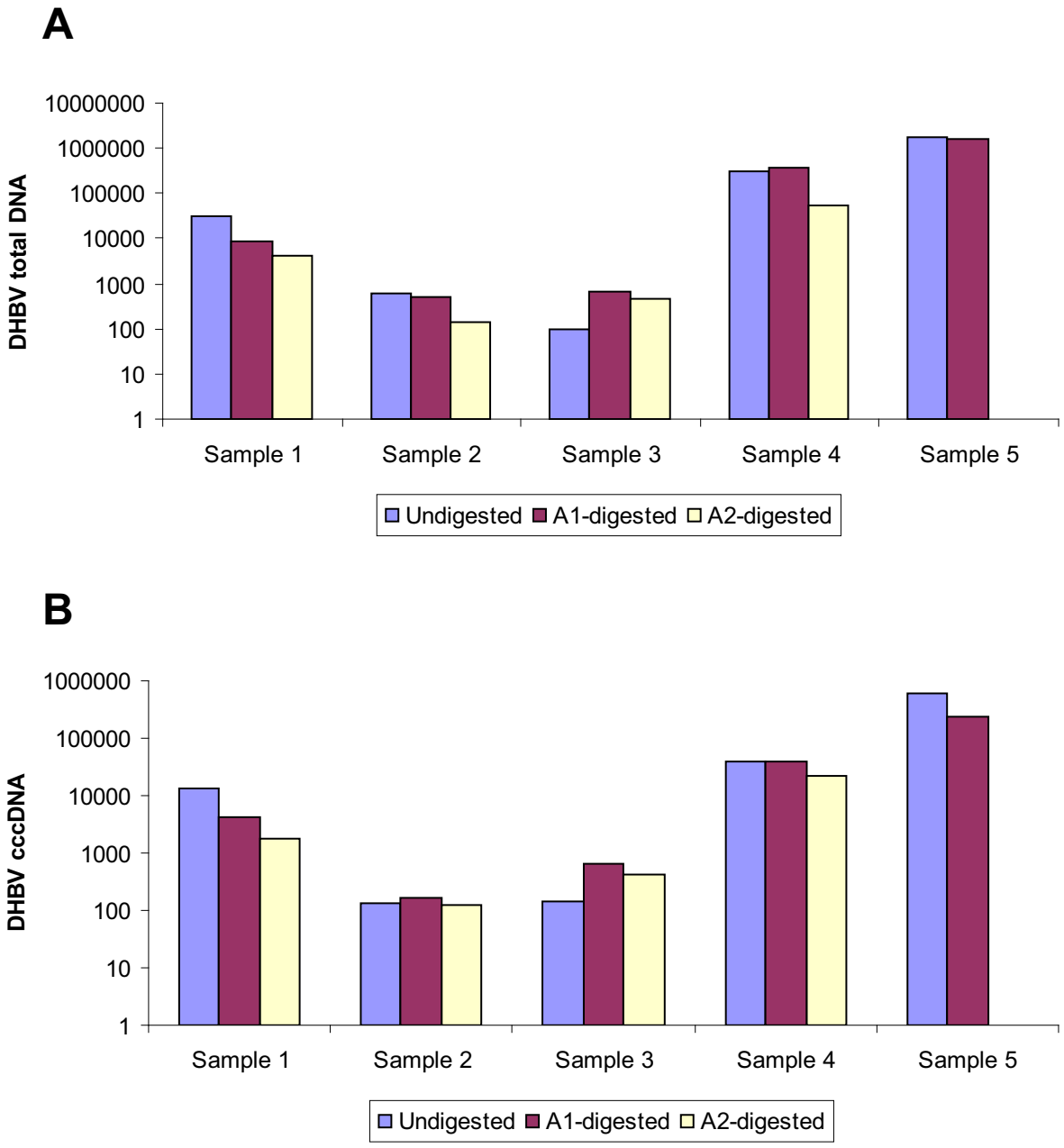


Figure 3.2.6: Levels of (A) DHBV total DNA and (B) DHBV cccDNA in duck liver Samples 1 to 5 quantitated from undigested, A1- and A2-digested duck liver DNA templates.

Samples 1 to 5 DNA were extracted from 5 DHBV-infected duck liver tissues using the DNeasy blood and tissue kit as described in Section 2.6.1, and A1- or A2-digested as described in Section 3.2.5. DHBV total and cccDNA qPCR assays were performed using the 423 – 576c or MG1 – CC2 primer sets respectively as described in Section 2.8.9, with qPCR standard curves generated using A1-digested pBL4.8x2 plasmid DNA templates.

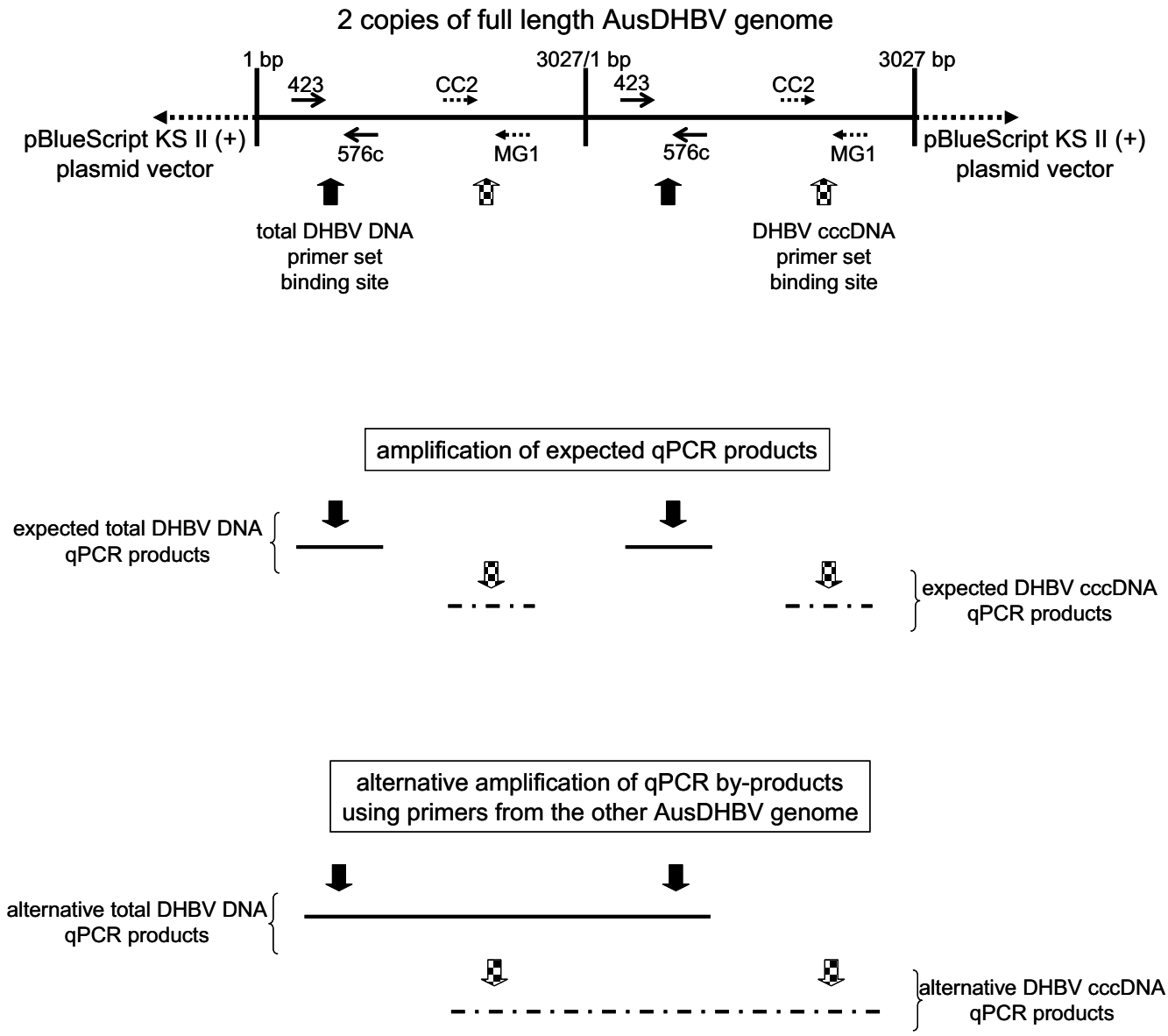


Figure 3.2.7: Illustration of the amplification of the expected and alternative DHBV total and cccDNA qPCR products from the pBL4.8x2 plasmid DNA template, using the 423 – 576c and MG1 – CC2 primer sets respectively.

The binding sites of qPCR primer sets, 423 – 576c and MG1 – CC2 on the pBL4.8x2 were shown (pBluescript KS II (+) plasmid vector not shown in this Figure). pBL4.8x2 was numbered (1 nt) from the *Eco*RI site at the 5' end of the AusDHBV.

Two qPCR products were expected for the amplification of both DHBV total and cccDNA from each pBL4.8x2 DNA template (157 bp and 154 bp in length respectively). However, using the other primer set from the other AusDHBV genome, an alternative AusDHBV qPCR by-product (~3180 bp) may also be amplified.

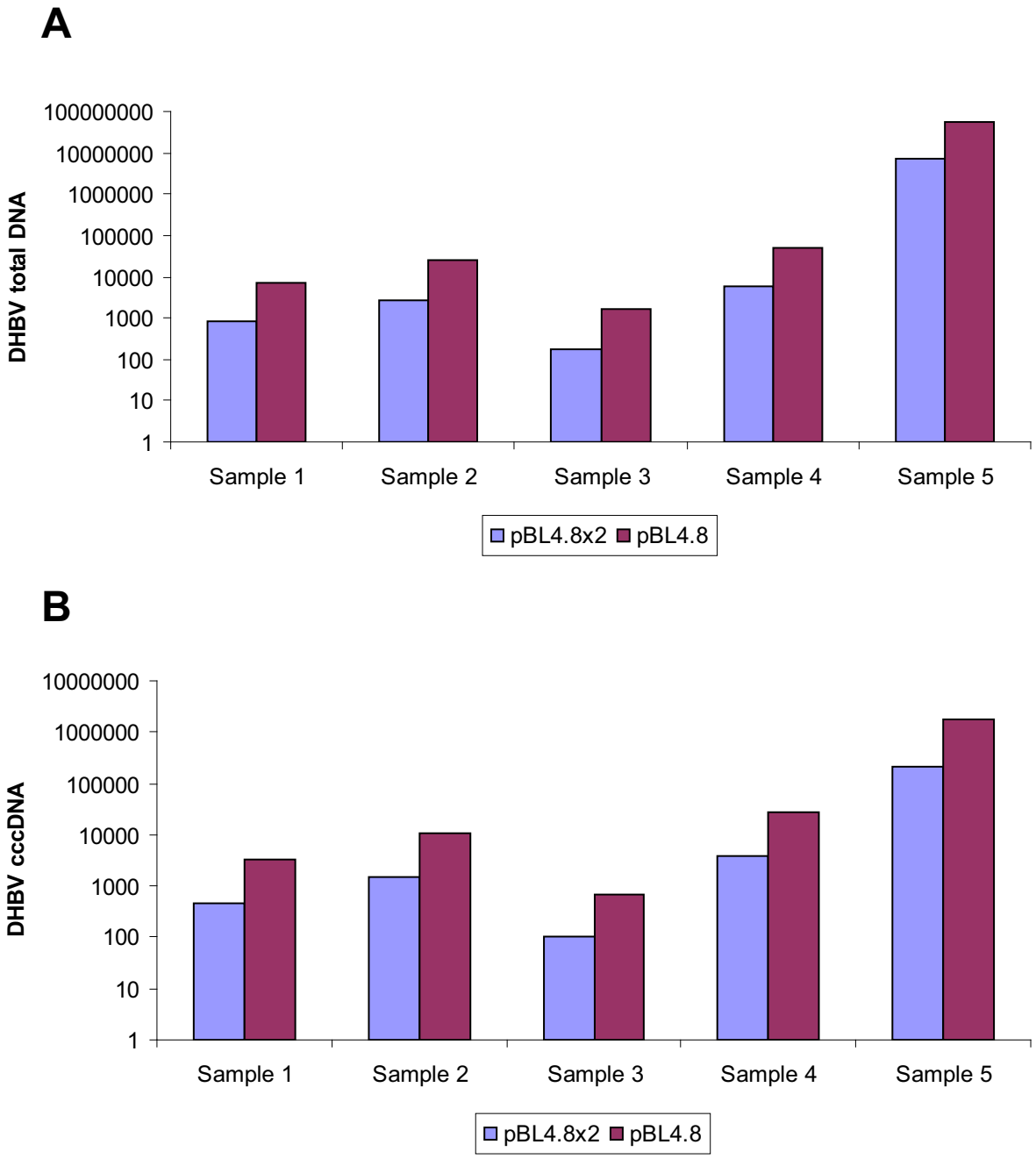


Figure 3.2.8: Levels of (A) DHBV total DNA and (B) DHBV cccDNA in duck liver Samples 1 to 5 quantitated based on qPCR standard curves generated using A1-digested pBL4.8x2 or pBL4.8 plasmid DNA templates.

qPCR standard curves were generated using A1-digested pBL4.8x2 or pBL4.8 plasmid DNA templates as described in Section 3.2.7.2. Samples 1 to 5 DNA were extracted from 5 DHBV-infected duck liver tissues using the DNeasy blood and tissue kit as described in Section 2.6.1. DHBV total and cccDNA qPCR assays were performed using the 423 – 576c or MG1 – CC2 primer sets respectively as described in Section 2.8.9.

Chapter 4: Development of Methods - Establishment and optimisation of qPCR assays for the detection of duck DNA

4.1. Aim

a) To amplify and sequence the duck genes, beta actin (β actin) and glyceraldehyde-3-phosphate dehydrogenase (GAPDH).
b) To clone the duck genes, β actin and GAPDH, into plasmid DNA vectors.
c) To establish and optimise qPCR assays for the detection of duck β actin and GAPDH.
d) To determine the copy number of the duck β actin and GAPDH genes per duck liver cell.

4.2. Introduction

Real-time qPCR assays have recently become one of the most common and effective assays used to quantify the relative or absolute copy number of a gene of interest present in a preparation of DNA. For example, the quantities of DHBV total and cccDNA present in a DNA sample could be determined by qPCR assays, as described in detail in Chapter 3.2. In qPCR assays, one of the issues faced is the variability in the actual amount of DNA added as template to each qPCR reaction. For instance, 150 ng of DNA prepared using standard protocols described in Section 2.8.9, and quantitated using Nanodrop spectrometry as described in Section 2.8.1, was used as DNA template for each qPCR reaction. However, the added DNA template may not correspond to 150 ng of duck liver DNA. This could be due to possible errors and inaccuracies during dilutions of the DNA sample, but more importantly could be due to the non-specific nature of the Nanodrop spectrometer that quantitates DNA by measuring absorbance at 260 nm, and thus DNA as well as RNA present in a sample would be measured. Therefore, the amount of actual DNA would vary from the quantitated amount, resulting in variable amounts of DNA template added to each qPCR reaction.

To overcome this issue, qPCR assays can be normalised against a reference gene (normally a housekeeping gene) found in the duck cell DNA. These reference genes are commonly referred to as the qPCR endogenous or internal controls, and are generally single copy genes present in every cell. Hence, the number of copies of the internal control gene present in a DNA extract can be used to calculate the number of cell equivalents present in each qPCR reaction, and by normalising the qPCR assays with the internal controls, variations in the amount of DNA template can be corrected to allow for accurate quantification of target genes.

Reverse transcription qPCR (RT-qPCR) assays have been routinely used to quantify gene expression in human studies, and some of the commonly used RT-qPCR internal controls include: β actin, GAPDH, hypoxanthine-guanine phosphoribosyl transferase I (HPRT1), albumin, and TATA-binding protein (TBP) (Huggett *et al.*, 2005; Fu *et al.*, 2009). The commonly used internal controls for RT-qPCR assays performed in chicken and duck animal models are the β actin (Bishop *et al.*, 2000; Ni *et al.*, 2006; De Boever *et al.*, 2008), and the GAPDH genes (Zhang *et al.*, 2008; Zimmerman *et al.*, 2008; Barber *et al.*, 2010).

In the Hepatitis Research Laboratory, internal controls for duck mRNA RT-qPCR assays were established by Dr. Georget Reaiche using duck β actin mRNA (GenBank Accession X00182) and GAPDH mRNA (GenBank Accession AY436595) (Reaiche, 2008). However, no internal controls had been established for duck cell DNA qPCR assays. This was partly due to the duck genome which has not been fully sequenced to date. Therefore, this Chapter aimed to amplify and sequence the duck β actin and GAPDH genes, and to develop qPCR assays using those genes. These qPCR assays could then be used as internal controls as well as to quantitate the amount of duck cell equivalents present in a DNA sample.

β actin and GAPDH are important housekeeping genes that are essential for the function and survival of cells. Briefly, the β actin gene encodes the β actin protein, which is one of the six isoforms of the actin protein (Vandekerckhove and Weber, 1978). Actins are one of the most abundant proteins present in most eukaryotic cells, and are highly conserved across most eukaryotes (Vandekerckhove and Weber, 1978; Bulinski, 2006). Mainly cytoplasmic, β actin proteins are essential cytoskeleton proteins that are involved in muscle contraction, cell mobility, cell motility, cytokinesis, and maintenance of cell shape and integrity (Ghosh *et al.*, 2008). Recently, actins have also been speculated to be involved in gene expression due to their ability to bind to nucleotides (Skarp and Vartiainen, 2010). On the other hand, the GAPDH gene encodes the tetrameric GAPDH protein (Biesecker *et al.*, 1977), which is highly conserved and constitutively expressed in many cell types, and especially high levels in fast-twitch muscle fibres (Stone *et al.*, 1985). Specifically, GAPDH is a glycolytic enzyme that catalyses the phosphorylation and oxidation of glyceraldehyde-3-phosphate to 1,3-biphosphoglycerate with the help of the coenzyme NAD^+ (nicotinamide adenine dinucleotide) during glycolysis (Sirover, 1999). Recently, the GAPDH protein has also been reported to play a role in various activities including apoptotic cell death and carcinogenesis, though the actual mechanisms of their involvement are still largely unknown (Colell *et al.*, 2009).

4.3. Amplification and sequencing of duck genes

4.3.1. Previous work performed to amplify and sequence the duck β actin gene

During work performed in my honours year, a ~1 kbp duck β actin gene was successfully amplified from NDL DNA using primer set β actin F – β actin R (Table 2.2). The primer set was designed by Bishop *et al.* (Bishop *et al.*, 2000) based on the chicken β actin mRNA sequence (GenBank Accession L08165), and had been used to amplify duck β actin mRNA Tduring RT-qPCR (Bishop *et al.*, 2000; Reaiche, 2003). The 1023 bp PCR product was subsequently sequenced, and the results were reported in my Honours thesis (Low, 2006). This duck β actin gene PCR product was used for further analysis in Section 4.4.1.

4.3.2. Amplification and sequencing of the duck GAPDH gene

Previously, attempts to amplify duck GAPDH from NDL DNA using primer set GAPDH F – GAPDH R (refer Table 2.2) were unsuccessful. The primers were designed by Dr. Georget Reaiche based on the conserved regions of human, chicken and pigeon GAPDH, and have been routinely used in the Hepatitis Research Laboratory to amplify a 801 bp region of the duck GAPDH mRNA (GenBank Accession AY436595) (Reaiche, 2003). These results were reported in my Honours thesis (Low, 2006) and will be further discussed in Section 4.3.2.2.

Subsequently, to amplify the duck GAPDH gene, PCR primers from another avian species, chicken (*Gallus gallus*), designed by Siegneres *et al.* (Seigneres *et al.*, 2003) were used. The chicken sequence was chosen as chickens have a close evolutionary relationship with ducks, both belonging in the same Aves class, as well as being classified under the same Galloanserae clade in the phylogenetic tree of birds (Hackett *et al.*, 2008). In addition, the chicken sequence is the most extensively analysed avian species, and is one of the first non-mammalian vertebrate to have its full genome sequenced (Schmid *et al.*, 2000; International Chicken Genome Sequencing Consortium, 2004; International Chicken Polymorphism Map Consortium, 2004). Therefore, PCR primers for duck genes have been commonly designed based on chicken sequence, including the β actin PCR primers as described in Section 4.3.1.

4.3.2.1. Amplification and sequencing of a short fragment of the duck GAPDH gene, using known chicken GAPDH primers

The primer set used by Siegneres *et al.* (Seigneres *et al.*, 2003) to amplify the chicken GAPDH cDNA, designated as chicken GAPDH F and chicken GAPDH R (Table 2.2), was used to amplify the duck GAPDH gene from NDL DNA as described in Section 2.8.5. The NDL DNA was extracted by the total DNA extraction method described in Section 2.6.3. After that, PCR products were visualised by gel electrophoresis as described in Section 2.8.7.

Results (data not shown) showed that a ~300 bp PCR product was successfully produced from the amplification of NDL DNA using the chicken GAPDH F – chicken GAPDH R primer set. The PCR product was subsequently sequenced as described in Section 2.8.10, and a 251 bp sequence was obtained. To ensure that the amplified and sequenced PCR product was indeed the expected duck GAPDH gene, the sequence was aligned with the duck GAPDH mRNA sequence (GenBank Accession AY436595). As reference, the amplified PCR product was also aligned with sequences from chicken, specifically the chicken GAPDH gene (GenBank Accession NC_006088), and the chicken GAPDH mRNA sequence (GenBank Accession K01458). The alignment of the four sequences was performed as described in Section 2.8.12.

As shown in Figure 4.1, the DNA sequence alignment scores indicated that the 251 bp sequenced PCR product had 99% coverage with 82% sequence similarity with the chicken GAPDH sequence, and 51% coverage with 93% sequence similarity (excluding gap regions) for the chicken GAPDH mRNA sequence. The high percentage of sequence coverage and similarity suggest a close evolutionary relationship between these two avian species, as well as the high conservation of the GAPDH genes across the two species, thus confirming that the chicken genomic sequences can indeed be a good reference for the still largely unknown duck genomic sequence. In addition, as the 251 bp sequenced PCR product had 56% coverage with 99% sequence similarity (excluding gap regions) for the duck GAPDH mRNA sequence, this also confirmed that the sequenced PCR product was indeed part of the duck GAPDH gene.

Based on the multiple sequence alignment (Figure 4.1), a “gap” was observed in the duck and the chicken GAPDH mRNA sequences between 110 to 220 nt of the duck and chicken GAPDH gene. This “gap” is likely to be a 111 bp intron site of the GAPDH gene, suggesting that the splice sites in the duck GAPDH gene were similar to the chicken GAPDH gene.

In summary, a 251 bp duck GAPDH gene was successfully amplified from NDL DNA using chicken GAPDH primer sets. The duck GAPDH gene showed a high level of sequence homology to the chicken GAPDH gene, and contained a 111 bp intron site that was also found in the chicken GAPDH gene. This also showed that the chicken GAPDH gene is a suitable reference sequence for further characterisation of the duck GAPDH gene

4.3.2.2. Amplification of a ~1 kbp fragment of the duck GAPDH gene, using primers designed based on the chicken GAPDH sequence

At least 1 kpb of the duck GAPDH gene was amplified using PCR primers designed based on the published chicken GAPDH sequence as reference. The amplified duck GAPDH gene is then to be cloned into plasmid vectors as DNA template to generate qPCR standard curves.

Alignment (alignment not shown) of chicken GAPDH gene (GenBank Accession NC006088) and chicken GAPDH mRNA sequence (GenBank Accession K01458) showed that the chicken GAPDH gene had frequent splice sites and consist of ~100 bp exons intermitted with ~100 bp introns. Therefore, it could be inferred that the duck GAPDH gene highly likely also contained similar patterns of short ~100 bp exons intermitted with short ~100 bp introns.

Based on the chicken GAPDH gene, new primers were designed to amplify ~1 kbp of the duck GAPDH gene, and were designated as duck GAPDH gF and duck GAPDH gR (refer Table 2.2). These primers were then used to amplify the duck GAPDH gene from NDL DNA as described in Section 2.8.9. As comparison, the primers were also used to amplify the duck GAPDH mRNA sequence from duck NDL cDNA prepared by Dr. Georget Reaiche (Reaiche, 2008). PCR products were visualised by gel electrophoresis as described in Section 2.8.7.

Results (data not shown) showed that the duck GAPDH gF – duck GAPDH gR primer set amplified a ~1 kbp PCR product from NDL DNA and a ~500 bp PCR product from duck cDNA. This once again confirms the high homology of the GAPDH sequence between the chicken and duck species. In addition, the difference in PCR product sizes produced from NDL DNA (genomic DNA) and cDNA (mRNA) suggests that there are up to 500 bp of introns present in this amplified fragment of duck GAPDH gene. Sequencing of both GAPDH PCR products using the same duck GAPDH gF and duck GAPDH gR primer set as described in Section 2.8.10 produced a 957 bp sequence for the duck GAPDH PCR product, and a 528 bp sequence for the duck GAPDH mRNA PCR product. Each sequence was analysed by aligning the duck GAPDH PCR product with the chicken GAPDH gene (GenBank Accession NC006088), and the duck GAPDH mRNA PCR product with the duck GAPDH sequence (GenBank Accession AY436595) as described in Section 2.8.12. As expected (alignment data not shown), alignment with the chicken GAPDH showed 99% coverage with 79% sequence similarity, while alignment with the duck GAPDH mRNA showed 50% coverage with 99% sequence similarity (excluding gap regions), confirming that the duck GAPDH sequence had been successfully amplified and sequenced from the NDL DNA and cDNA.

The successfully amplified duck GAPDH PCR product was subsequent used for further experiments and analysis as described in Sections 4.4.2.1 and 4.4.2.2 below.

In a separate note, based on the highly-spliced duck GAPDH gene, it was suggested that the failure of amplification of duck GAPDH using the duck GAPDH mRNA primers GAPDH F and GAPDH R mentioned in Section 4.3.1 was due to the primer(s), by chance, being designed across a duck GAPDH cDNA splice site. This means that the PCR primers would not be able to bind specifically and strongly onto the duck GAPDH sequences, resulting in the failure of PCR amplification of the duck GAPDH gene. However, by aligning the duck GAPDH mRNA primers with the chicken GAPDH gene, it was found that both the GAPDH F and GAPDH R primers did not bind across a duck GAPDH cDNA splice site, and should have been able to produce a 2089 bp duck GAPDH PCR product (alignment not shown). Hence, the failure of the first attempt to amplify duck GAPDH gene using the duck GAPDH mRNA primers GAPDH F and GAPDH R in Section 4.3.1 was likely due to technical problems, like insufficient PCR extension time used (1 min 30 sec instead of the optimal 2 min 30 sec for a ~2100 bp PCR product). To avoid similar problems in subsequent PCR reactions, longer PCR extension times will be used as described in Section 2.8.5.

4.4. Production and analysis of plasmids containing duck β actin and GAPDH genes

During qPCR assays, standard curves are generated using serial dilutions of known copy numbers of plasmids that contain the qPCR gene of interest. In the current study, to generate a qPCR assay for the duck β actin and GAPDH genes, plasmids that contain the duck β actin gene or the duck GAPDH gene were produced by cloning the amplified duck β actin PCR product (Section 4.3.1) and duck GAPDH PCR product (Section 4.3.2.2) into the plasmid vector TOPO pCR 2.1 as described below. After the plasmids were successfully cloned, glycerol stocks of the plasmids were produced as described in Section 2.9.3, and large scale plasmids extraction were carried out using Jetstar Maxiprep as described in Section 2.7.2.

4.4.1. Duck β actin gene

4.4.1.1. Production and analysis of pT2.1DgB plasmid containing duck β actin gene

The ~1 kbp duck β actin PCR product amplified from NDL DNA using primers β actin F and β actin R (described in Section 4.3.1) was purified using QIAquick PCR purification kit as described in Section 2.8.6, then observed by agarose gel electrophoresis as described in Section 2.8.7 (data not shown), to verify that the duck β actin PCR product was retained and was not lost during purification. After cloning into the pCR 2.1-TOPO plasmid vector (plasmid map shown in Figure 2.5) and transformation into *E. coli* as described in Section

2.9.1, ~30 white bacterial colonies were produced. Plasmid DNA was subsequently extracted from two of the white colonies using Qiagen Mini Prep kit as described in Section 2.7.1, and plasmid were designated as pT2.1DgB1 (from colony 1) and pT2.1DgB2 (from colony 2).

The extracted plasmid DNA was analysed as described in Section 2.9.2 by PCR amplification using the β actin F – T7 or β actin R – T7 primer sets (refer Table 2.2) to determine the orientation of the cloned DNA insert in relation to the *lacZ* promoter present in pCR 2.1-TOPO, and by *Eco*RI digestion to verify the size of the DNA insert. Finally the sequence of the cloned insert was determined as described in Section 2.9.2.

As shown in Figure 4.2 (only pT2.1DgB1 results shown), *Eco*RI digestion of both pT2.1DgB1 and pT2.1DgB2 plasmid produced a ~4000 bp and a ~1100 bp DNA band. This confirmed that in both of the plasmids, cloning of a ~1000 bp PCR product into the 3900 bp TOPO pCR2.1 plasmid vector had occurred. Based on PCR amplification of the duck β actin insert using either the β actin F – T7 or the β actin R – T7 primer sets (Figure 4.3A), it was determined that the duck β actin PCR product was cloned in the forward direction (in relation to the plasmid *lacZ* promoter) for pT2.1DgB1, and in the reverse direction for pT2.1DgB2. As the plasmids were not used for duck β actin protein production but only for qPCR assays in this study, the direction of cloning of the duck β actin PCR product was not critical and would not affect the qPCR assays to be performed. Lastly, sequencing of both plasmids in both forward and reverse directions using the T7 and M13 primers located ~90 bp away from the ends of the cloning site (as shown in Figure 2.5), yielded 1122 bp sequence of the duck β actin gene, which was 99 bp longer than the sequence previously described in Section 4.3.1.

4.4.1.2. Analysis of the cloned duck β actin gene sequence

The 1122 bp sequenced duck β actin gene (Section 4.4.1.1) was aligned with the duck β actin mRNA sequence (GenBank Accession DQ675572) to verify the β actin gene sequence as well as to determine possible mRNA splice sites in the duck β actin gene. As reference, the duck β actin gene sequence was also aligned with the chicken β actin gene (GenBank Accession X00182) and the chicken β actin mRNA sequence (GenBank Accession NM_205518). The alignment of these four sequences was performed as described in Section 2.8.12.

As shown in Figure 4.4, alignment of the sequences identified a “gap” in the duck and the chicken β actin mRNA sequences between 159 to 529 nt. The “gap” likely contains a 371 bp intron site, and shows that the duck and chicken β actin gene not only have high levels of sequence similarity, but also have similar mRNA splice sites. High levels of sequence

homology between the duck and chicken β actin sequences were also indicated by the DNA sequence alignment scores of 100% coverage with 83% sequence similarity.

Lastly, the homology of the duck β actin gene sequence was compared with the β actin gene sequences from other species. This was determined by aligning the 1122 bp duck β actin gene sequence with the β actin genes from humans (GenBank Accession NT_007819), chimpanzees (GenBank Accession NC_006474), mice (GenBank Accession NT_081055) and chickens (GenBank Accession X00182), as described in Section 2.8.12. Alignment with β actin sequences from other avian species, like geese and herons, were not performed as apart from chickens and ducks, no other avian β actin genes have been sequenced to date.

Based on the multiple sequence alignment shown in Figure 4.5, as expected, the duck β actin gene sequence had the highest homology with chickens at 100% sequence coverage with 83% sequence similarity. In comparison, the duck β actin sequence only had 54% coverage with humans and chimpanzees, and only 45% coverage with mice, with a sequence similarity of 79%, 79%, and 85% (excluding the many gap regions) respectively. These high percentages of sequence homology suggest that the β actin gene is relatively conserved across species. In addition, high sequence homology was observed between the closely-related human and chimpanzee β actin sequences, with 100% sequence coverage and 99% sequence similarity. These show that the β actin gene is relatively conserved, with higher sequence homology within the same animal class (in birds or mammals), as compared to the lower sequence homology found between species more distantly related in the evolutionary tree.

In summary, 1122 bp of the duck β actin gene had been successfully amplified, cloned into a plasmid vector, and sequenced. This duck β actin gene sequence contained a 371 bp intron site, and showed high levels of homology (83%) with the chicken β actin sequence. The newly cloned plasmids containing this fragment of duck β actin gene were designated as pT2.1DgB1 and pT2.1DgB2 plasmids, with the duck β actin gene sequence cloned in a forward and reverse direction in relation to the *lacZ* promoter present in pCR 2.1-TOPO respectively (refer Figure 4.6 for plasmid map). The duck β actin gene sequence has been submitted to GenBank and given the Accession number GU564232.

4.4.2. Duck GAPDH gene

4.4.2.1. Production and analysis of pT2.1DgG plasmid containing duck GAPDH gene

The ~1 kbp duck GAPDH PCR product amplified from NDL DNA using primers duck GAPDH gF and duck GAPDH gR (described in 4.3.2.2) was purified using QIAquick PCR

purification kit as described in Section 2.8.6, then observed by agarose gel electrophoresis as described in Section 2.8.7 (data not shown), to verify that the duck GAPDH PCR product was retained and was not lost during purification. After cloning into the pCR 2.1-TOPO plasmid vector (plasmid map shown in Figure 2.5) and transformation into *E. coli* as described in Section 2.9.1, only one white bacterial colony was produced. Plasmid DNA was subsequently extracted from that the white bacterial colony using Qiagen Mini Prep kit as described in Section 2.7.1, and the plasmid was designated as pT2.1DgG.

The extracted plasmid DNA was analysed as described in Section 2.9.2 by PCR amplification using the duck GAPDH gF – T7 or duck GAPDH gR – T7 primer sets (refer Table 2.2) to determine the orientation of the cloned DNA insert in relation to the *lacZ* promoter present in pCR 2.1-TOPO, and by *Eco*RI digestion to verify the size of the DNA insert. Finally, the sequence of the cloned insert was determined as described in Section 2.9.2.

As shown in Figure 4.2, *Eco*RI digestion of pT2.1DgG plasmid produced a ~4000 bp and a ~1050 bp DNA band. This confirmed the successful cloning of the ~1000 bp duck GAPDH PCR product into the 3900 bp TOPO pCR2.1 plasmid vector. Based on PCR amplification of the duck GAPDH insert using either the duck GAPDH gF – T7 primer set or the duck GAPDH gR – T7 primer set (Figure 4.3B), it was determined that the duck GAPDH PCR product was cloned in the reverse direction in relation to the plasmid *lacZ* promoter. Lastly, sequencing of the pT2.1DgG plasmid in both forward and reverse directions using the T7 and M13 primers located ~90 bp away from each end of the cloning site (as shown in Figure 2.5), yielded 1052 bp sequence of the duck GAPDH PCR product.

4.4.2.2. Analysis of the cloned duck GAPDH gene sequence

The 1052 bp sequenced duck GAPDH gene (Section 4.4.2.1) was aligned with two duck GAPDH mRNA sequences: the 738 bp published duck GAPDH mRNA sequence (GenBank Accession AY436595), and the 528 bp duck GAPDH mRNA that was amplified from duck cDNA using the same primer sets as the duck GAPDH, as described in Section 4.3.2.2. This comparison is to verify that the PCR products sequenced in Section 4.3.2.2 were the same as the published duck GAPDH mRNA sequence (GenBank Accession AY436595), as well as to determine possible mRNA splice sites present in the duck GAPDH gene. As reference, the duck GAPDH gene sequence was also aligned with the chicken GAPDH gene (GenBank Accession NC_006088) and the chicken GAPDH mRNA sequence (GenBank Accession K01458). The alignment of these five sequences was performed as described in Section 2.8.12.

As shown in Figure 4.7, multiple sequence alignment identified four distinct gaps in the duck and chicken GAPDH gene. These gaps were found between 89-173, 264-441, 554-665, and 749-921 nt of the duck and chicken GAPDH genes. These "gaps" likely indicate four ~100 bp introns in the GAPDH gene intermittent with ~100 bp of exons. These alignments once again showed high levels of sequence similarity between the duck and chicken GAPDH gene, and confirmed that the duck GAPDH gene contains similar frequently-occurring splice sites as observed in the chicken GAPDH gene (Section 4.3.2.2). On a separate note, the duck GAPDH mRNA amplified and sequenced in Section 4.3.2.2 showed 100% sequence homology with the published duck GAPDH mRNA sequence (GenBank Accession AY436595), confirming that the newly designed primers duck GAPDH gF and duck GAPDH gR could also be used to specifically amplify duck GAPDH mRNA sequence from duck cDNA libraries, and that no significant GAPDH sequence mutations were observed in the duck cDNA library stock.

Lastly, the homology of the duck GAPDH gene sequence was compared with the GAPDH gene sequences from other species. This was determined by aligning the 1052 bp duck GAPDH gene sequence with the GAPDH genes from humans (GenBank Accession NT_009759), chimpanzees (GenBank Accession NC_006479), mice (GenBank Accession NT_039353) and chickens (GenBank Accession NC_006088), as described in Section 2.8.12. Again, alignment with other avian species, like geese and herons, were not performed, as apart from chickens and ducks, no other avian GAPDH genes have been sequenced to date.

Based on the multiple sequence alignment shown in Figure 4.8, revealed, as expected, the duck GAPDH gene sequence had the highest homology with chicken at 99% sequence coverage and 79% sequence similarity. In comparison, the duck GAPDH gene sequence only has 62% coverage with humand and chimpanzees, and 53% coverage with mice, with a sequence similarity of 79%, 79%, and 85% (excluding the many gap regions) respectively. These high percentages of sequence homology suggest that the GAPDH gene is relatively conserved across species. In addition, high sequence homology was observed between the closely-related human and chimpanzee GAPDH sequences, with 100% sequence coverage and 99% sequence similarity. All these sequence homology percentages followed the same trend as the β actin gene (Section 4.4.1.2), confirming that higher sequence homology is observed within the same animal class (in birds or mammals), as compared to the lower sequence homology found between species more distantly related in the evolutionary tree.

In summary, 1052 bp of the duck GAPDH gene was successfully amplified, cloned into a plasmid vector, and sequenced. This duck GAPDH gene sequence contained four ~100 bp

intron sites intermittment with ~100 bp exons, and showed high levels of homology (79%) with the chicken GAPDH sequence. This fragment of duck GAPDH gene was cloned in a reverse direction in relation to the *lacZ* promoter present in pCR 2.1-TOPO, and the plasmid was designated as pT2.1DgG (refer Figure 4.9 for plasmid map). The duck GAPDH gene sequence has been submitted to GenBank and given the Accession number GU564233.

4.4.3. Establishment of qPCR assays for the detection of duck β actin and GAPDH

4.4.3.1. Optimisation of qPCR primers for duck β actin and GAPDH qPCR assays

First, the most suitable qPCR primers to be used to detect duck β actin and GAPDH genes were determined. The most suitable qPCR primers were chosen based on several criteria of the qPCR products produced. Firstly, the primer set should amplify only one qPCR product (high specificity) at the optimum qPCR product size that produces the highest detection sensitivity during qPCR, which is around 150 bp as recommended by the manufacturer of the qPCR machine, AB. In addition, to allow for a better direct comparison between the duck β actin and GAPDH qPCR assays, the qPCR product size, the melting temperature (Tm), guanine:cytosine (G:C) content, and molecular weight (MW) for each duck β actin and GAPDH qPCR product were preferably as similar as possible. By "standardising" these factors, the duck β actin and GAPDH qPCR reactions could have similar amplification sensitivity and efficiency even when quantifying different sequences of interest. An example of such comparisons was the optimisation of qPCR primers to detect DHBV total and cccDNA in duck DNA samples performed by Dr. Georget Reaiche (Reaiche *et al.*, 2010).

Several qPCR primer sets specific for the amplification of duck β actin and GAPDH genes were tested using the pT2.1DgB and pT2.1DgG plasmids (cloned in Sections 4.4.1 and 4.4.2) as qPCR templates, and using qPCR protocols optimised in Chapter 3.2 as described in Section 2.8.9. Examples of melt curves generated from qPCR reactions are shown in Figure 4.10. When the primer set successfully amplified only one qPCR product, only one Tm peak (~78.5^{o}C) was observed (Figure 4.10A). However, if multiple qPCR products, non-specific or no qPCR products were amplified, no distinct Tm peaks or multiple Tm peaks were observed (Figure 4.10B). Individual melt curve diagrams from Sections 4.4.3.1.1 and 4.4.3.1.2 are not shown, but the number of peaks and Tm for each peak produced are summarised in tables.

4.4.3.1.1. Optimisation of qPCR primers for the detection of duck β actin genes using pT2.1DgB plasmid as template

qPCR primers used in the Hepatitis Research Laboratory to detect duck β actin mRNA were the β actin RT F and β actin RT R primers (refer Table 2.2) optimised by Dr. Georget Reaiche

(Reaiche, 2003). However, this primer set would produce a 199 bp qPCR product using the pT2.1DgB plasmid as template, which would be slightly larger than the optimal 150 bp qPCR product size. Therefore, new primers were designed and tested in several primer sets to determine the most suitable qPCR primer sets to amplify duck β actin gene. A summary of qPCR primers used are listed in Table 4.1, while primer sets used are listed in Table 4.2.

Table 4.1: List of primers used to amplify the duck β actin gene from the pT2.1DgB plasmid during qPCR reactions

Primer name[a]	Primer sequence (5' – 3')	Primer position on the duck β actin sequence[b] (5' – 3')
β actin F[c]	aaactaccttcaactccatc	1-20
β actin R[c]	ccttcattcacatctatcac	1122-1103
β actin RT F[d]	ggatcagcaagcaggagtat	577-596
β actin RT R[d]	ccttcaccattccagttttt	775-756
Duck G β actin F	ccctgtgaataatggcattt	318-337
Duck G β actin R	gggagggaagaggtgctcag	490-471
Duck G β actin 2F	gccctgagctaaactcctac	227-246
Duck β actin RT F	gagcgcaagtactctgtctg	510-529
Duck β actin RT R	tcattttgtcacaagggtgt	679-660
Duck β actin RT R2	tgtgggtgttggtaacagtc	662-643

[a]For the primer names, F represents a forward primer, while R represents a reverse primer

[b]Nucleotide numbering were based on the duck β actin (GenBank Accession GU564232)

[c]Primer designed by Bishop *et al.* (Bishop *et al.*, 2000)

[d]Primer designed by Dr. Georget Reaiche (Reaiche, 2003)

Based on the summarised melt curve results in Table 4.2, most primer sets successfully produced a single qPCR product as only a single Tm peak was observed. In addition, based on the qPCR product sizes that were closest to the optimal qPCR product size of 150 bp, primer sets that were suitable were the Duck G β actin F – Duck G β actin R, Duck β actin RT F – Duck β actin RT R2, and Duck β actin RT F – Duck β actin RT R primer sets.

In summary, 3 qPCR primers sets were found to be suitable to be used to amplify duck β actin genes from pT2.1DgB plasmids during qPCR reactions. The most suitable primer set would be determined by the qPCR product that has the most similar Tm, G:C content, and MW with the duck GAPDH qPCR product described in Section 4.4.3.1.2 below.

4.4.3.1.2. Optimisation of qPCR primers for the detection of duck GAPDH genes using pT2.1DgG plasmid as template

qPCR primers used in the Hepatitis Research Laboratory to detect duck GAPDH mRNA were the GAPDH RT F and GAPDH RT R primers (refer Table 2.2) optimised by Dr. Georget Reaiche (Reaiche, 2003). However, the GAPDH RT R primer binding site spans across a duck GAPDH splice site, and thus was not suitable to be used for the detection of duck GAPDH gene. Therefore, new primers were designed and tested in several primer sets to determine the most suitable qPCR primer sets to amplify duck GAPDH gene. A summary of qPCR primers used are listed in Table 4.3, while primer sets used are listed in Table 4.4.

Table 4.3: List of primers used to amplify duck GAPDH from the pT2.1DgG plasmid during qPCR reactions

Primer name[a]	Primer sequence (5' – 3')	Primer position on the duck GAPDH sequence[b] (5' – 3')
GAPDH RT F[c]	tgctaagcgtgtcatcatct	452-471
Duck GAPDH R	tgacaattttcagggacttg	549-530
Duck GAPDH RT F	ggtcacattgagaaccctgt	319-338
Duck GAPDH RT R	gatgatgacacgcttagcac	470-451

[a]For the primer names, F represents forward primer, while R represents reverse primer

[b]Nucleutide numbering were based on the duck GAPDH (GenBank Accession GU564233)

[c]Primer designed by Dr. Georget Reaiche (Reaiche, 2003)

Based on the summarised melt curve results in Table 4.4, both primer sets successfully produced a single qPCR product as only a single Tm peak was observed. Both qPCR product sizes of 97 and 151 bp were also close to the optimal qPCR product size of 150 bp, making both primer sets suitable for qPCR reactions.

In summary, 2 qPCR primers sets were found to be suitable to be used to amplify duck GAPDH from pT2.1DgG plasmid during qPCR reactions.

Lastly, the duck β actin and GAPDH qPCR products produced by the qPCR primer sets found to be suitable in Sections 4.4.3.1.1 and 4.4.3.1.2 respectively were compared, to determine the duck β actin and GAPDH qPCR products that has the most similar product size, Tm, G:C content, and MW. All these information were calculated using the online program BioMath Calculators for Oligos (accessible through http://www.promega.com/biomath/calc11.htm).

Based on the data shown in Table 4.5, the duck β actin and GAPDH qPCR products that had the most similar qPCR product size, Tm, G:C content, and MW were produced by primer set Duck β actin RT F – Duck β actin RT R2 for duck β actin, and Duck GAPDH RT F – Duck GAPDH RT R for duck GAPDH. Their qPCR product size of 153 bp and 152 bp respectively were also the closest to the optimal qPCR product size of 150 bp, and had a Tm of 83^{o}C and 82^{o}C respectively. Therefore, these two primer sets were chosen to respectively amplify duck β actin and GAPDH for subsequent qPCR reactions in this study.

4.4.3.2. Calculation of plasmid copy numbers to generate qPCR standard curves

In qPCR assays, standard curves were commonly generated using a serial dilution of 10^8 – 10^1 copies of the gene of interest (usually cloned into a plasmid vector). Therefore, the pT2.1DgB and pT2.1DgG plasmids could be used to generate qPCR standard curves for the duck β actin and duck GAPDH genes respectively. Using the formula described in Section 2.8.9.3.1, it was calculated that 10^{10} copies of pT2.1DgB (5053 bp) was present in 55.4 ng of that plasmid, while 10^{10} copies of pT2.1DgG (4983 bp) was present in 55.5 ng of that plasmid.

4.4.3.3. Establishment of a qPCR standard curve for duck β actin and GAPDH using pT2.1DgB and pT2.1DgG plasmids

Standard curves for the qPCR detection of duck β actin and GAPDH genes were established using serial dilutions of pT2.1DgB and pT2.1DgG plasmids as template, allowing amplification of ~150 bp of the gene using specific primer sets (Duck β actin RT F – Duck β actin RT R2 or Duck GAPDH RT F – Duck GAPDH RT R) respectively.

All qPCR reactions were performed and analysed as described in Section 2.8.9. Briefly, ~2 µg of plasmid was digested with *Eco*RI as described in Section 2.8.2, and serially diluted with H_2O to 10^8 – 10^1 copies based on calculations shown in Section 4.4.3.2. qPCR reactions were then performed as described in Section 2.8.9, using primer set Duck β actin RT F – Duck β actin RT R2 for duck β actin amplification, or Duck GAPDH RT F – Duck GAPDH RT R for duck GAPDH amplification. qPCR results were then analysed using the StepOne Plus software. As previously defined in Chapter 3.2, the quality of generated qPCR standard curves were determined by 4 parameters of the standard curves, including the slope, the Y-intercept, the R^2 value, and the range of plasmid serial dilution points (from 10^8 – 10^1 copies) detectable during qPCR. Optimally, the standard curve should have slope value between -3.58 and -3.10, Y-intercept C_T value of ~40, R^2 value or coefficient of correlation of >0.99, while all the plasmid serial dilution copy numbers (10^8 – 10^1 copies) should be detected.

qPCR product amplification was specific for both qPCR assays, as a single melt curve Tm peak at 83^{o}C and 82^{o}C for duck β actin and GAPDH genes respectively was produced (Figure 4.11A). Standard curves for the duck β actin and GAPDH qPCR assays were also successfully generated (Figure 4.11B), with high efficiency of qPCR amplification (standard curve slope of -3.516 and -3.625 respectively), high sensitivity (C_T value of 33.169 and 35.778 respectively), and high coefficient of correlation (R^2 value 0.998 and 0.996 respectively). All the plasmid serial dilution copy numbers ($10^8 – 10^1$ copies) were also detected.

However, as shown in Figure 4.11B, the lines of both standard curves did not overlap, which was expected when the same amount of DNA template was quantitated. This suggest that there were still some differences in the sensitivity and efficiency in amplifying and detecting the duck β actin or GAPDH sequences, or that the amount of plasmid DNA template added to the reactions were not exact. Both qPCR assays will be further analysed in Section 4.4.4.

In conclusion, qPCR assays to detect duck β actin and duck GAPDH genes were successfully established using Duck β actin RT F – Duck β actin RT R2 primer set, or Duck GAPDH RT F – Duck GAPDH RT R primer set respectively. qPCR standard curves for duck β actin and GAPDH genes were also successfully established using pT2.1DgB and pT2.1DgG plasmids that contain a ~1 kbp duck β actin and GAPDH gene fragment respectively. Hence, the duck β actin and duck GAPDH genes could be used as internal controls for duck DNA qPCR assays, as well as to quantitate the amount of duck cell equivalents present in a DNA sample.

4.4.4. Determining the copy numbers of duck β actin and GAPDH genes in duck cells

It is unknown whether the duck β actin and GAPDH genes are present as single copy genes in the duck genome. Although these genes have been routinely used as relative internal controls during RT-qPCR assays, there are currently no publications regarding their copy number in ducks. In the chicken genome, it has been reported that chicken β actin (Cleveland *et al.*, 1980) and chicken GAPDH (Stone *et al.*, 1985) are present in chicken cells as single copy genes. Other identified single copy genes in chicken cells include chicken creatine kinase type B gene (Wirz *et al.*, 1990), PROCR endothelial protein C receptor gene (Maruoka *et al.*, 2005), and heart lactate dehydrogenase B-like protein (Hendriks *et al.*, 1988). In ducks, previously reported single copy genes include the duck heart lactate dehydrogenase B-like protein (Hendriks *et al.*, 1988) and the duck serum amyloid A protein (Guo *et al.*, 1996).

Therefore, this Section aims to determine the copy number of duck β actin and duck GAPDH present in liver cells of domestic ducks (*Anas platyrhynchos*), using several methods, including qPCR assays and fluorescence *in situ* hybridisation (FISH) assays.

4.4.4.1. Determining the copy number of duck β actin and GAPDH genes using qPCR

Using the duck β actin and GAPDH qPCR assays optimised in Section 4.4.3, the copy number of β actin and GAPDH gene in various samples of duck and chicken DNA were determined. The amounts of β actin and GAPDH gene quantitated by qPCR were then compared with the expected number of cells present in each sample in order to estimate the copy number of β actin and GAPDH genes, and to determine the fold difference (if any) of each gene present in the cells. Any differences observed would be expected to be in multiples of 2-fold differences, as the cells of ducks and chickens are diploid and therefore each cell would contain 2 homologous copies of each chromosome and hence 2 copies of the same gene. On a separate note, direct comparisons of the β actin and GAPDH qPCR assays could be performed, as qPCR assays for both genes had been "standardised" for possible variable factors that allowed for qPCR reactions with similar amplification sensitivity and efficiency (refer Section 4.4.3).

The duck liver samples used in this Section include NDL and DHBV-infected Pool 7 ducks congenitally infected with the Australian strain of DHBV (AusDHBV, GenBank Accession AJ006350) (Triyatni *et al.*, 2001). DNA was extracted from these liver tissues using the DNeasy blood and tissue kit as described in Section 2.6.1, the amount of DNA present was determined by Nanodrop spectrometry as described in Section 2.8.1, from which 10-fold serial dilutions of the extracted DNA were used as template for qPCR reactions as described in Section 2.8.9, using standard curves generated using the pT2.1DgB or pT2.1DgG plasmids. Based on calculations shown in Section 2.8.9.3.2, the estimated number of liver cells present in each qPCR reaction was determined and shown in Table 4.6.

The chicken DNA samples were extracted from the chicken hepatocellular carcinoma (HCC) cell line, LMH, and its derivative the dstet5 cell line. DNA was also extracted from primary duck hepatocytes (PDH) prepared from the liver of 1 – 2-week-old ducks. Briefly, the LMH cell line was established from a chicken HCC, and the LMH cells retained the differentiated phenotype of a chicken hepatocyte (Kawaguchi *et al.*, 1987); while the dstet5 cell line was produced by cloning plasmids containing the DHBV DNA sequence into LMH cells controlled by a tetracycline-regulated promoter (Guo *et al.*, 2003). Lastly, PDH were prepared by perfusing the liver of a duck before harvesting and culturing the PDH as described in Section 2.13.1. These 3 different cell cultures were specifically chosen in this Section, as the

number of cells in the cell cultures could be counted using present prior to extraction of DNA, thus providing a reliable estimation of the actual number of cells present in the sample.

The LMH, dstet5, and PDH cells were prepared, cultured and harvested with assistance from Dr. Georget Reaiche, Miss Catherine Scougall, Miss Cuixia Wang, and Mr. Qiao Qiao as described in Sections 2.13.1 and 2.13.2. Cells were counted using a haemocytometer as described in Section 2.13.3, before extracting DNA from the harvested cells using DNeasy blood and tissue kit as described in Section 2.13.4. The amount of extracted DNA was then quantified by Nanodrop spectrometry as described in Section 2.8.1, and 150 ng was used as template for each qPCR reaction as described in Section 2.8.9, using standard curves generated using pT2.1DgB or pT2.1DgG plasmid. The estimated number of cells present in each qPCR reaction was determined based on the viable cell counts and the total concentration of extracted DNA as described in Section 2.13.5, and are shown in Table 4.6.

Results (Table 4.6) showed that β actin and GAPDH were present ~5-fold lower and ~2-fold lower than the estimated number of cells present in the NDL DNA or Pool 7 DNA samples respectively. Lower quantifications of both genes were expected, as some losses of DNA were expected during DNA extraction, as well as inaccuracies during Nanodrop spectrometry and potential errors during dilutions, to result in less DNA template being added into each qPCR reaction than expected. By comparing the amount of β actin and GAPDH present in duck liver DNA, β actin was present at ~3-fold less than GAPDH on average. This suggests that GAPDH is present in duck liver cells in 2 – 3 times more copies than the β actin.

However, highly variable results were produced for the amount of β actin and GAPDH present in cell cultures (Table 4.6). It was found that β actin was present 200-fold higher than GAPDH in LMH cells, but was only present 2.4-fold higher than GAPDH in the dstet5 cells. Interestingly, GAPDH was 2.3-fold higher than β actin in PDH cells. The reasons for these observations are not known. It is speculated that the difference observed for LMH cells could be due to the difference in chicken and duck GAPDH sequences. As shown in Sections 4.4.1 and 4.4.2, β actin gene had 100% sequence coverage and 85% sequence similarities, while the GAPDH had 99% sequence coverage and 79% sequence similarities between the chicken and duck sequences. Therefore, the duck GAPDH qPCR assay developed in Section 4.4.3 may have been less specific and efficient for the chicken cells DNA due to some sequence variation, thus quantifying less of the GAPDH genes in LMH and dstet5 cells. If this was indeed a factor, the PDH cells derived from duck liver would then be the preferred DNA template to provide a more accurate comparison, as these cells would contain the same

genetic material as the NDL and Pool 7 liver tissues. Therefore, based on the qPCR results using PDH DNA as template, β actin was present 2.3-fold less than the GAPDH, an observation similar to that of the NDL and Pool 7 liver DNA qPCR results. However, there were obvious differences between the qPCR-quantitated genes and the estimated amount of cells present. It could be due to errors during cell counting as the cells tend to cluster together when cultured or large losses of DNA during DNA extractions (suggesting less efficiency of DNA extraction from cell cultures compared with DNA extraction from liver tissues). This showed that the theory of using cell cultures to provide a more reliable estimation of cells present in the qPCR DNA template was not as accurate as initially thought.

In conclusion, qPCR assays suggest that the β actin gene was present 2 to 3-fold less than the GAPDH gene in the duck liver cells. However, as there was ~5-fold less β actin and ~2-fold less GAPDH compared with the estimated number of cells present in the qPCR reaction, the exact copy number of genes present in each cell could not be determined.

4.4.4.2. Determining the copy numbers of duck β actin and GAPDH genes using FISH

The copy numbers of β actin and GAPDH genes in the duck genome were determined using the FISH assay. FISH or chromosomal painting, utilises a fluorescently-labelled DNA probe (usually BAC clones that are few Mbp in size) that when hybridised with the target cellular DNA in a chromosomal spread (mainly metaphase spread), could be visualised by fluorescent microscopy on their individual chromosomes, showing a physical map of the target DNA chromosomal locus and repetitive copies in the genome (Bayani and Squire, 2004; Pigozzi, 2007). Though more commonly used to determine localisation of genes on the chromosome (genetic mapping), FISH have been used to determine copy numbers of sequences in chicken (Pigozzi, 2007), and have been successfully applied to the mapping of the duck genome using chicken BAC clones (Yuan *et al.*, 2005; Fillon *et al.*, 2007).

In this Section, FISH was performed as described in Section 2.14 in an attempt to determine the copy number of duck β actin and GAPDH genes. Briefly, metaphase chromosome spreads of dstet5 and PDH cells were prepared by Dr. Georget Reaiche and Miss Layla Zhu, while probes were produced by fluorescently-labelling pT2.1DgB and pT2.1DgG plasmids for the detection of β actin and GAPDH genes respectively. The probes were then hybridised to the metaphase chromosome spreads with assistance from Dr. Georget Reaiche, and the slides were visualised using fluorescence microscopy with DAPI used as a counterstain.

Unfortunately, the FISH assay was not successful. No fluorescence was visible except the DAPI-stained metaphase chromosomes (data not shown). It is likely that the probe used was unsuitable as the cloned 1 kbp gene was too small in relation to the large chromosomes. As such, even if successful hybridisation with the chromosome spread had occurred, the fluorescent signal strength may be too weak to be detected under fluorescence microscopy.

FISH performed concurrently by Dr. Georget Reaiche using a ~3 kbp DHBV plasmid probe successfully produced specific fluorescence on chromosome spreads of the dstet5 cells that contain integrated DHBV DNA (data not shown). This confirmed that the FISH assay, both probe-labelling and hybridisation, had been successfully performed. As the fluorescence was visualised as very small dots, this suggest that at least 3 kbp of probe was needed for visible fluorescence. Unfortunately, as only ~1 kbp of the duck β actin and duck GAPDH gene had been sequenced, a larger probe was not available. A good alternative is to use large BAC clones (~3 Mbp) that span the gene of interest, as this would have a large area of hybridisation and thus produce stronger fluorescence signals. However, as there were no readily available duck (or chicken) BAC clones, the FISH assay was not further pursued in this study.

In conclusion, attempts to detect and quantify duck β actin and duck GAPDH genes using FISH assay were not successful. Despite that, with the correct probe, FISH would be a promising tool to accurately determine the exact copy numbers of both genes in the duck genome as the genes could be visualised clearly in the cell chromosomes. Possible future work includes sequencing up to 3 kbp of the duck β actin and GAPDH and cloning them into plasmids to produce bigger probes, or to try using β actin and GAPDH BAC clones from other species (e.g. chicken) as probes, if the duck BAC clones are not available.

4.5. Discussion

In previous studies using Southern blot hybridisation, it was found that β actin is a single copy gene in chickens (Cleveland *et al.*, 1980) and in Japanese pufferfish (Venkatesh *et al.*, 1996). However, in mammals like humans, rats and mice, the β actin genes are present in multiple copies in each genome, of which there is one functional copy and at least 19 pseudogenes present in the human genome (Ponte *et al.*, 1983; Ng *et al.*, 1985; Ng *et al.*, 1985).

On the other hand, in previous studies again using Southern blot hybridisation, it was found that GAPDH is a single copy gene in chickens (Alevy *et al.*, 1984; Stone *et al.*, 1985) and in quails (Weiskirchen *et al.*, 1993). Also, similar to the β actin gene mentioned above, in mammals like humans, hare, rats, mice, guinea pigs and Chinese hamsters, the GAPDH genes

are present in multiple copies in each genome, consisting of only one functional gene and multiple pseudogenes (Hanauer and Mandel, 1984; Piechaczyk *et al.*, 1984; Benham and Povey, 1989; Sabath *et al.*, 1990). Specifically, 10 – 40 pseudogenes have been found in humans, hares and guinea pigs; while 100 – 200 pseudogenes are thought to be present in the rats and mice (Hanauer and Mandel, 1984; Piechaczyk *et al.*, 1984).

Based on all that, it is expected that ducks, as part of the avian family, would also have a single copy of β actin and GAPDH gene. In this Chapter, although the exact copy number of each gene per liver cell could not be determined, based on the qPCR assay analysis (Section 4.4.4), the duck GAPDH genes were found to be present 2-fold to 3-fold more than the β actin gene. Thus, assuming that the duck β actin gene is present as a single copy gene in the liver cells, duck GAPDH genes may be present in multiple (2 – 3) copies in each liver cell.

It is unclear why the duck GAPDH gene may be present at higher copy numbers compared to the duck β actin gene. It is possible that there could be GAPDH pseudogenes present in the duck genome, which was thus co-amplified to produce the same qPCR product (as found in Section 4.4.4.1). To confirm this, Southern blot hybridisation of duck β actin and duck GAPDH genes could be performed on the total duck cell DNA (some digested by restriction enzymes), and probed using the pT2.1DgB2 and pT2.1DgG plasmids respectively.

Based on all the above, it was decided that the duck β actin gene would be used as an internal control for subsequent qPCR assays, as the β actin gene is a known single copy gene in avian species with no reported pseudogenes. This duck β actin qPCR assay successfully established in this Chapter using duck β actin gene cloned into plasmids, has since been routinely performed as internal control during duck DNA qPCR assays, including in this study (Sections 7.3.2.9 and 8.3.2.9), and Thorpe *et al.* (in preparation), and also been used to verify the presence of duck cell DNA in Feng *et al.* (Feng *et al.*, 2010). In addition, the duck β actin qPCR assay was performed to normalise the amount of duck cell DNA added to each qPCR reaction against a reference gene for accurate quantification of the target gene per duck cell, as well as to quantify the number of cells present extracted DNA samples (Section 5.1.4.4).

However, it should be noted that the β actin and GAPDH genes should only be used as internal controls for qPCR assays, and not for RT-qPCR assays that are used for quantitation of mRNA or gene expression. Despite being one of the most commonly-used internal controls for RT-qPCR assays, the β actin and GAPDH genes have been reported to have varying expression levels in different cell types (Warrington *et al.*, 2000) as well as altered levels of

gene expression during changes in cellular metabolism (Schmittgen and Zakrajsek, 2000). Thus, unlike the consistent number of genes present per genome, the inconsistent β actin and GAPDH mRNA levels would not be a reliable as internal controls. It is recommended that for RT-qPCR assays, the more stably-expressed HPRT1 gene (de Kok *et al.*, 2005) or TBP (Fu *et al.*, 2009) could be used as internal controls. Alternatively, several internal controls (up to three) could be used to generate a normalisation factor that would allow for more accurate normalisation of gene expression quantification to be produced (Vandesompele *et al.*, 2002).

In future studies, the absolute copy number of the duck β actin and GAPDH genes in the duck genome could be determined. This could be achieved by repeating the FISH assays using a larger-sized probe, like a BAC clone (few Mbp in size) spanning both genes, obtained from the chicken genome if the duck BAC clones are not commercially available. When successful, the exact copy number and even the chromosome in which each genes are present could be visualised using metaphase spreads of duck chromosomes. Alternatively, Southern blot hybridisation could also be performed, using the pT2.1DgB and pT2.1DgG as probes to detect each gene in the duck cell DNA that were digested using various restriction enzymes and separated using the agarose gel electrophoresis. If a single band was observed when the duck cell DNA was digested using restriction enzymes that do not cut the gene of interest, or if two bands were observed when the duck cell DNA digested using restriction enzymes that cut the gene of interest once, it is likely that the gene is present as a single copy in the genome.

4.6. Conclusion

In conclusion, ~1 kbp duck β actin and GAPDH were successfully amplified, sequenced, and cloned into plasmid vectors to produce the pT2.1DgB and pT2.1DgG plasmids. For the 1122 bp duck β actin gene that was sequenced, there was 83% homology with the chicken β actin and a 371 bp intron with the same splice sites as the chicken β actin gene. For the 1052 bp duck GAPDH gene that was sequenced, there was 79% homology with the chicken GAPDH and four ~100 bp introns, again with the same splice sites as the chicken GAPDH gene.

qPCR assays for the detection of the duck β actin and GAPDH genes were also established, and standard curves were optimised using the pT2.1DgB and pT2.1DgG plasmids with Duck β actin RT F – Duck β actin RT R2 or Duck GAPDH RT F – Duck GAPDH RT R primer sets, respectively. Hence, the duck β actin and GAPDH could be used as internal controls for duck cell DNA qPCR assays, as well as for the relative quantification of duck cells present.

Based on qPCR assay analysis, it is also suggested that the β actin gene was present 2 to 3-fold less than the GAPDH gene in duck liver cells. However, attempts to determine the copy number of β actin and GAPDH genes in duck liver cell were not successful.

Table 4.2: List of qPCR primer sets used for amplifying duck β actin from pT2.1DgB plasmid during optimisation of duck β actin qPCR assays, the expected qPCR product size produced by each qPCR primer sets, as well as observations of the melt curves generated by each qPCR reaction.

qPCR primers[a]		Expected product size[b] (bp)	Melt curve observation[c]
Forward primer	**Reverse primer**		
β actin F	β actin R	1122	Double peaks, Tm ~79, 86°C
Duck G β actin 2F	β actin RT R	549	Single peak, Tm ~87°C
β actin F	Duck G β actin R	490	Single peak, Tm ~86°C
Duck G β actin F	β actin RT R	458	Multiple peaks, Tm ~78, 83, 86°C
Duck G β actin 2F	Duck G β actin R	264	Single peak, Tm ~87°C
β actin RT F	β actin RT R	199	Single peak, Tm ~79°C
Duck G β actin F	Duck G β actin R	173	Single peak, Tm ~86°C
Duck β actin RT F	Duck β actin RT R2	153	Single peak, Tm ~82°C
β actin RT F	Duck β actin RT R	103	Single peak, Tm ~79°C
β actin RT F	Duck β actin RT R2	86	Single peak, Tm ~80°C

qPCR reactions were performed using pT2.1DgB plasmid as template as described in Section 2.8.9.

[a]Sequences and nucleotide binding site for each qPCR primer are shown in Table 4.1.
[b]Expected qPCR product sizes were calculated using the online program BioMath Calculators for Oligos by Promega (accessible through http://www.promega.com/biomath/calc11.htm).
[c]Melt curves were generated using the ABI Prism software, and observed as described in Figure 4.10.

Table 4.4: List of qPCR primer sets used for amplifying duck GAPDH from pT2.1DgG plasmid during optimisation of duck GAPDH qPCR assays, the expected qPCR product size produced by each qPCR primer sets, as well as observations of the melt curves generated by each qPCR reaction.

qPCR primers[a]		Expected product size[b] (bp)	Melt curve observation[c]
Forward primer	**Reverse primer**		
GAPDH RT F	Duck GAPDH R	97	Single peak, Tm ~85^{o}C
Duck GAPDH RT F	Duck GAPDH RT R	151	Single peak, Tm ~81^{o}C

qPCR reactions were performed using pT2.1DgG plasmid as template as described in Section 2.8.9.

[a]Sequences and nucleotide binding site for each qPCR primer are shown in Table 4.3.
[b]Expected qPCR product sizes were calculated using online program BioMath Calculators for Oligos by Promega (accessible through http://www.promega.com/biomath/calc11.htm).
[c]Melt curves were generated using the ABI Prism software, and observed as described in Figure 4.10.

Table 4.5: List of qPCR primer sets used for duck β actin and duck GAPDH qPCR assays with their corresponding qPCR product size, Tm, G:C content, and MW.

qPCR primers[a]		Expected product size[b] (bp)	Tm[b] (°C)	G:C content[b]	MW[b] (Da)
Forward primer	**Reverse primer**				
Duck β actin assay					
β actin RT F	β actin RT R	199	79	43.72	61457
β actin RT F	Duck β actin RT R	103	79	49.51	31595
Duck β actin RT F	Duck β actin RT R2	153	83	54.25	46930
Duck GAPDH assay					
GAPDH RT F	Duck GAPDH R	97	79	50.00	30143
Duck GAPDH RT F	Duck GAPDH RT R	152	82	51.32	47099

qPCR reactions were performed using pT2.1DgB and pT2.1DgG plasmid as template for the duck β actin and duck GAPDH qPCR assays respectively as described in Section 2.8.9.

[a]Sequences and nucleotide binding site for each qPCR primer are shown in Table 4.1 and Table 4.3.

[b]Expected qPCR product sizes, Tm, G:C content, and MW were calculated using the online program BioMath Calculators for Oligos (accessible through http://www.promega.com/biomath/calc11.htm).

Table 4.6: Comparison of the estimated number of cells present in the qPCR reactions with the results of duck β actin and duck GAPDH qPCR quantification determined using the duck β actin and duck GAPDH qPCR assays using various DNA templates, as well as the fold differences of the amount of β actin and GAPDH obtained.

qPCR template	Estimate number of cells present[c]	qPCR results (copies)		β actin and GAPDH fold difference
		β actin	GAPDH	
NDL DNA[a] 10-fold serial dilutions	5,357.1	1,307.78	4,185.06	3.2
	535.71	127.77	405.56	3.2
	53.571	14.16	35.89	2.5
	5.3571	1.16	3.28	2.8
LAD7 duck DNA[a] 10-fold serial dilutions	5,357.1	1,339.38	4,201.98	3.1
	535.71	144.18	393.58	2.7
	53.571	11.30	31.56	2.8
	5.3571	1.19	4.54	3.8
LMH[b]	700	8,657.17	43.12	200.8
Dstet5[b]	3,500	10,636.48	4,484.52	2.4
PDH[b]	7,000	9,966.26	22,519.77	2.3

qPCR reactions were performed using the qPCR primer sets Duck β actin RT F – Duck β actin RT R2 and Duck GAPDH RT F – Duck GAPDH RT R for the duck β actin and duck GAPDH qPCR assays respectively, as described in Section 2.8.9.

[a]DNA was extracted using the DNeasy blood and tissue kit as described in Section 2.6.1.
[b]DNA was extracted using the DNeasy blood and tissue kit as described in Section 2.13.4.
[c]The number of cells present was estimated as described in Section 2.8.9.3.2 for DNA extracted from duck liver tissues, and Section 2.13.5 for DNA extracted from cultured cells. Data for the original serial dilution of 150 ng duck liver DNA (53,571 cells) is not shown.

Figure 4.1: Multiple sequence alignment showing the 251 bp sequenced duck GAPDH PCR product aligned with the duck GAPDH mRNA sequence (GenBank Accession AY436595, REGION: 231-370), the chicken GAPDH gene (GenBank Accession NC006088, REGION: 80089632-80094155), and the chicken GAPDH mRNA sequence (GenBank Accession K01458, REGION: 385-524).

The duck GAPDH gene was amplified from NDL DNA using primer sets chicken GAPDH F – chicken GAPDH R (Seigneres *et al.*, 2003) (refer Table 2.2) as described in Section 2.8.5, and sequenced as described in Section 2.8.10. The multiple sequence alignment was performed using ClustalW2 program and output file viewed and arranged by Jalview program as described in Section 2.8.12.

Individual alignment scores of the reference genes with the duck GAPDH PCR product were obtained using the BLAST Align 2 Sequences programme as described in Section 2.8.12. The scores include: 56% coverage and 99% sequence similarity (excluding gap regions) for the duck GAPDH mRNA sequence; 99% coverage and 82% sequence similarity for the chicken GAPDH sequence; and 51% coverage and 93% sequence similarity (excluding gap regions) for the chicken GAPDH mRNA sequence.

Note:
REGION refers to the specific region of nucleotide sequence that was used for alignment in this multiple sequence alignment, and was based on the nucleotide numbering obtained from the respective GenBank sequences. REGIONs were chosen to match with the range of the target gene (duck GAPDH) sequence. The numbers shown in the multiple sequence alignment output Figure refer to the nucleotide numbering of the specified REGIONs.

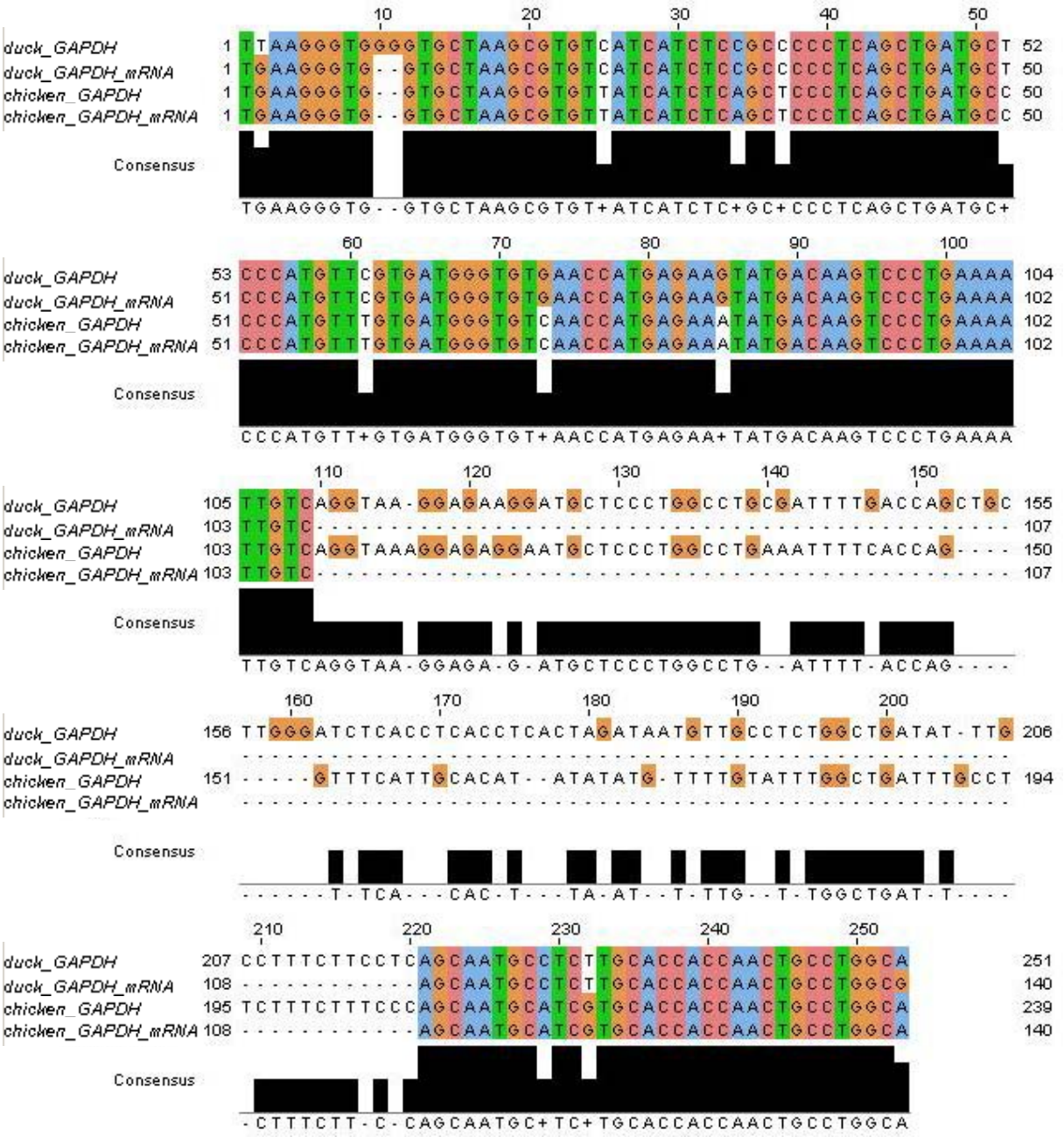

duck_GAPDH
duck_GAPDH_mRNA
chicken_GAPDH
chicken_GAPDH_mRNA
Consensus

Figure 4.1

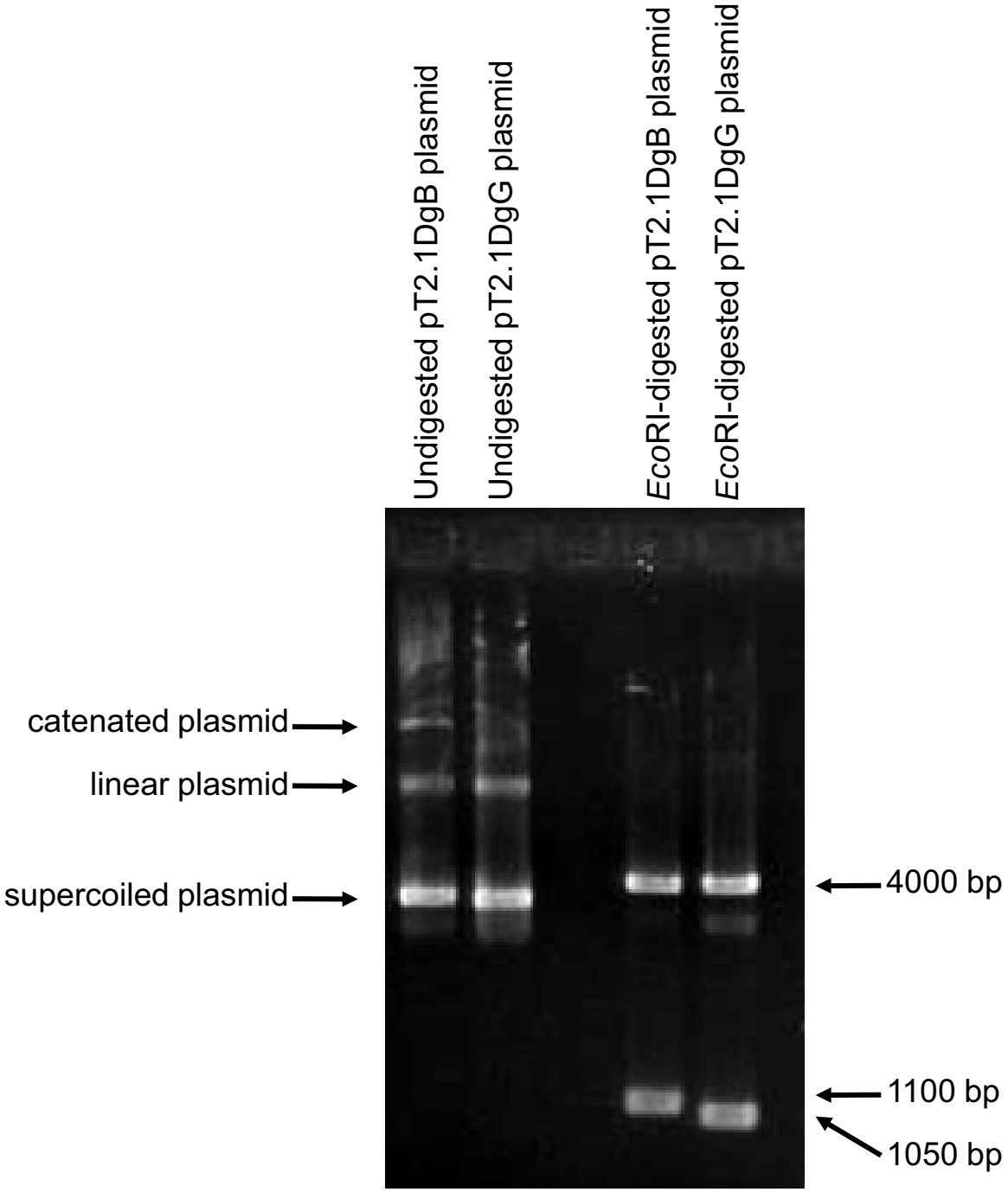


Figure 4.2: Undigested and *Eco*RI-digested plasmids pT2.1DgB and pT2.1DgG, visualised using agarose gel electrophoresis under 302 nm UV light.

DNA was visualised by GelRed-stained agarose gel electrophoresis as described in Section 2.8.7. The undigested plasmids were observed to migrate in the agarose gel electrophoresis in three forms: catenated, liner, or supercoiled forms. In the *Eco*RI-digested plasmids, the top ~4000 bp band corresponds to the plasmid vector, pCR 2.1-TOPO, while the bottom bands (~1100 bp and ~1050 bp) correspond to the cloned duck β actin gene and duck GAPDH genes respectively.

Figure 4.3: Cloned (A) duck β actin and (B) duck GAPDH PCR products amplified from DNA template pT2.1DgB plasmid and pT2.1DgG plasmid respectively, to determine the direction of the cloned duck β actin gene and duck GAPDH gene in relation to the plasmid *lacZ* promoter. Each PCR product was visualised using agarose gel electrophoresis under 302 nm UV light.

PCR amplification of pT2.1DgB was performed using the T7 primer with either the β actin F primer, or the β actin R primer, while the amplification of pT2.1DgG was performed using the T7 primer with either the duck GAPDH gF primer or the duck GAPDH gR primer (refer Table 2.2 for primer sequences), as described in Section 2.8.5.

As shown in Figure 4.3A, the 1200 bp duck β actin gene was cloned in pT2.1DgB1 in the forward direction in relation to the plasmid *lacZ* promoter, while the duck β actin gene was cloned in pT2.1DgB2 in the reverse direction in relation to the plasmid *lacZ* promoter, as a PCR product was successfully amplified using the β actin F – T7 primer set and β actin R – T7 primer set respectively (refer Figure 4.6 for location of primer binding sites on the plasmid).

As shown in Figure 4.3B, the 1150 bp duck GAPDH gene was cloned in pT2.1DgG in the reverse direction in relation to the plasmid *lacZ* promoter, as a PCR product was successfully amplified using the duck GAPDH gR – T7 primer set (refer Figure 4.9 for location of primers on the plasmid).

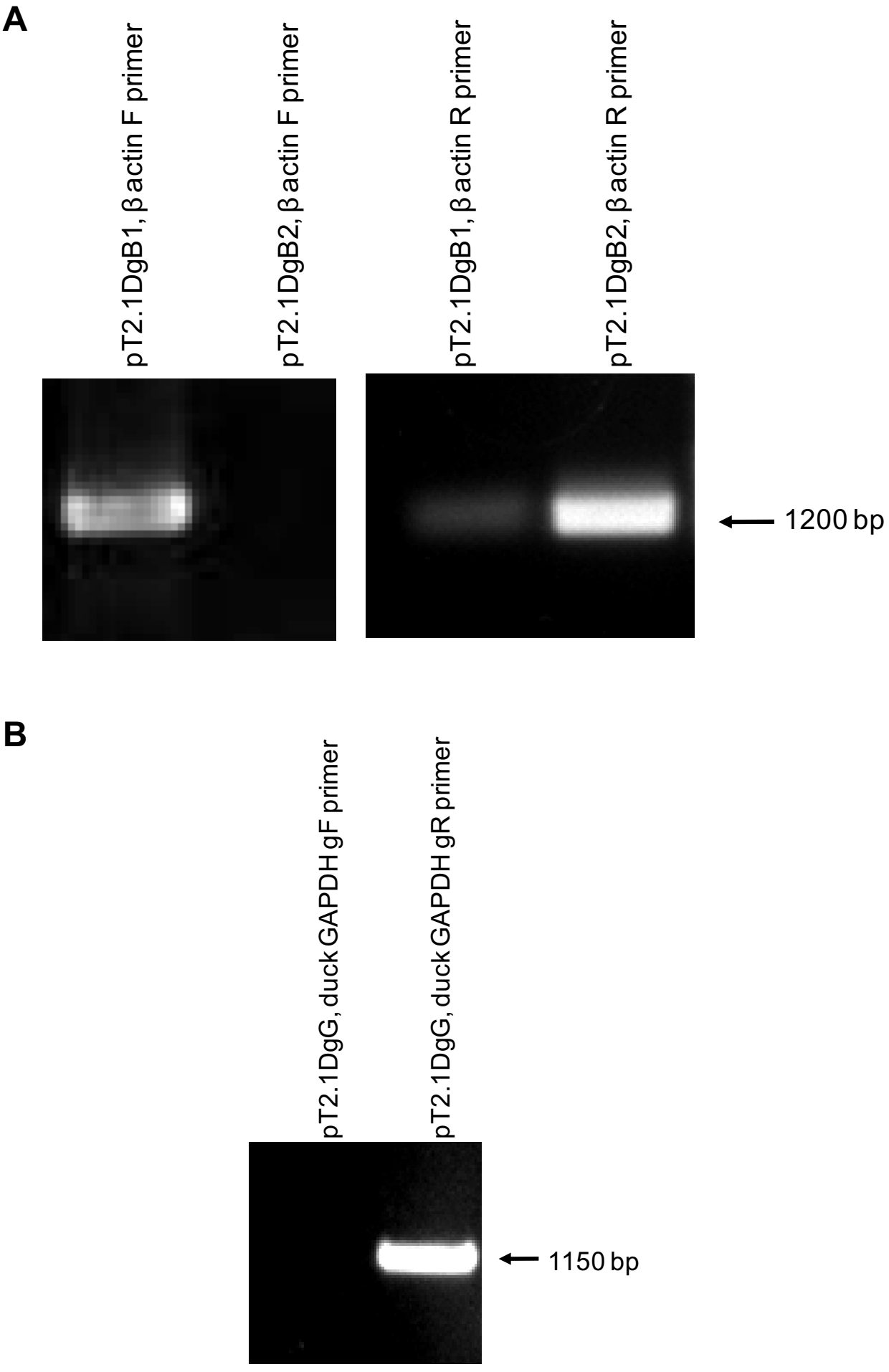

A
pT2.1DgB1, β actin F primer
pT2.1DgB2, β actin F primer
pT2.1DgB1, β actin R primer
pT2.1DgB2, β actin R primer
1200 bp
B
pT2.1DgG, duck GAPDH gF primer
pT2.1DgG, duck GAPDH gR primer
1150 bp

Figure 4.3

Figure 4.4: Multiple sequence alignment showing the 1122 bp sequenced duck β actin PCR product aligned with the chicken β actin gene (GenBank Accession X00182, REGION: 3519-4658), duck β actin mRNA sequence (GenBank Accession DQ675572) and chicken β actin mRNA sequence (GenBank Accession NM_205518, REGION: 895-1679).

The duck β actin gene was amplified from NDL DNA using primer sets β actin F – β actin R (refer Table 2.2) as described in Section 2.8.5, and sequenced as described in Section 2.8.10. The multiple sequence alignment was performed using ClustalW2 program and output file viewed and arranged by Jalview program as described in Section 2.8.12.

Individual alignment scores of the reference genes with the duck β actin PCR product were obtained using BLAST Align 2 Sequences programme as described in Section 2.8.12. The scores include: 100% coverage and 83% sequence similarity for the chicken β actin sequence; 64% coverage and 99% sequence similarity (excluding gap regions) for the duck β actin mRNA sequence; and 70% coverage and 94% sequence similarity (excluding gap regions) for the chicken β actin mRNA sequence.

Note:
REGION refers to the specific region of nucleotide sequence that was used for alignment in this multiple sequence alignment, and was based on the nucleotide numbering obtained from the respective GenBank sequences. REGIONs were chosen to match with the range of the target gene (duck β actin) sequence. The numbers shown in the multiple sequence alignment output figure refer to the nucleotide numbering of the specified REGIONs.

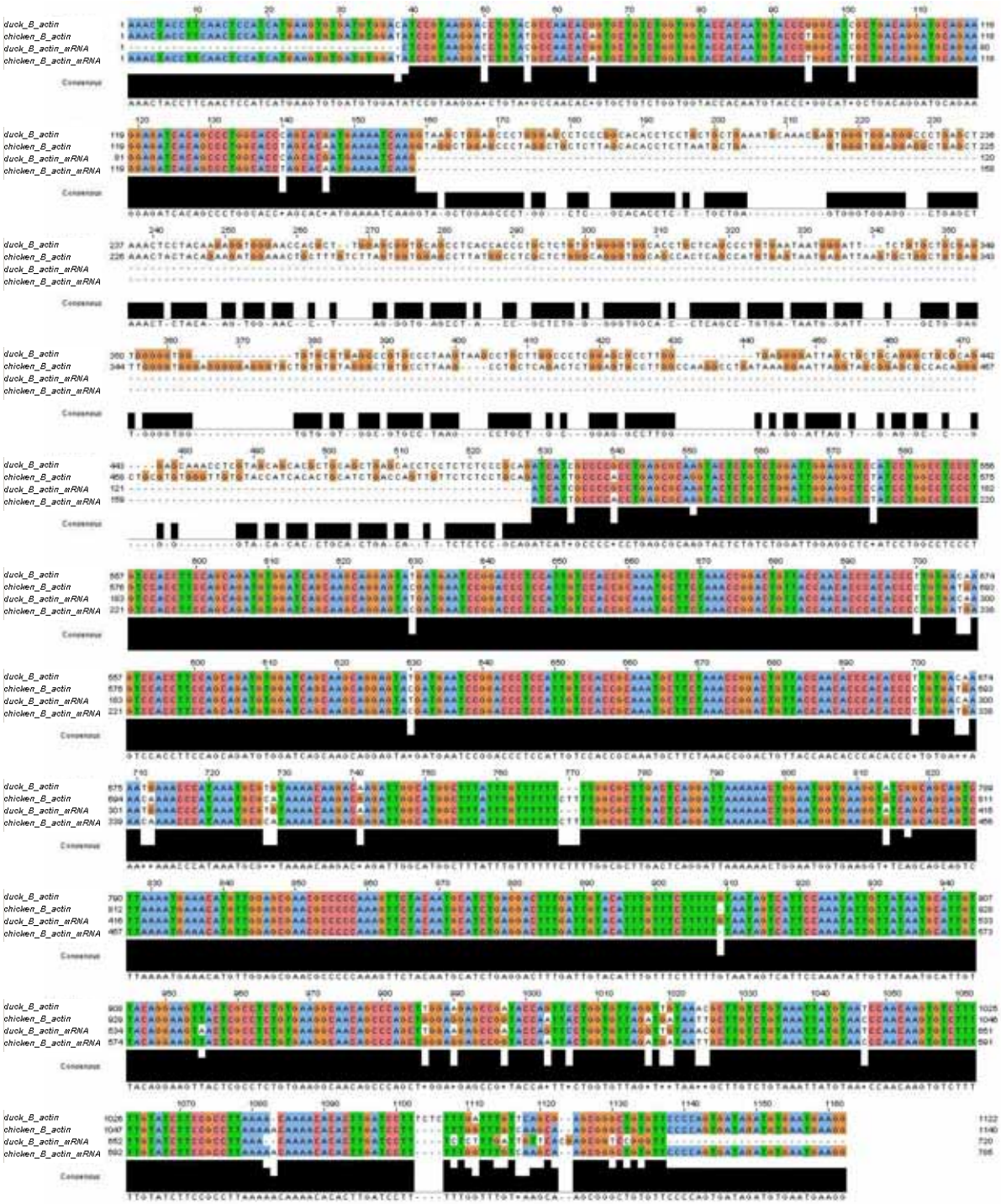

duck_B_actin
chicken_B_actin
duck_B_actin_mRNA
chicken_B_actin_mRNA
Consensus

Figure 4.4

Figure 4.5: Multiple sequence alignment showing the 1122 bp sequenced duck β actin PCR product aligned with chicken β actin gene (GenBank Accession X00182, REGION: 3519-4658), human β actin gene (GenBank Accession, NT_007819 REGION: 5557792-5556886 reverse complement), chimpanzee β actin gene (GenBank Accession NC_006474, REGION: 5518522-5518023 reverse complement) and mouse β actin gene (GenBank Accession NT_081055, REGION: 253157-254152 reverse complement).

The duck β actin gene was amplified from NDL DNA using primer sets β actin F – β actin R (refer Table 2.2) as described in Section 2.8.5, and sequenced as described in Section 2.8.10. The multiple sequence alignment was performed using ClustalW2 program and output file viewed and arranged by Jalview program as described in Section 2.8.12.

Individual alignment scores of the reference genes with the duck β actin PCR product were obtained using BLAST Align 2 Sequences programme as described in Section 2.8.12. The scores include: 100% coverage and 83% sequence similarity for the chicken β actin sequence; 54% coverage and 79% sequence similarity (excluding gap regions) for the human and chimpanzee β actin sequence; and 45% coverage and 85% sequence similarity (excluding gap regions) for the mouse β actin sequence.

Note:
REGION refers to the specific region of nucleotide sequence that was used for alignment in this multiple sequence alignment, and was based on the nucleotide numbering obtained from the respective GenBank sequences. REGIONs were chosen to match with the range of the target gene (duck β actin) sequence. The numbers shown in the multiple sequence alignment output figure refer to the nucleotide numbering of the specified REGIONs.

Reverse complement means that the sequence that was used for alignment in this multiple sequence alignment was the reverse complement of the sequence obtained from GenBank.

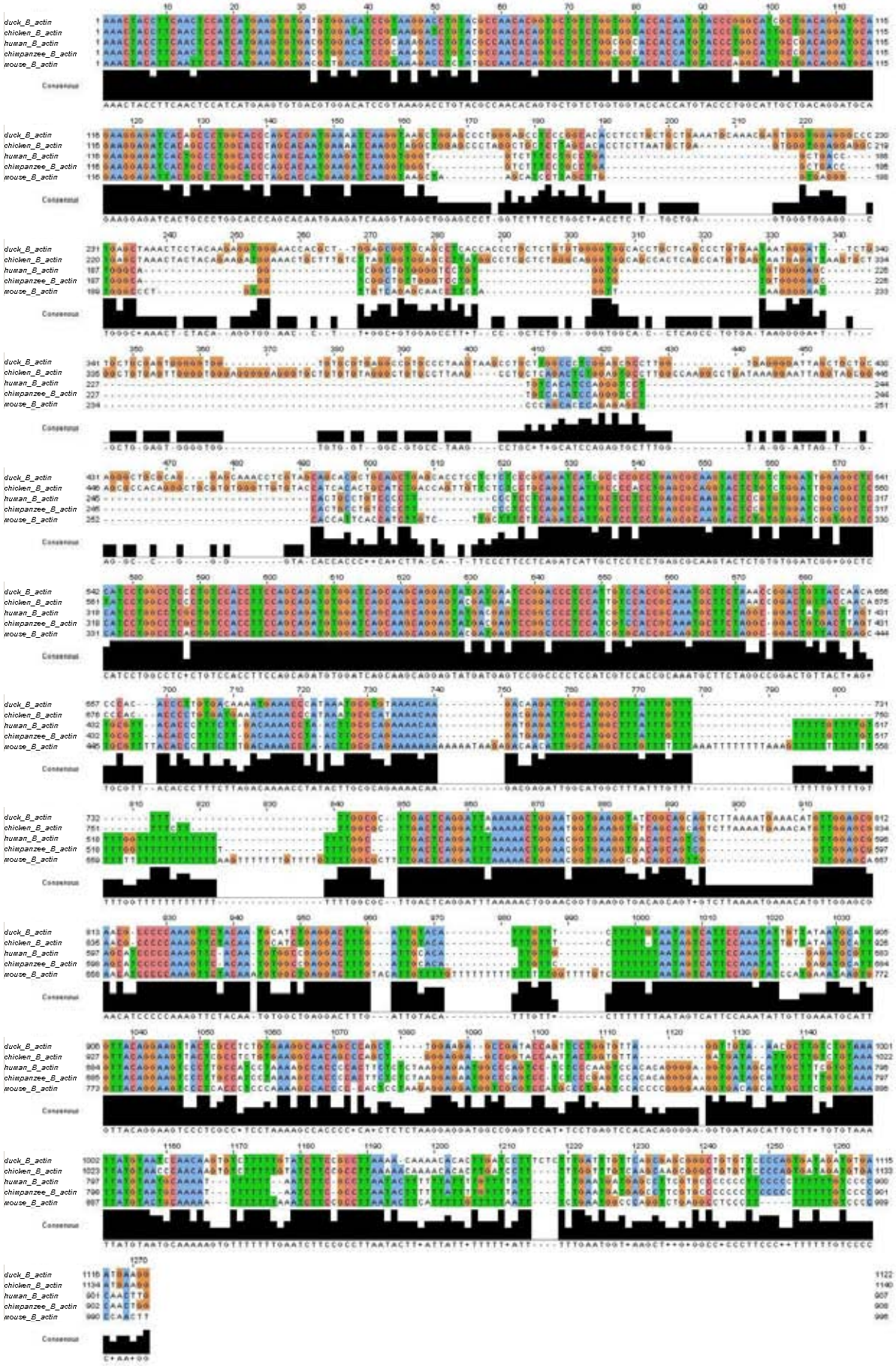

duck_B_actin
chicken_B_actin
human_B_actin
chimpanzee_B_actin
mouse_B_actin
Consensus

Figure 4.5

Figure 4.6: Map of the (A) pT2.1DgB1 and (B) pT2.1DgB2 plasmids.

The 1122 bp duck β actin gene sequence (GenBank Accession GU564232) was cloned into the pCR 2.1-TOPO plasmid vector near the *Eco*RI digestion sites, using the TOPO TA cloning kit (Invitrogen, USA) as described in Section 2.9.1. The detailed map of the pCR 2.1-TOPO plasmid vector is shown in Figure 2.5.

Arrow heads of the duck β actin gene represent the 5' – 3' direction of the duck β actin gene in relation to the *lacZ* promoter of the pCR 2.1-TOPO plasmid vector.

The approximate binding sites of the PCR primers β actin F, β actin R, M13 and T7 (refer Table 2.2) are also shown.

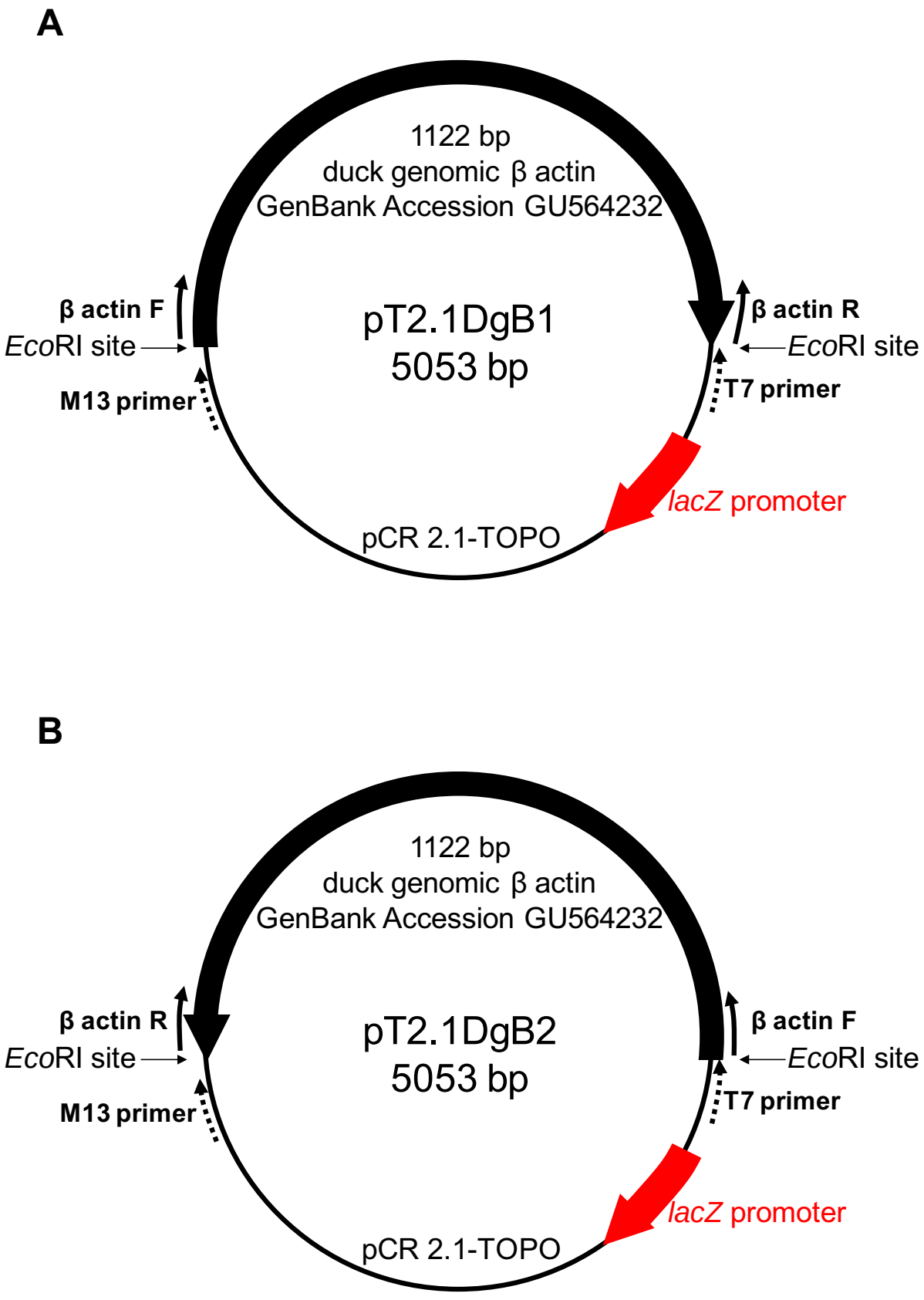

A
1122 bp
duck genomic β actin
GenBank Accession GU564232
pT2.1DgB1
5053 bp
β actin F
EcoRI site
M13 primer
β actin R
EcoRI site
T7 primer
lacZ promoter
pCR 2.1-TOPO
B
1122 bp
duck genomic β actin
GenBank Accession GU564232
pT2.1DgB2
5053 bp
β actin R
EcoRI site
M13 primer
β actin F
EcoRI site
T7 primer
lacZ promoter
pCR 2.1-TOPO

Figure 4.6

Figure 4.7: Multiple sequence alignment showing the 1052 bp sequenced duck GAPDH PCR product and the 528 bp sequenced duck GAPDH mRNA PCR product, aligned with the chicken GAPDH gene (GenBank Accession NC006088, REGION: 80089632-80094155), duck GAPDH mRNA sequence (GenBank Accession AY436595, REGION: 45-576) and chicken GAPDH mRNA sequence (GenBank Accession K01458, REGION: 199-726).

The duck GAPDH gene and the duck GAPDH mRNA sequence was amplified from NDL DNA using primer duck GAPDH gF – duck GAPDH gR (refer Table 2.2) as described in Section 2.8.5, and sequenced as described in Section 2.8.10. The multiple sequence alignment was performed using ClustalW2 program and output file viewed and arranged by Jalview program as described in Section 2.8.12.

Individual alignment scores of the reference genes with the duck GAPDH PCR product were obtained using BLAST Align 2 Sequences programme as described in Section 2.8.12. The scores include: 99% coverage and 79% sequence similarity for the chicken GAPDH sequence; 50% coverage and 99% sequence similarity (excluding gap regions) for the duck GAPDH mRNA PCR product; 50% coverage and 99% sequence similarity (excluding gap regions) for the duck GAPDH mRNA sequence; and 51% coverage and 93% sequence similarity (excluding gap regions) for the chicken GAPDH mRNA sequence.

Note:
REGION refers to the specific region of nucleotide sequence that was used for alignment in this multiple sequence alignment, and was based on the nucleotide numbering obtained from the respective GenBank sequences. REGIONs were chosen to match with the range of the target gene (duck GAPDH) sequence. The numbers shown in the multiple sequence alignment output figure refer to the nucleotide numbering of the specified REGIONs.

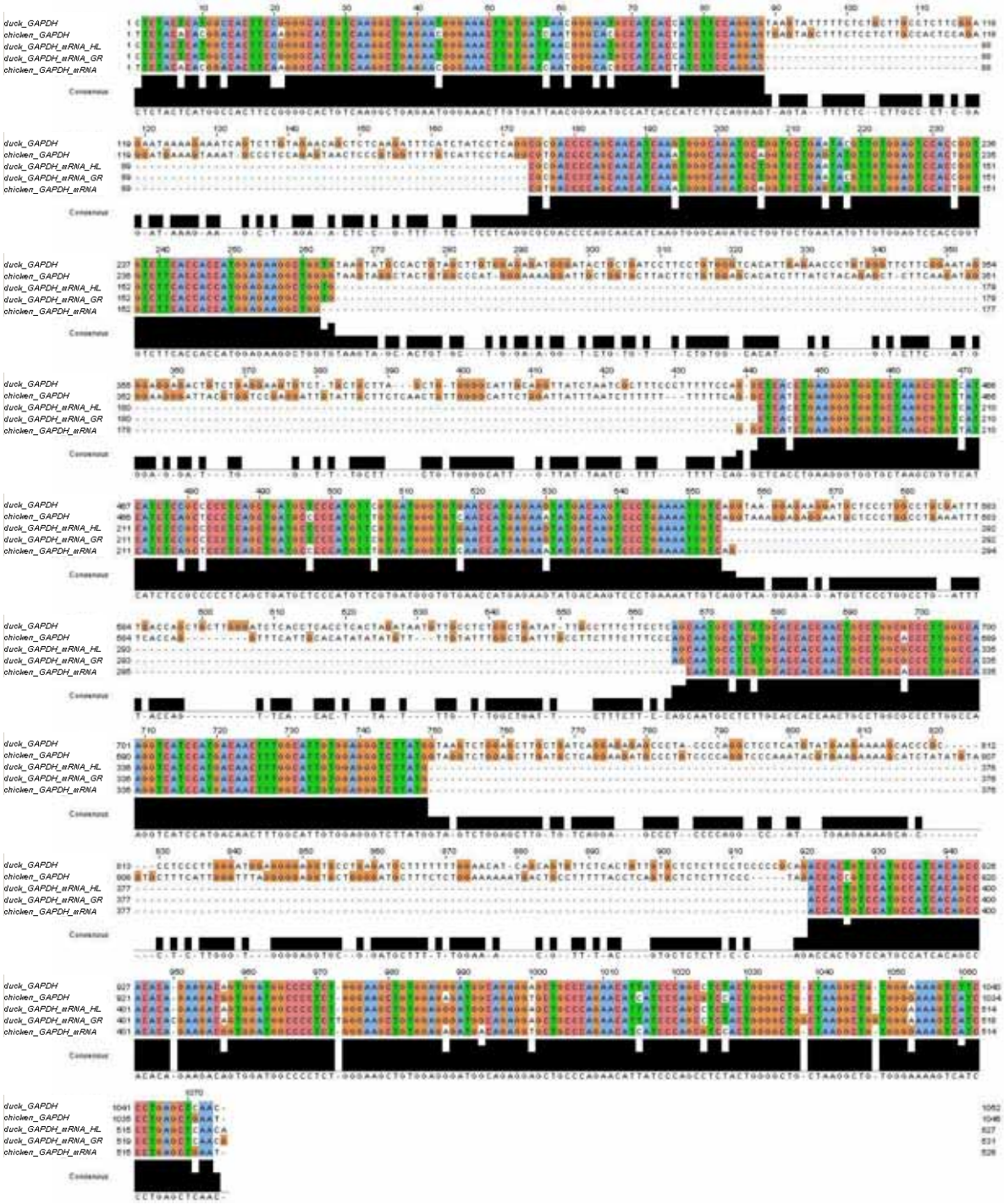

duck_GAPDH
chicken_GAPDH
duck_GAPDH_mRNA_HL
duck_GAPDH_mRNA_GR
chicken_GAPDH_mRNA
Consensus

Figure 4.7

Figure 4.8: Multiple sequence alignment showing the 1052 bp sequenced duck GAPDH PCR product aligned with chicken GAPDH gene (GenBank Accession NC006088, REGION: 80091152-80092199), human GAPDH gene (GenBank Accession NT_009759, REGION: 6585870-6586899), chimpanzee GAPDH gene (GenBank Accession NC_006479, REGION: 6758493-6759522) and mouse GAPDH gene (GenBank Accession NT_039353, REGION: 77426296-77425539 reverse complement).

The duck GAPDH gene was amplified from NDL DNA using primer duck GAPDH gF – duck GAPDH gR (refer Table 2.2) as described in Section 2.8.5, and sequenced as described in Section 2.8.10. The multiple sequence alignment was performed using ClustalW2 program and output file viewed and arranged by Jalview program as described in Section 2.8.12.

Individual alignment scores of the reference genes with the duck GAPDH PCR product were obtained using BLAST Align 2 Sequences programme as described in Section 2.8.12. The scores include: 99% coverage and 79% sequence similarity for the chicken GAPDH sequence; 62% coverage and 79% sequence similarity (excluding gap regions) for the human and chimpanzee GAPDH sequence; and 53% coverage and 85% sequence similarity (excluding gap regions) for the mouse GAPDH sequence.

Note:
REGION refers to the specific region of nucleotide sequence that was used for alignment in this multiple sequence alignment, and was based on the nucleotide numbering obtained from the respective GenBank sequences. REGIONs were chosen to match with the range of the target gene (duck GAPDH) sequence. The numbers shown in the multiple sequence alignment output figure refer to the nucleotide numbering of the specified REGIONs.

Reverse complement means that the nucleotide sequence that was used for alignment in this multiple sequence alignment was the reverse complement of the sequence obtained from GenBank.

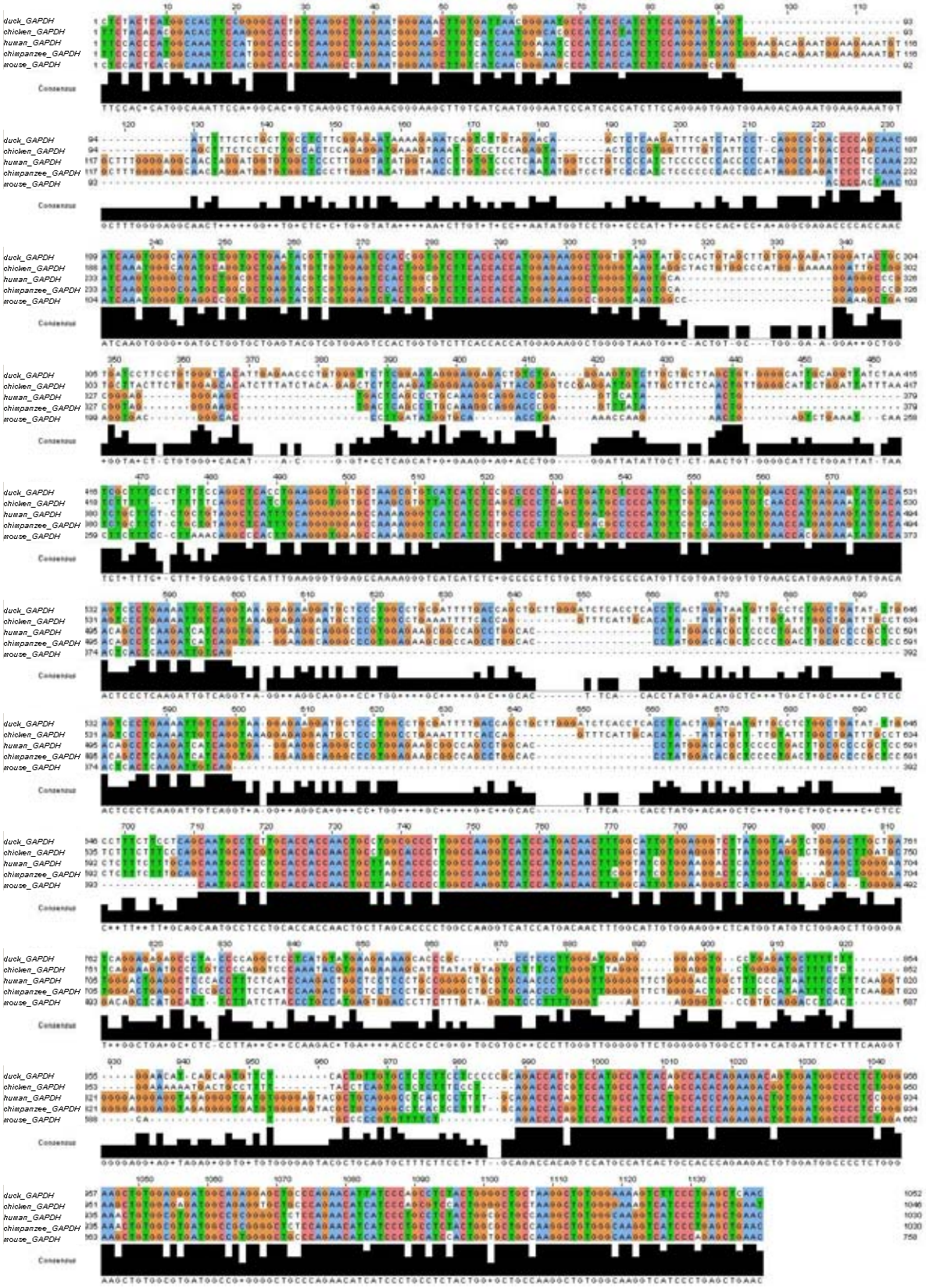

duck_GAPDH
chicken_GAPDH
human_GAPDH
chimpanzee_GAPDH
mouse_GAPDH
Consensus

Figure 4.8

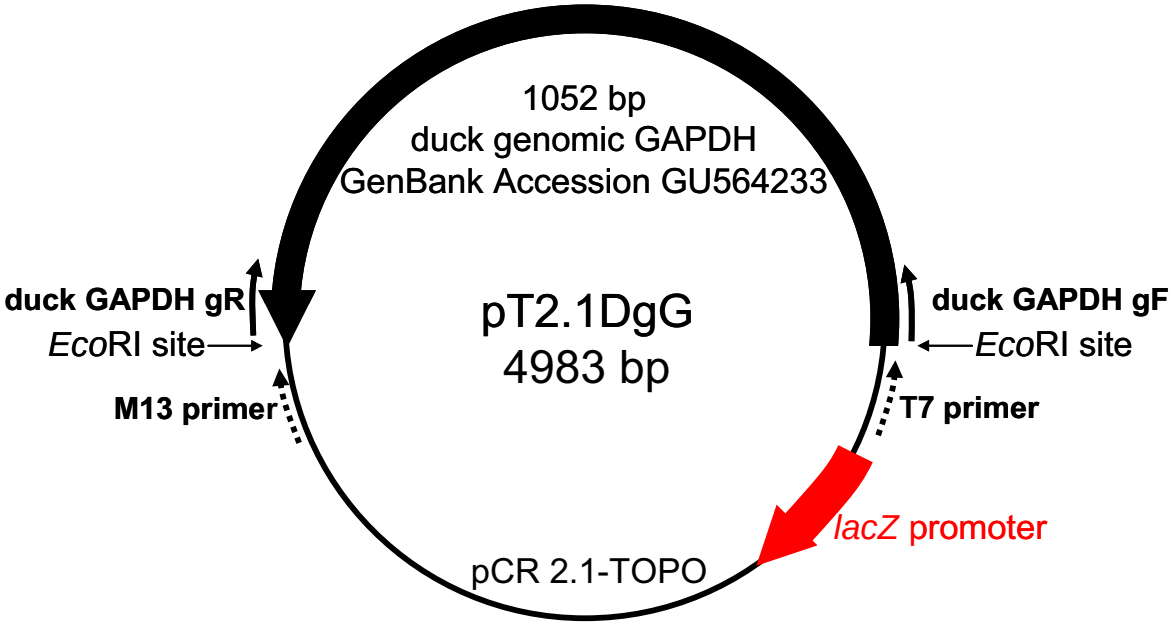


Figure 4.9: Map of the pT2.1DgG plasmid.

The 1052 bp duck GAPDH gene sequence (GenBank Accession GU564233) was cloned into the pCR 2.1-TOPO plasmid vector near the *Eco*RI digestion sites, using the TOPO TA cloning kit (Invitrogen, USA) as described in Section 2.9.1. The detailed map of the pCR 2.1-TOPO plasmid vector is shown in Figure 2.5.

Arrow heads of the duck GAPDH gene represent the 5' – 3' direction of the duck GAPDH gene in relation to the *lacZ* promoter of the pCR 2.1-TOPO plasmid vector.

The approximate binding sites of PCR primers duck GAPDH gF, duck GAPDH gR, M13 and T7 (refer Table 2.2) are also shown.

Figure 4.10: Examples of melt curves generated from qPCR reactions.

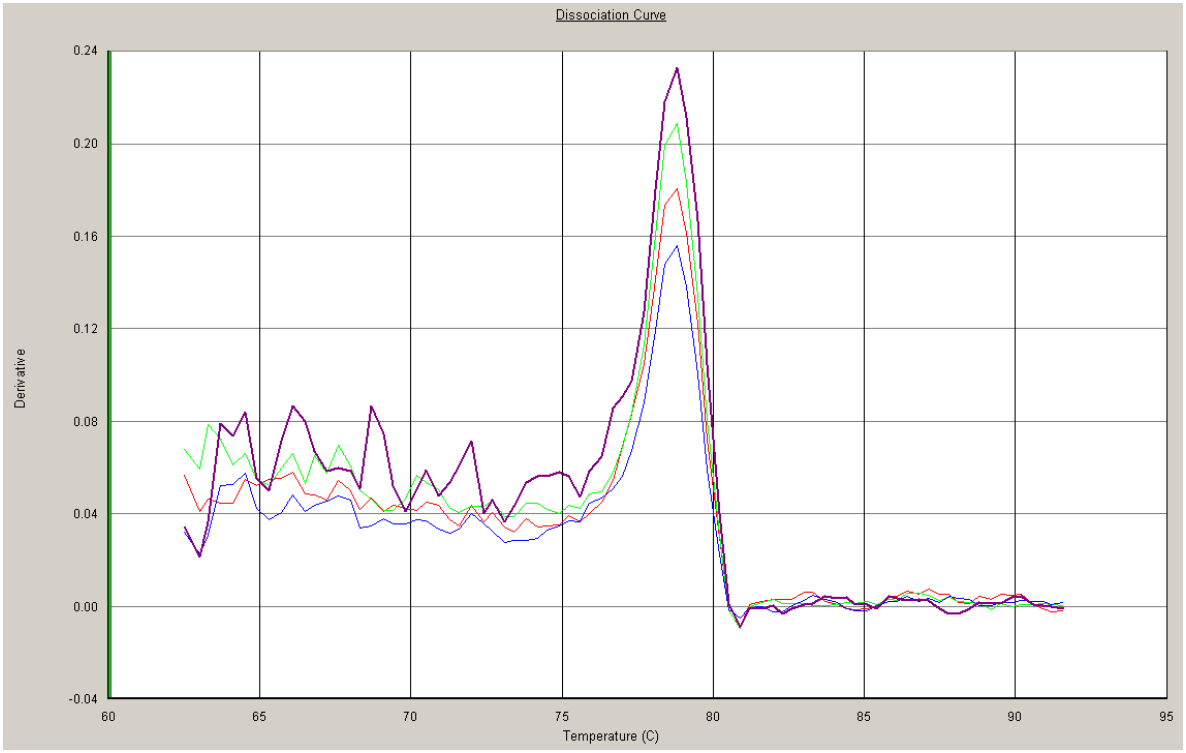
qPCR reactions were performed as described in Section 2.8.9, using pT2.1DgB1 plasmid as a DNA template. The qPCR melt curves were generated using the ABI Prism software (AB, USA). Each qPCR product amplified would have a specific Tm peak in the qPCR melt curve.

Figure 4.10A shows an example when only a single qPCR product was amplified in the qPCR reactions. The single Tm peak at ~78.5^{o}C corresponds to the Tm of the single qPCR product produced in the qPCR reaction.

Figure 4.10B shows an example when multiple qPCR products, or no/ non-specific qPCR products were amplified in the qPCR reactions. The multiple Tm peaks (blue and purple line) correspond to the Tm of multiple qPCR products produced in the qPCR reaction, while the non-distinct Tm peaks (red and green line) indicate that no specific qPCR products were produced in the qPCR reactions.

Multiple Tm peaks suggest that the qPCR primer sets used in the qPCR reactions were not specific enough and allowed for amplification of various by-products via random priming. On the other hand, the non-distinct peaks suggest that the failure to amplify any qPCR products in the qPCR reactions could be due to the absence of qPCR template, poor qPCR template quality, or qPCR primer sets were not specific for the qPCR template used.

A



B

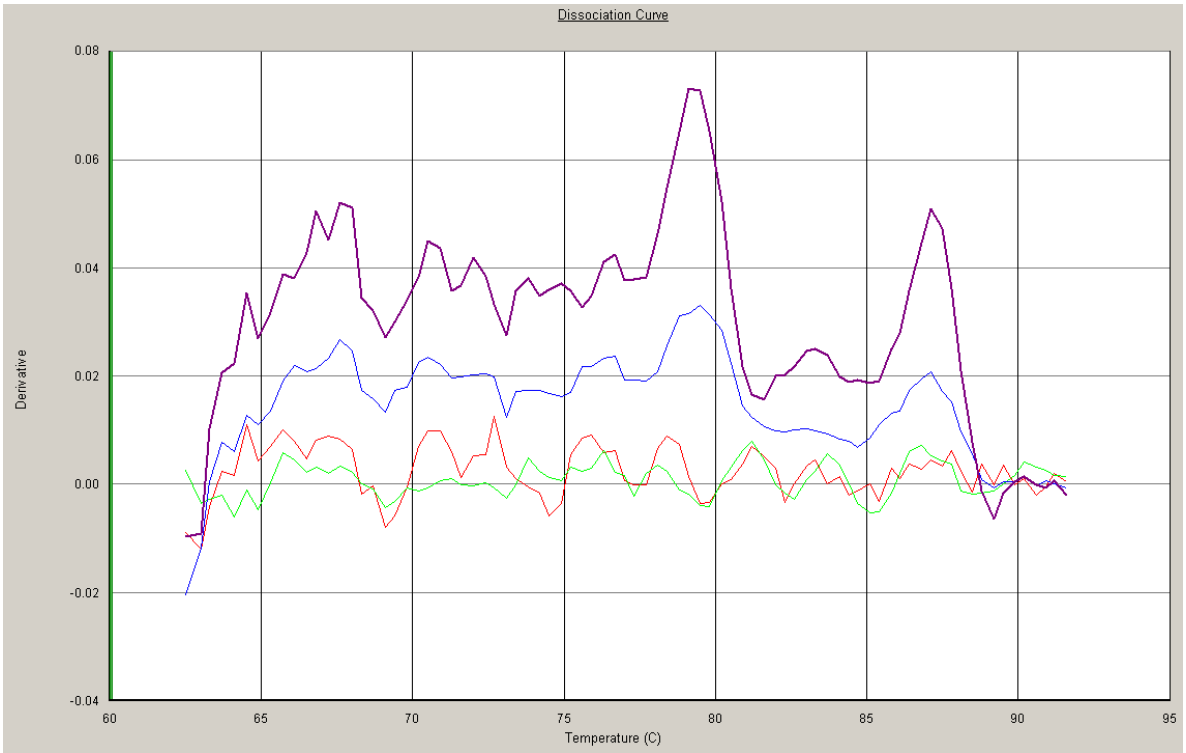


Figure 4.10

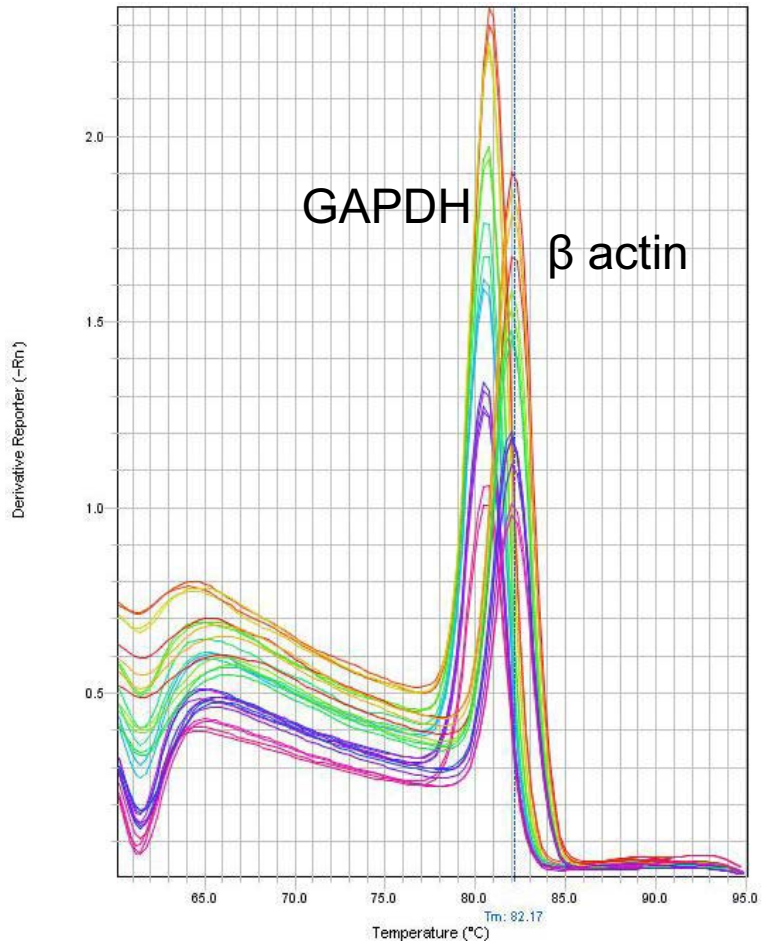
Figure 4.11: (A) Melt curves and (B) standard curves generated from the duck β actin and duck GAPDH qPCR assays.

qPCR reactions were performed using pT2.1DgB plasmid and pT2.1DgG plasmid as template, using the qPCR primer sets Duck β actin RT F – Duck β actin RT R2 or Duck GAPDH RT F – Duck GAPDH RT R for the duck β actin and duck GAPDH qPCR assays respectively, as described in Section 2.8.9. Melt curves and standard curves (along with the standard curves' slopes, Y-intercept, R^2 value, and plasmid serial dilution copy numbers detected) were generated and calculated using the StepOne Plus software.

Figure 4.11A shows that the duck β actin qPCR reactions produced a single melt curve Tm peak at 83^{o}C, while the duck GAPDH qPCR reactions produced a single melt curve Tm peak at 82^{o}C.

Figure 4.11B shows that the standard curve for the duck β actin qPCR assay had a slope of -3.516, Y-intercept C_T value of 33.169, R^2 value of 0.998, with all plasmid serial dilution copy numbers (10^8 – 10^1 copies) detected. On the other hand, the standard curve for the duck GAPDH qPCR assay had a slope of -3.625, Y-intercept C_T value of 35.778, R^2 value of 0.996, with all plasmid serial dilution copy numbers (10^8 – 10^1 copies) detected.

A



B

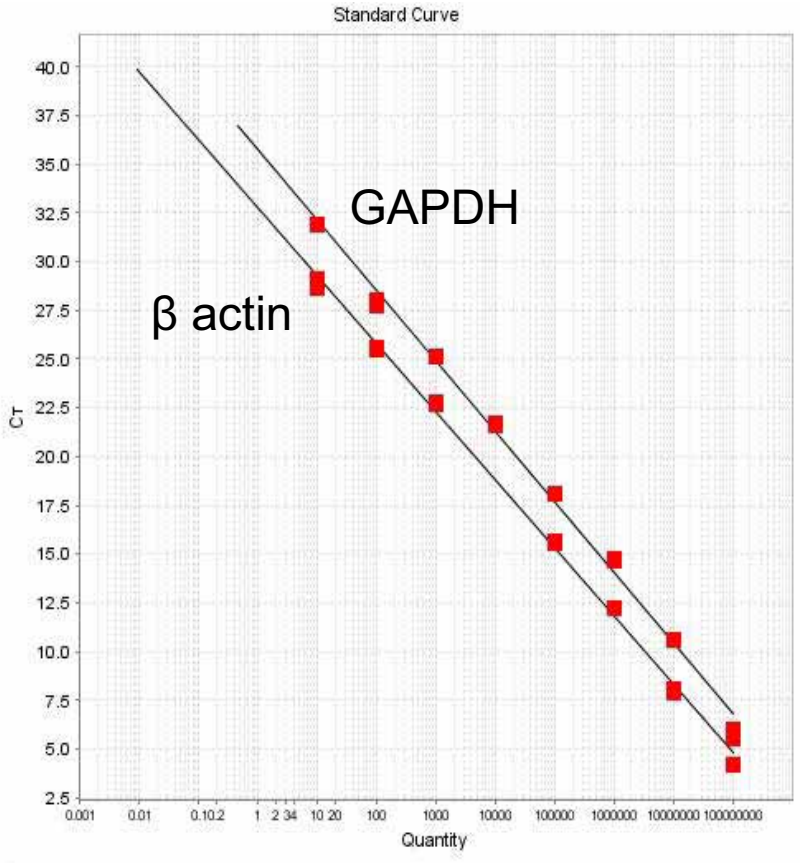


Figure 4.11

Chapter 5: Development of methods for the invPCR assay

Chapter 5.1: Extraction of cellular DNA from liver tissues

5.1.1. Aim

a) To establish methods to extract high MW DNA from small quantities of frozen liver.
b) To determine the DNA method that allows the most efficient recovery of high MW DNA with the least amount of DHBV RI DNA and cccDNA.

5.1.2. Introduction

Numerous DNA extraction methods are available to extract DNA from frozen liver samples. The extraction methods range from commercially available kits to selective and non-selective "manual" extraction methods. In this study, to ensure that the detection of integrated virus-cell junctions using the invPCR assay could be performed efficiently and effectively, the DNA template for the invPCR assay (high MW DNA), needed to be extracted from liver tissues with minimal losses, good DNA purity, and low levels of DNA degradation or shearing.

In addition, to reduce the levels of false positives detected during the invPCR assay, the DNA template for the invPCR assay should contain minimal amounts of viral RI DNA and cccDNA. This is because the PCR primers used in the invPCR assay are specific for the viral sequence, and thus could also amplify the viral DNA to generate false positives. Furthermore, especially in liver tissues collected from chronically infected individuals, viral cccDNA would generally be present at 1 – 50 copies per infected hepatocyte (Summers *et al.*, 1990; Zhang *et al.*, 2003), in contrast to the rare integrated virus-cell junctions that have been detected in only 0.1 – 10% of infected hepatocytes in woodchucks with acute and chronic WHV infection (Summers *et al.*, 2003; Summers and Mason, 2004). High levels of false positives have been observed in invPCR assays of liver tissue from DHBV-infected ducks, where out of 470 invPCR products sequenced by Yang and Summers (Yang and Summers, 1999), only ~6% were shown to be integrated virus-cell junctions, while ~42% were virus-virus false positive sequences and the remaining ~52% invPCR products could not be positively identified. Not only do the false positives interfere with the invPCR assay by greatly reducing the detection rate of integrated virus-cell junctions, ultimately leading to inaccurate quantitation of the number of integrated virus-cell junctions present in each liver tissue, but false positives also contribute to high sequencing costs and waste of reagents used.

In this Chapter, several DNA extraction methods were established, and the most suitable DNA extraction method fosr use prior to the invPCR assay was determined. In previous studies that applied the invPCR assay to detect integrated virus-cell junctions in liver tissues from humans (Mason *et al.*, 2010), chimpanzees (Mason *et al.*, 2009a), woodchucks (Summers *et al.*, 2003; Mason *et al.*, 2005), and ducks (Summers *et al.*, 1990) the most commonly used DNA extraction method was the total DNA extraction method described in Section 5.1.3.3 below. This extraction method been shown to be highly efficient in DNA from small quantities of frozen liver (1 – 10 mg), however, other forms of DNA, especially mitochondrial DNA and viral cccDNA, may also be extracted (Summers *et al.*, 1990).

To improve the detection of integrated virus-cell junctions as well as to reduce costs, DNA extraction methods that selectively extract the high MW DNA whilst removing most viral RI DNA and cccDNA were determined. Some selective DNA extraction methods that had been previously performed included pelleting of nuclei from liver homogenates without prior proteinase K digestion (Summers *et al.*, 2003), selective removal of non-protein bound DNA like cccDNA (Wu *et al.*, 1990; Jilbert *et al.*, 1992), and visualisation and purification of high MW DNA using low melting temperature agarose gel electrophoresis (Mason *et al.*, 2009a). However, although selective DNA extraction methods could effectively reduce the amount of extracted viral RI DNA and cccDNA, significant losses of genomic DNA may also occur. This would greatly reduce the chances of detecting the rare integrated virus-cell junctions, especially when only 1 – 10 mg liver tissues were obtained from liver biopsies. Therefore, a DNA extraction method which leads to minimal losses of genomic DNA, but with low levels of viral RI DNA and cccDNA, would be preferred for invPCR assays.

In addition, the DNA extraction method should also extract genomic DNA of good purity and without degradation or shearing. As the extracted DNA would be subjected to many downstream reactions including restriction enzyme digestions, ligation, and PCR, the extracted DNA should be free of impurities that may reduce the efficiency or interfere with any of the downstream reactions. On the other hand, when the genomic DNA is degraded or sheared, these DNA breaks could interrupt PCR amplification of integrated virus-cell junctions, and thus reducing the copy number of integrated virus-cell junctions detected.

Specifically, this Chapter will establish, analyse, and compare eight different DNA extraction methods to determine the DNA extraction method most suitable to extract DNA templates for invPCR assays. The DNA extraction methods used included the commercially available DNeasy blood and tissue kit (Section 5.1.3.1) and ChargeSwitch gDNA mini tissue kit

(Section 5.1.3.2), the non-selective total DNA extraction method (5.1.3.3), and the selective extractions low melting temperature agarose gel electrophoresis and purification of high MW cellular DNA extraction method (abbreviated as LM gel extraction method in this Chapter) (Section 5.1.3.4), nuclear DNA extraction method (Section 5.1.3.5), and high MW DNA extraction methods I (Section 5.1.3.6), II (Section 5.1.3.7) and III (Section 5.1.3.8).

All eight DNA extraction methods were performed on 1 – 25 mg of frozen liver tissues from the same Pool 7 duck (Triyatni *et al.*, 2001). After optimising all of the DNA extraction methods, all extracted DNA samples were then analysed using Nanodrop spectrometry to determine the amount of nucleic acid in the total extracts (Section 5.1.4.1), and examined by agarose gel electrophoresis to examine possible DNA degradation (Section 5.1.4.2). Possible contamination with inhibitory compounds was also examined by restriction enzyme digestion (Section 5.1.4.3.1) and PCR (Section 5.1.4.3.2). Lastly, the copy number of DHBV total DNA and duck cell DNA present in the extracts were determined by qPCR (Section 5.1.4.4).

5.1.3. Non-selective and selective DNA extraction methods

5.1.3.1. DNeasy blood and tissue kit

The DNeasy blood and tissue kit (Qiagen, Germany) is commonly used in the Hepatitis Research Laboratory to extract total cellular and viral DNA. It utilises direct lysis of tissues or cells using proteinase K, followed by binding of total DNA and RNA onto a silica-based membrane placed in a spin-column. DNA and RNA are then washed and eluted from the membrane. The DNeasy blood and tissue kit can be used to extract total DNA and RNA (genomic, mitochondrial or pathogenic), ranging from 100 bp – 50 kbp in size, from various sample sources, including frozen animal tissues and cells, blood, or bacteria, ranging from sample sizes of 100 – $5x10^6$ cells, with an expected yield of 10 – 30 μg of DNA from 25 mg of liver. As it is expected that 1 mg of duck liver would contain 1.75 μg of DNA (calculated in Section 2.8.9.3.2), this equates to an efficiency of extraction of ~22 – 66%.

The DNeasy blood and tissue kit was used to extract total DNA from ~25 mg of frozen liver tissues according to the instructions provided by the manufacturer as described in Section 2.6.1. The optional step of using RNase to digest RNA was included as liver cells generally contain high levels of RNA. RNA was preferentially removed, as although RNA would not interfere with downstream invPCR assays, it contributes to higher absorbance readings during spectrometry and result in over-estimates of the amount of of DNA present in the samples.

Several advantages of the DNeasy blood and tissue kit include its rapid and easy extraction method, which does not require mechanical homogenising of liver tissue and does not use hazardous chemicals like phenol or chloroform. As the buffer conditions were optimised for specific binding of DNA onto the silica-based membrane, contaminants including proteins and enzyme inhibitors like divalent cations are removed during the washing and centrifugation steps, allowing for extraction of highly pure DNA with a 1.7 – 1.9 ratio of absorbance at a wavelength of 260:280 nm using Nanodrop spectrometry. In addition, as the DNA sample is eluted in low-salt buffer, it could be readily used in various downstream applications without further treatments or the presence of potential inhibitors (Qiagen, 2010).

The disadvantages of this kit include its design to non-selectively extract all the DNA and RNA present in the liver tissues. Therefore, large quantities of viral RI DNA and cccDNA could also be extracted along with the liver cell DNA, and hence contribute to invPCR assay false positives. Moreover, the extracted DNA may contain silica residues originating from the column mesh from the kit, which would inhibit and interfere with downstream reactions.

5.1.3.2. ChargeSwitch gDNA mini tissue kit

The ChargeSwitch gDNA mini tissue kit (Invitrogen, USA) is another total DNA extraction kit that utilises a novel magnetic beads-based technology that has a changeable surface charge according to the pH of the buffer. The kit involves manual mechanical lysis of tissues by homogenisation, followed by binding of the negatively charged DNA backbone to the positively charged magnetic beads. The positive charges of the beads are maintained by the low pH conditions of the buffer solution. After DNA binding, contaminants and proteins can be washed away from the mixture by aqueous wash buffers without significant losses of DNA. Lastly, the purified DNA was eluted from the magnetic beads in the presence of a neutralising low salt elution buffer of pH 8.5. As reported by the manufacturer, the ChargeSwitch gDNA mini tissue kit can be used to extract genomic DNA >20 kbp in size from various tissue samples including 10 – 25 mg of liver, with an expected yield of ~30 µg of DNA from 25 mg of liver. As it is expected that 1 mg of duck liver would contain 1.75 µg of DNA (calculated in Section 2.8.9.3.2), this equates to an efficiency of extraction of ~66%.

The ChargeSwitch gDNA mini tissue kit was used to extract total DNA from ~25 mg of frozen liver tissues according to the instructions provided by the manufacturer as described in Section 2.6.2.

Several advantages of the ChargeSwitch gDNA mini tissue kit include its rapid and easy extraction method, the lack of requirement for centrifugation or vacuum steps, and do not require hazardous chemicals like phenol or chloroform. In addition, the DNA extracts contains only minimal RNA, and could be readily used in various downstream applications without further treatments or the presence of potential inhibitors (Invitrogen, 2010).

The disadvantages of this kit include its design to non-selectively extract all DNA present in the liver tissues to contribute to invPCR assay false positives, similar to the DNeasy blood and tissue kit as described in Section 5.1.3.1. In addition, as this method involved manual homogenisation of liver tissues, the number of concurrent extractions that could be performed is limited by the number of homogenizers available. Besides the recommended 1 mL mini glass homogenizer, other homogenizers suitable for lysis of 25 mg of liver tissues include Douce homogenizers and the autoclavable polypropylene pellet pestles used in this study.

5.1.3.3. Total DNA extraction

One of the most commonly used non-selective manual ("non-kit") total DNA extraction methods used prior to invPCR assays is the total DNA extraction described by Mason *et al.* (Mason *et al.*, 2009b). This method involves lysis of small liver tissues (1 – 5 mg) using proteinase K and SDS with vigorous vortexing, followed by phenol:chloroform extraction and ethanol precipitation. The DNA pellet could be dissolved in water or elution buffer from the DNeasy blood and tissue extraction kit.

The total DNA extraction method was used to extract total DNA from 1 – 10 mg of frozen liver tissues as described in Section 2.6.3. A flowchart of the steps involved in the total DNA extraction methods is shown in Figure 2.1.

Several advantages of the total DNA extraction method include the efficient lysis of small liver tissues without the need of mechanical homogenising, as well as its low losses of DNA as only one phenol:chloroform extraction was involved, to maximise the amount of DNA extracted from as little as 1 mg of liver tissues.

The disadvantages of this extraction method include performing only one organic solvent extraction, which could reduce the purity of extracted DNA due to possible carryover of proteins and organic solvents if the extractions were not performed carefully. In addition, as this extraction method would non-selectively extract all DNA and RNA present in the liver tissues, large quantities of viral RI DNA and cccDNA could also be extracted along with the

liver cell DNA, hence contributing to invPCR assay false positives. The large quantities of extracted RNA could also contribute to higher absorbance readings during spectrometry, resulting in over-estimates of the amount of DNA present in the samples.

5.1.3.4. Low melting temperature agarose gel electrophoresis and purification of high MW cellular DNA

High MW cellular DNA can also be separated from low MW DNA (viral RI DNA and cccDNA) using low voltage and low melting temperature agarose gel electrophoresis (abbreviated as LM gel extraction). The agarose used for this purpose has a low melting temperature of ~65^{o}C (Bio-Rad Laboratories, 2010). The method involves electrophoresis of the total DNA extracted from liver tissues as described in Section 5.1.3.3 using low melting temperature agarose gel electrophoresis. High MW DNA from 10 – 20 kbp and larger, including DNA trapped in the gel wells, were then excised from the gel as shown in Figure 5.1.1, and extracted using the QIAquick gel extraction kit (Qiagen, Germany).

In this study, high MW DNA was visualised and extracted from total DNA (extracted as described in Section 2.6.3), using the LM gel extraction method described in Section 2.6.4.

Several advantages of purifying high MW DNA using this method include the ability to visualise the DNA sample and to specifically select or excise only the high MW DNA. Moreover, the use of low melting temperature agarose allows the gel slices containing the high MW DNA to be used directly in the invPCR assay and to be digested with restriction enzymes directly in the gel mix, omitting the need to extract DNA from the gels. This can avoid losses of DNA to increase the chances of detecting integrated virus-cell junctions present in the genomic DNA. Full details of the invPCR assay protocols and the initial restriction enzyme digestions in the agarose gel mix are described in Section 2.10.2.

The disadvantages of this extraction method include the large quantities of DNA that may be lost during agarose gel electrophoresis from either incomplete separation during electrophoresis, or incomplete recovery of all the high MW DNA present. There is also a risk that DNA pyrimidine dimerisation may occur due to the UVB irradiation that occurs during visualisation of the DNA, and also DNA mutations that may occur after binding with the GelRed nucleic acid dyes, as explored in Section 3.1.4.2. Therefore, to prevent/reduce the UV-related DNA damage, the short-wavelength UVB light from the GelDoc XR imaging system, a known contributer to DNA pyrimidine dimerisation (Runger *et al.*, 2011), was converted to a longer-wavelength UVA light using a UV converter plate.

5.1.3.5. Nuclear DNA extraction

Another method used to selectively extract nuclear DNA, excluding cytoplasmic DNA and RNA as well as mitochondrial DNA, is the nuclear DNA extraction method described by Zhang *et al.* (Zhang *et al.*, 2003). This method involves physical disruption of the cell membrane by homogenisation, followed by low-speed centrifugation to pellet the nuclei. The nuclear membrane was lysed using proteinase K, allowing the nuclear DNA to be subsequently extracted by phenol:chloroform extractions and ethanol precipitation.

The nuclear DNA extraction method was optimised, established, and the extracted DNA was tested for its suitability for invPCR assays as described in Section 5.1.3.5.1 below. A flowchart of the steps involved in the nuclear DNA extraction method is shown in Figure 2.2.

One of the advantages of the nuclear DNA extraction includes its specificity in extracting large amounts of nuclear DNA whilst removing most of the cytoplasmic DNA and RNA. This "concentrates" the amount of genomic DNA present in the mixture relative to the amount of cytoplasmic viral DNA present, hence increasing the chance of detecting integrated virus-cell junctions during the invPCR assay. This also allows removal of cytoplasmic RNA by exclusion and not by RNase digestion, which may not be as complete.

However, one of the biggest flaws in the selectivity of this extraction method is that the viral cccDNA pool present in the nucleus will also be extracted to contribute to invPCR assay false positives. In addition, as this method relies on careful homogenisation of the liver tissue to lyse the cellular membrane whilst keeping the nuclear membrane intact, technical errors can occur due to insufficient or excessive homogenisation. Insufficient homogenisation would result in the cellular membrane remaining intact and therefore cytoplasmic as well is nuclear DNA would be extracted, while excessive homogenisation would in turn result in lysis of the nuclear membrane, thus leading to loss of nuclear DNA during centrifugation to pellet nuclei.

5.1.3.5.1. Optimisation of the nuclear DNA extraction method

The nuclear DNA extraction method published in Zhang *et al.* (Zhang *et al.*, 2003) was adapted and established to extract nuclear DNA from ~10 mg frozen duck liver tissues.

To ensure that each step of the nuclear DNA extraction method had been performed correctly and as expected, DNA was visualised during four steps of the extraction method (labelled A – E in Figure 2.2) using 4',6-diamidino-2-phenylindole (DAPI) fluorescent staining. This was

performed by spreading 100 µL of the DNA mixture onto a microscope slide, and adding one drop of ProLong Gold Anti-fade reagent with DAPI (Invitrogen, USA) onto the mixture. A glass coverslip was then gently lowered and placed onto the microscope slide, followed by sealing of the edges of the coverslip with clear nail polish, and lastly the DAPI-stained DNA was visualised at 358 – 461 nm using fluorescence microscopy, and photographed at 100X magnification. DAPI-bound DNA would be observed as dark blue/purple-stained DNA.

Figure 5.1.2 shows the DAPI-bound DNA during the nuclear DNA extraction method, each corresponding to the steps labelled A – E in Figure 2.2. Results suggest that after homogenisation of the liver tissue and prior to centrifugation (Figure 5.1.2A) most of the DNA was still bound in the nuclei as the DNA was observed as compact round circles. In addition, the cell membrane seemed to have been successfully disrupted, as clusters of nuclei were observed as indicated by the red arrow. After centrifugation to pellet the nuclei and the subsequent resuspension of the pellet in the homogenisation solution (Figure 5.1.2B), similar compact round circles of nuclei-bound DNA were still observed, suggesting that nuclei had been successfully retained during the washing of the pelleted nuclei, and that the nuclear membrane had not been disrupted during centrifugation and the first wash. However, after the second nuclei pellet wash (Figure 5.1.2C), strands of DNA could be observed as indicated by the purple arrow, suggesting that some disruption of the nuclear membrane had begun to occur, allowing the release of DNA previously tightly-contained within the nuclei. Nonetheless, some nuclei-bound DNA was still observed in the solution. Lastly after proteinase K lysis (Figure 5.1.2D), only strands of DNA were observed, suggesting that all the nuclei had been successfully lysed to release the nuclear DNA prior to phenol:chloroform extraction. However, as some smaller DNA strands and fragments were observed, some degradation or fragmentation of DNA may have occurred by this step.

To determine the amount of DNA loss that had occurred during washing of the pelleted nuclei, the wash supernatant was also stained with DAPI to visualise DNA. As shown in Figure 5.1.2E, some intact nuclei could be observed in the discarded wash supernatant, confirming that some nuclei were lost during washes as expected. By counting the total amounts of compact, round nuclei observed before and after each wash, there was an average of ~11% loss of nuclei per wash. Therefore, this showed that the majority of nuclei could be successfully retained after washing, with some losses as expected.

In summary, the nuclear DNA extraction method was successfully established, with retention of ~78% nuclei-bound DNA prior to proteinase K lysis. However, some degradation of DNA

had occurred after the second nuclei wash and proteinase K lysis. Therefore EDTA, a chelating agent commonly-used to reduce damage to DNA and proteins, was included in the digestion solution to prevent the degradation and fragmentation of DNA. The final optimised nuclear DNA extraction method with EDTA is described in Section 2.5.5.

5.1.3.6. High MW DNA extractions

Three DNA extraction methods developed by Dr. Jesse Summers from the University of New Mexico, USA (personal communication) that selectively extract high MW DNA from liver tissues were tested. These methods were based on commonly-used selective methods for the extraction of viral cccDNA (Summers and Mason, 1982; Wu *et al.*, 1990; Jilbert *et al.*, 1992).

Briefly, the cccDNA extraction method (described in Section 2.6.7) involves SDS-KCl precipitation of cell lysates that pellets proteins and K-SDS-protein-DNA complexes, which include cellular DNA and viral RI DNA, to obtain a supernatant containing non-protein-bound DNA, which includes viral cccDNA. cccDNA is then extracted from the supernatant by standard phenol and phenol:chloroform extraction followed by ethanol precipitation (Wu *et al.*, 1990; Jilbert *et al.*, 1992). Thus conversely, to selectively extract DNA while excluding viral cccDNA, a high MW DNA extraction method was developed by Dr. Summers to extract the protein-bound DNA from the precipitated K-SDS-protein-DNA complexes.

Three high MW DNA extraction methods (I, II and III), developed by Dr. Summers (personal communication), were used to extract DNA from ~25 mg frozen liver tissues as described in Sections 2.5.6, 2.5.7 and 2.5.8 respectively. A flowchart of the steps involved in the high MW DNA extraction methods, as well as when the deviations of methods occurred, is shown in Figure 2.3. All three methods share the same initial manual mechanical lysis of small liver tissues by homogenisation in a buffer containing NP40 detergent (known to disrupt the cellular membrane but is not aggressive enough to disrupt the nuclear membrane). This was followed by SDS-KCl precipitation of K-SDS-protein-DNA complexes, which includes the histone-bound host cellular DNA and viral polymerase-bound viral rcDNA, with were subsequently pelleted by centrifugation. After discarding the viral cccDNA-rich supernatant, high MW DNA could then be extracted from the pellet using three different methods.

The first method of extracting high MW DNA from the pellet (high MW DNA extraction I) involved digesting the proteins present in the pellet using Pronase, followed by extraction of DNA using phenol:chloroform. However, this method may extract the viral rcDNA and RI DNA that is covalently bound to the viral polymerase. Hence, the second method (high MW

DNA extraction II) omits the Pronase digestion step, and directly extracts DNA with phenol:chloroform followed by a phenol extraction. Although phenol:chloroform extraction is able to efficiently remove most proteins, a subsequent phenol extraction step was included as phenol may help remove the viral rcDNA present in the pellet, thus reducing the amount of viral DNA extracted (Summers, personal communication). Lastly, as proteins would be present in the original pellet, to further ensure that all proteins were completely removed during extraction, a third method (high MW DNA extraction III) included a subsequent Pronase digestion step followed by a final third phenol extraction. Finally, DNA was then precipitated in all of three methods using standard ethanol precipitation.

A major advantage of these high MW DNA extraction methods includes the exclusion of most viral cccDNA present in the liver tissues, greatly reducing false positives during invPCR assays. The use of Pronase digestion or additional organic solvent extraction steps would also increase the purity of extracted DNA, as these steps ensure that no carryover of proteins would be present in the DNA extract samples.

However, although these methods exclude viral cccDNA, protein-bound viral RI DNA would also be extracted along with the genomic DNA, and thus could still contribute to false positives during invPCR assay. Another disadvantage is that more DNA could be lost during the additional organic solvent extraction steps included in the methods. In addition, as these methods require manual homogenisation of liver tissues, the number of DNA extractions that can be concurrently performed are thus limited to the number of homogenizers available.

5.1.4. Analysis of extracted DNA

5.1.4.1. Amount and purity of total extracts

The amount of DNA extracted from liver tissues using the eight extraction methods described in Section 5.1.3 was determined using the Nanodrop spectrometer as described in Section 2.8.1. The Nanodrop spectrometer can also be used to measure the purity of DNA based on the ratio of the absorbance of nucleic acid at 260 nm wavelength against the absorbance of proteins, phenol or other contaminants at 280 nm wavelength. The A_{260}:A_{280} ratio of 1.8 – 2.0 is generally accepted as a "pure" DNA sample (Thermo Fisher Scientific, 2008).

As RNA also absorbs light at 260 nm, the presence of RNA could contribute to higher concentration of DNA measured using the Nanodrop spectrometer. Hence, the determination of the concentration would not refer to the absolute concentration of DNA present in the sample, but rather the concentrations of all nucleic acids (DNA and RNA) present. The

presence of RNA in the sample can be visualised using agarose gel electrophoresis as described in Section 2.8.7, and can be removed by the addition of an RNase digestion step.

The SpectraMax M2 microplate and cuvette reader (Molecular Devices, USA) has been routinely used in Hepatitis Research Laboratory to measure the concentration of DNA. Similar with the Nanodrop spectrometer, it measures the concentration of nucleic acids based on absorbance at 260 nm wavelength. However, while the Nanodrop spectrometer only requires 1 µL of the sample to be loaded directly onto the stage, the SpectraMax spectrometer requires up to 100 µL of each diluted sample to be loaded into a cuvette tube. To compare the accuracy of absorbance readings measured with each spectrometer, the DNA concentrations of several serial dilutions of two different plasmid samples ranging from 30 – 400 ng/µL were measured using both spectrometers. Results showed that, on average, the DNA concentrations measured by the Nanodrop spectrometer were only 4.75% more than the DNA concentrations measured by the SpectroMax spectrometer (data not shown). Therefore this suggests that the accuracy of the Nanodrop spectrometer in measuring DNA concentration was comparable with the SpectroMax spectrometer, confirming the Nanodrop spectrometer as a reliable instrument that can replace the SpectraMax to measure DNA concentrations in this study.

Using the Nanodrop spectrometer, the amount of DNA extracted from Pool 7 duck liver tissues using the eight extraction methods described in Section 5.1.3 were determined. Knowing that duck liver contains $7x10^8$ cells/gram (Jilbert *et al.*, 1992) and that each cell contains approximately 2.5 pg of cellular DNA (Tiersch and Wachtel, 1991; Krishan *et al.*, 2005), the calculated amount of cellular DNA in 25 and 10 mg of liver would be ~43.8 µg and ~17.5 µg respectively (Section 2.8.9.3.2). However, these figures could only serve as a rough guide of the expected amounts of extracted DNA, as the weight of the initial liver tissues used was neither exact nor identical, and some losses are expected during the extraction process.

Results (Table 5.1.1) showed that both commercially-available DNA extraction kits, DNeasy blood and tissue kit and ChargeSwitch gDNA mini tissue kit, successfully extracted 36.31 µg and 24.45 µg of DNA from ~25 mg of liver respectively, corresponding to ~83% and ~70% extraction efficiency. The higher levels of efficiency of extraction were expected as both kits have been optimised by their respective manufacturers to non-selectively extract all DNA from the tissue samples while removing most RNA by the use of an RNase digestion step in the protocol. The ChargeSwitch gDNA mini tissue kit, which uses magnetic beads for extraction, yielded less DNA than the column-based DNeasy blood and tissue kit. This may be due to the lower binding efficiency of DNA to the magnetic beads, or could be simply due

to slightly less starting liver tissue used for the ChargeSwitch gDNA mini tissue kit. On the other hand, the purity of DNA extracted from the ChargeSwitch gDNA mini tissue kit was higher than the DNeasy blood and tissue kit, with A_{260}:A_{280} of 1.92 and 1.68 respectively. It was suspected that the purity may have been affected by silica residues derived from the DNeasy blood and tissue kits' column mesh that were eluted with the DNA. This was especially seen in several batches of the DNeasy blood and tissue kit, where the eluted DNA solution looked "cloudy" or "mirky" due to the presence of silica, which also interfered with subsequent spectrometry readings. The manufacturer of the kit, Qiagen, acknowledged the issue, and recommended the removal of the silica from eluted DNA by precipitating the silica by centrifugation at 18,000 g for at least 30 min, while retaining the DNA-containing supernatant. Although up to half of the eluted DNA may be lost in this process, this precipitation step has been shown to improve DNA purity as measured using the Nanodrop spectrometer (data not shown). Hence, this precipitation step was performed whenever "cloudy" DNA was eluted, and when the spectrometry readings showed poor DNA purity. In summary, both commercially-available DNA extraction kits DNeasy blood and tissue kit and ChargeSwitch gDNA mini tissue kit were able to efficiently extract large quantities of good quality DNA from 25 mg of liver quickly and without the use of hazardous organic solvents.

For the manual non-selective total DNA extraction method, 18.53 μg of DNA was extracted from 10 mg of liver, which was ~106% of the expected DNA present (refer Table 5.1.1). Minimal loss of DNA was expected for this method, as there was only one phenol:chloroform extraction step involved. But as the amount of extracted DNA was more than expected, this could be because more than 10 mg liver tissue being used, or due to the higher levels of RNA present in the mixture that contributed to high absorbance readings measured using the Nanodrop spectrometer. To obtain a more accurate measurement of the amount of DNA, RNase digestion could be used to remove the RNA present in the extract, or the amount could be estimated by visualising using agarose gel electrophoresis. In addition to greater amounts of extracted DNA, the purity of the extracted DNA was also good with A_{260}:A_{280} of 1.9. As one of the concerns for this extraction method was the potential carryover of phenol, chloroform, or proteins present in the phenol:chloroform-aqueous interface if the phenol:chloroform extraction was not performed accurately, this showed that it is possible to obtain a relatively pure DNA using only one phenol:chloroform step when performed with good technical skills. In summary, as the total DNA extraction method could efficiently extract large quantities of high quality DNA from even small liver tissues (down to 1 of mg), this would be a suitable method to extract total DNA especially from small liver tissues.

Moving on to selective extraction methods, when LM gel extraction was performed to selectively extract high MW DNA from a total DNA extract, only 1.12 μg or ~6.4% of the total DNA (A_{260}:A_{280} of 1.86) was obtained. The lower extraction efficiency could be due to high MW DNA constituting only a small portion of the total DNA (and RNA) present in the total DNA extract, or that the extraction method was not efficient and large quantities of DNA were lost along the multiple processes. However, as the extracted DNA was of good purity, this suggests that this method was able to extract DNA with minimal protein contamination. In summary, although large amounts of high MW DNA were lost by LM gel extraction, the good DNA purity and convenience of the invPCR first cut restriction enzyme performed directly in the gel mix makes this method suitable to be used for DNA samples with a lot of viral RI DNA and cccDNA, or when large amounts of starting DNA were available.

The nuclear DNA extraction method on the other hand extracted 7.43 μg of good DNA purity (A_{260}:A_{280} of 1.98) from 10 mg liver, corresponding to a 42.5% extraction efficiency. This good extraction efficiency of good DNA purity suggests that the nuclear DNA extraction method is so far the most suitable selective extraction method. However, the method was not easily repeated, and variable extraction outcomes were often observed between each extraction, and sometimes even losing the entire DNA samples during extractions (data not shown). This could be due to several variable steps in the nuclear DNA extraction method, which include the homogenisation of liver tissues to lyse the cellular membrane whilst keeping the nuclear membrane intact, and the efficiency of precipitation of nuclei without disrupting the nuclear membrane. On top of that, the quality of the liver tissues has to be good, as weak cellular and nuclear membrane could lead to DNA losses during the nuclei pelleting steps. It is thus recommended that the nuclear DNA extractions be performed in at least duplicates for each sample. In summary, the nuclear DNA extraction method can efficiently extract nuclear DNA of good purity, but is not very consistently reproducible.

Lastly, the three variations of high MW DNA extraction, methods I, II, III, extracted 3.55 μg, 1.85 μg and 1.20 μg of DNA from 10 mg of liver, corresponding to 20.3%, 10.5% and 6.9% extraction efficiency respectively. As expected, when more phenol:chloroform or phenol extraction steps were included, the loss of DNA was increased, as seen in the 2-fold difference of the amount of DNA extracted using method I and II, and the 1.5-fold difference between methods II and III. The purity of extracted DNA with the use of Pronase to remove proteins in methods I and III was also similar when no Pronase was used in method II, suggesting that the additional Pronase step was not necessary, with the organic solvents being sufficient. On top of that, the purity of extracted DNA as determined by A_{260}:A_{280} was only

increased slightly with additional phenol:chloroform or phenol extraction steps, suggesting that additional extraction steps were not necessary. In summary, the high MW DNA extraction methods with multiple phenol:chloroform and phenol steps would not be the necessary and required to be used in invPCR assays.

5.1.4.2. Quality of extracts

To confirm the results obtained by Nanodrop spectrometry in Section 5.1.4.1, the quality of each sample of extracted DNA was visualised using agarose gel electrophoresis. Briefly, ~200 ng of each extracted DNA sample was electrophoresed in a 1% agarose gel, and visualised under UV light after GelRed staining as described in Section 2.8.7.

As shown in Figure 5.1.3, all extractions successfully extracted high MW DNA, with some RNA extracted by the total DNA extraction (lane 3) and nuclear DNA extraction (lane 8). High MW DNA was also observed trapped in the wells of the gel for all extraction methods except the LM gel extraction (lane 4) and nuclear DNA extraction (lane 8). Some degradation of DNA was observed using the DNeasy blood and tissue kit (lane 1) and LM gel extraction (lane 4), as seen by the DNA smears in both lanes, as compared to a tight high MW DNA band seen in other lanes. On the other hand, smears of smaller sized DNA were observed for high MW DNA extraction methods I, II, III (lanes 5 – 7), suggesting that a lot of degradation of DNA or RNA had occurred. The best quality of extracted DNA was found to have been extracted using the ChargeSwitch gDNA mini tissue kit (lane 2), as the extracted DNA formed a tight high MW DNA with little degradation of DNA and no RNA present.

On a separate note, the high levels of RNA observed in the DNA extracted by the total DNA extraction (lane 3) and the nuclear DNA extraction (lane 8) may indeed have contributed to high amounts of DNA measured by the Nanodrop spectrometer for both samples, as previously suspected in Section 5.1.4.1. Therefore, the actual amount of DNA and the extraction efficiency (%) would be less than as reported in Section 5.1.4.1.

In summary, all extraction methods successfully extracted high MW DNA from duck liver tissues, with the ChargeSwitch gDNA mini tissue kit showing the greatest quality of extracted DNA. These agarose gel electrophoresis observations also confirmed the purity of DNA that was determined by the Nanodrop spectrometer in Section 5.1.4.1.

5.1.4.3. Inhibition of downstream reactions

As the extracted DNA was to be used as template in invPCR assays, it was important to check that the DNA extracts did not contain any carryover proteins or contaminants that could inhibit downstream reactions, including restriction enzyme digestions, PCR and qPCR. Previously, inhibition of downstream restriction enzyme reactions have been observed especially from DNA extracted using the high MW DNA extraction methods (unpublished data). Potential inhibitors include carryover of organic solvents, SDS detergent, contaminating chemicals from impure reagents used like EDTA and alcohol. High salt levels present in the extracted DNA can also alter the solution environment and subsequently reduce the efficiency of the digestion by salt-sensitive restriction enzymes. Therefore, to ensure that downstream reactions will not be inhibited, restriction enzyme digestions (Section 5.1.4.3.1) and PCR (Section 5.1.4.3.2) were performed using all extracted DNA as DNA template.

5.1.4.3.1. Restriction enzyme digestion

To ensure the extracted DNA samples did not inhibit downstream restriction enzyme digestions, each DNA sample was "spiked" with pBL4.8x2 plasmid DNA. If no inhibition had occurred, the plasmid DNA would be successfully digested to form linear DNA, and the changes in plasmid forms and DNA sizes can be visualised using agarose gel electrophoresis.

To achieve this aim, 200 ng of pBL4.8x2 plasmid (refer Figure 3.2.1A for plasmid map) were added to 200 ng of DNA extracted using each of the eight extraction methods described in Section 5.1.3. Keeping aside a total of 100 ng of the DNA mixture (containing both plasmid and extracted DNA), the rest of the DNA mixture was digested using 5 U of *Eco*RI overnight as described in Section 2.8.2. After that, 100 ng of each DNA sample before and after restriction enzyme digestion was subsequently visualised by agarose gel electrophoresis as described in Section 2.8.7. It is expected that for the undigested DNA mixture, the high MW DNA pattern similar to Figure 5.1.3, as well as at least 2 bands from the undigested circular plasmid DNA corresponding to the supercoiled and relaxed circular DNA forms of the plasmid will be observed. Conversely, for the digested DNA mixture, many smaller DNA fragments of varying sizes from the randomly-digested cellular DNA would be observed as smears, with the linear form of the *Eco*RI-digested pBL4.8x2 plasmid expected to produce three fragments the sizes of 2091, 3027 and 3027 bp each.

As shown in Figure 5.1.4A, the undigested DNA mixture showed that all extracted DNA samples were "spiked" with equal amounts of circular pBL4.8x2 plasmid. This was shown by the high MW DNA and two forms of plasmid DNA observed in each lanes. After *Eco*RI

digestion (Figure 5.1.4B), the high MW DNA and plasmid DNA forms were no longer present. Instead, a ~3 kbp band and small DNA fragments or smears were observed in each lane. This showed that both the high MW DNA and the pBL4.8x2 plasmid had been successfully digested by *Eco*RI, therefore confirming that DNA samples from all eight extraction methods produced do not inhibit downstream restriction enzymes digestions.

In summary, none of the DNA samples extracted using the eight extraction methods described in Section 5.1.3 inhibited downstream restriction enzyme activities.

5.1.4.3.2. PCR

To ensure that the extracted DNA did not inhibit downstream PCR reactions, standard PCR was performed using each extracted DNA sample as DNA template. Briefly, standard PCR reactions were performed to amplify the duck β actin gene, a housekeeping gene found in the duck DNA, using the primer set Duck β actin RT F – Duck β actin RT R2 (refer Table 2.2), using ~50 ng of each of the extracted DNA samples as template, as described in Section 2.8.5. PCR products were subsequently visualised using agarose gel electrophoresis as described in Section 2.8.7, and were expected to produce a 151 bp PCR product.

As shown in Figure 5.1.5, the duck β actin gene was successfully amplified from all extracted DNA samples, as the expected 151 bp PCR product was produced in all samples.

In summary, none of the DNA extracted using the eight extraction methods described in Section 5.1.3 inhibited PCR reactions, and thus could be used for downstream invPCR assays.

5.1.4.4. Quantitation of DHBV DNA and genomic DNA

Lastly, the amount of DHBV DNA present in the extracted DNA was quantified using qPCR. Sections 5.1.4.1 to 5.1.4.3 had shown that all extraction methods could extract good quality and pure DNA that do not inhibit downstream reactions. However, the amount of DHBV DNA and duck cellular DNA present in the each sample were not determined. As the invPCR assay is designed to detect integrated DHBV DNA in the genome, the optimal DNA template for invPCR assays should have the maximum amount of cellular DNA and the minimum amount of extra-chromosomal DHBV DNA, to reduce the levels of false positives detected.

qPCR was performed using 100 ng of extracted DNA (without *Eco*RI digestion) as DNA template as described in Section 2.8.9, using primer sets 423 – 576c to amplify DHBV total

DNA, and Duck β actin RT F – Duck β actin RT R2 to amplify the duck β actin gene as an internal control, as established in Chapter 4 (refer Table 2.2 for primer sequences).

100 ng of extracted duck DNA is estimated to correspond to ~$3.57x10^5$ duck liver cell equivalents of DNA (calculations as shown in Section 2.8.9.3.2). Therefore, assuming that the duck β actin gene is present in the duck genome as a single copy gene, there would be ~$7.14x10^5$ copies of duck β actin gene in each diploid duck cell. It is also estimated that there would be at least 500 copies of DHBV total DNA in the form of either RI DNA and/or DHBV cccDNA in the congenitally chronic DHBV infected Pool 7 ducks (Jilbert *et al.*, 1992).

Interestingly, results (Table 5.1.2) showed that variable amounts of duck β actin were observed in 100 ng of DNA from each extraction method. This could be due the various levels of RNA present in the DNA samples (as seen in Figure 5.1.3) that would be measured by the Nanodrop spectrometry to give an under-measurement of the actual DNA amounts. Thus, it was not surprising that the amount of DHBV total DNA normalised with β actin was higher than the DHBV total DNA calculated based on the expected amount of cells present. However, as the trend of the amount of DHBV total DNA is similar for both calculations, this validates the duck β actin qPCR assay established in Chapter 4 (Section 4.4.4) as an internal control.

Based on the amount of DHBV total DNA normalised to duck β actin (Table 5.1.2), it was observed that the non-selective extraction methods, which include both kits (DNeasy blood and tissue kit and ChargeSwitch gDNA mini tissue kit) and the total DNA extraction method, contained similar amounts of DHBV total DNA (averaging 307 copies). As this is less than the expected ~500 copies of DHBV total DNA, it might be possible that some DHBV DNA was lost during the extraction process, to suggest some form of extraction selectivity.

A clear contrast was seen in DNA extracted by the selective extraction method, LM gel extraction, which contained only 10.55 copies of DHBV total DNA. This suggests that physical separation of high MW cellular DNA and the lower MW DHBV DNA using agarose gel electrophoresis were efficient, and by excising only the high MW DNA from the agarose gel, this selectively and effectively exclude most of the lower MW DHBV total DNA.

On the other hand, DNA extracted by another selective extraction method, nuclear DNA extraction, was found to contain 83.35 copies of DHBV total DNA. As the copy number of DHBV DNA was less than the non-selective methods mentioned above, some selectivity had definitely occurred to exclude DHBV DNA. The DHBV DNA extracted by this method was

likely to be the DHBV cccDNA that is found in the nucleus, which could be 1 – 17 copies in each infected hepatocyte nucleus during chronic DHBV infection (Zhang *et al.*, 2003).

For the remaining selective high MW DNA extraction methods, the extraction method with the greatest copy number of DHBV total DNA was the high MW DNA extraction I with 645.37 copies. This suggests that the Pronase digestion before phenol:chloroform extraction did indeed allow for the co-extraction of virus polymerase-bound rcDNA, thus resulting in high levels of extracted DHBV DNA. High levels of DHBV total DNA (225.31 copies) were also seen in the high MW DNA extraction III that also used Pronase digestion of proteins, although the Pronase digestion was performed in between phenol extractions. As the level of DHBV total DNA was lower than high MW DNA extraction I, this suggests that the phenol extraction step before Pronase digestion can reduce the amount of extracted DHBV DNA. However, when compared with the high MW DNA extraction II, only 25.15 copies of DHBV total DNA were detected. This amount was comparable with the DHBV total DNA levels found in the LM gel extraction, showing that the high MW DNA extraction II could efficiently and selectively extract high MW DNA while removing DHBV total DNA. In summary, the digestion of proteins by Pronase during extraction resulted in the extraction of more DHBV DNA and thus would not be suitable for invPCR assays. In addition, it was shown that using phenol and phenol:chloroform extractions alone were sufficient in extracting duck cellular DNA while removing most of the DHBV total DNA present in the liver.

Summarising Section 5.1.4, as DNA extracted using all eight extraction methods were of good quality and did not inhibit downstream reactions, the most suitable DNA extraction method to be used for downstream invPCR assays would be determined by the DNA extraction method that extracts genomic DNA with minimal losses, good DNA purity, least DNA degradation or shearing, and containing the least amount of viral RI DNA and cccDNA in the extract. Comparing the commercially-available DNA extraction kits, as several batches of the DNeasy blood and tissue kit had silica residue problems, ChargeSwitch gDNA mini tissue kit would be the preferred kit. However, as at least 20 mg of liver tissue has to be used, the ChargeSwitch gDNA mini tissue kit would not be suitable when only small amounts of starting liver tissue are available. For manual extractions, total DNA extraction would be one of the best extraction methods as it has good extraction efficiency, the levels of extracted DHBV total DNA (normalised to duck β actin gene) were most similar to the kits, and can be used on as little as 1 mg of liver tissue. Although the LM gel extraction method has the lowest levels of DHBV total DNA, as it has poor extraction efficiency, this method would be suitable when large amounts of starting liver is available or when the removal of DHBV DNA is

essential to justify the large losses of cellular DNA. The nuclear DNA extraction on the other hand, although having acceptable extraction efficiency, is not consistently reproducible and had extracted high levels of DHBV total DNA. Thus this method would not be suitable for the downstream invPCR assays. Lastly, the high MW DNA extractions I, II, III had poor extraction efficiency, and except for method II, has high copies of DHBV total DNA. Hence, all three high MW DNA extraction methods would not be used for downstream invPCR assay.

5.1.5. Conclusion

In conclusion, the total DNA extraction method was found to be the most suitable method to extract DNA for downstream invPCR assays in this study, as the method was able to extract good quality cellular DNA from small quantities of liver tissue, with relatively good extraction efficiency. The Invitrogen ChargeSwitch gDNA mini tissue kit was also suitable for extracting DNA from larger liver tissues (up to 20 mg). However, when the removal of DHBV DNA was essential, LM gel extraction method would be performed, but with the compromise of losing large quantities of cellular DNA during the process.

Table 5.1.1: Analysis of the total amount, purity and percentage extraction efficiency of DNA extracted from Pool 7 duck liver tissues using eight different DNA extraction methods.

DNA extraction method[a]	Liver tissue[b] (mg)	Total amount of extracted DNA[c] (µg)	Extraction efficiency[d] (%)	A_{260}:A_{280}[e]
DNeasy blood and tissue kit	25	36.31	83.0	1.68
ChargeSwitch gDNA mini tissue kit	20	24.45	70.0	1.92
Total DNA extraction	10	18.53	106.0	1.90
LM gel extraction	10	1.12	6.4	1.86
Nuclear DNA extraction	10	7.43	42.5	1.98
High MW DNA extraction I	10	3.55	20.3	1.66
High MW DNA extraction II	10	1.85	10.5	1.74
High MW DNA extraction III	10	1.20	6.9	1.75

[a]DNA was extracted from frozen liver tissues from the same chronic DHBV-infected Pool 7 duck, using eight different DNA extraction methods as described in Sections 2.6.1 to 2.6.6.

[b]Estimated weight of frozen liver tissue used for each extractions. Some variations of the exact amount of liver tissue may occur.

[c]Total amount of extracted DNA was calculated from the concentration of extracted DNA determined using the Nanodrop spectrometer as described in Section 2.8.1 (data not shown), and the volume of final eluted DNA.

[d]Extraction efficiency refers to the percentage of the total amount of extracted DNA in relation to the expected amount of DNA present in 25 mg and 10 mg of liver. Based on calculations in Section 2.8.9.3.2, 25 mg and 10 mg of liver tissue would contain ~43.8 µg and ~17.5 µg of cellular DNA respectively.

[e]A_{260}:A_{280} is the ratio of absorbance readings of the DNA sample using the Nanodrop spectrometer at 260 nm (A_{260}) to 280 nm (A_{280}) wavelength. It refers to the purity of the DNA sample, of which the A_{260}:A_{280} of 1.8 – 2.0 is generally accepted as a "pure" DNA sample.

Table 5.1.2: Copy number of DHBV total DNA and duck β actin genes in DNA samples extracted using various DNA extraction methods as quantified by qPCR.

DNA extraction method[a]	DHBV total DNA[b]	Duck β actin[c]
DNeasy blood and tissue kit	12,001,287.50	73,717.50
ChargeSwitch gDNA mini tissue kit	3,483,593.00	24,170.31
Total DNA extraction	3,375,316.13	27,255.14
LM gel extraction	289,577.22	54,904.95
Nuclear DNA extraction	711,725.84	17,078.98
High MW DNA extraction I	14,207,370.00	44,028.77
High MW DNA extraction II	408,509.60	32,485.93
High MW DNA extraction III	2,721,699.13	24,159.26

DNA extraction method[a]	DHBV total DNA per cell[d]	DHBV total DNA normalised to β actin[e]
DNeasy blood and tissue kit	336.04	325.60
ChargeSwitch gDNA mini tissue kit	97.54	288.25
Total DNA extraction	94.51	247.68
LM gel extraction	8.11	10.55
Nuclear DNA extraction	19.93	83.35
High MW DNA extraction I	397.81	645.37
High MW DNA extraction II	11.44	25.15
High MW DNA extraction III	76.21	225.31

[a]DNA was extracted from frozen liver tissues from the same chronic DHBV-infected Pool 7 duck, using eight different DNA extraction methods as described in Sections 2.6.1 to 2.6.6.

[b]DHBV total DNA was quantified by qPCR using primer set 423 – 576c (refer Table 2.2) and 100 ng of extracted DNA (without *Eco*RI digestion) as template, and using standard curves generated from serial dilutions of pBL4.8 plasmid as described in Section 2.8.9.

[c]The duck β actin gene was quantified by qPCR using primer set Duck β actin RT F – Duck β actin RT R2 (refer Table 2.2) and 100 ng of extracted DNA (without *Eco*RI digestion) as template, and using standard curves generated from serial dilutions of pT2.1DgB2 plasmid, as described in Section 2.8.9. The duck β actin gene was used as a qPCR internal control.

[d]DHBV total DNA per cell was calculated based on the expected amount of 35,714 cells present in 100 ng of DNA, as calculated in Section 2.8.9.3.2.

[e]DHBV total DNA per cell was calculated by normalising the qPCR-quantified DHBV total DNA with the qPCR-quantified duck β actin gene. This calculation assumes that duck β actin gene is a single copy gene, and present in 2 copies per diploid duck cell.

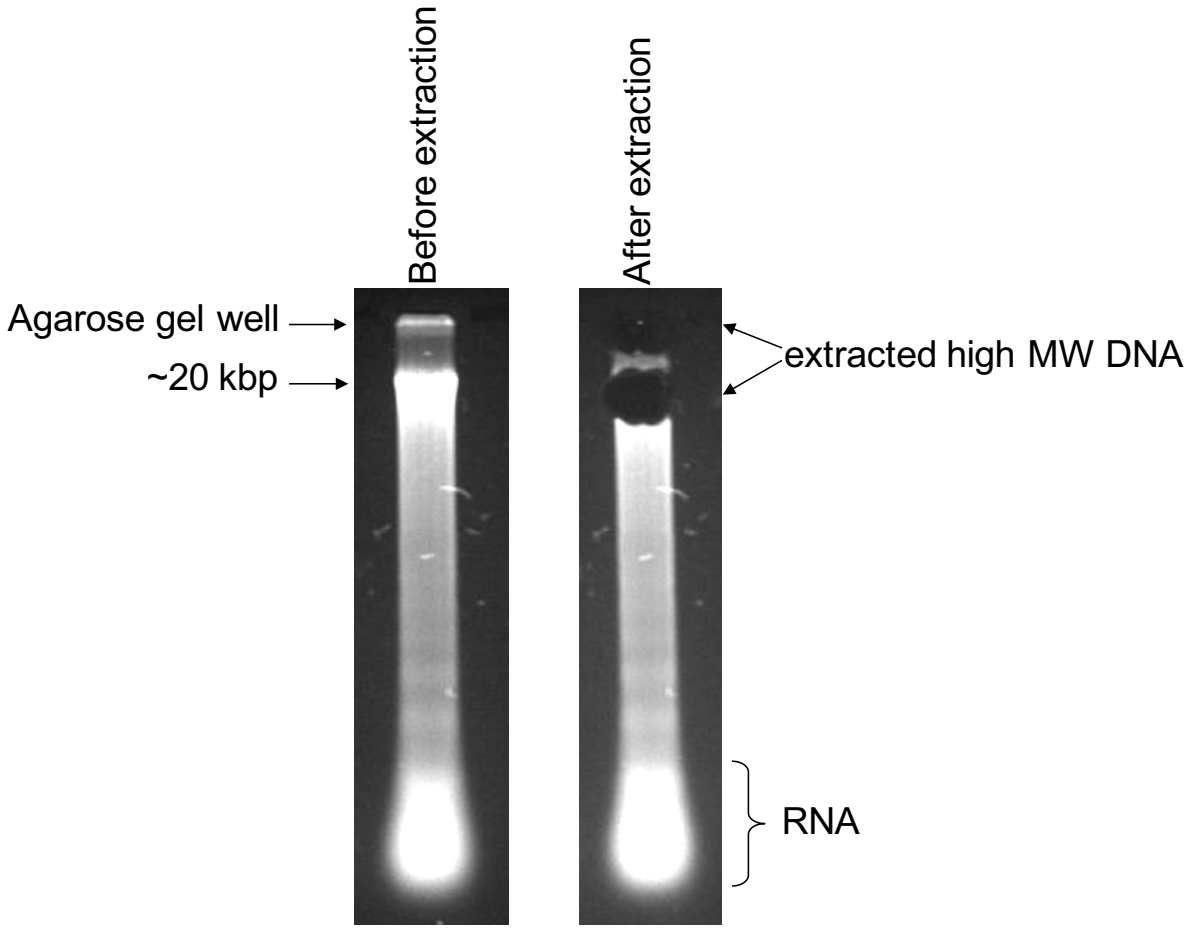


Figure 5.1.1: Separation and purification of high MW DNA using low melting temperature agarose gel electrophoresis, visualised under 302 nm UV light.

Total DNA extracted as described in Section 5.1.3.3 was subjected to low melting temperature agarose gel electrophoresis, and visualised under UV after GelRed post-staining as described in Section 2.6.4.

The extracted total DNA was shown to consist of high MW DNA (tight dense band at ~20 kbp) at the top of the gel, some lower MW DNA (including possibly viral cccDNA and RI DNA) smears and fragmented DNA, and large quantities of RNA at the bottom of the gel.

High MW DNA, which include the DNA trapped at the gel wells and DNA around 10 – 20 kbp and larger, were then excised from the gel into clean 1.5 mL tubes, leaving behind the lower MW DNA and RNA.

Figure 5.1.2: Visualisation of fluorescent DAPI-stained DNA during various steps of the nuclear DNA extraction method under 358 – 461 nm light.

DNA was extracted from liver tissues using the nuclear DNA extraction method as described in Section 5.1.3.5.1. All pictures were viewed using fluorescence microscope and photographed at 100X magnification.

In Figure 5.1.2A, after homogenisation of the liver tissues, DNA was found to be still bound in the nuclei as DNA were observed as compact round circular dots. Clustering of nuclei as indicated by the red arrow also suggest that the cellular membrane of cells had been successfully lysed, hence allowing the released nuclei to cluster together.

In Figure 5.1.2B, after the first nuclei pellet wash, the DNA was found to be successfully retained, comparable with the DNA prior to washing (Figure 5.1.2A), with similar nuclei-bound DNA observed as compact round circular dots and clustering of nuclei as indicated by the red arrow.

In Figure 5.1.2C, after the second nuclei pellet wash, some strands of DNA were found as indicated by the purple arrow, suggesting that some disruption of the nuclear membrane had begun to occur, releasing strands of DNA previously tightly-bound in the nuclei. However, some nuclei-bound DNA was still observed as compact round circular dots as indicated by the red arrow.

In Figure 5.1.2D, after proteinase K lysis, DNA was no longer nuclei bound and was observed as strands of DNA. However, some small DNA strands and fragments were found, suggesting that some degradation or fragmentation of DNA may have occurred.

In Figure 5.1.2E, some nuclei-bound DNA could be observed in the discarded supernatant of the nuclei pellet washes, showing that low quantities of DNA were being lost during each washing step. By calculating the amount of nuclei-bound DNA present in the wash supernatant, it was estimated that up to ~11% of nuclei were lost per wash.

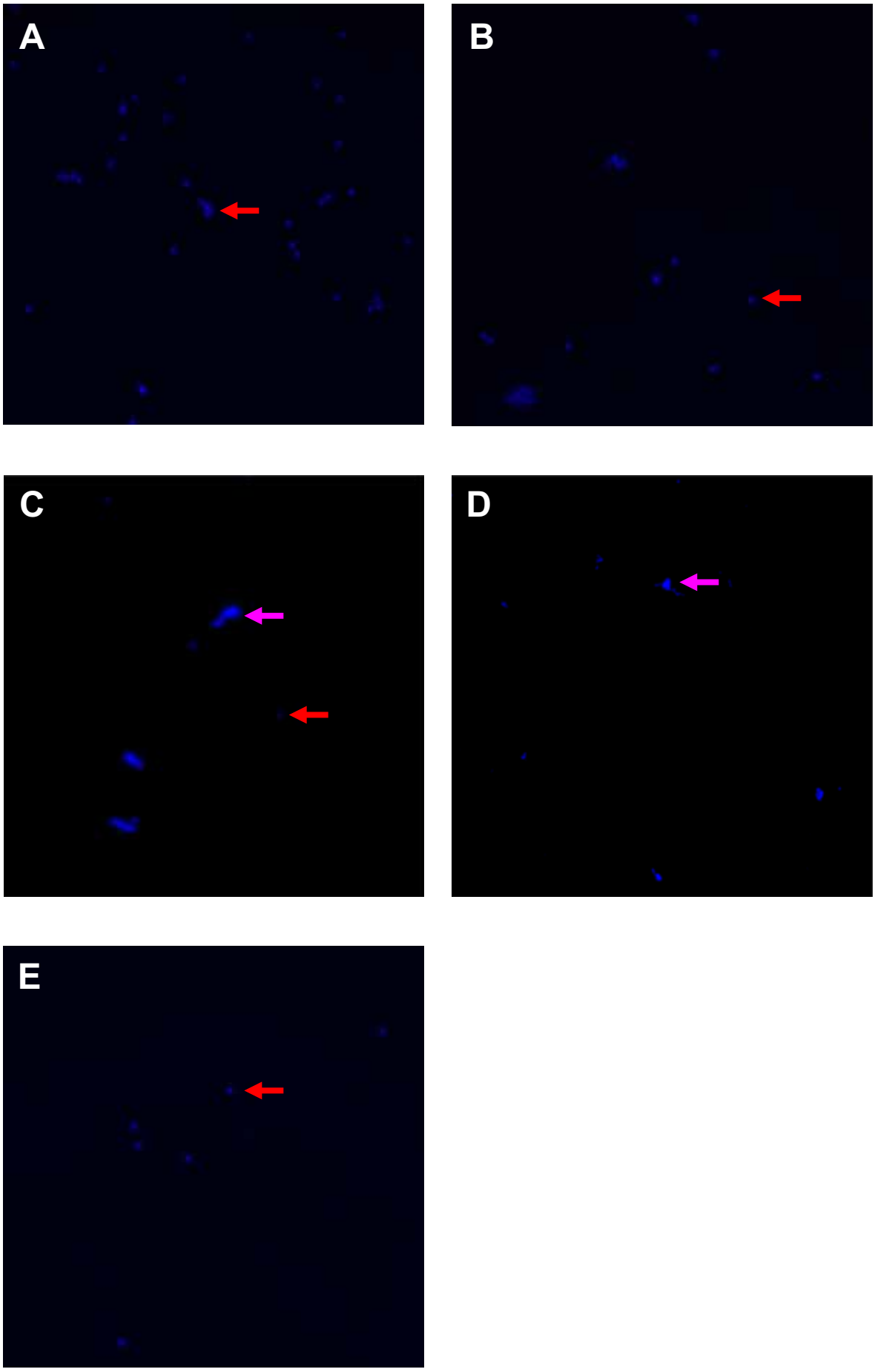


Figure 5.1.2

Figure 5.1.3: The quality and content of DNA samples extracted using various DNA extraction methods visualised using agarose gel electrophoresis under 302 nm UV light.

All DNA samples were extracted from frozen liver tissues from the same chronic DHBV-infected Pool 7 duck, using eight different DNA extraction methods as described in Section 2.6.1 to 2.6.6. The concentration of DNA was then measured using the Nanodrop spectrometer as described in Section 2.8.1, from which 200 ng were ran on 1% agarose gel electrophoresis, and visualised under UV after GelRed post-staining as described Section 2.8.7.

All DNA samples were shown to contain the ~20 kbp high MW DNA, some of which was still trapped in the agarose gel wells. Some degradation of DNA could be observed as smearing of the high MW DNA band for example in DNA extracted using the DNeasy blood and tissue kit (lane 1), or as fragmented DNA or smearing of lower MW DNA for example in DNA extracted using high MW DNA extraction III (lane 7). RNA was also observed in samples extracted by total DNA extraction (lane 3) and nuclear DNA extraction (lane 8).

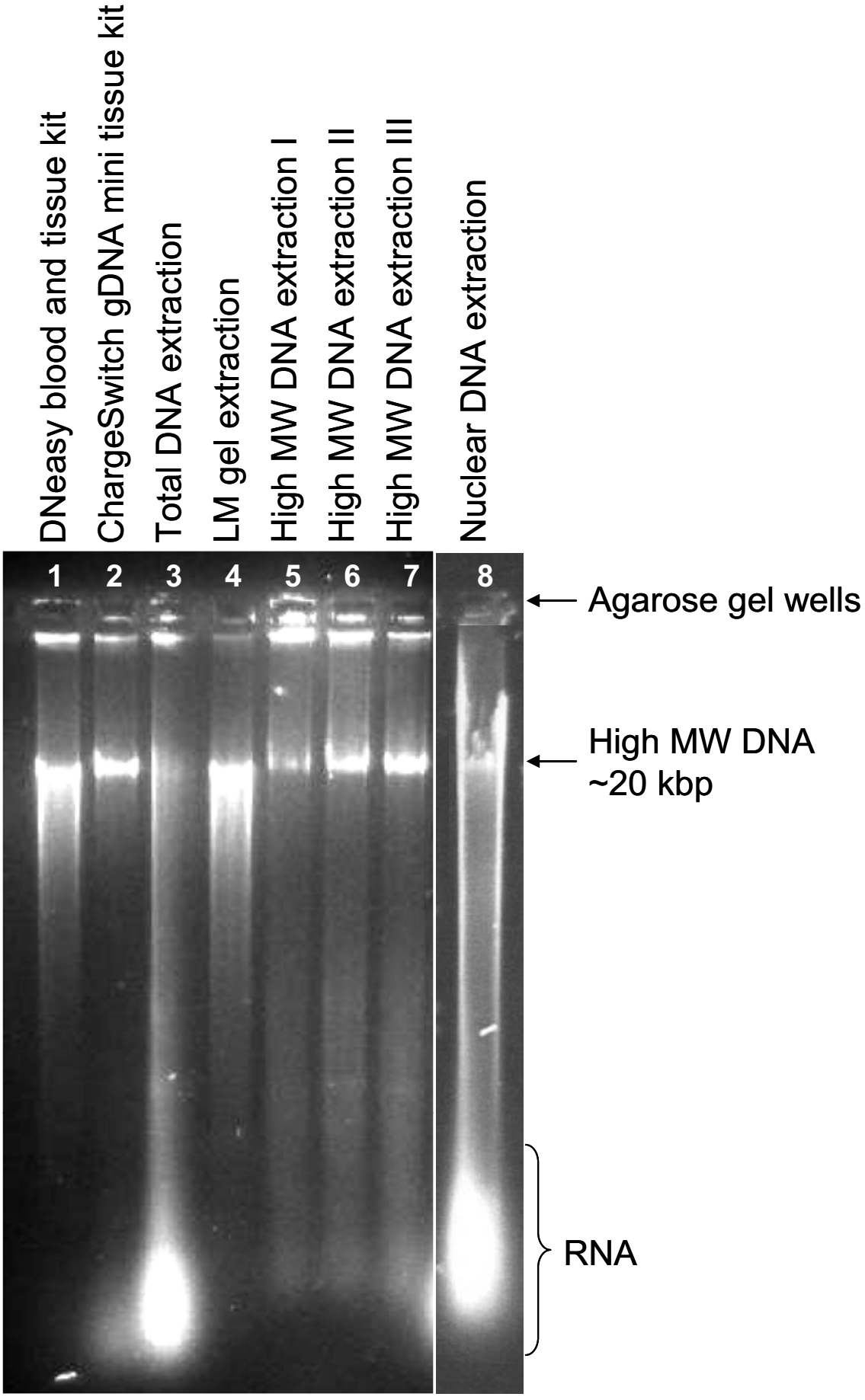

DNeasy blood and tissue kit
ChargeSwitch gDNA mini tissue kit
Total DNA extraction
LM gel extraction
High MW DNA extraction I
High MW DNA extraction II
High MW DNA extraction III
Nuclear DNA extraction
1
2
3
4
5
6
7
8
Agarose gel wells
High MW DNA
~20 kbp
RNA

Figure 5.1.3

Figure 5.1.4: Restriction enzyme digestion of DNA mixture containing DNA extracted from liver samples using various extraction methods and pBL4.8x2 plasmid, to determine the possible inhibition of downstream restriction enzyme activities.

All DNA samples were extracted from frozen liver tissues from the same chronic DHBV-infected Pool 7 duck, using eight different DNA extraction methods as described in Section 2.6.1 to 2.6.6. The concentration of DNA was then measured using the Nanodrop spectrometer as described in Section 2.8.1, and 200 ng of pBL4.8x2 plasmid was added to 200 ng of extracted DNA to produce a DNA mixture. Up to 100 ng of DNA mixture was then subjected to 1% agarose gel electrophoresis and visualised under UV after GelRed post-staining, as described Section 2.8.7 (Figure 5.1.4A). A total of 300 ng of the DNA mixture was also digested with 5 U of *Eco*RI overnight as described in Section 2.8.2, from which 100 ng of DNA mixture after *Eco*RI digestion was then was then subjected to 1% agarose gel electrophoresis and visualised under 302 nm UV after GelRed post-staining as described Section 2.8.7 (Figure 5.1.4B).

In Figure 5.1.4A, high MW DNA and two forms of plasmid DNA (relaxed circular plasmid and supercoiled plasmid) were observed in each DNA mixture. These suggest that all extracted DNA samples were "spiked" with equal amounts of circular pBL4.8x2 plasmid.

In Figure 5.1.4B, a ~3 kbp band and small DNA fragments or smears were observed in each DNA mixture, corresponding to the expected 2091, 3027 and 3027 bp fragments of the *Eco*RI-digested pBL4.8x2 plasmid. These suggest that both the high MW DNA and the pBL4.8x2 plasmid had been successfully digested by *Eco*RI to produce fragmented DNA and the expected ~3 kbp band respectively.

No inhibition of downstream restriction enzyme activities was observed in any of the DNA mixtures.

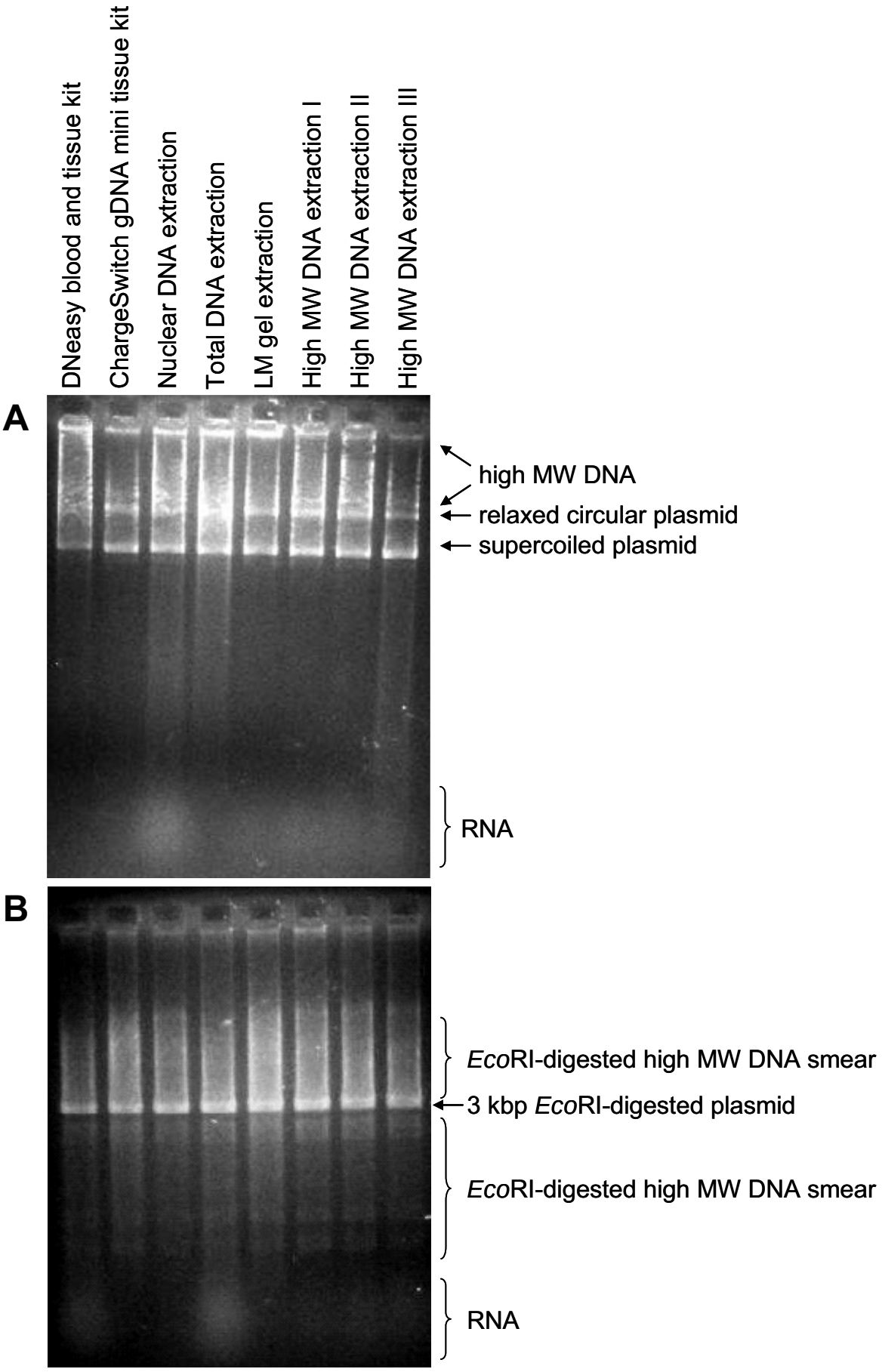

DNeasy blood and tissue kit
ChargeSwitch gDNA mini tissue kit
Nuclear DNA extraction
Total DNA extraction
LM gel extraction
High MW DNA extraction I
High MW DNA extraction II
High MW DNA extraction III
A
high MW DNA
relaxed circular plasmid
supercoiled plasmid
RNA
B
EcoRI-digested high MW DNA smear
3 kbp EcoRI-digested plasmid
EcoRI-digested high MW DNA smear
RNA

Figure 5.1.4

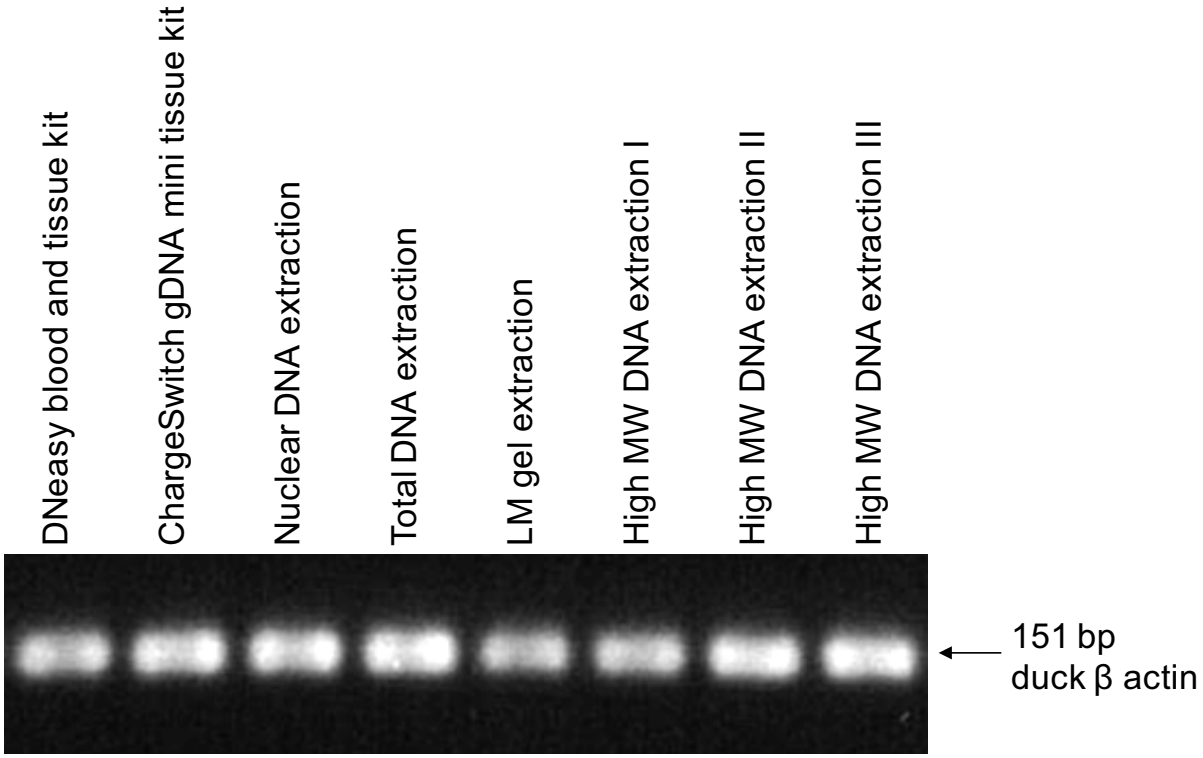


Figure 5.1.5: PCR amplification of duck β actin gene using DNA samples extracted from liver samples using various DNA extraction methods as template, to determine the possible inhibition of downstream PCR reactions.

All DNA samples were extracted from frozen liver tissue from the same chronic DHBV-infected Pool 7 duck, using eight different DNA extraction methods as described in Sections 2.6.1 to 2.6.6. The concentration of DNA was then measured using the Nanodrop spectrometer as described in Section 2.8.1. Up to 50 ng of DNA was then used as template for PCR reactions performed using the primer set Duck β actin RT F – Duck β actin RT R2 (refer Table 2.2), as described in Section 2.8.5. PCR products were subjected to 1% agarose gel electrophoresis and visualised under 302 nm UV after GelRed post-staining as described Section 2.8.7. The PCR reaction is expected to amplify 151 bp of the duck β actin gene.

All reactions successfully produced a 151 bp PCR product that corresponds to the size of the expected duck β actin gene PCR product. No inhibition of downstream PCR activities was observed in any of the DNA mixtures.

Chapter 5.2: The use of locked nucleic acid (LNA) oligonucleotides to increase the specificity of invPCR assays

5.2.1. Aim

a) To design and synthesise locked nucleic acid (LNA) oligonucleotides specific for AusDHBV DNA.
b) To use LNA oligonucleotides to block amplification of DHBV DNA during PCR.
c) To use LNA oligonucleotides to block or reduce the amplification of DHBV false positives during invPCR assays, in order to increase the specificity of the detection of integrated DHBV-cell junctions in duck liver tissues.

5.2.2. Introduction

In previous studies, one of the main problems encountered during the invPCR assay was the high level of false positives. These false positives were virus-virus sequences, contributed mainly by the viral DNA present in the liver that had been inverted and ligated by the invPCR assay, and subsequently amplified as virus-specific primers were used during nested PCR. This was a significant problem as the levels of viral DNA in the liver, in both RI DNA and cccDNA forms, were present in a greater abundance than integrated viral DNA. Therefore, more virus-virus sequences were likely to be detected instead of the rare integrated virus-cell junctions. High levels of virus-virus false positives have been reported in various previous studies, for instance, as high as 41.7% of the total invPCR reactions performed in chronic DHBV-infected ducks were false positives (Yang and Summers, 1999); 23.6% false positives in chronic WHV-infected woodchucks (Mason *et al.*, 2005); and 38.7% false positives in chronic HBV-infected chimpanzees, (Mason *et al.*, 2009a). This high level of false positives not only greatly reduces the efficiency of detection of true integrated virus-cell junctions using the invPCR assay, but also wastes resources including reagents, money, time and effort.

As it is essential to reduce the number of false positives detected in the invPCR assay, several methods could be used, including the selective DNA extraction methods described in Chapter 5.1. These selective methods aim to remove viral RI DNA and cccDNA from the liver cell DNA extracts, to physically reduce the main contributors to the virus-virus false positives. However, by performing selective DNA extraction methods, a proportion of liver cell DNA would be lost along with some of the integrated virus-cell junctions present (Chapter 5.1). Another approach has been to use one or more restriction enzymes to digest viral DNA to prevent nested PCR amplification. These restriction enzymes were designated as cccDNA

destroying enzymes, and were chosen to specifically digest any viral DNA formed after the inversion process at sites not present in the inverted DNA fragments, therefore preventing viral DNA from being amplified (refer to Figures 2.6 and 2.7 for schematic representation of the cccDNA destroying enzymes digestion sites). However, the cccDNA destroying enzymes may still potentially digest the liver cell DNA near the integration site, effectively preventing the amplification and detection of integrated virus-cell junctions by invPCR assay.

Therefore, this Section aims to reduce virus-virus false positives detected during invPCR assay using locked nucleic acid (LNA) oligonucleotides. LNA oligonucleotides are structurally similar to normal nucleic acids: water soluble, stable, and easy to handle (Petersen and Wengel, 2003). LNA oligonucleotides contain at least one LNA monomer, which is a 2'-O,4'-C-methylene-β-D-ribofuranosyl nucleotide, and virus-specific nucleic acid sequences can be synthesised with various structural analogues and configurational isomers. Sequence-specific LNA oligonucleotides have strong hybridisation affinity or binding efficiency to complementary DNA (and RNA), and can bind with high potency as antisense molecules in both *in vitro* and *in vivo* systems (Vester and Wengel, 2004). This is because LNA oligonucleotides can bind to double-stranded DNA or RNA by the formation of triple-helical complexes or by single-strand targeting that effectively displaces the other DNA strand. Hence, this strong binding would induce high thermal stability and high melting temperature of the LNA:DNA or LNA:RNA complexes (Vester and Wengel, 2004). Conversely, due to the strong hybridisation affinity, even single nucleotide differences in the target DNA or RNA may significantly alter the melting temperature of the complexes (Petersen and Wengel, 2003).

Based on these unique characteristics, LNA oligonucleotides have been extensively used in many areas of research, diagnostics and therapeutics. Some significant uses include the large scale detection of single-nucleotide polymorphisms during genotyping using real-time PCR for allelic discrimination of heritable genetic defects (Johnson *et al.*, 2004), to increase sensitivity and success of amplification during real-time PCR when incorporated into PCR primers (Ballantyne *et al.*, 2008), and as high emission fluorescent probes for the detection of DNA or RNA in FISH assays (Ostergaard *et al.*, 2010). Recently, LNA oligonucleotides have also shown potential as antisense oligonucleotide therapeutic agents, by being able to be readily taken up into cells and to bind mRNAs with high affinity, resulting in inhibition of gene expression and subsequent protein translation, to down-modulate of oncogenic-related proteins in mouse models (Zhang *et al.*, 2010), as well as reducing HBV DNA, HBsAg and HBcAg antigen levels in transgenic mouse models (Deng *et al.*, 2009).

In this Section, LNA oligonucleotides were used in an attempt to block amplification of DHBV DNA during PCR. By generating LNA:DHBV DNA complexes with melting temperatures of >95^{o}C, the complexes will not be dissociated during the PCR denaturation step and thus subsequently dislodge or block the Taq polymerase to prevent amplification. If successful, LNA oligonucleotides could specifically reduce the amplification of virus-virus DNA fragments during nested PCR, and greatly reduce invPCR assay false positives.

The advantages of using LNA oligonucleotides over selective DNA extraction methods and cccDNA destroying enzymes would be reduce either losing liver cell DNA during extraction or digesting inverted DNA fragments containing integrated virus-cell junctions.

However, there are also several potential disadvantages for the use of LNA oligonucleotides to reduce false positives during invPCR assay. Due to the high binding specificity of LNA oligonucleotides, even single nucleotide mutations present in the DHBV genome could prevent hybridisation, rendering the LNA oligonucleotide ineffective in blocking PCR amplifications. In addition, as high levels of DHBV DNA would be present in most liver tissues, an equally high amount of LNA oligonucleotide would need to be added in each PCR mix so that every viral DNA molecule present would be bound. If not enough LNA oligonucleotide were added, the remaining unbound DHBV DNA could still be amplified by PCR, subsequently resulting in the amplification of even small amounts DHBV DNA present. Lastly, one of the biggest disadvantages of using LNA oligonucletides is the high cost involved in its synthesis, as each LNA nucleotide (~6 μM) could cost up to $20 to synthesise.

In this Section, two DHBV-specific LNA oligonucleotides were designed to bind to separate regions of the DHBV genome, which were not part of the inverted DNA fragments used as DNA template for the detection of integrated DHBV-cell junctions during the invPCR assay. Optimisation was carried out using the pBL4.8x2 plasmid as the DNA template for PCR amplification (further explained in Section 5.2.4 below). Differing amounts of LNA oligonucleotide were then added to the PCR mix to determine whether LNA oligonucleotides could be used to effectively block the amplification of DHBV DNA during PCR.

5.2.3. Designing DHBV-specific LNA oligonucleotides

The LNA oligonucleotides were designed to bind to highly conserved regions of the AusDHBV genome sequence (GenBank Accession AJ006350) to prevent mismatching. In general, LNA oligonucleotides are designed to be 15 – 20 nt long with a guanine:cytosine (GC) content of 40% – 50%. Specifically, the LNA oligonucleotides were designed to be

downstream of the first cut restriction enzyme digestion site during the detection of integrated virus-cell left hand end junctions (refer Figure 2.6), and upstream of the first cut restriction enzyme digestion site during the detection of integrated virus-cell right hand end junctions (refer Figure 2.7). It was previously reported that the most probable 5' end (left hand end) of the integrated DHBV genome is at the 2485 nt while the most probable 3' end (right hand end) of the integrated DHBV genome is at the 2537 nt (Yang and Summers, 1999). Based on that, two DHBV-specific LNA oligonucleotides were designed with the assistance of Dr. Miao Yang, and were designated as LNA DHBV RH (2614 – 2630 nt of the AusDHBV genome, 5' cctttggtatgtaccat 3') and LNA DHBV LH (2917 – 2933 nt of the AusDHBV genome, 5' tatctcattcagcacga 3'). Both of the LNA oligonucleotides were synthesised by TIB Miobiol (Germany), dissolved to 100 μM stock with H_2O and stored at -20^oC until use.

5.2.4. The use of LNA oligonucleotides to block amplification of DHBV DNA from plasmid DNA templates

To determine whether LNA oligonucletides were able to block the amplification of DHBV DNA during PCR, pBL4.8x2 plasmid that contained two head-to-tail, full-length DHBV genomes (refer Figure 3.2.1A for plasmid map) was used as DNA template. Plasmids were used to ensure that all the DHBV DNA sequences were identical, as single nucleotide alterations in the DHBV genome were likely to be present in a population (quasispecies) of DHBV DNA extracted from liver tissues. Furthermore, the use of a plasmid as DNA template allows the amount of DHBV DNA added per PCR reaction to be determined and controlled.

The LNA DHBV RH binds to 2614 – 2630 nt of the DHBV genome, while LNA DHBV LH binds to 2917 – 2933 nt of the DHBV genome. Thus, LNA DHBV RH was used to block amplification of a 252 bp region of the DHBV genome from 2462 – 2713 nt using the primer set CC2 – DLK R2; while LNA DHBV LH was used to block amplification of a 282 bp region of the DHBV genome from 2798 – 52 nt using the primer set DLK F1 – R2. The sequences of all PCR primers are shown in Table 2.2, and the positions of each LNA and primer sets on the plasmid pBL4.8x2 are shown in Figure 5.2.1.

All PCR amplifications were performed as described in Section 2.8.5, using AmpliTaq Gold as the polymerase in 40 μL final volume with an annealing temperature of 55^oC and extension time of 30 sec. Up to 5 ng of pBL4.8x2 was used as DNA template, with LNA oligonucleotides added to the PCR mixture in various molar ratios. A positive control of the amplification of pBL4.8x2 without added LNA oligonucleotide was also performed. All PCR products were then visualised by agarose gel electrophoresis as described in Section 2.8.7.

5.2.5. Results and discussion

Preliminary experiments using a molar ratio of LNA:plasmid DNA of 0.1:1 – 10:1 failed to block amplification of pBL4.8x2 using either primer set (data not shown). Hence, higher molar ratios of LNA:plasmid DNA were evaluated.

As shown in Figure 5.2.2, results showed that LNA DHBV RH failed to block the amplification of pBL4.8x2 at all molar ratios of LNA:plasmid DNA, while LNA DHBV LH successfully blocked amplification of pBL4.8x2 when added at molar ratios of 50,000:1 or higher, with partial blocking when added at the molar ratios of 1000:1 – 10,000:1, and failed to block amplification when added at molar ratios of 100:1 and lower.

It was unclear why LNA DHBV RH failed to even partially block or reduce the amplification of pBL4.8x2 in this study. Some of the possible reasons include base pair mutations that may have occurred in some of the pBL4.8x2 sequence, which would result in base pair mis-matchings when bound with LNA oligonucleotide, and thus the failure to from strong hybridisation complexes to block PCR amplification. Alternatively, the LNA sequence chosen may simply not be optimal for forming complexes with the pBL4.8x2 plasmid DNA and may not have increased the melting temperature of the complex to >95^{o}C. These LNA oligonucleotides had been designed by Dr. Miao Yang manually without using any primer design software, and thus it was possible that some characteristics of the oligonucleotide sequences, for instance having non-specific binding sites in other regions of the plasmid or having high chances of self-complementarity, may have been overlooked. Therefore, with the assistance of primer design software, like the Primer3 online primer design tool (accessible at http://biotools.umassmed.edu/bioapps/primer3_www.cgi), more suitable and optimal LNA sequences could be designed. However, it was also likely that as two LNA DHBV RH binding sites are present on each pBL4.8x2 plasmid (as shown in Figure 5.2.1), the efficiency of two LNA oligonucleotides binding to each plasmid and subsequently forming complexes may be affected by the close proximity of the LNA binding. Therefore, it was likely that one of the two LNA:plasmid complexes may be more readily disrupted, thus allowing the PCR amplification to occur. No further work was performed to investigate this matter in this thesis.

On the other hand, LNA DHBV LH failed to block the amplification of pBL4.8x2 at a molar ratio of LNA:plasmid DNA of 100:1 and lower, and only blocked amplification of pBL4.8x2 when a molar ratio of 50,000:1 or higher was used. In this study, theoretically, two LNA oligonucleotides would be required to bind to each pBL4.8x2 DNA template, as each plasmid

contains two copies of the DHBV genome. Hence, assuming 100% binding efficiency, a molar ratio of 2:1 LNA:plasmid DNA should be enough to block all PCR amplification. However, it is highly likely that not all the DHBV DNA present in the pBL4.8x2 plasmids will be complexed with LNA oligonucleotides before PCR amplification began. Thus, with each PCR cycle, an exponential increase in the number of DHBV DNA fragments would be generated, which would in turn require much more LNA oligonucleotides to bind with every DHBV DNA present. Therefore, as shown in Figure 5.2.2, it could be assumed that at a molar ratio of LNA:plasmid DNA of 100:1 and lower, there was insufficient LNA oligonucleotides to bind with the pBL4.8x2 template as well as the subsequent DHBV DNA fragments generated by PCR, resulting in subsequent "normal" amplification of DHBV DNA. However, when LNA oligonucleotide was added at a molar ratio of 1000:1, a significant number of the PCR-generated DHBV DNA fragments were complexed with LNA oligonucleotides, effectively blocking most of the subsequent PCR amplification. Only when excessive amounts of LNA oligonucleotide were added (molar ratio of 50,000:1 or higher), "complete" blocking of PCR amplifications of all pBL4.8x2 template and PCR-generated DHBV DNA fragments by complexing with LNA oligonucleotide were observed.

cccDNA was extracted from duck liver tissues using the cccDNA extraction method (Section 2.6.7) and was ready to be used to test whether LNA DHBV LH could block or reduce the amplification of DHBV DNA in liver tissues during PCR. However, due to several concerns described below, this was decided to not be pursued any further in this thesis.

One of the main concerns was the large molar excess of LNA oligonucleotide required to completely block PCR amplification. As shown in Figure 5.2.2, to effectively block and reduce amplification, a molar ratio of LNA:plasmid DNA of at least 10,000:1 had to be used in each PCR reaction. Therefore, when performing 96-well PCR reactions with each well containing more than 1 copy of DHBV DNA, large amounts of the LNA oligonucleotide would have to be added to effectively block DHBV DNA amplification. However, the cost of LNA oligonucleotide synthesis was expensive, with $20 per LNA nucleotide to synthesise ~6 μM of oligonucleotide. Hence, it would not be economical to routinely use large amounts of LNA oligonucleotide in the 96-well PCR reactions to be performed in the invPCR assays.
In addition, as mentioned in Section 5.2.2 above, due to the high binding specificity of the LNA oligonucleotide, even single base pair mutations in the DHBV genome could prevent the formation of LNA:DHBV DNA complex, rendering the LNA oligonucleotide unable to block PCR amplification of DHBV DNA. Being a reverse transcribing virus, DHBV has been reported to have a mutation rate of $0.8 \times 10^{-5} – 4.5 \times 10^{-5}$ per nucleotide per generation, or one

base pair mutation per 7 – 42 viral genomes synthesised (Pult *et al.*, 2001). Based on that, it is estimated that mutations may occur in the 17 bp binding site of the LNA oligonucleotide in every ~1250 – 7500 DHBV virions produced. And knowing that chronic DHBV-infected ducks may contain 100 – 1000 copies of DHBV DNA per hepatocyte (Noordeen, 2009), as ~0.5 mg of liver ($3.5x10^5$ hepatocytes) is analysed per invPCR assay, $3.5x10^7$ – $3.5x10^8$ copies of DHBV DNA may be present in the extracted DNA analysed per invPCR assay, of which 4500 – 280,000 (0.01% – 0.08%) may contain a mutation in the 17 bp binding site of the LNA oligonucleotide. Hence, the effectiveness of LNA oligonucleotide to block amplification of DHBV DNA during invPCR would be highly dependent on the quasispecies population of DHBV present in the liver tissues. Therefore, it may be more efficient to use for instance restriction enzymes which are more affordable and less sensitive to single base-pair mutations to reduce virus-virus false positives during invPCR.

Future studies could explore alternative cheaper oligonucleotides from other sources that have similar strong binding affinities, or could further optimise the hybridisation efficiency of LNA to DHBV DNA to close to a molar ratio of LNA:plasmid DNA of 1:1, for instance by designing more optimal oligonucleotides using primer design softwares. For more accurate testing of the efficiency of LNA in blocking PCR amplifications, qPCR assays could be used as they can detect down to 10 copies of PCR products. In addition, the plasmids used as PCR template DNA could be first linearised by restriction enzymes, to remove any secondary forms of the circular plasmids that may block the binding of LNA to the DNA sequences.

5.2.6. Conclusion

Two LNA oligonucleotides were designed to bind specifically to the AusDHBV sequence to block amplification of the DHBV DNA during PCR. Using pBL4.8x2 plasmid as DNA template, only one LNA (LNA DHBV LH) successfully blocked most amplification when added at a molar ratio of LNA:plasmid DNA of 50,000:1 or higher. However, due to the high cost of LNA oligonucleotides as well as the high binding specificity of LNA oligonucleotides, the use of LNA oligonucleotides to block or reduce the amplification of DHBV DNA during invPCR assays was not pursued further in this study.

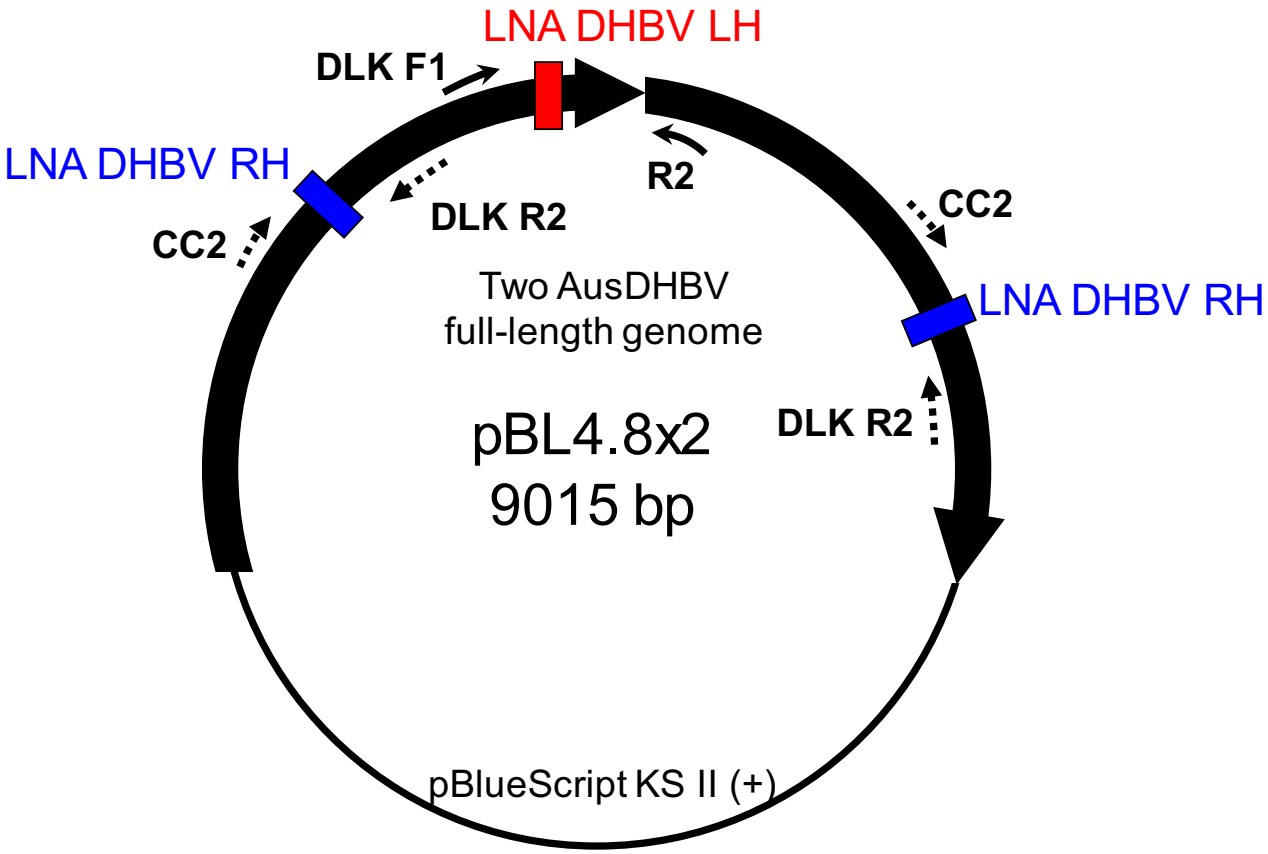


Figure 5.2.1: Approximate binding sites of LNA DHBV RH and LNA DHBV LH oligonucleotides that were designed to specifically block the amplification of DHBV DNA on the pBL4.8x2 plasmid.

The approximate binding sites of PCR primer sets (CC2 – DLK R2 and DLK F1 – R2) that were used to amplify the region of DHBV DNA flanking both LNA oligonucleotides are also shown. It was expected that the PCR amplification using the CC2 – DLK R2 primer set would produce a 252 bp PCR product, while the DLK F1 – R2 primer set would produce a 282 bp PCR product.

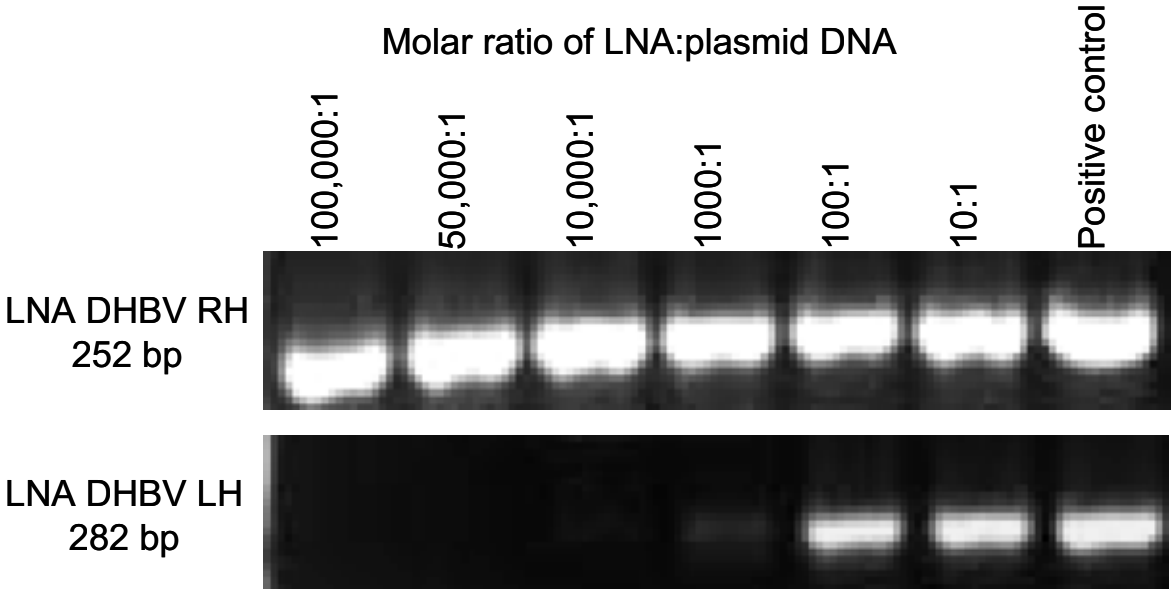


Figure 5.2.2: The use of varying various amounts of LNA oligonucleotides to block the amplification of pBL4.8x2 plasmid by PCR.

LNA DHBV RH and LNA DHBV LH oligonucleotides were designed to specifically bind to 2614 – 2630 nt and 2917 – 2933 nt of the AusDHBV genome (GenBank Accession AJ006350) as described in Section 5.2.3.

Varying amounts of LNA oligonucleotides were added to the PCR mixture that ranged from a molar ratio of LNA:plasmid DNA of 10:1 – 100,000:1, followed by PCR amplification of DHBV DNA as described in Section 5.2.4. No LNA oligonucleotides were added in the positive control. All PCR products were visualised by agarose gel electrophoresis as described in Section 2.8.7.

LNA DHBV RH failed to block the amplification of pBL4.8x2 at all molar ratios, while LNA DHBV LH partially blocked the amplification of pBL4.8x2 at a molar ratio of LNA:plasmid DNA of 1000:1 – 10,000:1, with "complete" blocking (lower than sensitivity of agarose gel electrophoresis) at a molar ratio of LNA:plasmid DNA of 50,000:1 LNA:plasmid DNA or higher.

Chapter 5.3: Using linker ligation assay to detect integrated virus-cell junctions

5.3.1. Aim

a) To evaluate the use of linker ligation assay as an alternative assay to the invPCR assay to detect integrated virus-cell junctions.
b) To perform linker ligation assay on WHV-infected woodchuck liver tissues.
c) To establish and perform linker ligation assay on DHBV-infected duck liver tissues.

5.3.2. Introduction

As previously described in Introduction Chapter 1.8.1, integrated virus-cell junctions present in the liver genome can be detected using several molecular assays. These assays include the invPCR assay (Yang and Summers, 1999), Southern blot hybridisation (Hino *et al.*, 1985), *Alu*-PCR (Kawai *et al.*, 2001), *in situ* hybridisation using biotinylated probes (Negro *et al.*, 1985), and linker ligation assay (Summers *et al.*, 2003). As an alternative assay to the invPCR assay widely used in this study, this Section explores the use of linker ligation assay to detect integrated virus-cell junctions. The linker ligation assay was previously described in Section 1.8.1, and a schematic representation of the steps involved is shown as Figure 2.9.

Linker ligation assay has an advantage over the invPCR assay as only two restriction enzyme were used compared to three during invPCR assay, thus reducing the number of DNA fragments produced, which could potentially reduce the amount of virus-virus false positives detected. By using a restriction enzyme that does not cut the viral DNA as the first cut restriction enzyme, this also prevents the digestion of viral DNA before the ligation step, to avoid the generation of virus-virus fragments. In addition, unlike invPCR assays where there is the probability that the insert liver cell DNA could be digested by the cccDNA destroying restriction enzyme, this situation would be prevented using linker ligation assay, and thus potentially having a much broader range of integrated virus-cell junctions detected. Furthermore, as the first linker ligation assay PCR reaction uses the specific linker – virus linker primer set, this amplification step would specifically select for the amplification of integrated virus-cell junctions only, further reducing the detection of virus-virus false positives, which have been one of the main problems and limitations of the invPCR assay.

However, compared to invPCR assay, numerous steps and different reagents and components are involved in the linker ligation assay protocol. This makes linker ligation assay a more

labour intensive molecular assay, which is more complicated to perform and with a higher chance of making mistakes during the protocol. The cost of performing linker ligation assay is also higher, and considering that this molecular assay would have to be performed multiple times, this would significantly increase the overall cost involved in this study. In addition, the efficiency of linker ligation assay may be lower than invPCR assay, as it has several extra steps compared to invPCR assay, including two purification steps using the QIAquick PCR purification kit, during which losses of DNA would occur. It is also dependent on blunt end ligation of the linkers to the DNA fragments, and subsequent circularisation of the DNA fragments after removal of the linkers. Therefore, if the quality of results obtained from linker ligation assay is comparable to invPCR assay, the invPCR assay would be the preferred molecular assay used in this study for the detection of integrated virus-cell junctions.

In this Section, linker ligation assay was performed on WHV-infected woodchuck and DHBV-infected duck liver tissues. The results obtained using the linker ligation assay will be compared to the results obtained using the invPCR assay in Chapters 5.5 and 6 respectively.

5.3.3. Using linker ligation assay to detect integrated virus-cell junctions in WHV-infected woodchuck liver tissues

5.3.3.1. Woodchuck liver tissues

Liver tissues from woodchuck 559 (133 dpi) were provided by Dr. William Mason. Briefly, woodchuck 559 was 1 year old when it was inoculated with 1 mL of serum from a chronic WHV-infected woodchuck (virus titre ~10^9 per mL). Blood samples were then collected weekly, and wedge liver biopsies were performed at 35, 70, 98 and 133 dpi. By 35 dpi, woodchuck 559 had a viraemia of 6.72×10^9 WHV DNA genomes per mL of serum and >95% of hepatocytes were WHV core antigen-positive. By 133 dpi, woodchuck 559 was found to have resolved the WHV infection, with levels of viraemia dropping below the limit of detection, and <0.001% of hepatocytes WHV core antigen-positive. The full serological and histological analysis of woodchuck 559 were reported by Mason *et al.* (Mason *et al.*, 2009b).

Liver biopsy tissue from woodchuck 559 at 133 dpi was dissected to obtain 4 x ~1 mg fragments (designated as 559-1, 559-2, 559-3 and 559-4), and DNA was extracted from the liver tissues using the total DNA extraction method as described in Section 2.6.3. Extracted DNA from ~0.9 mg of each liver fragment was then used as DNA templates for linker ligation assay performed as described in Section 2.12. The woodchuck linker ligation assay design used was designed by Dr. William Mason based on the design previously used in Summers *et al*. (Summers *et al.*, 2003), and is summarised in detail in Table 2.4.

5.3.3.2. Woodchuck linker ligation assay results

Figure 5.3.1A shows an example of an integrated virus-cell junction DNA sequencing result, which consisted of an insert DNA flanked by WHV DNA; while Figure 5.3.1B shows an example of a virus-virus false positive DNA sequencing result, which consisted of only WHV DNA sequences. Individual DNA sequencing results were not shown in this Section.

The results of all linker ligation assays are summarised in Table 5.3.1. Out of a total of 672 linker ligation nested PCR reactions performed in DNA extracted from ~0.9 mg of 559-1, 559-2, 559-3 and 559-4 liver tissues, 60 linker ligation assay products were sequenced. Among these, 41 of the sequences were integrated virus-cell junctions, 10 were virus-virus false positive sequences, 4 were unknown sequences (defined in this thesis as insert DNA sequences that were either too short (<15 bp) or did not show homology to any known sequences during the BLAST searches), and 5 DNA sequencing reactions failed to produce any readable sequences. No linker ligation assay products were produced from 559-3 and 559-4 liver tissues. It should be noted that as the woodchuck genome has not been fully sequenced, in this thesis, insert DNA that showed homology to other mammalian "non-woodchuck" genome sequences would also be considered as integrated virus-cell junctions.

In the 559-1 liver tissue, out of the 21 integrated virus-cell junctions detected, 14 of the junctions were unique, with 1 of the junctions repeated 5 times, and 3 of the other junctions repeated 2 times each. Detailed analysis of the 21 integrated virus-cell junctions are summarised in Table 5.3.2. In the 559-2 liver tissue, out of the 20 integrated virus-cell junctions detected, 13 of the junctions were unique, with 1 of the junctions repeated 5 times, and another 1 of the junctions repeated 4 times. Detailed analysis of the 20 integrated virus-cell junctions is summarised in Table 5.3.3, and it was found that none of these integrated virus-cell junctions were similar to the junctions found in the 559-1 liver tissue.

On a separate note, it was found that most of the insert DNA sequenced did not have 100% of BLAST analysis query coverage, with only parts of the insert DNA showing homology to a known sequence. Most of the sequences also did not have detectable flanking virus sequences. These suggest that additional sequences may have been added, or that some rearrangements of the genome sequences may have occurred during the production of inverted DNA fragments. Alternatively, the integrated virus-cell junction may have been to close to the primers used in the nested PCR, resulting in the failure to sequence the flanking viral sequences.

5.3.3.3. Discussion

Based on the results summarised in Tables 5.3.2 and 5.3.3, it was found that the 5' end of the WHV dslDNA that joined to the woodchuck genome during integration, forming the left hand end integrated virus-cell junction, ranged between 1935 – 2084 nt of the WHV genome (GenBank Accession M18752), with a median at 1935 nt. This was consistent with the published 5' end of the WHV dslDNA at 1935 nt (Summers *et al.*, 2003), and the range of integrated virus-cell junctions previously compiled from 1202 junctions (Mason *et al.*, 2009b).

In addition, based on the BLAST analysis of the insert DNA found in this Section, there were no significant patterns or preference of integration sites in the woodchuck genome, and it appeared that the WHV dslDNA had integrated randomly into different regions of the woodchuck genome, consistent with published results (Tokino and Matsubara, 1991).

As 6 of the integrated virus-cell junctions were repeated 2 – 5 times (average 3.3 times), this suggests that there were at least 6 hepatocyte clones present in these liver tissues. It could also be inferred that ~2 rounds of clonal proliferation of hepatocytes had occurred in the liver.

When the results obtained using linker ligation assay were compared to the results obtained using the invPCR assay (Chapter 5.5.3), despite using liver samples from the different woodchuck 522, it was found that the total amount and number of repeats of integrated virus-cell junctions were similar. The 5' end of the WHV dslDNA was found to be similar (1935 nt by linker ligation assay and 1944 nt by invPCR assay), thus validating both molecular assays for the detection of integrated WHV DNA. The integration patterns of the WHV dslDNA into the woodchuck genome were also similar, as both assays showed random integration sites in the woodchuck genome with no significant patterns or preference of integration sites.

On the other hand, the amount of virus-virus false positives detected using linker ligation assay was lower compared to invPCR assay, as 10 in 60 of the linker ligation assay products sequenced (17%), while 49 in 144 of the invPCR assay products sequenced (34%), were virus-virus sequences. Although different woodchuck samples were used, both woodchucks had undetectable levels of viraemia when the liver biopsy tissues were obtained (Mason *et al.*, 2009b), thus it was assumed that the amount of WHV DNA present were similar. Based on that, results suggest that the amount of virus-virus false positives detected could be reduced using the linker ligation assay, due to several factors previously discussed in Section 5.3.2.

However, the quality of the inverted DNA fragments sequences that were produced using linker ligation assay were poorer compared to invPCR assay, as the insert DNA had a low % of query coverage during BLAST analysis (average 60%), compared to >80% of query coverage using the invPCR assay. Furthermore, the detection of flanking virus sequences was also less frequent in the linker ligation assay. This makes the analysis of the linker ligation assay products harder, as without the ability to detect the flanking virus sequences, the DNA sequences obtained could not be confidently said to be integrated virus-cell junctions, as they could be false positives or artefacts generated during linker ligation assay or DNA sequencing.

In summary, the results of the woodchuck linker ligation assay were comparable to the results of the invPCR assays (Chapter 5.5.3). This showed that both molecular assays could be effectively used to detect integrated virus-cell junctions in WHV-infected woodchuck livers.

5.3.4. Using linker ligation assay to detect integrated virus-cell junctions in DHBV-infected duck liver tissues

5.3.4.1. Duck liver tissues

Liver tissues from 4 ducks with chronic DHBV infection were obtained from previous studies performed in the Hepatitis Research Laboratory. These ducks included: Pool 7 (Jilbert *et al.*, 1996), DM32:33 (Miller *et al.*, 2006), and FN76 and FN77 (Noordeen, 2009).

Briefly, Pool 7 duck livers were obtained from a flock of congenitally DHBV-infected ducks infected with the AusDHBV strain (GenBank Accession AJ006350), collected at 34 dpi (Jilbert *et al.*, 1996). Duck DM32:33 was inoculated with $5x10^8$ vge of Pool 7 serum at 18 days of age, and liver tissues were obtained at 29 dpi (Miller *et al.*, 2006). Both ducks had widespread and persistent DHBV infection with >95% DHBsAg-positive hepatocytes at the time of liver collection and viraemia up to $5x10^9$ vge/mL. Ducks FN76 and FN77 were inoculated with $5x10^8$ vge Pool 8 serum at 14 days of age, and were treated with 5 mg/kg tenofovir (TFV) and 100 mg/kg emtricitabine (FTC) by daily intraperitoneal injections until 41 dpi. Liver tissues were collected at 41 dpi, and the ducks had an average of ~9.9% of hepatocytes DHBsAg-positive and a viraemia of ~$5x10^3$ copies of DHBV DNA at the time of liver collection (Noordeen, 2009). Pool 7 and DM32:33 duck liver tissues have widespread DHBV infection with high levels of active DHBV replication (~96 copies of DHBV total DNA per cell), while FN76 and FN77 were antiviral-treated, and thus have lower levels of active DHBV replication and DHBV DNA in the liver (average of 2.34 copies of DHBV total DNA per cell). By using these different groups of ducks, it can be determined whether the amounts of DHBV DNA present in the liver samples contribute to virus-virus false positives.

DNA were extracted from all four duck liver tissues using the total DNA extraction method as described in Section 2.6.3. In addition, DNA was extracted from Pool 7 and DM32:33 liver tissues using the nuclear DNA extraction method as described in Section 2.6.5. The linker ligation assay was performed as described in Section 2.12, with the duck linker ligation assay designed based on the AusDHBV genome (GenBank Accession AJ006350) with assistance from Dr. William Mason, and is summarised in detail in Table 2.4.

5.3.4.2. Duck linker ligation assay results

Figure 5.3.2A shows an example of an integrated virus-cell junction DNA sequencing result, which consisted of an insert DNA flanked by DHBV DNA; while Figure 5.3.2B shows an example of a virus-virus false positive DNA sequencing result, which consisted of only DHBV DNA sequences. Individual DNA sequencing results were not shown in this Section.

The results of all linker ligation assays are summarised in Table 5.3.4. Out of a total of 864 linker ligation assay nested PCR reactions performed on 2370.75 ng of DNA from 4 ducks, 94 linker ligation assay products were sequenced. Among these, 10 of the sequences were integrated virus-cell junctions, 47 were virus-virus false positive sequences, 5 were unknown sequences, and 32 DNA sequencing reactions failed to produce any readable sequences. No linker ligation assay products were produced in the FN77 liver tissue. In the FN76 liver tissue, out of the 9 integrated virus-cell junctions detected, 7 junctions were unique, with 2 of the junctions repeated 2 times. Detailed analysis of the 10 integrated virus-cell junctions detected are summarised in Table 5.3.5. It should be noted that as the duck genome has not been fully sequenced, in this thesis, insert DNA that showed homology to other avian or mammalian "non-duck" genome sequences would also be considered as integrated virus-cell junctions.

It was found that the amount of virus-virus false positives detected in the Pool 7 and DM32:33 were higher (40 out of 62 linker ligation assay products sequenced) compared to the FN76 and FN77 (7 out of 33 linker ligation assay products sequenced). This confirmed that the levels of viral DNA present in the liver do affect the levels of virus-virus false positives detected, with higher viral DNA levels resulting in higher virus-virus false positives detected.

On a separate note, it was found that most of the insert DNA sequenced did not have 100% of BLAST analysis query coverage, with only parts of the insert DNA showing homology to a known sequence. In addition, a significant number of the virus-virus false positive sequences were found to contain the linker LL 1415 sequence (shown in Table 2.2) at the 3' end of the

sequence (data not shown). This suggests that the *Pvu*II digestion performed to remove the linkers (refer Section 2.12 for detailed methods) may be incomplete.

5.3.4.3. Discussion

Based on the results summarised in Table 5.3.5, it was found that the 5' end of the DHBV dslDNA that joined to the duck genome during integration, forming the left hand end integrated virus-cell junctions, ranged between 1863 – 2600 nt of the AusDHBV genome (GenBank Accession AJ006350), with a median at 2543 nt. This was similar to the published 5' end of the DHBV dslDNA at 2485 nt (Yang and Summers, 1999).

In addition, based on the BLAST analysis of the insert DNA found in this Section, there were no significant patterns or preference of integration sites in the duck genome, and it appeared that the DHBV dslDNA, like the WHV dslDNA, integrated randomly into different regions of the duck genome, consistent with published results (Tokino and Matsubara, 1991).

As it was found that 2 of the integrated virus-cell junctions were repeated 2 times in FN76, this suggests that there were at least 2 hepatocyte clones present in this liver tissue. It could also be inferred that 1 round of clonal proliferation of hepatocytes had occurred in the liver.

When the results obtained using linker ligation assay in this Section were compared to the results obtained using the invPCR assay in the 3 same duck liver tissues extracted using the same DNA extraction methods (Chapter 6), it was found that the number of integrated virus-cell junctions detected using the linker ligation assay was higher than the invPCR assay. Using the linker ligation assay, when 2370.75 ng of duck liver DNA were analysed, 10 integrated virus-cell junctions were detected, of which 8 of the junctions were unique, and 2 of the junctions were repeated 2 times (Table 5.3.4); while using the invPCR assay, when 14,929 ng of duck liver DNA were analysed, 7 integrated virus-cell junctions were detected (Tables 6.1 and 6.3), of which none of the junctions were repeated. This suggests that the linker ligation assay was much more efficient than the invPCR assay in detecting integrated DHBV-cell junctions in DHBV-infected duck liver tissues. Furthermore, the amount of virus-virus false positives detected using linker ligation assay was lower compared to invPCR assay, as 47 in 94 of the linker ligation assay products sequenced were virus-virus sequences (50%) (Table 5.3.4), while 365 in 509 of the invPCR products sequenced were virus-virus sequences (72%) (Tables 6.1 and 6.3). This again suggests that the amount of virus-virus false positives detected could be reduced using the linker ligation assay (Section 5.3.2).

Despite that, using both assays, the 5' end of the DHBV dslDNA was found to be similar (2543 nt by linker ligation assay and 2537 nt by invPCR assay), thus validating both assays for the detection of integrated DHBV DNA. The integration patterns of the DHBV dslDNA into the duck genome were also similar, as both assays displayed random integration sites in the duck genome with no significant patterns or preferences of integration sites.

However, the quality of inverted DNA fragments sequences that were produced using the linker ligation assay were poor compared to the invPCR assay, as insert DNA had low % of query coverage during BLAST analysis (average 47%), compared to >80% of query coverage for insert DNA detected using the invPCR assay, similar to observations in Section 5.3.3.

In summary, the results obtained using the duck linker ligation assay were better than the results obtained using the invPCR assays (Chapter 6), thus the linker ligation assay may be more suitable to detect integrated virus-cell junctions in DHBV-infected duck liver tissues.

5.3.5. Conclusion

In conclusion, using the woodchuck linker ligation assay, in the woodchuck 559 livers, 60 integrated virus-cell junctions were detected, of which 27 were unique; using the duck linker ligation assay, in the Pool 7, DM32:33, FN76 and FN77 duck livers, 10 integrated virus-cell junctions were detected, of which 8 were unique.When compared to the results obtained using the invPCR assay, the efficiency of detecting integrated virus-cell junctions were similar in the WHV-infected woodchuck livers, but lower in the DHBV-infected duck livers.

Although the results outlined above would suggest that the linker ligation assay is more efficient, linker ligation assay is more complicated to perform, involves more steps, more time consuming, and has a higher cost compared to the invPCR assay. Thus, linker ligation assay would not be further used to detect integrated virus-cell junctions in this study. However, if high levels of virus-virus false positives were detected using the invPCR assay, linker ligation assay could be performed to increase the detection of integrated virus-cell junctions.

Table 5.3.1: Linker ligation assay results obtained using liver samples from woodchuck 559 at 133 dpi after recovery from an acute WHV infection.

Liver fragment	Total nested PCR reactions[a]	Number of linker ligation assay products sequenced[b]	Integrated virus-cell junctions detected[c]	Virus-virus sequences detected[d]	Unknown sequences detected[e]
559-1	192	24	21	1	-
559-2	192	36	20	9	4
559-3	96	0	-	-	-
559-4	192	0	-	-	-
Total	**672**	**60**	**41**	**10**	**4**

The woodchuck linker ligation assay was performed on ~0.9 mg of woodchuck 559 liver tissues as described in Section 2.12 based on the woodchuck linker ligation design (refer Table 2.4). DNA sequencing results were analysed as described in Section 2.8.12.

[a]Total nested PCR reactions refers to the total number of nested PCR reactions performed in individual PCR wells.

[b]From all the nested PCR reactions performed, only reactions that produced clear nested PCR product bands were extracted from the agarose gel and sequenced. The number of total linker ligation assay PCR products observed on the agarose gels was not shown.

[c]An example of an integrated virus-cell junction is shown in Figure 5.3.1A.

[d]An example of a virus-virus false positive sequence is shown in Figure 5.3.1B.

[e]Unknown sequences were defined as insert DNA that were either too short (<15 bp) or did not show homology to any known sequences during the BLAST searches.

Table 5.3.2: Summary of the 21 integrated virus-cell junctions detected by linker ligation assay using DNA extracted from woodchuck 559-1 liver tissue.

No	Virus junction 1	Virus junction 2	Insert DNA size (bp)	BLAST homology	GenBank Accession	Nucleotide position (5' – 3')	Query coverage[a] %
1	1935	2039	506	*Rhinolophus ferrumequinum* genomic sequence	NT_113341	491246-/-525511[b]	62
2	1935	2250	475	*Rhinolophus ferrumequinum* genomic sequence	NT_113341	491246-/-525511	58
3	1935	ND[c]	471	*Rhinolophus ferrumequinum* genomic sequence	NT_113341	491246-/-525511	62
4	1935	ND	504	*Rhinolophus ferrumequinum* genomic sequence	NT_113341	491246-/-525511	59
5	1935	2245	469	*Rhinolophus ferrumequinum* genomic sequence	NT_113341	491246-/-525511	56
6	2084	ND	230	*Pongo abelii* chromosome 16 genomic scaffold, P_pygmaeus_2.0.2	NW_002888150	18596-18648	23
7	2084	ND	229	*Pongo abelii* chromosome 16 genomic scaffold, P_pygmaeus_2.0.2	NW_002888150	18596-18648	23
8	1935	2250	95	*Oryctolagus cuniculus* breed Thorbecke inbred unplaced genomic scaffold, OryCun2.0 chrUn0469	NW_003159793	81512-81541	31
9	1935	2250	95	*Oryctolagus cuniculus* breed Thorbecke inbred unplaced genomic scaffold, OryCun2.0 chrUn0469	NW_003159793	81512-81541	31
10	2078	2257	548	*Spermophilus tridecemlineatus* genomic sequence	NT_166732	139717-139527	45
11	2078	2257	552	*Spermophilus tridecemlineatus* genomic sequence	NT_166732	139717-139527	44
12	ND	2250	393	*Spermophilus tridecemlineatus* genomic sequence	NT_166768	1261717-1261559	59

Table 5.3.2 continued

13	2047	2258	188	*Equus caballus* breed thoroughbred chromosome 5 genomic scaffold	NW_001867416	11635402-11635293	58
14	1935	ND	383	*Pongo abelii* chromosome 2A, P_pygmaeus_2.0.2	NC_012592	29642426-29642668	76
15	1935	2249	118	*Cavia porcellus* strain inbred line 2N unplaced genomic scaffold	NT_176419	68712842-68712783	80
16	2021	2250	257	*Macaca mulatta* chromosome 1 genomic scaffold, Mmul_051212	NW_001111147	1958948-1959119	67
17	ND	2250	301	*Cricetulus griseus* unplaced genomic scaffold, CriGri_1.0 scaffold221	NW_003613759	1272552-1272494	19
18	1945	2250	458	*Homo sapiens* chromosome 1 genomic contig	NW_001838533	17746214-17745771	97
19	1936	ND	442	*Spermophilus tridecemlineatus* genomic sequence	NT_166696	179077-179276	52
20	1988	2235	192	*Spermophilus tridecemlineatus* genomic sequence	NT_166671	501020-501187	87
21	1935	2250	346	*Equus caballus* breed thoroughbred chromosome 18, EquCab2.0	NC_009161	66587652-66587358	85

The woodchuck linker ligation assay was performed on ~0.9 mg of woodchuck 559-1 liver tissues as described in Section 2.12 based on the woodchuck linker ligation assay design (refer Table 2.4). DNA sequencing results were analysed as described in Section 2.8.12, based on examples shown in Figures 5.3.1A and 5.3.1B.

The coloured highlights show the different groups of repeated integrated virus-cell junctions.

[a]Query coverage (%) refers to the % of insert DNA sequence that were aligned with their respective GenBank DNA sequences at the nucleotide positions shown.

[b]The symbol "-/-" was used when the nucleotide positions of the insert DNA had gaps (not continuous).

[c]The virus junction was not detected (ND) in the DNA sequence.

Table 5.3.3: Summary of the 20 integrated virus-cell junctions detected by linker ligation assay using DNA extracted from woodchuck 559-2 liver tissue.

No	Virus junction 1	Virus junction 2	Insert DNA size (bp)	BLAST homology	GenBank Accession	Nucleotide position (5' – 3')	Query coverage[a] %
1	1937	ND[b]	36	*Oreochromis niloticus* unplaced genomic scaffold, Orenil1.0 scaffold00605	NT_167 981	141268-141287	100
2	1937	2251	33	*Oreochromis niloticus* unplaced genomic scaffold, Orenil1.0 scaffold00605	NT_167 981	141268-141287	60
3	1937	2250	35	*Oreochromis niloticus* unplaced genomic scaffold, Orenil1.0 scaffold00605	NT_167 981	141268-141287	57
4	1937	2250	35	*Oreochromis niloticus* unplaced genomic scaffold, Orenil1.0 scaffold00605	NT_167 981	141268-141287	57
5	1937	2250	35	*Oreochromis niloticus* unplaced genomic scaffold, Orenil1.0 scaffold00605	NT_167 981	141268-141287	57
6	1944	2257	66	*Oryctolagus cuniculus* breed Thorbecke inbred chromosome 8 genomic scaffold, OryCun2.0	NW_003 159268	48511570-48511506	98
7	1944	ND	108	*Oryctolagus cuniculus* breed Thorbecke inbred chromosome 8 genomic scaffold, OryCun2.0	NW_003 159268	48511570-48511499	66
8	1944	2250	73	*Oryctolagus cuniculus* breed Thorbecke inbred chromosome 8 genomic scaffold, OryCun2.0	NW_003 159268	48511570-48511499	98
9	1944	2250	73	*Oryctolagus cuniculus* breed Thorbecke inbred chromosome 8 genomic scaffold, OryCun2.0	NW_003 159268	48511570-48511499	98
10	2028	ND	710	*Homo sapiens* chromosome 1 genomic contig	NW_001 838523	3396385-3397008	88
11	2065	ND	567	*Spermophilus tridecemlineatus* genomic sequence	NT_166 705	861353-861644	51

Table 5.3.3 continued

12	2028	ND	454	*Equus caballus* breed thoroughbred chromosome 2 genomic scaffold	NW_001 867403	6450678-6450244	88
13	1937	2250	40	*Rattus norvegicus* strain BN/SsNHsdMCW chromosome 18 genomic scaffold, RGSC_v3.4	NW_047 512	4773890-4773870	52
14	2029	2250	96	*Cricetulus griseus* unplaced genomic scaffold, CriGri_1.0 scaffold2166	NW_003 615451	107596-107574	23
15	2077	ND	626	*Pan troglodytes* chromosome 8, Pan_troglodytes-2.1.4	NC_006 475	2713849-2713648	39
16	1937	2250	38	*Ailuropoda melanoleuca* unplaced genomic scaffold, AilMel_1.0	NW_003 217449	28584-28560	65
17	2028	ND	189	*Callithrix jacchus* chromosome 7 genomic scaffold, Callithrix jacchus-3.2	NW_003 183698	3497280-3497444	83
18	2077	2250	603	*Loxodonta africana* unplaced genomic scaffold, Loxafr3.0 scaffold_31	NW_003 573451	8170125-8170086	6
19	ND	2250	306	*Loxodonta africana* unplaced genomic scaffold, Loxafr3.0 scaffold_10	NW_003 573430	51479511-51479589	25
20	1946	2242	30	*Pongo abelii* chromosome 1 genomic scaffold, P_pygmaeus_2.0.2	NW_002 875635	334813-334794	66

The woodchuck linker ligation assay was performed on ~0.9 mg of woodchuck 559-2 liver tissues as described in Section 2.12 based on the woodchuck linker ligation assay design (refer Table 2.4). DNA sequencing results were analysed as described in Section 2.8.12, based on examples shown in Figures 5.3.1A and 5.3.1B.

The coloured highlights show the different groups of repeated integrated virus-cell junctions.

[a]Query coverage (%) refers to the % of insert DNA sequence that were aligned with their respective GenBank DNA sequences at the nucleotide positions shown.

[b]The virus junction was not detected (ND) in the DNA sequence.

Table 5.3.4: Linker ligation assay results obtained using liver samples from 4 ducks with chronic DHBV infection.

DNA extraction	Duck	Total nested PCR reactions [a]	Total DNA analysed (ng)[b]	Number of linker ligation assay products sequenced[c]	Integrated virus-cell junctions detected[d]	Virus-virus sequences detected[e]	Unknown sequences detected[f]
Total DNA extraction	**Pool 7**	96	471.71	24	-	6	1
Nuclear DNA extraction		96	634.02	24	1	21	2
Total DNA extraction	**DM 32:33**	96	339.34	7	-	7	-
Nuclear DNA extraction		96	634.02	6	-	6	-
Total DNA extraction	**FN76**	288	194.44	33	9	7	2
Total DNA extraction	**FN77**	192	97.22	0	-	-	-
Total		**864**	**2370.75**	**94**	**10**	**47**	**5**

The duck linker ligation assay was performed on 4 duck liver samples as described in Section 2.12 based on the duck linker ligation assay design (refer Table 2.4). DNA sequencing results were analysed as described in Section 2.8.12.

[a]Total nested PCR reactions refers to the total number of nested PCR reactions performed in individual PCR wells.

[b]The amount of DNA analysed was estimated according to the amount of DNA added per linker ligation reaction, which was based on the amount of liver used after DNA extraction.

[c]From all the nested PCR reactions performed, only reactions that produced a clear invPCR product band was extracted from the agarose gel and sequenced. The number of total linker ligation assay PCR products observed on the agarose gels was not shown.

[d]An example of an integrated virus-cell junction is shown in Figure 5.3.2A.

[e]An example of a virus-virus false positive sequence is shown in Figure 5.3.2B.

[f]Unknown sequences were defined as insert DNA that were either too short (<15 bp) or did not show homology to any known sequences during the BLAST searches.

Table 5.3.5: Summary of the 10 integrated virus-cell junctions by linker ligation assay using DNA extracted from duck liver tissues.

No	Virus junction 1	Virus junction 2	Insert DNA size (bp)	BLAST homology	GenBank Accession	Nucleotide position (5' – 3')	Query coverage[a] %
1	2534	12	101	*Gallus gallus* BAC clone CH261-48J8 from chromosome z	AC188941	27708-27623	88
2	1863	12	39	*Mus musculus* BAC clone RP23-339P15 from chromosome 8	AC131107	115220-115238	48
3	1863	12	39	*Mus musculus* BAC clone RP23-339P15 from chromosome 8	AC131107	115220-115238	48
4	2545	12	236	*Gallus gallus* DNA, BAC clone: 77C10 and 108G03, MHC region, from WLA homozygote chicken	AP011531	166442-166395	20
5	2545	12	124	*Gallus gallus* DNA, BAC clone: 77C10 and 108G03, MHC region, from WLA homozygote chicken	AP011531	166442-166395	38
6	2600	3025	29	*Mus musculus* BAC clone RP23-372I18 from chromosome 7	AC125050	56925-56907	65
7	2539	ND[b]	412	*Gallus gallus* BAC clone CH261-65D3 from chromosome w	AC239877	29637-30028	94
8	2541	12	115	*Gallus gallus* radical fringe mRNA	GGU82088	712-686	23
9	2557	ND	470	Mouse DNA sequence from clone RP23-167I12 on chromosome 4	AL807796	21022-21058	8
10	2559	ND	48	*Mus musculus* chromosome 1, clone RP24-392K18	AC102297	134132-134114	39

The duck linker ligation assay was performed on Pool 7 and FN76 liver tissues as described in Section 2.12 based on the duck linker ligation design (refer Table 2.4). DNA sequencing results were analysed as described in Section 2.8.12, based on examples shown in Figures 5.3.2A and 5.3.2B. Integrated virus-cell junction no. 1 was detected in DNA extracted using the nuclear DNA extraction method from Pool 7, while no. 2 – 10 were detected in DNA extracted using the total DNA extraction method from FN76, as shown in Table 5.3.4.

The coloured highlights show the different groups of repeated integrated virus-cell junctions.

[a]Query coverage (%) refers to the % of insert DNA sequence that were aligned with their respective GenBank DNA sequences at the nucleotide positions shown.

[b]The virus junction was not detected (ND) in the DNA sequence.

Figure 5.3.1: Example of DNA sequencing results (5' – 3') obtained from the linker ligation assay to detect integrated WHV-cell junctions in WHV-infected woodchuck liver tissues.

The linker ligation assay was performed as described in Section 2.12 based on the woodchuck linker ligation assay design (refer Table 2.4), with Figure 2.9 showing a schematic representation of the major steps involved during linker ligation assay.

Figure 5.3.1A shows an example of the DNA sequencing result for an integrated virus-cell junction. BLAST analysis showed that the 692 bp sequence consisted of a 470 bp insert DNA (black font) flanked by WHV genome (GenBank Accession M18752) 2121 – 1935 nt (blue bold font) and 2250 – 2217 nt (red bold font). This was consistent with the expected inverted DNA fragment that will be produced by the woodchuck linker ligation assay design, to confirm that this DNA sequence obtained was an integrated virus-cell junction. Based on this, 1935 nt is known as virus junction 1 (the 5' end of the WHV dslDNA), and 2250 nt is known as virus junction 2 (the 5' end of the virus linker primer BM 1246). Further BLAST analysis showed that the insert DNA shared homology with the *Rhinolophus ferrumequinum* (Greater Horseshoe bat) genomic sequence (GenBank Accession NT_113341), 491284 – 491506 nt and 525454 – 525511 nt, with a 167 bp gap (bold font) which did not show any significant BLAST homology.

Figure 5.3.1B shows an example of the DNA sequencing result for a virus-virus sequence, which was a false positive result. BLAST analysis showed that the 165 bp sequence consisted of 2 fragments of WHV genome (GenBank Accession M18752), 2125 – 1993 (blue bold font) and 2251 – 2217 (black bold font). This suggests that this virus-virus false positive fragment was likely to be formed by the ligation of 2 fragmented WHV DNA sequences.

A

GCAGTGTCCACCAAAGCATTAAGGTCAGAAAAAAGTCCAAAGGAAG
AAAATTCAACAACTGATAAGATGAACCAAATTCTTTATAGGGATCT
ATGTCCATGCCCCAAAGCCACCCAAGGCACAGCTTGGAGGCTTGAA
AAGTAGGACATGGAACACAGGCAAAAACAAGGCACAGGTGAAAAAG
ATTTTGGTTCATCTACTTTAAACAACAACTCTTTGTTGATTTTTTG
CATTGTATTCTTATTCTCTATTTCATTAACTTTGGTTTTGGATTAT
ATTTCTTCTCATTTTGGGAATGGTTCATTTTTGTTTTTCTAAGATT
GTGAGGTGATTTATTTGGGCATTTCTTATATAGGCATTTATAGATA
TAAAATTTCCTCTTAAAATTGCTTTTACTGTGTATCAAAGATTTTG
GTTTGATGCTAAGAATTATAAATTTTATCTTCTTTATTGACCGCCC
CTGTCATCATTCAAAAGTTATTGAATCTTCCTGTGTTTATATAGCT
TCTATATTTTTTCTTGCTGTTAATTTCTAACTTCATTCTATTATAA
TGTTATAACATGCAGTAAATGTTATCATCCTTTACGGATTTGTGAT
GACTTGTTTTGTGGCCCAAGATGTGATTGATCTATTTTGGATAAAG
TTCCATGAACAGGTTATGTTAGAGCTCATCCAAGCTATCNAATTNA
GA

B

GAGTAGCAGTGTCCACCAAAGCATTAAGGTCAGGAAAAAAGTCCAA
AGGAAGAAAATTCAACAACTGATAAGATGAACCAAATTCTTTATAG
GGATCTATGTCCATGCCCCAAAGCCACCCAAGGCACAGGTTATGTT
AGAGCTCATCCAAGCTATCAATTTAGA

Figure 5.3.2: Example of DNA sequencing results (5' – 3') obtained from the linker ligation assay to detect integrated DHBV-cell junctions in DHBV-infected duck liver tissues.

The linker ligation assay was performed as described in Section 2.12 based on the duck linker ligation assay design (refer Table 2.4), with Figure 2.9 showing a schematic representation of the major steps involved during linker ligation assay.

Figure 5.3.2A shows an example of the DNA sequencing result for an integrated virus-cell junction. BLAST analysis showed that the 272 bp sequence consisted of a 101 bp insert DNA (black font) flanked by AusDHBV genome (GenBank Accession AJ006350) 2675 – 2534 nt (blue bold font) and 12 – 3011 nt (red bold font). This was consistent with the expected inverted DNA fragment that will be produced by the duck linker ligation assay design, to confirm that this DNA sequence obtained was an integrated virus-cell junction. Based on this, 2534 nt is known as virus junction 1 (the 5' end of the DHBV dslDNA), and 12 nt is known as virus junction 2 (the 5' end of the virus linker primer LL 1329). Further BLAST analysis showed that the insert DNA shared homology with *Gallus gallus* (chicken) BAC clone CH261-48J8 from chromosome z sequence (GenBank Accession AC188941), 27708-27623 nt.

Figure 5.3.2B shows an example of the DNA sequencing result for a virus-virus sequence, which was a false positive result. BLAST analysis showed that the 151 bp sequence consisted of 2 fragments of the AusDHBV genome (GenBank Accession AJ006350), 2678 – 2565 (blue bold font) and 12 – 3011 (black bold font). This suggests that this virus-virus false positive fragment was likely to be formed by the ligation of 2 fragmented DHBV DNA sequences.

A

GCTCTAGAGCATTGATATCCATATATAAGCAAGAATCATAAACAATG
GTACATACCAAAGGTACAGTCAAGGCTGACAACAGCAATGTAGACGT
AAAAATACCTTGGCAGGCAGCTCCGAAGGAGAGGGGTGTAATTCTTA
CAGTGACAGAGCACTGGAACAGGCTGCCCAGAGACGCTGTGGAGTCT
CCTCTGCAGATATTCCCAATCCACCTGGGTGCCATCCTGTGCAGTCT
GTCCCAGTAGGTGTGCATGAATTCTTGCCGTAATCGA

B

CTTGGCAAGGCTCTAGAGCATTGATATCCATATATAAGCAAGAATC
ATAAACAATGGTACATACCAAAGGTACAGTCAAGGCTGACAACAGC
AATGTAGACGTAAAAATACCTTGGCAGTAGGTGTGCATGAATTCTT
GCCGTAATCGATA

Figure 5.3.2

Chapter 5.4: Performing invPCR assays on plasmid DNA as a model system

5.4.1. Aim

a) To establish invPCR assays using plasmid DNA as a model system.
b) To use the plasmid DNA invPCR assay as a model system to determine the sensitivity and efficiency of invPCR assays.

5.4.2. Introduction

Established by Yang and Summers (Yang and Summers, 1999), the invPCR assay has been used to detect integrated virus-cell junctions in liver tissues of HBV-infected humans (Mason *et al.*, 2010) and chimpanzees (Mason *et al.*, 2009a), WHV-infected woodchucks (Mason *et al.*, 2005), and DHBV-infected ducks (Yang and Summers, 1999). The invPCR assay was reported by to be able to detect integrated virus-cell junctions from as little as ~1.2 ng of DNA template with a 20% efficiency, sensitive enough to yield detectable invPCR products from a single DNA template, and is able to amplify individual invPCR products from a mixture of DNA templates when the template was diluted out to a single copy per reaction.

In order to verify that the invPCR assay currently used in the Hepatitis Research Laboratory was as effective and sensitive as published (Yang and Summers, 1999), the efficiency of the invPCR assay was determined using plasmid DNA as a model system. Briefly, invPCR assays were designed to specifically detect known plasmid DNA sequences, in the same way that randomly integrated virus-cell junctions are detected in the liver cell DNA. Based on the expected invPCR products, the specificity and accuracy of the DNA inversion step and the nested PCR steps could be determined. Furthermore, as the amount of DNA template added could be controlled, the limit of sensitivity and the efficiency of detection for each invPCR assay could be determined. In addition, the model system could also be used to determine if preferential amplification (competition) of shorter templates occurs during PCR amplification, or if any points of interference had occurred along the invPCR assay protocols.

However, the model system outlined above would only serve as a general guideline for the efficiency of the invPCR assay. Each invPCR assay is designed for the specific detection of a particular integrated virus-cell junction. Therefore, as each invPCR design will be unique with its own restriction enzymes and PCR primers, the efficiency of each different restriction enzyme digestion and PCR primer amplification could affect the overall sensitivity and efficiency of each invPCR assay. Furthermore, unlike the defined model system, virus integration occurs at random sites in the host cellular DNA. This means that the restriction

enzyme digestion sites on the host cellular DNA will occur at different distances and will produce DNA templates of varying lengths. Templates larger than ~3 kbp will not be easily detected by the nested PCR as it been designed to detect products up to 3 kbp. Due to these variables, the exact efficiency for each invPCR assay could not be determined. However, the model system could provide a valuable guideline of the overall sensitivity and efficiency of the invPCR assays in a closed, controlled system, and can be used as a reference for the invPCR assay used to detect virus-cell integration junctions in liver tissues in this study.

5.4.3. Plasmid DNA as invPCR assay model system

An invPCR assay was designed and established specifically for two known plasmid DNA sequences to produce different sized invPCR products from each plasmid DNA template. The plasmids used were pBL4.8 (Figure 5.4.2) and pBlueScript SK II (-) (pBsSK) (Figure 5.4.1). Briefly, pBL4.8 plasmid consists of a full-length AusDHBV genome (GenBank Accession AJ006350) cloned into a pBlueScript KS II (+) (pBsKS) plasmid vector at the *Eco*RI site (Triyatni, 1998), while the pBsSK is "vector-only" and does not contain any DHBV genome. The pBsSK and pBsKS plasmids contain the same sequences and only differ in the orientation of the f1 origin of replication (to allow for the replication of single stranded DNA in bacteriophage), and the orientation of the *Kpn*I to *Sac*I restriction enzyme sites in the multiple cloning site (MCS), in relation to the direction of the *lazZ* gene of the plasmid.

The invPCR assay involves two steps which need to be designed specifically for each DNA template. In the first step for inverting the invPCR template, a restriction enzyme needs to be chosen to cut out a fragment of DNA from the template, and after circularising the fragment using DNA ligase, another restriction enzyme needs to be chosen to subsequently linearise the circular DNA to invert the DNA fragment. The inversion step will be discussed in detail in Section 5.4.4 below. After inversion, the second step is a nested PCR reaction of the inverted DNA fragment, during which two sets of PCR primers, an outer and inner primer set, need to be designed. The nested PCR reaction will be discussed in detail in Section 5.4.5 below.

In this Section, an invPCR assay specific for the pBL4.8 and pBsSK plasmid DNA was established. Due to the differences in orientation of the pBsSK and pBsKS plasmid DNA sequences, different invPCR products would be produced using the same invPCR assay design. Using these two plasmid model systems, the sensitivity and efficiency of the invPCR assay were determined, as well as other parameters like the preference of amplification of different PCR product sizes, the interference of duck cell DNA on the invPCR assay, and the difference of nested PCR amplification using various combinations of PCR polymerases.

5.4.4. Establish invPCR assay – plasmid DNA template inversion step

5.4.4.1. Restriction enzyme digestion of plasmid DNA

The first step of the invPCR assay is to invert the template DNA, and this involves three parts: firstly to digest the invPCR template into fragments of DNA by first cut restriction enzyme digests, secondly to self-ligate the fragments to form circular DNA, and thirdly to linearise the circular DNA by a single second cut restriction enzyme digest to invert the template DNA fragments (refer to Figures 2.6 and 2.7 for schematic representation of inversion).

Therefore, to design the plasmid invPCR assay, two restriction enzymes had to be chosen specifically for the inversion of pBsSK and pBL4.8 plasmidss. The restriction enzymes preferably have 6 bp recognition sites rather than 4 bp recognition sites, as this will result in less frequent restriction digestion sites, based on the estimation that in a random sequence of bases, restriction enzyme sites is estimated to be present once in every 4096 bp (4^6) or 256 bp (4^4) for restriction enzymes with a 6 bp and 4 bp recognition sites respectively (Nelson and Williams, 2007). In addition, the restriction enzymes should be non-methylation sensitive, and should not contain a lot of degenerate bases (non-specific base pairing) at the recognition site. Ideally, the first restriction enzyme digestion should leave an overhang to allow for subsequent efficient ligations of the digested DNA fragment, while the second restriction enzyme should only digest once in the circular DNA fragment generated after ligation.

Based on those selection requirements, restriction enzyme *Tsp*45I was chosen as the first cut restriction enzyme, while *Afl*III was chosen as the second cut restriction enzyme.

To ensure that the various restriction enzyme digestion reactions were complete with no observable star activities (resulting from relaxed or altered specificity of the restriction enzyme), 5 µg of plasmid pBsSK and pBL4.8 were digested with *Tsp*45I or *Afl*III, or double-digested with *Tsp*45I and *Afl*III. Restriction enzyme digests were performed as described in Section 2.8.2, using restriction enzyme reagents and conditions as described in Table 2.1. For the *Tsp*45I and *Afl*III double digestion, the restriction enzyme digestion mix contained NEBuffer 4 and 1x BSA, and was incubated at 37^{o}C for 1 hr followed by incubation at 65^{o}C for 1 hr. Approximately 1 µg of digested plasmid was then visualised by agarose gel electrophoresis as described in Section 2.8.7. The expected sizes of DNA fragments after the above restriction enzyme digestions of pBsSK and pBL4.8 are summarised in Table 5.4.1.

As shown in Figure 5.4.3, for pBsSK digestion, the undigested pBsSK (lane 1) was observed in three forms of a circular plasmid as expected. These include the concatenated, relaxed

circular, and supercoiled forms. When digested with *Tsp*45I (lane 2), three of the four expected products were present, of which the 532 and 504 bp products could be seen as the large ~500 bp band due to the inability of the agarose gel electrophoresis to separate bands that were ~50 bp apart. As marked by the red box, a larger band of ~3000 bp was also present, suggesting that some incomplete digestion of the plasmid had occurred possibly due to the large quantity of DNA (5 μg) used in the digestion. It was also possible that the ~1500 bp band also contained some incomplete digestion of the plasmid, as the band was thicker than expected. When pBsSK was digested with *Afl*III (lane 3), a ~3000 bp band was present, as expected. However, as marked by the blue box, the ~2000 bp band may be a by-product of some *Afl*III star activity resulting in non-specific digestion, or could be due to incomplete digestion of the plasmid. Lastly, when pBsSK was double-digested with *Tsp*45I and *Afl*III (lane 4), three of the five expected products were present. Again, the 565, 532, and 504 bp bands could be seen as the thicker ~550 bp band due to limitations of the gel electrophoresis.

On the other hand, as shown in Figure 5.4.4, for pBL4.8 digestion, the undigested pBL4.8 (lane 1) was observed in three forms of circular plasmid as expected and described above. When digested with *Tsp*45I (lane 2), four of the eight expected products were present, of which the 848 and 808 bp products, the 592 and 591 bp products, and 251, 211 and 188 bp products could be seen as ~800 bp, ~600 bp and ~200 bp bands respectively due to limitations of the gel electrophoresis. When digested with *Afl*III (lane 3), three of the four expected products were present, of which the 629 and 573 bp products could be seen as the ~600 bp thicker band. As marked by the red box, some larger ~5000 and ~4000 bp bands were present in the *Tsp*45I and *Afl*III-digested pBL4.8, suggesting that some incomplete digestion of the plasmid had occurred. Also, as marked by the blue box, the ~1250 bp band present may be a by-product of some *Afl*III star activity resulting in non-specific digestion. Lastly, when pBL4.8 was double-digested with *Tsp*45I and *Afl*III (lane 4), five of the twelve expected products were present. The 454, 434, 415 and 355 bp products could be seen as the ~400 bp band, while the other five products shorter than 251 bp could be seen as the ~200 bp band.

In summary, pBsSK and pBL4.8 were successfully digested by the restriction enzymes *Tsp*45I and *Afl*III in both single and double-digestion reactions, and were able to produce the expected restriction enzyme digestion products. Thus these two restriction enzymes could be used to invert the plasmids during invPCR assays. However, undigested plasmids were observed during *Tsp*45I digestion of both plasmids, with some undigested plasmids also observed during *Afl*III digestion of pBL4.8. Furthermore, it would appear that some star

activity was observed for *Afl*III. This may be due to a number of factors including long digestion times at multiple temperatures during double digests, or high enzyme concentrations.

5.4.4.2. Inversion of plasmid DNA

After choosing suitable restriction enzymes for the invPCR inversion step (Section 5.4.4.1), the plasmids were inverted to produce inverted plasmid fragments, which were to be used as template for the invPCR nested PCR step. The inversion process for pBsSK and pBL4.8 are shown as a flowchart in Figures 5.4.5 and 5.4.6 respectively, with the expected inverted plasmid fragment sizes produced to be 1714 bp and 2500 bp respectively, and each containing a "junction" of interest (*Eco*RI digestion site) that is to be detected by the invPCR assay.

To ensure that the restriction enzyme digestions and ligation of plasmids had occurred as expected, DNA was visualised after each digestion and ligation step during the inversion protocol. Using *Tsp*45I as first cut restriction enzyme and *Afl*III as second cut restriction enzyme, pBsSK and pBL4.8 were inverted similar to the invPCR inversion protocol described in Section 2.10.1. During this process, samples were removed and stored at four different steps of the inversion protocol. In detail, ~1 µg of plasmid was digested with *Tsp*45I in a 30 µL final volume as described in Section 2.8.2 using restriction enzyme reagents and conditions described in Table 2.1, from which 5 µL of digested DNA was kept in a separate sterile tube. The remaining DNA was then purified using the QIAquick PCR purification kit as described in Section 2.8.6, from which 5 µL of the 40 µL eluted DNA was kept in a separate sterile tube. DNA was then ligated using T4 DNA ligase as described in Section 2.8.3 in a final volume of 400 µL at RT for 2 hr, followed by heat inactivation at 75^{o}C for 10 min. This step produces self-ligated circular plasmid forms essential for generating the inverted DNA. After that, 50 mM NaCl and 1 µL of 20 mg/µL dextran (as carrier) was added, and the DNA was precipitated with 2X volumes of 100% ethanol and incubation at -20^{o}C overnight. After centrifugation and washing of the pellet with 100% ethanol, the pelleted DNA was dissolved in 35 µL H_2O, from which 15 µL of the dissolved DNA was digested with second cut restriction enzyme *Afl*III in a final volume of 30 µL as described in Section 2.8.2 using restriction enzyme reagents and conditions as described in Table 2.1. This final step produces the inverted plasmid fragments used as template for subsequent nested PCR.

DNA samples from four steps during inversion were visualised by agarose gel electrophoresis as described in Section 2.8.7. These steps include after the first cut restriction enzyme *Tsp*45I digestion ("*Tsp*45I-digested"), after QIAquick PCR purification ("*Tsp*45I-digested after purification"), after dissolving the pelleted DNA which is the ligated circular plasmid form

("ligated circular plasmid"), and finally after the second cut restriction enzyme *Afl*III digestion to produce the linear inverted plasmid fragments ("inverted plasmid fragments").

As shown in Figure 5.4.7, during the inversion of pBsSK, the undigested (lane 1) and *Tsp*45I-digested pBsSK (lane 2) produced the same products as observed in Figure 5.4.3, with complete *Tsp*45I-digestion observed possibly due to the smaller amount of pBsSK digested (1 μg instead of 5 μg in Figure 5.4.3). After purification using the QIAquick PCR purification kit (lane 3), some losses of DNA was observed while retaining the same digestion products, with no observable degradation of DNA. After ligation (lane 4), the circular products were now slightly larger than the *Tsp*45I-digested products with an additional band observed. This showed that ligation of the digested products had generated various forms of circular plasmids that had slower gel electrophoresis migration. After digesting the ligated circular products with *Afl*III (lane 5), the circular plasmids were no longer observed, but two products that were similar in size to the *Tsp*45I-digested products were observed. This was as expected, because if the *Tsp*45I-digested products were successfully self-ligated and linearised again by *Afl*III, the inverted products should have the same sizes as the initial *Tsp*45I-digested products. In addition, the brightest ~1700 bp band coincided with the expected pBsSK inverted plasmid fragment size of 1714 bp, confirming that pBsSK had been successfully inverted.

As shown in Figure 5.4.8, during the inversion of pBL4.8, the undigested pBL4.8 (lane 1) and *Tsp*45I-digested pBL4.8 (lane 2) produced the same products as observed in Figure 5.4.4, with complete *Tsp*45I-digestion observed possibly due to the smaller amount of pBL4.8 digested (1 μg instead of 5 μg in Figure 5.4.4). After purification using the QIAquick PCR purification kit (lane 3), some losses of DNA were observed while retaining the same digestion products, with no observable degradation of DNA. After ligation (lane 4), the smaller circular products were observed to be similar in size to the *Tsp*45I-digested products, while multiple larger circular product bands were observed. As the small circular plasmid forms do not generate high resistance during gel electrophoresis compared to larger circular plasmids, they migrate at essentially the same molecular weight as the linear *Tsp*45I-digested products. On the other hand, multiple bands were seen for the circularised large ~2500 bp *Tsp*45I-digested product, suggesting that ligation had generated various forms of circular plasmids. After digesting the ligated circular products with *Afl*III (lane 5), the multiple bands were no longer observed, but all the *Tsp*45I-digested products were observed, with some losses of the ~200 bp product. Again, this was as expected if the *Tsp*45I-digested products were successfully self-ligated and linearised again by *Afl*III, the inverted products should have the same sizes as the initial *Tsp*45I-digested products. In addition, the brightest ~2500 bp

band coincided with the expected pBL4.8 inverted plasmid fragment size of 2500 bp, confirming that pBL4.8 had been successfully inverted. However, an additional unexplained ~1500 bp band was present after inversion (lane 5), suggesting that some additional non-specific *Afl*III digestion of the 2499 bp DNA, or intermolecular ligations of two or more *Tsp*45I-digested DNA fragments had occurred, resulting in an inversion by-product.

In summary, during the inversion step of invPCR assay using pBsSK and pBL4.8 plasmids, *Tsp*45I as first cut restriction enzyme and *Afl*III as second cut restriction enzyme were shown to successfully invert both plasmids, generating inverted plasmid fragments suitable to be used as DNA template for subsequent nested PCR reactions during the invPCR assay.

5.4.5. Establish invPCR assay – nested PCR step

5.4.5.1. Design of nested primer sets for inverted plasmid DNA

The second step of the invPCR assay is to perform nested PCR reactions using the inverted plasmid fragments generated in Section 5.4.4 as DNA templates. Nested PCR consists of two rounds of PCR to specifically amplify the region of interest. Briefly, a first round PCR using an outer primer set specific for the region of interest (*Eco*RI digestion site) in the inverted plasmid fragments was performed. The PCR product was then used as the DNA template for a second round PCR using an inner primer set, selectively re-amplifying a shorter fragment of the region of interest as well as producing higher quantities of the PCR products.

Therefore, two sets of PCR primers were designed specifically for the pBsSK and pBL4.8 inverted fragments using the online Primer3 program with the primer criteria as described in Section 2.8.4. Primers pBS F1 and pBS R1 were designed as the outer primer set, while pBS F2 and pBS R2 were designed as the inner primer set (refer Table 2.2 for primer sequences). The inner primer set was designed to not overlap the outer primer set, but to bind ~100 bp away from the 5' or 3' end of the first PCR product. This not only increases the specificity of the nested PCR by amplifying a shorter second PCR product, but also accommodates for any degradation or damages that may have occured at the 5' and 3' ends of the first PCR product.

5.4.5.2. Nested PCR amplifications of inverted plasmid DNA

Both primer sets designed in Section 5.4.5.1 were used to amplify non-inverted and inverted pBsSK and pBL4.8 in single or nested PCR reactions. For the non-inverted plasmid, as shown in Figures 5.4.1 and 5.4.2, both primer sets would bind specifically onto the region between the ColE1 *E. coli* origin of replication and the start of the *lacZ* gene on the same pBlueScript sequence that is present in both plasmids. On the other hand, after inverting the plasmids

using *Tsp*45I and *Afl*III as described in Section 5.4.4, the primer sets would amplify the inverted plasmid fragments that contain the region of interest (*Eco*RI digestion site) as shown in Figure 5.4.9. All the expected PCR product sizes are summarised in Table 5.4.2.

The second restriction enzyme digestion was performed as it was reported that circular templates may not be as efficiently amplified compared to linear templates (Chen *et al.*, 2007; Hou *et al.*, 2010; Lin *et al.*, 2011). However, additional restriction enzyme digestion steps during the invPCR assay potentially digest the cellular DNA contained in the inverted fragments and prevent its amplification. Therefore, the efficiency and differences in using a circular or a linear DNA template during nested PCR amplifications will also be compared in this Section, to determine whether the linearisation of ligated circular DNA fragments were essential during the invPCR assay. As summarised in Table 5.4.2, both the circular and linear plasmid templates are expected to produce the same PCR products. It should be noted that in the invPCR assay established by Yang and Summers (Yang and Summers, 1999), additional restriction enzymes were routinely used not only to linearise the circular DNA fragments, but also as cccDNA destroying enzymes that digest cccDNA to reduce virus-virus false positives.

All PCR amplifications were performed as described in Section 2.8.5 using GoTaq Flexi polymerase, and each PCR cycle had extension times of 6 min 30 sec. The pBsSK and pBL4.8 plasmids (10 – 20 ng) were used as DNA templates in three different forms: non-inverted (circular), inverted by *Tsp*45I and *Afl*III as described in Section 5.4.4, or ligated circular fragments (inverted by *Tsp*45I and ligated as described in Section 5.3.4.2 only, without linearisation by *Afl*III). Three sets of PCR amplifications were performed: using outer primer set only (pBS F1 – pBS R1), using inner primer set only (pBS F2 – pBS R2), and nested PCR (two rounds of PCR amplification: a first round PCR using outer primer set, then flame pin transfer PCR products to a second round PCR using the inner primer set). All PCR products were visualised by agarose gel electrophoresis as described in Section 2.8.7.

As shown in Figure 5.4.10, using the outer primer set, PCR amplification of the non-inverted pBsSK produced two ~1800 bp and ~3000 bp PCR products instead of the expected 2238 bp PCR product. The reasosn for this are unknown. In contrast, PCR amplification of the non-inverted pBL4.8 produced the expected ~5500 bp PCR product. PCR amplification of both inverted plasmid fragments produced PCR products of ~1000 bp for pBsSK and ~1800 bp for pBL4.8, showing that specific PCR amplification of invPCR plasmid fragment had successfully occurred as a 991 bp and 1776 bp PCR product was expected for each inverted plasmid fragment respectively. Similar PCR products were also observed for the ligated

circular plasmids, with additional ~3000 bp and ~4000 bp PCR by-products produced during the PCR amplification of ligated circular pBsSK. It is likely that these PCR by-products were produced from amplifications of various forms of ligated circular pBsSK artefacts, which could be produced by the intermolecular ligation of different *Tsp*45I-digested pBsSK fragments rather than the expected intramolecular ligation and circularisation of the pBsSK. Thus, by linearising the ligated circular pBsSK with *Afl*III, the ligation artefacts would be digested and no longer able to be amplified, as seen in the "inverted pBsSK" lane where only the expected PCR products were amplified from the inverted pBsSK fragments.

On the other hand, using the inner primer set, PCR amplification of the non-inverted pBsSK and pBL4.8 produced a ~1900 bp and ~5000 bp PCR product respectively, indicating that PCR amplification had successfully occurred, as a 1784 bp and 4811 bp PCR products was expected for each non-inverted plasmid fragment. Similarly, PCR amplification of the inverted pBsSK and pBL4.8 fragments also produced ~500 bp and ~1400 bp PCR products respectively, again indicating that PCR amplifications had successfully occurred, as a 537 bp and 1322 bp PCR product was expected for each inverted plasmid fragment. Similar PCR products were also observed for the ligated circular plasmids, with additional ~3000 bp and ~3500 bp PCR by-products produced during the PCR amplification of ligated circular pBsSK, and additional ~2500 bp PCR by-products produced during the PCR amplification of ligated circular pBL4.8. Again, it is likely that these PCR by-products were produced from amplifications of various forms of ligated circular plasmids as described previously.

As nested PCR amplifications of the ligated circular plasmids were shown to produce the same PCR products as the inverted plasmid fragments (linear), these suggest that PCR amplifications of linear and circular templates had a similar efficiency. However, as by-products were produced during the first round nested PCR (e.g. in PCR reactions of circular ligated pBsSK in Figure 5.4.10), these suggest that the circular template may not be as specifically amplified compared to a linear template. Thus, it was decided that the ligated circular plasmids produced during the inversion process of the invPCR assay would first be linearised by restriction enzyme digestion prior to nested PCR reactions.

When nested PCR amplifications were performed (data not shown), PCR products similar to PCR amplifications using the inner primer set were produced. None of the PCR by-products observed during the PCR amplification of ligated circular plasmids or the non-inverted pBsSK were produced. These suggest that that second round nested PCR amplification does

increase the specific of PCR amplifications, as it selectively amplifies only the expected PCR product, while eliminating any by-products produced during the first round PCR amplification.

All of these results suggest that the four plasmid invPCR assay PCR primers designed in Section 5.4.5.1 were able to bind specifically to the non-inverted and inverted pBsSK and pBL4.8, and produce the expected PCR products in nested PCR reactions. Hence, the outer (pBS F1 – pBS R1) and inner primer sets (pBS F2 – pBS R2) could be used during plasmid invPCR assay to amplify the region of interest of pBsSK and pBL4.8 plasmids.

In conclusion, an invPCR assay was successfully designed and established using the pBsSK and pBL4.8 plasmids. It is expected that a 537 bp product would be produced for pBsSK, while a 1322 bp product would be produced for pBL4.8. The schematic representation of the plasmid invPCR assay designs for pBsSK and pBL4.8 plasmids as well as the expected invPCR assay products are shown in Figures 5.4.11 and 5.4.12 respectively. The invPCR design is also summarised in Table 2.3 and designated as invPCR design P1.

5.4.6. Parameters of invPCR assays assessed

After successfully designing and establishing invPCR assays for the pBsSK and pBL4.8 plasmids in Sections 5.4.4 and 5.4.5, the plasmid invPCR assays was used as a model system to determine the the sensitivity and efficiency of invPCR assays. To do this, invPCR assays were performed using known amounts of starting plasmid as DNA template. Also, by combining both plasmids in a single invPCR assay, the preference and PCR amplification competition that may have occurred due to the different PCR product sizes produced could be determined. Extracted normal duck liver (NDL) DNA was also added to the plasmid DNA template to determine the potential interference of large quantities of duck cell DNA on the invPCR assay. Lastly, different combinations of PCR Taq polymerase were used during nested PCR reactions to determine the optimal Taq polymerase combination for nested PCR.

Briefly, 1 μg of pBsSK and pBL4.8 plasmids were inverted as described in Section 5.4.4, and used as DNA templates for nested PCR reactions as described in Section 2.10.3. AmpliTaq Gold polymerase and the outer primer set pBS F1 – pBS R1 were used in the first round PCR reaction, and following flamed pin transfer of the first round PCR products, GoTaq polymerase and inner primer set pBS F2 – pBS R2 were used in the second round PCR reaction. Both PCR reactions were performed in a 10 μL final volume, with a PCR cycle extension time of 2 min 30 sec. Lastly, all PCR products were visualised using agarose gel

electrophoresis as described in Section 2.8.7. It is expected that pBsSK would produce a 537 bp PCR product, while pBL4.8 would produce a 1322 bp PCR product.

The copy numbers of each plasmid could be calculated using the formula described in Section 2.8.9.3.1. Based on that, to get 10^{10} copies of plasmid, 32.5 ng of pBsSK was needed, while 65.6 ng of pBL4.8 was needed. The copy numbers of inverted plasmid fragments were then estimated as being the same as the copy numbers of plasmids used during the inversion step. As this estimation assumed that no loss or degradation of plasmid DNA had occurred during the inversion steps, and that 100% efficiency of inversion had occurred, it is highly likely that this would be an over-estimation of the actual inverted plasmid fragments copy numbers.

As the restriction enzymes and PCR primers used were the same for both pBsSK and pBL4.8 plasmids, the efficiencies of the restriction enzyme digestions and PCR amplifications were assumed to be the same, although the restriction enzyme digestion sites and PCR primer binding sites would be different on both plasmids due to the different sequence orientations as explained in Section 5.4.3. It should also be noted that that PCR reactions were assumed to be sensitive enough to amplify from a single copy of DNA template (AB, 2009; Roux, 2009). Therefore, the efficiency of PCR amplification was not taken into account in this Section.

5.4.6.1. The sensitivity of detection of the invPCR assay

To determine the sensitivity of the plasmid invPCR assay established in Sections 5.4.4 and 5.4.5, serial dilutions of the inverted pBsSK and pBL4.8 fragments produced in Section 5.4.4 were used as DNA templates for nested PCR (Section 5.4.6). A total of eight 10-fold serial dilutions were performed to obtain a range of 10^{10} – 10^{-2} copies of DNA template

Results (data not shown) showed that for the pBsSK plasmid invPCR assay, the expected 537 bp PCR product was produced from 10^{10} – 10^{1} copies of inverted pBsSK fragments, a faint PCR product was produced from 10^{0} copies of inverted pBsSK fragments, and no PCR products were produced from 10^{-1} – 10^{-2} copies of inverted pBsSK fragments. On the other hand, results (data not shown) showed that for the pBL4.8 plasmid invPCR assay, the expected 1322 bp PCR product was produced from 10^{10} – 10^{2} copies of inverted pBL4.8 fragments, a faint PCR product was produced from 10^{1} copies of inverted pB4.8 fragments, and no PCR products were produced from 10^{0} – 10^{-2} copies of inverted pBL4.8 fragments.

The invPCR assay was slightly more sensitive for pBsSK possibly due to the smaller plasmid (2961 bp), shorter inverted pBsSK fragment (1715 bp) and nested PCR product (537 bp),

compared to the pBL4.8 plasmid that was larger (5988 bp), has longer inverted pBL4.8 fragment (2500 bp) and longer nested PCR product (1322 bp). It is thought that during the inversion process, shorter DNA fragments may be more efficiently self-ligated; while during nested PCR, shorter PCR products were more efficiently and easily amplified, and were thus were seen as a bright PCR product band by agarose gel electrophoresis. However, as the invPCR assay was not able to produce a clear visible product from a single copy of inverted pBsSK fragment and less than 10 copies of inverted pBL4.8 fragment, these suggest that the plasmid invPCR assays were slightly less sensitive compare to the published invPCR assays (Yang and Summers, 1999). Alternatively, this could also be due to the over-estimation of inverted plasmid fragment copy numbers mentioned in Section 5.4.6, which would result in lower actual copy numbers of inverted plasmid fragments added as DNA templates.

In summary, results suggest that the plasmid invPCR assays established in Sections 5.4.4 and 5.4.5 were sensitive enough to detect and produce a PCR product from a single copy of inverted pBsSK fragment or 10 copies of inverted pBL4.8, albeit only as a faint band.

5.4.6.2. The efficiency of the invPCR assay

To determine the efficiency of aliquoting or distributing DNA templates to more PCR wells (schematically represented as step C in Figure 2.8), 10 copies of the inverted pBsSK and pBL4.8 fragments produced as described in Section 5.4.4 were aliquoted to 12 individual PCR reaction wells for nested PCR performed as described in Section 5.4.6. If equal distribution of DNA templates were achieved in all the PCR wells, PCR products would be amplified in 10 of the 12 PCR wells. However, as equal distribution of DNA by aliquoting is almost impossible in practice, less than 10 wells were expected to contain PCR products.

Results (data not shown) showed that for the pBsSK plasmid, the expected 537 bp PCR product was produced in all 12 PCR wells, while for the pBL4.8 plasmid, the expected 1322 bp PCR product was produced in only 5 of the 12 PCR wells. The intensity of the pBsSK PCR product bands were strong, while the the pBL4.8 PCR product bands were faint.

The results for the pBL4.8 plasmid was as expected, and showed that the inverted pBL4.8 fragments had been distributed to other PCR wells. However, for the pBsSK plasmid invPCR assay, results suggest that there may in fact be more than 12 copies of inverted pBsSK fragment present rather than the estimated 10 copies. This may explain faint band observed from the amplification of 10^0 copies of inverted pBsSK fragments in Section 5.4.6.1.

In summary, by aliquoting DNA templates to more PCR wells, it was possible to distribute the DNA template to as little as a single copy per PCR well, which can be subsequently amplified by nested PCR. In addition, it was suggested that the smaller pBsSK plasmid may have higher efficiency of inversion and amplification compared to the larger pBL4.8 plasmid.

5.4.6.3. Product size preference during the invPCR assay

To examine competition between products of various sizes during invPCR assays, the inverted pBsSK and pBL4.8 fragments were mixed together and used as DNA templates for the plasmid invPCR assays. To achieve this, 0.5 μg of each pBsSK and pBL4.8 plasmid were inverted in the same tube as described in Section 5.4.4, and serially diluted from 10^9 to 10^{-2} copies (of each of the plasmids) in a 96-well PCR tray as described in Section 5.4.6.1. The contents of the PCR well which was expected to contain 10^1 copies of each inverted plasmid fragments were also aliquoted out to 12 PCR wells as described in Section 5.4.6.2. Nested PCR was subsequently performed as described in Section 5.4.6.

Results (data not shown) showed that only the 537 bp pBsSK invPCR product was produced from 10^9 to 10^0 copies of each inverted plasmid fragments, while a faint pBsSK PCR product agarose gel electrophoresis band was produced at 10^{-1} copies of each inverted plasmid fragments. For the 12 aliquoted PCR wells, all wells also contained only the 537 bp pBsSK PCR product. These results suggest that the invPCR assay showed preferential detection of shorter invPCR products, as only the shorter pBsSK invPCR product was observed.

To determine whether the longer pBL4.8 invPCR products were present in the first round PCR, PCR products from each round of the amplification of 10^4 to 10^{-1} copies of each inverted pBsSK and pBL4.8 fragments were visualised by agarose gel electophoresis as described in Section 2.8.7. As comparison, PCR products from serial dilutions of 10^4 to 10^{-1} copies of either inverted pBsSK or pBL4.8 fragments only were also visualised.

As shown in Figure 5.4.13, using individual inverted pBsSK or pBL4.8 fragments as DNA template only, first round PCR had successfully amplified the expected 991 bp and 1776 bp products respectively, followed by the expected 537 bp and 1322 bp products respectively after performing nested PCR amplifications. Interestingly, reducing amounts of invPCR products correlating to the reducing amounts of serially diluted DNA templates added were produced in the first round PCR, as seen by the reducing intensities of the bands. However, after nested PCR amplifications using the first round PCR products as DNA template, almost

equal amounts of nested PCR products were produced in all reactions. On top of that, invPCR products were only observed after nested PCR amplification of 10^0 copies of inverted pBsSK fragment, although no invPCR product could be observed during the first round PCR. All these show that nested PCR amplification was able to specifically and efficiently amplify the first round PCR products, as well as increasing the sensitivity of detection of DNA templates.

When a mixture of pBsSK and pBL4.8 was used as DNA template for the invPCR assay, in the first round PCR, only the pBsSK invPCR product was observed at 10^4 and 10^3 copies of DNA template. It was only when the copies of template was reduced (10^2 – 10^0 copies), that the pBL4.8 inbPCR product could be observed in addition to the pBsSK invPCR product. However, only the pBsSK invPCR product was observed after nested PCR amplification. These show that during the first round PCR, when the DNA templates were present in abundance (>10^3 copies), the shorter PCR product would be preferentially amplified; but when lesser amounts of DNA templates were present (<10^2 copies), the two different DNA templates present in the PCR mix could both be amplified. However, after nested PCR amplifications, only the shorter PCR product would be preferentially amplified, even when only ~1 copy of the shorter DNA template was present in the mixture.

Previously, Yang and Summers (Yang and Summers, 1999) reported that by performing 40 nested PCR reactions each containing 0.6 copies of two different plasmids, they detected a total of 8 PCR products, 5 of which were from one plasmid while 3 were from the other plasmid. Hence they concluded that at endpoint dilutions of DNA templates, nested PCR reactions were able to efficiently amplify and produce nested PCR products from individual DNA templates present. Therefore, the nested PCR reactions were repeated using mixed inverted pBsSK and pBL4.8 fragment aliquoted out to 50 PCR wells, so that each well would contain ~0.5 copies of each inverted plasmid fragment. Results (data not shown) showed that a total of 24 PCR products were produced, 15 of which were the pBsSK invPCR product, while 9 were the pBL4.8 invPCR product. Based on that, this suggests that similar to the published invPCR assay (Yang and Summers, 1999), the invPCR assay established in this Section was also able to amplify and detect different individual DNA templates present in a mixture when the DNA template was diluted to approximately one copy per PCR well.

In summary, when more than one DNA template was present, the invPCR assay preferably detects the shorter invPCR products, or from the DNA template that was present in larger quantities. By aliquoting out a mixture of DNA templates so that only a single copy of each

DNA template was present in each PCR well, individual DNA templates present in the mixture could be detected using the invPCR assay.

5.4.6.4. The interference of duck cell DNA with the invPCR assay

In the extracted liver cell DNA samples, invPCR assay has to detect the rare specific integrated virus-cell junctions that are present amongst the much more abundant liver cell DNA. Therefore, to determine whether the invPCR assay would be affected by the presence of large amounts of DNA, duck liver cell DNA was added to the plasmid DNA templates during the plasmid invPCR assay. Specifically, duck liver cell DNA was extracted from NDL or from DHBV-infected duck livers (Pool 7 ducks) (Triyatni *et al.*, 2001) using the DNeasy blood and tissue kit as described in Section 2.6.1. After that, 1 μg of duck liver cell DNA was added to the plasmid DNA before performing the inversion step, and the experiments described in Sections 5.4.6.1, 5.4.6.2, and 5.4.6.3 were repeated to test the sensitivity, efficiency, and product size preference of the invPCR assay in the presence of duck liver cell DNA. The addition of 1 μg of duck liver cell DNA was to represent the amount of total DNA normally added during invPCR assays. The Pool 7 duck liver cell DNA was expected to contain at least 500 copies of DHBV total DNA in the form of either RI DNA and/or DHBV cccDNA (Jilbert *et al.*, 1992), and 1 – 17 copies of DHBV cccDNA (Zhang *et al.*, 2003). Therefore, these experiments were also used to determine whether the presence of DHBV RI DNA and cccDNA on top of the duck cell DNA would have any effects on the invPCR assays.

For the invPCR assay sensitivity test, when compared with the results obtained in Section 5.4.6.1, results (data not shown) showed that the addition of NDL or Pool 7 DNA did not affect the pBsSK invPCR assay results. However, the addition of NDL or Pool 7 DNA had reduced the sensitivity of pBL4.8 invPCR assay, as the PCR product was produced from only 10^{10} – 10^{3} copies of inverted pBL4.8 fragments as compared to 10^{10} – 10^{2} copies in Section 5.4.6.1, while a faint PCR product was produced from 10^{2} copies as compared to 10^{1} copies in Section 5.4.6.1. When compared with the results in Section 5.4.6.3, the addition of NDL or Pool 7 DNA did not alter the preferential amplification of the shorter pBsSK invPCR product.

For the invPCR assay efficiency test, when compared with the results obtained in Section 5.4.6.2, results (data not shown) showed that the addition of NDL or Pool 7 DNA had slightly affected the pBsSK invPCR assay, by producing PCR products in 10 or 8 wells respectively out of the 12 PCR wells, as compared to PCR products in all 12 wells in Section 5.4.6.2. However, the addition of NDL or Pool 7 DNA did not affect the pBL4.8 invPCR assay as PCR products were both similarly produced in 5 out of the 12 PCR wells as found in Section

5.4.6.2. When compared with the results in Section 5.4.6.3, the addition of NDL or Pool 7 DNA had again slightly affected the efficiency of the pBsSK and pBL4.8 mixture invPCR assay, by both preferentially producing the pBsSK PCR product in 9 out of the 12 PCR wells, as compared to the pBsSK invPCR product in all 12 wells in Section 5.4.6.3.

Therefore, the results suggest that the presence of either NDL or Pool 7 DNA may slightly reduce the sensitivity and efficiency of the plasmid invPCR assay. The reduction in sensitivity of the pBL4.8 invPCR assay in the presence of either NDL or Pool 7 DNA may be contributed by the saturation of reagents by the duck liver cell DNA and DHBV DNA present. The pBL4.8 invPCR assay may have been more affected as the size of the pBL4.8 plasmid and expected invPCR product was larger than the pBsSK plasmid as described in Section 5.4.6.1. On the other hand, the reduction in efficiency could be due to less efficient aliquoting and equal distribution of the short inverted pBsSK and pBL4.8 fragments (2500 bp and 1715 bp respectively) in the presence of greater amounts and much longer fragments of duck cell DNA (1.05 – 1.38 billion base pairs) (International Chicken Genome Sequencing Consortium, 2004; Kraus *et al.*, 2011). On the other hand, as no differences were observed betwen the addition of either NDL or Pool 7 DNA (which contained RI DNA and cccDNA), these suggest that the presence of the smaller DHBV RI DNA and cccDNA (~3027 bp) would not greatly affect the efficiency of the invPCR assay. Rather, it was the presence of longer duck cell DNA that would slightly affect the efficiency of the invPCR assay.

In summary, the plasmid invPCR products were efficiently amplified in the presence of duck cellular DNA, although slightly lower amounts of invPCR products were generated, as the sensitivity and efficiency of the invPCR assays were found to be slightly reduced.

5.4.6.5. Taq polymerases combinations during nested PCR

To determine which combination of Taq polymerase would be most efficient during invPCR assay, nested PCR reactions were performed using different Taq polymerase combinations. This was in response to non-specific amplifications observed by collaborator Dr. William Mason (personal communication) when the same Taq polymerase was used in both round of the nested PCR amplifications. Two of the commonly used PCR Taq polymerases in the Hepatitis Research Laboratory, namely the AmpliTaq Gold (AB, USA), and GoTaq Flexi (Promega, Australia) polymerases, were tested. Specifically, inverted pBsSK fragments produced as described in Section 5.4.4, were serially diluted from 10^6 – 10^1 copies, and subsequently amplified by nested PCR reactions as described in Section 5.4.6. Four combinations of the polymerases were used: AmpliTaq Gold – AmpliTaq Gold, AmpliTaq

Gold – GoTaq Felxi, GoTaq Flexi – AmpliTaq Gold, and GoTaq Flexi – GoTaq Flexi. All PCR products were visualised using agarose gel electrophoresis as described in Section 2.8.7

Results (data not shown) showed that all four Taq polymerase combinations successfully produced the expected 537 bp pBsSK PCR product for all serial dilutions of DNA template. Comparing the intensities of the PCR product bands produced, AmpliTaq Gold – AmpliTaq Gold produced the faintest bands, followed by GoTaq Flexi – GoTaq Flexi. Both GoTaq Flexi – AmpliTaq Gold and GoTaq Flexi – GoTaq Flexi had similar strongest intensity bands.

As AmpliTaq Gold – GoTaq Flexi produced bands with less DNA smearing compared to the GoTaq Flexi – AmpliTaq Gold (data not shown), the AmpliTaq Gold – GoTaq Flexi combination would be the preferred Taq polymerase combination used during invPCR assay. These findings were consistent with results obtained by collaborator Dr. William Mason, who had chosen to use the same AmpliTaq Gold – GoTaq Flexi Taq combinations during invPCR assays in his recently published studies (Mason *et al.*, 2009a; Mason *et al.*, 2009b; Mason *et al.*, 2010). In addition, the GoTaq Flexi PCR reagents were ideal to be used during the second round PCR reactions, as the Green GoTaq Flexi PCR buffer (Promega, Australia) that was used in the PCR reaction mix already contains an agarose gel electrophoresis loading dye. Therefore, this allowed for the loading of PCR products directly onto the agarose gels, eliminating the extra step of adding 1/10 volume of 10X TAE loading buffer to each sample. The optimised nested PCR methods are described in detail in Section 2.10.3.

5.4.7. InvPCR assays detecting duck cellular genes as a model system

Another model system that can be used to determine the efficiency of an invPCR assay is by detecting a known cellular gene, preferably a single copy gene for easier quantitation, that can also be inverted using the same restriction enzymes used in the invPCR assay, therefore serving as an "internal control" for the invPCR assay.

For instance, the first cut restriction enzyme for the woodchuck invPCR assay, *Sac*I, could also digest a 892 bp fragment of the woodchuck *hcr* gene. After the inversion step of the invPCR assay, in addition to detecting the integrated virus-cell junctions using WHV-specific PCR primers, PCR primers specific for the 892 bp fragment of the *hcr* gene were also used to amplify the inverted *hcr* gene. Thus, by measuring the amount of *hcr* gene that was successfully inverted, the efficiency of the invPCR assay could be estimated. Using this method, the efficiency of the inversion reaction in the woodchuck invPCR assay was reported to be as high as 80% by Mason *et al.* (Mason *et al.*, 2005).

The advantages of using known cellular genes as an invPCR assay model system over using plasmid DNA as a model system, include eliminating the differences in digestion efficiencies of individual restriction enzymes as the same restriction enzymes with the actual invPCR assays were used. In addition, the control gene could be amplified from the same invPCR assay's inverted DNA template mix to more accurately determine the efficiency of that assay.

However, the biggest challenge in using duck cellular genes an invPCR assay model system is that the duck genome has not been as fully sequenced as compared to mammalian genomes like humans or chimpanzees. This greatly limits the search and choices of suitable single copy duck genes that could be used. For example, none of the currently known single copy duck genes, the duck heart lactate dehydrogenase B-like protein (Hendriks *et al.*, 1988), the duck serum amyloid A protein (Guo *et al.*, 1996), duck β actin and GAPDH (Chapter 4), could be inverted using the duck invPCR assays D1 – D5 summarised in Table 2.3.

To increase the choices of suitable genes, single copy genes from the closely-related chicken species (*Gallus gallus*) were used instead. The chicken sequence was chosen as chickens have a close evolutionary relationship with ducks, both belonging in the same Aves class, as well as being classified under the same galloanserae clade in the phylogenetic tree of birds (Hackett *et al.*, 2008). Chapter 4 had also confirmed the suitability of using chicken genes by showing that most duck genes had high homology to the corresponding chicken genes.

From the chicken genome, it was found that the chicken Or1 sex determining region Y-box 5 SOX5 gene (GenBank Accession FJ548633.1) could be inverted by the duck invPCR assay design D3 (Table 2.3) to produce a 2355 bp inverted SOX5 fragment. Based on the chicken sequence, nested PCR primer sets were designed to detect the inverted SOX5 fragments, and were designated as chSOX5 F1 – chSOX5 R1 for the outer primer set and chSOX5 F2 – chSOX5 R2 for the inner primer set (refer Table 2.2 for primer sequences). In addition, PCR primer sets were also designed to detect the normal or non-inverted (normal) SOX5 gene, and were designated as chSOX5 F – chSOX5 R primer set (refer Table 2.2 for primer sequences).

Duck liver cell DNA was extracted from Pool 7 (Triyatni *et al.*, 2001) and DM32:33 ducks (Miller *et al.*, 2006) using the total DNA extraction method as described in Section 2.6.3. The duck liver cell DNA was subsequently inverted based on the invPCR assay design D3 as described in Section 2.10.1. The chSOX5 F1 – chSOX5 R1 and chSOX5 F2 – chSOX5 R2 primer sets were then used to detect the inverted SOX5 gene using nested PCR amplification,

while the chSOX5 F – chSOX5 R primer set was used to detect the non-inverted (normal) SOX5gene from both inverted and non-inverted extracted duck liver DNA.

Unfortunately, no SOX5 PCR products were detected (data not shown). Also, no PCR products were detected when the chSOX5 F – chSOX5 R primer set was used to detect the SOX5 gene from the non-inverted Pool 7 and DM32:33 DNA (data not shown). These suggest that the SOX5 primers designed were unsuitable to detect the SOX5 equivalent gene in the duck genome, either due to great differences in the chicken and duck SOX5 genes that would cause mis-matching of primer sequences so that the duck SOX5 gene could not be PCR amplified, or it could also be that the duck genome does not contain the SOX5 gene.

Due to time limitations and the success of the plasmid DNA as a model system for the invPCR assay (Section 5.4.6), further attempts to establish other chicken genes as an invPCR assay model system were not pursued in this study.

In summary, attempts to use duck cellular genes as a model system to determine the efficiency of the invPCR assay were not successful partly due to the limited number of published and sequenced duck genome.

5.4.8. Conclusion

In conclusion, a plasmid invPCR assay was successfully designed and established for pBsSK and pBL4.8 plasmids as shown in Figures 5.4.11 and 5.4.12, and was able to amplify a 537 bp invPCR product from pBsSK, and a 1322 bp invPCR product from pBL4.8.

The plasmid invPCR assay was found to be able to detect a single copy of the DNA template after efficient serial dilution and aliquoting (equal distribution of DNA templates amongst PCR wells) of the inverted plasmid fragments. Furthermore, when one template is in excess, the invPCR assay preferably detects the smaller invPCR product, or the DNA templates that were present in larger quantities. However, this bias could be overcome by diluting and aliquoting the DNA templates so that only a single copy of each DNA template is present in each PCR well. Lastly, it was found that the presence of large amounts of duck cell DNA might slightly reduce the total number of invPCR products detected.

Table 5.4.1: Expected DNA products generated by restriction enzyme digestion of plasmid DNA.

Plasmid	Restriction enzyme digestion[a]	Expected DNA products of plasmid DNA[b] (bp)
pBsSK	*Tsp*45I	1714, 532, 504, 211
pBsSK	*Afl*III	2961
pBsSK	*Tsp*45I and *Afl*III	1149, 565, 532, 504, 211
pBL4.8	*Tsp*45I	2499, 848, 808, 592, 591, 251, 211, 188
pBL4.8	*Afl*III	2751, 2035, 629, 573
pBL4.8	*Tsp*45I and *Afl*III	1350, 1149, 848, 453, 434, 415, 355, 251, 211, 188, 176, 158

[a]Up to 5 μg of each plasmid DNA was digested by restriction enzyme(s) as described in Section 5.4.4.1.

[b]Expected DNA products after complete restriction enzyme digestion of plasmid DNA were obtained using NEBcutter V2.0 online free software (accessible through http://tools.neb.com/NEBcutter2/index.php).

Table 5.4.2: Expected PCR product sizes produced from PCR amplification of circular (non-inverted) and inverted pBsSK and pBL4.8 plasmids, using the plasmid invPCR assay outer or inner primer sets.

invPCR assay PCR primer set[a]	**Plasmid**[b]		**Expected PCR product size**[c] **(bp)**
Outer primer set pBS F1 – pBS R1	pBsSK	Non-inverted	2238
	pBL4.8		5265
	pBsSK	Inverted	991
	pBL4.8		1776
Inner primer set pBS F2 – pBS R2	pBsSK	Non-inverted	1784
	pBL4.8		4811
	pBsSK	Inverted	537
	pBL4.8		1322

[a]invPCR assay PCR primer sets were designed as described in Section 5.4.5 (refer Table 2.2 for primer sequences).

[b]Plasmids were inverted using the restriction enzymes *Tsp*45I and *Afl*III as described in Section 5.4.4.

[c]Expected PCR product sizes were calculated based on primer binding sites on each plasmid as shown in Figures 5.4.1, 5.4.2 and 5.4.9. The expected PCR product sizes for inverted (linear) plasmid and the ligated circular plasmid are the same.

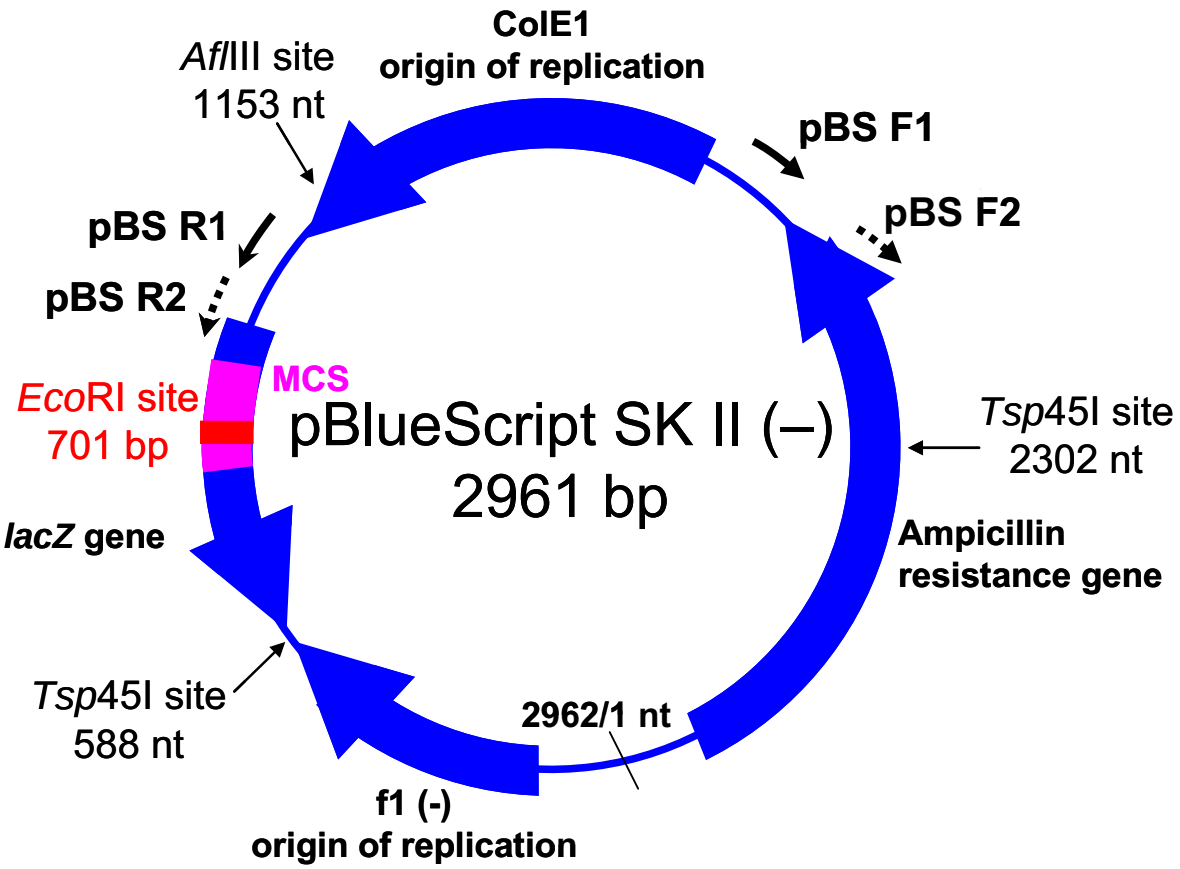


Figure 5.4.1: Orientation and position of the binding sites of four PCR primers designed for the plasmid invPCR assay on the circular (non-inverted) plasmid. Figure was adapted from the pBsSK plasmid map (GenBank Accession X52330) provided by the manufacturer, Stratagene, USA.

Two sets of invPCR assay nested PCR primers were designed in Section 5.4.5.1: outer primer set that consisted of pBS F1 and pBS R1, and inner primer set that consist of pBS F2 and pBS R2 (refer Table 2.2 for primer sequences). Base pair numberings shown in the Figure were based on the pBsSK sequence (GenBank Accession X52330).

During PCR amplification of pBsSK, the outer primer set is expected to produce a 2238 bp PCR product, while the inner primer set is expected to produce a 1784 bp PCR product.

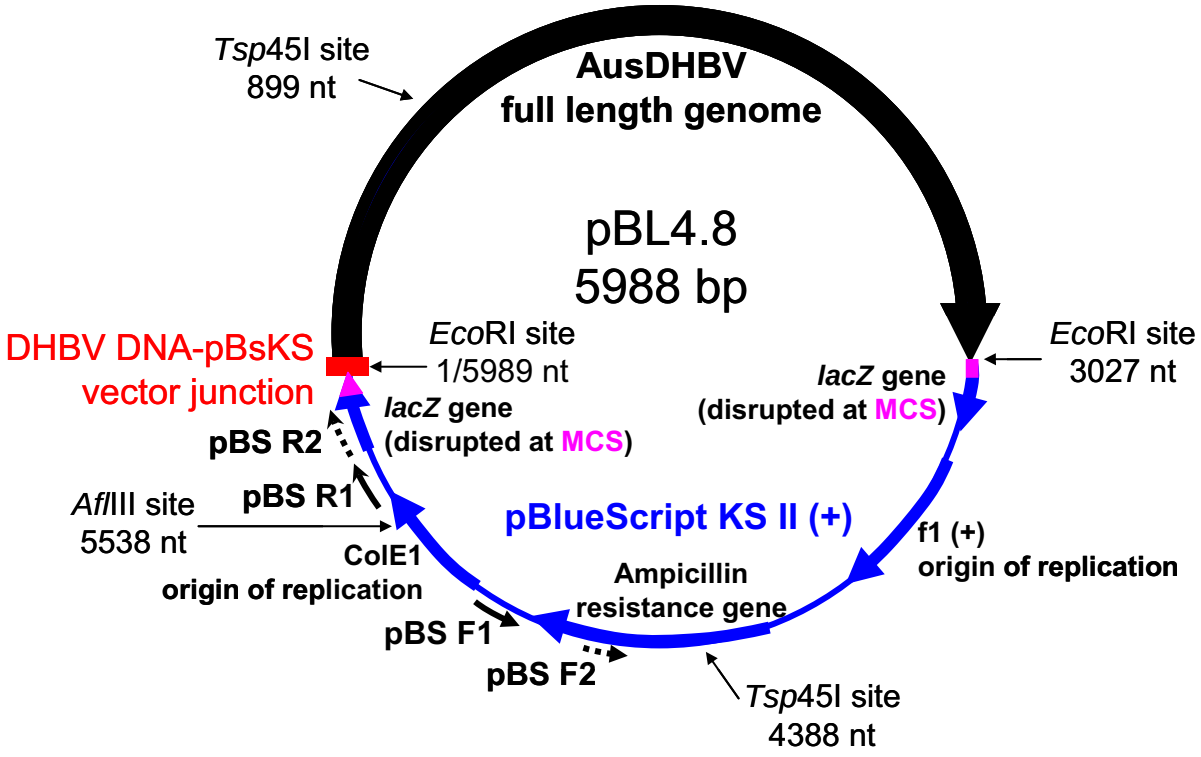


Figure 5.4.2: Orientation and position of the binding sites of four PCR primers designed for the plasmid invPCR assay on the circular (non-inverted) plasmid pBL4.8. The pBsKS plasmid map was adapted from the pBsKS plasmid map (GenBank Accession X52327) provided by the manufacturer, Stratagene, USA.

Two sets of invPCR assay nested PCR primers were designed in Section 5.4.5.1: outer primer set that consist of pBS F1 and pBS R1, and inner primer set that consist of pBS F2 and pBS R2 (refer Table 2.2 for primer sequences). Base pair numberings shown in the Figure were based on the AusDHBV (GenBank Accession AJ006350) *Eco*RI site as 1 nt, followed by the pBsKS sequence (GenBank Accession X52327) but in the 3' – 5' order.

During PCR amplification of pBL4.8, the outer primer set is expected to produce a 5265 bp PCR product, while the inner primer set is expected to produce a 4811 bp PCR product.

Figure 5.4.3: *Tsp*45I and *Afl*III restriction enzyme-digested pBsSK plasmid.

Up to 5 µg of pBsSK plasmid was digested with *Tsp*45I (lane 2) or *Afl*III (lane 3), or double-digested with *Tsp*45I and *Afl*III (lane 4) as described in Section 5.4.4.1. Approximately 1 µg of undigested and digested plasmid DNA was visualised by 1% agarose gel electrophoresis as described in Section 2.8.7.

Based on the expected DNA product sizes after restriction enzyme digestion of pBsSK (Table 5.4.1), three of the four expected products were present after *Tsp*45I digestion (lane 2), all expected products were present after *Afl*III digestion (lane 3), and three of the five expected products were present after double digestion (lane 4). Products ~60 bp apart in size could not be separated by this agarose gel electrophoresis.

The red box (lane 2) indicates that some incomplete digestion of plasmid may have occurred. The blue box (lane 3) indicates the presence of smaller DNA fragments that may be due to restriction enzyme star activities.

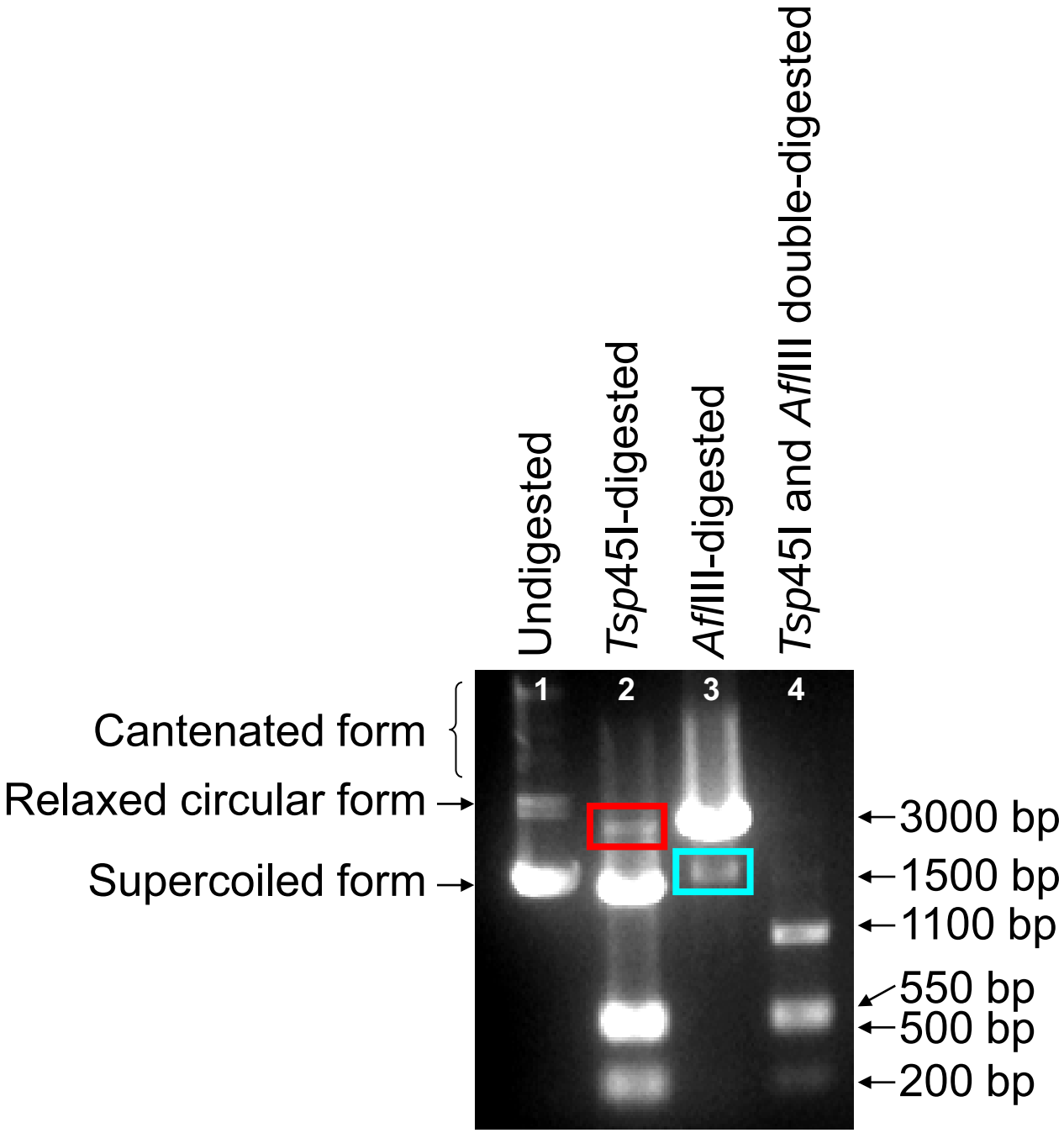

Undigested
Tsp45I-digested
AflIII-digested
Tsp45I and AflIII double-digested
1
2
3
4
Cantenated form
Relaxed circular form
Supercoiled form
3000 bp
1500 bp
1100 bp
550 bp
500 bp
200 bp

Figure 5.4.3

Figure 5.4.4: *Tsp*45I and *Afl*III restriction enzyme-digested pBL4.8 plasmid.

Up to 5 µg of pBL4.8 plasmid was digested with *Tsp*45I (lane 2) or *Afl*III (lane 3), or double-digested with *Tsp*45I and *Afl*III (lane 4) as described in Section 5.4.4.1. Approximately 1 µg of undigested and digested plasmid DNA were visualised by 1% agarose gel electrophoresis as described in Section 2.8.7.

Based on the expected DNA product sizes after restriction enzyme digestion of pBL4.8 (Table 5.4.1), four of the eight expected products were present after *Tsp*45I digestion (lane 2), three of the four expected products were present after *Afl*III digestion (lane 3), and five of the twelve expected products were present after double digestion (lane 4). Products ~100 bp apart in size could not be separated by this agarose gel electrophoresis.

The red box (lanes 2 and 3) indicate that some incomplete digestion of plasmid may have occurred. The blue box (lane 3) indicates the presence of smaller DNA fragments that may be due to restriction enzyme star activities.

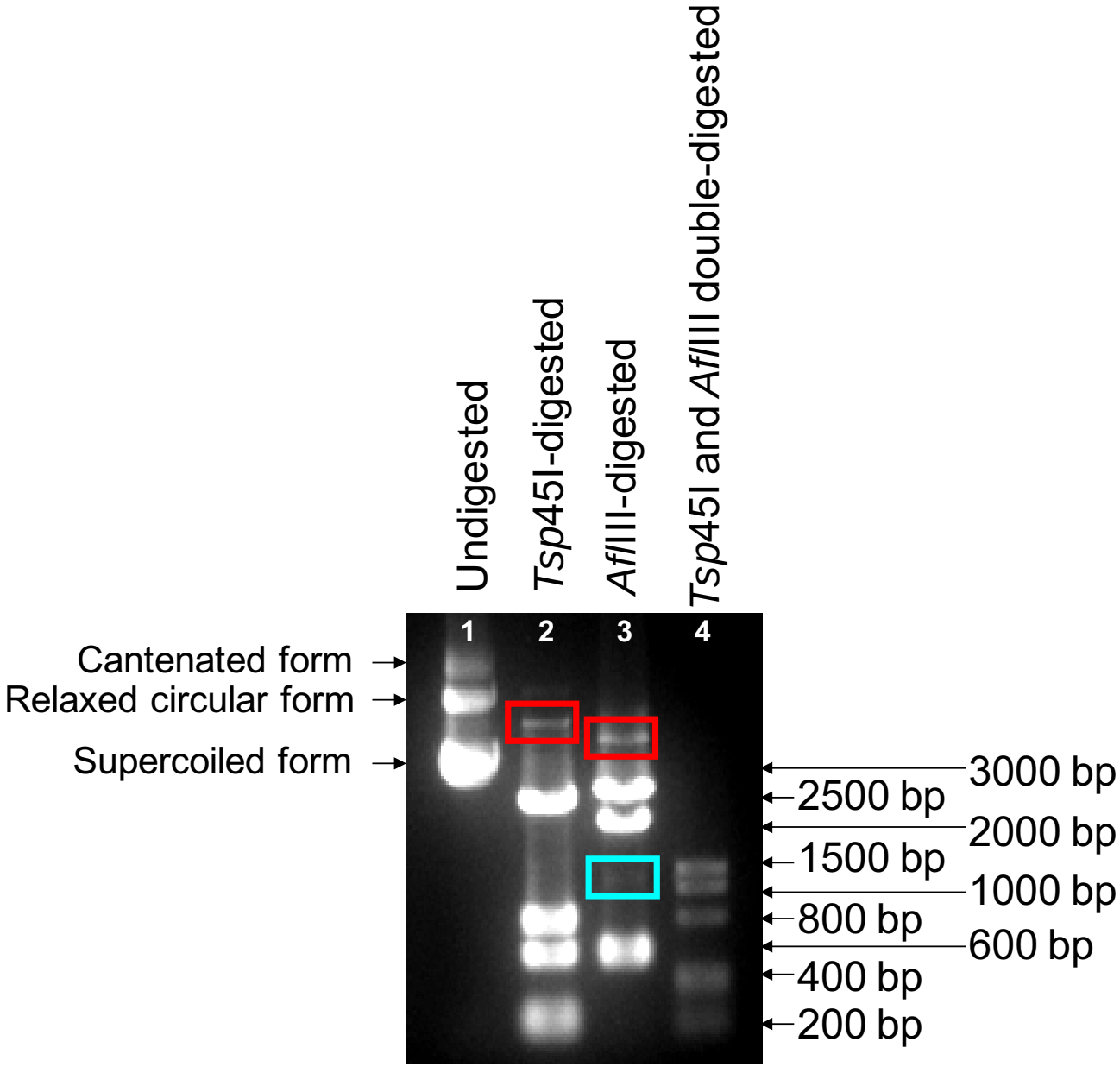

Undigested
Tsp45I-digested
AflIII-digested
Tsp45I and AflIII double-digested
1
2
3
4
Cantenated form
Relaxed circular form
Supercoiled form
3000 bp
2500 bp
2000 bp
1500 bp
1000 bp
800 bp
600 bp
400 bp
200 bp

Figure 5.4.4

Figure 5.4.5: Flowchart of the steps involved in the pBsSK plasmid DNA inversion during pBsSK invPCR assay, using *Tsp*45I and *Afl*III restriction enzymes as the first and second cut restriction enzymes respectively.

Restriction enzymes to be used for plasmid invPCR assay were chosen as described in Section 5.4.4.1. The DNA inversion was performed as described in Section 2.10.1.

Figure 5.4.5A shows the 2961 bp circular pBsSK plasmid DNA (refer Figure 5.4.1), with the first cut restriction enzyme, *Tsp*45I, digestion site, the second cut restriction enzyme, *Afl*III, digestion site, and the "junction" of interest (*Eco*RI digestion site).

Figure 5.4.5B shows the 1714 bp plasmid fragment that would be formed after digestion with *Tsp*45I. The DNA fragment would contain the "junction" of interest.

Figure 5.4.5C shows the circularised plasmid fragment that would be formed after DNA ligation. The plasmid would still be 1714 bp in size.

Figure 5.4.5D shows the 1714 bp linearised inverted plasmid fragment that would be formed after digestion with *Afl*III. The inverted plasmid fragment consists of the pBsSK 1153 nt – 2302/588 nt ligation junction – 1153 nt, and contain the "junction" of interest.

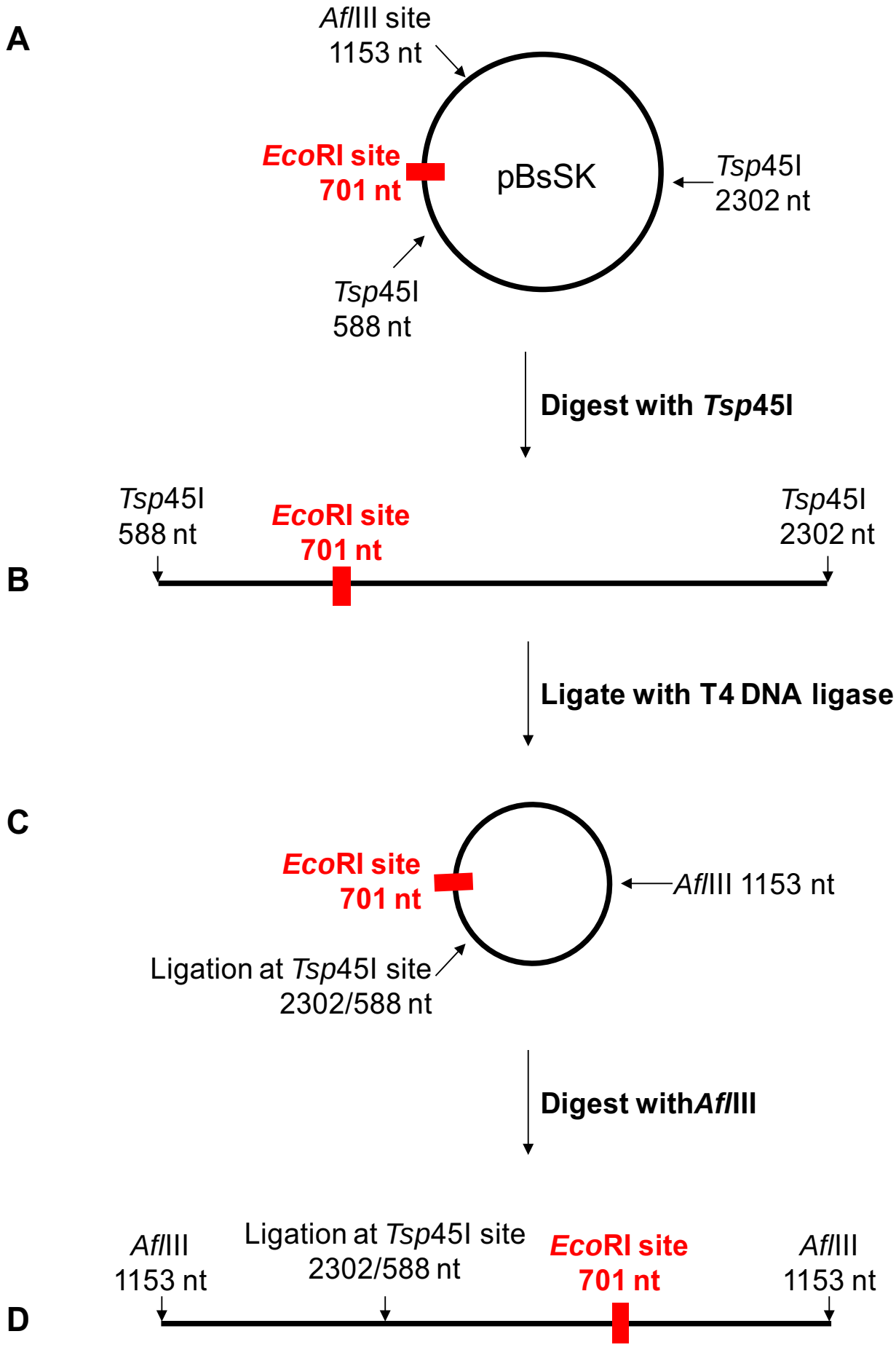

A
AflIII site
1153 nt
EcoRI site
701 nt
pBsSK
Tsp45I
2302 nt
Tsp45I
588 nt
Digest with Tsp45I
B
Tsp45I
588 nt
EcoRI site
701 nt
Tsp45I
2302 nt
Ligate with T4 DNA ligase
C
EcoRI site
701 nt
AflIII 1153 nt
Ligation at Tsp45I site
2302/588 nt
Digest withAflIII
D
AflIII
1153 nt
Ligation at Tsp45I site
2302/588 nt
EcoRI site
701 nt
AflIII
1153 nt

Figure 5.4.5

Figure 5.4.6: Flowchart of the steps involved in the pBL4.8 plasmid DNA inversion during pBL4.8 invPCR assay, using *Tsp*45I and *Afl*III restriction enzymes as the first and second cut restriction enzymes respectively

Restriction enzymes to be used for plasmid invPCR assay were chosen as described in Section 5.4.4.1. The inversion was performed as described in Section 2.10.1.

Figure 5.4.6A shows the 5988 bp circular pBL4.8 plasmid DNA (refer Figure 5.4.2), with the first cut restriction enzyme, *Tsp*45I, digestion site, the second cut restriction enzyme, *Afl*III, digestion site, and the "junction" of interest (the DHBV DNA-pBsKS vector junction at 5989/1 nt, which is also an *Eco*RI digestion site).

Figure 5.4.6B shows the 2500 bp plasmid fragment that would be formed after digestion with *Tsp*45I. The DNA fragment would contain the "junction" of interest.

Figure 5.4.6C shows the circularised plasmid fragment that would be formed after DNA ligation. The plasmid would still be 2500 bp in size.

Figure 5.4.6D shows the 2500 bp linearised inverted plasmid fragment that would be formed after digestion with *Afl*III. The inverted plasmid fragment consists of the pBL4.8 plasmid 5538 nt – 899/4388 nt ligation junction – 5538 nt, and contain the "junction" of interest.

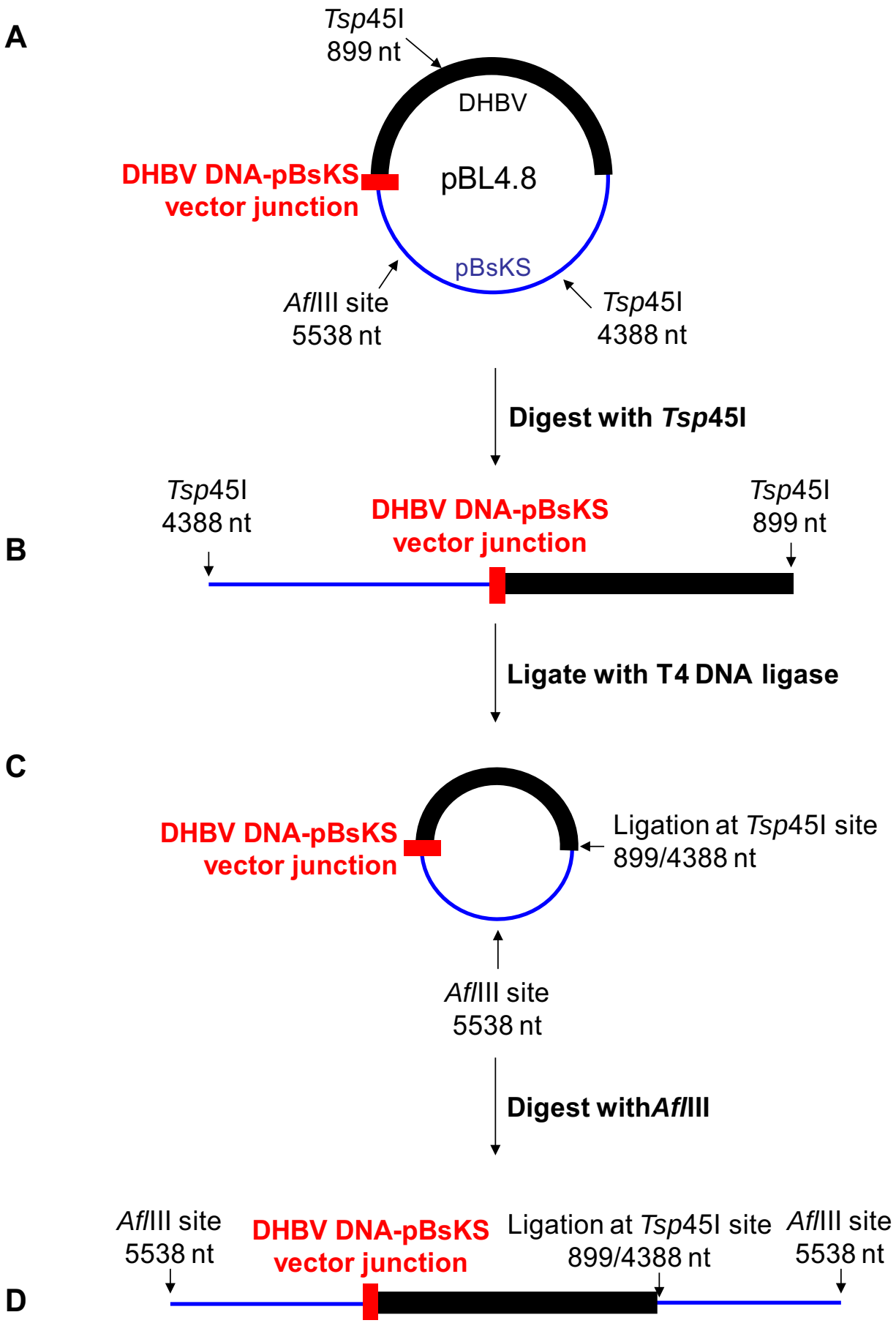

A
Tsp45I
899 nt
DHBV
pBL4.8
DHBV DNA-pBsKS
vector junction
pBsKS
AflIII site
5538 nt
Tsp45I
4388 nt
Digest with Tsp45I
B
Tsp45I
4388 nt
DHBV DNA-pBsKS
vector junction
Tsp45I
899 nt
Ligate with T4 DNA ligase
C
DHBV DNA-pBsKS
vector junction
Ligation at Tsp45I site
899/4388 nt
AflIII site
5538 nt
Digest withAflIII
D
AflIII site
5538 nt
DHBV DNA-pBsKS
vector junction
Ligation at Tsp45I site
899/4388 nt
AflIII site
5538 nt

Figure 5.4.6

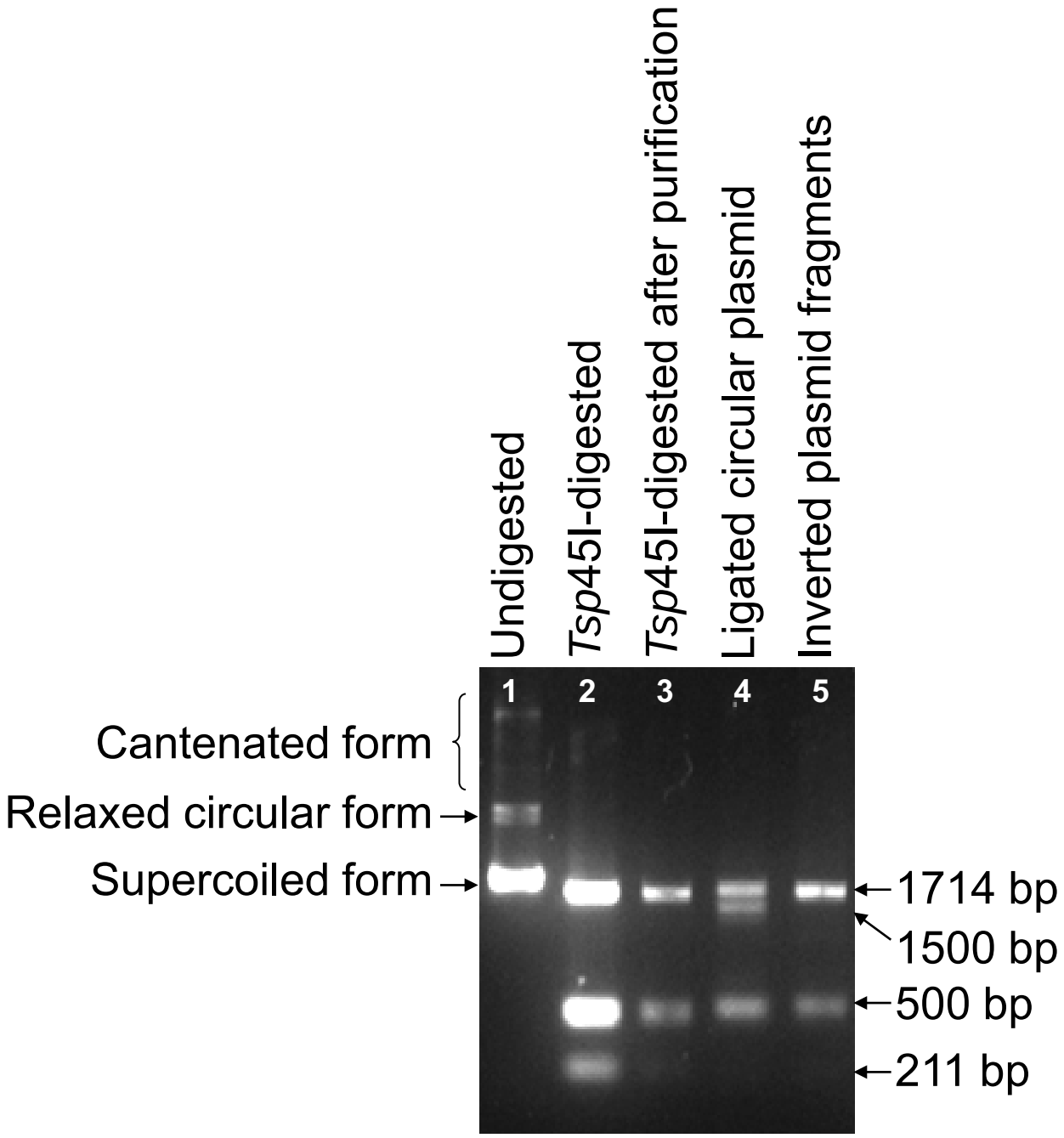


Figure 5.4.7: pBsSK plasmid DNA collected during four steps of the invPCR assay inversion protocol.

Up to 1 μg of pBsSK was inverted as described in Section 5.4.4, and 100 – 110 ng DNA from each of the four steps during the inversion protocol were visualised by 1% agarose gel electrophoresis as described in Section 2.8.7.

The digestion of pBsSK with *Tsp*45I (lane 2) yielded 3 bands (1714 bp, ~500 bp, 211 bp) as expected. Some losses of DNA had occurred during QIAquick PCR purification (lane 3). Successful ligation of the *Tsp*45I-digested pBsSK was indicated by the presence of multiple bands (lane 4). The ligated DNA was linearised by *Afl*III digestion to produce the expected 1714 bp and ~500 bp bands (lane 5).

Figure 5.4.8: pBL4.8 plasmid DNA collected during four steps of the invPCR assay inversion protocol.

Up to 1 µg pBL4.8 was inverted as described in Section 5.4.4, and 100 – 110 ng DNA from each of the four steps along the inversion protocol were visualised by 1% agarose gel electrophoresis as described in Section 2.8.7.

The digestion of pBL4.8 with *Tsp*45I (lane 2) yielded 4 bands (2499 bp, ~800 bp, ~600 bp, ~200 bp) as expected. This *Tsp*45I digestion was more complete when compared to Figure 5.4.4 (lane 2). Some losses of DNA had occurred during QIAquick PCR purification (lane 3). Successful ligation of the *Tsp*45I-digested pBL4.8 was indicated by the presence of multiple bands (lane 4). The ligated DNA was linearised by *Afl*III digestion to produce the expected 2499 bp, ~800 bp, ~600 bp bands (lane 5). The additional ~1500 bp band in lane 5 may be due to non-specific *Afl*III digestions of the 2499 bp DNA, or artefacts formed by intermolecular ligations.

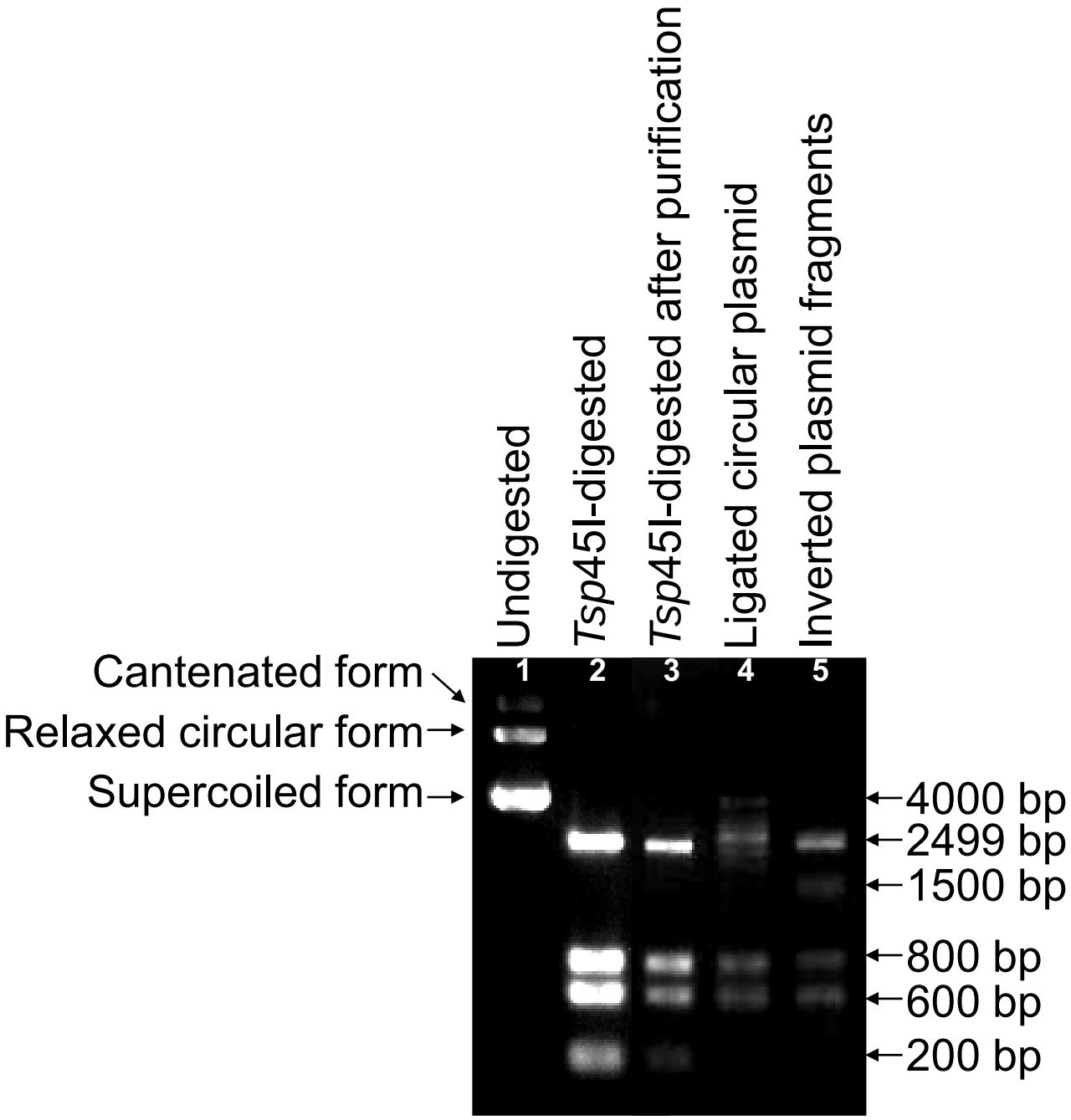

Undigested
Tsp45I-digested
Tsp45I-digested after purification
Ligated circular plasmid
Inverted plasmid fragments
1
2
3
4
5
Cantenated form
Relaxed circular form
Supercoiled form
4000 bp
2499 bp
1500 bp
800 bp
600 bp
200 bp

Figure 5.4.8

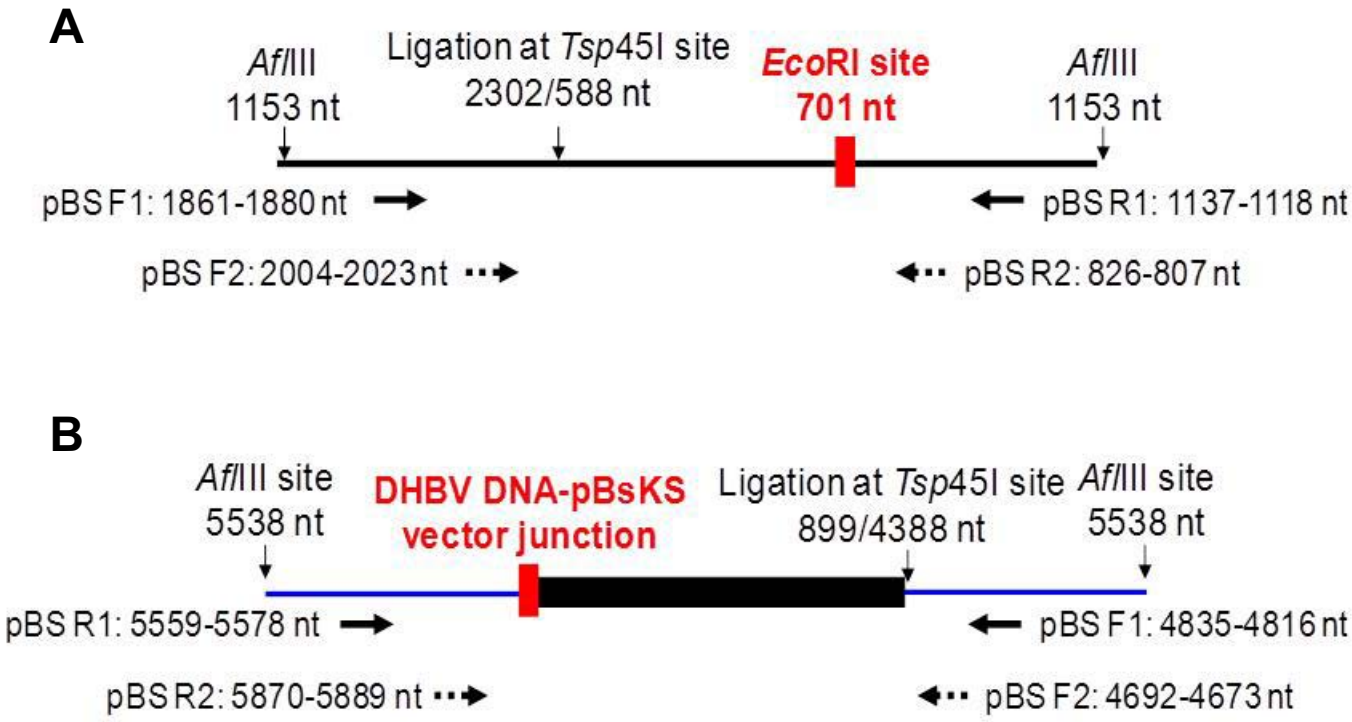


Figure 5.4.9: Orientation and position of the binding sites of four PCR primers designed for the plasmid invPCR assay on the inverted pBsSK (Figure 5.4.9A) and inverted pBL4.8 (Figure 5.4.9B) fragments.

Both pBsSK and pBL4.8 plasmids were inverted by *Tsp*45I and *Afl*III as described in Section 5.4.4 to produce a 1714 bp and 2500 bp inverted plasmid fragments respectively.

Two sets of invPCR assay PCR primers were designed in Section 5.4.5: outer primer set that consist of pBS F1 and pBS R1, and inner primer set that consist of pBS F2 and pBS R2 (refer Table 2.2 for primer sequences). Both primer sets binds to the inverted plasmid fragments to amplify most of the fragment, including the region of interest represented as the red box in the figures.

During PCR amplification of the inverted pBsSK fragment, a 991 bp PCR product is expected to be produced using the outer primer set during the first round PCR, while a 537 bp PCR product is expected to be produced using the inner primer set during the second round PCR. Conversely, during PCR amplification of the inverted pBL4.8 fragment, a 1776 bp PCR product is expected to be produced using the outer primer set during the first round PCR, while a 1322 bp PCR product is expected to be produced using the inner primer set during the second round PCR.

Figure 5.4.10: PCR amplification products produced using the invPCR assay outer primer set (pBSF1 – pBS R1) or inner primer set (pBS F2 – pBS R2) on three forms of each plasmid pBsSK and pBL4.8 (non-inverted, inverted, ligated circular) as DNA template.

Plasmids were inverted by *Tsp*45I and *Afl*III as described in Section 5.4.4. PCR amplification was performed as described in Section 5.4.5.2, using the invPCR assay outer primer set (pBS F1 – pBS R1) or inner primer set (pBS F2 – pBS R2). PCR products were visualised by 1% agarose gel electrophoresis as described in Section 2.8.7. Expected PCR product sizes are summarised in Table 5.4.2.

The "non-inverted" samples were amplified using full-length circular plasmid DNA as the DNA template. The "inverted" samples were amplified using linear inverted plasmid fragments produced as described in Section 5.4.4.2 as the DNA template. The "ligated circular" samples were amplified using the circular ligated plasmids (described in Section 5.4.4.2) as the DNA template.

All PCR reactions using the outer primer set produced the expected PCR products summarised in Table 5.4.2, except for the "non-inverted pBsSK" lane which had produced two ~1800 bp and ~3000 bp bands instead of the expected 2238 bp band, and the "ligated circular pBsSK" lane which had additional ~3000 bp and ~4000 bp bands.

All PCR reactions using the inner primer set produced the expected PCR products summarised in Table 5.4.2, except for the "ligated circular pBsSK" lane, which had produced additional ~3000 bp and ~3500 bp bands, and the "ligated circular pBL4.8" lane, which had produced an additional ~2500 bp band.

As PCR by-products were observed, PCR amplification from a circular template may not be as specific as from a linear template.

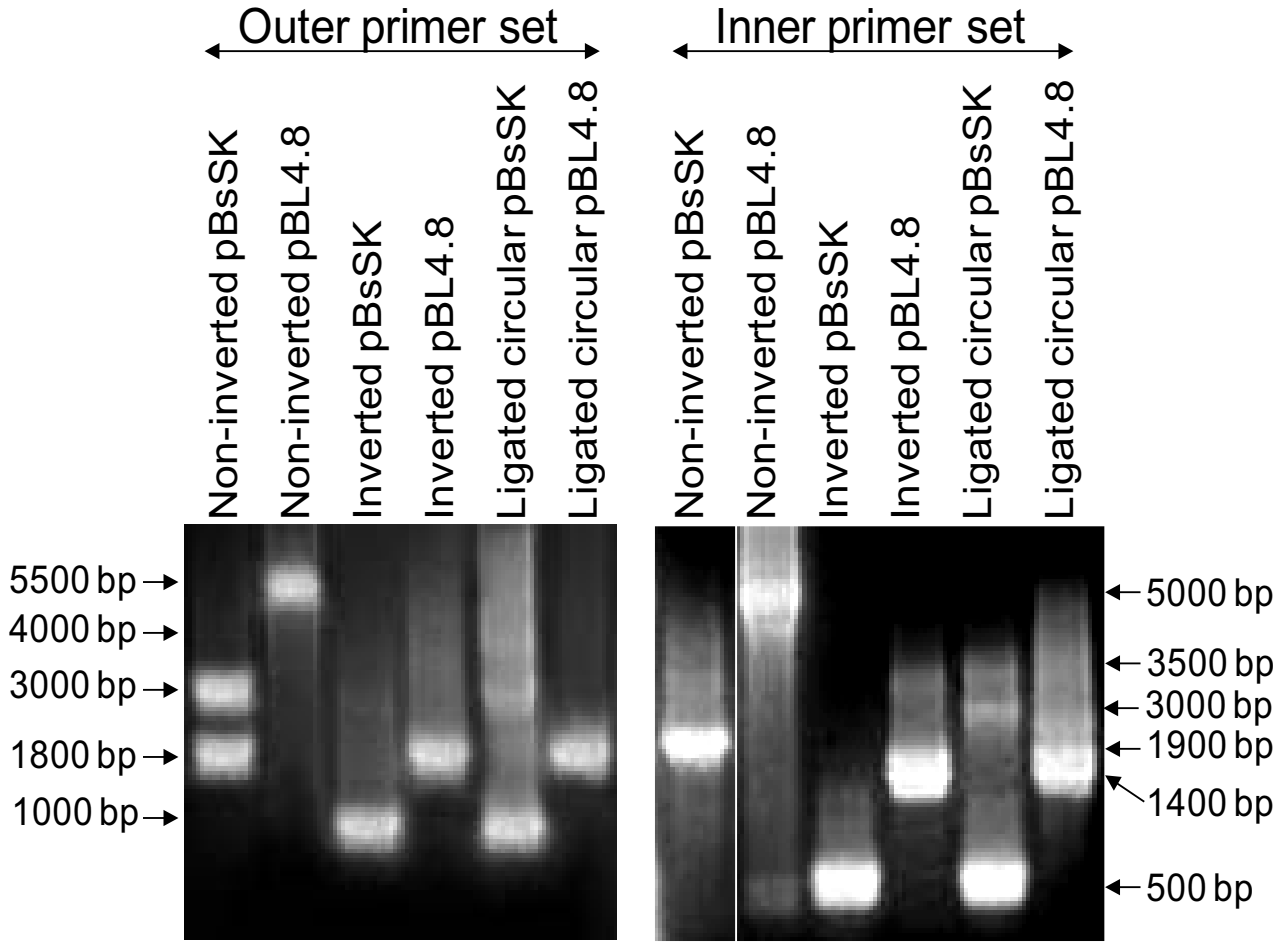

Outer primer set
Inner primer set
Non-inverted pBsSK
Non-inverted pBL4.8
Inverted pBsSK
Inverted pBL4.8
Ligated circular pBsSK
Ligated circular pBL4.8
Non-inverted pBsSK
Non-inverted pBL4.8
Inverted pBsSK
Inverted pBL4.8
Ligated circular pBsSK
Ligated circular pBL4.8
5500 bp
4000 bp
3000 bp
1800 bp
1000 bp
5000 bp
3500 bp
3000 bp
1900 bp
1400 bp
500 bp

Figure 5.4.10

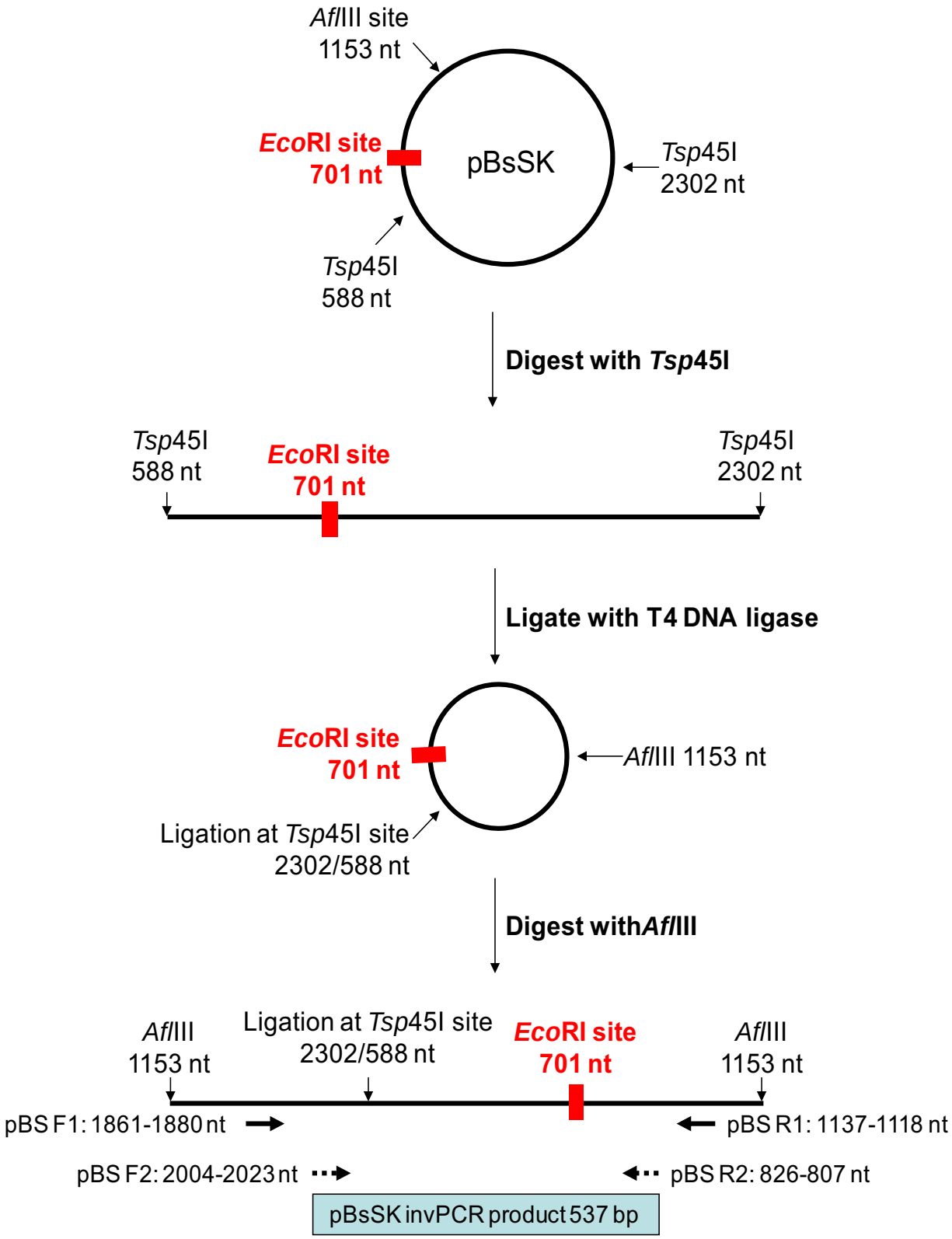


Figure 5.4.11: Schematic representation of the pBsSK invPCR assay design, showing the plasmid DNA inversion process, the nested PCR reaction primer binding sites, and the expected pBsSK invPCR assay product.

pBsSK invPCR assay restriction enzymes were chosen as described in Section 5.4.4, and nested PCR primers were designed as described in Section 5.4.5.

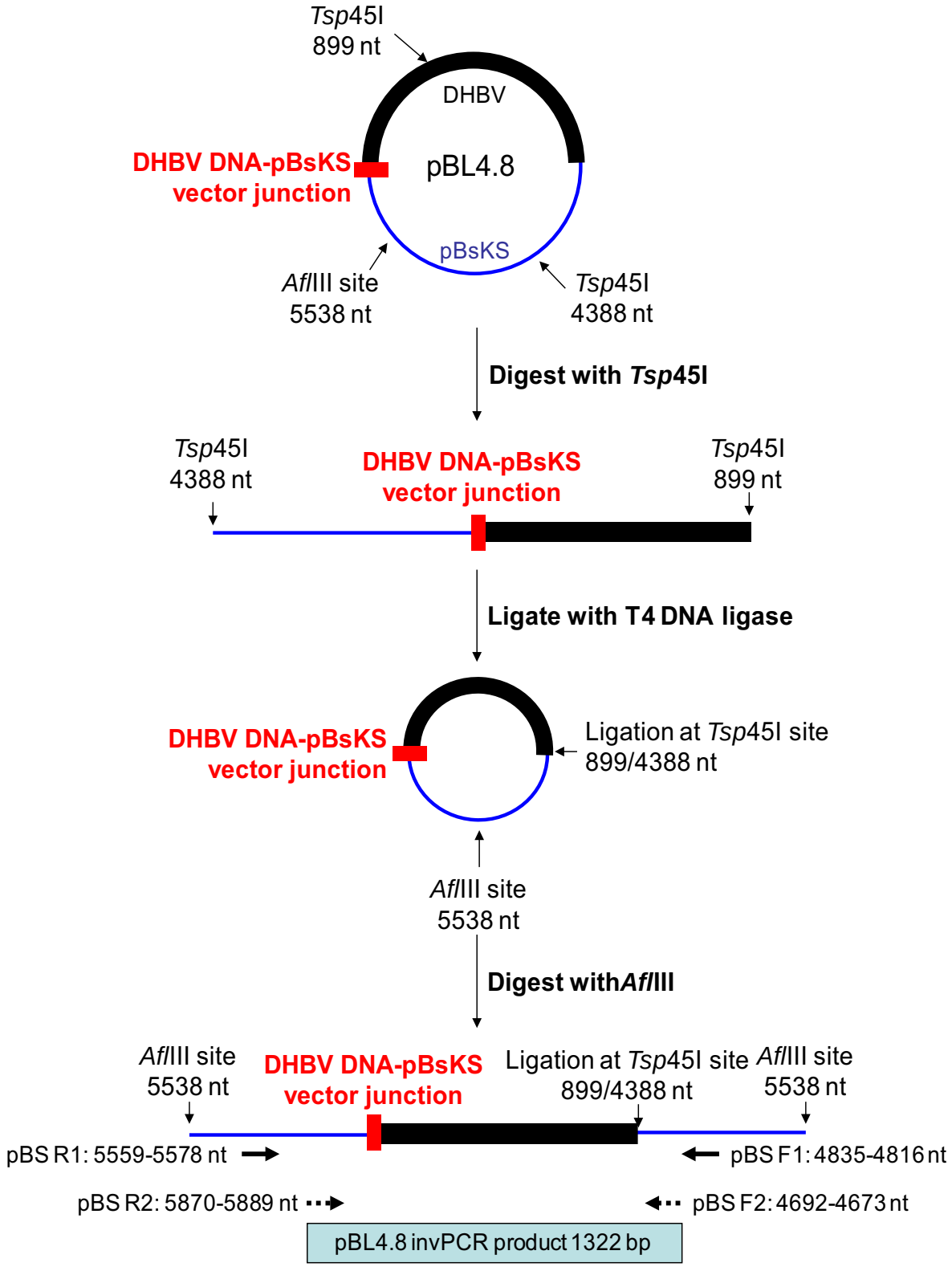


Figure 5.4.12: Schematic representation of the pBL4.8 invPCR assay design, showing the plasmid DNA inversion process, the nested PCR reaction primer binding sites, and the expected pBL4.8 invPCR assay product.

pBL4.8 invPCR assay restriction enzymes were chosen as described in Section 5.4.4, and nested PCR primers were designed as described in Section 5.4.5.

Figure 5.4.13: PCR products produced from first round PCR amplification and nested PCR amplification using serial dilutions of inverted pBsSK, pBL4.8, and pBsSK mixed with pBL4.8 fragments as DNA template.

Plasmids were inverted by *Tsp*45I and *Afl*III as described in Section 5.4.4. Inverted plasmid templates were serially diluted and amplified by nested PCR as described in Section 5.4.6.3. PCR products were visualised by 1% agarose gel electrophoresis as described in Section 2.8.7. The expected PCR product sizes are summarised in Table 5.4.2.

In the first round PCR, the expected 991 bp PCR product was observed for "pBsSK only", the 1776 bp PCR product was observed for "pBL4.8 only", while both PCR products were observed for "pBsSK and pBL4.8 mixture". After nested PCR, the expected 537 bp PCR product was observed for "pBsSK only", the 1322 bp PCR product was observed for "pBL4.8 only", but only the pBsSK PCR product was observed for "pBsSK and pBL4.8 mixture".

Reducing amounts of PCR products were observed along the serially diluted DNA templates in the first round PCR reactions, detecting down to 10^1 copies for "pBsSK only" and "pBL4.8 only", and 10^0 copies for the pBsSK and pBL4.8 mixture. After nested PCR, equal amounts of PCR products were observed in all the serially diluted DNA templates, detecting down to 10^0 copies for "pBsSK and pBL4.8 mixture", 10^0 copies for "pBsSK only", and 10^1 copies for "pBL4.8 only".

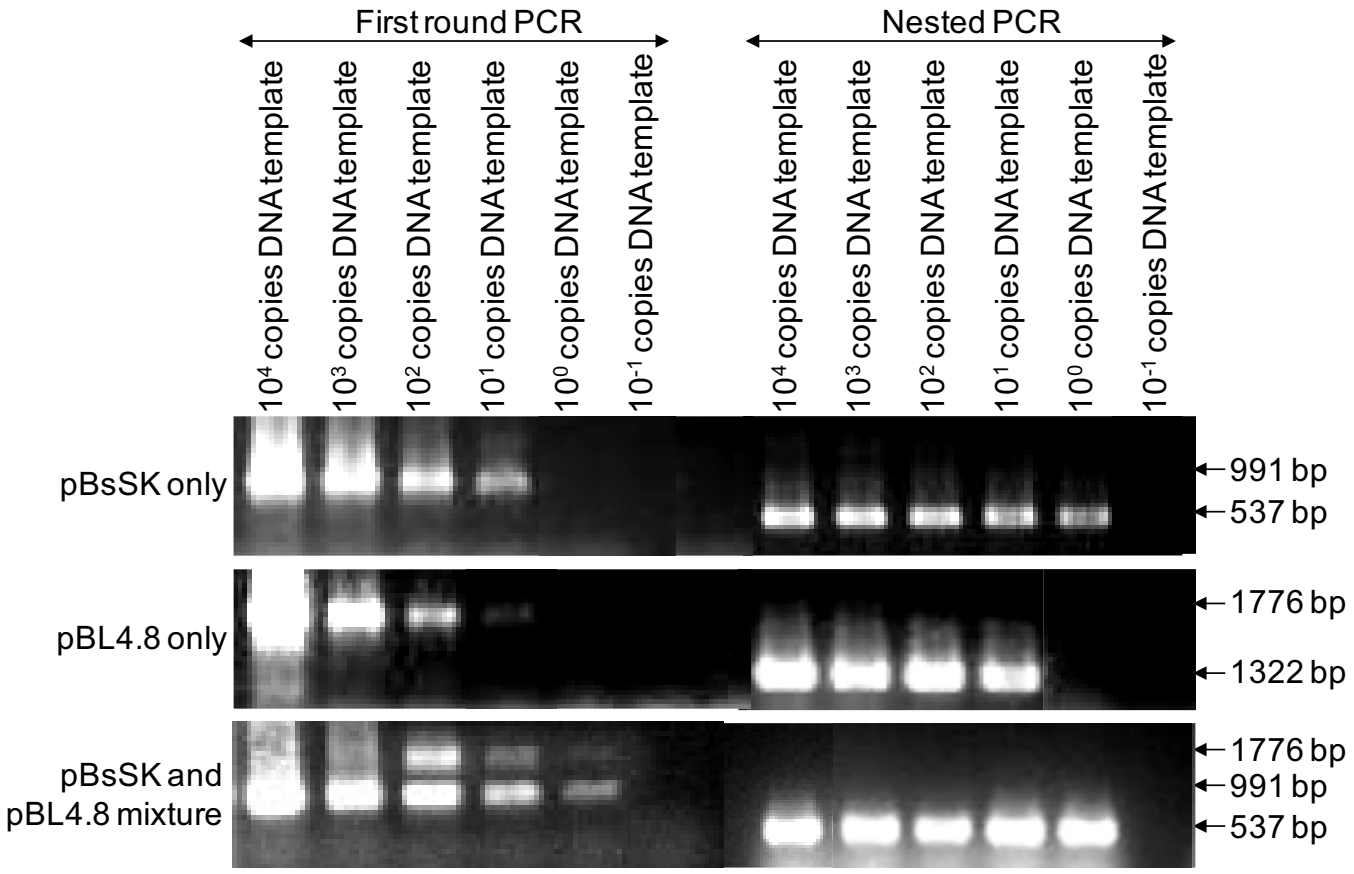

First round PCR
Nested PCR
10^4 copies DNA template
10^3 copies DNA template
10^2 copies DNA template
10^1 copies DNA template
10^0 copies DNA template
10^-1 copies DNA template
10^4 copies DNA template
10^3 copies DNA template
10^2 copies DNA template
10^1 copies DNA template
10^0 copies DNA template
10^-1 copies DNA template
pBsSK only
991 bp
537 bp
pBL4.8 only
1776 bp
1322 bp
pBsSK and
pBL4.8 mixture
1776 bp
991 bp
537 bp

Figure 5.4.13

Chapter 5.5: Performing invPCR assays on WHV-infected woodchuck and HBV-infected chimpanzee liver tissues

5.5.1. Aim

a) To perform invPCR assays specific for WHV-infected woodchuck and HBV-infected chimpanzee liver tissues.
b) To compare the results obtained from invPCR assays in this study with the results obtained from the well established invPCR assays in our collaborator's laboratory.

5.5.2. Introduction

The invPCR assay has been routinely performed by Dr. William Mason's laboratory at the Fox Chase Cancer Center (FCCC), Philadelphia, USA, to detect integrated virus-cell junctions in ducks (Yang and Summers, 1999), woodchucks (Mason *et al.*, 2005), chimpanzees (Mason *et al.*, 2009a), and human liver tissues (Mason *et al.*, 2010). The same invPCR assay was then established as described in Chapters 3 and 5, which involved extensive molecular assays, such as the DNA inversion (Section 2.10.1), 96-well nested PCR (Section 2.10.3), 96-well agarose gel electrophoresis (Section 2.10.4), 96-well gel extraction (Section 2.10.5), 96-well DNA sequencing (Section 2.10.6) and subsequent 96-well cleanup of DNA sequencing products (Section 2.10.7). These were novel methods established in this study that had not been previously performed in the Hepatitis Research Laboratory.

In order to ensure that the invPCR assay established in this study was of a comparable quality with the invPCR assay that was well established in FCCC, two invPCR assays were performed in parallel with studies conducted by our collaborators at FCCC to allow for direct comparison of the quality of invPCR assay results obtained. Specifically, these studies were for the detection of clonal expansion of hepatocytes in woodchucks with acute WHV infection and in chimpanzees with chronic HBV infection. Integrated virus-cell junctions were detected by myself and by Dr. William Mason, using invPCR assays that were designed by Dr. William Mason specifically for the WHV and HBV sequences. The quantity and types of integrated virus-cell junctions detected in both studies were then compared.

5.5.3. Woodchuck invPCR assay

5.5.3.1. Woodchuck liver tissues

Liver tissues from woodchuck 522 (112 dpi) were provided by collaborator Dr. William Mason. Woodchuck 522 was 3 years old when it was inoculated with 1 mL of serum from a

chronic WHV-infected woodchuck (virus titre ~10^9 per mL). Blood samples were then collected weekly, and wedge liver biopsies were performed at 49, 84 and 112 dpi. By 49 dpi, woodchuck 522 had a viraemia of 2.96x10^9 WHV DNA genomes per mL serum and >95% of WHV core antigen-positive hepatocytes. Treatment with entecavir (ETV) (Bristol-Myers Squibb, USA) was carried out at a daily oral dose of 0.5 mg per kg body weight till the end of the experiment. By 112 dpi, woodchuck 522 was found to have resolved WHV infection, with no detectable levels of viraemia and <0.001% of WHV core antigen-positive hepatocytes. The full serological and histological analysis were reported in detail by Mason *et al*, 2009b.

Liver biopsy tissues from woodchuck 522 at 112 dpi was dissected to obtain 2 x 1.7 mg fragment (designated as 522-2 and 522-3), and DNA was extracted from both liver tissues using the total DNA extraction method as described in Section 2.6.3. Most of the extracted DNA (from ~1.4 mg of each liver fragment) was then used as DNA templates for WHV invPCR assay as described in Section 5.5.3.3 below.

5.5.3.2. Woodchuck invPCR assay design

As described in Section 1.8.1, the most probable left and right hand ends of the dslDNA sequences of the integrated viral DNA are generally used to design invPCR assays. As published studies showed that the 5' and 3' end of the WHV dslDNA is at 1935 nt and 2118 nt (GenBank Accession M18752) respectively (Summers *et al.*, 2003), Dr. William Mason designed the woodchuck invPCR assay W1, using *Sac*I as first cut restriction enzyme, *Hind*III as second cut restriction enzyme, *Afl*III as cccDNA destroying enzyme, with WHV P4 – WHV P5 as outer primer set and WHV P3 – WHV P6 as inner primer set (refer Table 2.3). A schematic representation of the woodchuck W1 invPCR assay design is shown in Figure 5.5.1.

5.5.3.3. Woodchuck invPCR assay results

The woodchuck W1 invPCR assay (Table 2.3) was performed on woodchuck liver DNA samples 552-2, 552-3 (Section 5.5.3.1). Specifically, the woodchuck liver DNA samples were inverted as described in Section 2.10.1 and shown in Figure 5.5.1, and 96-well nested PCR was performed as described in Section 2.10.3 by evenly distributing the inverted DNA fragments as DNA templates to all the PCR wells. To visualise the invPCR products, 96-well agarose gel electrophoresis was performed as described in Section 2.10.4. Figure 5.5.2 shows an example of the invPCR products obtained from the woodchuck invPCR assay, when the inverted DNA fragments were evenly distributed to all PCR wells. The invPCR products observed were extracted as described in Section 2.10.5, and 96-well DNA sequencing was then performed as described in Section 2.10.6 using the WHV P3 primer (Table 2.2), with

cleanup of 96-well DNA sequencing products subsequently performed as described in Section 2.10.7. The DNA sequencing results were then analysed as described in Section 2.8.12.

Figure 5.5.3A shows an example of an integrated virus-cell junction DNA sequencing result, which consisted of an insert DNA flanked by WHV DNA. As mentioned in Section 5.3.3.2, in this thesis, insert DNA that showed homology to other mammalian "non-woodchuck" genome sequences would also be considered as integrated virus-cell junctions. Figure 5.5.3B shows an example of a virus-virus false positive DNA sequencing result, which consisted of only WHV DNA sequences. Individual DNA sequencing results are not shown in this Section.

Out of a total of 180 invPCR reactions performed in DNA extracted from ~1.4 mg of woodchuck 522-2 liver, 63 invPCR products were sequenced. Among these, 26 of the sequences were integrated virus-cell junctions, 9 were virus-virus false positive sequences, and 21 were unknown sequences (defined in this thesis as insert DNA sequences that were either too short (<15 bp) or did not show homology to any known sequences during the BLAST searches), and 7 DNA sequencing reactions failed to produce any readable sequences. Out of the 26 integrated virus-cell junctions, 17 of the integrated virus-cell junctions were unique, with 1 of the junctions repeated 5 times, another 1 of the junctions repeated 3 times, and 3 of the junctions repeated 2 times. Detailed analysis of the 26 integrated virus-cell junctions detected are summarised in Table 5.5.1.

Out of a total of 180 invPCR reactions performed in DNA extracted from ~1.4 mg of woodchuck 522-3 liver, 81 invPCR products were sequenced. Among these, 33 of the sequences were integrated virus-cell junctions, 40 were virus-virus false positive sequences, and 3 were unknown sequences, and 5 DNA sequencing reactions had failed to produce any readable sequences. Out of the 33 integrated virus-cell junctions, 28 of the integrated virus-cell junctions were unique, with 1 of the junctions repeated 3 times, and 3 of the junctions repeated 2 times. None of these integrated virus-cell junctions found were repeats of the junctions found in woodchuck 522-2 liver fragment as shown in Table 5.5.1. Detailed analysis of the 33 integrated virus-cell junctions detected are summarised in Table 5.5.2.

5.5.3.4. Discussion

Based on the results summarised in Tables 5.5.1 and 5.5.2, it was found that the 5' end of the WHV dslDNA that joined to the woodchuck genome during integration, forming the left hand end integrated virus-cell junctions, ranged between 1738 – 2103 nt of the WHV genome (GenBank Accession M18752), with a median at 1944 nt. This was similar to the published 5'

end of the WHV dslDNA at 1935 nt (Summers *et al.*, 2003), as well as the range of integrated virus-cell junctions compiled from 1202 integrated virus-cell junctions (Mason *et al.*, 2009b).

In addition, based on the BLAST analysis of the insert DNA found in this Section, there were no significant patterns or preference of integration sites in the genome, and it appeared that the WHV dslDNA had integrated randomly into different regions of the woodchuck genome, consistent with published results (Tokino and Matsubara, 1991) observations in Chapter 5.3.

As 9 of the integrated virus-cell junctions were repeated 2 – 5 times (average 2.5 times), this suggests that there were at least 9 hepatocyte clones present in these liver tissues. It could also be inferred that ~2 rounds of clonal proliferation of hepatocytes had occurred in the liver.

When the same woodchuck invPCR assay was performed by Dr. William Mason at FCCC, USA, out of a total of 180 invPCR reactions performed in DNA extracted from ~1.4 mg of woodchuck 522-1 liver tissue, 23 integrated virus-cell junctions were detected, out of which 10 of the integrated virus-cell junctions were unique (Mason *et al.*, 2009b). Comparing Dr. Mason's results with the results obtained in this study (Tables 5.5.1, 5.5.2), it was found that both studies had detected similar numbers of integrated virus-cell junctions from the woodchuck 522 liver tissues, with comparable number of unique and repeated integrated virus-cell junctions. Therefore, this showed that the invPCR assay techniques established in this study was comparable with well established invPCR assays in FCCC.

5.5.3.5. Conclusion

In conclusion, using the woodchuck W1 invPCR assay, in the woodchuck 522-2 and 522-3 liver tissues, 59 integrated virus-cell junctions were detected, of which 45 of the integrated virus-cell junctions were unique. These results were comparable to the results of collaborator Dr. Mason from FCCC. The woodchuck invPCR assay results obtained was subsequently included as a subset of the data and was published collaboratively in Mason *et al*., 2009b.

5.5.4. Chimpanzee invPCR assay

5.5.4.1. Chimpanzee liver tissues

Liver cell DNA extracted from three chimpanzee liver biopsy tissues were provided by collaborator Dr. William Mason. These chimpanzees, which include chimpanzee 4x136, 4x222 and 4x506, were all biopsied in 2006. The full clinical history as well as histological and serological analysis of these chimpanzees were reported in detail by Mason *et al.*, 2009a.

Briefly, chimpanzee 4x136 was 37 years old at the time of biopsy, and had chronic HBV infection for least 29 years. This animal had viraemia of $2.8x10^3$ genome equivalents (GE)/mL, 0.2 copies of HBV DNA per liver cell, no fibrosis (based on the Ishak fibrosis scoring), but had severe portal and lobular hepatitis. Chimpanzee 4x222 was 44 years old at the time of biopsy, with at least 27 years of chronic HBV infection. This animal had a viraemia of $2.9x10^2$ GE/mL, 0.06 copies of HBV DNA per liver cell, no fibrosis (based on the Ishak fibrosis scoring), and normal liver histology. Lastly, chimpanzee 4x506 was 27 years old at the time of biopsy, with at least 25 years of chronic HBV infection. This animal had viraemia of $1.4x10^3$ GE/mL, 175 copies of HBV DNA per liver cell, had a fibrosis score of 2 based on the Ishak fibrosis scoring (showing fibrous expansion of most portal areas, with or without short fibrous septa), and had mild portal and lobular hepatitis.

At the Regional Primate Center in San Antonio, Texas, USA, Dr. Robert Lanford and colleagues dissected the liver biopsy tissues obtained from each chimpanzee to multiple ~1 mg fragments. Liver DNA was then extracted from 2 liver fragments from each chimpanzee by Dr. William Mason using the total DNA extraction method as described in Section 2.6.3, and sent to the Hepatitis Research Laboratory in a dried DNA pellet form for parallel invPCR assay analysis. A total of 6 DNA samples extracted from liver fragments from chimpanzee 4x136 (designated as 4x136-2, 4x136-3), chimpanzee 4x222 (designated as 4x222-3, 4x222-4) and chimpanzee 4x506 (4x506-3, 4x506-4) were obtained. The DNA pellets were redissolved in 70 μL of EB (Qiagen, Germany), and the quality of the DNA samples were determined by agarose gel electrophoresis (Section 2.8.7). As shown in Figure 5.5.4, all the DNA samples still retained good quality genomic DNA as observed by the tight high molecular weight (MW) bands with little degradation as there were no significant DNA smears observed. Each DNA sample had an estimated DNA concentration of <10 ng/μL, with little RNA observed.

5.5.4.2. Chimpanzee invPCR assay design

As described in Section 1.8.1, invPCR assays are generally designed based on the most probable left and right hand ends of the dslDNA sequences of the integrated viral DNA. Therefore, to design chimpanzee invPCR assays, the HBV sequences near the 5' end and 3' end of the dslDNA in these chimpanzees were first determined. Based upon published studies showing that the 5' end of the HBV pregenomic DNA is around1820 nt, and that the 3' end of the HBV pregnomic DNA is around 1970 nt (Jilbert *et al.*, 2008a), a region near the 1820 nt and 1970 nt of the HBV DNA present in each chimpanzee were amplified and sequenced.

Using the chimpanzee liver DNA from Section 5.5.4.1, a 729 bp region of the HBV DNA present in each chimpanzee was amplified using the ch TL66 cF – ch TL67 cR primer set (refer Table 2.2) as described in Section 2.8.5. The PCR products were purified as described in Seciton 28.6, and sequenced using primer ch TL66 cF as described in Section 2.8.10, with subsequent cleanup of DNA sequencing products as described in Section 2.8.11.2.

Based on the multiple sequence alignment shown as Figure 5.5.5, the HBV sequence present in chimpanzees 4x136, 4x222 and 4x506 showed high homology (~98.5%) to the reference HBV sequence (GenBank Acccession AF222323), which was used to design the primers ch TL66 cF and ch TL67 cR. Therefore, this suggests that the chimpanzee invPCR assay could be designed based on the reference HBV sequence (GenBank Acccession AF222323).

As the 5' end of the HBV dslDNA is at 1820 nt (Mason *et al.*, 2009a), Dr. William Mason designed the chimpanzee invPCR assay C1, using *Bgl*II as first cut restriction enzyme, *Bsa*WI as second cut restriction enzyme, *Bsa*BI as cccDNA destroying enzyme, with HBV F1 – HBV R1b as outer primer set and HBV F2 – HBV R2b as inner primer set (refer Table 2.3). A schematic representation of the chimpanzee C1 invPCR assay design is shown in Figure 5.5.6.

5.5.4.3. Chimpanzee invPCR assay results

The chimpanzee C1 invPCR assay (Table 2.3) was performed on all 6 chimpanzee liver DNA samples (Section 5.5.4.1). Specifically, the high MW DNA was purified using the low melting temperature agarose gel electrophoresis as described in Section 2.10.2. After that, DNA was inverted as described in Section 2.10.1 and shown in Figure 5.5.6, and 96-well nested PCR was performed as described in Section 2.10.3, either using 1/3 serially dilution of the inverted DNA fragments as DNA templates as described in Section 2.10.3 and shown in Figure 2.8, or by evenly distributing the inverted DNA fragments as DNA templates to all of the PCR wells without dilution. To visualise the invPCR products, 96-well agarose gel electrophoresis was performed as described in Section 2.10.4.

Figure 5.5.7 shows an example of the PCR products obtained from the chimpanzee invPCR assay, when the inverted DNA fragments were serially diluted (Figure 5.5.7.A) or were evenly distributed to all PCR wells (Figure 5.5.7.B). The invPCR products observed were extracted as described in Section 2.10.5, and 96-well DNA sequencing was then performed as described in Section 2.10.6 using the HBV R2b primer (Table 2.2), and cleanup of 96-well DNA sequencing products was subsequently performed as described in Section 2.10.7. The DNA sequencing results were then analysed as described in Section 2.8.12.

Figure 5.5.8A shows an example of an integrated virus-cell junction DNA sequencing result, which consisted of an insert DNA flanked by HBV DNA. It should be noted that due to the close evolutionary relationship and high genomic homology between chimpanzees and humans, insert DNA that showed homology to either chimpanzee or human genome sequences would be considered as integreated virus-cell junctions. Figure 5.5.8B shows an example of a virus-virus false positive DNA sequencing result, which consisted of only HBV DNA. Individual DNA sequencing results are not shown in this Section.

The results of all invPCR assay are summarised in Table 5.5.3. Out of a total of 1068 invPCR reactions performed on a total of 7825 ng DNA, 49 invPCR products were sequenced. Among these, 32 of the sequences were integrated virus-cell junctions, 3 were virus-virus false positives, and 14 were unknown sequences. None of the DNA sequencing reactions failed to produce a readable sequence. Out of the 32 integrated virus-cell junctions, 20 of the integrated virus-cell junctions were unique, with 4 of the junctions each repeated 3 and 2 times. Detailed analysis of the 32 integrated virus-cell junctions detected are summarised in Table 5.5.4.

5.5.4.4. Discussion

Based on the results summarised in Table 5.5.4, it was found that the 5' end of the HBV dslDNA that joined to the host genome during integration, forming the integrated virus-cell junctions, ranged mainly between 1819 – 1892 nt of the HBV genome (GenBank Accession AF222323), with a median at 1828 nt. This was similar to the published 5' end of the HBV dslDNA at 1820 nt (Jilbert *et al.*, 2008a), as well as the range of integrated virus-cell junctions compiled from 176 integrated virus-cell junctions (Mason *et al.*, 2009a).

In addition, based on the BLAST analysis of the insert DNA found in this Section, there were no significant patterns or preference of integration sites in the genome, and it appeared that the HBV dslDNA had, as expected, integrated randomly into different regions of the chimpanzee genome, consistent with the published results (Tokino and Matsubara, 1991).

As 8 of the integrated virus-cell junctions were repeated 3 or 2 times (average 2.5 times), this suggests that there were at least 8 hepatocyte clones present in these liver tissues. It could also be inferred that ~1 round of clonal proliferation of hepatocytes had occurred in the liver.

In addition, as 1/3 serial dilution of the chimpanzee inverted DNA fragments were performed during the 96-well nested PCR of chimpanzee liver tissue 4x222-3 and 4x506-3, the sizes of the hepatocyte clones found in these tissues could be determined by the number of repeats found at the highest dilution times the dilution factor (Mason *et al.*, 2005), which had been

incorporated into a Monte Carlo-based mathematical calculation software designed by Samuel Litwin and Dr. William Mason from the FCCC, USA (personal communication). For instance, the integrated virus-cell junctions numbered 7 – 9 from the 4x222-3 liver fragment (Table 5.5.4) was detected from a 0.16 fraction of the total extracted DNA, and the junction was repeated once in Row A (1/3 serial dilution) and twice in Row C (1/27 serial dilution) (refer Figure 2.8 for schematic representation of the serial dilution). Using this software (Monte Carlo program set to 95% confidence and 1000 runs), it was estimated that this hepatocyte clone could be 4 – 45 cells in size. Applying this software with the same parameters, it was estimated that the integrated virus-cell junctions numbered 10 – 11 from the 4x222-3 liver fragment (Table 5.5.4) detected from a 0.16 fraction of the total extracted DNA, and found repeated once in Row B (1/9 serial dilution) and once in Row F (1/729 serial dilution), could be 3 – 170 cells in size; while the integrated virus-cell junction numbered 29 – 30 from the 4x506-3 liver fragment (Table 5.5.4) detected from a 0.16 fraction of the total extracted DNA, and found repeated once in Row A (1/3 serial dilution) and once in Row C (1/27 serial dilution), could be 3 – 48 cells in size.

When the same chimpanzee invPCR assay was performed by Dr. William Mason at FCCC, USA, from chimpanzee 4x136 (liver fragment 4x136-1 and 4x136-4), 42 integrated virus-cell junctions were detected, out of which 6 of the integrated virus-cell junctions were unique. From chimpanzee 4x222 (liver fragment 4x222-1 and 4x22-2), 20 integrated virus-cell junctions were detected, out of which 14 of the integrated virus-cell junctions were unique. From chimpanzee 4x506 (liver fragment 4x506-1 and 4x506-2), 28 integrated virus-cell junctions were detected, out of which 26 of the integrated virus-cell junctions were unique (Mason *et al.*, 2009a; Mason, personal communication). Comparing Dr. Mason's results with the results obtained in this study (Tables 5.5.3, 5.5.4), it was found that both studies had detected similar numbers of integrated virus-cell junctions from the chimpanzee liver tissues, with comparable number of unique and repeated integrated virus-cell junctions. Therefore, like the woodchuck invPCR assay (Section 5.5.3), this again showed that the invPCR assay established in this study was comparable with well established invPCR assays in in FCCC.

5.5.4.5. Conclusion

In conclusion, using the chimpanzee C1 invPCR assay, in 6 of the liver tissues from chimpanzees 4x136, 4x222 and 4x506, 32 integrated virus-cell junctions were detected, among which 20 of the junctions were unique. These results were comparable to the results of collaborator Dr. Mason from FCCC. The chimpanzee invPCR assay results obtained was subsequently included as a subset of the data published collaboratively in Mason *et al*., 2009a.

Table 5.5.1: Summary of the 26 integrated virus-cell junctions detected by invPCR assay using DNA extracted from woodchuck 522-2 liver tissue.

No	Virus junction 1	Virus junction 2	Insert DNA size (bp)	BLAST homology	GenBank Accession	Nucleotide position (5' – 3')
1	1818	2255	412	*Homo sapiens* chromosome 16 clone RP11-432I5	AC009097	27056-27469
2	1818	2241	401	*Homo sapiens* chromosome 16 clone RP11-432I5	AC009097	27056-27431
3	1818	2241	401	*Homo sapiens* chromosome 16 clone RP11-432I5	AC009097	27056-27431
4	1818	2241	401	*Homo sapiens* chromosome 16 clone RP11-432I5	AC009097	27056-27431
5	1818	2241	401	*Homo sapiens* chromosome 16 clone RP11-432I5	AC009097	27056-27431
6	1978	ND[a]	379	*Homo sapiens* chromosome 8 clone RP11-21J9	AC009635	10920-11222
7	1978	ND	692	*Homo sapiens* chromosome 8 clone RP11-21J9 *Spermophilus tridecemlineatus* clone VMRC20-244I10	AC009635 AC190469	10920-11398 50891-50991
8	1978	ND	614	*Homo sapiens* chromosome 8 clone RP11-21J9	AC009635	10921-11397
9	1937	ND	473	*Homo sapiens* BAC clone RP11-89C12 from 2	AC013262	81743-81193
10	1937	ND	341	*Homo sapiens* BAC clone RP11-89C12 from 2	AC013262	81743-81425
11	1980	2241	422	*Spermophilus tridecemlineatus* clone VMRC20-410J16	AC192323	86166-85736
12	1980	2241	422	*Spermophilus tridecemlineatus* clone VMRC20-410J16	AC192323	86166-85736
13	2043	ND	586	*Marmota monax* lymphotoxin-beta, TNF, and lymphotoxin-alpha genes	AF096268	8829-8663
14	2043	2241	557	*Marmota monax* lymphotoxin-beta, TNF, and lymphotoxin-alpha genes	AF096268	8829-8663
15	1855	ND	624	*Marmota monax* lymphotoxin-beta, TNF, and lymphotoxin-alpha genes	AF096268	12370-/-12810[b]
16	2031	2241	108	*Mus saxicola* haptoglobin mRNA	L10353	175-75
17	1943	2241	441	*Pongo pygmaeus abelii* BAC clone CH276-365M4	AC210534	50228-50499
18	1935	ND	644	*Homo sapiens* breast cancer metastasis-suppressor 1 gene	AF281036	4892-4633

Table 5.5.1 continued

19	1758	2241	312	*Spermophilus tridecemlineatus* clone XX-28522957A7	AC175448	32403-32275
20	1939	ND	689	*Homo sapiens* chromosome 10 clone RP11-254K3	AC069021	99978-/-100990
21	2010	ND	667	*Homo sapiens* chromosome 8 clone RP11-212F11	AC112673	135570-135182
22	1936	ND	410	*Homo sapiens* chromosome 5 clone RP11-1006G2	AC116339	61729-62057
23	1738	ND	310	*Spermophilus tridecemlineatus* clone XX-28682257A7	AC172103	22145-22018
24	1738	ND	253	*Rhesus Macaque* BAC CH250-271I18	AC143915	102593-102729
25	2071	ND	790	Pig DNA sequence from clone CH242-82N3 on chromosome 14	CU062407	16521-15723
26	ND	ND	617	Human DNA sequence from clone RP11-199O14 on chromosome 20	AL162504	66932-66369

The woodchuck W1 invPCR assay was performed on ~1.4 mg of woodchuck 552-2 liver sample as described in Section 5.5.3.3. DNA sequencing results were analysed as described in Section 2.8.12, based on examples shown in Figures 5.5.3A and 5.5.3B.

The coloured highlights show the different groups of repeated integrated virus-cell junctions.

[a]The virus junction was not detected (ND) in the DNA sequence.

[b]The symbol "-/-" was used when the nucleotide positions of the insert DNA had gaps (not continuous).

Table 5.5.2: Summary of the 33 integrated virus-cell junctions detected by invPCR assay using DNA extracted from woodchuck 522-3 liver tissue.

No	Virus junction 1	Virus junction 2	Insert DNA size (bp)	BLAST homology	GenBank Accession	Nucleotide position (5' – 3')
1	1807	2241	282	*Equus caballus* breed thoroughbred chromosome 6 genomic scaffold	NW_001867422	19172338-19172033
2	1807	2241	282	*Equus caballus* breed thoroughbred chromosome 6, EquCab2.0 scaffold_43	NW_001867422	19172338-19172033
3	1807	2241	282	*Equus caballus* breed thoroughbred chromosome 6, EquCab2.0 scaffold_43	NW_001867422	19172338-19172033
4	1941	2241	186	*Homo sapiens* chromosome 4 genomic contig, GRCh37.p5	NT_016354	103720193-103729975
5	1941	2241	186	*Homo sapiens* chromosome 4 genomic contig, GRCh37.p5	NT_016354	103720193-103729975
6	2024	2241	99	*Pan troglodytes* chromosome 14, Pan_troglodytes-2.1.4	NW_003457865	613237-613274
7	2020	2441	95	*Pan troglodytes* chromosome 14, Pan_troglodytes-2.1.4.1 *Macaca mulatta* chromosome 8 genomic scaffold, Mmul_051212	NW_003457865 NW_001122906	613237-613274 12949861-1294984
8	2040	2241	419	*Equus caballus* breed thoroughbred chromosome 14, EquCab2.0	NC_009157	10617134-10616756
9	2040	2241	419	*Equus caballus* breed thoroughbred chromosome 14, EquCab2.0 scaffold_1	NC_009157	10617134-10616795
10	1954	2241	341	*Spermophilus tridecemlineatus* genomic sequence	NT_ 166762	474540-474620
11	ND[a]	ND	838	*Pongo abelii* chromosome 22	NW_002891657	241688-241867
12	1945	2241	399	*Equus caballus* breed thoroughbred chromosome 8	NW_001867430	25857221-25857522
13	2042	ND	71	*Mus musculus* strain C57BL/6J chromosome 18 genomic contig MGSCv37 C57BL/6J	NT_039678	4759913-4759860

Table 5.5.2 continued

14	1886	ND	549	*Homo sapiens* doublecortin, RefSeqGene on chromosome X	NG_011750	4447-4974
15	2095	2241	217	*Homo sapiens* chromosome 5 genomic contig	NW_001838952	28118973-28118940
16	1936	2241	55	*Spermophilus tridecemlineatu*s genomic sequence, ENCODE region ENm003	NT_166595	485339-485393
17	1937	2241	108	*Drosophila melanogaster* chromosome X	NC_004354	15627671-15627601
18	1984	ND	558	*Equus caballus* breed thoroughbred chromosome 17, EquCab2.0 scaffold_8	NW_001867383	34012319-34011811
19	2011	2241	311	*Pongo abelii* chromosome 11, P_pygmaeus_2.0.2	NW_002885325	9922-10225
20	1940	2241	540	*Macaca mulatta* chromosome 12 genomic scaffold, Mmul_051212	NW_00109816	8198076-8197544
21	1940	ND	551	*Nomascus leucogenys*, Nleu1.0 scaffold_62	NW_003501432	2892834-2892316
22	2103	2241	138	*Sus scrofa* breed mixed chromosome 1, Sscrofa10.2	NW_003534167	80659-80615
23	1957	2241	351	*Homo sapiens* chromosome 12 genomic contig, GRCh37.p5 Primary Assembly	NT_029419	16126313-16126057
24	1940	2241	111	*Caenorhabditis remanei* Scfld02_431 genomic scaffold	NW_003319269	15407-15327
25	1945	2241	273	*Homo sapiens* chromosome 15, clone RP11-540N15	AC087482	137039-137276
26	2034	ND	329	*Spermophilus tridecemlineatus* clone VMRC20-433G18	AC182361	83871-83933
27	1944	ND	663	*Spermophilus tridecemlineatus* genomic sequence *Equus caballus* breed thoroughbred chromosome 7, EquCab2.0	NT_166614 NC_009150	389484-38978 8339123-83391073
28	1947	2241	166	*Homo sapiens* chromosome 7 genomic contig	NW_001839063	4404891-4405062

Table 5.5.2 continued

29	2012	2241	212	*Nomascus leucogenys* unplaced genomic scaffold, Nleu1.0 scaffold_2	NW_003501372	25252197 -/- 60824976[b]
30	1935	2241	242	*Canis lupus familiaris* chromosome 19, CanFam3.1	NC_006601	15617923- /-21388393
31	1952	2241	445	*Equus caballus* breed thoroughbred chromosome 27, EquCab2.0 scaffold_24	NW_001867398	15725633- 15726048
32	1800	ND	540	*Nomascus leucogenys* unplaced genomic scaffold, Nleu1.0 scaffold_56	NW_003501426	3686277- 3685779

The woodchuck W1 invPCR assay was performed on ~1.4 mg of woodchuck 552-3 liver sample as described in Section 5.5.3.3. DNA sequencing results were analysed as described in Section 2.8.12, based on examples shown in Figures 5.5.3A and 5.5.3B.

The coloured highlights show the different groups of repeated integrated virus-cell junctions.

[a]The virus junction was not detected (ND) in the DNA sequence.

[b]The symbol "-/-" was used when the nucleotide positions of the insert DNA had gaps (not continuous).

Table 5.5.3: InvPCR assay products obtained using liver tissues from 3 chimpanzees with chronic HBV infection.

Chimpanzee liver sample	Total nested PCR reactions[a]	Total amount of DNA analysed (ng)[b]	Number of invPCR products sequenced[c]	Integrated virus-cell junctions detected[d]	Virus-virus junctions detected[e]	Unknown sequences detected[f]
4x136-2	180	725.1	5	5	-	-
4x136-3	180	309.3	5	1	-	4
4x222-3	174	2239.2	11	8	1	2
4x222-4	180	1588.0	16	14	-	2
4x506-3	174	917.4	2	-	-	2
4x506-4	180	2046.0	8	2	2	4
Total	**1068**	**7825.0**	**47**	**30**	**3**	**14**

The chimpanzee C1 invPCR assay was performed on the DNA extracted from chimpanzee liver tissues as described in Section 5.5.4.3. DNA sequencing results were analysed as described in Section 2.8.12, based on examples shown in Figures 5.5.8A and 5.5.8B.

[a]Total nested PCR reactions refers to the total number of nested PCR reactions performed in individual PCR wells.

[b]The amount of DNA analysed were estimated according to the amount of inverted DNA added per invPCR reaction, which was based on the amount of liver used during DNA extraction.

[c]From all the nested PCR reactions performed, only reactions that produced clear invPCR products bands were extracted from the agarose gel and sequenced. The number of total invPCR products observed on the agarose gels was not shown.

[d]An example of an integrated virus-cell junction is shown in Figure 5.5.8A.

[e]An example of a virus-virus false positive sequence is shown in Figure 5.5.8B.

[f]Unknown sequences were defined as insert DNA that were either too short (<15 bp) or did not show homology to any known sequences during the BLAST searches.

Table 5.5.4: Summary of the 32 integrated virus-cell junctions detected by invPCR assay using DNA extracted from the chimpanzee liver tissues.

No	Chimpanzee liver sample	Virus junction 1	Virus junction 2	Insert DNA size (bp)	BLAST homology	GenBank Accession	Nucleotide position (5' – 3')
1	4x136-2	1828	2430	32	*Pongo abelii* chromosome 5 genomic scaffold, P_pygmaeus_2.0.2	NW_002880105	1085-1115
2		1828	2430	31	*Pongo abelii* chromosome 5 genomic scaffold, P_pygmaeus_2.0.2	NW_002880105	1085-1115
3		1828	2430	31	*Pongo abelii* chromosome 5 genomic scaffold, P_pygmaeus_2.0.2	NW_002880105	1085-1115
4		1835	2117	323	*Macaca mulatta* chromosome 15 unlocalized genomic scaffold, Mmul_051212	NW_001101697	25750-24538
5		1823	2430	450	*Pan troglodytes* chromosome 7, Pan_troglodytes-2.1.4	NC_006474	12113652-12113204
6	4x136-3	1820	ND[a]	112	*Pan troglodytes* chromosome 6 genomic scaffold, Pan_troglodytes-2.1.4	NW_003457130	114009-113966
7	4x222-3	1861	ND	603	*Homo sapiens* chromosome 21 genomic contig, GRCh37.p5	NT_011512	13819061-13819664
8		1861	ND	700	*Homo sapiens* chromosome 21 genomic contig, GRCh37.p5	NT_011512	13819061-13819721
9		1861	ND	680	*Homo sapiens* chromosome 21 genomic contig, GRCh37.p5	NT_011512	13819061-13819728
10		1875	ND	811	*Pan troglodytes* chromosome 19 genomic scaffold, Pan_troglodytes-2.1.4	NW_003458428	7629-6827
11		1875	ND	820	*Pan troglodytes* chromosome 19 genomic scaffold, Pan_troglodytes-2.1.4	NW_003458428	7629-6827

Table 5.5.4 continued

12		1849	ND	873	Pan troglodytes chromosome 15, Pan_troglodytes-2.1.4	NC_006482	57834191-57835058
13		1822	ND	560	*Pan troglodytes* chromosome 11, Pan_troglodytes-2.1.4	NC_006478	117009414 - 117009947
14		1821	ND	192	*Pan troglodytes* chromosome 19, Pan_troglodytes-2.1.4	NC_006486	61045756-61045607
15	4x222-4	416	ND	66	*Pan troglodytes* chromosome 22, Pan_troglodytes-2.1.4	NC_006489	34099962-34099926
16		416	2430	541	Pan troglodytes chromosome 22, Pan_troglodytes-2.1.4	NC_006489	34099962-34099452
17		416	2430	541	*Pan troglodytes* chromosome 22, Pan_troglodytes-2.1.4	NC_006489	34099962-34099451
18		1825	2430	467	Pan troglodytes chromosome 15, Pan_troglodytes-2.1.4	NC_006482	39099177-39099643
19		1825	2430	467	*Pan troglodytes* chromosome 15, Pan_troglodytes-2.1.4	NC_006482	39099177-39099650
20		1825	2430	467	*Pan troglodytes* chromosome 15, Pan_troglodytes-2.1.4	NC_006482	39099177-39099643
21		1848	ND	158	Pan troglodytes chromosome 2A, Pan_troglodytes-2.1.4	NC_006469	13756415-13756277
22		1848	ND	164	Pan troglodytes chromosome 2A, Pan_troglodytes-2.1.4	NC_006469	13756415-13756277
23		ND	2430	311	*Pan troglodytes* chromosome 7, Pan_troglodytes-2.1.4	NC_006474	159667067 - 159666764
24		ND	2430	310	*Pan troglodytes* chromosome 7, Pan_troglodytes-2.1.4	NC_006474	159667067 - 159666764

Table 5.5.4 continued

25		1837	ND	880	*Pan troglodytes* chromosome 3, Pan_troglodytes-2.1.4	NC_006490	190616709 - 190617564
26		1841	ND	76	*Pan troglodytes* chromosome 15, Pan_troglodytes-2.1.4	NC_006482	66252353-66252426
27		1841	ND	120	*Macaca mulatta* chromosome 2 genomic scaffold, Mmul_051212	NW_001112557	5598477-5598387
28		1819	2430	314	*Pan troglodytes* chromosome 15, Pan_troglodytes-2.1.4	NC_006482	62409152-62409450
29	4x506-3	1820	2430	85	*Pan troglodytes* chromosome 4, Pan_troglodytes-2.1.4	NC_006471	171379143 - 171379227
30		1820	2430	85	*Pan troglodytes* chromosome 4, Pan_troglodytes-2.1.4	NC_006471	171379143 - 171379227
31	4x506-4	1820	2430	227	*Pan troglodytes* chromosome 9, Pan_troglodytes-2.1.4	NC_006476	96604435-96604647
32		1892	2430	145	*Pan troglodytes* chromosome 7, Pan_troglodytes-2.1.4	NC_006474	159688027 - 159687883

The chimpanzee C1 invPCR assay was performed on the DNA extracted from chimpanzee liver tissues as described in Section 5.5.4.3. DNA sequencing results were analysed as described in Figure 5.5.8, based on examples shown in Figures 5.5.8A and 5.5.8B.

The coloured highlights show the different groups of repeated integrated virus-cell junctions.

[a]The virus junction was not detected (ND) in the DNA sequence.

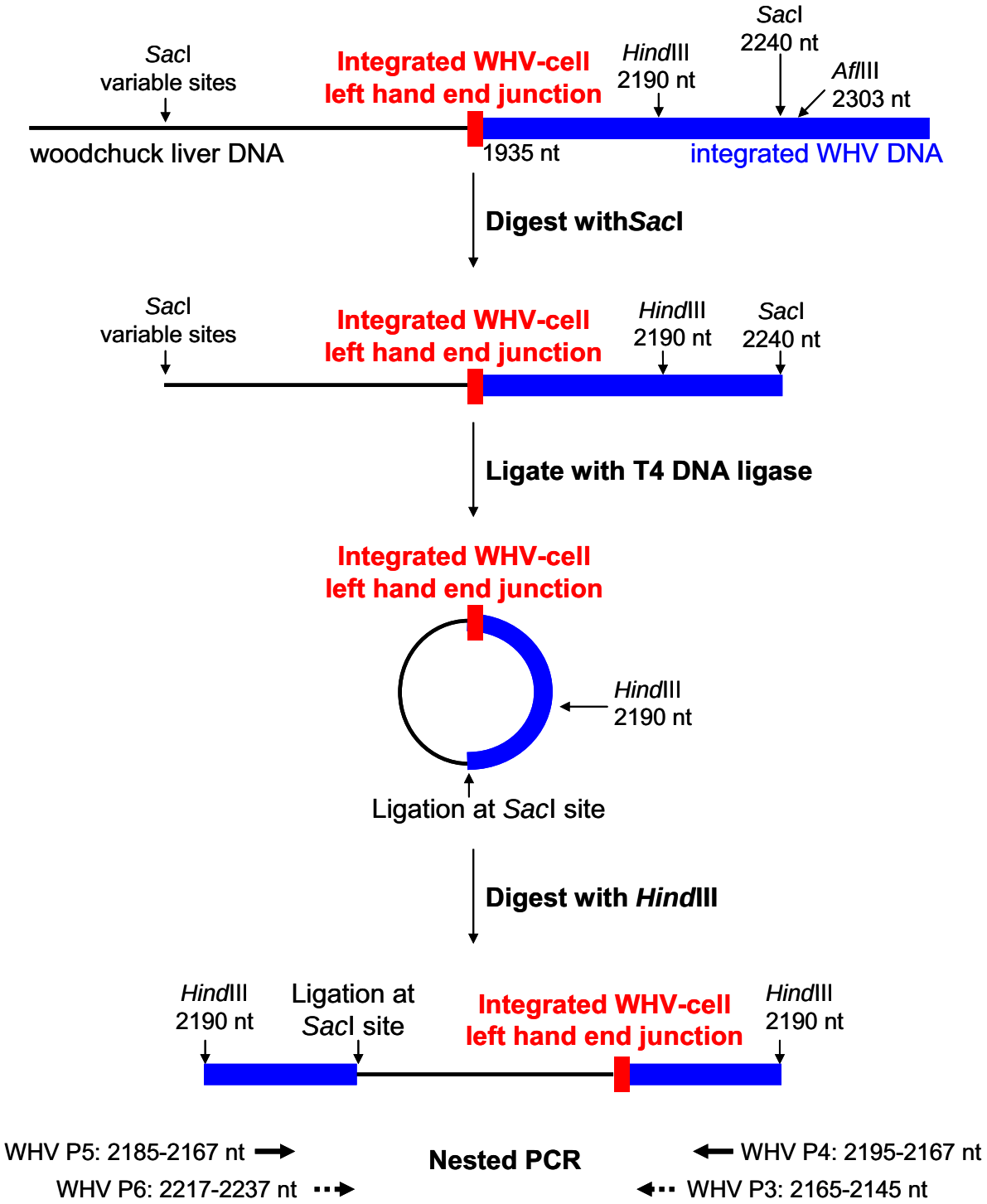


Figure 5.5.1: Schematic representation of the woodchuck W1 invPCR assay design, showing the DNA inversion process, and the nested PCR reaction primer binding sites.

The woodchuck W1 invPCR assay (refer Table 2.3) was designed by Dr. William Mason based on the WHV genome (GenBank Accession M18752) (Mason *et al.*, 2009b).

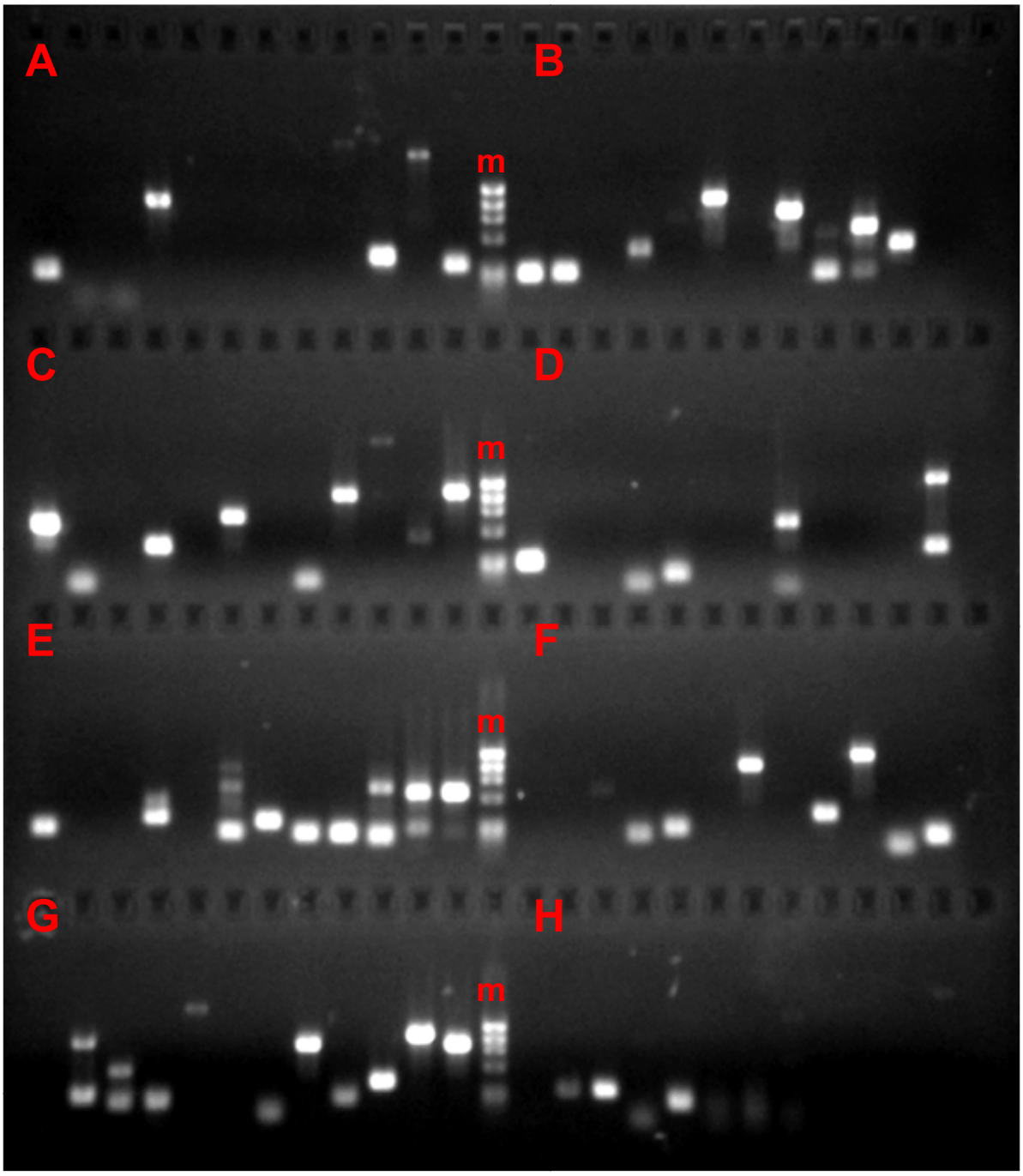


Figure 5.5.2: Example of the nested PCR products obtained from the woodchuck invPCR assay.

The woodchuck W1 invPCR assays were performed as described in Section 5.5.3, and products were visualised using 96-well agarose gel electrophoresis under 302 nm UV light.

The letters A – H refer to the rows of the PCR wells. The DNA marker used (at the lanes labelled "m") was 0.5 µg of the φX174 RF DNA/*Hae* III Fragments (Invitrogen, USA).

Figure 5.5.3: Example of DNA sequencing results obtained from the woodchuck invPCR assay.

The woodchuck W1 invPCR assays were performed as described in Section 5.5.3.

Figure 5.5.3A shows an example of the DNA sequencing result for an integrated virus-cell junction. BLAST analysis revealed that the 653 bp sequence consisted of a 577 bp insert DNA (black font) flanked by the WHV genome (GenBank Accession M18752) 2125 – 2043 nt (blue bold font) and 2244 – 2231 nt (red bold font) at the *Sac*I first cut restriction enzyme site (underline). This was consistent with the expected inverted DNA fragment that will be produced by the woodchuck W1 invPCR assay design (refer Figure 5.5.1). Based on this, 2043 nt is known as virus junction 1, and 2244 nt is known as virus junction 2. Further BLAST analysis showed that the insert DNA shared homology with the *Marmota monax* (woodchuck) lymphotoxin-beta, tumor necrosis factor (TNF), and lymphotoxin-alpha genes (GenBank Accession AF096268), confirming that the DNA sequence obtained was an integrated virus-cell junction in the woodchuck genome.

Figure 5.5.3B shows an example of the DNA sequencing result for a virus-virus sequence, which was a false positive result. BLAST analysis showed that the 209 bp sequence consisted of 2 fragments of the WHV genome (GenBank Accession M18752), 2124 – 1942 (blue bold font) and 2245 – 2217 (black bold font), joined at the *Sac*I restriction enzyme site (underline). This suggests that this virus-virus false positive fragment was likely to be formed by the ligation of 2 WHV DNA fragments that were digested by *Sac*I.

A

GAGTAGCAGTGTCCACCAAAGCATTAAGGTCAGGAAAAAAGTCCAAAG
GAAGAAAATTCNNCAACtGATAAGATGAACCAAATTTGAAGGGGTACA
GGACATTGATTATTTTGACCACTAAAATATCATTCACCTGCTTCAAGT
AATTGCCCCCAATTTTTTGACGTGTCCTTCTCTCTCCCCAAGTCATCC
CCTGATTCAGAGCTAAAGCAAGTGACAGGTGTAAGTCAATCATGGCTG
CTTGTTCCTCTGTCCCCAGAAATTGGGCATGTGGCTCAACCAGAAGCA
ACGAGGCACAAAGAGCATTTCTGGGGTTCTGAGAGAGAAGTGGTTGTT
TCTTCCCTCTATTCTTATTATATGGAGCCCAAGACCTCATGGAGAAAG
GCAGAGTTAAAAGATGAAGATAGCTGGGTGCGGTGGCGCATGCCTGTA
ATCCCAGAGGCTCGGGAGGCTGAGGCAGGAGGACCACAAGTTCAAAGC
CAGCTTAGCAACTTAGCAAGGCCCTAAGCAATTTAGTGAGACCCTGTC
TCTAAATAAAAAAATAAAAATGGCTGGGATGTGGCTCAGTGATTAAGC
GCCTCTGGGTTCAGTCTCTAGTACAAAAATAAATAAATAAATAAATAA
AGATGAAGACAGTATTT**GAGCTCATCCAC**

B

GTAGCAGTGTCCACCAAAGCATTAAGGTCAGGAAAAAAGTCCAAAGGA
AGAAAATTCAACAACTGATAAGATGAACCAAATTCTTTATAGGGATCT
ATGTCCATGCCCCAAAGCCACCCAAGGCACAGCTTGGAGGCTTGAAAA
GTAGGACATGGAACACAGGCAAAAACAAGGCACAGGTGAGAGCTCATC
CAAGCTATCAATTTAGA

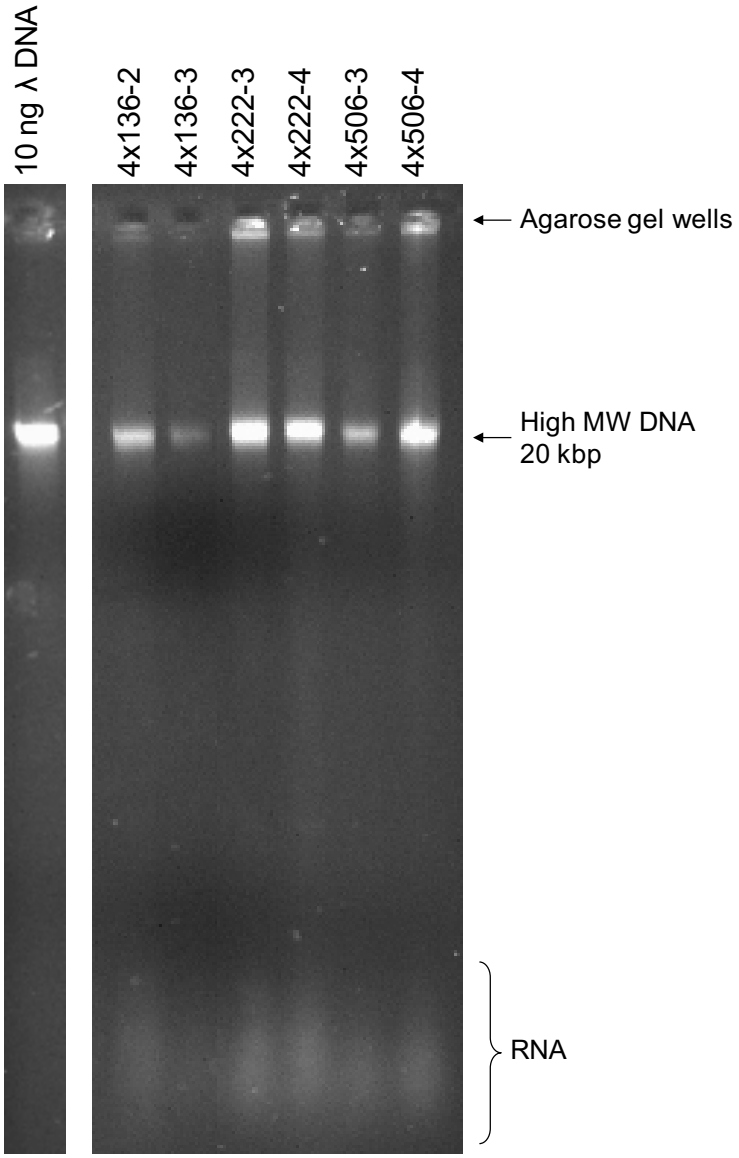


Figure 5.5.4: The quality and content of chimpanzee liver DNA samples that were extracted by Dr. William Mason at the FCCC, USA, and redissolved in the Hepatitis Research Laboratory.

Liver DNA were extracted from ~1 mg fragments of chimpanzee liver biopsy tissues by Dr. William Mason using the total DNA extraction method as described in Section 2.6.3. Dried DNA pellets were sent to the Hepatitis Research Laboratory and resuspended in 70 µL EB (Qiagen, Germany), from which 1 µL of the redissolved DNA samples were visualised using agarose gel electrophoresis as described in Section 2.8.7.

All DNA samples were shown to contain ~20 kbp high MW DNA, with little DNA smears observed. By comparing to the λ DNA, all DNA samples had less than 10 ng/µL of DNA concentration. Only little RNA were observed in all DNA samples.

Figure 5.5.5: Multiple sequence alignment showing the 650 bp sequenced region of the HBV genome from chimpanzees 4x136, 4x222 and 4x506, aligned with the HBV genome (GenBank Accession AF222323, REGION 1797-2446).

The PCR product was amplified from DNA extracted from 4x136, 4x222 and 4x506 chimpanzee liver tissues using primer set ch TL66 cF – ch TL67 cR (refer to Table 2.2) as described in Section 5.5.4.2. The multiple sequence alignment was performed using ClustalW2 program and output file viewed and arranged by Jalview program as described in Section 2.8.12.

Individual alignment scores of the HBV sequence (GenBank Acccession AF222323) with other three sequenced PCR products were obtained using BLAST Align 2 Sequences programme as described in Section 2.8.12. The HBV DNA sequence present in all chimpanzees showed a high level of homology (average of 98.5% sequence similarity) with the HBV genome.

Note:
REGION refers to the specific region of nucleotide sequence that was used for alignment in this multiple sequence alignment, and was based on the nucleotide numbering obtained from the HBV (GenBank Accession AF222323) sequence. REGION was chosen to match with the range of the amplified and sequenced target gene (HBV genome). The numbers shown in the multiple sequence alignment output figure refer to the nucleotide numbering of the specified REGIONs.

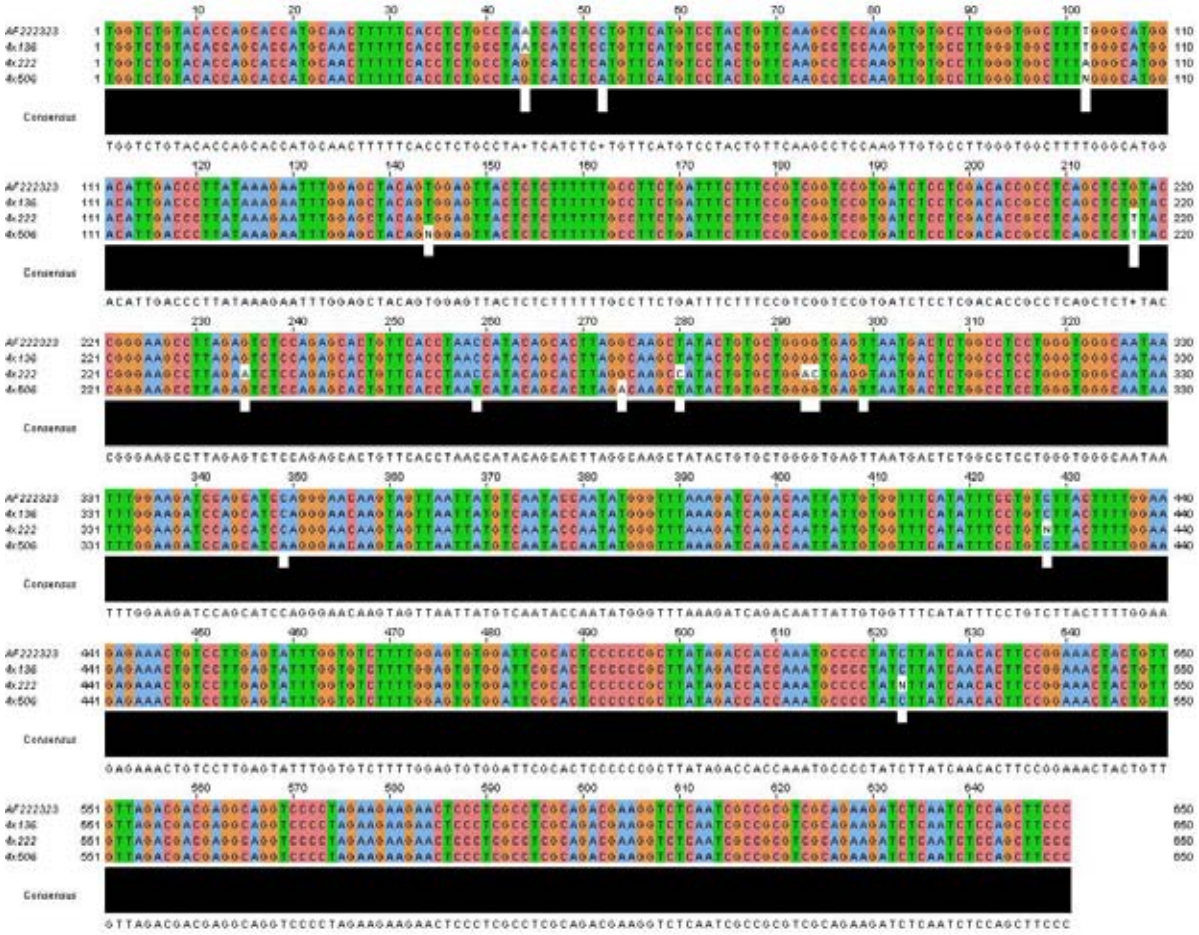


Figure 5.5.5

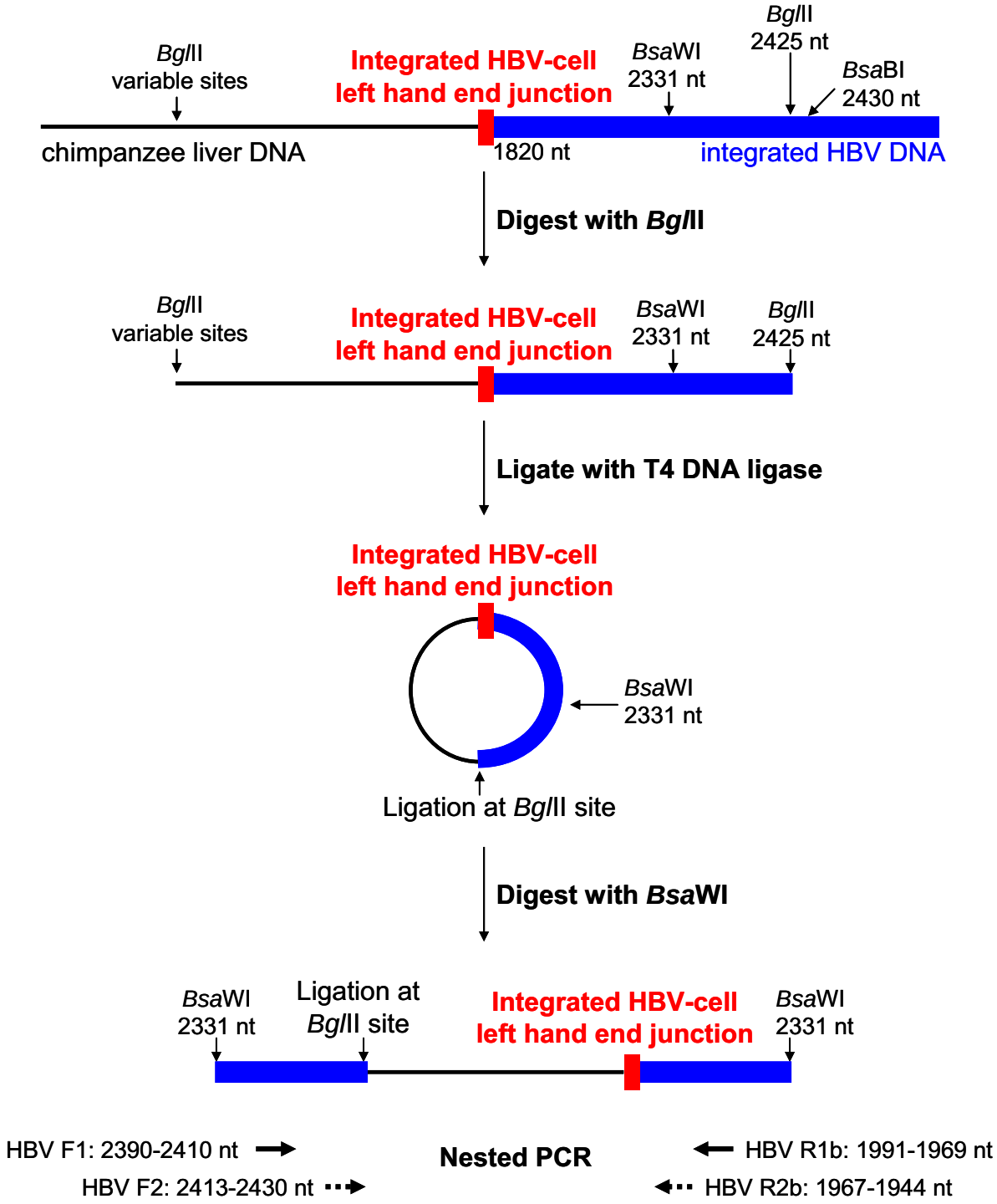


Figure 5.5.6: Schematic representation of the chimpanzee C1 invPCR assay design, showing the DNA inversion process, and the nested PCR reaction primer binding sites.

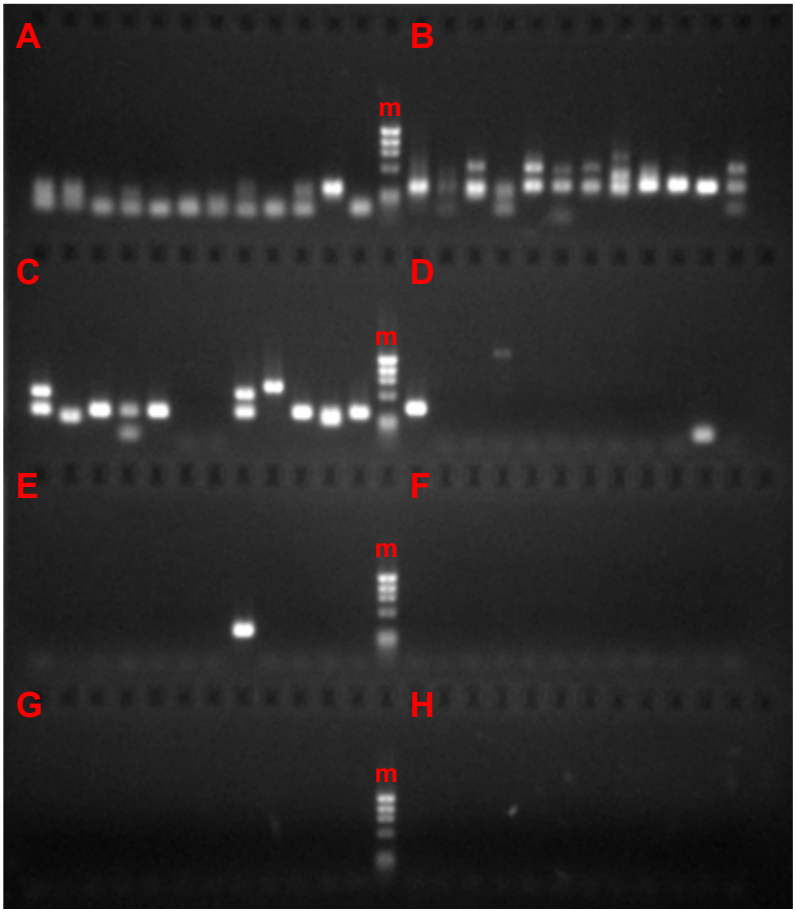
The chimpanzee C1 invPCR assay (refer Table 2.3) was designed by Dr. William Mason based on the HBV genome (GenBank Accession AF222323) (Mason *et al.*, 2009a).

Figure 5.5.7: Examples of invPCR products obtained from the chimpanzee invPCR assays.

The chimpanzee C1 invPCR assays were performed as described in Section 5.5.4, and products were visualised using 96-well agarose gel electrophoresis under 302 nm UV light.

The letters A – H refer to the rows of the PCR wells. The DNA marker used in Figure 5.5.7A (at the lanes labelled "m") was 0.5 μg of the φX174 RF DNA/*Hae* III Fragments (Invitrogen, USA). The DNA marker used in Figure 5.5.7B (at the lanes labelled "m") was 1 μg of the GeneRuler 1 kb Plus DNA Ladder (Thermo Fisher Scientific, Canada).

A



B

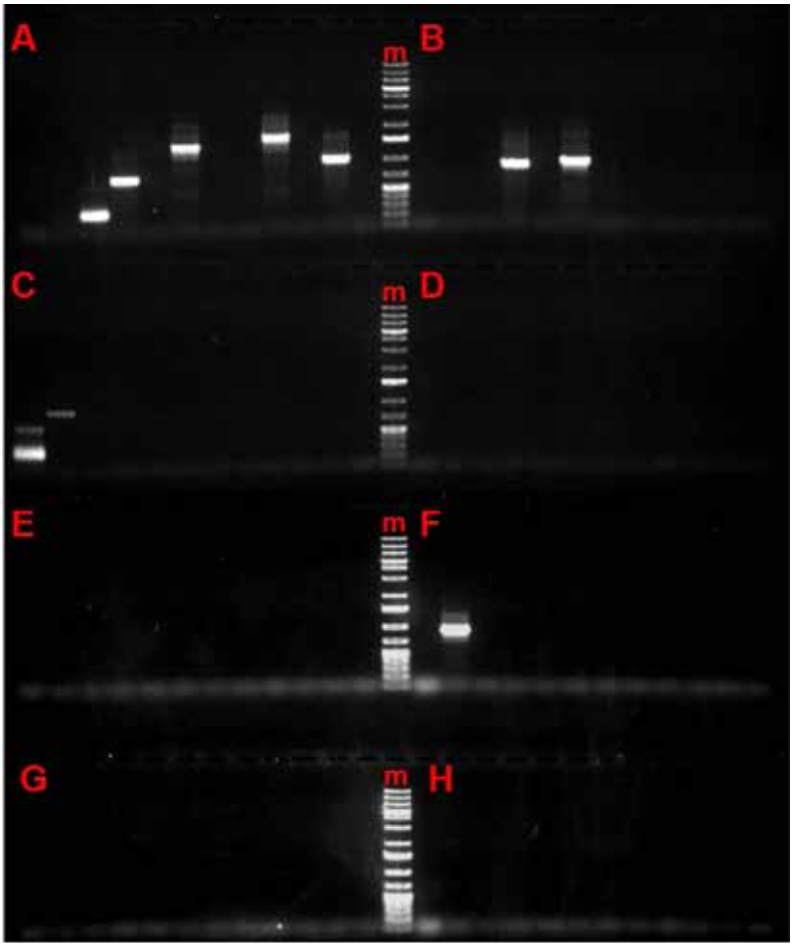


Figure 5.5.7

Figure 5.5.8: Example of DNA sequencing results obtained from the chimpanzee invPCR assay.

The chimpanzee C1 invPCR assays were performed as described in Section 5.5.4.

Figure 5.5.8A shows an example of the DNA sequencing results for an integrated virus-cell junction. BLAST analysis showed that the 578 bp sequence consisted of a 451 bp insert DNA (black font) flanked by the HBV genome (GenBank Accession AF222323) 1927 – 1823 nt (blue bold font) and 2433 – 2413 nt (red bold font) at the *Bgl*II first cut restriction enzyme site (underline). This was consistent with the expected inverted DNA fragment that will be produced by the chimpanzee C1 invPCR assay design (refer Figure 5.5.6). Based on this, 1823 nt is known as virus junction 1, and 2433 nt is known as virus junction 2. Further BLAST analysis showed that the insert DNA shared homology with part of the *Pan troglodytes* (chimpanzee) chromosome 7 (GenBank Accession NC_006474) 12113652 – 12113206 nt, to further confirm that the DNA sequence obtained was an integrated virus-cell junction formed by the integration of the HBV into the chimpanzee genome.

Figure 5.5.3B shows an example of the DNA sequencing result for a virus-virus sequence, which was a false positive result. BLAST analysis showed that the 632 bp sequence consisted of 2 fragments of the HBV genome (GenBank Accession AF222323), 1927 – 1765 nt (blue bold font) and 2886 – 2423 (black bold font). It was not known how this virus-virus false positive fragment was formed, as there were no detectable restriction enzyme sites at the ligation site of both HBV fragments.

A

CGTACTCATTCTTTATAGGGTCAtGTCCATGCCCAAAAGCCACCCAAG
GCACAACTTGGAGGCTTGAACAGTAGGACATGAACATGAGATGACTAG
GCAGAGGTGAAAAACAGGGACTCTTTTTCCCATTGATTGTTTTTGTCA
GCTTTGTCAAAGATCAGATGGTCACAGATATGTGGTTTATTTCTGGGA
CCTCTATTCTGTTCCACTGATACATGTGCTTGTTTTTGTACCACTACC
ATGCTTTGTTACTGTAGTCCTTTAGTATAAAGTCGGGTAACGTGATGC
CTTCAACTTTGTTCTTTTTGCTTAAAGTTGCCCTGGCTATTCAGGCTC
TTTTTTGGTTCCTTATGAATTTTAAAATAGTTTTTTCTAGTTATGTGA
AAAATGGCATTGGTAGCTTGATAGGAATAATATTAAATCTGAAAGTTG
CTTTGGGCAGTATAGCCACGTTAATGATATTGATTCTTTCTATCCATG
AGCATGGAATTTGTGTGCATGTGTATCTTCTCTGATTTCCTTGAGTAG
TGTTTTGTAATTCTCATTGTTTCTCATTGTAGAGATCTTCTGCGACGC
GG

B

GTACTCATTCTTTATAAGGGTCaTGTCCATGCCCAAAAGCCACCCAAG
GCACAACTTGGAGGCTTGAACAGTAGGACATGAACATGAGATGACTAG
GCAGAGGTGAAAAAGTTGCATGGTGCTGGTGTACAGACCAATTTATGC
CTGCAGCCTCCTAATACAAAGACCATCCCAGCGGATTGCTGGTGGAAA
GATTCTGCCCCATGCTGTAGCTCTTGTTCCCAAGAATATGGTGACCCA
CAGAATGAAGCGCTATGTGTGGTTTCTCTCTTATATAAAATGCCTGCC
TGCCATAGAGTATGTAAATAGTGTCTAGTTTGGAAGTAATGATTAACT
ACATTATCTGGATAATAGGGTTTTATACCTTTCTCTAGAGGCAAATAC
TTGGTAGAATTTGGATAAAATCTGGCAGGCATTACTAACTTCAATCTT
CTTTTTTCATTAACCGTAAGAGGGCCCACAAACTGTTCACACTTGTTA
ATAATATCTTGGTGCAAATGAATATCAGGGAAAGAAGGAGTTTGCCAG
TTAGGGTTAAAGACAGGTAGAGTAGAAAAATAAAGCCCAGTAAAATTT
CCCACCTTATGAGTCCAAGGAATACTAACATTGGGAAGCTGGAGATTG
AGATCTTC

Chapter 6: Establishment of invPCR assays to detect integrated virus-cell junctions in DHBV-infected duck liver tissues

6.1. Aim

a) To establish invPCR assays specific for the detection of integrated virus-cell junctions in DHBV-infected duck liver tissues.
b) To perform preliminary invPCR assays in DHBV-infected duck liver tissues collected previously in other studies.
c) To explore the efficiency of invPCR assays in detecting integrated virus-cell junctions in DHBV-infected duck liver tissues.

6.2. Introduction

The invPCR assay involves three main steps as described in Section 1.8.1 and schematically shown in Figures 2.6 and 2.7. The first step is the extraction of liver cellular DNA from liver tissues (usually small amounts, ~1 – 25 mg) using the total DNA extraction method optimised in Chapter 5.1. This is followed by the second step of DNA inversion by a series of restriction enzyme digestions and DNA ligation, to produce inverted DNA fragments containing the integrated virus-cell junction. Lastly, the third step is nested PCR reactions performed on dilutions or aliquots of the inverted DNA fragments (shown in Figure 2.8), with the invPCR assay products subsequently analysed by agarose gel electrophoresis and DNA sequencing.

Methods used during the invPCR assay were developed and established in Chapter 5.4, and are described in detail in Section 2.10. The invPCR assay was also subsequently used to detect integrated virus-cell junctions in WHV-infected woodchuck and HBV-infected chimpanzee liver tissues as described in Chapter 5.5. It was found that the invPCR assays established in this study had comparable efficiency with previous invPCR assays used in our collaborator's laboratory at the Fox Chase Cancer Center (FCCC), Philadelphia, USA.

Subsequently, in order to apply the developed invPCR assay to this study of ducks with acute and chronic DHBV infection, several invPCR assays specific for the detection of integrated AusDHBV DNA (GenBank Accession AJ006350) were established in this Chapter. Preliminary invPCR assays were also preformed on several duck liver tissues collected previously in the laboratory from ducks with acute or chronic DHBV infection. For the purposes of this study, in this thesis, ducks which have cleared DHBV infection from the liver with <0.001% of DHBsAg-positive hepatocytes as detected by immuno-staining by 10 dpi are

defined as having “acute DHBV infection”; while ducks which have persistent and widespread DHBV infection in the liver with >95% of DHBsAg-positive hepatocytes after 10 dpi until the last time-point of a study are defined as having “chronic DHBV infection”.

6.3. Establishment of invPCR assays specific for the detection of integrated virus-cell junctions in DHBV-infected duck liver tissues

6.3.1. Duck liver tissues collected in previous studies

Liver tissues from 3 ducks with chronic DHBV infection were collected from previous studies: Pool 7 from Dr. Miriam Triyatni (Triyatni *et al.*, 2001), and DM30:31 and DM32:33 from Dr. Darren Miller (Miller *et al.*, 2006). Pool 7 and DM32:33 have been previously described in Section 5.4.3.1, while DM30:31 was inoculated with the same dose of virions and had the same infection outcome as DM32:33 (Miller *et al.*, 2006).

These ducks were chosen as they have long periods of active DHBV replication (34 days for Pool 7 s and 29 days for DM30:31 and DM32:33). Therefore, it is expected that there would be high levels of integrated DHBV DNA in these duck liver tissues (~1 integration per 10^3 liver cells as previously reported by Yang and Summers, 1999). In addition, as the ducks grow bigger, the liver containing the infected hepatocytes would also grow and proliferate to form hepatocyte clones in the liver. It was reported that the average liver mass of ducks increases ~20-fold from 1 – 37 days old, with a mean hepatocyte proliferation index declining from ~0.2% between 1 – 7 days old, to ~0.01% between 28 – 35 days old (Thorpe, 2007). Assuming that the liver grows by mitosis of mature hepatocytes, and not liver stem cells, this suggests that each hepatocyte would undergo ~4.3 rounds of mitosis between 1 – 35 days old, and are predicted to stochastically form hepatocyte clones on average up to 58 cells in size, based on mathematical modelling of the hepatocyte clone size after exponential growth of the liver developed by Tu (in preparation). Thus, it is expected that hepatocyte clones up to ~58 cells in size, identifiable as repeats of the unique integrated virus-cell junctions, could be present in these duck liver tissues. However, as there are high levels of DHBV replication in these ducks, it is expected that the high levels of DHBV RI DNA and cccDNA present would contribute to high levels of virus-virus false positives detected during invPCR assays.

6.3.2. Determining the sequence of the most probable left and right hand end junctions of the integrated DHBV DNA

As described in Section 1.8.1, in order to choose suitable restriction enzymes and to design PCR primers for the duck invPCR assay to specifically amplify and detect the integrated virus-cell junctions in DHBV-infected ducks, the DHBV sequences near the 5’ and 3’ end of

the dslDNA had to be first determined. As previous studies have found that the 5' and 3' end of the DHBV pregnomic DNA is each around 2485 and 2537 nt (Yang and Summers, 1999), a ~1 kbp region spanning 2485 – 500 nt of the DHBV genome was amplified and sequenced in this Section. This region roughly corresponds to the DHBcAg ORF on the DHBV genome.

In this study, DHBV-inoculation of ducks was performed using a pool of serum collected from 2 groups of congenitally AusDHBV-infected ducks (Pool 7 or Pool 8) as described in Section 2.2. Thus, DHBV genome was extracted from tissues of pooled serum and liver from the Pool 7 and Pool 8 ducks, and the mentioned ~1 kbp DHBV genome region was sequenced. In addition, to determine whether the sequence of DHBV genome mutates or changes significantly after "passaging" or being used to experimentally infect ducks as described in Section 2.3.1 (for example ducks DM30:31 and DM32:33), liver DNA was also extracted from DM30:31 and the same ~1 kbp DHBV genome region was also sequenced.

Specifically, total DNA was extracted from Pool 7 and DM30:31 liver tissues using the total DNA extraction method described in Section 2.6.3. DNA was also extracted from Pool 8 serum using the ChargeSwitch gDNA 1 mL serum kit as described in Section 2.5.1. Up to 150 ng of extracted DNA was then used as template for PCR amplification as described in Section 2.8.5. Specifically, the PCR reactions were performed using GoTaq polymerase, PCR cycle extension time of 2 min, and using PCR primers DHBV preC F – DHBV C R (Table 2.2) which were designed based on the AusDHBV sequence (GenBank Accession AJ006350). PCR products were then visualised using agarose gel electrophoresis as described in Section 2.8.7. It is expected that a 991 bp PCR product would produced. The PCR product was then purified using the QIAquick PCR purification kit as described in Section 2.8.6, and sequenced using both forward and reverse primers as described in Section 2.8.10 with subsequent purification of the DNA sequencing products using isopropanol as described in Section 2.8.11.1. DNA were sent to the Division of Molecular Pathology, IMVS/SA Pathology for sequencing, and the sequencing results were analysed as described in Section 2.8.12.

Results (data not shown) showed that a ~1 kbp PCR product was successfully produced from all amplifications of DNA extracted from Pool 7 and DM30:31 liver, and Pool 8 serum. From these PCR products, ~915 bp was successfully sequenced. Subsequent alignment of these DHBV DNA sequences (Figure 6.1) showed that they had 99% sequence homology to the published AusDHBV genome. This indicates that even after passage through ducks, the DHBV genome would not mutate and change significantly from its original DHBV sequence. Most mutations were found in the first 35 and last 20 nucleotides of the sequenced DHBV,

which was expected as base pair mismatches may be introduced near the 5' and 3' end of a PCR product due to the instability of the DNA near the ends. Interestingly, a guanine to thymine mutation at 502 nt was found in Pool 8 serum, but not in Pool 7 or DM30:31 liver. Based on this detected nucleotide mutation, restriction enzymes with digestion sites at 502 nt should not be chosen for the duck invPCR assays, as restriction enzymes are base pair specific; while PCR primers amplifying across 502 nt could still be designed, as a single base pair change would not significantly inhibit or affect the efficiencies of PCR amplification.

In summary, the sequence of the most probable left and right hand junction of integrated DHBV DNA was determined, and was shown to be 99% similar to the published AusDHBV sequence. Therefore, all subsequent studies using ducks experimentally infected with the DHBV stock from Pool 7 or Pool 8 could use the AusDHBV sequence as a reliable reference.

6.3.3. Design of invPCR assays

Based on the AusDHBV sequence, several invPCR assays were designed specific for the detection of either the right or the left hand end integrated virus-cell junctions. The restriction enzyme and nested PCR primers were chosen based on criterias described in Chapter 5.4 using plasmid DNA as a model system. In addition to the criteria for restriction enzymes described in Section 5.4.4.1, the first cut restriction enzyme should have minimal restriction sites in the DHBV genome to reduce the production of DHBV DNA fragments which could be ligated to form DHBV-DHBV false positives, and should also preferably not have a cytosine-guanine (CG) recognition sequence, because CG sequences are under-represented in eukaryotic DNA. Thus, less frequent restriction enzymes digestion sites are expected in the duck genome, which would in turn limit the detection of integrated virus-cell junctions. Conversely, the second cut restriction enzyme should preferably have a CG recognition sequence to avoid the chances of digesting the duck genome. Lastly, the third cccDNA destroying enzyme digestion site was chosen to be located immediately downstream and as close as possible to the first cut restriction enzyme digestion site in the DHBV genome, as well as preferably to have a CG recognition sequence to avoid digestion of the duck genome.

A total of 5 invPCR assays were designed. The invPCR assay D1 was designed to detect the right hand end integrated virus-cell junction, while the D2 invPCR assay was designed to detect the left hand end integrated virus-cell junction. Two invPCR assays D3 and D4 were also designed by our collaborator Dr. William Mason to detect the left hand end integrated virus-cell junction. As a control, the invPCR assay D5 was designed by Dr. William Mason to

detect the left hand end integrated virus-cell junction of the DHBV16 strain (GenBank Accession AF047045). All invPCR assay designs are summarised in Table 2.3.

6.3.4. Extraction of liver cell DNA

Several DNA extraction methods were used to extract liver cell DNA from the various frozen duck liver tissues described in Section 6.3.1. The extraction methods include the non-selective DNeasy blood and tissue kit (Section 2.6.1), total DNA extraction (Section 2.6.3), the selective nuclear DNA extraction (Section 2.6.5) and high molecular weight (MW) DNA extraction II (Section 2.6.6.2). The non-selective DNA extractions methods were expected to extract all of the DNA present in the liver tissues, including the duck liver cell DNA, DHBV RI DNA and cccDNA. The selective DNA extraction methods were expected to extract the duck liver cell DNA while removing most of the DHBV RI DNA and cccDNA present.

The concentration of extracted liver cell DNA was measured by Nanodrop spectrometry (Section 2.8.1), and 1.75 μg of DNA, which is the amount of DNA expected in 1 mg of duck liver (calculated in Section 2.8.9.3.2), was used as DNA template for each invPCR assay.

6.3.5. Performing the invPCR assay

Using the duck liver cell DNA extracted as described in Section 6.3.4, the duck invPCR assay designs D1, D2, D3, D4 and D5 (Table 2.3) were performed. Firstly, low melting temperature agarose gel electrophoresis and purification of high MW cellular DNA, and DNA inversion were performed as described in Section 2.10.2. After inversion, 96-well nested PCR was performed as described in Section 2.10.3, firstly with 1/3 serial dilutions of the inverted DNA fragments (schematically shown in Figure 2.8), in order to determine the optimal amount of inverted DNA fragments to be used as the DNA template for the nested PCR reactions. The optimal amount of inverted DNA fragment was determined by the amount of inverted DNA fragment that can produce a single PCR product in most of the PCR wells. Subsequent 96-well nested PCR were performed by evenly distributing the optimal amount of inverted DNA fragments to all PCR wells as described in Section 2.10.3. To visualise the PCR products, 96-well agarose gel electrophoresis was performed as described in Section 2.10.4.

Figure 6.2 shows examples of invPCR products visualised by agarose gel electrophoresis when the inverted DNA fragments were serially diluted (Figure 6.2A) or were evenly distributed (Figure 6.2B) to all PCR wells. Individual agarose gel electrophoresis results are not shown in this Chapter. The invPCR products observed were subsequently extracted by 96-well agarose gel extraction as described in Section 2.10.5, 96-well DNA sequencing was then

performed as described in Section 2.10.6 using the inner primer set reverse primer R2 (Table 2.2), and cleanup of 96-well DNA sequencing products was subsequently performed as described in Section 2.10.7. The DNA sequencing results were lastly analysed as described in Section 2.8.12, focusing on detecting the flanking DHBV DNA sequences and the insert duck liver cell DNA, to determine the integrated virus-cell junction of that inverted DNA fragment.

6.3.6. Establishing the duck invPCR assay

Firstly, all the invPCR assay designs D1, D2, D3 and D4 were performed on DNA extracted from Pool 7 duck liver tissues (refer Section 6.3.1) using the total DNA extraction method as described in Section 2.6.3. This was to determine which of the 4 invPCR assays designed specifically based on the AusDHBV sequence was more effective. The Pool 7 duck liver tissue was used as it was expected to contain the highest amount of integrated virus-cell junctions, and the non-selective total DNA extraction method was used as it was previously found to be the most suitable extraction method for the invPCR assay in Chapter 5.1.

Figure 6.3A shows an example of an integrated virus-cell junction DNA sequencing result, which consisted of an insert DNA flanked by DHBV DNA. As mentioned in Section 5.3.4.2, in this thesis, insert DNA that showed homology to other avian or mammalian "non-duck" genome sequences would also be considered as integrated virus-cell junctions. Figure 6.3B shows an example of a virus-virus false positive DNA sequencing result, which consisted of only DHBV DNA. Individual DNA sequencing results are not shown in this Chapter.

As summarised in Table 6.1, from invPCR assays no. 1 – 4, out of a total of 1270 invPCR reactions performed on a total of 7726 ng of DNA, 303 invPCR products were sequenced. Among these, 5 were integrated virus-cell junctions, 256 were virus-virus false positive sequences, 5 were unknown sequences (defined in this thesis as insert DNA sequences that were either too short (<15 bp) or did not show homology to any known sequences during the BLAST searches), and 37 DNA sequencing reactions failed to produce any readable sequences. All 5 integrated virus-cell junctions detected were unique sequences. Detailed analysis of these 5 integrated virus-cell junctions are summarised in Table 6.2.

Out of the 5 integrated virus-cell junctions detected, 2 were detected using the D1 and D3 invPCR assay design, while 1 was detected using the D4 invPCR assay design. As up to 5 times larger amounts of DNA were analysed using the D3 invPCR assay design, these suggest that the D1 invPCR assay design was more effective. In addition, high levels of virus-virus false positives were detected in all invPCR assays, which was expected as high levels of

DHBV replication were occurring in the Pool 7 duck, and thus high levels of DHBV RI DNA and cccDNA would be present and extracted by the total DNA extraction method.

As the D2 invPCR assay design failed to detect any integrated virus-cell junctions but had only detected virus-virus false positive sequences, the design was further performed on Pool 7 DNA that was extracted using other DNA extraction methods. These methods include the non-selective DNeasy blood and tissue (Section 2.6.1), and the selective high MW DNA extraction method II (Section 2.6.6.2). Using the high MW DNA extraction method II, it is expected that the amount of DHBV DNA present in the extracted DNA will be reduced, and thus would in turn reduce the amount of virus-virus false positives detected.

As summarised in Table 6.1, from invPCR assays no. 7 and 8, out of a total of 336 invPCR reactions performed on a total of 1340.5 ng of DNA, 55 invPCR products were sequenced. Among these, 7 of the sequences were integrated virus-cell junctions, 36 were virus-virus false positive sequences, 1 was an unknown sequence with an insert DNA that was shorter than 15 bp, and 11 DNA sequencing reactions failed to produce any readable sequences. All of the 7 integrated virus-cell junctions detected were unique. Detailed analysis of these 7 integrated virus-cell junctions detected are summarised in Table 6.2.

As invPCR assays performed on DNA extracted using the DNeasy blood and tissue kit only produced 3 invPCR products and none of them were integrated virus-cell junctions, this suggests that the liver cell DNA extracted using this kit was not suitable to be used for invPCR assay. Therefore, DNeasy blood and tissue extraction kit would not be further used in this thesis to extract DNA from liver tissues prior to the invPCR assay. On the other hand, invPCR assays performed on DNA extracted using the high MW DNA extraction method II successfully detected 7 integrated virus-cell junctions. This suggests that this selective extraction method was highly effective and suitable to extract DNA from liver tissues to be used in subsequent invPCR assays. However, as virus-virus false positive sequences were still detected, the selective high MW DNA extraction method II could not completely remove DHBV DNA, but could reduce the false positive levels detected per amount of DNA analysed. To further confirm that high amounts of integrated virus-cell junctions could be detected from DNA extracted using the high MW DNA extraction method II, invPCR assays were performed on DNA extracted from duck DM30:31 (refer Section 6.3.1) using the high MW DNA extraction method II. High amounts of integrated virus-cell junctions were expected to be present in the DM30:31 liver tissue, as similar to Pool 7 ducks, DM30:31 had widespread chronic DHBV infection. The D2 invPCR assay design was performed, and for comparison,

the D1 invPCR assay design that previously detected integrated virus-cell junctions was also performed. Specifically, the D2 invPCR assay detects the integrated left hand end junction, while the D1 invPCR assay detects the integrated right hand end junction.

As summarised in Table 6.1, from invPCR assays no. 9 and 10, out of a total of 252 invPCR reactions performed on a total of 1165 ng of DNA, 19 invPCR products were sequenced. Among these, 9 of the sequences were virus-virus (false positive) sequences, and 4 were unknown sequences, and 6 DNA sequencing reactions failed to produce any readable sequences. None of the invPCR products sequenced were integrated virus-cell junctions.

The failure to detect any integrated virus-cell junctions, even though more DM30:31 DNA was analysed compared to Pool 7, was not expected. As explained in Chapter 5.1, although the high MW DNA extraction method II was able to reduce the levels of DHBV DNA extracted from the liver tissues, there would be high losses of duck cell DNA during this selective extraction. Hence, a lot of the integrated virus-cell junctions may have been lost during extraction, resulting in the failure to detect any junctions. Based on this, it was decided that non-selective DNA extraction methods, like the total DNA extraction method, would be used to prevent the loss of integrated virus-cell junctions during extraction. If the reduction of DHBV DNA were necessary, the low melting temperature agarose gel electrophoresis and purification of high MW cellular DNA (described in Section 2.6.4) would be performed.

Next, the invPCR assay design that was most effective in detecting integrated virus-cell junctions was determined. Previously, when all the D1, D2, D3 and D4 invPCR assays were performed on Pool 7 DNA extracted using the total DNA extraction method, it was found that the D1, D3 and D4 invPCR assays successfully detected integrated virus-cell junctions. The D2 invPCR assay design also subsequently detected integrated virus-cell junctions in Pool 7 DNA extracted using the high MW DNA extraction method II. Based on previous studies, it was found that the invPCR assays that detect the left hand end integration junctions in duck liver tissues were more efficient and could successfully detect more integrated virus-cell junctions per amount of DNA analysed compared to invPCR assays that detect the right hand end integration junctions (Yang and Summers, 1999). In addition, most of the invPCR assays performed on chimpanzee (Mason *et al.*, 2009a) and woodchuck (Mason *et al.*, 2005; Mason *et al.*, 2009b) liver tissues detect the left hand end integration junctions. Based on that, it was decided that the D1 invPCR assays that detect the right hand end integration junctions in ducks would not be further used in this thesis. Next, as the first cut restriction enzyme used in the D2 invPCR assay, *Kpn*I (Table 2.1), could not be heat inactivated, an additional step using

the QIAquick PCR purification kit (described in Section 2.8.6) would be necessary during the DNA inversion step in order to remove the restriction enzyme prior to DNA ligation. This additional step would result in additional DNA losses during the DNA inversion. Hence, it was decided that the D2 invPCR assay would not be the preferred invPCR assay in this thesis.

To determine whether the D3 or D4 invPCR assay was more efficient in detecting integrated virus-cell junctions, both invPCR assays were performed on DNA extracted from DM32:33 liver tissues (refer Section 6.3.1) using the total DNA extraction method (Section 2.6.3). High amounts of integrated virus-cell junctions were expected to be present in the DM32:33 liver tissue, as similar to Pool 7, DM32:33 had widespread chronic DHBV infection.

As summarised in Table 6.1, from invPCR assays no. 5 and 6, out of a total of 1032 invPCR reactions performed on a total of 4092.8 ng of DNA, 143 invPCR products were sequenced. Among these, 1 of the sequences was an integrated virus-cell junction, 102 were virus-virus false positive sequences, 21 were unknown sequences, and 18 DNA sequencing reactions failed to produce any readable sequences. Detailed analysis of the only integrated virus-cell junctions detected is summarised in Table 6.2.

Using the D3 invPCR assay design, 1 integrated virus-cell junction in addition to 21 unknown sequences were detected. This suggests that the D3 invPCR assay may be more efficient in detecting integrated virus-cell junctions compared to the D4 invPCR assay, which had detected mainly virus-virus false positives. Therefore, it was decided that the D3 invPCR assay would be the preferred invPCR assay design used to detect integrated virus-cell junctions in DHBV-infected duck liver tissues in this thesis.

On top of that, the D3 invPCR assay was also performed on DNA extracted from Pool 7 and DM32:33 liver tissues using the selective nuclear DNA extraction method as described in Section 2.6.5. In addition to further confirming that the D3 invPCR assay was suitable to detect integrated virus-cell junctions, this was to determine whether the amounts of virus-virus false positives could be reduced using the selective nuclear DNA extraction method. It was expected that most of the DHBV RI DNA would not be extracted, and thus less virus-virus false positives would be detected during invPCR assay.

As summarised in Table 6.1, from invPCR assays no. 11 and 12, out of a total of 720 invPCR reactions performed on a total of 5098 ng of DNA, 256 invPCR products were sequenced. Among these, 4 of the sequences were integrated virus-cell junctions, 180 were virus-virus

false positive sequences, and 72 DNA sequencing reactions failed to produce any readable sequences. Among the 4 integrated virus-cell junctions detected, 3 of the junctions were unique, with 1 of the junctions repeated 2 times. Interestingly, the same insert DNA was also detected in the invPCR assay no. 1 (Table 6.1), performed on DNA extracted from the same Pool 7 liver tissue but using the total DNA extraction method. Detailed analysis of these 4 integrated virus-cell junctions detected are summarised in Table 6.2, while further analysis of the same insert DNA detected is later discussed in Section 6.5.

As 1 of the integrated virus-cell junctions was repeated 2 times, this suggests that there was at least 1 hepatocyte clone present in the Pool 7 liver tissue. This was expected, as mentioned in Section 6.3.1, hepatocytes clones ~58 cells in size could be present in this liver tissue, as the ducks were congenitally infected and liver mass was estimated to have increased ~20-fold from the time of DHBV infection.

Based on these results, by using the nuclear DNA extraction method, the levels of virus-virus false positives detected using the invPCR assay could not be significantly reduced as expected. This suggests that most of the virus-virus sequences were contributed not by the DHBV RI DNA, but by the DHBV cccDNA present in the nucleus in a pool of 5 – 50 copies per infected hepatocyte (Summers *et al.*, 1990; Zhang *et al.*, 2003). Therefore, the nuclear DNA extraction would not be used to extract DNA from liver tissues during the invPCR assay in this thesis. In addition, as expected, the number of integrated virus-cell junctions detected increased when the total amount of DNA analysed increased. Hence, the key to detecting more integrated virus-cell junctions may be simply to analyse more amounts of liver cell DNA. However, integrations were expected to occur once in every 2.5 ng of DNA, as calculated by the reported frequency of integration that was 1 in every 10^3 cells (Yang and Summers, 1999), and that each cell contains ~2.5 pg of DNA (Tiersch and Wachtel, 1991; Krishan *et al.*, 2005). Therefore, the low amounts of integrated virus-cell junctions detected in this Section may also reflect the low efficiency of the duck invPCR assay, which may not have been fully optimised. This would be further discussed later in Section 6.6.

In summary, invPCR assay specific for the detection of integrated virus-cell junctions in DHBV-infected duck liver tissues was established, by first using the total DNA extraction method to extract the liver cell DNA, followed by performing the D3 invPCR assay. A schematic representation of the D3 invPCR assay design is shown in Figure 6.4.

6.4. Perform preliminary invPCR assays to detect integrated virus-cell junctions in DHBV-infected duck liver tissues

Integrated virus-cell junctions were detected in duck liver tissues using the invPCR assay established in Section 6.3, as preliminary experiments for the main studies performed in Chapters 7 and 8. Briefly, DNA was extracted from the duck liver tissues using the total DNA extraction method as described in Section 2.6.3, followed by low melting temperature agarose gel electrophoresis and purification of high MW cellular DNA as described in Section 2.6.4. Next, the invPCR assays were performed as described in Section 2.10, using the D3 invPCR assay design described in Table 2.3 and shown schematically in Figure 6.4. The DNA sequencing results were analysed as described in Section 2.8.12.

6.4.1. Detecting integrated virus-cell junctions in livers tissues collected from ducks with acute DHBV infection

6.4.1.1. Duck liver tissues collected from previous studies

A total of 12 liver tissues from 8 ducks with acute DHBV infection were collected from previous studies: CQ4B.1 and CQ4B.4 from Chee Quin Teoh (Teoh, unpublished), GR134, GR136, GR137, GR140, GR141, and GR142 from Dr. Georget Reaiche (Reaiche *et al.*, 2010).

Briefly, ducks CQ4B.1 and CQ4B.4 were pre-treated with 500 μg of each 3 DHBV DNA vaccines (pcDNA3-preS/S, pcDNA3-S, pcDNA3-C) (Feng *et al.*, 2010) at 14 and 28 days of age, before being experimentally infected at 6 weeks of age by intravenous inoculation with a dose of $4.5x10^{10}$ vge of Pool 8 serum (refer Section 2.2). Liver tissues were obtained at 4, 14 and 31 dpi. At 4 dpi, these ducks were shown to have an average of 4.7% of DHBsAg-positive hepatocytes in the liver, and by 14 and 31 dpi, there were <0.001% of DHBsAg-positive hepatocytes in the liver. There were no detectable levels of viraemia throughout infection, suggesting that the vaccines had successfully primed the duck immune responses to quickly control or inhibit DHBV replication during early stages of infection, thus preventing the spread of infection, and leading to the successful clearance by 14 dpi (Teoh, unpublished).

Ducks GR134, GR136, GR137, GR140, GR141, GR142 were experimentally infected at 6 weeks of age by intravenous inoculation with a dose of $1.5x10^{10}$ vge of Pool 8 serum (refer Section 2.2). GR134, GR136 and GR137 subsequently received oral treatment with the nucleoside analogue antiviral drug entecavir (ETV) (Bristol-Myers Squibb, USA) at a dose of 1 mg/kg/day from 126 – 316 dpi, in order to inhibit replication of any residual DHBV DNA. GR140, GR141, GR142 did not receive any antiviral treatment, thus allowing for residual DHBV DNA replication or rebound of DHBV infection to occur (Reaiche *et al.*, 2010). At 4

dpi, all of the ducks had an average of 3.7% DHBsAg-positive hepatocytes in the liver and a viraemia of $1.6x10^6$ DHBV total DNA per mL of serum. From 60 – 316 dpi, all the ducks had <0.001% of DHBsAg-positive hepatocytes in the liver and undetectable levels of viraemia. No further active DHBV replication was reported in all ducks, and most of the remaining DHBV DNA persisting in the liver was found to be in the form of DHBV cccDNA (Reaiche *et al.*, 2010). Liver tissues collected at 316 dpi were used in this Section.

These ducks were chosen to be used for preliminary invPCR assays for Chapter 7, which aims to explore the mechanisms involved during the clearance of DHBV-infected hepatocytes during acute DHBV infection. Hence, liver tissues obtained from ducks CQ4B.1 and CQ4B.4 at 4, 14 and 31 dpi were used, as these liver tissues were collected during different early stages of acute DHBV infection. Therefore, this allows for the complexity of the integrated virus-cell junctions present in the liver of the same animal to be directly compared during various stages of acute DHBV clearance. If integrated virus-cell junctions were present in the liver at 4 dpi but not after resolution of acute DHBV infection like at 31 dpi, this suggests that cytolytic hepatocyte killing had occurred; conversely, if the amount of integrated virus-cell junctions present in the liver at 4 dpi were similar to 14 and 31 dpi, this suggests that non-cytolytic hepatocyte curing had occurred. On the other hand, liver tissues obtained from GR134, GR136, GR137, GR140, GR141, GR142 were used as they were collected at 316 dpi, which was a late stage after clearance of DHBV infection. Therefore, this allows for the complexity of the integrated virus-cell junctions present in the liver long after the clearance of acute DHBV infection to be determined. If hepatocyte curing occurs, it is expected that large clones containing repeats of the integrated virus-cell junctions would be present in the liver, as several liver turnovers would have occurred, allowing for the copy number of the unique integrated virus-cell junctions to increase as the hepatocytes had underwent multiple mitosis.

For CQ4B.1 and CQ4B.4, as ~4.7% of the hepatocytes were DHBsAg-positive, it is expected that integrated virus-cell junctions could be detected once every $\sim4.7x10^5$ cells. For GR134, GR136, GR137, GR140, GR141 and GR142, as ~3.7% of the hepatocytes were DHBsAg-positive, it is expected that integrated virus-cell junctions could be detected once every $\sim3.7x10^5$ cells. During early stages of acute DHBV infection (1 – 14 dpi), as high amounts of DHBV replication is occurring, it is expected that high levels of virus-virus false positives would be detected, with integrated virus-cell junctions present at low frequencies due to low percentage of DHBV-infected hepatocytes and short period of time allowed for integrations to occur. After clearance of DHBV infection, as there would only be residual levels of DHBV cccDNA present, it is expected that few virus-virus false positives would be detected.

6.4.1.2. Results and discussion

As summarised in Table 6.3, from invPCR assays no. 1 – 6, out of a total of 540 invPCR reactions performed on a total of 4575 ng of DNA on all time-points of CQ4B.1 and CQ4B.4 duck liver tissues, only 13 invPCR products were sequenced. Among which, 8 were virus-virus false positive sequences, and 5 DNA sequencing reactions failed to produce any readable sequences. As these ducks were vaccinated before experimentally infected with DHBV, it was likely that the immune system had been primed for a quick response against DHBV infection, resulting in low levels of DHBV replication and DHBV integrations. Based on that, these vaccinated duck liver tissues were not used for further analysis in this thesis.

To increase the chances of detecting integrated virus-cell junctions, as suggested in Section 6.3.6, increased amounts of DNA were analysed from the GR134, GR136, GR137, GR140, GR141, GR142 liver tissues. As summarised in Table 6.3, from invPCR assays no. 7 – 12, out of a total of 486 invPCR reactions performed on a total of 44,060 ng of DNA, 81 invPCR products were sequenced. Among which, only 1 integrated virus-cell junction was detected, 57 were virus-virus false positives, 5 were unknown sequences, and 18 DNA sequencing reactions failed to produce any readable sequences. Detailed analysis of the integrated virus-cell junction detected is summarised in Table 6.4. Surprisingly, high levels of virus-virus false positives were detected despite the ducks having no reported active DHBV replication, and contained an average of ~0.0015 DHBV total DNA per cell (Reaiche *et al.*, 2010). These suggest that the invPCR assay is highly sensitive and able to detect DNA present at low levels in the liver, and that DHBV cccDNA is a major contributor to virus-virus false positives.

In summary, as no integrated virus-cell junctions were detected at early time-points during acute DHBV infection, no definite conclusions could be made regarding the mechanisms involved during the clearance of DHBV-infected hepatocytes during acute DHBV infection. As an integrated virus-cell junction was detected 316 dpi, this suggests that non-cytolytic hepatocyte curing may have occurred during resolution of DHBV infection. On the other hand, the absence of integrated virus-cell junctions could also suggest that the majority of DHBV-infected hepatocyes had been cytolytically killed during resolution of DHBV infection.

6.4.2. Detecting integrated virus-cell junctions in liver tissues collected from ducks with chronic DHBV infection

6.4.2.1. Duck liver tissues collected from previous studies

Liver tissues from 11 ducks with chronic DHBV infection and treated with antiviral drugs were collected from previous studies: HT102/149, HT103/132, HT106/129, HT115/128,

HT122/131 from Hugh Trahair (Trahair, 2008), and FN1, FN2, FN3, FN76, FN77, and FN78 from Dr. Faseeha Noordeen (Noordeen, 2009). The antiviral drugs are expected to inhibit DHBV polymerases' reverse transcription, to stop DHBV replication and DHBV antigens production/expression, as well as to prevent the synthesis of new cccDNA in the liver.

Briefly, ducks HT102/149, HT103/132, HT106/129, HT115/128 and HT122/131 were experimentally infected at 14 days of age by intravenous inoculation with $5x10^8$ vge of Pool 8 serum (refer Section 2.2). The DHBV infection was allowed to spread for 5 days, before being treated with 500 μg of pcDNA3 vector (Invitrogen, USA) DNA vaccines by intramuscular injection, and at 12 dpi, the ducks were treated with $6x10^7$ plaque forming units (pfu) of FPV-M3, a commercially available live-attenuated vaccine strain of fowlpox virus (Fort Dodge Animal Health, Australia) by intramuscular injection (Feng *et al.*, 2010). From 5 – 19 dpi, the ducks also received daily oral treatment with 1 mg/kg of ETV. Liver tissues were obtained at 19 dpi, and these ducks showed an average of 8.5% of DHBsAg-positive hepatocytes in the liver and ~10 μg/mL DHBsAg in the serum. By 33 dpi, these ducks showed a slight decrease of DHBV infection with an average 7.69% of DHBsAg-positive hepatocytes in the liver and ~2 μg/mL DHBsAg in the serum (Trahair, 2008).

Ducks FN1, FN2, FN3, FN76, FN77, and FN78 were experimentally infected at 14 days of age by intravenous inoculation with $5x10^8$ vge of Pool 8 serum (refer Section 2.2). The DHBV infection was allowed to spread for 14 days before starting treatment from 14 – 41 dpi, and liver tissues were obtained at 41 dpi. For FN1, FN2 and FN3, the ducks were treated daily with 5 mg/kg of tenofovir (TFV) (Gilead Sciences, USA) by intraperitoneal injection. At 41 dpi, and these ducks showed an average of 10% of DHBsAg-positive hepatocytes in the liver and no detectable serum DHBsAg. For FN76, FN77 and FN78, the ducks were treated daily with 5 mg/kg of TFV and 100 mg/kg of emtricitabine (FTC) (Gilead Sciences, USA) by intraperitoneal injection. At 41 dpi, and these ducks showed an average of 9.9% of DHBsAg-positive hepatocytes and ~2 μg/mL of DHBsAg in the serum (Noordeen, 2009).

These ducks were chosen to be used in preliminary invPCR assays for Chapter 8, which aims to access the levels of clonal proliferation of hepatocytes during chronic DHBV infection. Briefly, clonal proliferation of hepatocytes could be assessed by determining the copy number (repeats) of unique integrated virus-cell junctions, to also allow the calculation of the size of any hepatocyte clones, and to estimate the number of rounds of hepatocyte proliferation that had occurred (Summers *et al.*, 2003; Mason *et al.*, 2009a; Mason *et al.*, 2009b).

Hence, liver tissues obtained from both of these groups of ducks were used, as DHBV infection was allowed persist for 5 and 14 days respectively, before starting antiviral therapy. This was crucial as it allowed time for DHBV integration to occur. As ~10% of the hepatocytes were DHBsAg-positive in these duck liver tissues, it is expected that integrated virus-cell junctions could be detected once every ~10^4 cells. In addition, these ducks had received antiviral therapy that inhibits DHBV replication. Thus, the levels of DHBV DNA would be reduced, and in turn reduce the levels of virus-virus false positives detected. This was specially expected for FN76, FN77 and FN78 that were treated with combination therapy, therefore much lower levels of DHBV DNA replication would be expected these liver tissues.

6.4.2.2. Results and discussion

As summarised in Table 6.3, from invPCR assays no. 13 – 17, out of a total of 540 invPCR reactions performed on a total of 400 ng of DNA, 75 invPCR products were sequenced. Among which, 65 were virus-virus false positive sequences, 1 was an unknown sequence that did not show homology to any known sequences during the BLAST searches, and 9 DNA sequencing reactions failed to produce any readable sequences. None of the sequences were integrated virus-cell junctions. It was possible that as DHBV infection was allowed to spread for only 5 days before the ducks were treated, and as the liver tissues were obtained at 19 dpi, the short time frame did not allow for enough integrations and clonal proliferation of hepatocytes to occur. Future studies could look into analysing the 33 dpi liver tissues from this study (final time-point), to determine whether more integrated virus-cell junctions could be detected after an additional 12 days of infection after treatment was terminated.

On the other hand, as summarised in Table 6.3, from invPCR assays no. 18 – 23, out of a total of 1530 invPCR reactions performed on a total of 4177 ng of DNA, 88 invPCR products were sequenced. Among which, 20 were integrated virus-cell junctions, 26 were virus-virus false positive sequences, 20 were unknown sequences, and 22 DNA sequencing reactions failed to produce any readable sequences. Detailed analysis of the integrated virus-cell junctions detected are summarised in Table 6.4. Results suggest that TFV antiviral treatment had indeed reduced the levels of DHBV DNA, and by reducing the number of virus-virus false positives, it may have increased the detection of integrated virus-cell junctions. Additionally, as DHBV infection was allowed to spread for 14 days before the ducks were treated, this may have allowed for more DHBV DNA integrations to occur. As 1 of the integrated virus-cell junctions detected in FN1 was repeated twice, this suggests that there were at least 1 hepatocyte clone present in the FN1 liver tissue that was at least 2 cells in size, and that at least 1 round of clonal proliferation of hepatocytes had occurred in the liver by 41 dpi. These

liver tissues were not further analysed in this thesis, but future work could continue analysing these liver samples to observe the possible effects of antiviral therapy on viral integration, clonal proliferation of hepatocytes, and formation of hepatocyte clones.

Interestingly, no invPCR products were detected at all for FN76, FN77 and FN78, with only smears observed in all the lanes in the agarose gel electrophoresis of invPCR products (data not shown). Similar smears were still observed after repeating the invPCR assay multiple times, and when using different batches of extracted FN76, FN77 and FN78 liver DNA as template (data not shown). It was unclear why invPCR reactions were not successful for these samples. A possibility could be that the residual FTC, a cytosine nucleoside analogue, or in combination with the TFV, an adenosine nucleoside analogue, may have interfered with the PCR Taq polymerases during nested PCR amplifications, resulting in the failure to amplify any invPCR products from these liver tissues. The effects of nucleoside analogue loads present in the tissue samples on PCR amplifications were not pursued further in this thesis.

In summary, hepatocyte clones could be detected in ducks with chronic DHBV infection as early as 41 dpi. The detection of integrated virus-cell junctions was also found to be more effective when less DHBV DNA that contributes to virus-virus false positives were present.

6.5. Analysis of the integrated virus-cell junctions detected

Based on all the 38 integrated virus-cell junctions detected in this Chapter (shown in Tables 6.1 and 6.3), the 5' end of the DHBV dslDNA that joined to the host genome during integration, forming the integrated virus-cell junctions, was found to range between 2515 – 2841 nt with a median at 2537 nt; while the 3' end of the DHBV dslDNA was found to be either 2470 or 2478 nt of the DHBV genome (GenBank Accession AJ006350). This was similar to the published 5' end of the DHBV dslDNA at 2485 or 2529 nt (depending on the dslDNA form), and the 3' end of the DHBV dslDNA at 2537 nt (Yang and Summers, 1999). The compiled distribution map of the left hand end of DHBV dslDNA is shown as Figure 6.5.

In addition, based on the BLAST analysis of insert DNA, there were no significant patterns or preferences of integration sites in the duck genome, and the DHBV dslDNA had integrated randomly into different regions of the duck genome, similar to observations in Chapter 5.3. An exception is shown in Table 6.2, where the DHBV dslDNA was found in two cases to have integrated into the *Anas platyrhynchos* (Pekin duck) major histocompatibility complex class I region (GenBank Accession AY885227.1), but at different nucleotide positions. The repeated integrated virus-cell junction from invPCR assay no. 11, which detects the left hand

end integration junction, was from a hepatocyte clone as discussed in Section 6.3.6, as both the inverted DNA fragments were almost identical, showing that integration had occurred at 2608 nt of the DHBV genome and 33396 nt of the duck gene. However, the integrated virus-cell junction from invPCR assay no. 1, which detects the right hand end integration junction, showed that integration had occurred at 2478 nt of the DHBV genome and 33430 nt of the duck gene. As the integration site in the duck gene was ~430 nt apart, this suggests that both these integrated virus-cell junctions were not from the same hepatocyte clone.

The integration sites of hepadnavirus dslDNA into host liver genome have been previously found to be mainly random (Tokino and Matsubara, 1991). However, sites of the liver genome that are fragile or prone to DNA damage, with gaps or double-stranded breaks, have been shown to be targets for integration (Bill and Summers, 2004; Hu *et al.*, 2010), as integration occurs mainly via the non homologous end joining (Yang and Summers, 1995). In some cases, high frequency integration into certain genome sites has been reported. For example, integration of WHV DNA has been commonly reported to occur in N-*myc* gene in the woodchuck liver genome (Fourel *et al.*, 1990). However, integration of WHV into the N-*myc* gene has also been associated with oncogene activation, and is found in >50% of woodchuck liver tumours (Fourel *et al.*, 1994a). Therefore, it was highly likely that the high frequency of WHV integration was not due to the N-*myc* gene being a preferred site for WHV integration, but was due to the oncogenic effects triggered by the integration event.

Several fragile sites prone to breakage have been reported in the chicken genome (Gordon *et al.*, 2007). However, as the genome analysis for ducks or chickens are not complete, it could not be determined whether the duck major histocompatibility complex class I region gene was a fragile site. As this gene was reported to be involved with duck immune responses against infection (Mesa *et al.*, 2004) and not oncogenic activation, it was unlikely that the integrated virus-cell junctions detected was from a "duck liver tumour", as DHBV-infected Pekin ducks were also not reported to develop liver tumours after DHBV infection (Zoulim *et al.*, 2008).

Based on all that, the integration of DHBV into 2 different nucleotide positions in the duck major histocompatibility complex class I region gene would either be because the gene was a genetic fragile site, or it was pure coincidence that the random integration events had occurred in close proximity. No further work had been performed in this thesis to pursue this matter.

6.6. Discussion on the efficiency of invPCR assay in detecting integrated virus-cell junctions in DHBV-infected duck liver tissues

Based on the invPCR assay results summarised in Tables 6.1 and 6.3 and discussed in Sections 6.3.6 and 6.4, the number of integrated virus-cell junctions detected was less than the expected amount of junctions present in the respective liver tissues. For example, in the Pool 7 and DM30:31, DM32:33 ducks that had long periods of chronic DHBV infection, it was expected that integrated virus-cell junctions would be present once every 10^3 cells, with clone sizes reaching up to 15 cells in size (as explained in Section 6.3.1). However, only 17 integrated virus-cell junctions were detected in 19.4 μg of DNA, or ~$7.8x10^6$ cells (as calculated in Section 2.8.9.3.2) that were analysed in Section 6.4. This equals a 0.02 frequency of detection of integrated virus-cell junctions per 10^4 cells.

In previous studies by Yang and Summers, two invPCR assays designed to detect the right hand end or left hand end integrated virus-cell junctions were performed on liver tissues collected at 6 dpi from 3 ducks experimentally infected at 4 days of age with $5x10^9$ genomes of DHBV16 (GenBank Accession AF047045). Out of a total of 840 invPCR reactions performed on 477 ng of DNA or ~$1.9x10^5$ cells, 470 invPCR products were sequenced. Among these, 29 of the sequences were integrated virus-cell junctions, 196 were virus-virus false positive sequences, and the remaining 245 sequences were DNA sequencing reactions that had failed to produce any readable sequences, had the presence of multiple products in a DNA sequence, or had unidentifiable integration junctions. This equals a frequency of detection of integrated virus-cell junctions of 1 per 10^3 – 10^4 cells (Yang and Summers, 1999).

As Pool 7 ducks were similar in age compared to the ducks used by Yang and Summers and had more days of DHBV infection (34 days compared to 6 days respectively), more integrated virus-cell junctions would be expected for the Pool 7 ducks. Thus, the stark difference in the frequency of detection of integrated virus-cell junctions in this Chapter compared to published studies (Yang and Summers, 1999) suggests that the duck invPCR assay established in this Chapter may not have been fully optimised and established. This was unexpected, as the parallel invPCR assays performed on WHV-infected woodchuck and HBV-infected chimpanzee liver tissues in Chapter 5.5 had confirmed that the techniques involved in the invPCR assays established in this thesis was comparable with the quality of the invPCR assay that had been well established by our collaborator Dr. William Mason in FCCC, USA.

To investigate whether the low detection of integrated virus-cell junctions in this Chapter were due to any technical issues, Dr. Mason kindly performed the same invPCR assays on DNA extracted from FN1 and FN76 liver tissues as described in Section 6.4. All experiments were performed in the Hepatitis Research Laboratory. According to Dr. Mason (personal communication) and as summarised in Table 6.5, from invPCR assays no. 1 and 2, out of the 384 invPCR reactions performed on a total of 393.1 ng of DNA, 23 invPCR products were sequenced. Among these, only 1 of the sequences was an integrated virus-cell junction, 13 were virus-virus false positive sequences, 4 were unknown sequences, and 5 DNA sequencing reactions failed to produce any readable sequences. For FN76, only smears were observed in all the lanes in the agarose gel electrophoresis of invPCR products (data not shown).

Next, Dr. Mason again kindly performed the same invPCR assays on DNA extracted from Pool 7 duck liver tissues using the total DNA extraction method as described in Section 6.3.6. DNA was extracted in the Hepatitis Research Laboratory and sent to FCCC in dried DNA pellets for analysis. Subsequent low melting temperature agarose gel electrophoresis and purification of high MW cellular DNA, invPCR assays and analysis of invPCR products, were performed at FCCC. Both the duck D3 and D4 invPCR assay designs were performed. According to Dr. Mason (personal communication) and as summarised in Table 6.5, from invPCR assays no. 3 and 4, out of the 192 invPCR reactions performed on a total of ~18 ng of DNA, 82 invPCR products were sequenced. Among these, 21 of the sequences were integrated virus-cell junctions, 56 were virus-virus false positive sequences, and 6 DNA sequencing reactions had failed to produce any readable sequences.

When compared directly to the invPCR assays performed in Section 6.3, only 3 integrated virus-cell junctions and 185 virus-virus false positive sequences were detected in 224 invPCR reactions sequenced from 6016 ng of Pool 7 DNA analysed using the duck D3 and D4 invPCR assay designs (Table 6.1). These results suggest that there were some differences between the qualities of invPCR assays performed in the two laboratories. As the same DNA template and invPCR assay design was used in both laboratories, this suggests that the problems likely lie with the quality of reagents or equipments used in the DNA inversion steps, the nested PCR reaction steps, or the sequencing reaction steps.

The DNA inversion steps and the nested PCR reaction steps were optimised and established in Chapter 5.4, which showed that the invPCR assay was sensitive enough to detect a single copy of DNA template, but the presence of large amounts of duck cell DNA may slightly affect the efficiency of detection of invPCR assay products. Thus, it was likely that these had

reduced the amounts of integrated virus-cell junctions detected in this Chapter. Alternatively, there could have been high losses of DNA during the DNA inversion step during the DNA precipitation step (refer Section 2.10.1). To improve this step, a different dextran DNA carrier could be used to improve the precipitation of DNA. The DNA pellet washes should also be performed with greater care to avoid DNA losses. In addition, DNA pellets could be dried in a heated vacuum dryer, so that the time needed to dry the pellet could be reduced to prevent any possible (but unlikely) degradation of DNA due to long periods of exposure during drying.

On the other hand, results showed that 6 out of 82 invPCR products sequenced by Dr. Mason in FCCC had failed to produce any readable sequences (6%), while 31 out of 224 invPCR products sequenced in the Hepatitis Research Laboratory had failed (14%). The failed DNA sequencing reactions may be due to poor qualities of the inverted DNA fragments, 96-well nested PCR products produced, the 96-well agarose gel extraction methods, the 96-well DNA sequencing reactions, or the subsequent cleanup of 96-well DNA sequencing products steps. Hence, despite using the same protocols as Dr. Mason in FCCC, further optimisation and improvisation were required for these downstream steps.

Based on all that, several improvements could be made to the invPCR assay. During low melting temperature agarose gel electrophoresis and purification of high MW cellular DNA (methods shown in Section 2.6.4), to reduce degradation of DNA by UV light, a UV converter plate would be used to convert the 302 nm UVB light from the GelDoc XR system to a longer wavelength of 365 nm UVA light. For the 96-well agarose gel extraction (methods shown in Section 2.10.5), more wash steps on the QIAEX II beads were performed using the QX1 buffer and PE buffer, to ensure that all traces of the agarose gel and other contaminating reagents present in the mixture would be removed. The QIAEX II beads were also allowed to air dry between 30 – 60 min, until the beads had fully dried (turned white) to allow for more efficient elution of the DNA from the beads. For the 96-well DNA sequencing reaction (methods shown in Section 2.10.6), based on the work performed in Chapter 3.1, up to 1X BigDye Terminator mix could be added in each DNA sequencing reaction to increase the quality of the DNA sequences obtained. In addition, DNA sequencing reactions could be performed at 20 μL of final volume instead of 10 μL to prevent evaporation of reagents during sequencing. Lastly, for the cleanup of 96-well DNA sequencing products (methods shown in Section 2.10.7), only new CleanSeq magnetic beads should be used, as the beads only have a short shelf lifespan of 6 months. The beads were also ensured not to over-dry to avoid degradation of DNA or subsequent inefficient elution of DNA from the beads. To prevent carryover of the magnetic beads in the solution sent for DNA sequencing analysis, the 96-well

tray could be centrifuged to ensure that the beads were collected at the bottom of the tray, before carefully removing part of the supernatant for DNA sequencing. All the improved methods are described in Chapter 2, and these changes have been successful in reducing the sequencing failure rate from 19% during preliminary invPCR assays in Section 6.2, to 1% at later stages of this study (Chapters 7 and 8). Nevertheless, more improvments could be done to achieve the ideal 0% DNA sequencing failure rate.

To further investigate whether the low detection of integrated virus-cell junctions in this Chapter was due to poorly extracted liver cell DNA, invPCR assays were performed on DNA extracted from liver tissues of 2 congenitally DHBV-infected ducks (2069 and 2071) by Dr. Mason at FCCC (Fourel *et al.*, 1994c). Liver tissues were obtained at ~6 weeks of age, before the ducks received treatments of 10 μg/kg of 2' carbodeoxyguanosine (2' CDG), an inhibitor of HBV synthesis (Price *et al.*, 1992) orally from ~9 weeks of age onwards every other day. Before treatment, the ducks had an average viraemia of $1.1x10^9$ virions per mL of serum, with >95% of DHBsAg-positive hepatocytes in the liver (Mason *et al.*, 1994).

DNA was extracted from ~1 mg of liver tissue using the total DNA extraction method as described in Section 2.6.3 by Dr. Mason, and was subsequently sent to the Hepatitis Research Laboratory for parallel invPCR assay analysis. Specifically, low melting temperature agarose gel electrophoresis and purification of high MW cellular DNA were performed as described in Section 2.6.4, followed by duck D5 invPCR assay (Table 2.3) performed as described in Section 2.10, and invPCR assay products were analysed as described in Section 2.8.12.

As summarised in Table 6.3, from invPCR assays no. 24 and 25, out of a total of 504 invPCR reactions performed on a total of ~800 ng of DNA, 39 invPCR products were sequenced. Among which, 9 were virus-virus false positive sequences, 20 were unknown sequences, and 10 DNA sequencing reactions failed to produce any readable sequences. None of the sequences were integrated virus-cell junctions.

When the same invPCR assay was performed by Dr. Mason at FCCC (personal communication), as summarised in Table 6.5, from invPCR assays no. 5 and 6, 81 invPCR products were sequenced. Among which, 10 were integrated virus-cell junction, 36 were virus-virus false positive sequences, 20 were unknown sequences, and 15 DNA sequencing reactions failed to produce any readable sequences.

Comparing the results obtained in both laboratories, the difference between the invPCR products detected was similar as previously described in this Section. These suggest that the low detection of integrated virus-cell junctions in this Chapter were not likely due to poor qualities of DNA extracted from the liver tissues, but were likely due to the lower efficiencies of the downstream DNA inversion steps, the nested PCR reaction steps, or the sequencing reaction steps as discussed above. To improve the extraction of DNA from liver tissues, smaller fragments of frozen liver tissues could be used to ensure that the cells could be properly lysed by the lysis buffers, or alternatively the frozen liver tissues could be first homogenized to physically lyse the cells and release the DNA without shearing via vortexing

On a separate note, as summarised in Table 6.5, Dr. Mason had also found high levels of virus-virus false positives in his invPCR assays, totalling 105 out of 186 invPCR products sequenced (56.5%) from ~411.1 ng of DNA analysed. In comparison, as summarised in Tables 6.1 and 6.3, this thesis found that 201 out of 298 invPCR products sequenced (67.4%) from ~7,616 ng of DNA analysed were virus-virus false positives. These suggest that the detection of high levels of virus-virus false positives were not due to poorly optimised invPCR assays or the invPCR assay design used, but were due to the high levels of DHBV RI DNA and cccDNA present in the liver tissues. Nonetheless, the detection of high levels of virus-virus false positives would significantly reduce the detection of integrated virus-cell junctions, as while each hepatocyte may contain 1 – 17 copies of DHBV cccDNA (Zhang *et al.*, 2003) and at least 500 copies of DHBV RI DNA (Jilbert *et al.*, 1992), integrated virus-cell junctions would be present at comparatively lower numbers in the liver, as integrations were rare occurrences expected to occur once in every ~2.5 ng of DNA (as shown in Section 6.3.6).

Much additional work could be done and improvements could be made to reduce the levels of DHBV RI DNA and cccDNA extracted from the liver tissue, in order to increase the amount of integrated virus-cell junctions detected. Chapter 5.1 explored several selective DNA extraction methods, and found that low melting temperature agarose gel electrophoresis and purification of high MW cellular DNA (Section 2.6.4) was efficient in removing most of the DHBV RI DNA and cccDNA. Thus, this step was performed in most subsequent invPCR assays in this thesis. In addition, other DNA extraction methods could also be explored, for instance the single nuclei sorting and DNA extraction method using the MoFlo cytometer and high speed cell sorter Cytomation (MoFlo, USA) (Zhang *et al.*, 2003). By first isolating the nuclei of the hepatocytes, this would remove most of the DHBV RI DNA present in the hepatocyte cytoplasm. However, the DHBV cccDNA would still be present in the nuclei and thus would also be extracted during subsequent DNA extractions.

To specifically target the majority of virus-virus false positives detected in these studies, all the sequenced virus-virus fragments could be compiled and analysed to try and identify any sequence similarities as well as any potential common mutations or quasispecies. This would provide information and further understanding as to whether these virus-virus junctions were artefacts during the DNA inversion process, or were detected due to base mutations to escape restriction enzyme digestion, or non-specific primer bindings. Based on the information obtained, it will thus be possible to redesign more specific primers, in addition to choosing cccDNA destroying enzymes that could digest the majority of the virus-virus fragments formed, to subsequently prevent their amplification during nested PCR. More than one cccDNA destroying enzymes could also be used to ensure more thorough digestions of DHBV DNA. However, this would increase the possibilities for digestion of the duck insert DNA, and thus may end up reducing the number of integrated virus-cell junctions detected.

On the other hand, Chapter 5.2 explored the use of locked nucleic acid (LNA) oligonucleotides to block the amplifications of DHBV DNA, which due to the high cost of LNA synthesis, could not be routinely used in this thesis. If alternative cheaper LNA oligonucleotides, or any other oligonucleotides with similar properties could be found, this would be a efficient and specific tool to reduce false positives during invPCR assay, without compromising high losses of DNA using selective DNA extraction methods, or compromising on digesting actual integrated virus-cell junctions using cccDNA destroying enzymes.

In summary, the invPCR assays performed in this Chapter were found to be slightly less efficient in detecting integrated virus-cell junctions compared to published studies as well as the invPCR assays performed by Dr. Mason at FCCC. This was not likely due to poor personal laboratory techniques or poor qualities of DNA extracted from liver tissues. Thus, more optimisation may be required for the downstream DNA inversion steps, the nested PCR reaction steps, and the sequencing reaction steps. Future work should also focus on reducing the levels of DHBV RI DNA and cccDNA in the DNA extracted from liver tissues, in order to reduce the levels of virus-virus false positives detected during invPCR assays.

6.7. Conclusion

In conclusion, invPCR assays specific for the detection of integrated virus-cell junctions in DHBV-infected duck liver tissues were established. DNA was extracted from liver tissues using the total DNA extraction method, followed by low melting temperature agarose gel electrophoresis and purification of high MW cellular DNA. The duck D3 invPCR assay, designed to detect the left hand end integrated virus-cell junction was then performed.

During the establishment of invPCR assays, 17 integrated virus-cell junctions were detected in 3 chronic DHBV-infected duck liver tissues. Preliminary invPCR assays performed on 12 acute DHBV-infected duck liver tissues detected only 1 integrated virus-cell junction; while 20 integrated virus-cell junctions were detected from 11 antiviral-treated chronic DHBV-infected duck liver tissues. A total of 3 hepatocytes clones at least 2 cells in size were detected. The most probable 5' end of the DHBV dslDNA was found to be at 2537 nt, while the most probable 3' end of the DHBV dslDNA was found to be at 2470 or 2478 nt, and it was found that the DHBV integration sites in the duck genome was random.

However, the invPCR assays performed may be slightly less efficient in detecting integrated virus-cell junctions compared to published studies as well as the invPCR assays performed by Dr. Mason at FCCC. Thus, more work would be required to improve the DNA inversion steps, the nested PCR reaction steps, and the sequencing reaction steps during invPCR assay, in addition to exploring more methods to reduce the levels of virus-virus false positives detected during invPCR assays.

Legend for Table 6.1

To detect integrated virus-cell junctions, DNA was extracted from duck liver tissues as described in Section 6.3.4, duck invPCR assays were performed as described in Section 6.3.5, and the invPCR assay products were analysed as described in Section 6.3.6.

[a]Liver DNA were extracted from duck liver tissues using one of the 4 extraction methods described in Section 6.3.4.

[b]InvPCR assays were designed specifically based on the AusDHBV sequence (GenBank Accession AJ006350) as described in Section 6.3.3, and summarised in Table 2.3.

[c]Total nested PCR reactions refers to the total number of nested PCR reactions performed in individual PCR wells.

[d]The amount of DNA analysed was estimated according to the amount of inverted DNA added per PCR reaction, which were based on the amount of liver used during DNA extraction as calculated in Section 2.8.9.3.2. As losses of DNA were expected during extraction and inversion steps, a 50% loss of DNA were included in the calculations.

[e]From all the nested PCR reactions performed, only reactions that produced clear invPCR product bands were extracted from the agarose gel and sequenced. The number of total invPCR products observed on agarose gels was not shown. The number of sequencing reactions that failed to produce a readable product was also not shown.

[f]An example of an integrated virus-cell junction is shown in Figure 6.3A.

[g]An example of a virus-virus false positive sequence is shown in Figure 6.3B.

[h]Unknown sequences are defined as having insert DNA that were either too short (<15 bp) or did not show homology to any known sequences during the BLAST searches.

Table 6.1: Summary of the invPCR assay products detected using chronic DHBV-infected duck liver tissues during the establishment of the duck invPCR assay.

No.	DNA extraction[a]	Duck	InvPCR assay design[b]	Total nested PCR reactions[c]	Total amount of DNA analysed (ng)[d]	Number of invPCR products sequenced[e]	Integrated virus-cell junctions detected[f]	Virus-virus junctions detected[g]	Unknown sequences detected[h]
1	Total DNA extraction	Pool 7	D1	168	1170.0	31	2	28	0
2			D2	252	540.0	48	0	43	0
3			D3	682	5756.0	185	2	151	5
4			D4	168	260.0	39	1	34	0
5		DM32:33	D3	612	3805.0	68	1	34	21
6			D4	420	287.8	36	0	34	0
7	DNeasy blood and tissue kit	Pool 7	D2	84	1265.0	3	0	2	1
8	High molecular weight DNA extraction II	Pool 7	D2	252	75.5	52	7	34	0
9		DM30:31	D1	84	290.0	10	0	5	3
10			D2	168	875.0	9	0	4	1
11	Nuclear DNA extraction	Pool 7	D3	540	3018.0	189	4	125	0
12		DM32:33	D3	180	2080.0	67	0	55	0
Total				**3610**	**19422.3**	**737**	**17**	**549**	**31**

Table 6.2: Summary of integrated virus-cell junctions detected from the duck invPCR assays shown in Table 6.1.

No[a]	Virus junction 1	Virus junction 2	Insert DNA size (bp)	BLAST homology	GenBank Accession	Nucleotide position (5' – 3')
1	2478	1881	315	*Anas platyrhynchos* major histocompatibility complex class I region	AY885227.1	33430-33159
	2470	1882	26	*Pan troglodytes* BAC clone CH251-272H6 from chromosome 17	AC193771.2	159168-159136
3	2572	3027	45	*Xanthomonas perforans* genes for amino acid transporter, hypothetical protein, bacteriocin-B	AB302849.1	5925-5881
	2590	3027	74	*Nematostella vectensis* NEMVEscaffold_306 genomic scaffold	NW_001834108.1	29932-30005
4	2542	ND[b]	291	Chicken c-myb proto-oncogene 5'region exons 1-5	GGMYB15	8066-7799
5	2535	3027	16	*Schistosoma mansoni* strain Puerto Rico chromosome 4	HE601627.1	30378754 - 30378769
8	2651	2906	21	*Gallus gallus* BAC clone CH261-10O11 from chromosome z	AC186363.2	39958-39943
	2655	2908	27	*Arabidopsis thaliana* chromosome 1 BAC F23A5 sequence	F23A5	43678-43696
	2583	2875	20	*Homo sapiens* BAC clone RP11-439K15 from 4	AC098593.2	101198-101215
	2841	2898	18	*Monodelphis domestica* similar to LOC446287 protein	XM_001380266.1	88-72
	2524	2909	18	*Oryza sativa* (japonica cultivar-group) genomic	AP008216.1	15502962 - 15502947
	2653	2909	18	*Gallus gallus* similar to T-Brain-1 (LOC429029	XR_026840.1	172-159
	2653	2883	51	*Aeromonas salmonicida* subsp. salmonicida A449	CP000644.1	792937-792961

Table 6.2 continued

11	2608	38	151	*Anas platyrhynchos* major histocompatibility complex class I region	AY885227.1	33396-33245
	2608	38	157	*Anas platyrhynchos* major histocompatibility complex class I region	AY885227.1	33396-33243
	2515	3027	62	*Anas platyrhynchos* 28S ribosomal RNA gene	EF552792.1	572-633
	2535	3027	22	*Trypanosoma brucei gambiense* DAL972 chromosome 8	FN554971.1	2118990-2118973

DNA was extracted from duck liver tissues as described in Section 6.3.4, followed by duck invPCR assays performed as described in Section 6.3.5, and analysis of invPCR assay products as described in Section 6.3.6.

The yellow coloured highlights show the group of repeated integrated virus-cell junctions.

[a]The invPCR assay numbers are based on Table 6.1. The integrated virus-cell junction in assay 5 was detected in duck DM32:33, while all the rest were detected in Pool 7 duck liver tissues.

[b]The virus junction was not detected (ND) in the DNA sequence.

Legend for Table 6.3

DNA was extracted from duck liver tissues using the total DNA extraction method as described in Section 2.6.3, duck D3 invPCR assays were performed as described in Section 2.10, and the invPCR assay products were analysed as described in Section 2.8.12.

[a]Duck liver tissues used were collected from previous studies as described in Sections 6.4.1.1 and 6.4.2.1.

[b]Total invPCR reactions refers to the total number of nested PCR reactions performed in individual PCR wells.

[c]The amount of DNA analysed was estimated according to the amount of inverted DNA added per invPCR reaction, which were based on the amount of liver used during DNA extraction as calculated in Section 2.8.9.3.2. As losses of DNA were expected during extraction and inversion steps, a 50% loss of DNA were included in the calculations.

[d]From all the nested PCR reactions performed, only reactions that produced clear invPCR product bands were extracted from the agarose gel and sequenced. The number of total invPCR products observed on agarose gels was not shown. The number of sequencing reactions that failed to produce a readable product was also not shown.

[e]An example of an integrated virus-cell junction was shown in Figure 6.3A.

[f]An example of a virus-virus false positive junction was shown in Figure 6.3B.

[g]Unknown sequences were defined as insert DNA that were either too short (<15 bp) or did not show homology to any known sequences during the BLAST searches.

[h]Total DNA extraction from the liver were performed by our collaborator Dr. William Mason at FCCC, USA. The duck D5 invPCR assay design (Table 2.3) was performed.

Table 6.3: Summary of the invPCR assay products detected using DHBV-infected duck liver tissues during preliminary duck invPCR assays.

No	Duck[a]	Total nested PCR reactions[b]	Total amount of DNA analysed (ng)[c]	Number of invPCR products sequenced[d]	Integrated virus-cell junctions detected[e]	Virus-virus junctions detected[f]	Unknown sequences detected[g]
	Acute DHBV-infected ducks						
	Vaccinated						
1	CQ4B.1-4 dpi	90	265	0	0	0	0
2	CQ4B.1-14 dpi	90	335	7	0	7	0
3	CQ4B.1-31 dpi	90	2520	0	0	0	0
4	CQ4B.4-4 dpi	90	510	5	0	1	0
5	CQ4B.4-14 dpi	90	335	0	0	0	0
6	CQ4B.4-31 dpi	90	610	1	0	0	0
	Antiviral drug treated						
7	GR134	168	4660	34	0	24	3
8	GR136	78	6575	15	1	13	0
9	GR137	78	8750	12	0	9	1
10	GR140	54	8010	9	0	5	1
11	GR141	54	7475	7	0	4	0
12	GR142	54	8590	4	0	2	0
	Chronic DHBV-infected ducks						
	Antiviral treatment started at 5 dpi						
13	HT102/149	180	130	18	0	14	0
14	HT103/132	90	60	13	0	13	0
15	HT106/129	90	70	14	0	12	0
16	HT115/128	90	85	21	0	18	1
17	HT122/131	90	55	9	0	8	0
	Antiviral treatment started at 14 dpi						
18	FN1	360	700	35	13	7	9
19	FN2	360	1455	19	0	11	6
20	FN3	360	1710	34	7	8	14
21	FN76	270	100	0	0	0	0
22	FN77	90	170	0	0	0	0
23	FN78	90	42	0	0	0	0
	Non-treated						
24	2069[h]	168	200.0	13	0	7	1
25	2072[h]	336	600.0	26	0	2	19
	Total	**3600**	**54,012**	**296**	**21**	**165**	**55**

Table 6.4: Summary of integrated virus-cell junctions detected from the duck invPCR assays as summarised in Table 6.3.

No [a]	Virus junction 1	Virus junction 2	Insert DNA size (bp)	BLAST homology	GenBank Accession	Nucleotide position (5' – 3')
8	2653	411	21	*Leishmania* major strain Friedlin complete genome, chromosome 25	FR796421.1	295225-295209
18	2537	3027	122	*Aspergillus fumigatus* Af293 chromosome 6	NC_007199.1	232626-232554
	2537	3027	118	*Aspergillus fumigatus* Af293 chromosome 6	NC_007199.1	232626-232554
	2681	3027	181	*Anas platyrhynchos* microsatellite DNA, locus CAM047	FR750429.1	769-708
	2537	3027	52	*Escherichia coli* 536, complete genome	NC_008253.1	8016-8067
	2640	3027	330	*Plasmodium vivax* SaI-1 scf_6908 genomic scaffold	NW_001850074.1	1097-856
	2537	3027	114	Human G protein-coupled receptor gene	HSU13667	35-/-1308[b]
	2537	2037	247	*Mus musculus* transketolase gene	MMU90889	15446-15224
	2534	3027	102	*Schistosoma mansoni* strain Puerto Rico chromosome W Zebrafish DNA sequence from clone CH73-48E2	HE601631.1 FP340248.7	52123552-52123524 72728-72700
	2534	3027	294	*Bos taurus* breed Hereford chromosome 19	NC_007317.5	49249936-49250125
	2523	3027	325	*Plasmodium vivax* SaI-1 scf_6908 genomic scaffold	NW_001850074.1	264-/-715
	2523	ND[c]	1056	*Cryptosporidium hominis* TU502 chromosome 5 CHRO015097	NW_666290.1	203-890
	2537	3027	504	*Bacillus cereus* m1550 chromosom	NZ_CM000722.1	5191062-5191286
	ND	3027	55	*Dictyostelium discoideum* AX4 chromosome 6 chromosome	NC_007092.3	2002146-2002093

Table 6.4 continued

20	2537	3027	272	*Escherichia coli* 'BL21-Gold(DE3)pLysS AG' chromosome	NC_012947.1	3012287-/-3025512
	2537	3027	271	*Escherichia coli* 'BL21-Gold(DE3)pLysS AG' chromosome	NC_012947.1	3012287-/-3025512
	2535	3027	338	*Gallus gallus* breed Red Jungle fowl	NC_006088.3	175800208-17580053 9
	2521	3027	482	*Gallus gallus* breed Red Jungle fowl	NC_006111.3	4307784-4308033
	2537	3027	223	*Prevotella nigrescens ATCC 33563 genomic scaffold*	NZ_GL982482.1	238-6
	2537	3027	20	*Zebrafish DNA sequence from clone CH211-112K18*	BX276117.5	87784-87800

DNA was extracted from duck liver tissues as using the total DNA extraction method as described in Section 2.6.3, duck D3 invPCR assays were performed as described in Section 2.10, and the invPCR assay products were analysed as described in Section 2.8.12.

The coloured highlights show the different groups of repeated integrated virus-cell junctions.

[a]The invPCR assay numberings were based on Table 6.3.

[b]The virus junction was not detected (ND) in the DNA sequence.

[c]The symbol "-/-" was used when the nucleotide positions of the insert DNA had gaps (not continuous).

Table 6.5: Summary of the invPCR assay products detected by Dr. William Mason using DHBV-infected duck liver tissues.

No	Duck[a]	invPCR assay design[b]	Total nested PCR reactions[c]	Total amount of DNA analysed (ng)[d]	Number of invPCR products sequenced[e]	Integrated virus-cell junctions detected[f]	Virus-virus junctions detected[g]	Unknown sequences detected[h]
1	FN1	D3	192	325.8	23	1	13	4
2	FN76	D3	192	67.3	0	0	0	0
3	Pool 7	D3	96	9	20	6	13	0
4		D4	96	9	62	15	42	0
5	2069[i]	D5	N/A[j]	N/A	41	6	21	5
6	2072[i]	D5	N/A	N/A	40	4	15	15
Total			**576**	**477.2**	**186**	**21**	**105**	**34**

DNA was extracted from duck liver tissues using the total DNA extraction method as described in Section 2.6.3, followed by low melting temperature agarose gel electrophoresis and purification of high MW cellular DNA as described in Section 2.6.4. Duck invPCR assays were performed as described in Section 2.10, and the invPCR assay products were analysed as described in Section 2.8.12.

[a]Duck liver tissues used were described in Sections 6.4.1.1 and 6.4.2.1.

[b]InvPCR assays were designed specifically based on the AusDHBV sequence as described in Section 6.3.3, and summarised in Table 2.3.

[c]Total invPCR reactions refers to the total number of nested PCR reactions performed in individual PCR wells.

[d]The amount of DNA analysed were estimated according to the amount of inverted DNA added per invPCR reaction, which were based on the amount of liver used during DNA extraction as calculated in Section 2.8.9.3.2.

[e]From all the nested PCR reactions performed, only reactions that produced clear invPCR product bands were extracted from the agarose gel and sequenced. The number of total invPCR products observed on agarose gels was not shown. The number of sequencing reactions that failed to produce a readable product was also not shown.

[f]An example of an integrated virus-cell junction is shown in Figure 6.3A.

[g]An example of a virus-virus false positive sequence is shown in Figure 6.3B.

[h]Unknown sequences were defined as insert DNA that were either too short (<15 bp) or did not show homology to any known sequences during the BLAST searches.

[i]DNA was extracted from liver tissues by Dr. William Mason in FCCC, USA.

[j]Information was not available (N/A).

Figure 6.1: Multiple sequence alignment showing the sequenced ~1 kbp region of the DHBV genome from Pool 7 and DM30:31 duck liver and Pool 8 duck serum aligned with AusDHBV (GenBank Accession AJ006350, REGION: 2520 – 407), to determine the most probable left and right hand end junction of the integrated DHBV DNA.

The PCR product was amplified from DNA extracted from Pool 7 and DM30:31 duck liver tissues and Pool 8 duck serum using primer set DHBV preC F – DHBV C R (refer to Table 2.2), and sequenced as described in Section 6.3.2. The multiple sequence alignment was performed using ClustalW2 program and output file viewed and arranged by Jalview program as described in Section 2.8.12.

Individual alignment scores of the AusDHBV sequence with other three sequenced PCR products were obtained using BLAST Align 2 Sequences programme as described in Section 2.8.12. The scores include: 100% coverage and 99% sequence similarity (excluding gap regions) for the Pool 7 sequence; 99% coverage and 99% sequence similarity (excluding gap regions) for the DM30:31 sequence; 99% coverage and 99% sequence similarity (excluding gap regions) for the Pool 8 sequence.

Note:
REGION refers to the specific region of nucleotide sequence that was used for alignment in this multiple sequence alignment, and was based on the nucleotide numbering obtained from the AusDHBV (GenBank Accession AJ006350) sequence. REGION was chosen to match with the range of the other DHBV sequences. The numbers shown in the multiple sequence alignment output figure refers to the nucleotide numbering of the specified REGION.

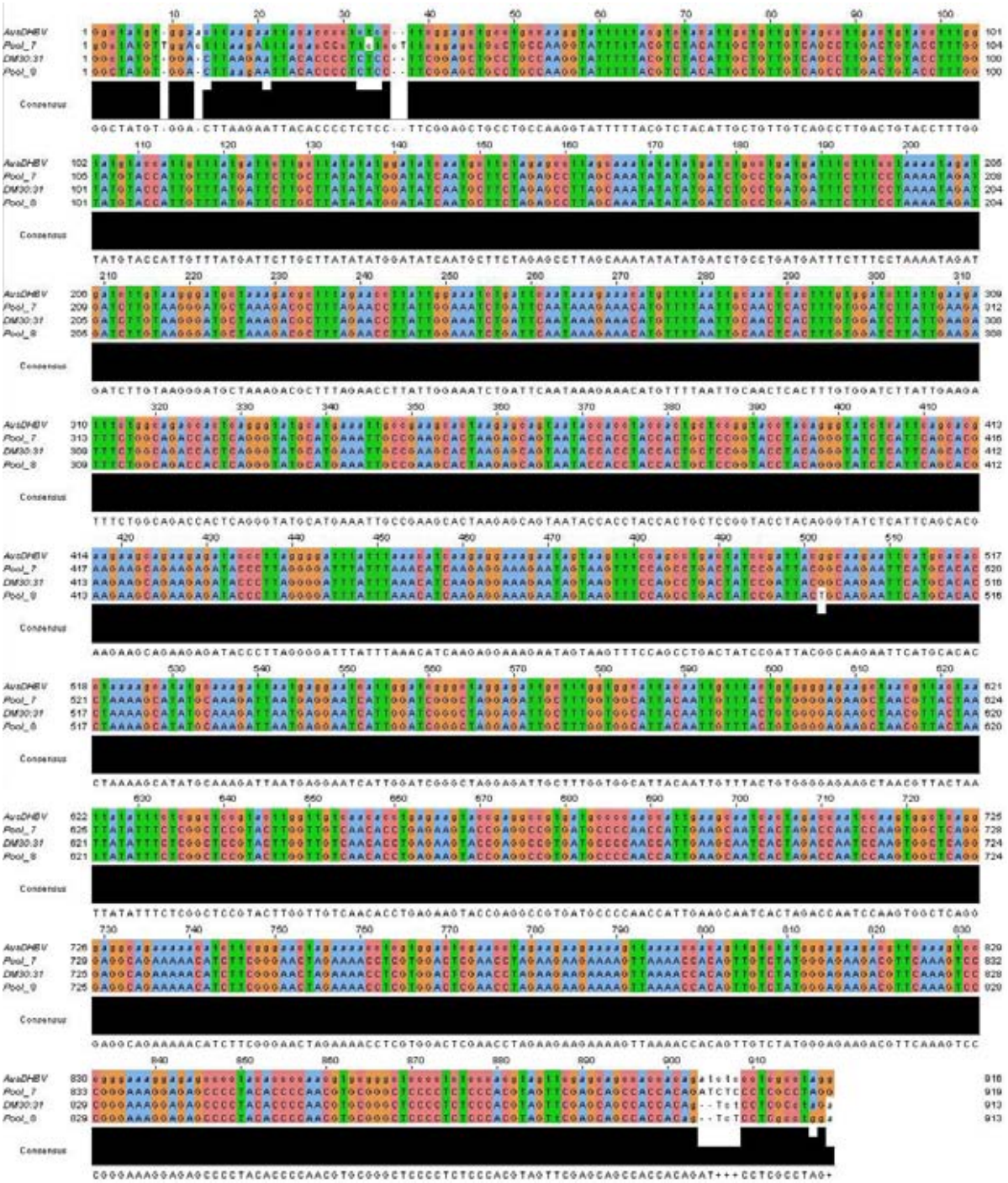


Figure 6.1

Figure 6.2: Examples of invPCR products obtained from the duck invPCR assays.

DNA was extracted from duck liver tissues as described in Section 6.3.4, and inverted as described in Section 6.3.5. The inverted DNA fragments were either 1/3 serially diluted in the 96-well PCR tray as shown in Figure 2.8 (Figure 6.2A), or was distributed evenly to all 96 PCR wells (Figure 6.2B), as DNA templates during nested PCR. invPCR products were visualised using 96-well agarose gel electrophoresis under 302 nm UV light.

The letters A – H refer to the rows of the PCR wells. The DNA marker used (at the lanes labelled "m") was 1 μg of the GeneRuler 1 kb Plus DNA Ladder (Thermo Fisher Scientific, Canada). Wells H7 – H12 (marked by red box) that did not contain any DNA templates were used as PCR negative controls (-ve).

Based on Figure 6.2A, the optimal amount of inverted DNA fragment that can produce a single invPCR product in most of the PCR wells, was the amount of DNA in between Rows E and F.

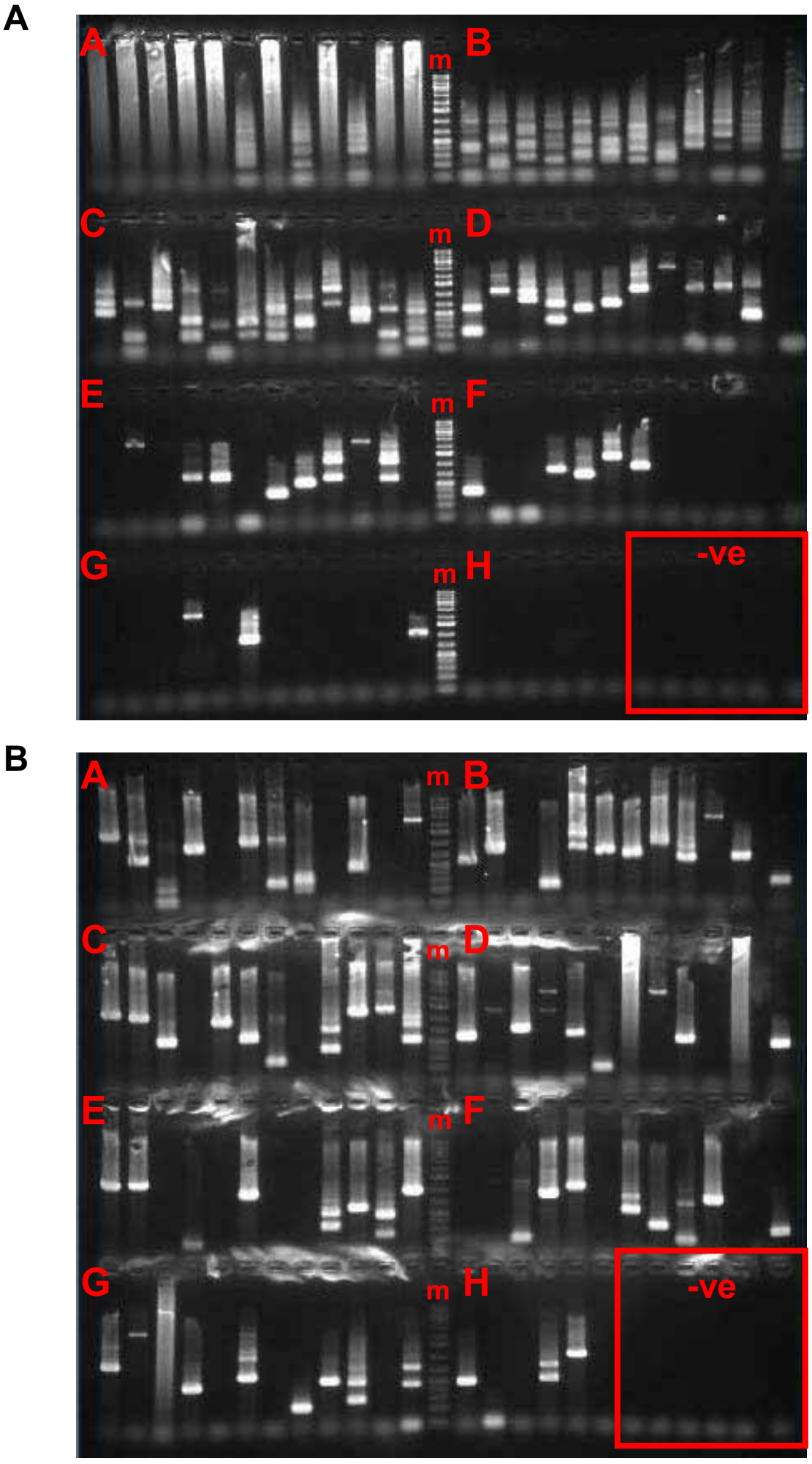


Figure 6.2

Figure 6.3: Example of DNA sequencing results obtained from the duck D3 invPCR assay.

DNA was extracted from duck liver tissues as described in Section 6.3.4, and duck D3 invPCR assays were performed as described in Section 6.3.5.

Figure 6.3A shows an example of the DNA sequencing results for an integrated virus-cell junction. BLAST analysis showed that the 472 bp sequence consisted of a 332 bp insert DNA (blank font) flanked by the DHBV genome (GenBank Accession AJ006350) 2654 – 2535 nt (blue bold font) and 3027 – 3011 nt (red bold font) at the *Eco*RI first cut restriction enzyme site (underlined). This was consistent with the expected inverted DNA fragment that will be produced by the duck D3 invPCR assay design (refer Figure 6.4). 2535 nt is known as virus junction 1, and 3027 is known as virus junction 2. Further BLAST analysis showed that the insert DNA shared homology with the *Gallus gallus* (chicken) breed Red Jungle fowl (GenBank Accession NC_006088.3).

Figure 6.3B shows an example of the DNA sequencing result for a virus-virus sequence, which was a false positive result. BLAST analysis showed that the 817 bp sequence consisted of 2 fragments of the DHBV genome (GenBank Accession AJ006350), 2675 – 1872 nt (blue bold font) and 3027 – 3011 nt (black bold font), joined at the *Eco*RI restriction enzyme site (underlined). This shows that the virus-virus false positive sequence was likely to be formed by the ligation of 2 DHBV DNA fragments that were digested by *Eco*RI.

A

ATATATAAGCAAGAATCATAAACAATGGTACATACCAAAGGTACAGTC
AAGGCTGACAACAGCAATGTAGACGTAAAAATACCTTGGCAGGCAGCT
CCGAAGGAGAGGGGTGTAATTCTTCTGATTCACCTTCTCACTTAAAGT
AGTTTATTGTACTACATTATTACTAATTTCAGGCTTTAAACATTTCAT
TTTTGAGTAGCCTTCTTGAAACAAATGTCAGATTCACATTCTTCAAAA
TATTTTCCATAAAAAGAAACATGAAACAATGGAAGAAACAACAACGTC
CCACTGAAATTCTTATATTTTTAAATAAGATTTCTCATCCATTAACAT
AATTCAGTCCTCCTTGTTACCTTCCTTTTTACTGAGATATCTCTTTAG
GAAAAGATTTGCACCCCTGAAATTCAGTAAAGGTTCACAGATCGCACA
ATACAAGTGCTCGCTGTACTGAATTCTTGCCGTAATCGAA

B

GCTCTAGAGCATTGATATCCATATATAAGCAAGAATCATAAACAATGG
TACATACCAAAGGTACAGTCAAGGCTGACAACAGCAATGTAGACGTAA
AAATACCTTGGCAGGCAGCTCCGAAGGAGAGGGGTGTAATTCTTAAGT
TCCACATAGCCTATGTGGAATATATATTGCTTTCGAGAGAGGGGTGTA
TGTAAGAGCCGTCCAATCAGGCGGTTTGTGCCTGGATGGGCCGTCAGC
AGGATTATATTTACTCGGAACAAAGTACAATTGTATAGGAGATAACAA
TTGTTTGGCCAACATAGCAAAATGCCATGGTAACGTCTGATAACGTTT
GTGACAAACAAAGGTAGAATCGGAAAGTATACATCTGGGTTTAATCAT
TATCCTAGCTAAACATACCATCAGCAATTCCTGTATATGTATATCTCT
GACCTTTGAAAAAGCAAACACTGCGCTCCCGCCGGTGATATGGGATAT
TGCGCCATGTGTTGGAGTAGCATCTGTGGCTACACGTGGCAAAGGTAC
AGAGGACTTTGGTCTAATGGCTAATTTACAAACACCCATGGTTAGTTT
ATACAATAAAGTCCTATATGCAGAAGAGAAGCTAAAGTTAACTTTGTT
AGTAATAGCAGCATACATTGGTTTTAACATTTCAATATTACCCTTAGT
GAAAGGTAACACGAAATTCAAATGCCCGACAAATCTTTGAATACATTT
CCAATCATACCACGCGCCAATTTTTATTTTCTTAATAACAGTCCTTAA
TTCTTTCCATCTGCTTTCTTCGATCTTCATGAATTCTTGCCGTAATCG
A

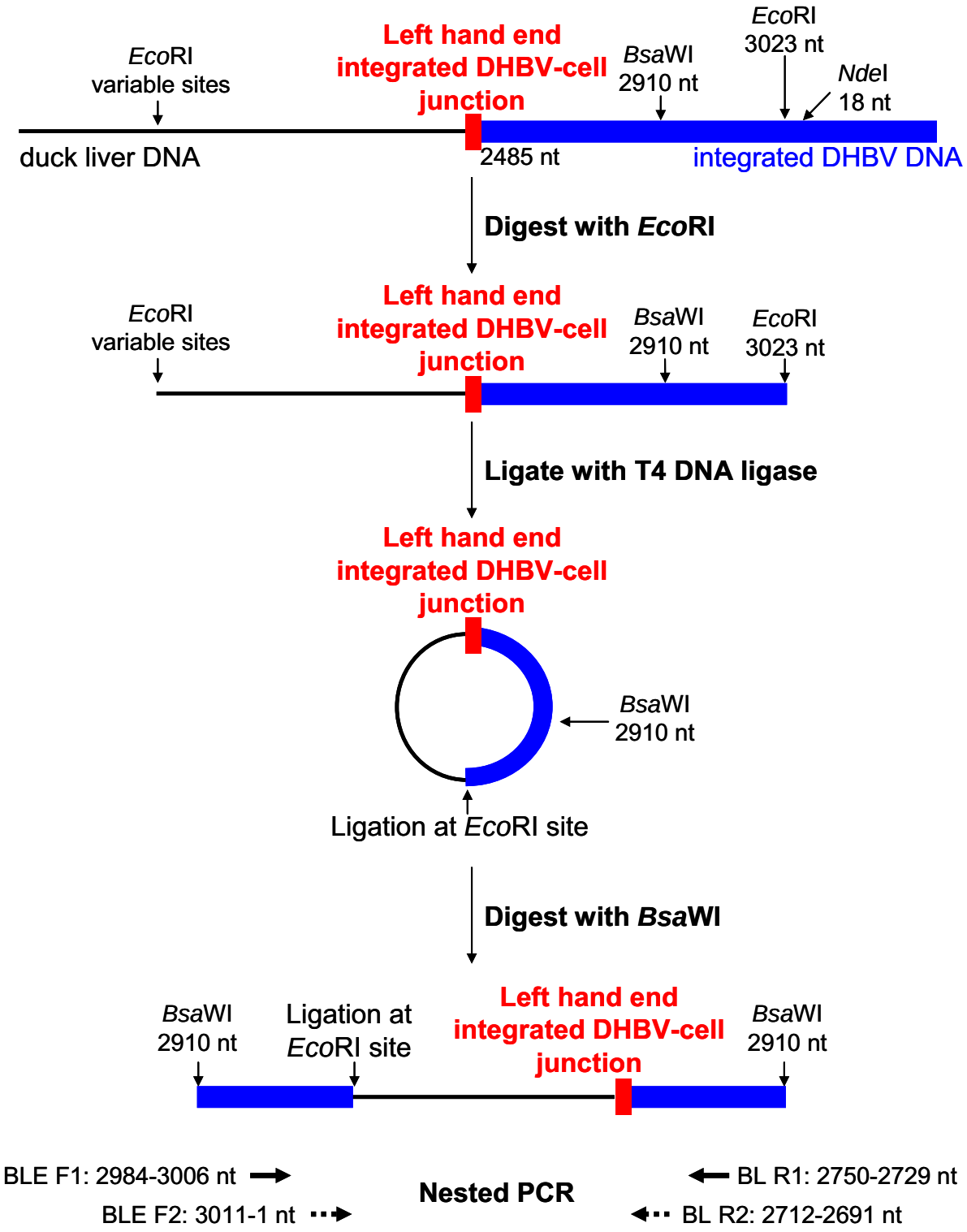


Figure 6.4: Schematic representation of the duck D3 invPCR assay design, showing the DNA inversion process, and the nested PCR reaction primer binding sites.

The DHBV invPCR assays specific for the detection of integrated virus-cell junctions were designed as described in Section 6.3.3 based on the AusDHBV genome (GenBank Accession AJ006350).

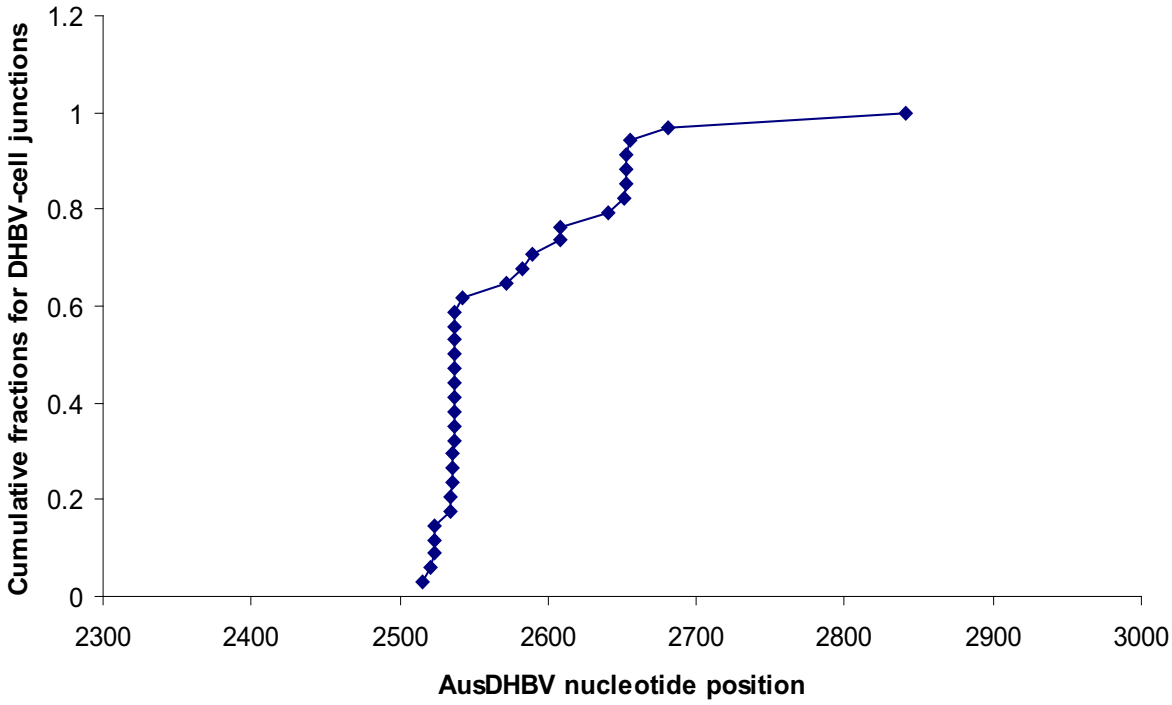


Figure 6.5: Distribution map of the left hand end (5' end) of the DHBV dslDNA detected using the invPCR assays.

The left hand end of the DHBV dslDNA is the 5' end DHBV nucleotide that joined to the duck genome during integration, forming the integrated virus-cell junction. The data was a compilation of 36 left hand end integrated virus-cell junctions detected from DHBV-infected duck liver tissues using the invPCR assay in this Chapter.

Chapter 7: The use of invPCR assays to explore the mechanisms involved in clearance of DHBV-infected hepatocytes during acute DHBV infection

7.1. Aims

a) To establish and monitor acute DHBV infection in ducks.
b) To characterise histological and serological changes occurring during various stages of acute DHBV infection.
c) To detect integrated virus-cell junctions during various stages of acute DHBV infection using the invPCR assay.
d) To determine the mechanisms involved in clearance of DHBV-infected hepatocytes during acute DHBV infection.

7.2. Introduction

As mentioned in Chapter 1, acute HBV infection occurs when an individual infected with HBV clears HBsAg from the serum and develops anti-HBs antibodies within 6 months after infection (Andersson and Dienstag, 2008). It is now clear that HBV may not be completely cleared during the resolution of acute HBV infection, and traces of HBV DNA and antigens are often still present. HBV may reactivate if the person becomes severely immunosuppressed (Raimondo *et al.*, 2007). As the DNA that persists in the liver is predominantly in the cccDNA form (Michalak *et al.*, 1999; Le Mire *et al.*, 2005), and since cccDNA is the main template for transcription of HBV pregenomic RNA and other mRNA forms (Summers and Mason, 1982), it is therefore essential to clear all traces of HBV cccDNA from the nucleus in order to achieve complete resolution of HBV infection.

The exact mechanisms of clearance of HBV cccDNA from infected hepatocytes are still relatively undetermined. As discussed in Section 1.6, two mechanisms have been proposed for clearance of cccDNA. The first mechanism is cytolytic hepatocyte killing, involving HBV-specific CTL attack on infected hepatocytes and killing of the infected hepatocyte population, thus destroying all HBV DNA and antigens contained within the infected hepatocytes. The second mechanism is non-cytolytic hepatocyte curing, where HBV RI DNA, cccDNA and antigens are removed by the action of inflammatory antiviral cytokines without physically killing the infected hepatocytes. The cytokines involved include IFN-β and IFN-γ (Wieland *et al.*, 2005), secreted mainly by CTL and NK cells (Visvanathan, 2008).

It is important to gain further understanding of the possible mechanisms of clearance of cccDNA from infected hepatocytes, as this may assist in the development of new antiviral therapies for chronic HBV infection. As discussed in Section 1.5.2, current antiviral therapies include pegylated IFN-α, and a range of antiviral drugs that include the nucleoside and nucleotide analogues ETV, TFV, adefovir, and lamivudine (Lai *et al.*, 2002; Dienstag, 2008). Although these antiviral drugs efficiently prevent further HBV replication, pre-existing pools of cccDNA in the nucleus are not directly targeted (Krastev, 2006). This not only results in an inability of these antiviral therapies to clear HBV infection, but the persistence of cccDNA would pre-dispose for rebound of HBV infection after discontinuation of treatment (Osborn and Lok, 2006). It is hoped that by determining whether cytolytic hepatocyte killing or non-cytolytic hepatocyte curing are involved in the removal of cccDNA, new therapies can be developed to focus on activation of HBV-specific CTL and NK cells that have the capacity to cytolytically kill the HBV-infected hepatocytes, or on boosting the immune response to produce cytokines that have the ability to non-cytolytically cure HBV-infected hepatocytes.

Therefore, the studies described in this Chapter aim to determine the mechanisms of DHBV RI DNA and cccDNA clearance from DHBV-infected hepatocytes, to observe whether cytolytic hepatocyte killing or non-cytolytic hepatocyte curing play a greater role during the clearance of acute DHBV infection. This study focuses on using the invPCR assay to detect integrated virus-cell junctions present in the duck liver during the course of acute DHBV infection. As mentioned in Section 1.8, the unique integrated virus-cell junctions can be used as genetic markers for individual infected hepatocytes, allowing the fate of the individual hepatocytes to be tracked during various stages of acute DHBV infections.

Several studies have used integrated WHV-cell junctions in woodchucks with acute WHV infection in order to determine the mechanisms of clearance of WHV-infected hepatocytes. However, those studies, some of which are described below, showed conflicting conclusions. In the studies performed by Summers *et al.*, integrated virus-cell junctions were detected in 3 woodchucks with acute WHV infection at 16 weeks post infection. Out of a total of 129 integrated virus-cell junctions detected, 69 of the junctions were unique, corresponding to a junction complexity of 0.53. Using mathematical modelling and calculations, these corresponded to ~1.8 complete turnovers of the population of infected hepatocytes, of which >95% of hepatocytes were WHV-DNA positive at 4 and 8 dpi. Furthermore, the copy number of unique integrated virus-cell junctions had increased as the hepatocytes had clonally proliferated to replace the killed hepatocytes, forming hepatocytes clones larger than 4 cells in size. Hence, these findings suggest that cytolytic hepatocyte killing was significant and

directly involved in the clearance of WHV infection (Summers *et al.*, 2003). On the other hand, in studies performed by Mason *et al.*, integrated virus-cell junctions were detected in 2 groups of woodchucks with acute WHV infection. The first group, Group 1, had 4 woodchucks which were not drug treated, while the second group, Group 2, had 3 woodchucks which were treated orally with 0.5 mg/kg/day of ETV to inhibit WHV replication from 4 or 7 weeks post infection. In all woodchucks, at 2 weeks post infection, >95% of the hepatocytes in the liver were found to be WHV DNA-positive, but this level dropped to <0.002% at 16 weeks post infection. In the Group 1 untreated woodchucks, at 16 or 19 weeks post infection, out of a total of 1019 integrated virus-cell junctions detected, 385 of the junctions were unique, corresponding to a junction complexity of 0.41. On the other hand, in the Group 2 ETV-treated woodchucks, at 16 weeks post infection, out of a total of 378 integrated virus-cell junctions detected, 278 of the junctions were unique, corresponding to a junction complexity of 0.73. As the junction complexity in the Group 1 untreated woodchucks was lower than the Group 2 ETV-treated woodchucks, these results suggest that greater levels of cytolytic hepatocyte killing would occur when there was a delay in the immune response in inhibiting or reducing the levels of WHV replication. However, using mathematical modelling and calculations, it was found that the levels of hepatocyte turnover in all these woodchucks were more consistent with the levels of hepatocyte turnover expected when non-cytolytic hepatocyte curing of WHV-infected hepatocytes occurs, hence suggesting that that non-cytolytic hepatocyte curing in addition to some cytolytic hepatocyte killing was involved in the clearance of WHV infection (Mason *et al.*, 2009b).

One of the disadvantages of using the WHV-infected woodchuck model, or even the HBV-infected chimpanzee model for these studies, is that acute WHV and HBV infections have relatively long incubation periods and an extended time course of acute WHV and HBV infection (15 – 20 weeks) (Murray *et al.*, 2005; Mason *et al.*, 2009b). In addition, the WHV and HBV infections spread to infect >95% of hepatocytes in the liver during the early stages of infection (Summers *et al.*, 2003; Murray *et al.*, 2005). This means that potentially every hepatocyte could contain an integrated virus-cell junction. Therefore, as there may not be any available uninfected hepatocytes to replace the hepatocytes that were killed during clearance of infection, the complexity of the integrated virus-cell junctions had to be calculated in order to try to determine whether cytolytic hepatocyte killing or non-cytolytic hepatocyte curing had occurred. To complicate things further, as the efficiency of detection of integrated virus-cell junctions using invPCR assay is not always 100%, more mathematical calculations had to be performed to take into account the estimated efficiency of invPCR assays to obtain the "actual" complexity of the population of integrated virus-cell junctions (Mason *et al.*, 2009b).

Currently, there are no related studies in other animal models besides the WHV-infected woodchucks that have been published. It is also extremely difficult to perform this type of study in HBV-infected humans, as it is almost impossible to obtain frequent liver biopsy samples from human patients with acute HBV infection. Hence, the DHBV-infected duck model would be an alternative animal model to provide a more empirical approach for this study. Unlike acute WHV and HBV infections in woodchucks and chimpanzees, DHBV infections have relatively short incubation periods and a short time course of DHBV infection (14 – 30 days) (Reaiche, 2008). The initial percentage of DHBV-infected hepatocytes can also be controlled and limited in ducks by the dose of DHBV inoculated to the ducks as well as the age of the ducks at the time of infection (Jilbert *et al.*, 1998). For instance the intravenous inoculation of 6-week-old ducks with $1.5x10^{10}$ vge of DHBV resulted in only ~3.5% DHBV-positive hepatocytes at 4 dpi (Reaiche *et al.*, 2010). In addition, in the duck model there is greater flexibility to obtain liver biopsy samples at various stages of acute DHBV infection, which is more difficult in woodchucks and chimpanzees and almost impossible for human samples. On top of that, by using 6-week-old ducks, there should be lower levels of normal hepatocyte proliferation occurring due to the growth or expansion of liver mass. Thus, any hepatocyte proliferation observed in the liver would be more likely to be compensatory hepatocyte proliferation to replace neighbouring hepatocytes that were killed.

For the study in this Chapter, DHBV infection will be established in 6-week-old ducks resulting in the infection of <10% of hepatocytes. The invPCR assay will then be used to determine the complexity of the population of integrated virus-cell junctions, or the fraction of unique to total integration junctions detected, during and after the resolution of acute DHBV infection. The D3 duck invPCR assay (Table 2.3) will be performed as established and described in Chapter 6, to detect the left hand end integrated virus-cell junction. As mentioned in Section 6.2, in this thesis, ducks that cleared DHBV infection by 10 dpi are defined as having “acute DHBV infection”, while ducks with widespread DHBV infection from 10 dpi until the last time-point of a study are defined as having “chronic DHBV infection”.

It is expected that during the early stages of acute DHBV infection, there would be a pool of unique integrated virus-cell junctions with a high junction complexity, generated from individual integration events and not due to clonal proliferation of infected hepatocytes. During the resolution of acute DHBV infection, DHBV-infected hepatocytes would then, based on the two mechanisms proposed for clearance of cccDNA described above, either be cytolytically killed, or be non-cytolytically cured. If cytolytic hepatocyte killing occurs, integrated virus-cell junctions would no longer be present in the liver after resolution of acute

DHBV infection, as the individual DHBV-infected hepatocytes would be selectively destroyed and replaced by neighbouring uninfected hepatocytes that do not contain any integrated DHBV DNA. Conversely, if non-cytolytic hepatocyte curing occurs, integrated virus-cell junctions would still be present in the liver after resolution of acute DHBV infection, with similar junction complexities expected before and after resolution of infection. Most of the integrated virus-cell junctions are expected to be present as single copies, since most of the infected cells will not be destroyed and will not proliferate to replace hepatocytes that are being killed. If the infected hepatocytes have proliferated during clearance, the copy number of each unique integrated virus-cell junction could provide an estimation of the extent of hepatocyte proliferation that had occurred in the liver. It should also be noted that some hepatocyte proliferation in this experiment will also occur due to natural growth of the liver, which was estimated using incorporation of proliferating cell nuclear antigen (PCNA) to be around 0.94% – 2.2% per day in 3 – 12-month-old ducks (Reaiche *et al.*, 2010).

There are however, several challenges in this study design. Firstly, the rate of detection of integrated virus-cell junctions in ducks was found in previous studies to be low, at 1 integrated virus-cell junctions per 10^3 – 10^4 cells (Yang and Summers, 1999). Preliminary invPCR assays performed on duck liver tissues in Chapter 6 also only detected 1 integrated virus-cell junction in a total of 48.6 μg of DNA analysed (~$1.9x10^7$ cells calculated as described in Section 2.8.9.3.2). Thus, larger amounts of liver tissue may have to be analysed, and many invPCR assay reactions may need to be performed, in order to be able to detect the rare integrated virus-cell junctions. Secondly, if cytolytic hepatocyte killing occurs, it is expected that no integrated virus-cell junctions would be present in the liver after resolution of acute DHBV infection. Hence, this expected negative result would be hard to verify, as the results may be misinterpreted as unsuccessful invPCR assay reactions.

7.3. To establish and monitor acute DHBV infection in ducks

7.3.1. To establish acute DHBV infection in ducks

Six 6-week-old Pekin-Aylesbury ducks (Section 2.1) were experimentally infected with $1.5x10^{10}$ vge of Pool 8 DHBV virus stock (Section 2.2) as described in Section 2.3.1. This virus dose was chosen based on previous studies, where inoculation of 6-week-old ducks with this viral dose had led to DHBV infection in ~4% – 6% of hepatocytes in the liver by 4 dpi, with ~70% of the inoculated ducks subsequently developed acute DHBV infection, while the remaining ~30% developed chronic DHBV infection (Jilbert *et al.*, 1998; Reaiche, 2008).

In this study, liver biopsy tissues were collected from the ducks at 4 and 18 dpi as described in Section 2.3.3.1. The percentage of DHBsAg-positive hepatocytes was then determined by immuno-staining of DHBsAg in liver tissue sections as described in Section 2.4.2. At 18 dpi, in three ducks (numbered 337, 339, 342), <0.15% of the hepatocytes were DHBsAg-positive (Section 7.3.2.1); while in the other three ducks (numbered 338, 343, 350), >95% of the hepatocytes were DHBsAg-positive. These findings suggest that ducks 337, 339, and 342 developed acute DHBV infection, whilst ducks 338, 343, and 350 developed chronic DHBV infection. Ducks 338, 343 and 350 will be described in detail in Chapter 8.

Ducks 337, 339 and 342 were further monitored until 45 dpi, where liver autopsy tissues were collected as described in Section 2.3.3.2. All collected liver tissues were either snap frozen in liquid nitrogen and stored at -80^{o}C, or fixed in ethanol:acetic acid (EAA), formalin or 70% ethanol, were subsequently embedded and sectioned onto glass microscope slides as described in Section 2.3.4.1, and used for various histological analyses as described in Section 2.4. In addition, DNA was extracted from the liver tissues using the ChargeSwitch gDNA mini tissue kit as described in Section 2.6.2, to determine the levels of DHBV total and cccDNA present in the liver by qPCR as described in Section 2.8.9.2. On top of that, blood samples were obtained twice a week from by venipuncture as described in Section 2.3.2.1, and serum was collected as described in Section 2.3.2.2. Serum was then analysed by ELISA to determine the levels of DHBsAg and anti-DHBc and anti-DHBs antibodies as described in Section 2.5.2 to 2.5.4, and to determine levels of DHBV total DNA by qPCR as described in Section 2.8.9.1.

As there were no control ducks in this study, uninfected duck liver tissue was obtained from a previous study conducted by Dr. Georget Reaiche (Reaiche *et al.*, 2010) for comparison. The duck, designated as duck 138, was hatched from the same commercial hatchery as this study (as described in Section 2.1), and was inoculated with normal duck serum (NDS) at 6 weeks of age, and thus could be used as an uninfected duck control to allow for comparison of age matched ducks with or without DHBV challenge. H&E-staining of formalin-fixed liver tissue sections of duck 138 was previously prepared by Dr. Reaiche (Reaiche *et al.*, 2010). The 3 ducks with chronic DHBV infection described in Chapter 8 would also be used for comparison of events occurring during acute and chronic DHBV infections.

7.3.2. Characterisation of histological and serological changes occurring during various stages of acute DHBV infection

7.3.2.1. DHBsAg-positive hepatocytes in the liver

EAA-fixed and embedded duck liver tissue sections prepared as described in Section 2.3.4.1 were stained with anti-DHBV pre-S monoclonal antibody, 1H.1, as described in Section 2.4.2, to determine the percentage of DHBsAg-positive hepatocytes present. Sections of DHBsAg-stained liver were photographed at each time-point and compiled as Figure 7.1.

DHBsAg-staining (Figure 7.1) showed that at 4 dpi, ducks 337, 339 and 342 had 4.2%, 5.8%, and 3.1% DHBsAg-positive hepatocytes respectively (an average of 4.4%). These results were similar to the average 4.1% DHBsAg-positive hepatocytes found in ducks 338, 343 and 350 that developed chronic DHBV infection (Section 8.3.2.1). At 18 dpi, ducks 337 and 342 had <0.001% DHBsAg-positive hepatocytes while duck 339 had 0.15%. In comparison, the ducks that developed chronic DHBV infection all showed >95% DHBsAg-positive hepatocytes by 18 dpi (Section 8.3.2.1). These findings suggest that acute DHBV infection was established in ducks 337, 339 and 342, as DHBV infection was initially detected in a low percentage of hepatocyte and this was followed by rapid clearance of DHBsAg-positive hepatocytes by 18 dpi. These observations were consistent with the infection outcome observed previously in ducks that developed acute DHBV infection (Jilbert *et al.*, 1998; Reaiche, 2008). Finally by 45 dpi, all ducks had <0.001% DHBsAg-positive hepatocytes, suggesting that resolution of acute DHBV infection had been achieved by 45 dpi.

7.3.2.2. Levels of inflammation in the liver

Formalin-fixed and embedded duck liver tissue sections were H&E-stained, viewed, and analysed as described in Section 2.4.1, to determine the levels of inflammation (portal and lobular) in the liver. The H&E-stained liver tissue sections were photographed at each time-point and compiled as Figure 7.2, with detailed analysis summarised in Table 7.1A.

It is expected that upon DHBV infection the 6-week-old ducks would be able to mount a rapid and strong immune response to control the DHBV infection by 18 dpi, when <0.15% of DHBsAg-positive hepatocytes were present in the liver (Section 7.3.2.1). Previous studies have also reported moderate to severe portal and lobular inflammation in 4-month-old ducks at 12 dpi (Jilbert and Kotlarski, 2000), while 6-week-old ducks showed normal portal and lobular inflammation at 4 dpi, and normal – mild portal and lobular inflammation after clearance of DHBV infection (60 – 316 dpi) (Table 7.1B; Reaiche *et al.*, 2010).

As summarised in Table 7.1A, at 4 dpi, the duck livers showed low levels of inflammation: 0.69% of the liver contained inflammatory cells, portal inflammation (pointed out by black arrows in Figure 7.2) was present in some portal tracts (with areas of portal inflammation up to 10 cells in diameter), and with no observable lobular inflammation. These findings were similar to previous studies (Table 7.1B; Reaiche *et al.*, 2010), suggesting that at 4 dpi, the CMI of the ducks had not been fully activated or were just starting to be activated, in response to the low levels of DHBV infection (an average of 4.4% DHBsAg-positive hepatocytes as shown in Section 7.3.2.1). Vacuolated hepatocytes (pointed out by green arrows in Figure 7.2) were also observed in duck 342, suggesting that steatosis, or accumulation of triglyceride fat droplets in the liver hepatocytes (Crawford, 2007), had occurred. Similar steatosis has been observed in 40% of 8-month-old ducks with chronic DHBV infection and in one 6-week-old uninfected duck (Freiman *et al.*, 1988), and is likely due to liver injury from various non-viral causes, like liver toxicity by Aflatoxins (Mason *et al.*, 1994; Augesse-Germon *et al.*, 1998). As all the ducks in this study were housed together and thus would be exposed to the same environmental toxins, it was likely that duck 342 may be more sensitive or susceptible towards the toxins to result in these liver injuries not observed in the other ducks 337 and 339.

At 18 dpi, the duck livers all showed elevated levels of inflammation: 1.69% of the liver contained inflammatory cells, portal inflammation (pointed out by black arrows in Figure 7.2) was present in most portal tracts (with areas of portal inflammation up to 30 cells in diameter), and scarce patches of lobular inflammation (pointed out by blue arrows in Figure 7.2) in 1 duck (up to 13 cells in diameter). These were similar to results from previous studies (Jilbert *et al.*, 1998), and suggest that CMI responses had been activated, resulting in infiltration of lymphocytes into the liver. It is assumed that the immune response had protected further infection of hepatocytes and successfully cleared the DHBV infection from the liver, as <0.15% of hepatocytes were DHBsAg-positive at 18 dpi (Section 7.3.2.1).

At 45 dpi, the livers of ducks 337 and 339 showed slightly lower levels of inflammation compared to 18 dpi, with an average of 1.26% of the liver containing inflammatory cells; while duck 342 only had 0.61%, similar to levels seen at 4 dpi. However, portal inflammation (pointed out by black arrows in Figure 7.2) was present in some portal tracts (with areas of portal inflammation up to 30 cells in diameter), and scarce patches of lobular inflammation (pointed out by the blue arrows in Figure 7.2) (up to 22 cells in diameter), were observed in liver tissues from all ducks. These were similar to results from previous studies in ducks with acute DHBV infection at 60 dpi (Table 8.1B; Reaiche *et al.*, 2010), suggesting that persistent mild levels of inflammation may be maintained in the liver after clearance of DHBV infection.

When compared to the liver inflammation in the age matched ducks (6-week-old) that developed chronic DHBV infection (ducks 338, 343 and 350 as shown in Table 8.1), at 4 dpi, 2 of the ducks (ducks 338 and 343) showed higher levels of inflammation (but not statistically significant): 1.68% of the liver contained inflammatory cells, portal inflammation was present in some portal tracts (with areas of portal inflammation up to 16 cells in diameter, and scarce patches of lobular inflammation in duck 343 (up to 26 cells in diameter). At 18 dpi, even higher levels of inflammation were also observed in all of the ducks that developed chronic DHBV infection (but still not statistically significant): 2.44% of the liver contained inflammatory cells, large areas of portal inflammation were observed in almost all the portal tracts (with areas of portal inflammation up to 32 cells in diameter), and the frequent presence of lobular inflammation (up to 19 cells in diameter). These were expected, as it was reported that in humans with chronic HBV infection, denser and more extensive portal and lobular inflammation are often observed during chronic HBV infection (Theise *et al.*, 2007). But at later stages of infection, the lower levels of liver inflammation in ducks with acute DHBV infection (45 dpi) were similar to the ducks with chronic DHBV infection (60 dpi).

Interestingly, as shown in Table 7.1B, the uninfected control duck 138 showed that in the absence of DHBV infection, varying levels of inflammation could occur in the liver, with 0.66% of the liver containing inflammatory cells at 4 dpi, and an average of 1.46% from 60 – 316 dpi. The liver tissues also showed persistent portal inflammation in some portal tracts (with areas of portal inflammation up to 18 cells in diameter), but no lobular inflammation was observed. This was consistent with other studies that also found mild portal inflammation in ~33% of the uninfected control ducks (Freiman *et al.*, 1988; Cullen *et al.*, 1989), suggesting that these were normal occurrences in ducks possibly due to environmental exposure. Therefore, as the mild levels of inflammation observed in ducks 337, 339 and 342 was not significantly different compared to uninfected ducks, these suggest that either the infiltration of lymphocytes may not be the key immune response involved during clearance of DHBV infection, or that mild levels of infiltration of lymphocytes were sufficient to clear the DHBV infection. As previous studies found that bursectomized ducks that showed increased levels of inflammation had mostly developed persistent DHBV infection, while thymectomized ducks that showed normal – mild levels of inflammation mostly cleared infection (Vickery *et al.*, 2006), these strongly suggest that the levels of liver inflammation are a poor indicator of the ability of the ducks to clear DHBV infection. Rather, the key to the ability to clear DHBV infection may lie in the quality and specificity of the infiltrating lymphocytes (Vickery *et al.*, 2006), the activation of innate immune responses, the production

of cytokines like IFN-α (Tohidi-Esfahani *et al.*, 2010), and seroconversion to anti-DHBs antibodies (Jilbert and Kotlarski, 2000; Vickery *et al.*, 2006).

7.3.2.3. Levels of hepatocyte apoptosis in the liver

The same H&E-stained duck liver tissue sections described in Section 7.3.2.2 were also viewed using light microscopy to determine the levels of hepatocyte apoptosis. Photographs showing examples of apoptotic cells observed are compiled in Figure 7.3, and findings are summarised in Table 7.2A. It is expected that higher levels of hepatocyte apoptosis would be observed when levels of liver inflammation (Section 7.3.2.2) were elevated and during clearance of DHBV infection (4 – 18 dpi) (Guo *et al.*, 2000), and then return to normal levels after clearance of DHBV infection (45 dpi). This was seen in previous studies where 6-week-old ducks showed 2.1% of apoptotic cells per total hepatocytes at 4 dpi, but only an average of 0.83% after clearance of DHBV infection (60 – 317 dpi) (Table 7.2B; Reaiche *et al.*, 2010).

As shown in Table 7.2A, at 4 dpi, an average of 1.57% of hepatocyte apoptosis were detected (Figure 7.3B). At 18 dpi, there was a slight increase in the levels of hepatocyte apoptosis to an average of 1.94%. This was expected, as all these ducks showed elevated levels of inflammation at 18 dpi (Section 7.3.2.2), which is commonly associated with an increase in apoptosis (Goodman, 2008). These suggest that the duck immune responses had been activated and were actively clearing the DHBV infection by apoptosis. At 45 dpi, the levels of hepatocyte apoptosis reduced back to an average of 1.57%. This was again expected, as the DHBV infection had been successfully cleared in these ducks by 45 dpi, thus only normal levels of apoptosis would be present as the duck immune responses were no longer stimulated.

When compared to the levels of apoptosis in age matched ducks (6-week-old) that developed chronic DHBV infection (ducks 338, 343 and 350 as shown in Table 8.2A), 2 – 3-fold higher (but not statistically significant) levels of hepatocyte apoptosis were observed, with 2.1% and 2.9% of hepatocyte apoptosis at 4 and 18 dpi respectively. At 60 dpi, the levels of hepatocyte apoptosis were significantly higher in ducks with chronic DHBV infection compared to ducks with acute DHBV infection (45 dpi), presumably due to the constant activation of immune responses in the ducks with chronic DHBV infection, while only "basal" levels of hepatocyte apoptosis were occurring in the ducks with acute DHBV infection after resolution of infection.

Interestingly, as shown in Table 7.2B, analysis of the liver tissues from the 6-week-old uninfected control duck 138 showed that the levels of hepatocyte apoptosis varied between 0.54% – 1.26% from 4 – 316 dpi. By taking this as the normal levels of apoptosis in the duck

liver, this further supports that the levels of apoptotic hepatocytes would increase when the immune responses are actively clearing DHBV infection (4 – 18 dpi), although not to statistically significant levels, and return to normal levels after clearance of infection (45 dpi).

7.3.2.4. Levels of Kupffer cell infiltration and activation in the liver

Formalin-fixed and embedded duck liver tissue sections were stained with Periodic acid-Schiff diastase (PAS-D) as described in Section 2.4.3, and viewed using light microscopy to observe the levels of Kupffer cell infiltration and activation. Kupffer cells are resident liver macrophages which remove hepatocyte debris by phagocytosis, causing the Kupffer cells to increase in size and to be stained strongly for PAS-D and/or acid-fast pink/brown pigments due to the accumulation of phagocytosed material (Roskams *et al.*, 2007). While the presence of many PAS-D-positive Kupffer cells usually indicates recent hepatitis (Geller *et al.*, 2007), Kupffer cells are long-lived and can persist in the liver parenchyma for weeks to months (Crawford, 2007). Examples of Kupffer cells without phagocytosed materials (termed "unactivated Kupffer cells") and with phagocytosed materials (termed "activated Kupffer cells") are shown in Figure 7.4, with detailed analysis summarised in Table 7.3A.

It is expected that the levels of Kupffer cell infiltration and activation would increase during clearance of DHBV infection (4 – 18 dpi), and be maintained at normal levels after clearance of DHBV infection (45 dpi). This was seen in previous studies in 6-week-old ducks where 1.92% of the total cells in the liver were Kupffer cells, and up to two thirds of the Kupffer cells contained phagocytosed materials (activated). After clearance of DHBV infection (60 – 316 dpi), the levels of Kupffer cells were maintained at an average of 3.85% of total liver cell with up to two thirds of the total Kupffer cells activated (Table 7.3B; Reaiche *et al.*, 2010).

As shown in Table 7.3A, at 4 dpi, an average of 6.37% of the total liver cells was comprised of Kupffer cells, with slightly more than half of the Kupffer cells containing some phagocytosed materials (activated) (shown as Figure 7.4A). These findings support previous observations (Sections 7.3.2.2 and 7.3.2.3) that the immune responses of the ducks had not been fully activated or were just starting to be activated at 4 dpi. At 18 dpi, there was an increase in the levels of Kupffer cells to an average of 7.97% of the total liver cells. The Kupffer cells also increased in size, and up to two thirds of the Kupffer cells were activated and contained PAS-D positive (shown as Figure 7.4B) and some acid-fast pink/brown pigmented (shown as Figure 7.4C) phagocytosed materials. These again support previous observations (Sections 7.3.2.2 and 7.3.2.3) that the immune responses of the ducks were now

fully activated, as most of the Kupffer cells contained phagocytosed debris, presumably from hepatocytes that underwent apoptosis, to allow the ducks to control and clear DHBV infection.

At 45 dpi, the levels of Kupffer cells in the liver were similar to 18 dpi, with an average of 8.58% of the total liver cells comprised of Kupffer cells. Most of the Kupffer cells were medium-sized and almost all the Kupffer cells were activated and contained PAS-D positive and some acid-fast pink/brown pigmented phagocytosed materials. These suggest that after clearance of DHBV infection, there would not be an increase in levels of Kupffer cell infiltration in the liver, but with slight increase in activation of Kupffer cells to continue removing hepatocyte debris. The levels of Kupffer cells did not decrease after clearance of DHBV infection, as Kupffer cells are long-lived and would persist in the parenchyma for weeks to months even after activation and phagocytosis (Crawford, 2007).

When compared to the levels of Kupffer cells in the age matched ducks (6-week-old) that developed chronic DHBV infection (ducks 338, 343 and 350 as shown in Table 8.3A), surprisingly, the levels of Kupffer cells present in the liver were lower in ducks with chronic DHBV infection, varying from 4.14% – 8.93% at 4 dpi (not significantly different) and 6.91% or 4.4% at 18 or 60 dpi (significantly lower), and also with less proportions of activated Kupffer cells (not significantly different). This was unexpected, as the levels of inflammation (Section 8.3.2.2) and apoptosis (Section 8.3.2.3) were 2 – 3-fold higher in the ducks that developed chronic DHBV infection, and thus it would be expected that higher levels of Kupffer cells would be activated in response to the hepatocyte death occurring in the liver. It was only during later stages of chronic DHBV infection (60 – 327 dpi) that there were similar levels of Kupffer cells in the liver (up to 7.81% of total cells in the liver) which were mostly activated (5.39% out of the 7.81% Kupffer cells). It was unclear why there was a delayed response in the infiltration and activation of Kupffer cells during chronic DHBV infection, despite the higher levels of liver inflammation and apoptosis. As Kupffer cells are known to be activated by cytokines and chemokines like TNF-α and IFN-γ (Smedsrod *et al.*, 1994; Kolios *et al.*, 2006), it may be possible that there were delayed secretion of these cytokines/chemokines, resulting in the delay of Kupffer cells infiltration and activated.

Interestingly, as shown in Table 7.3B, the age matched uninfected control duck 138 showed varying levels of Kupffer cells from 4 – 316 dpi, ranging from 1.95% – 5.98% of total liver cells, thus showing that variable levels of Kupffer cell infiltration are natural occurances in the duck liver. However, the almost statistically higher levels of Kupffer cell infiltration (p =

0.06) and activation ($p = 0.05$) in the ducks with acute DHBV infection suggest that Kupffer cells do play an essential role in clearance of DHBV infection (Tohidi-Esfahani *et al.*, 2010).

7.3.2.5. Levels of DHBsAg in the serum

The levels of DHBsAg in the serum of ducks were measured by rapid qualitative ELISA as described in Section 2.5.2. DHBsAg levels act as a marker for the levels of "active" viraemia, as this DHBsAg ELISA was designed to detect DHBV virions that are not complexed to anti-DHBs antibodies (Miller *et al.*, 2004). It is expected that in ducks with acute DHBV infection, DHBV virions would be released from infected hepatocytes could be detected by DHBsAg ELISA. However, when the DHBV virions are complexed by anti-DHBs antibodies during clearance, it would not be detectable by this ELISA (Jilbert *et al.*, 1998; Reaiche, 2008).

As shown in Figure 7.5A, the levels of DHBsAg in the serum of all three ducks were below the limit of detection throughout this study (0 – 45 dpi). This suggests that low levels of viraemia had occurred in these ducks, which was expected as only 4.4% of hepatocytes were DHBsAg-positive at 4 dpi (Section 7.3.2.1). In addition, the adaptive immune responses could also have been rapidly activated, producing anti-DHBs antibodies that complex to the DHBsAg and preventing their detection by ELISA. To test for the activation of the adaptive immune response to DHBV infection, levels of anti-DHBc and anti-DHBs antibodies were detected in the serum of these ducks as described in Sections 7.3.2.6 and 7.3.2.7 respectively.

When compared to the levels of DHBsAg in the serum of age matched ducks that developed chronic DHBV infection (Section 8.3.2.5) (ELISAs were performed concurrently for both groups of ducks), DHBsAg was found to persist at 0.6 – 20 μg/mL from 8 – 327 dpi, indicative of continuous low levels of "active" viraemia and the failure of anti-DHBs antibodies to complex with all the virions. Therefore, this further confirmed that low levels of viraemia or rapid production of anti-DHBs antibodies had occurred in ducks 337, 339, 342.

7.3.2.6. Levels of anti-DHBc antibodies in the serum

The levels of anti-DHBc antibodies in the serum of ducks were measured by quantitative ELISA as described in Section 2.5.3. The detection of anti-DHBc antibodies is commonly used as a marker of current or past DHBV infection, and could be detected ~7 – 30 dpi in ducks that developed acute DHBV infection (Jilbert *et al.*, 1998; Reaiche, 2008). It is expected that the ability to mount specific adaptive immune responses against DHBV early after infection is crucial for the clearance of DHBV infection.

As shown in Figure 7.5B, anti-DHBc antibodies could be detected in the serum of all three ducks by 4 dpi at titres of 590 – 6450 until 32 dpi, before decreasing to titres of 520 – 1050 from 36 – 45 dpi.

When compared to the levels of anti-DHBc antibodies in the serum of age matched ducks (6-week-old) that developed chronic DHBV infection (Section 8.3.2.6) (ELISAs were performed concurrently for both groups of ducks), anti-DHBc antibodies were also detectable by 4 dpi, and were maintained at higher titres of 1375 – 2900 until after 36 dpi, indicative of continuous stimulation of the adaptive immune responses due to the persistent DHBV infections in the ducks to keep producing higher levels of anti-DHBc antibodies.

7.3.2.7. Levels of anti-DHBs antibodies in the serum

The levels of anti-DHBs antibodies in the serum of ducks were measured by quantitative ELISA as described in Section 2.5.4. The anti-DHBs antibodies ELISA performed in this study had been designed to detect mainly the free circulating anti-DHBs antibodies, but could also detect anti-DHBs antibodies that are complexed to DHBsAg (Miller *et al.*, 2004). As the rabbit anti-duck IgY secondary antibodies used in this ELISA were generated using rabbits challenged with total IgY purified from duck egg yolks (Bertram, 1997), it is expected that both forms of the duck IgY, which are the full-length IgY and the smaller IgY(ΔFc) (Ng and Higgins, 1986; Lundqvist *et al.*, 2006), would be detected by this ELISA.

The detection of anti-DHBs is commonly used as a marker of immunity as well as of resolution of DHBV infection, as the seroconversion to detectable levels of anti-DHBs antibodies reflects high protective immunity against DHBV infection by preventing the binding of DHBV to hepatocytes (Pugh *et al.*, 1995), and neutralization of circulating DHBV virions (Vickery *et al.*, 1989). Anti-DHBs antibodies could be detected in most ducks with acute DHBV infection from ~7 – 21 dpi (Jilbert *et al.*, 1998). It is expected that the ability to mount specific adaptive immune responses against DHBV early after infection is crucial for the clearance of DHBV infection.

As shown in Figure 7.5C, anti-DHBs antibodies could be detected in the serum of all ducks by 11 dpi at titres of 135 – 1150, with spikes of antibodies titres up to 12,500 at 32, 36 and 43 dpi. These showed that adaptive immune responses had been activated to produce anti-DHBs antibodies from the onset of DHBV infection, and likely contributed to the rapid clearance of DHBV from the serum by complexing with the DHBsAg and to prevent further DHBV binding and infection of the hepatocytes, as no viraemia was detected in these ducks (Section

7.3.2.5). After clearance of infection, detectable levels of anti-DHBs antibodies would remain to provide protection against further DHBV infections (Jilbert *et al.*, 1998; Reaiche, 2008).

7.3.2.8. Levels of DHBV DNA in the serum

The levels of DHBV DNA present in the serum were determined by qPCR as described in Section 2.8.9.1. The primer set 423 – 576c (refer Table 2.2) was designed to amplify all forms of DHBV DNA (Reaiche *et al.*, 2010) and was used in this assay to amplify DHBV DNA in its rcDNA form packaged into progeny DHBV virions. All DNA templates were extracted from the serum using the ChargeSwitch gDNA 1 mL serum kit as described in Section 2.5.1. The levels of serum DHBV DNA detected would represent the levels of viraemia in these ducks, showing the ongoing active DHBV replication occurring in the liver.

It is expected that in ducks with acute DHBV infection, serum DHBV DNA levels may peak at 4 – 7 dpi (up to 10^6 copies per mL) due to ongoing DHBV replication in the liver that resulted in detectable levels of viraemia. During clearance phase, DHBV DNA levels would be expected to drop (up to ~10-fold) by 10 dpi, and lastly would not be detectable by 21 – 30 dpi after clearance of DHBV infection (Le Mire *et al.*, 2005; Reaiche *et al.*, 2010).

As shown in Figure 7.6A, no serum DHBV DNA was detected at 0 dpi, indicating that the ducks did not have viraemia prior to being experimentally infected. Low levels of serum DHBV DNA were detected at 4 dpi only in duck 339 ($5.7x10^3$ copies per mL), with serum DHBV DNA levels peaking at 11 – 14 dpi in ducks 337 and 339 (up to $2x10^6$ copies per mL). A small spike of serum DHBV DNA ($1x10^4$ copies per mL) was detected at 36 dpi in duck 337, which may be due to a slight rebound of DHBV infection that was rapidly resolved as subsequently no more serum DHBV DNA was detected for the rest of the study. These results were consistent with the expected serum DHBV DNA levels during acute DHBV infection, showing a peak of viraemia during the early stages of infection, that rapidly resolved by 21 – 30 dpi. However, the peak viraemia at 11 – 14 dpi was much later than the expected peak a4 – 7 dpi) in previously published age matched ducks (Le Mire *et al.*, 2005; Reaiche *et al.*, 2010). On a separate note, no serum DHBV DNA were detected for duck 342, with only low levels of serum DHBV DNA detected just below the limit of detection at 11 dpi. As these serum samples were analysed concurrently with the other duck 337 and 339 samples, there should not have been errors during qPCR. Furthermore, as the highest levels of serum DHBV DNA detected in this study ($2x10^6$ copies per mL) was similar to the peak serum DHBV DNA levels reported in previous studies (~10^6 copies per mL) (Reaiche *et al.*, 2010), this suggests that qPCR assays performed in this study was not less efficient or less sensitive compared to

the published assays to result in poor detection of serum DHBV DNA in duck 342. As DHBV DNA was still detectable in the liver of duck 342 (Section 7.3.2.9), this confirmed that duck 342 had been infected with DHBV, and may have cleared the DHBV infection effectively with low levels of viraemia, resulting in such low levels of serum DHBV DNA.

When compared to the levels of serum DHBV DNA in age matched ducks that developed chronic DHBV infection (Section 8.3.2.8), the highest level of serum DHBV DNA detected in ducks that develop acute DHBV infection was ~2 logs lower than the average serum DHBV DNA levels during chronic DHBV infection ($5x10^8$ copes per mL), which were as expected.

7.3.2.9. Levels of DHBV DNA in the liver

The levels of total and cccDNA present in the liver were determined by qPCR using primer sets 423 – 576c and CC2 – MG1 respectively (refer Table 2.2) as described in Section 2.8.9.2.

It is expected that in the liver of ducks with acute DHBV infection, during early stages of infection (4 dpi), higher levels of DHBV total and cccDNA would be detected due to high levels of DHBV replication which produces DHBV RI DNA and the formation of cccDNA pools in the liver. However, there would be lower levels of DHBV cccDNA compared to the DHBV total DNA, as the cccDNA pool is still being generated from the rcDNA that were transported to the nucleus (refer to Section 1.2.4 for detailed description of viral replication). During clearance of DHBV infection (18 dpi), as DHBV replication was controlled and inhibited, the levels of DHBV total DNA would be significantly reduced, while the DHBV cccDNA levels also start to decline as DHBV infection is cleared from the liver. After clearance of DHBV infection (45 dpi), only residual DHBV DNA, predominantly in the cccDNA form, would be detected in the liver (Reaiche *et al.*, 2010), and as no active DHBV replication would be occurring, the levels of DHBV total and cccDNA would be similar.

As shown in Figure 7.6B, at 4 dpi, each cell contained ~7 and ~0.16 copies copies of DHBV total and cccDNA. As the DNA used as qPCR template was extracted from both DHBsAg-positive and -negative hepatocytes present in the liver, and knowing that ~4.4% of hepatocytes were DHBsAg-positive (Section 7.3.2.1), it could be calculated that each DHBsAg-positive hepatocyte would on average contain ~159 copies of DHBV total DNA and ~3.6 copies of DHBV cccDNA. These levels were similar to the DHBV DNA levels found in the age matched ducks that had similar percentage of DHBsAg-positive hepatocytes (chronic DHBV-infected ducks at 4 dpi described in Section 8.3.2.9, and Reaiche *et al.*, 2010).

After that, during the clearance phase (18 dpi), the DHBV DNA levels began to drop ~100-fold to ~0.06 copies of DHBV total DNA and ~16-fold to ~0.01 copies of DHBV cccDNA by 18 dpi. This was as expected, as the duck immune responses were now activated to control and inhibit further DHBV replication, thus greatly reducing the DHBV RI DNA levels, and to a lesser extent, the DHBV cccDNA levels either by hepatocyte killing or curing (as discussed in Section 7.2). Finally, after clearance of infection (45 dpi), only ~0.02 and ~0.01 copies copies of DHBV total and cccDNA were detected (cccDNA levels for duck 339 was below the limit of detection). As no more active DHBV replication should be occurring, all the remaining DHBV DNA present would be residual DHBV DNA predominantly (~50%) in the cccDNA form (Reaiche *et al.*, 2010). All these results were consistent with the expected DHBV DNA levels during acute DHBV infection (Jilbert *et al.*, 1992; Reaiche *et al.*, 2010).

7.4. Using invPCR assay to detect integrated virus-cell junctions during various stages of acute DHBV infection

7.4.1. Sequence of the DHBV genome present in ducks

As described in Section 1.8.1, invPCR assays are generally designed based on the most probable left and right hand ends of the dslDNA sequences of the integrated viral DNA. In Chapter 6, the most probable left and right hand end junctions of DHBV dslDNA were determined, and preliminary studies found that the duck D3 invPCR assay (shown in Table 2.3) designed based on the AusDHBV sequence (GenBank Accession AJ006350) was most suitable to detect integrated virus-cell junctions in DHBV-infected ducks this study.

To ensure that the duck D3 invPCR assay was suitable to detect integrated virus-cell junctions in ducks 337, 339 and 342, the most probable left hand end junction of the integrated DHBV DNA (~2485 nt of the AusDHBV genome) in these ducks was sequenced. To achieve this, DNA was extracted from all duck liver tissues using the total DNA extraction method as described in Section 2.6.3. A region of the DHBV DNA (2349 – 52 nt) was then amplified by PCR as described in Section 2.8.5. Specifically, PCR reactions were performed using GoTaq polymerase, PCR cycle extension time of 1 min, and DRS F2 – R2 primers (refer Table 2.2). PCR products were visualised by agarose gel electrophoresis as described in Section 2.8.7, and results (data not shown) showed that the expected 731 bp region of the DHBV DNA was amplified in all three ducks. Next, the amplified DHBV DNA were sequenced using both the DRS F2 (forward) and R2 (reverse) primers as described in Section 2.8.10, with cleanup of DNA sequencing products as described in Section 2.8.11.2. The samples were sent to AGRF for sequencing, and the DNA sequences were analysed as described in detail in Section 2.8.12.

It should be noted that specific proof-reading polymerase was not used in this Section, as although some base pair mutations may be introduced by the non-proof-reading GoTaq polymerase used, the PCR products and subsequent sequences produced in this Section were only used to check and verify the DHBV strains present in the ducks in this study. In addition, as natural DHBV quasispecies were expected to be present in each duck, it was therefore not critical to proof-read the PCR products for sequencing in this Section.

As shown in Figure 7.7, the multiple sequence alignment of DHBV genome present in all ducks showed high homology with the AusDHBV genome, with 100% sequence coverage and 99% sequence similarity. Specifically, there was a thymine to cytosine mutation at 418 nt in all ducks, and an adenine nucleotide deletion at 17 nt in ducks 339 and 342. However, these mutations did not occur in regions of restriction enzyme digestion or PCR primer binding sites present in the duck D3 invPCR assay design.

In summary, the duck D3 invPCR assay that was designed in Chapter 6 based on the AusDHBV sequence is suitable and specific to detect integrated virus-cell junctions in the liver of ducks 337, 339 and 342 that developed acute DHBV infection in this study.

7.4.2. Detection of integrated virus-cell junctions during various stages of acute DHBV infection using the invPCR assay

The invPCR assays were performed as optimised in Chapter 6. Specifically, liver cell DNA was extracted from all frozen liver tissues using the total DNA extraction method as described in Section 2.6.3. The extracted DNA samples were then inverted based on the duck D3 invPCR assay design (Table 2.3) as described in Section 2.10.1, followed by nested PCR and visualisation of PCR products using agarose gel electrophoresis as described in Sections 2.10.3 and 2.10.4. An example of the invPCR products produced from serial dilution of DNA template is shown in Figure 7.8A, while an example of the invPCR products produced from the equal distribution of the "optimal" DNA template into each PCR well is shown in Figure 7.8B. The "optimal" amount of inverted DNA to be used as template during nested PCR reactions was chosen from the amount of inverted DNA that would produce a single PCR product in each PCR well, as shown in Figure 7.8A. Lastly, invPCR products that were produced in single PCR wells were extracted from the agarose gel and sequenced as described in Sections 2.10.5 to 2.10.7. Analysis of the obtained DNA sequences was performed as described in Section 2.8.12, focusing on detecting integrated virus-cell junctions, which would be seen as the duck liver cell insert DNA flanked by DHBV DNA sequences.

7.4.3. InvPCR assay results

Figure 7.9A shows an example of an unknown sequence DNA sequencing result, which is defined in this thesis as insert DNA sequences that were either too short (<15 bp) or did not show homology to any known sequences during the BLAST searches. Figure 7.9B shows an example of a virus-virus false positive DNA sequence result, which consisted of only DHBV DNA. Individual DNA sequencing results were not shown in this Section.

All invPCR assay results obtained are summarised in Table 7.4. Unfortunately, no integrated virus-cell junctions were successfully detected in this Chapter. For all three duck liver tissues, a total of 24.31 μg DNA were analysed by performing 180 invPCR reactions on DNA extracted at 4 and 18 dpi, and 90 invPCR reactions on DNA extracted at 45 dpi. Specifically, at 4 dpi, a total of 278 invPCR products were sequenced, among which 211 were virus-virus false positive sequences, 5 were unknown sequences, and 62 DNA sequencing reactions failed to produce any readable sequences. At 18 dpi, only 3 invPCR products were sequenced, all of which failed to produce any readable sequences. Lastly at 45 dpi, only 8 invPCR products were sequenced, among which 5 were virus-virus false positive sequences, 1 was an unknown sequence that did not show homology to any known sequences during the BLAST searches, and 2 DNA sequencing reactions failed to produce any readable sequences.

7.5. Discussion

7.5.1. Characterisation of histological and serological changes occurring during acute DHBV infection

In summary, based on the histological and serological characterisations in Sections 7.3.2.1 to 7.3.2.9, it was found that in ducks experimentally infected with $1.5x10^{10}$ vge of DHBV virions at 6 weeks of age that eventually cleared the DHBV infection (developed acute DHBV infection), DHBV infection was established in ~4.4% of hepatocytes during the early stages of infection (4 dpi) with active DHBV replication in the liver (~159 and ~3.6 copies of DHBV total and cccDNA per infected hepatocyte). This was accompanied with low levels of liver inflammation, hepatocyte apoptosis, some increase in infiltration of Kupffer cells, and the production of anti-DHBc antibodies by 4 dpi, followed by the neutralising anti-DHBs antibodies by 11 dpi. At 18 dpi, DHBV replication was successfully controlled (~0.06 copies of DHBV total DNA per liver cell) and mostly cleared from the liver (<0.15% of hepatocytes were DHBsAg-positive) with only residual DHBV cccDNA in the liver (~0.01 copies per liver cell) and no detectable viraemia. As expected, elevated levels of liver inflammation, hepatocyte apoptosis, and infiltration and activation of Kupffer cells were observed during DHBV clearance, but reduced back to “basal” levels when the DHBV infection was cleared

(45 dpi). By 45 dpi, DHBsAg-positive hepatocytes and viraemia were no longer detectable, with only residual DHBV DNA predominantly in the cccDNA form found in the liver (~0.02 and ~0.01 copies of DHBV total and cccDNA per liver cell).

In addition, attempts were made to determine the levels of proliferating hepatocytes by the use of proliferating cell nuclear antigen (PCNA) staining as described in Section 2.4.4. This was performed to determine the levels of hepatocyte proliferation occurring in the liver, as well as to observe and confirm that the hepatocytes were indeed proliferating to replace neighbouring hepatocytes that were killed during clearance (compensatory hepatocyte proliferation), rather than being replaced by proliferating and differentiating bile duct cells. Unfortunately, the PCNA staining was not successful despite numerous attempts in the Hepatitis Research Laboratory as well as by the Tissue Pathology Laboratories, IMVS/SA Pathology and Hanson Institute Centre for Neurological Diseases. Hence, attempts to observe and calculate hepatocyte proliferation during acute DHBV infection were not successful in this study.

7.5.2. Detection of integrated virus-cell junctions using the invPCR assay

The failure to detect any integrated virus-cell junctions in this study was not expected. It is expected that during early stages of acute DHBV infection (4 dpi), low levels of integration would be detected in the liver, as in previous studies, integration has been reported to occur at a rate of ~1 in 10^3 – 10^4 cells by 6 dpi in ducks experimentally infected at 3 – 5 days of age (Yang and Summers, 1999). Based on that, out of the 734 ng of 4 dpi DNA analysed in this study (approximately 2.9×10^5 cells calculated as described in Section 2.8.9.3.2), ~4.4% of which were DHBsAg-positive (Section 7.3.2.1), it is expected that at least 1 – 12 integrated virus-cell junction would be detected. During later stages of DHBV infection, if non-cytolytic hepatocyte curing occurs, more integration junctions would be expected to be detected (40 – 428 based on ~24 μg of DNA analysed), with the possible formation of hepatocyte clones (seen as repeats of the unique integrated virus-cell junction) as hepatocytes undergo mitosis. This was observed in preliminary invPCR assays performed in ducks with acute DHBV infection in Chapter 6, where 1 integrated virus-cell junction was detected at 316 dpi. In addition, as mentioned in Section 7.2, in woodchucks with acute WHV-infection, up to 385 integration junctions could be detected at 16 or 19 weeks post infection, with hepatocyte clones up to 21 cells in size (Mason *et al.*, 2009b).

The failure to detect any integrated virus-cell junctions in this study could be due to various reasons. Firstly, high levels of virus-virus false positives have been detected, comprising up to 75.5% of the total invPCR products sequenced in this study as shown in Table 7.4. These

virus-virus sequences were not only a huge waste of resources and time when performing and analysing invPCR products, but could also overwhelm the invPCR assay and greatly reduce the frequency of detecting actual integrated virus-cell junctions present in the liver tissues. For instance, at 4 dpi, almost all the invPCR products sequenced were virus-virus sequences. This was expected due to the high levels of DHBV replication occurring in the liver that produces a range of "non-integrated DHBV DNA", including the cytoplasmic DHBV rcDNA and RI, and the nuclear DHBV cccDNA. All of these forms of DHBV DNA could contribute to virus-virus sequences detected during the invPCR assay as discussed in Section 5.1.2. As these DHBV DNA could be present in up to 159 copies (Section 7.3.2.9) compared to 1 copy of integrated virus-cell junction per liver cell, these high levels of non-integrated DHBV DNA would therefore reduce the chance of detecting the integrated virus-cell junctions.

To reduce the levels of non-integrated DHBV DNA, the selective low melting temperature agarose gel electrophoresis and purification of high MW cellular DNA was performed on total DNA extracted from the 4 dpi liver tissues from ducks 337, 339 and 342, followed by DNA inversion as described in Section 2.10.2, and subsequent invPCR assay steps as performed previously in Section 7.4.2. However, no invPCR products were detected out of 90 invPCR reactions performed for each duck liver tissue (data not shown). InvPCR assays performed on DNA for ducks with chronic DHBV infection extracted using the same low melting temperature agarose gel electrophoresis protocols were also not successful (Section 8.5.2). The low melting temperature agarose gel electrophoresis and purification of high MW cellular DNA protocols have been optimised and improved in Chapters 5.1 and 6, therefore the failure to detect any invPCR products should not be due to the poorly optimised protocols or the presence of any PCR amplification inhibitors. However, as high losses of DNA (60% – 85%) have been shown to occur using this protocol (Chapter 5.2; Mason, personal communication), it was likely that the few integration junctions present had been lost during the extraction process, resulting in the failure to detect any integration junctions in both Chapters.

In future studies, the levels of DHBV DNA could be reduced using various methods as described in Section 6.6. These include alternative selective DNA extraction methods, the use of locked nucleic acid (LNA) oligonucleotides to specifically block the amplification of DHBV DNA, and using specific cccDNA destroying enzymes to digest the majority of virus-virus sequences detected. For instance, in this study, most of the virus-virus sequences detected were shown to contain the *Nde*I cccDNA destroying enzyme digestion site (Figure 7.9B). This showed that the current *Nde*I cccDNA destroying enzyme used in the duck D3 invPCR assay design was not efficient in digesting the virus-virus sequences formed, and thus

did not prevent the amplification of the virus-virus sequences during the invPCR assay as expected. Hence, future studies could establish a new invPCR assay design using alternative cccDNA destroying enzymes, like *Ase*I and *Mfe*I, as their digestion sites have been found in the majority of the virus-virus sequences detected in this study (Figure 7.9B).

Secondly, the failure to detect any integrated virus-cell junctions in this study could be due to the large proportion of invPCR products that had failed to produce any readable sequences (22.4%). For instance, at 18 and 45 dpi, as only low levels of DHBV DNA would remain in the liver, most of which would be residual cccDNA in the nucleus (~0.04 copies per liver cell as shown in Section 7.3.2.9), low levels of virus-virus false positives would be expected to be produced, thereby should greatly increase the chances of detecting the integrated virus-cell junctions. This was observed, as out of the ~23.6 µg of 18 and 45 dpi DNA analysed, only 11 invPCR products were produced (Table 7.4). However, 5 of the invPCR products had failed to produce readable DNA sequences, which almost halved the chances of the invPCR assay to detect the integrated virus-cell junctions. Therefore, in future studies, the DNA sequencing reactions could be further optimised as previously described in Section 6.6.

Thirdly, the failure to detect integrated virus-cell junctions could be due to their true absence in the liver. As described in Section 7.2, the cytolytic hepatocyte killing theory suggests that to completely clear DHBV infections, the DHBV-infected hepatocytes have to be killed. Therefore, integrated virus-cell junctions would no longer be present in the liver after clearance of DHBV infection. Hence, this failure to detect any integrated virus-cell junctions could be interpreted to support the cytolytic hepatocyte killing theory. To ensure that the failure to detect any integrated virus-cell junctions was due to their true absence and not the failure of the invPCR assay, the duck liver cell DNA could be spiked with plasmid DNA that could produce an invPCR product using the same duck invPCR assay design, similar to the model system described in Section 5.4.7. Hence, if the plasmid DNA invPCR products were observed, this would confirm that the invPCR assays had been performed properly.

7.6. Conclusion

The aims of this Chapter were to establish and characterise histological and serological changes during various stages of acute DHBV infection, and to determine the mechanisms involved in clearance of DHBV-infected hepatocytes, using the invPCR assay to detect integrated virus-cell junctions in the liver during various stages of acute DHBV infection. By gaining understanding of viral clearance from infected hepatocytes, new therapeutic directions could be determined for chronic HBV infection, and to prevent reactivation of HBV infection.

Acute DHBV infections were successfully established in three 6-week-old Pekin ducks (337, 339, 342). At 4 dpi, active DHBV replication was occurring (~159 copies of DHBV total DNA per infected hepatocyte) with ~4.4% of DHBsAg-positive hepatocytes in the liver. At 45 dpi, <0.001% of hepatocytes were DHBsAg-positive, with residual DHBV DNA predominantly (50%) in the cccDNA form remaining in the liver (~0.02 copies and ~0.01 copies of DHBV total and cccDNA per liver cell). Histological characterisation of liver tissues showed elevated levels of liver inflammation (both portal and lobular), apoptosis, and Kupffer cell infiltration and activation during clearance of infection (4 and 18 dpi), returning to "basal" levels after clearance of infection (45 dpi). Serological characterisation showed that the ducks produced anti-DHBc antibodies by 4 dpi and anti-DHBs antibodies by 11 dpi. The neutralizing anti-DHBs antibodies would have removed DHBV virions from the serum by forming antibody-antigen complexes, as no viraemia were detected. The anti-DHBs antibodies were also found to be continuously produced at high levels even after resolution of infection (45 dpi), to provide protection against further DHBV infection.

Using the duck D3 invPCR assay that was shown to be suitable to detect integrated virus-cell junctions in these ducks, up to 24.3 μg of DNA were analysed from liver tissues at 4, 18 and 45 dpi. However, no integrated virus-cell junctions were detected at any stages of acute DHBV infection, with most of the invPCR products sequenced were found to be virus-virus sequences (75.5% of the total invPCR products sequenced). Therefore, the mechanisms involved during the clearance of DHBV-infected hepatocytes during acute DHBV infection could not be conclusively determined in this Chapter.

Legend for Table 7.1

(A) Formalin-fixed and embedded duck liver tissue sections were H&E-stained and viewed under light microscopy as described in Section 2.4.1. Examples of portal and lobular inflammation are shown in Figure 7.2.

(B) Duck 138 is an uninfected control duck inoculated with 3 mL of NDS at 6 weeks of age as described in Section 7.3.1. Liver tissues were formalin-fixed, paraffin-embedded, sectioned at 6 μM thick, and H&E-stained by Dr. Georget Reaiche (Reaiche *et al.*, 2010), who then generously provided the H&E-stained slides for use in this study.

(C) Statistical analysis of the average % of total area of liver containing inflammatory cells. Ducks with acute DHBV infection include ducks 337, 339, 342; duck with chronic DHBV infection include 339, 343, 350 (Chapter 8); the uninfected duck is duck 138. The p-value of <0.05 is considered statistically significant.

[a]DHBsAg-positive hepatocytes were determined from Figure 7.1 or Reaiche *et al.*, 2010.
[b]Total area of liver tissues were examined as described in Section 2.4.1.
[c]Percentage of the examined area of liver tissues that contained inflammatory cells.
[d]Thickness of the largest inflammation observed from the examined area of liver tissues.
[e]The grading of portal and lobular inflammation was adapted from Mason *et al.* (Mason *et al.*, 1994) and Bedossa and Poynard (Bedossa and Poynard, 1996), and described in detail in Section 2.4.1.
[f]P-value was calculated using the Student's unpaired *t*-test, set to two-tailed distribution and two-sample unequal variance (heteroscedastic). The difference of the levels of inflammation between ducks with acute and chronic DHBV infection at each time-point was not significant.
[g]As there were only 1 uninfected duck sample (duck 138), the Student's unpaired *t*-test was performed comparing data from all time-points of the different groups as an array/data set. The difference of the levels of inflammation between ducks with acute DHBV infection and an uninfected duck was not significant.

Table 7.1: Summary of portal and lobular inflammation observed in H&E-stained duck liver sections.

A) Portal and lobular inflammation in ducks with acute DHBV infection

Duck	Dpi	DHBsAg-positive hepatocytes[a]	Area of liver analysed (mm^2)[b]	Inflammatory cells (% of total area of liver)[c]	Inflammation (cell thickness)[d]		Inflammation grading[e]	
					Portal	Lobular	Portal	Lobular
337	**4**	4.2%	24.48	0.47	8	ND	1	1
	18	<0.001%	43.20	1.77	21	13	3	2
	45	<0.001%	92.16	1.19	20	ND	2	1
339	**4**	5.8%	34.56	0.88	10	ND	2	1
	18	0.15%	40.32	1.86	30	ND	3	1
	45	<0.001%	108.00	1.33	30	22	2	2
342	**4**	3.1%	21.60	0.73	6	ND	1	1
	18	<0.001%	36.00	1.44	6	20	2	2
	45	<0.001%	113.76	0.61	16	19	2	2

B) Portal and lobular inflammation in negative control duck

Duck	Dpi	DHBsAg-positive hepatocytes[a]	Area of liver analysed (mm^2)[b]	Inflammatory cells (% of total area of liver)[c]	Inflammation (cell thickness)[d]		Inflammation grading[e]	
					Portal	Lobular	Portal	Lobular
138	**4**	<0.0001%	41.76	0.66	12	ND	2	1
	60	<0.0001%	24.48	1.59	18	ND	2	1
	221	<0.0001%	24.48	1.35	12	10	2	1
	316	<0.0001%	79.20	1.44	5	ND	2	1

C) Statistical analysis of the average % of total area of liver containing inflammatory cells

Group	Dpi						
	4		18		45 or 60		
Acute	0.69	⌋ 0.40[f]	1.69	⌋ 0.30[f]	1.04	⌋ 0.72[f]	⌋ 0.6[g]
Chronic	1.22		2.44		1.23		
Uninfected	0.66		N/A		1.59		

ND: not detected

N/A: not available

Legend for Table 7.2

(A) Formalin-fixed and embedded duck liver tissue sections were H&E-stained and viewed under light microscopy as described in Section 2.4.1.

(B) Duck 138 is an uninfected control duck inoculated with 3 mL of NDS at 6 weeks of age, as described in Section 7.3.1. Liver tissues were formalin-fixed, paraffin-embedded, sectioned at 6 μM thick, and H&E-stained by Dr. Georget Reaiche (Reaiche *et al.*, 2010), who then generously provided the H&E-stained slides for use in this study.

(C) Statistical analysis of the average % of apoptotic hepatocytes. Ducks with acute DHBV infection include ducks 337, 339, 342; duck with chronic DHBV infection include 339, 343, 350 (Chapter 8); the uninfected duck is duck 138. The p-value of <0.05 is considered statistically significant.

[a]Hepatocytes were counted as described in Section 2.4.1.
[b]Apoptotic cells were counted and expressed as a percentage of total hepatocytes. Examples of apoptotic hepatocytes are shown in Figure 7.3B.
[c]P-value was calculated using the Student's unpaired *t*-test, set to two-tailed distribution and two-sample unequal variance (heteroscedastic). Only the difference in the levels of hepatocyte apoptosis between ducks with acute and chronic DHBV infection at 45 dpi was significant ($p < 0.05$).
[d]As there were only 1 uninfected duck sample (duck 138), the *t*-test was performed comparing data from all time-points of the different groups as an array/data set. The difference of the levels of hepatocyte apoptosis between ducks with acute DHBV infection and an uninfected duck 138 was not significant.

Table 7.2: Summary of hepatocyte apoptosis observed in H&E-stained duck liver sections.

A) Hepatocyte apoptosis in ducks with acute DHBV infection

Duck	Dpi	Total hepatocytes analysed (cells)[a]	Apoptotic cells (% of total hepatocytes)[b]
337	**4**	3252	1.45
	18	3618	2.32
	45	4044	1.53
339	**4**	4062	1.40
	18	3630	1.68
	45	3114	1.67
342	**4**	4386	1.87
	18	4182	1.82
	45	2532	1.50

B) Hepatocyte apoptosis in negative control duck

Duck	Dpi	Total hepatocytes analysed (cells)[a]	Apoptotic cells (% of total hepatocytes)[b]
138	**4**	3360	0.68
	60	5562	0.54
	221	3846	0.68
	316	3726	1.26

C) Statistical analysis of the average % of apoptotic hepatocytes

Group	**Dpi**						
	4		**18**		**45 or 60**		
Acute	1.57	⌋ 0.56[c]	1.94	⌋ 0.064[c]	1.57	⌋ <0.040[c]	⌋ 0.070[d]
Chronic	2.10		2.89		2.57		
Uninfected	0.68		N/A		0.54		

N/A: not available

Legend for Table 7.3

(A) Formalin-fixed and embedded duck liver tissue sections were PAS-D stained and viewed under light microscopy as described in Section 2.4.3. Examples of unactivated and activated Kupffer cells are shown in Figure 7.4.

(B) Duck 138 is an uninfected control duck inoculated with 3 mL of NDS at 6 weeks of age, as described in Section 7.3.1. Liver tissues were formalin-fixed, paraffin-embedded and sectioned at 6 μM thick by Dr. Georget Reaiche (Reaiche *et al.*, 2010), who then generously provided the tissue slides for use in this study. Slides were PAS-D stained as described in Section 2.4.3.

Statistical analysis of the average % of (C) total Kupffer cells, (D) unactivated Kupffer cells, and (E) activated Kupffer cells. Ducks with acute DHBV infection include ducks 337, 339, 342; duck with chronic DHBV infection include 339, 343, 350 (Chapter 8); the uninfected duck is duck 138. The p-value of <0.05 is considered statistically significant.

[a]Total liver cells were counted as described in Section 2.4.3.

[b]Percentage of Kupffer cells observed out of the total liver cells analysed. The percentage of total Kupffer cells were further categorised into unactivated or activated Kupffer cells.

[c]Unactivated Kupffer cells do not contain PAS-D positive phagocytosed materials.

[d]Activated Kupffer cells contained PAS-D positive phagocytosed materials and/or acid-fast pink/brown pigmented phagocytosed materials.

[e]P-value was calculated using the Student's unpaired *t*-test, set to two-tailed distribution and two-sample unequal variance (heteroscedastic). The difference of levels of total Kupffer cells between ducks with acute and chronic DHBV infection at 18 and 45 dpi was significant ($p < 0.05$).

[f]As there were only 1 uninfected duck sample (duck 138), the *t*-test was performed comparing data from all time-points of the different groups as an array/data set. The differences of levels of activated Kupffer cells between ducks with acute DHBV infection and the uninfected duck 138 was almost significant ($p = 0.05$).

Table 7.3: Analysis of Kupffer cells detected in PAS-D-stained duck liver sections.

A) Analysis of Kupffer cells in ducks with acute DHBV infection

Duck	Dpi	Total cells analysed (cells)[a]	Kupffer cells (% of total liver cells)[b]			Size of activated Kupffer cells
			Total	Unactivated[c]	Activated[d]	
337	4	5736	6.73	2.74	3.99	Small
	18	4812	7.77	2.39	5.38[e]	Small
	45	4314	9.85	2.13	7.72	Medium
339	4	4836	7.09	2.48	4.61	Small
	18	4338	7.91	2.07	5.83[e]	Medium
	45	4194	8.63	1.50	7.13	Medium
342	4	5310	6.38	2.22	4.16	Small
	18	4404	8.24	3.29	4.95	Medium
	45	3702	7.27	2.08	5.19[e]	Medium

B) Analysis of Kupffer cells in negative control duck

Duck	Dpi	Total cells analysed (cells)[a]	Kupffer cells (% of total liver cells)[b]			Size of activated Kupffer cells
			Total	Unactivated[c]	Activated[d]	
138	4	6258	3.68	1.31	2.36	Small
	60	9294	1.95	0.85	1.10	Small
	221	5130	3.02	1.07	1.95	Small
	316	4662	5.98	1.05	4.93	Small

C) Statistical analysis of the average % of total Kupffer cells

Group	Dpi						
	4		18		45 or 60		
Acute	6.73	⌋ 0.91[e]	7.97	⌋ <0.01[e]	8.58	⌋ 0.02[e]	⌋ 0.06[f]
Chronic	6.92		6.91		4.40		
Uninfected	3.68		N/A		1.95		

D) Statistical analysis of the average % of unactivated Kupffer cells

Group	Dpi						
	4		18		45 or 60		
Acute	2.42	⌋ 0.23[e]	2.02	⌋ 0.50[e]	2.53	⌋ 0.057[e]	⌋ 0.09[f]
Chronic	3.99		2.50		1.21		
Uninfected	1.31		N/A		0.85		

E) Statistical analysis of the average % of activated Kupffer cells

Group	Dpi						
	4		18		45 or 60		
Acute	5.70	⌋ 0.11[e]	5.886	⌋ 0.18[e]	4.77	⌋ 0.13[e]	⌋ 0.05[f]
Chronic	2.93		4.40		3.19		
Uninfected	2.36		N/A		1.10		

N/A: not available

Table 7.4: Summary of invPCR assay products obtained using liver tissues from ducks with acute DHBV infection.

Duck	Dpi	Total invPCR reactions[a]	Total amount of DNA analysed (ng)[b]	Number of invPCR products sequenced[c]	Virus-cell junctions detected[d]	Virus-virus junctions detected[e]	Unknown sequences detected[f]
337	**4**	180	208	85	-	63	2
	18	180	5890	3	-	-	-
	45	90	1970	0	-	-	-
339	**4**	180	221	80	-	50	3
	18	180	5890	0	-	-	-
	45	90	1970	4	-	4	-
342	**4**	180	305	113	-	98	-
	18	180	5890	0	-	-	-
	45	90	1970	4	-	1	1
Total		**1350**	**24314**	**286**	**0**	**216**	**6**
% of total invPCR products sequenced					**0**	**75.5**	**2.1**

The duck D3 invPCR assays were performed as described in Section 7.4.2.

[a]Total invPCR reactions refers to the total number of nested PCR reactions performed in individual PCR wells.

[b]The amount of DNA analysed was estimated according to the amount of inverted DNA added per invPCR reaction, which was based on the amount of liver used during DNA extraction as calculated in Section 2.8.9.3.2. As losses of DNA were expected during extraction and inversion steps, a 50% loss of DNA was included in the calculations.

[c]From all the nested PCR reactions performed, only reactions that produced a clear invPCR product band was extracted from the agarose gel and sequenced. The number of total invPCR products observed on agarose gels was not shown. 64 of the sequencing reactions failed to produce a readable product (22.4% of total invPCR products sequenced).

[d]An example of an integrated virus-cell junction is shown in Figure 6.3A.

[e]An example of a virus-virus false positive junction is shown in Figure 7.9B.

[f]Unknown sequences are defined as insert DNA that were either too short (<15 bp) or did not show homology to any known sequences during the BLAST searches. An example of an unknown sequence is shown in Figure 7.9A.

Figure 7.1: Detection of DHBsAg-positive hepatocytes in liver sections prepared from ducks 337, 339 and 342 with acute DHBV infection at 4, 18 and 45 dpi.

EAA-fixed and embedded duck liver tissue sections were stained with pre-S monoclonal antibody, 1H.1, as described in Section 2.4.2, and photographed using light microscopy at 100X magnification, magnification bar = 200 μM. DHBsAg-positive hepatocytes are stained dark brown, while nuclei are counter-stained blue-purple using haematoxylin.

The percentage of DHBsAg-positive hepatocytes was determined by counting the total number of DHBsAg-positive hepatocytes per ~$1x10^5$ hepatocytes, examined at 200X magnification using an eyepiece graticule and a 600 μM x 600 μM grid. Likewise, the lower limit of sensitivity of detection (<0.001%) was calculated based on the percentage of 1 DHBsAg-positive hepatocyte in a total of $1x10^5$ hepatocytes.

The black arrow shows DHBsAg observed in non-hepatocyte cells located in the portal tract.

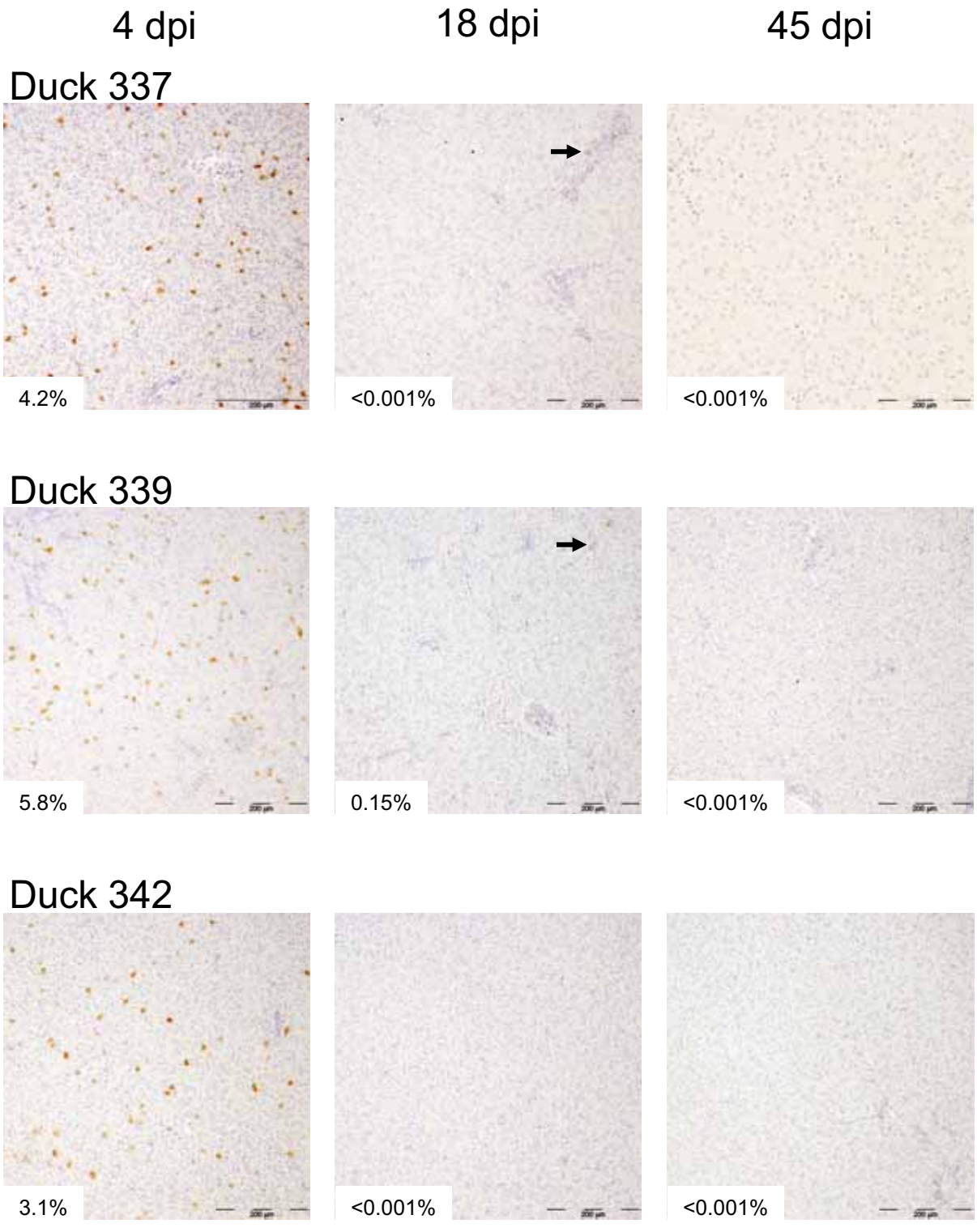

4 dpi
18 dpi
45 dpi
Duck 337
4.2%
<0.001%
<0.001%
Duck 339
5.8%
0.15%
<0.001%
Duck 342
3.1%
<0.001%
<0.001%

Figure 7.1

Figure 7.2: Detection of liver inflammation in H&E-stained liver sections prepared from ducks 337, 339 and 342 with acute DHBV infection at 4, 18 and 45 dpi.

Formalin-fixed and embedded duck liver tissue sections were H&E-stained as described in Section 2.4.1, and photographed using light microscopy at 100X magnification, magnification bar = 200 μM. Inflammatory cells are stained dark purple, while nuclei are counter-stained blue-purple using haematoxylin.

The black arrows show portal inflammation, while the blue arrows show lobular inflammation observed in the liver. Green arrows point out some vacuolated hepatocytes in the liver of duck 342.

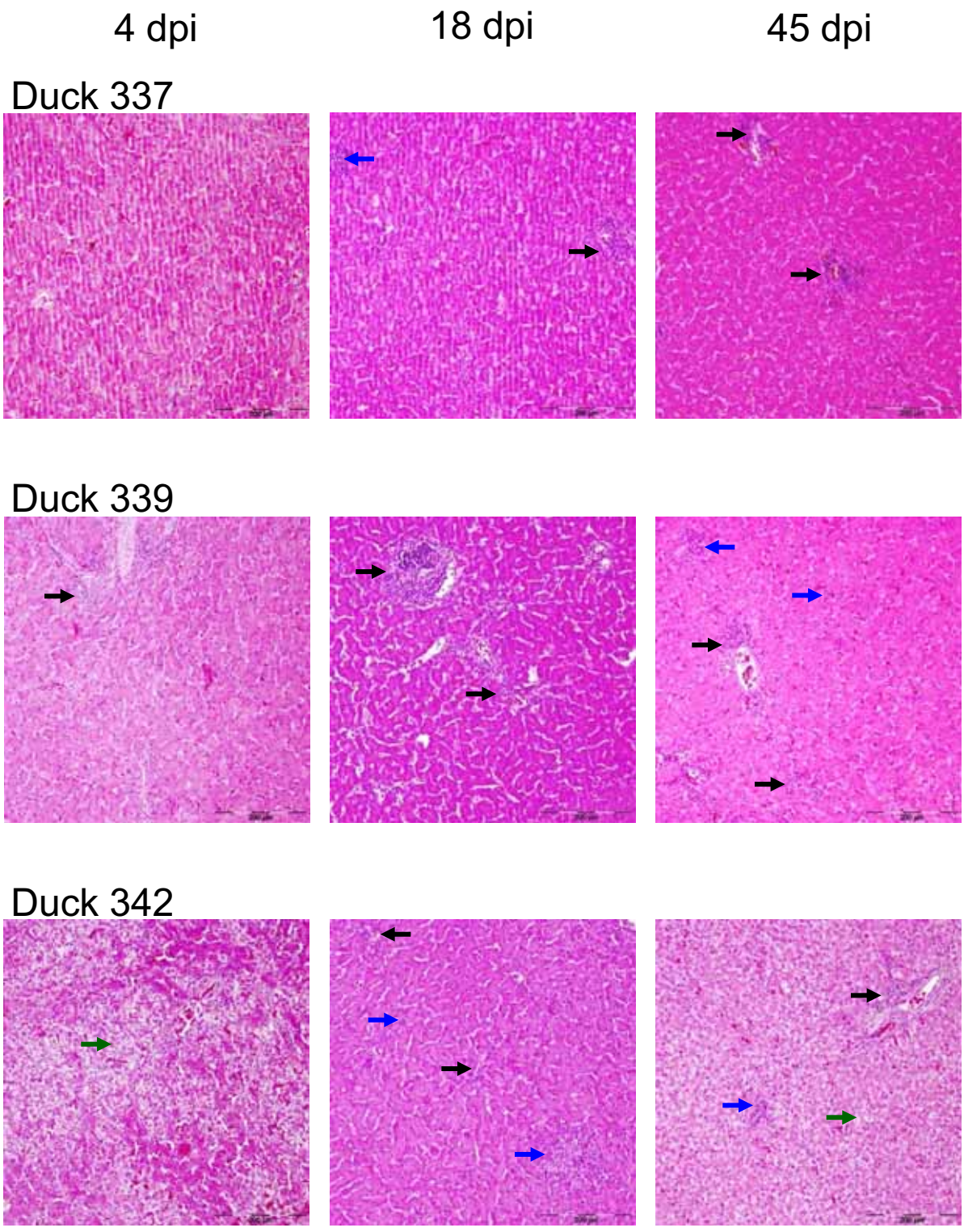


Figure 7.2

Figure 7.3: Detection of apoptotic hepatocytes and other histological features observed in H&E-stained liver sections prepared from ducks with acute DHBV infection.

Formalin-fixed and embedded duck liver tissue sections were H&E-stained as described in Section 2.4.1. Eosinophilic structures like proteins will be stained as various shades of red – pink, while nuclei are counter-stained blue-purple using haematoxylin.

Figure 7.3A shows an example of a portal tract, consisting of the portal vein, hepatic arteriole, and bile ducts. Photograph was taken from the liver of duck 339 at 18 dpi at 200X magnification, magnification bar = 100 μM.

Figure 7.3B shows examples of apoptotic hepatocytes emphasised by black arrows. In the apoptotic cells, chromatin condensation and cellular fragmentation form small apoptotic bodies, commonly referred to as acidophilic Councilman bodies, which can be seen as black dots in the ovoid-shaped hepatocyte cytoplasm that had turned thick and refractile. Apoptotic hepatocytes can also show cytoplasmic shrinkage, cell membrane blebbing, and may not contain nuclear remnants (Crawford, 2007). Photograph was taken from the liver of duck 342 at 18 dpi at 400X magnification, magnification bar = 50 μM.

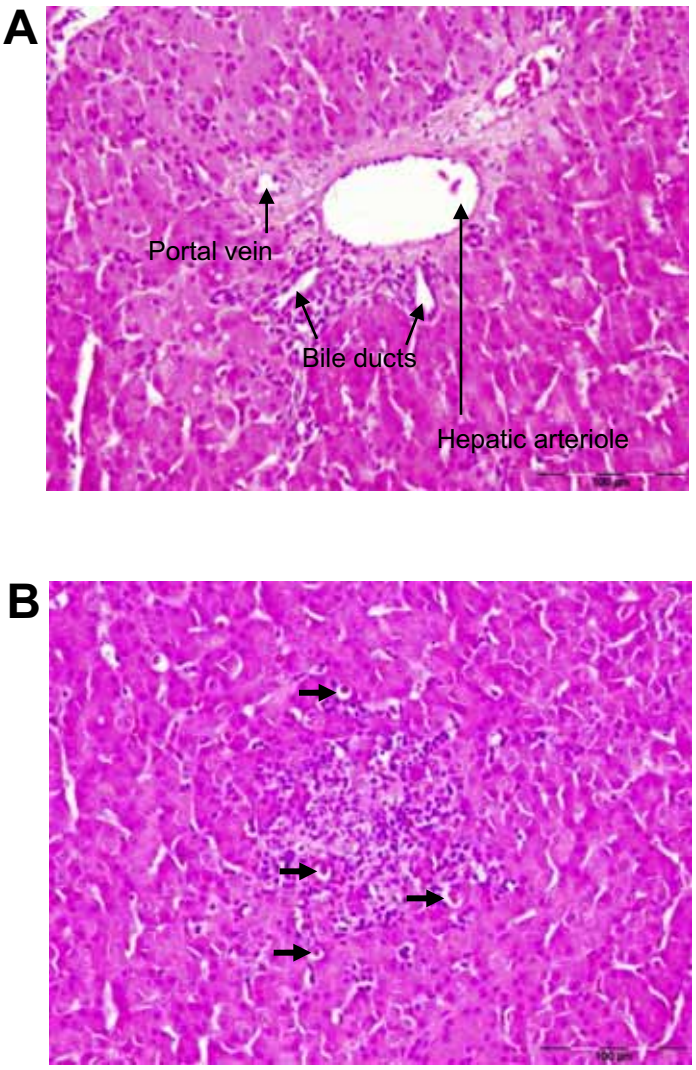


Figure 7.3

Figure 7.4: Detection of Kupffer cells during various stages of activation in PAS-D-stained liver sections prepared from ducks with acute DHBV infection.

Formalin-fixed and embedded duck liver tissue sections were PAS-D stained as described in Section 2.4.3, and photographed using light microscopy at 400X magnification, magnification bar = 50 μM. Kupffer cells will be stained purple-bright pink for lipid-rich ceroid PAS-D positive phagocytosed materials, and pink/brown granular aggregates acid-fast phagocytosed materials (like bile), while nuclei are counter-stained blue-purple using haematoxylin.

Figure 7.4A shows examples of Kupffer cells that mostly do not contain phagocytosed materials (termed as "unactivated") (emphasised by black arrows). Photograph was taken from the liver of duck 339 at 4 dpi.

Figure 7.4B shows examples of medium-sized Kupffer cells that mostly contain PAS-D positive materials (termed as "activated") (emphasised by blue arrows), with some unactivated Kupffer cells still present (emphasised by black arrows). Photograph was taken from the liver of duck 339 at 45 dpi.

Figure 7.4C shows examples of medium-sized mostly activated Kupffer cells that contain acid-fast pink/brown pigments (emphasised by blue arrows), with some unactivated Kupffer cells still present (emphasised by black arrows). Photograph was taken from the liver of duck 339 at 18 dpi.

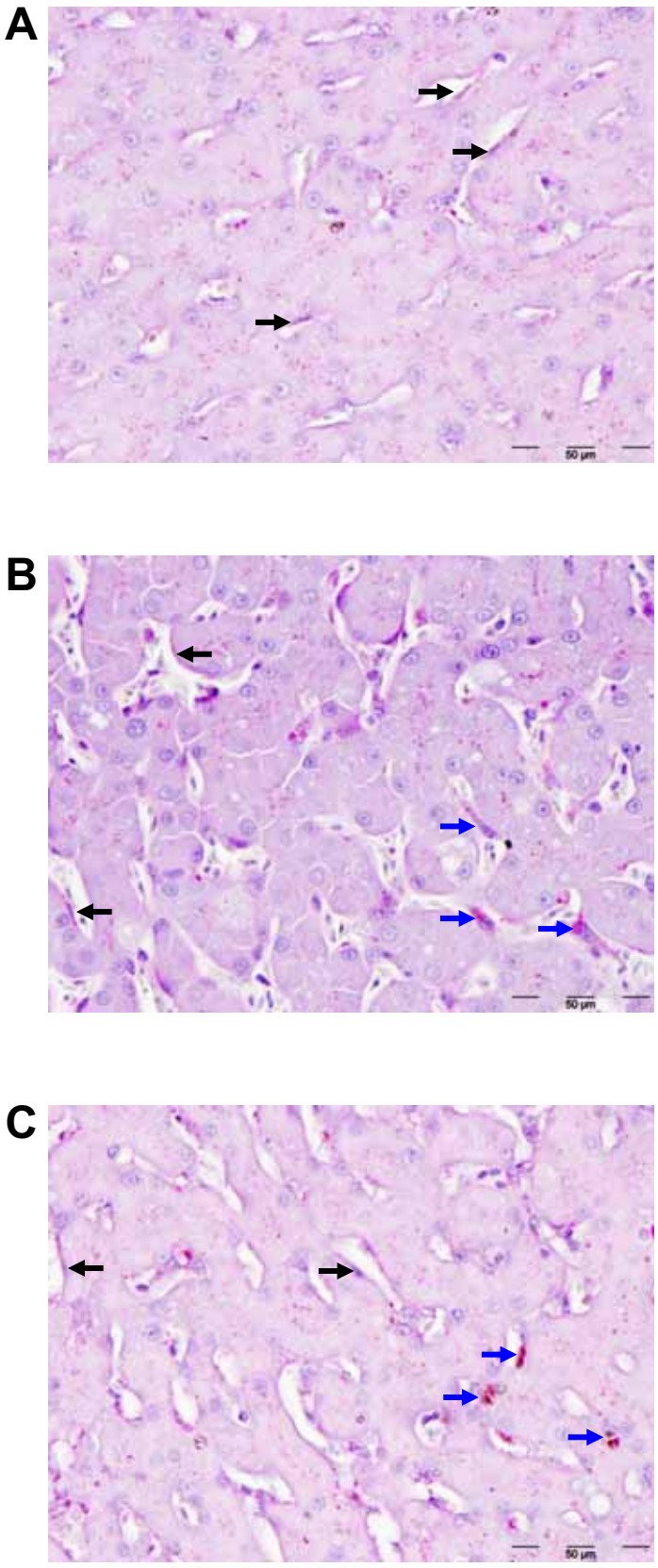


Figure 7.4

Figure 7.5: Levels of DHBsAg (A), anti-DHBc antibodies (B), and anti-DHBs antibodies (C) in the serum of ducks 337, 339, 342 with acute DHBV infection as detected by ELISA.

The levels of DHBsAg present in the serum were detected by rapid qualitative ELISA as described in Section 2.5.2, and were calculated based on standard curves generated using the Pool 8 serum containing 50 μg/mL of DHBsAg (Jilbert *et al.*, 1996). The background level of the DHBsAg ELISA was determined by the mean optical density (OD) readings of normal duck serum (NDS) plus two standard deviations. The background reading (0.63 μg/mL of DHBsAg) is shown as dotted line in Figure 7.5A, and used as the limit of detection for all these assays.

The levels of anti-DHBc antibodies present in the serum were detected by quantitative ELISA as described in Section 2.5.3. Titres of anti-DHBc antibodies are expressed as the reciprocal of the serum dilution required to achieve an OD of 0.47 at 490 nm. The negative cut-off for anti-DHBc-positive samples is set at two standard deviations above the average background obtained by assaying all 6 ducks in this study (337, 338, 339, 342, 343, 350) at 0 dpi (Miller *et al.*, 2004). As the minimum serum dilution was 1/500, the minimum titre is 500 (shown as the dotted line in Figure 7.5B), with values under 500 represented as "1" (Foster *et al.*, 2005).

The levels of anti-DHBs antibodies present in the serum were detected by quantitative ELISA as described in Section 2.5.4. Titres of anti-DHBc antibodies are expressed as the reciprocal of the serum dilution required to achieve an OD of 0.24 at 490 nm. The negative cut-off for anti-DHBc-positive samples is set at two standard deviations above the average background obtained by assaying all 6 ducks in this study (337, 338, 339, 342, 343, 350) at 0 dpi (Miller *et al.*, 2004). As the minimum serum dilution was 1/100, the minimum titre is 100 (shown as the lower dotted line in Figure 7.5C), with values under 100 represented as "1". As the maximum serum dilution was 1/12,500, the maximum titre is 12,500 (shown as the upper dotted line in Figure 7.5C) (Foster *et al.*, 2005).

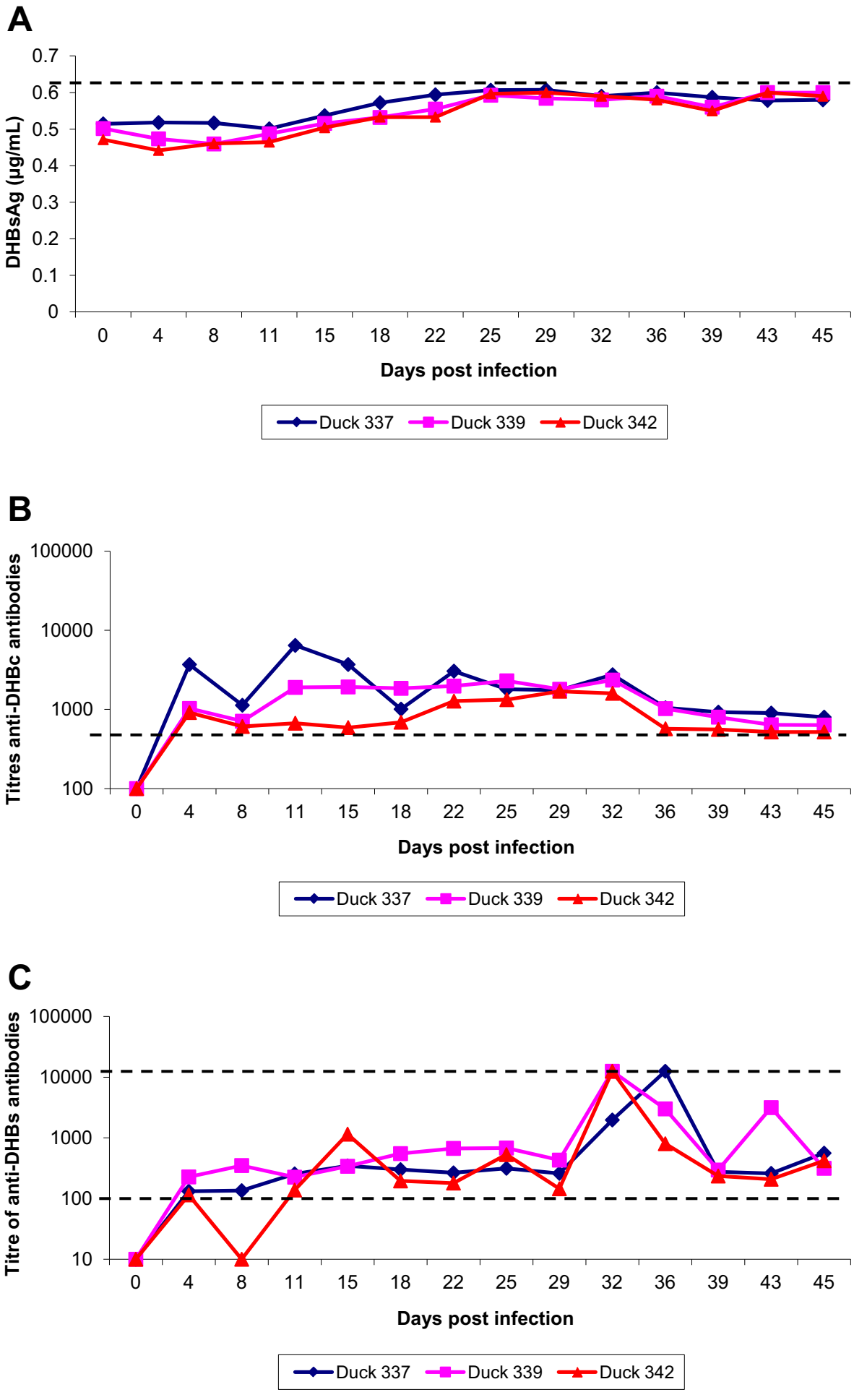
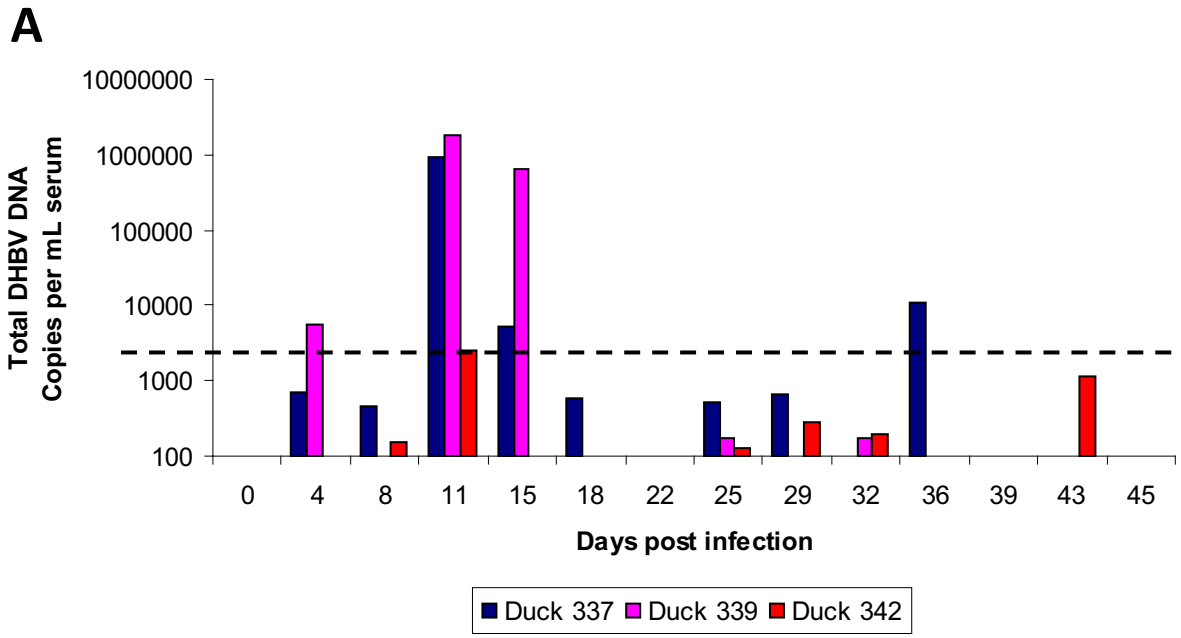

A
0.7
0.6
0.5
0.4
0.3
0.2
0.1
0
DHBsAg (µg/mL)
0 4 8 11 15 18 22 25 29 32 36 39 43 45
Days post infection
Duck 337 Duck 339 Duck 342
B
100000
10000
1000
100
Titres anti-DHBc antibodies
0 4 8 11 15 18 22 25 29 32 36 39 43 45
Days post infection
Duck 337 Duck 339 Duck 342
C
100000
10000
1000
100
10
Titre of anti-DHBs antibodies
0 4 8 11 15 18 22 25 29 32 36 39 43 45
Days post infection
Duck 337 Duck 339 Duck 342

Figure 7.5

Figure 7.6: Levels of DHBV total DNA present in the serum (A), and levels of DHBV total and cccDNA present in the liver (B) of ducks 337, 339 and 342 with acute DHBV infection as detected by qPCR reactions.

The levels of DHBV total DNA present per mL serum was determined as described in Section 2.8.9.1 using the primer set 423 – 576c (Table 2.2). The limit of detection of the assay shown as the dotted line in Figure 7.6A is determined by the limit of sensitivity of the qPCR machine which does not accurately detect less than 10 copies of DHBV total DNA per 4 μL of serum, or 2500 copies of DHBV total DNA per mL of serum.

The levels of DHBV total and cccDNA in the liver were determined as described in Section 2.8.9.2 using the primer sets 423 – 576c and CC2 – MG1 respectively (Table 2.2). The levels of DHBV DNA per cell were calculated as described in Section 2.8.9.3.2. The limit of detection of the assay shown as the dotted line in Figure 7.6B is determined by the limit of sensitivity of the qPCR machine which does not accurately detect less than 10 copies of DHBV total and cccDNA per 53,571 cells, or 0.00019 copies of DHBV DNA per cell.


A
Total DHBV DNA
Copies per mL serum
10000000
1000000
100000
10000
1000
100
0
4
8
11
15
18
22
25
29
32
36
39
43
45
Days post infection
Duck 337
Duck 339
Duck 342

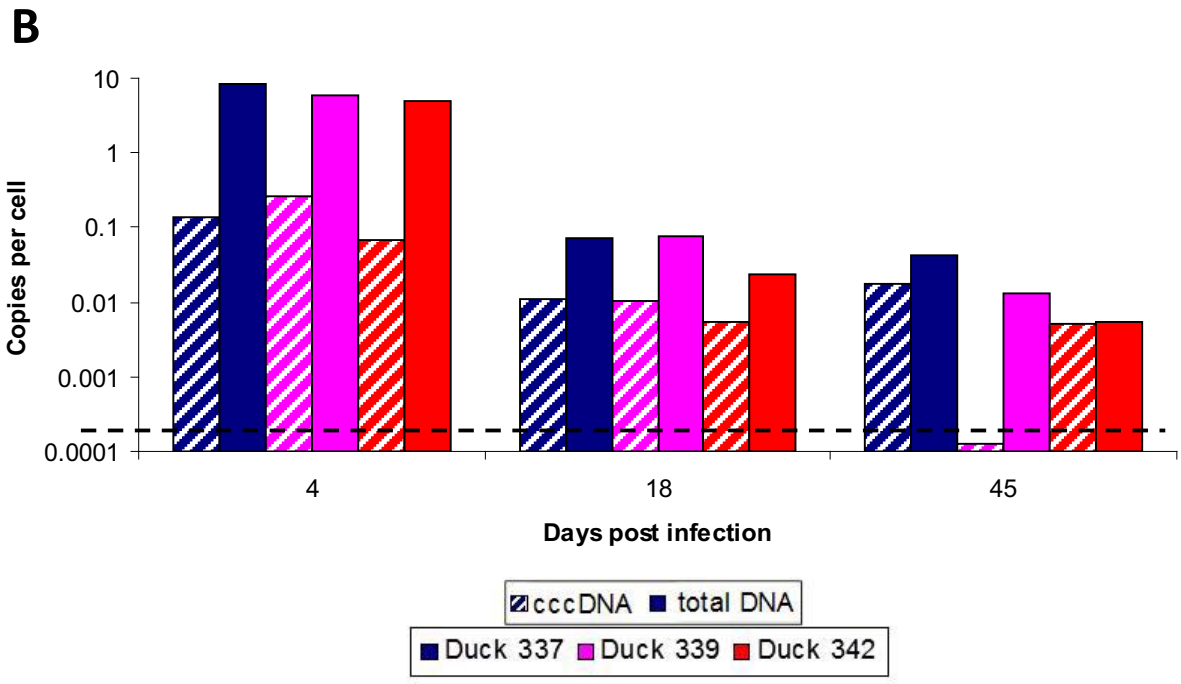

B
Copies per cell
10
1
0.1
0.01
0.001
0.0001
4
18
45
Days post infection
cccDNA
total DNA
Duck 337
Duck 339
Duck 342

Figure 7.6

Figure 7.7: Multiple sequence alignment showing the 640 bp sequenced region of the DHBV genome from ducks 337, 339 and 342 with acute DHBV infection, aligned with the duck AusDHBV genome (GenBank Accession AJ006350, REGION: 2388 – 3027).

DNA was extracted from duck liver tissues using total DNA extraction method as described in Section 2.6.3, and was used as template for PCR reactions using primer set DRS F2 – R2 (refer Table 2.2), and sequenced as described in Section 7.4.1. The multiple sequence alignment was performed using ClustalW2 program and output file viewed and arranged by Jalview program as described in Section 2.8.12.

Individual alignment scores of the AusDHBV and the DHBV DNA sequence were obtained using the BLAST Align 2 Sequences programme as described in Section 2.8.12. The scores were 100% coverage and 99% sequence similarity for all ducks 337, 339 and 342.

Note:
REGION refers to the specific region of nucleotide sequence that was used for alignment in this multiple sequence alignment, and was based on the nucleotide numbering obtained from the AusDHBV (GenBank Accession AJ006350) sequence. REGION was chosen to match with the range of the amplified and sequenced target gene (DHBV genome). The numbers shown in the multiple sequence alignment output figure refer to the nucleotide numbering of the specified REGIONs.

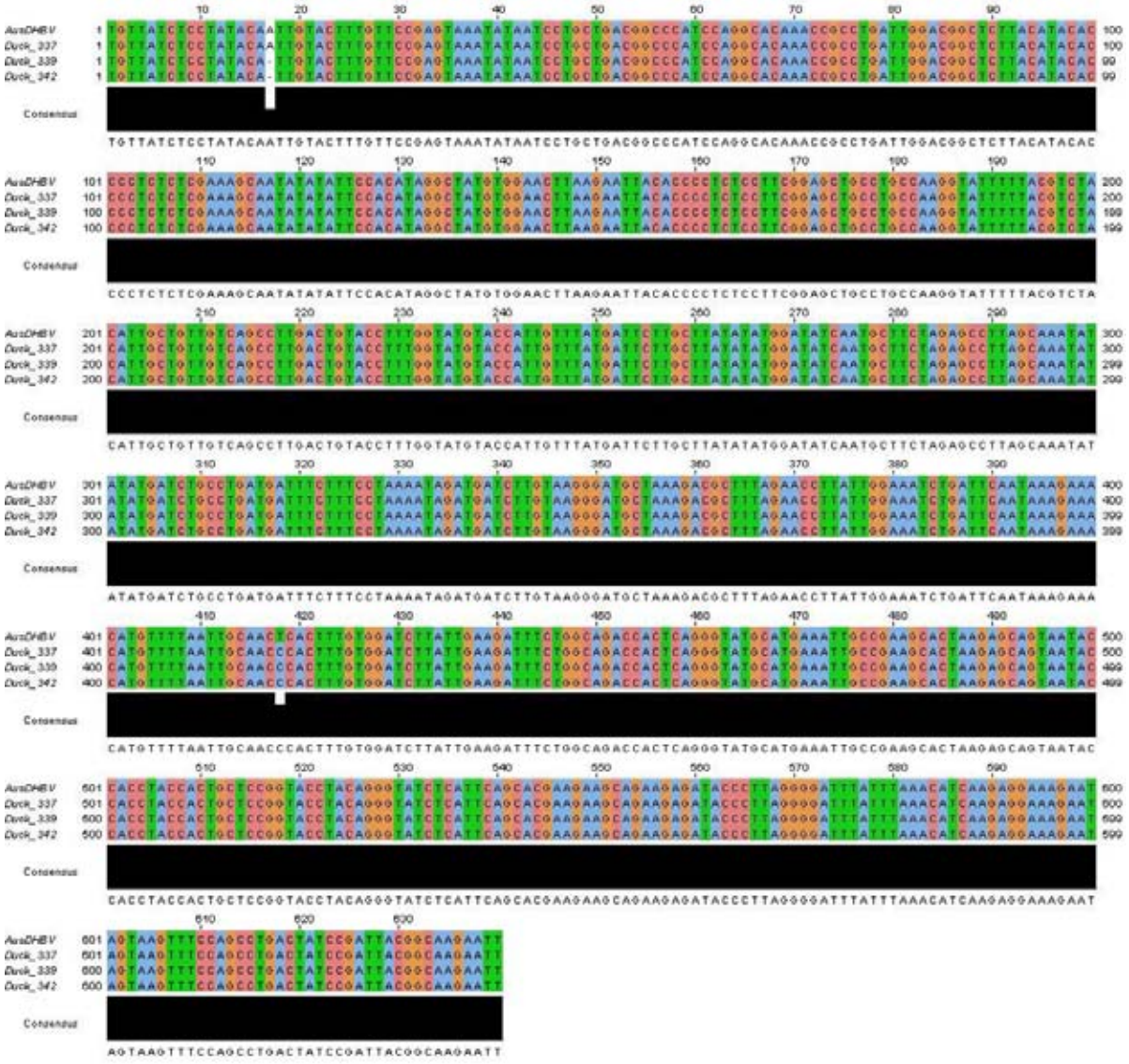


Figure 7.7

Figure 7.8: Examples of invPCR products obtained from the duck invPCR assays.

DNA was extracted from duck liver tissues and inverted as described in Section 7.4.2. The inverted DNA fragments were either 1/3 serially diluted in the 96-well PCR tray as shown in Figure 2.8 (Figure 7.8A), or were distributed evenly to all 96 PCR wells (Figure 7.8B), as DNA templates during nested PCR. Products were visualised using 96-well agarose gel electrophoresis as under 365 nm UV light as described in Section 2.10.5.

The letters A – H refer to the rows of the PCR wells. The DNA marker used (at the lanes labelled "m") was 1 μg of the GeneRuler 1 kbp Plus DNA Ladder (Thermo Fisher Scientific, Canada). Wells H7 – H12 (marked by red box) that did not contain any DNA templates were used as PCR negative controls (-ve).

Based on Figure 7.8A, the optimal amount of inverted DNA fragment that can produce a single invPCR product in most of the PCR wells, was the amount of DNA in between Rows D and E.

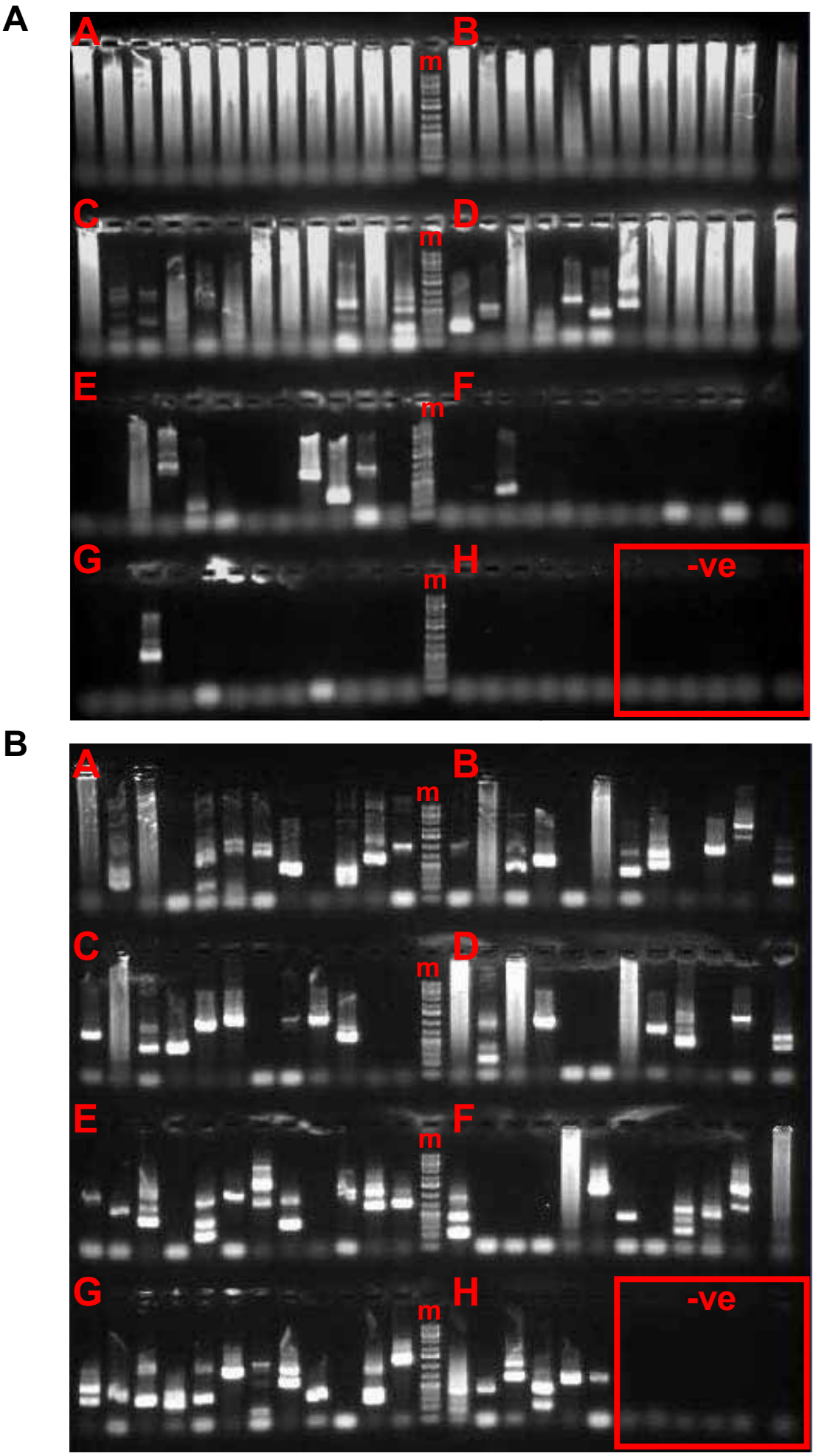


Figure 7.8

Figure 7.9: Example of DNA sequencing results obtained from invPCR assays performed using liver tissues from ducks with acute DHBV infection.

The duck D3 invPCR assays were performed as described in Section 7.4.2.

Figure 7.9A shows an example of the DNA sequencing results for an unknown sequence. BLAST analysis showed that the 463 bp sequence consisted of a 9 bp insert DNA (black font) flanked by the DHBV genome (GenBank Accession AJ006350) 2750 – 2688 nt that is joined to 2590 – 2534 nt (blue bold font) and 299 – 3011 nt (red bold font). The *Eco*RI first cut restriction enzyme site is underlined.

Figure 7.9B shows an example of the DNA sequencing result for a virus-virus sequence, which was a false positive result. BLAST analysis showed that the 353 bp sequence consisted of 2 fragments of the DHBV genome (GenBank Accession AJ006350), 2682 – 2535 nt (blue bold font) and 190 – 3011 nt (black bold font). This shows that the virus-virus false positive sequence was likely to be formed by the ligation of 2 DHBV DNA fragments. The *Eco*RI first cut restriction enzyme digestion site is underlined, while the *Nde*I cccDNA destroying enzyme digestion site is underlined and italicized

A

GCACTCTTGCCGTATCGAATATCTGGCTGGAATCTGCGTCTTTGGCAT
CCCTTACAGAACGGCTATTGTTGACAAGAAATCATGTAGAAGATCAAA
TCCTTGGCAGGTGAATCCGAAGGAGAGGGGTGTAATTCTTAGGGGTGG
CTTAGGCAGCTGTTGATTTATCGTTTCTTCGTCTAGGGTCAGAACCAC
TGCGTTTTCTAGGTGCCCTGCATGTTTTCTGCCTCCCTGAGCCACTTG
GATTGGTCTAGTGATTGCTTCAATGGTTGGGGGATCACGGCCTCGGTA
CTTCTCAGGTGTTGACAACCAAGTACGGAGCCGAGAAATATAATTAGT
AACGTTAGCTTCTCCCCACAGTAAACAATTGTAATGCCACCAAAGCAA
TCTCCTAGCCCGATCCAATGATTCCTCATTAATCTTTGCATATGCTTT
TAGGTGTGCATGAATTCTTGCCGTAATCGAA

B

TGCTAGGCTCTAGAAGCATTGATATCCATATATAAGCAAGAATCATAA
ACAATGTTACATACCAAAGGTACAGTCAAGGCTGACAACAGCAATGTA
GACGTAAAAATACCTTGGCAGGCAGCTCCGAAGGAGAGGGGTGTAATT
CTTGCTTCAATGGTTGGGGCATCACGGCCTCGGTACTTCTCAGGTGTT
GACAACCAAGTACGGAGCCGAGAAATATAATTAGTAACGTTAGCTTCT
CCCCACAGTAAACAATTGTAATGCCACCAAAGCAATCTCCTAGCCCGA
TCCAATGATTCCTCATTAATCTTTG*CATATG*CTTTTAGGTGTGCATGA
ATTCTTGCCGTAATCGA

Chapter 8: The use of invPCR to assess levels of clonal proliferation of hepatocytes during various stages of chronic DHBV infection

8.1. Aims

a) To establish and monitor chronic DHBV infection in ducks.
b) To characterise histological and serological changes occurring during various stages of chronic DHBV infection.
c) To detect integrated virus-cell junctions during various stages of chronic DHBV infection using the invPCR assay.
d) To determine the extent of clonal proliferation of hepatocytes that occurred in the ducks during chronic DHBV infection.

8.2. Introduction

As discussed in Chapter 1.7, clonal proliferation of hepatocytes refers to clonal expansion of a hepatocyte undergoing multiple rounds of proliferation to replace neighbouring hepatocytes that have been killed, thus forming hepatocyte clones in the liver. Clonal proliferation may play a pivotal role during liver regeneration, clearance of HBV-infected hepatocytes, and contributing to the formation of HCC and tumours in the liver. Several methods have been previously used to detect clonal proliferation, including Southern blot hybridisation analysis of integrated HBV DNA, X chromosome-linked methylation patterns, *p53* gene mutations, DNA fingerprinting, and patterns of loss of chromosomal alleles (Ochiai *et al.*, 2000).

Using the Southern blot hybridisation method as described in Section 1.8.1, it was found that ~30% of cirrhotic nodules present in the livers of human HBV carriers were comprised of hepatocyte clones larger than 10^5 cells in size (Yasui *et al.*, 1992). Although this method is specific and could differentiate different clones based on bands of HBV DNA created by restriction enzyme digestion patterns of DNA, Southern blot hybridisation it is not highly sensitive and could only efficiently detect clones larger than 10^5 cells. Furthermore, as hepatocyte clones that do not contain integrated HBV DNA would not be detected by this method, the true rate of clonal proliferation of hepatocytes would not be determined.

Clonal proliferation of hepatocytes can also be detected by observing gene methylation patterns or gene inactivation patterns on X chromosomes. Methylation of genes can be determined by digesting the DNA using methylation-sensitive restriction enzymes like *Hpa*II, and then observing the DNA restriction enzyme digestion patterns produced using Southern

blot hybridisation or PCR amplification (Vogelstein *et al.*, 1987; Kawai *et al.*, 1995). As only a single X chromosome is activated in somatic cells, during embryogenesis either the maternal or paternal X chromosome-linked gene would be inactivated by methylation, thus producing individual gene inactivation patterns for each cell. If a tissue contains cells that are clonal or derived from clonal proliferation of a single cell only, they would all contain the same gene inactivation pattern, and thus would produce a consistent banding pattern when analysed using this method. On the other hand, tissues that are polyclonal would contain various gene inactivation patterns, and thus would produce multiple or inconsistent banding patterns (Ochiai *et al.*, 2000). Using this technique, it was found that most liver regenerative nodules (suspected to precede hepatocarcinogenesis) were polyclonal (Ochiai *et al.*, 2000), while most HCC nodules larger than 25 mm in diameter were clonal or likely to have derived from a single cell (Kawai *et al.*, 1995). Although the methylation approach is sensitive and could be used for small liver tissues or for DNA extracted from paraffin-embedded microdissected tissue samples for higher specificity, this technique can only be applied to genders that have two of the same sex chromosome. Specifically, the technique would be limited to mammalian females that have two X chromosomes, or avian males that have two Z chromosomes (Ellegren, 2001). Furthermore, this methylation approach assumes that the gene inactivation patterns are retained in the progeny cells, and could also produce false polyclonal results if samples were contaminated by DNA extracted from other cell types, like connective tissue or white blood cells, which are polyclonal (Vogelstein *et al.*, 1987; Ochiai *et al.*, 2000).

Lastly, clonal proliferation of hepatocytes can also be detected by the invPCR assay using integrated virus-cell junctions present in liver cell DNA as genetic markers to track clonal proliferation of hepatocytes and to determine the size of any hepatocyte clones detected. As mentioned in Chapter 1.8.1, every integration event produces a unique integrated virus-cell junction, which upon clonal proliferation of that hepatocyte, would form hepatocytes clones that contained the same integrated virus-cell junctions (Ochiai *et al.*, 2000). Thus, the frequency of each unique integrated virus-cell junction detected would allow for the calculation of the size of the hepatocyte clone, and to determine how many times a single hepatocyte has proliferated (Summers *et al.*, 2003; Mason *et al.*, 2009a; Mason *et al.*, 2009b).

InvPCR assays have been used to detect clonal proliferation of hepatocytes during chronic infection in liver tissues from DHBV-infected ducks (Yang and Summers, 1999), WHV-infected woodchucks (Mason *et al.*, 2005), HBV-infected chimpanzees (Mason *et al.*, 2009a), and HBV-infected humans (Mason *et al.*, 2010). In long-term studies, in liver tissue collected from 2.4 year old WHV-infected woodchucks, at least 2% of the liver consisted of hepatocyte

clones larger than 1000 cells, with the largest clone found to be up to 26,000 cells in size (Mason *et al.*, 2005). Similarly, in HBV-infected chimpanzees, 50 hepatocyte clones ranging from 35 to 10,000 cells in size were found in a sample size of ~3 x 10^7 hepatocytes (Mason *et al.*, 2009a). While in the HBV-infected human liver tissues, 1 – 8 hepatocyte clones of 100 – 60,000 cells were found in 1 – 3 mg of each liver tissue (Mason *et al.*, 2010). Currently no studies had been published on the clonal proliferation of hepatocytes in ducks with long-term chronic DHBV infection. Therefore, this Chapter aims to use invPCR assays to detect clonal proliferation of hepatocytes in chronic DHBV-infected ducks up to 1 year post infection.

It is expected that during the early stages of DHBV infection, the low levels of DHBV integrations events would generate a pool of unique integrated virus-cell junctions with no or few hepatocyte clones (Yang and Summers, 1999). Throughout later stages of infection, as DHBV replication continues and DHBV infection spreads to >95% of hepatocytes (Jilbert *et al.*, 1998), more integration events would occur to generate more integrated virus-cell junctions. Hepatocyte clones would also be formed due to clonal proliferation of hepatocytes to replace the neighbouring DHBV-infected hepatocytes killed by the host immune response, or by normal hepatocyte proliferation during the natural growth or expansion of the liver mass.

In this study, 6-week-old ducks were used, as it is expected that older ducks would be able to mount stronger immune responses compared to younger ducks (e.g. 1-day-old) during DHBV infection. With stronger immune responses, it is expected that a higher rate of liver turnover would occur and larger hepatocytes clones could be formed. On top of that, as the progression of chronic DHBV infection in ducks infected at 6 weeks of age has not been extensively studied and published, this Chapter also aims to characterise the histological and serological changes occurring during different stages of chronic DHBV infection in ducks. As mentioned in Section 6.2, in this thesis, ducks that cleared DHBV infection by 10 dpi are defined as having "acute DHBV infection", while ducks with widespread DHBV infection from 10 dpi until the last time-point of a study are defined as having "chronic DHBV infection".

8.3. To establish and monitor chronic DHBV infection in ducks

8.3.1. To establish chronic DHBV infection in ducks

Similar with the study performed in Chapter 7 and as described in Section 7.3.1, six, 6-week-old Pekin-Aylesbury ducks (Section 2.1) were experimentally infected with 1.5x10^{10} vge of Pool 8 DHBV virus stock (Section 2.2) as described in Section 2.3.1.

In this study, liver biopsy tissues were collected from the ducks at 4 and 18 dpi as described in Section 2.3.3.1. The percentage of DHBsAg-positive hepatocytes was then determined by immuno-staining of DHBsAg in liver tissue sections as described in Section 2.4.2. At 18 dpi, in three ducks (numbered 338, 343 and 350), >95% of the hepatocytes were DHBsAg-positive (Section 8.3.2.1); while in the other three ducks (numbered 337, 339 and 342), <0.15% of the hepatocytes were DHBsAg-positive. These findings suggest that widespread and possibly persistent DHBV infection had been established in ducks 338, 343 and 350 by 18 dpi, while ducks 337, 339, and 342 had acute DHBV infection as described in Chapter 7.

Ducks 338, 343 and 350 were further monitored, with liver biopsy tissues collected at 60 and 196 dpi, and liver autopsy tissues collected at 327 dpi as described in Section 2.3.3.2. However, as duck 343 unfortunately fell ill due to DHBV infection-unrelated causes, this duck was euthanased and autopsy was performed at 165 dpi. All collected liver tissues were either snap frozen in liquid nitrogen and stored at -80^{o}C, or fixed in EAA, formalin or 70% ethanol, and subsequently embedded and sectioned onto glass microscope slides, as described in Section 2.3.4.1, to be used for various histological analyses as described in Section 2.4. DNA was also extracted from the liver tissues using the ChargeSwitch gDNA mini tissue kit, as described in Section 2.6.2, to determine the levels of DHBV total and cccDNA present in the liver by qPCR as described in Section 2.8.9.2. In addition, blood samples were obtained periodically from the ducks by venipuncture as described in Section 2.3.2.1, and serum was collected as described in Section 2.3.2.2. Specifically, blood samples were collected twice weekly until 116 dpi, weekly till 170 dpi, fortnightly till 196 dpi, at 224 dpi and finally at 327 dpi. Blood samples were collected from duck 343 at the same timings but with the final sample collected at 165 dpi. Serum was then analysed by ELISA to determine the levels of DHBsAg and anti-DHBc and anti-DHBs antibodies as described in Section 2.5.2 to 2.5.4, and to determine levels of DHBV total DNA by qPCR as described in Sections 2.8.9.1.

As there were no control ducks in this study, 4 duck liver tissues were obtained from a previous study conducted by Dr. Georget Reaiche (Reaiche *et al.*, 2010). These include duck 138 (described previously in Section 7.3.1) inoculated with NDS at 6 weeks of age as an age matched uninfected duck control, and 3 ducks (designated as ducks 140, 141 and 142) as age matched ducks for comparison of events occurring during acute and chronic DHBV infections. Ducks 140, 141 and 142 were hatched from the same commercial hatchery as this study (as described in Section 2.1), was inoculated with the same $1.5x10^{10}$ vge of DHBV virus stock (Pool 8), and subsequently developed acute DHBV infection with <0.001% DHBsAg-positive hepatocytes by 60 dpi. H&E-staining of formalin-fixed liver tissue sections of these 4 ducks

were previously prepared by Dr. Reaiche (Reaiche *et al.*, 2010). In addition, the 3 ducks with acute DHBV infection described in Chapter 7 would also be used for short-term comparison (the study in Chapter 7 was terminated at 45 dpi compared to 327 dpi in this Chapter).

8.3.2. Characterisation of histological and serological changes occurring during various stages of chronic DHBV infection

8.3.2.1. DHBsAg-positive hepatocytes in the liver

EAA-fixed and embedded duck liver tissue sections prepared as described in Section 2.3.4.1 were stained with anti-DHBV pre-S monoclonal antibody, 1H.1, as described in Section 2.4.2, to determine the percentage of DHBV-infected hepatocytes present. Sections of DHBsAg-stained liver were photographed at each time-point and compiled as Figure 8.1.

DHBsAg-staining (Table 8.1) showed that at 4 dpi, ducks 338, 343 and 350 had 5.2%, 3.0% and 4.1% of DHBsAg-positive hepatocytes respectively (an average of 4.1%). These results were similar to the average 4.4% of DHBsAg-positive hepatocytes found in ducks 337, 339 and 342 that developed acute DHBV infection (Section 7.3.2.1). At 18 dpi, ducks 338, 343 and 350 had >95% of DHBsAg-positive hepatocytes, compared to only ~0.2% of DHBsAg-positive hepatocytes found in the ducks with acute DHBV infection (Section 7.3.2.1). These suggest that chronic DHBV infection was established in these ducks, as the initial DHBV infection was not cleared or controlled, resulting in a widespread DHBV infection in the liver by 18 dpi. These observations are consistent with the infection outcome observed previously in ducks that developed chronic DHBV infection (Jilbert *et al.*, 1998; Miller *et al.*, 2008).

As some ducks have been shown to be able to spontaneously resolve widespread DHBV infection after 31 dpi (Reaiche, 2008), DHBV levels in these ducks were further monitored. As shown in Figure 8.1 and Table 8.1, ducks 338, 343 and 350 had >95% of DHBsAg-positive hepatocytes at all subsequent time-points, and thus confirmed that chronic DHBV infection had been established in these ducks throughout this study.

8.3.2.2. Levels of inflammation in the liver

Formalin-fixed and embedded duck liver tissue sections were H&E-stained, viewed, and analysed as described in Section 2.4.1, to determine the levels of inflammation (portal and lobular) in the liver. The H&E-stained liver tissue sections were photographed at each time-point are compiled as Figure 8.2, with detailed analysis summarised in Table 8.1A.

Currently, there have been no reported long-term studies of 6-week-old ducks that were experimentally infected with DHBV and subsequently developed chronic DHBV infection. In previous studies showing long-term characterisation of the livers from 1-day-old ducks experimentally infected with DHBV to develop chronic DHBV infection, it was found that moderate portal inflammation and some lobular inflammation was only detected in 35% – 66% of the infected ducks at 21 – 42 dpi, likely due to the "immunologically tolerant" 1-day-old ducks that had not fully developed their immune responses until 2 – 6 weeks of age (Marion *et al.*, 1984; Cullen *et al.*, 1989). From 70 – 644 dpi, most ducks showed persistent mild – moderate portal inflammation with little lobular inflammation. However, some control uninfected ducks also showed similar mild portal inflammation with the chronic DHBV-infected ducks, with no significant differences between the inflammation levels in both groups of ducks before ~21 dpi (when ducks were still "immuno-tolerant") and after 84 dpi (Freiman *et al.*, 1988; Cullen *et al.*, 1989). On the other hand, another previous study of 4-month-old ducks experimentally infected with DHBV to develop chronic DHBV infection showed extensive portal and lobular inflammation at 12 dpi (Jilbert *et al.*, 1998). Based on that, it is expected that in this study, these ducks would be able to mount strong immune responses against DHBV infection, and thus should result in moderate portal and lobular inflammation as early as 12 dpi, which would persist as mild portal and lobular inflammation throughout the duration of chronic DHBV infection until the end of the study (327 dpi).

As summarised in Table 8.1A, at 4 dpi, the ducks livers showed varying inflammation levels, from normal inflammation levels in duck 350 where only 0.32% of the liver contained inflammatory with almost no portal and lobular inflammation; to mild levels of inflammation in ducks 338 and 343 where an average of 1.68% of the liver contained inflammatory cells, with portal inflammation (pointed out by black arrows in Figure 8.2) in some portal tracts (with areas of portal inflammation up to 16 cells in diameter), and scarce patches of lobular inflammation (pointed out by blue arrows in Figure 8.2) (up to 26 cells in diameter).

At 18 dpi, the ducks livers all showed elevated levels of inflammation: 2.44% of the liver contained inflammatory cells, large portal inflammation was present in almost all the portal tracts (with areas of portal inflammation up to 32 cells in diameter), and frequent lobular inflammation (up to 19 cells in diameter). These were similar to results from previous studies (Jilbert *et al.*, 1998), and suggest that the immune response of the ducks had been activated, resulting in infiltration of lymphocytes to the liver. However, the activated immune responses were unable to clear the DHBV infection, resulting in the spread of DHBV infection to >95% of hepatocytes in the liver at 18 dpi as described in Section 8.3.2.1.

At 60 dpi, the duck livers showed reduced levels of inflammation compared to 18 dpi, varying from 0.64% – 2.04% of the liver containing inflammatory cells, portal inflammation in some portal tracts (with areas of portal inflammation up to 22 cells in diameter), and scarce patches of lobular inflammation (up to 25 cells in diameter). Similar levels of mild liver inflammation subsequently persisted throughout the later stages of chronic DHBV infection (165, 196, 327 dpi) in all ducks: an average of 1.52% of the liver contained inflammatory cells, portal inflammation present in some portal tracts (with areas of portal inflammation up to 38 cells in diameter), and scarce patches of lobular inflammation (up to 22 cells in diameter). These were as expected, as ongoing low level immune responses would be maintained throughout chronic DHBV infection due to continuous DHBV replication, resulting in persistent mild liver inflammation (Cullen *et al.*, 1989). Interestingly, lobular inflammation persisted in these ducks, something not previously observed in ducks experimentally infected at a younger age (1-day-old) (Freiman *et al.*, 1988; Cullen *et al.*, 1989). Hence, these showed that stronger immune responses would be activated and maintained in older ducks during long-term DHBV infection, to result in higher levels of portal and lobular inflammation in the liver.

When compared to the liver inflammation in the age matched ducks (6-week-old) that developed acute DHBV infection (ducks 337, 339 and 342 as shown in Table 7.1A and 140, 141 and 142 as shown in Table 8.1B), it was found that all ducks had lower levels of liver inflammation at all time-points. Although the differences were not statistically significant (p-value >0.05), the thickness of inflammation was mostly smaller, and scarce patches of lobular inflammation were often not present in the ducks with acute DHBV infection. These findings were similar to observations in humans, where humans with chronic HBV infection were reported to have denser and more severe portal inflammation and more frequent lobular inflammation compared to humans with acute HBV infection (Theise *et al.*, 2007).

Interestingly, as shown in Table 7.1B and described in Section 7.3.2.2, the age matched uninfected control duck 138 showed that in the absence of DHBV infection, varying levels of portal inflammation were still observed in the liver. Although these differences with ducks with chronic DHBV infection were not statistically significant (p-value >0.05), it was difficult to be confident about the significance of this data due to the small number of animals analysed. Interestingly, no lobular inflammation was observed in duck 138 at any time-point.

8.3.2.3. Levels of hepatocyte apoptosis in the liver

The same H&E-stained duck liver tissue sections described in Section 8.3.2.2 were also viewed to determine the levels of hepatocyte apoptosis. Photographs showing examples of

apoptotic cells observed are compiled in Figure 8.3, and findings are summarised in Table 8.2A. It is expected that higher levels of hepatocyte apoptosis would be observed when the levels of liver inflammation (Section 8.3.2.2) were elevated (Guo *et al.*, 2000).

As shown in Table 8.2A, at 4 dpi, an average of 2.1% of hepatocyte apoptosis were detected (Figure 8.3B). At 18 dpi, there was only a slight increase in the levels of hepatocyte apoptosis to an average of 2.89%. During later stages of chronic DHBV infection (60, 196, 327 dpi), the duck livers showed similar levels of hepatocyte apoptosis as observed at 4 dpi (an average of 2.24%). These higher levels of hepatocyte apoptosis may reflect ongoing immune responses against DHBV-infected hepatocytes due to the persistent and active DHBV infections.

On a separate note, for duck 343 which had to be euthanized at 165 dpi due to DHBV infection-unrelated illness, it was found that there were high levels of hepatocyte apoptosis (4.84%), with vacuolated hepatocytes (shown in Figure 8.4C), suggesting that steatosis, or accumulation of triglyceride fat droplets in the liver hepatocytes (Crawford, 2007) had occurred. Similar steatosis had been previously observed in 40% of 1-day-old ducks with chronic DHBV infection after 8 months post infection as well as in one age matched uninfected duck (Freiman *et al.*, 1988), and is likely due to liver injury from various non-viral causes like liver toxicity by Aflatoxins (Mason *et al.*, 1994; Augesse-Germon *et al.*, 1998).

When compared to the levels of hepatocyte apoptosis in the age matched ducks (6-week-old) that developed acute DHBV infection (ducks 337, 339 and 342 as shown in Table 7.2A and 141 as shown in Table 8.2B), it was found that all ducks had lower levels of hepatocyte apoptosis at all time-points. The differences were not statistically significant from 4 – 60 dpi (p-value >0.05), but were statistically different at later time-points of 196 – 327 dpi (p-value = 0.01), likely due to the ongoing immune responses in the ducks with chronic DHBV infection compared to “basal” levels of immune responses in ducks after clearance of DHBV infection.

Interestingly, as shown in Table 7.2B and described in Section 7.3.2.3, the uninfected control duck 138 showed that in the absence of DHBV infection, varying levels of hepatocyte apoptosis between 0.54% – 1.26%. Although the differences with ducks with chronic DHBV infection were statistically significant (p-value <0.01), it was difficult to be confident about the significance of this data due to the small number of animals analysed. Nonetheless, these showed that levels of hepatocyte apoptosis would increase during chronic DHBV infection.

Additionally, many of the classic liver pathologies commonly observed in humans with chronic HBV infections were not found in these duck liver tissues. These pathologies include bridging necrosis, ground glass hepatocytes, fibrosis, cirrhosis and even HCC (Theise *et al.*, 2007). Chronic DHBV infections do not generally cause liver diseases in ducks which results in cirrhosis and HCC (Funk *et al.*, 2007; Zoulim *et al.*, 2008). This may be due to differences in the pathogenesis of avian and mammalian hepadnavirus infection, or due to the shorter lifespan of ducks compared to humans that did not allow for the further development of more severe DHBV-induced liver diseases (Jilbert, 2005). The only few reported cases of DHBV-related HCC in Pekin ducks were in a 88-week-old duck chronically infected with DHBV at 1 day of age (Cullen *et al.*, 1989), and 5 DHBV-infected Indian domestic Pekin ducks, though the latter may also be induced by environmental toxins like Aflatoxin (Sridhar *et al.*, 1993). In addition, as hepatocellular adenoma (benign nodules) have been reported in a Pekin duck (1 – 3 years of age) with no detectable DHBV (Yokosuka *et al.*, 1985), and liver fibrosis has been reported in ducks infected with a mutant G133E strain (Lenhoff *et al.*, 1999; Meier *et al.*, 2003), these showed that liver diseases can occur in Pekin ducks, and thus the absence of these liver diseases during DHBV infection were not due to physiological differences of Pekin duck livers preventing their formation. However, as previous studies have observed HCC in ~61% of naturally DHBV-positive Chinese brown ducks (Duflot *et al.*, 1995), but only 2 out of 20 of the Pekin ducks experimentally infected with the same DHBV strain showed significant fibrosis but no HCC (Omata *et al.*, 1984), these observations suggest that Pekin ducks may indeed have some reduced susceptibility to DHBV-induced HCC compared to other duck species. On a separate note, secondary amyloidosis, a common liver disease in Pekin ducks after 7 months of age (Guo *et al.*, 1996) was not found any of these three ducks.

8.3.2.4. Levels of Kupffer cell infiltration and activation in the liver

Formalin-fixed and embedded duck liver tissue sections were PAS-D-stained as described in Section 2.4.3, and viewed to observe the levels of Kupffer cell infiltration and activation, as described in Section 7.3.2.4. Examples of Kupffer cells without phagocytosed materials (termed “unactivated Kupffer cells”) and with phagocytosed materials (termed “activated Kupffer cells) are shown in Figure 8.4, with detailed analysis summarised in Table 8.3A.

Currently, as emphasized previously, there have been no reported characterisations of 6-week-old ducks experimentally infected with DHBV that went on to develop long-term chronic DHBV infection. Knowing that Kupffer cells are involved in clearance of hepatocyte debris, it is expected that the levels of Kupffer cell infiltration and activation would continue to increase after DHBV infection, and will be maintained at moderate levels throughout

infection, due to the constant liver inflammation and apoptosis in the liver caused by the immune response occurring during persistent and active DHBV infections.

As shown in Table 8.3A, at 4 dpi, an average of 8.31% of the total liver cells in ducks 338 and 350 were Kupffer cells, while only 4.14% of the total cell in the liver of duck 343 were Kupffer cells. However, the Kupffer cells were mainly small-sized, and only a few Kupffer cells contained some phagocytosed materials ("activated") (2.93%) compared to Kupffer cells without observable phagocytosed materials ("unactivated") (3.99%) (shown in Figure 8.4A). At 18 dpi, all ducks showed similar levels of Kupffer cells, with an average of 6.91% of the total cells in the liver were Kupffer cells, but with higher numbers of activated Kupffer cells (4.4%) compared to unactivated Kupffer cells (2.5%). There was a slight increase in the Kupffer cells sizes to small- to medium-sized, with most Kupffer cells containing PAS-D positive phagocytosed materials (shown in Figure 8.4B). This was unexpected, as the levels of inflammation (Section 8.3.2.2) and apoptosis (Section 8.3.2.3) had greatly increased at 18 dpi.

During later stages of chronic DHBV infection (60, 196, 327 dpi), varying levels of Kupffer cells were observed (2.78% – 7.81%). Almost all of the Kupffer cells increased in size, and mostly contained PAS-D positive (shown in Figure 8.4B) and some acid-fast pink/brown pigments (shown in Figure 8.4C). This supports previous observations (Sections 8.3.2.2 and 8.3.2.3) that the immune responses of the ducks had been activated, with ongoing low levels of immune responses maintained throughout chronic DHBV infection. Thus, as there was ongoing hepatocyte apoptosis (Section 8.3.2.3), there would also be ongoing infiltration and activation of Kupffer cells to clear the hepatocyte debris.

For duck 343 which had to be euthanized at 165 dpi due to DHBV infection-unrelated illness, it was found that 11.48% of total liver cells were Kupffer cells, most of which were large-sized and contained PAS-D positive and some acid-fast pink/brown pigments (9.34%). This was expected as high levels of hepatocyte apoptosis were also observed in the liver (Section 8.3.2.3). As Kupffer cells are also known to be activated by bacterial lipopolysaccarides and muramyl peptides (Smedsrod *et al.*, 1994; Kolios *et al.*, 2006), these may indicate that duck 343 may had some form of bacterial infection. No further studies were performed to pursue the exact cause of illness and liver injuries in duck 343 in this thesis.

When compared to the levels of Kupffer cell in the age matched ducks (6-week-old) that developed acute DHBV infection (ducks 337, 339 and 342 as shown in Table 7.3A and 141 as shown in Table 8.3B), it was found that the levels of total and unactivated Kupffer cells were

similar between ducks with acute and chronic DHBV infection (p-value >0.05), with the exception of the difference of levels of total Kupffer cells at 18 dpi between both groups of ducks that were statistically significant (p-value <0.01). It was also found that chronic DHBV-infected ducks had lower levels of activated Kupffer cells from 4 – 60 dpi compared to acute DHBV-infected ducks, but had similar levels from 196 – 327 dpi, although the differences were not statistically significant at all time-points (p-value >0.05). It was unclear why the levels of Kupffer cell infiltration and activation in chronica DHBV-infected ducks were similar to acute DHBV-infected ducks despite higher levels of liver inflammation (Section 8.3.2.2) and hepatocyte apoptosis (Section 8.3.2.3), or why there was a slight delayed activation of Kupffer cells. As Kupffer cells are known to be activated by cytokines and chemokines like TNF-α and IFN-γ (Smedsrod *et al.*, 1994; Kolios *et al.*, 2006), it may be possible that there were delayed secretion of these cytokines/chemokines, or the Kupffer cells had slower activation by these cytokines/chemokines. It is likely that due to the inability of the ducks' immune system to rapidly activate Kupffer cells after DHBV challenge, the ducks were unable to control and clear DHBV infection, resulting in chronic DHBV infections.

Interestingly, as shown in Table 8.3B and described in Section 7.3.2.4, the age matched uninfected control duck 138 showed that in the absence of DHBV infection, varying levels of Kupffer cells were observed in the liver from 4 – 316 dpi, ranging from 1.95% – 5.98% of total liver cells, with most of the Kupffer cells not containing much phagocytosed materials until 221 dpi. These showed that variable levels of Kupffer cell infiltration and activation were normal occurances in the duck liver, and that the levels were lower compared to the reported normal levels of Kupffer cells found in normal rat livers (up to 15% of total liver cells were Kupffer cells) (Bouwens *et al.*, 1986). But at 316 dpi, there were 5.98% of Kupffer cells per total cells in the liver, most of which were large-sized and contained phagocytosed materials (4.93%). Coupled with the almost 2-fold increase in apoptotic cells (Table 8.2B), these suggest that shortly before 316 dpi, duck 138 was likely naturally exposed to some environmental toxins which resulted in activation of immune responses, causing higher levels of apoptosis and prompting the increase in infiltration and activation of Kupffer cells to clear the hepatocyte debris. Despite these variable levels, the levels Kupffer cells infiltration and activation were still on average higher in the ducks throughout chronic DHBV infection.

8.3.2.5. Levels of DHBsAg in the serum

The levels of DHBsAg in the serum of ducks were measured by rapid qualitative ELISA as described in Section 2.5.2 and explained in Section 7.3.2.5. It is expected that in ducks with

chronic DHBV infection, DHBsAg could be detected by 7 dpi and will persist throughout infection at 10 – 100 μg/mL (Jilbert *et al.*, 1998; Foster *et al.*, 2005).

As shown in Figure 8.5A, DHBsAg could be detected in ducks 338 and 350 by 8 dpi, and persisted at 0.6 – 20 μg/mL throughout infection. However in duck 343, less than 1 μg/mL of DHBsAg were detected from 4 – 22 dpi, before increasing to 7 μg/mL from 71 dpi onwards.

The DHBsAg levels in the serum were found to be 10-fold lower than the expected levels based on a previous study where $9.5x10^9$ vge/mL of DHBV was inoculated into 7-day-old ducks (Foster *et al.*, 2003). One possibility may be that adaptive immune responses were rapidly activated in the 6-week-old ducks to produce neutralising anti-DHBs antibodies that could complex with the DHBV virions in the serum, rapidly reducing the levels of viraemia and DHBsAg in these ducks (Vickery *et al.*, 1989). To test this possibility, levels of anti-DHBs antibodies were detected in the serum of these ducks as described in Section 8.3.2.7.

When compared to the levels of DHBsAg in the serum of age matched ducks that developed acute DHBV infection (Section 7.3.2.5) (ELISAs were performed concurrently for both groups of ducks), DHBsAg levels were below the level of detection throughout infection. Therefore, these showed that continuous low levels of "active" viraemia had occurred in ducks 338, 343 and 350 throughout the duration of this study (4 – 327 dpi), indicative of chronic DHBV infection and the failure of the duck to control and clear the DHBV infection.

8.3.2.6. Levels of anti-DHBc antibodies in the serum

The levels of anti-DHBc antibodies in the serum of ducks were measured by quantitative ELISA as described in Section 2.5.3 and explained in Section 7.3.2.6. In previous studies, anti-DHBc antibodies have been detected from as early as 9 – 14 dpi in ducks that develop chronic DHBV infection and with similar levels of anti-DHBc antibodies maintained throughout infection (Jilbert *et al.*, 1998; Noordeen, 2009). As the levels of anti-DHBc antibodies were expected to be maintained at similar levels once the adaptive immune responses were established, the anti-DHBc antibody levels were measured in the serum of ducks from 0 – 45 dpi only instead of the whole duration of this study (to 327 dpi).

As shown in Figure 8.5B, anti-DHBc antibodies could be detected in the serum of all three ducks at all time-points after 4 dpi, and were maintained at titres of 3,000 – 34,000 until 45 dpi (last time-point of testing), as expected.

When compared to the levels of anti-DHBc antibodies in the serum of age matched ducks (6-week-old) that developed acute DHBV infection (Section 7.3.2.6) (ELISAs were performed concurrently for both groups of ducks), anti-DHBc antibodies were also detectable by 4 dpi, but decreased in titres to 1050 after 36 dpi when DHBV infection had been cleared.

8.3.2.7. Levels of anti-DHBs antibodies in the serum

The levels of anti-DHBs antibodies in the serum of ducks were measured by quantitative ELISA as described in Section 2.5.4 and explained in Section 7.3.2.7. In ducks with chronic DHBV infection, low titres of anti-DHBs antibodies could be detected from 7 – 29 dpi, and fluctuated in titres throughout infection. Co-detection of DHBsAg which was not complexed to the antibodies was also observed (Jilbert *et al.*, 1998; Foster *et al.*, 2005; Miller *et al.*, 2008), suggesting that DHBsAg were present in excess to anti-DHBs antibodies. As the levels of anti-DHBs antibodies were expected to be maintained at similar levels once the adaptive immune responses were established, the anti-DHBs antibody levels were measured in the serum of ducks from 0 – 45 dpi only instead of the whole duration of this study (to 327 dpi).

As shown in Figure 8.5C, anti-DHBs antibodies could be detected in the serum of ducks 343 and 350 by 4 dpi at titres of 115 – 290 and then fluctuated between undetectable levels and titres of 12,500 until 32 dpi; while it could only be detected in duck 338 at 11 dpi at a titre of 195, and fluctuated between undetectable levels and titres of 3,250 until 32 dpi. From 36 – 45 dpi, the titres were maintained at 100 – 775 in all ducks. All these showed that the ducks' adaptive immune responses were able to be activated to produce anti-DHBs antibodies almost from the onset of DHBV infection. However, the antibodies were not sufficient in protecting the hepatocytes against further DHBV infection. In addition, co-detection of DHBsAg (Section 8.3.2.5) and anti-DHBs antibodies were observed, similar to previous studies (Jilbert *et al.*, 1998; Foster *et al.*, 2005; Miller *et al.*, 2008). These again confirmed that the levels of circulating DHBV virions (DHBsAg) were present in excess to the anti-DHBs antibodies, as the DHBsAg ELISA could not detect DHBsAg that was bound to the anti-DHBs antibodies.

When compared to the levels of anti-DHBs antibodies in the serum of the age matched ducks that developed acute DHBV infection (Section 7.3.2.7) (ELISAs were performed concurrently for both groups of ducks), anti-DHBs antibodies were detectable in all ducks only by 11 dpi at titres of 135 – 1150, and also with spikes of antibodies titres up to 12,500 at 32, 36 and 43 dpi. These showed that the more rapid and higher production of anti-DHBs antibodies may have contributed to the control and clearance of DHBV infection (Zhang and Summers, 2004).

8.3.2.8. Levels of DHBV DNA in the serum

The levels of DHBV DNA present in the serum were determined by qPCR as described in Section 2.8.9.1 and as explained in Secion 7.3.2.8. It is expected that in ducks with chronic DHBV infection, viraemia would persist in these ducks throughout infection with serum DHBV DNA of ~$1x10^5$ – $1x10^9$ copies per mL (Noordeen, 2009).

As shown in Figure 8.6A, no serum DHBV DNA was detected at 0 dpi, indicating that the ducks did not have viraemia prior to beign experimentally infected. By 4 dpi, serum DHBV DNA was detected in all ducks, and in ducks 338 and 350, serum DHBV DNA levels were maintained at $1x10^6$ – $1x10^9$ copies of DHBV DNA per mL from 18 – 327 dpi. Interestingly, for duck 343, the serum DHBV DNA levels were 1 – 2 logs lower than the other two ducks, varying from $1x10^4$ – $1x10^8$ copies of DHBV DNA per mL from 18 – 165 dpi, with a drop to 4,150 copies at 39 dpi, and with decreasing serum DHBV DNA levels after 116 dpi, finally dropping below the limit of detection at 127 dpi and 148 dpi. However, at 165 dpi, the liver still showed >95% DHBsAg-positive hepatocytes (Section 8.3.2.1), constant levels of DHBsAg in the serum from 71 – 165 dpi (Section 8.3.2.5), as well as high levels of DHBV total and cccDNA in the liver (Section 8.3.2.9), suggesting that DHBV infection had not been cleared in duck 343. As the serum samples from duck 343 were analysed concurrently with the other duck 338 and 350 samples, there should not have been errors during the qPCR instrument run to result in the low detection of serum DHBV DNA levels. Coupled with the undetermined DHBV-unrelated illness that duck 343 contracted around 165 dpi, the causes of the reduction of serum DHBV DNA levels in duck 343 were not pursued further in this thesis.

8.3.2.9. Levels of DHBV DNA in the liver

The levels of total and cccDNA present in the liver were determined by qPCR using primer sets 423 – 576c and CC2 – MG1 respectively (refer Table 2.2) as described in Section 2.8.9.2.

It is expected that in the liver of ducks with chronic DHBV infection, due to continuous DHBV replication, all forms of DHBV DNA, including the DHBV RI, rcDNA and DHBV cccDNA would be detected throughout infection. Specifically, during early stages of infection (4 dpi), there would be lower levels of DHBV cccDNA compared to the DHBV total DNA, as the cccDNA pool is still being generated from the rcDNA that was transported to the nucleus (refer to Section 1.2.4 for detailed description of viral replication). As chronic DHBV infection gradually establishes with continuous DHBV replication, increasing levels of both DHBV total and cccDNA would be detected, until a plateau occurs when maximum liver capacity is reached. In a fully established chronic DHBV infection, it is expected that up to 17

copies of DHBV cccDNA (Zhang *et al.*, 2003), and up to 100X more copies of total DHBV DNA could be found in each hepatocyte (Jilbert *et al.*, 1992; Noordeen, 2009).

As shown in Figure 8.6B, at 4 dpi, each cell contained ~9 and ~0.15 copies of DHBV total and cccDNA. As the DNA used as qPCR template was extracted from both DHBsAg-positive and -negative hepatocytes present in the liver, and knowing that ~4.1% of hepatocytes were DHBsAg-positive (Section 8.3.2.1), it could be calculated that each DHBsAg-positive hepatocytes would contain ~219.5 and ~3.7 copies of DHBV total and cccDNA. These levels were also similar to the DHBV DNA levels found in age matched ducks (6-week-old) that had similar percentage of DHBsAg-positive hepatocytes at 4 dpi but developed acute DHBV infection as described in Section 7.3.2.9, as well as in previous studies (Reaiche *et al.*, 2010). After DHBV infection was established in >95% of hepatocytes, DHBV DNA levels increased to ~298 and ~5 copies of DHBV total and cccDNA per cell at 18 dpi and 60 dpi, and were maintained at ~181 and ~9 copies of DHBV total and cccDNA at 165, 196 and 327 dpi. At this stage, it is likely that maximum liver capacity would have been reached, with a pool of DHBV cccDNA maintained stably in the hepatocytes (Zhang *et al.*, 2003).

8.4. Using invPCR assay to detect integrated virus-cell junctions during various stages of DHBV chronic infection

8.4.1. Sequence of the DHBV genome present in ducks

As described in Section 1.8.1, invPCR assays are generally designed based on the most probable left and right hand ends of the dslDNA sequences of the integrated viral DNA, and as described in Section 7.4.1, the duck D3 invPCR assay (shown in Table 2.3) was found to be most suitable to detect integrated virus-cell junctions in DHBV-infected ducks this study (Chapter 6). To ensure that the duck D3 invPCR assay established was suitable to detect integrated virus-cell junctions in ducks 338, 343 and 350, the most probable left hand end junction of the integrated DHBV DNA (~2485 nt of the AusDHBV genome) in these ducks was sequenced. To achieve this, total DNA was extracted from liver tissues of ducks 338, 343 and 350 using the total DNA extraction method as described in Section 2.6.3. A region of the DHBV DNA (2349 – 52 nt) was then amplified by PCR as described in Section 7.4.1. Results (data not shown) showed that the expected 731 bp region of the DHBV DNA was successfully amplified in all the three ducks. Next, the amplified DHBV DNA were sequenced as described in Section 7.4.1, and as explained, the use of specific proof-reading polymerase was not necessary for this study, and thus was not used in this Chapter.

As shown in Figure 8.7, the multiple sequence alignment of DHBV genome present in all ducks showed high homology with the AusDHBV genome, with 100% sequence coverage and 99% sequence similarity. Specifically, there was a cytosine to adenine mutation at 417 nt in all ducks, and an adenine to guanine mutation at 472 nt in duck 350. However, these mutations did not occur in regions of restriction enzyme digestion or PCR primer binding sites present in the duck D3 invPCR assay design.

In summary, the duck D3 invPCR assay that was designed in Chapter 6 based on the AusDHBV sequence is suitable and specific to detect integrated virus-cell junctions in the liver of ducks 338, 343 and 350 that developed chronic DHBV infection in this study.

8.4.2. Detection of integrated virus-cell junctions during various stages of chronic DHBV infection using the invPCR assay

The invPCR assays were performed as optimised in Chapter 6 and as described in Section 7.4.2. An example of the invPCR products produced from serial dilution of DNA template is shown in Figure 8.8A, while an example of the invPCR products produced from the equal distribution of the "optimal" DNA template into each PCR well is shown in Figure 8.8B. The "optimal" amount of inverted DNA to be used as template during nested PCR reactions was chosen from the amount of inverted DNA that would produce a single PCR product in each PCR well, as shown in Figure 8.8A.

8.4.3. InvPCR assay results

All invPCR assay results obtained are summarised in Table 8.4. Unfortunately, no clones or repeats of the same integrated virus-cell junctions were successfully detected in this Chapter. For all three duck liver tissues, a total of ~22.77 μg of DNA were analysed by performing 90 – 270 invPCR reactions on liver cell DNA extracted from each duck at each time-point, only 3 integrated virus-cell junctions were detected. Specifically, at 4 dpi, a total of 285 invPCR products were sequenced, among which 1 of the sequence was an integrated virus-cell junction, 207 were virus-virus false positive sequences, 6 were unknown sequences (defined in this thesis as insert DNA sequences that were either too short (<15 bp) or did not show homology to any known sequences during the BLAST searches), and 2 DNA sequencing reactions had failed. At 18 dpi, a total of 54 invPCR products were sequenced, among which none were integrated virus-cell junctions, 43 were virus-virus false positive sequences, and 11 DNA sequencing reactions had failed; while at 60 dpi, a total of 251 invPCR products were sequenced, among which none were integrated virus-cell junctions, 217 were virus-virus false positive sequences, and 2 were unknown sequences. For duck 343 at 165 dpi, 33 invPCR

products were sequenced, among which 30 of the sequences were virus-virus false positive sequences, 1 was an unknown sequence that was too short (<15 bp), and 2 DNA sequencing reactions had failed. Lastly for ducks 338 and 350, at 196 dpi, a total of 15 invPCR products were sequenced, among which 1 of the sequences was an integrated virus-cell junction, but the others (14) were virus-virus false positive sequences; while at 327 dpi, a total of 47 invPCR products were sequenced, among which 1 of the sequences was an integrated virus-cell junction, but the others (46) were virus-virus false positive sequences.

Detailed analysis of the 3 integrated virus-cell junctions detected are shown in Figure 8.9; while Figure 8.10A shows an example of an unknown sequence, and Figure 8.10B shows an example of a virus-virus false positive sequence, which consisted of only DHBV DNA.

8.5. Discussion

8.5.1. Characterisation of histological and serological changes occurring during chronic DHBV infection

In summary, based on the histological and serological characterisations in Sections 8.3.2.1 to 8.3.2.9, it was found that in ducks experimentally infected with $1.5x10^{10}$ vge of DHBV at 6 weeks of age that eventually developed widespread and persistent DHBV infection (chronic DHBV infection), DHBV infection was established in ~4.1% of hepatocytes at 4 dpi, with active DHBV replication, or ~219.5 and ~3.7 copies of DHBV total and cccDNA per infected hepatocyte. This was accompanied with slightly elevated levels of liver inflammation, hepatocyte apoptosis, some increase in infiltration of Kupffer cells, and the production of anti-DHBc antibodies by 4 dpi, followed by low titres of anti-DHBs antibodies from 4 – 11 dpi. Compared to age matched ducks with acute DHBV infection, it was found that the activation of Kupffer cells and the production of anti-DHBs antibodies were delayed in these ducks. Thus, these suggest that the early activation of Kupffer cells and production of neutralising anti-DHBs antibodies may be one of the keys to the early control and resolution of DHBV infection (Vickery *et al.*, 1989; Pugh *et al.*, 1995; Tohidi-Esfahani *et al.*, 2010).

DHBV replication continued to occur in these ducks, and DHBV infection was almost fully established from 18 dpi until 165 or 327 dpi, with >95% of DHBsAg-positive hepatocytes, continuous high levels of DHBV replication (181 – 298 copies of total DNA per cell), high levels of viraemia (0.6 – 20 μg/mL DHBsAg; $1x10^6$ – $1x10^9$ copies of DHBV DNA per mL of serum), and the establishment of a pool of 5 – 9 copies of DHBV cccDNA in each hepatocyte. The immune response was also continuously activated, resulting in marked increasing levels of liver inflammation at 18 dpi, which reduced to milder levels during the later stages of

infection (60 – 327 dpi), persistent elevated levels of apoptosis and activated Kupffer cells, but with varying levels of Kupffer cells infiltration.

On a separate note, as described in Section 7.5.1, attempts to determine the levels of proliferating hepatocytes by using PCNA staining as described in Section 2.4.4 was also not successful for these duck liver samples. Hence, attempts to observe and calculate hepatocyte proliferation during chronic DHBV infection were not successful in this study.

8.5.2. Detection of integrated virus-cell junctions using the invPCR assay

The low rate of detection of integrated virus-cell junctions in this study was not expected. It is expected that during early stages of chronic DHBV infection, low levels of integration would be detected in the liver, as in previous studies, integration has been reported to occur at a rate of ~1 in 10^3 – 10^4 cells by 6 dpi in ducks experimentally infected at 3 – 5 days of age (Yang and Summers, 1999). During later stages of infection, due to ongoing DHBV replication, hepatocyte death from the activated duck immune responses, and subsequent clonal proliferation of hepatocytes to replace the killed hepatocytes, higher levels of integration and large hepatocyte clones (containing the same integrated virus-cell junctions) would be detected. These had been observed in previous studies in human, chimpanzee and woodchuck with long-term chronic HBV or WHV infections, with 1% – 2% of the hepatocytes reported to contain integrated virus sequences, and the formation of hepatocyte clone sizes ranging from 35 – 60,000 cells (Mason *et al.*, 2005; Mason *et al.*, 2009a; Mason *et al.*, 2010).

Based on that, in the ~22.77 μg of DNA analysed in this study (approximately $8x10^6$ cells as calculated in Section 2.8.9.3.2), assuming that the rate of integration is 1 in 10^3 – 10^4 cells, it is expected that 800 – 8000 integrated virus-cell junctions could be detected. However, this would be an overestimation, as that rate of integration was obtained from a study performed in 6-day-old ducks, and thus the number of integration events may be different in rapidly growing young ducks compared to adult ducks. In addition, as the rate of proliferation of hepatocytes during chronic DHBV infection has been reported to be 0.5% – 1.5% daily (Fourel *et al.*, 1994b), by 327 dpi, it could be estimated that the hepatocyte population could have turned over at least 3 times, allowing the production of hepatocyte clones at least 8 cells in size. Even preliminary invPCR assays performed in ducks with chronic DHBV infection in Chapter 6 detected up to 37 integrated virus-cell junctions, with 3 of the integrated virus-cell junctions repeated 2 times, indicating the presence of hepatocyte clones at least 2 cells in size.

Despite all that, the detection of 3 integrated virus-cell junctions in this study, even at a low rate, confirmed that integration of DHBV into the duck liver genome does occur during chronic DHBV infection, and that the duck D3 invPCR assay can be successfully used for the specific detection of integrated virus-cell junctions in AusDHBV-infected ducks.

The low rate of detection of integrated virus-cell junctions in this study could be due to various reasons. Firstly, high levels of virus-virus false positives have been detected, comprising up to 81.3% of the total invPCR products sequenced in this study as shown in Table 8.4. This was expected, as high levels of DHBV replication are continuously occurring in the liver of ducks with chronic DHBV infection, to produce a range of "non-integrated DHBV DNA", including the cytoplasmic RI DNA and rcDNA, and the nuclear cccDNA. All of these forms of DHBV DNA could contribute to virus-virus sequences detected during the invPCR assay as discussed in Section 5.1.2.

To reduce the levels of non-integrated DHBV DNA, the selective low melting temperature agarose gel electrophoresis and purification of high MW cellular DNA was performed on total DNA extracted from the 4 dpi liver tissues from ducks 338, 343 and 350, followed by DNA inversion as described in Section 2.10.2, and subsequent invPCR assay steps as performed previously in Section 8.4.2. However, no invPCR products were detected out of 90 invPCR reactions performed for each duck liver tissue (data not shown). InvPCR assays performed on DNA for ducks with acute DHBV infection extracted using the same low melting temperature agarose gel electrophoresis were also not successful (Section 7.5.2). As discussed in Section 7.5.2, these results may be due to the high losses of DNA during the extraction method.

Based on all these, future studies could explore alternative methods to reduce the levels of DHBV DNA in the extracted DNA samples, as described in Sections 6.6 and 7.5.2. Briefly, these include the use of LNA oligonucleotides to specifically block the amplification of DHBV DNA, and using alernative cccDNA destroying enzymes, as the *Nde*I digestion site have been found in most of the virus-virus sequences detected in this study (Figure 8.10B).

Secondly, the low rate of detection of integrated virus-cell junctions in this study could be due the large proportion of invPCR products that had failed to produce readable DNA sequences (16.9%). Therefore, in future studies, the DNA sequencing reactions could be further optimised in various steps as described in Sections 6.6 and 7.5.2.

Lastly, the low rate of detection of integrated virus-cell junctions in duck liver tissues could also be due to physiological differences in using the duck model as compared to mammalian models, which did not allow for high levels of DHBV integration or the formation or large hepatocyte clones in the duck livers. For instance, the final time-point of the ducks in this study was 327 dpi, which were much shorter compared to the mammalian models, which had 22 – 28 months WHV-infected woodchucks (Mason *et al.*, 2005), and at least 20 years of chronic HBV infection in chimpanzees (Mason *et al.*, 2010) and humans (Mason *et al.*, 2010). Hence, the levels of liver turnover and clonal proliferation of hepatocytes are likely to be lower in ducks, and in turn would result in much smaller hepatocyte clones present in the liver. In addition, as DHBV infections do not seem to induce cirrhosis or HCC in ducks like in woodchucks, chimpanzees and humans, there may be differences in the natural history of DHBV infection in ducks which may result in lower integration rates of DHBV DNA.

Alternatively, as the duck genome consists of 40 chromosome pairs (2n = 80) that consist of a few macrochromosome pairs, Z and W sex chromosomes, and numerous indistinguishable microchromosomes (microsatellites) (Fillon *et al.*, 2007; Huang *et al.*, 2009; Skinner *et al.*, 2009), these microchromosomes and microsatellites may reduce the frequency of DHBV integration, as well as reduce the efficiency of the invPCR assay to detect integrated virus-cell junctions from DNA fragments. The duck genome is also smaller than the mammalian genome (2.5 pg per cell in ducks compared to 7 pg per cell in humans) (Gregory *et al.*, 2007), thus potentially further reducing the rate of DHBV integration events. Furthermore, it is unknown whether the isolated breeding of ducks used in this study may have resulted in a genetic makeup that has a natural reduction for integration of DHBV DNA into the genome.

To ensure that the low detection of integrated virus-cell junctions were not due to poor laboratory techniques, our collaborator Dr. William Mason kindly performed the same duck D3 invPCR assays using DNA samples extracted from duck 338 liver collected at 196 dpi, as a comparison. DNA was extracted from the duck liver tissue by total DNA extraction in the Hepatitis Research Laboratory, and Dr. Mason performed the subsequent low melting temperature agarose gel electrophoresis and purification of high MW cellular DNA, inversion and nested PCR on DNA from ~50,000 cells. Dr. Mason successfully detected 85 invPCR products, among which 20 of the sequences were integrated virus-cell junctions (23.5% of total invPCR products sequenced), 50 were virus-virus false positive sequences (58.8% of total invPCR products sequenced), and 14 were unknown sequences (16.5% of total invPCR products sequenced). Two of the integrated virus-cell junctions were identical, indicating the presence of a hepatocyte clone (Mason, personal communication).

As up to 20 integrated virus-cell junctions were successfully detected in that duck liver tissue, this shows that the integrated virus-cell junctions were present in the duck liver genome, and was just not able to be detected with the same sensitivity in this study. As the same duck D3 invPCR assay design was used by Dr. Mason, this confirms that the invPCR design is specific for the detection of the integrated virus-cell junctions in AusDHBV-infected ducks.

There are several differences between the invPCR assay performed in this thesis and by Dr. Mason. Firstly, the low melting temperature agarose gel electrophoresis and purification of high MW cellular DNA was successfully performed by Dr. Mason, and thus may have resulted in much lower amounts of false positives were detected (58.8% compared to 81.3% in this study). This confirmed that by reducing the levels of non-integrated DHBV DNA from the extracted liver cell DNA samples, this would in turn reduce the number of virus-virus sequences detected, and may increase the detection of integrated virus-cell junctions. Thus future studies should look into further optimising the low melting temperature agarose gel electrophoresis methods, and apply this additional step to all chronic duck liver samples. Some of the improvements that could be made include extracting only minimal amounts of low melting temperature gel, so that the final volume of first cut restriction enzyme digestion could be reduced, incubating the gel with restriction enzyme buffer overnight with proper shaking, and increasing the amount of first cut restriction enzyme added and the incubation time for digestion to ensure that complete first cut digestions had occurred.

Secondly, none of the DNA sequences performed by Dr. Mason had failed to produce a readable sequence. When compared to the 16.9% of failed DNA sequencing reactions out of the total invPCR products sequenced in this study, this confirmed that further optimisation for the agarose gel extraction, DNA sequencing reactions and subsequent purification of DNA sequencing products should be peformed, as described in Section 6.6. The agarose gel-extracted invPCR products could also be directly sent for sequencing to determine whether the DNA sequencing facilities could help to perform more optimal DNA seqeuencing reactions compared to this study, and to assist in improving the DNA sequencing reactions currently performed in the Hepatitis Research Laboratory. Alternatively, different DNA sequencing facilities with different DNA sequencing platforms could be explored, to find out whether for instance next generation sequencing platforms would be more suitable to sequencing low quantities and possible low quality of invPCR products from this study.

8.6. Conclusion

The aims of this Chapter were to establish and characterise histological and serological changes occurring during various stages of chronic DHBV infection, and to assess the levels of clonal proliferation of hepatocytes and calculate the number and size of hepatocyte clones formed during chronic DHBV infection, using the invPCR assay to detect integrated virus-cell junctions in the liver during various stages of chronic DHBV infection. By gaining understanding of clonal proliferation of hepatocytes, further understanding of the development of HCC could be determined for earlier identification of the formation of pre-neoplastic liver nodules, and potential therapeutic directions for HCC.

Chronic DHBV infections were successfully established in three 6-week-old Pekin ducks (338, 343, 350). At 4 dpi, active DHBV replication was occurring (~219.5 copies of total DHBV DNA per infected hepatocyte) with ~4.1% of DHBsAg-positive hepatocytes in the liver. At 18 dpi, the DHBV infection spread to >95% of hepatocytes in the liver, and was maintained throughtout the study, with continuous high levels of DHBV replication (181 – 298 copies of total DNA per liver cell) and viraemia (0.6 – 20 μg/mL DHBsAg; $1x10^6$ – $1x10^9$ copies of DHBV DNA per mL of serum), and the establishment of a pool of 5 – 9 copies of DHBV cccDNA per liver cell. Histological characterisation of liver tissues showed that the ducks' innate immune responses were activated almost from the onset of DHBV challenge, with elevated the levels of liver inflammation (both portal and lobular) and apoptosis, but with low levels of Kupffer cells infiltration and activation at 4 dpi. After widespread of DHBV infection, marked liver inflammation were observed at 18 dpi, but reduced to milder levels throughout infection. In addition, apoptosis levels and activated Kupffer cells levels were persistently elevated throughout infection, but with varying levels of Kupffer cells infiltration. As the activation of Kupffer cells was slower and at lower levels, these suggest that the delayed response in the infiltration and activation of Kupffer cells may have contributed to the failure of these ducks to resolve DHBV infection. Serological characterisation showed that the ducks' adaptive immune responses were also activated, producing moderate titres of anti-DHBc antibodies by 4 dpi, followed by anti-DHBs antibodies. However, the neutralizing anti-DHBs antibodies were not sufficient to complex to and remove the DHBV virions from the serum, as "active" viraemia were also detected, indicating that the levels of circulating DHBV virions in the serum were in excess to the anti-DHBs antibodies. As anti-DHBs antibodies were produced earlier and at higher titres in ducks that developed acute DHBV infection, these suggest that the ability of ducks to rapidly produce anti-DHBs antibodies were essential in the control and clearance of DHBV infection.

Using the duck D3 invPCR assay that was shown to be suitable to detect integrated virus-cell junctions in these ducks, up to 22.8 μg of DNA were analysed from liver tissues at 4, 18 and 60, 165, 196, 327 dpi. Three integrated virus-cell junctions were detected, but no hepatocyte clones were found. Most of the invPCR products sequenced were found to be virus-virus false postives (81.3% of the total invPCR products sequenced). Therefore, the levels of clonal proliferation of hepatocytes and the number and size of hepatocyte clones formed during chronic DHBV infection could not be conclusively determined in this Chapter.

Legend for Table 8.1

ND: not detected
N/A: not available

(A) Formalin-fixed and embedded duck liver tissue sections were H&E-stained and viewed under light microscopy as described in Section 2.4.1. Examples of portal and lobular inflammation are shown in Figure 8.2.

(B) Ducks 140, 141 and 142 were 3 ducks with acute DHBV infection by inoculation with $1.5x10^{10}$ vge of Pool 8 DHBV virus stock at 6 weeks of age, each from a previous study (Reaiche *et al.*, 2010) as described in Section 8.3.1. Liver tissues were formalin-fixed, paraffin-embedded, sectioned at 6 μM thick and H&E-stained by Dr. Georget Reaiche (Reaiche *et al.*, 2010), who generously provided the H&E-stained slides for use in this study.

(C) Statistical analysis of the average % of total area of liver containing inflammatory cells. Ducks with chronic DHBV infection include ducks 339, 343, 350; ducks with acute DHBV infection include ducks 337, 339, 342 (Chapter 7), 140, 141, 142; the uninfected duck is duck 138 (described in Table 7.1B). The p-value of <0.05 is considered statistically significant.

[a]DHBsAg-positive hepatocytes were determined from Figure 8.1 or Reaiche *et al.*, 2010.
[b]Total area of liver tissues were examined as described in Section 2.4.1.
[c]Percentage of the examined area of liver tissues that contained inflammatory cells.
[d]Thickness of the largest inflammation observed from the examined area of liver tissues.
[e]The grading of portal and lobular inflammation was adapted from Mason *et al.* (Mason *et al.*, 1994) and Bedossa and Poynard (Bedossa and Poynard, 1996), and described in detail in Section 2.4.1.
[g]P-value was calculated using the Student's unpaired *t*-test, set to two-tailed distribution and two-sample unequal variance (heteroscedastic). The difference of the levels of inflammation between ducks with chronic and acute DHBV infection at each time-point was not significant.
[h]As there was only 1 uninfected duck sample (duck 138), the Student's unpaired *t*-test was performed comparing data from all time-points of the different groups as an array/data set. The difference of the levels of inflammation between ducks with chronic DHBV infection and an uninfected duck 138 was not significant.

Table 8.1: Summary of portal and lobular inflammation observed in H&E-stained duck liver sections.

A) Portal and lobular inflammation in ducks with chronic DHBV infection

Duck	Dpi	DHBsAg-positive hepatocytes [a]	Area of liver analysed (mm^2)[b]	Inflammatory cells (% of total area of liver)[c]	Inflammation (cell thickness)[d]		Inflammation grading[e]	
					Portal	Lobular	Portal	Lobular
338	4	5.2%	41.76	2.03	7	ND	2	1
	18	>95%	38.88	2.85	28	15	4	3
	60	>95%	21.60	1.00	9	7	2	2
	196	>95%	56.16	2.64	29	12	3	3
	327	>95%	80.64	1.41	38	22	2	2
343	4	3.0%	36.00	1.32	16	26	2	2
	18	>95%	30.24	3.10	32	19	3	3
	60	>95%	38.88	2.04	22	25	3	2
	165	>95%	116.64	1.26	23	18	2	2
350	4	4.1%	27.36	0.32	3	ND	1	1
	18	>95%	31.68	1.36	24	12	2	2
	60	>95%	40.32	0.64	14	7	2	2
	196	>95%	80.64	1.36	22	20	2	2
	327	>95%	61.92	0.95	21	14	2	2

B) Portal and lobular inflammation in acute DHBV-infected ducks

Duck	Dpi	DHBsAg-positive hepatocytes [a]	Area of liver analysed (mm^2)[b]	Inflammatory cells (% of total area of liver)[c]	Inflammation (cell thickness)[d]		Inflammation grading[e]	
					Portal	Lobular	Portal	Lobular
140	4	2.8%	59.04	0.29	5	ND	1	1
	60	<0.0001%	17.28	1.58	21	ND	2	1
	221	<0.0001%	38.88	0.78	15	12	2	2
	316	<0.0001%	76.32	0.74	16	ND	2	1
141	4	1.8%	72.00	0.36	3	8	1	2
	60	<0.0001%	20.16	1.50	9	7	2	2
	221	<0.0001%	38.88	1.19	17	8	3	2
	316	<0.0001%	11.52	1.13	10	ND	2	1
142	4	3.2%	59.04	0.32	9	ND	1	1
	60	<0.0001%	28.80	1.30	18	8	2	2
	221	<0.0001%	34.56	1.88	20	8	2	2
	316	<0.0001%	33.12	1.00	8	ND	2	1

C) Statistical analysis of the average % of total area of liver containing inflammatory cells

Group	Dpi										
	4		18		45 or 60		196 or 221		316 or 327		
Chronic	1.22	0.28[g]	2.44	0.30[g]	1.23	0.64[g]	2.00	0.36[g]	1.18	0.95[g]	0.62[h]
Acute	0.51		1.69		1.25		1.03		1.21		
Uninfected	0.66		N/A		1.59		1.35		1.44		

Legend for Table 8.2

(A) Formalin-fixed and embedded duck liver tissue sections were H&E-stained and viewed under light microscopy as described in Section 2.4.1.

(B) Duck 141 was a duck with acute DHBV infection by inoculation with $1.5x10^{10}$ vge of Pool 8 DHBV virus stock at 6 weeks of age, each from a previous study (Reaiche *et al.*, 2010) as described in Section 7.3.1. Liver tissues were formalin-fixed, paraffin-embedded, sectioned at 6 μM thick, and H&E-stained by Dr. Georget Reaiche (Reaiche *et al.*, 2010), who then generously provided the H&E-stained slides for use in this study.

(C) Statistical analysis of the average % of apoptotic hepatocytes. Ducks with chronic DHBV infection include ducks 339, 343, 350; ducks with acute DHBV infection include ducks 337, 339, 342 (Chapter 7), 141; the uninfected duck is duck 138 (described in Table 7.2B). The p-value of <0.05 is considered statistically significant.

[a]Hepatocytes were counted at as described in Section 2.4.1.
[b]Apoptotic cells were counted and expressed as a percentage of total hepatocytes. Examples of apoptotic hepatocytes are shown in Figure 8.3B.
[c]P-value was calculated using the Student's unpaired *t*-test, set to two-tailed distribution and two-sample unequal variance (heteroscedastic). The difference of the levels of hepatocyte apoptosis between ducks with chronic and acute DHBV infection at 4, 18 and 60 dpi was not significant.
[d]As there were only 1 uninfected duck sample (duck 138) and 1 acute DHBV-infected duck sample for 221 and 316 dpi (duck 141), the *t*-test was performed comparing data from all time-points of the different groups as an array/data set. The levels of hepatocyte apoptosis was significantly higher in ducks with chronic DHBV infection compared to ducks with acute DHBV infection or the uninfected duck 138.

Table 8.2: Summary of hepatocyte apoptosis observed in H&E-stained duck liver sections.

A) Hepatocyte apoptosis in ducks with chronic DHBV infection

Duck	Dpi	Total hepatocytes analysed (cells)[a]	Apoptotic cells (% of total hepatocytes)[b]
338	**4**	4368	2.22
	18	3714	2.85
	60	3210	2.99
	196	4314	2.04
	327	3852	1.48
343	**4**	4392	2.12
	18	4212	3.42
	60	4158	2.28
	165	3660	4.84
350	**4**	3618	1.96
	18	3792	2.40
	60	3504	2.45
	196	3228	2.01
	327	2838	2.43

B) Hepatocyte apoptosis in acute DHBV-infected duck

Duck	Dpi	Total hepatocytes analysed (cells)[a]	Apoptotic cells (% of total hepatocytes)[b]
141	**4**	3522	2.10
	60	6126	0.95
	221	5034	0.91
	316	5034	0.91

C) Statistical analysis of the average % of apoptotic hepatocytes

Group	Dpi								
	4		**18**		**45 or 60**		**196 or 221**	**316 or 327**	
Chronic	2.10	] 0.28[c]	2.89	] 0.30[c]	2.57	] 0.64[c]	2.03	1.96	] 0.01[d]
Acute	1.71		1.94		1.41		0.91	0.81	
Uninfected	0.68		N/A		0.54		0.68	1.26	<0.01[d]

N/A: not available

Table 8.3: Analysis of Kupffer cells detected in PAS-D-stained duck liver sections.

A) Analysis of Kupffer cells in ducks with chronic DHBV infection

Duck	Dpi	Total cells analysed (cells)[a]	Kupffer cells (% of total liver cells)[b]			Size of activated Kupffer cells
			Total	Unactivated[c]	Activated[d]	
338	4	4686	7.68	4.37	3.31	Small
	18	5040	6.88	3.37	3.51	Small
	60	4638	2.78	0.84	1.94	Small
	196	5544	3.77	0.99	2.78[e]	Small
	327	5088	4.40	0.59	3.80	Medium
343	4	5118	4.14	2.21	1.93	Small
	18	4848	7.20	2.70	4.50	Medium
	60	4896	5.21	0.96	4.25	Medium
	165	4572	11.48	2.14	9.34	Large
350	4	4278	8.93	5.38	3.55	Small
	18	5196	6.64	1.44	5.20	Small
	60	5562	5.20	1.82	3.38	Small
	196	4674	7.81	2.42	5.39	Small
	327	3954	6.30	1.24	5.06	Small

B) Analysis of Kupffer cells in acute DHBV-infected duck

Duck	Dpi	Total cells analysed (cells)[a]	Kupffer cells (% of total liver cells)[b]			Size of activated Kupffer cells
			Total	Unactivated[c]	Activated[d]	
141	4	7716	1.92	0.64	1.28	Medium
	60	7854	3.21	1.24	1.97	Small
	221	6480	3.21	0.94	2.27	Large
	316	6132	5.12	1.57	3.56	Small

C) Statistical analysis of the average % of total Kupffer cells

Group	Dpi								
	4		18		45 or 60		196 or 221	316 or 327	
Chronic	6.92	] 0.50[e]	6.91	] <0.01[e]	4.40	] 0.15[e]	5.79	5.35	] 0.95[f]
Acute	5.53		7.97		7.24		3.21	5.12	
Uninfected	3.68		N/A		1.95		3.02	5.98	0.11[f]

D) Statistical analysis of the average % of unactivated Kupffer cells

Group	Dpi								
	4		18		45 or 60		196 or 221	316 or 327	
Chronic	3.99	] 0.15[e]	2.50	] 0.50[e]	1.21	] 0.11[e]	1.71	0.92	] 0.61[f]
Acute	1.98		2.02		2.21		0.94	1.57	
Uninfected	1.31		N/A		0.85		1.07	1.05	0.30[f]

Table 8.3 continued

E) Statistical analysis of the average % of activated Kupffer cells

Group	Dpi									
	4		18		45 or 60		196 or 221	316 or 327		
Chronic	2.93	] 0.32[e]	4.40	] 0.18[e]	3.19	] 0.42[e]	4.09	4.44	] 0.71[f]	
Acute	4.59		5.86		4.07		2.27	3.56		
Uninfected	2.36		N/A		1.10		1.95	4.93	0.30[f]	

N/A: not available

(A) Formalin-fixed and embedded duck liver tissue sections were PAS-D stained and viewed under light microscopy as described in Section 2.4.3. Examples of unactivated and activated Kupffer cells are shown in Figure 8.4.

(B) Duck 141 was a duck with acute DHBV infection by inoculation with $1.5x10^{10}$ vge of Pool 8 DHBV virus stock at 6 weeks of age, each from a previous study (Reaiche *et al.*, 2010) as described in Section 7.3.1. Liver tissues were formalin-fixed, paraffin-embedded and sectioned at 6 μM thick by Dr. Reaiche (Reaiche *et al.*, 2010), who generously provided the tissue slides for use in this study. Slides were PAS-D stained as described in Section 2.4.3.

Statistical analysis of the average % of (C) total Kupffer cells, (D) unactivated Kupffer cells, and (E) activated Kupffer cells. Ducks with chronic DHBV infection include ducks 339, 343, 350; ducks with acute HBV infection include ducks 337, 339, 342 (Chapter 7), 141; the uninfected duck is duck 138 (described in Table 7.3B). The p-value of <0.05 is considered statistically significant.

[a]Total liver cells were counted as described in Section 2.4.3.

[b]Percentage of Kupffer cells observed out of the total liver cells analysed. The percentage of total Kupffer cells were further categorised into unactivated or activated Kupffer cells.

[c]Unactivated Kupffer cells do not contain PAS-D positive phagocytosed materials.

[d]Activated Kupffer cells contained PAS-D positive phagocytosed materials and/or acid-fast pink/brown pigmented phagocytosed materials.

[e]P-value was calculated using the Student's unpaired *t*-test, set to two-tailed distribution and two-sample unequal variance (heteroscedastic). Only the difference of levels of total Kupffer cells between ducks with chronic and acute DHBV infection at 18 dpi was significant.

[f]As there were only 1 uninfected duck sample (duck 138) and 1 acute DHBV-infected duck sample for 221 and 316 dpi (duck 141), the *t*-test was performed comparing data from all time-points of the different groups as an array/data set. The differences of the levels of Kupffer cells (total, unactivated, activated) in ducks with chronic DHBV infection compared to ducks with acute DHBV infection or an uninfected duck were not significant.

Table 8.4: Summary of invPCR assay products obtained using liver tissues from ducks with chronic DHBV infection.

Duck	Dpi	Total invPCR reactions[a]	Total amount of DNA analysed (ng)[b]	Number of invPCR products sequenced[c]	Virus-cell junctions detected[d]	Virus-virus junctions detected[e]	Unknown sequences detected[f]
338	**4**	180	208	109	-	84	3
	18	90	1950	27	-	22	-
	60	180	1115	72	-	65	-
	196	270	2994.5	10	1	9	-
	327	270	1987.75	20	-	20	-
343	**4**	180	221	78	-	68	1
	18	90	1950	13	-	9	-
	60	180	2.23	96	-	87	-
	165	180	4045	33	-	30	1
350	**4**	180	265	98	1	55	2
	18	90	1950	14	-	12	-
	60	180	1115	83	-	65	2
	196	270	2994.5	5	-	5	-
	327	180	1972.65	27	1	26	-
Total		**2520**	**22770.63**	**685**	**3**	**557**	**9**
% of total invPCR products sequenced					**0.6**	**81.3**	**1.2**

The duck D3 invPCR assays were performed as described in Section 8.4.2.

[a]Total invPCR reactions refers to the total number of nested PCR reactions performed in individual PCR wells.

[b]The amount of DNA analysed was estimated according to the amount of inverted DNA added per invPCR reaction, which was based on the amount of liver used during DNA extraction as calculated in Section 2.8.9.3.2. As losses of DNA were expected during extraction and inversion steps, a 50% loss of DNA was included in the calculations.

[c]From all the nested PCR reactions performed, only reactions that produced a clear invPCR product bands was extracted from the agarose gel and sequenced. The numbers of total invPCR products observed on agarose gels was not shown. 116 of the sequencing reactions failed to produce a readable product (16.9% of total invPCR products sequenced).

[d]Integrated virus-cell junctions are shown in Figure 8.9.

[e]An example of a virus-virus false positive junction is shown in Figure 8.10B.

[f]Unknown sequences are defined as insert DNA that were either too short (<15 bp) or did not show homology to any known sequences during the BLAST searches. An example of an unknown sequence is shown in Figure 8.10A.

Figure 8.1: Detection of DHBsAg-positive hepatocytes in liver sections prepared from ducks 338, 343 and 350 with chronic DHBV infection at 4, 18, 60, 165, 196 and 327 dpi.

EAA-fixed and embedded duck liver tissue sections were stained with pre-S monoclonal antibody, 1H.1, as described in Section 2.4.2, and photographed using light microscopy at 100X magnification, magnification bar = 200 μM. DHBsAg-positive hepatocytes are stained dark brown, while nuclei are counter-stained blue-purple using haematoxylin.

The percentage of DHBsAg-positive hepatocytes was determined by counting the total number of DHBsAg-positive hepatocytes per ~$1x10^5$ hepatocytes, examined at 200X magnification using an eyepiece graticule and a 600 μM x 600 μM grid. Liver tissue sections where all observed hepatocytes are positive for DHBsAg were recorded as having >95% of DHBsAg-positive hepatocytes.

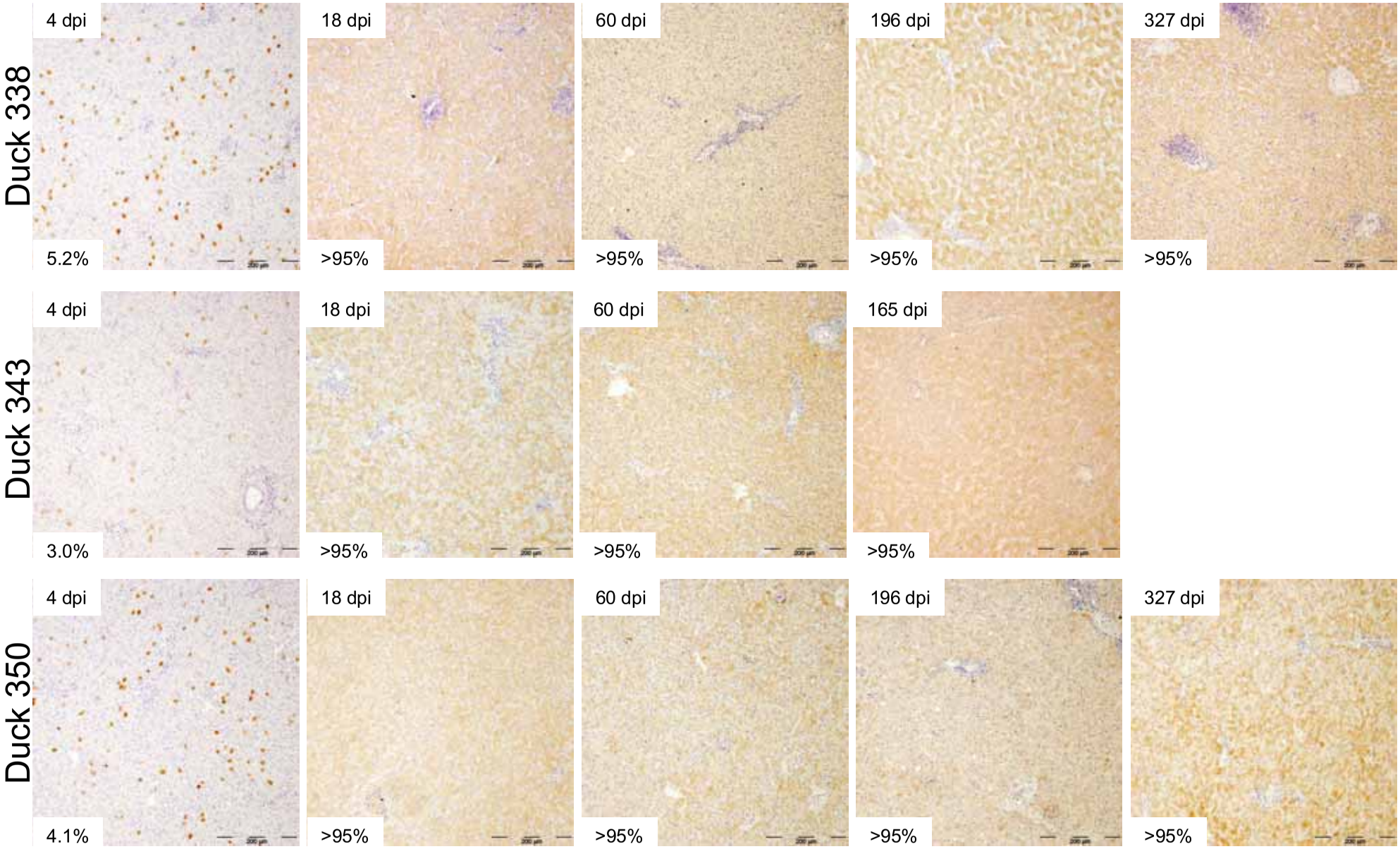

Duck 338
4 dpi
5.2%
18 dpi
>95%
60 dpi
>95%
196 dpi
>95%
327 dpi
>95%
Duck 343
4 dpi
3.0%
18 dpi
>95%
60 dpi
>95%
165 dpi
>95%
Duck 350
4 dpi
4.1%
18 dpi
>95%
60 dpi
>95%
196 dpi
>95%
327 dpi
>95%

Figure 8.1

Figure 8.2: Detection of liver inflammation in H&E-stained liver sections prepared from ducks 338, 343 and 350 with chronic DHBV infection at 4, 18, 60, 165, 196 and 327 dpi.

Formalin-fixed and embedded duck liver tissue sections were H&E-stained as described in Section 2.4.1, and photographed using light microscopy at 100X magnification, magnification bar = 200 μM. Inflammatory cells are stained dark purple, while nuclei are counter-stained blue-purple using haematoxylin.

The black arrows show portal inflammation, while the blue arrows show lobular inflammation observed in the liver.

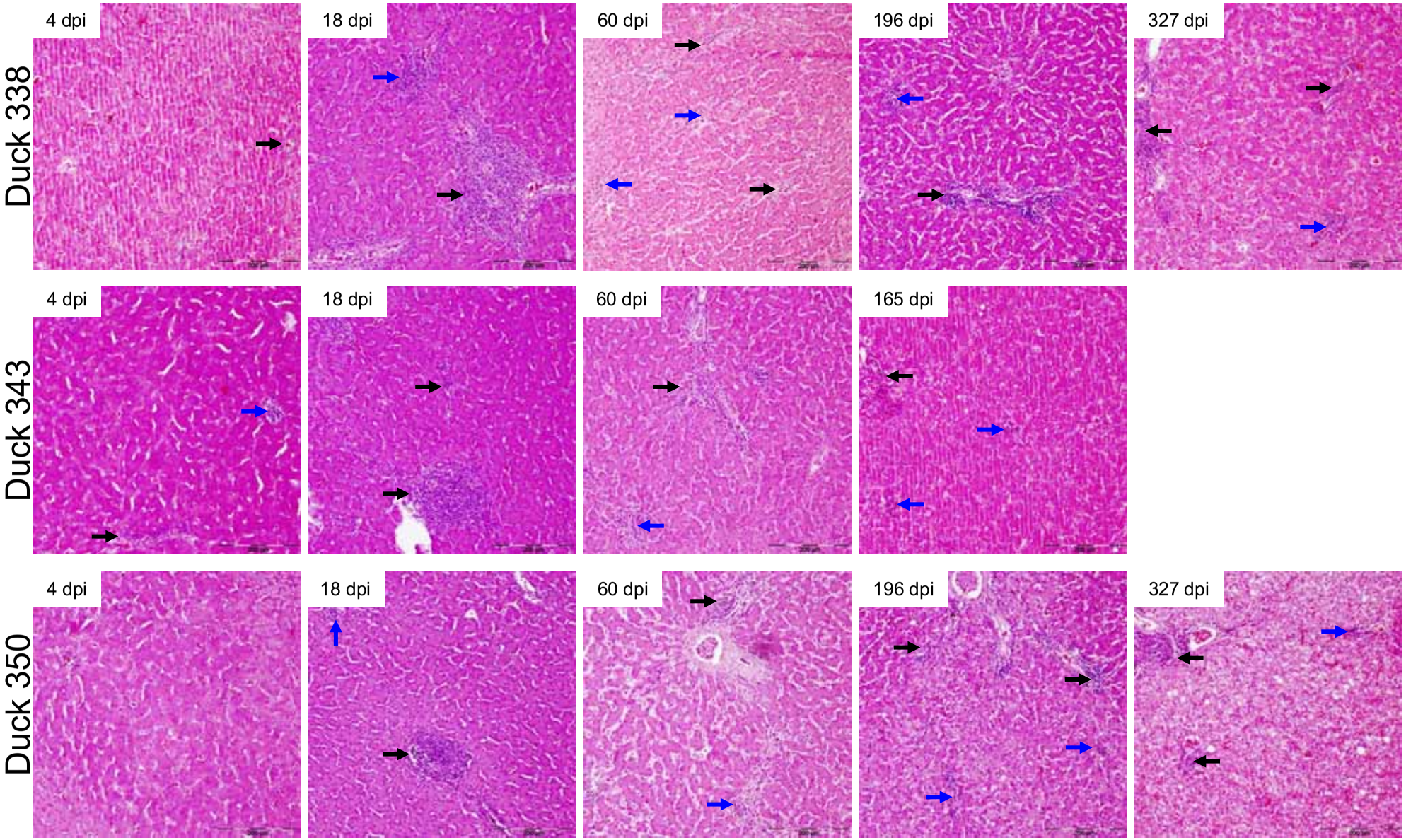

Duck 338
4 dpi
18 dpi
60 dpi
196 dpi
327 dpi
Duck 343
4 dpi
18 dpi
60 dpi
165 dpi
Duck 350
4 dpi
18 dpi
60 dpi
196 dpi
327 dpi

Figure 8.2

Figure 8.3: Detection of apoptotic hepatocytes and other histological features observed in H&E-stained liver sections prepared from ducks with chronic DHBV infection.

Formalin-fixed and embedded duck liver tissue sections were H&E-stained as described in Section 2.4.1. Eosinophilic structures like proteins will be stained as various shades of red – pink, while nuclei are counter-stained blue-purple using haematoxylin.

Figure 8.3A shows an example of a portal tract, consisting of the portal vein, hepatic arteriole, and bile ducts. Photograph was taken from the liver of duck 338 at 4 dpi at 200X magnification, magnification bar = 100 μM.

Figure 8.3B shows examples of apoptotic hepatocytes emphasised by black arrows. In the apoptotic cells, chromatin condensation and cellular fragmentation to form small apoptotic bodies, commonly referred to as acidophil Councilman bodies, which can be seen as black dots in the ovoid-shaped hepatocyte cytoplasm that had turned thick and refractile. Apoptotic hepatocytes can also show cytoplasmic shrinkage, cell membrane blebbing, and may not contain nuclear remnants (Crawford, 2007). Photograph was taken from the liver of duck 343 at 4 dpi at 400X magnification, magnification bar = 50 μM.

Figure 8.3C shows an example of steatosis, or the accumulation of triglyceride fat droplets in the liver hepatocytes (Crawford, 2007), observable as vacuolated hepatocytes (emphasised by black arrows). Photograph was taken from the liver of duck 343 at 165 dpi at 100X magnification, magnification bar = 200 μM.

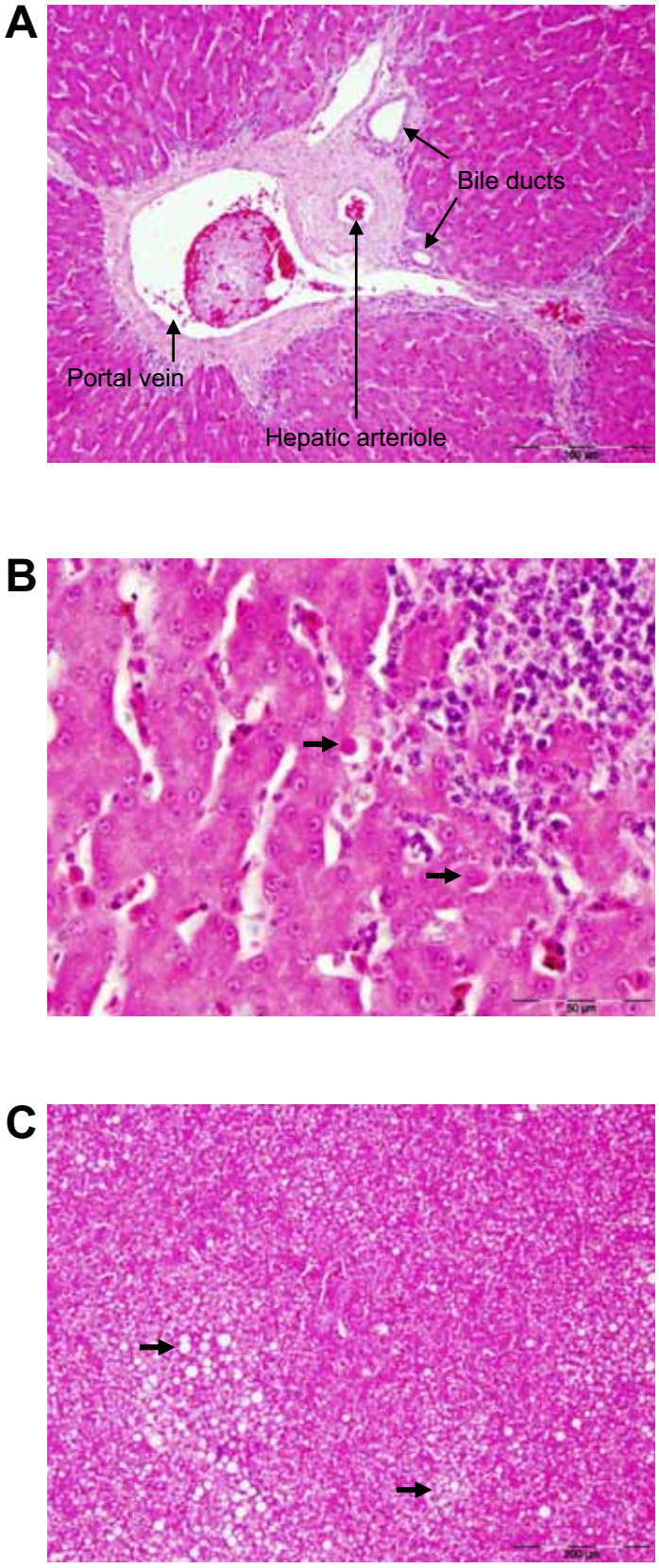


Figure 8.3

Figure 8.4: Detection of Kupffer cells during various stages of activation in PAS-D-stained liver sections prepared from ducks with chronic DHBV infection.

Formalin-fixed and embedded duck liver tissue sections were PAS-D stained as described in Section 2.4.3, and photographed using light microscopy at 400X magnification, magnification bar = 50 μM. Kupffer cells will be stained purple-bright pink for lipid-rich ceroid PAS-D positive phagocytosed materials, and pink/brown granular aggregates acid-fast phagocytosed materials (like bile), while nuclei are counter-stained blue-purple using haematoxylin.

Figure 8.4A shows examples of Kupffer cells that mostly do not contain phagocytosed materials (termed as "unactivated") (emphasised by black arrows). Photograph was taken from the liver of duck 343 at 4 dpi.

Figure 8.4B shows examples of medium-sized Kupffer cells that mostly contain PAS-D positive materials (termed as "activated") (emphasised by blue arrows), with some unactivated Kupffer cells still present (emphasised by black arrows). Photograph was taken from the liver of duck 343 at 18 dpi.

Figure 8.4C shows examples of medium-sized mostly activated Kupffer cells that contain acid-fast pink/brown pigments (emphasised by blue arrows), with some unactivated Kupffer cells still present (emphasised by black arrows). Photograph was taken from the liver of duck 343 at 60 dpi.

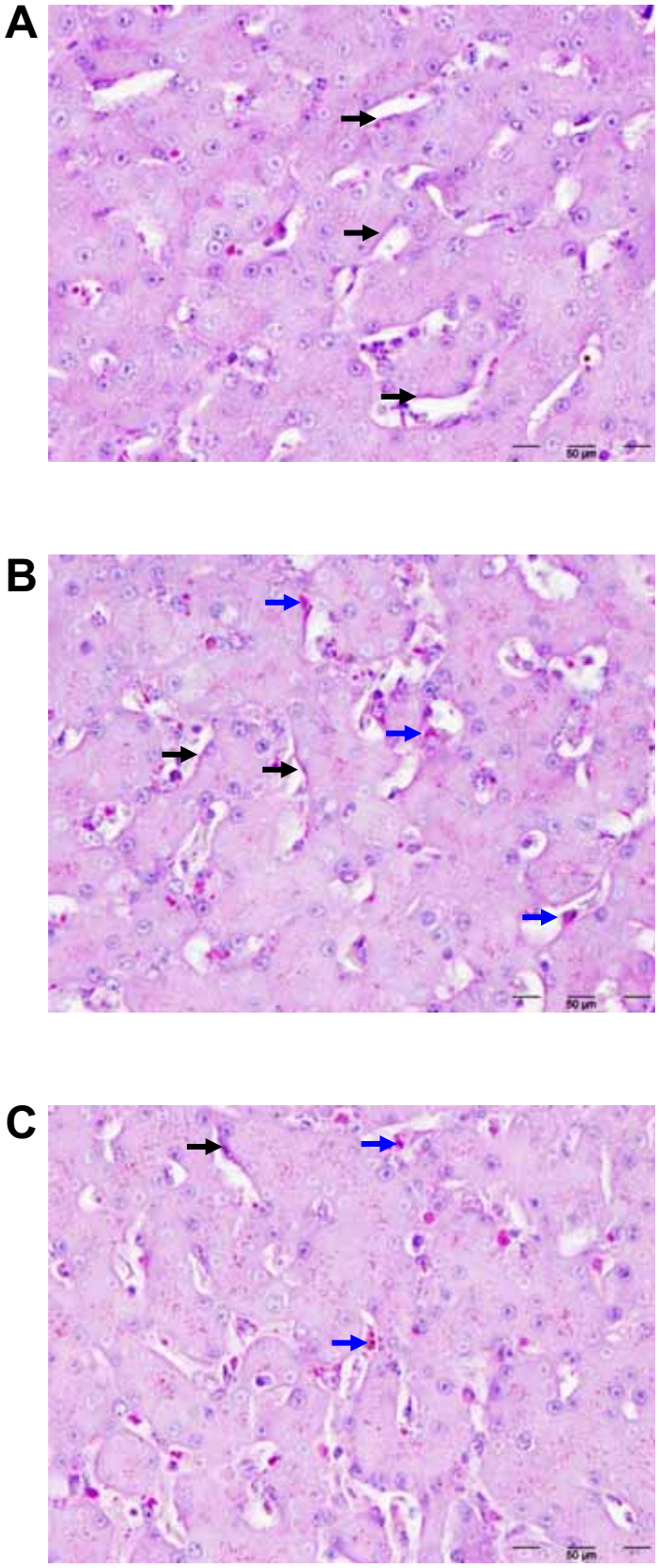


Figure 8.4

Figure 8.5: Levels of DHBsAg (A), anti-DHBc antibodies (B), and anti-DHBs antibodies (C) in the serum of ducks 338, 343 and 350 with chronic DHBV infection as detected by ELISA.

The levels of DHBsAg present in the serum were detected by rapid qualitative ELISA as described in Section 2.5.2, and were calculated based on standard curves generated using the Pool 8 serum containing 50 μg/mL of DHBsAg (Jilbert *et al.*, 1996). The background level of the DHBsAg ELISA was determined by the mean optical density (OD) readings of normal duck serum (NDS) plus two standard deviations. The background reading (0.63 μg/mL of DHBsAg) is shown as dotted line in Figure 8.5A, and is used as the limit of detection for all these assays.

The levels of anti-DHBc antibodies present in the serum were detected by quantitative ELISA as described in Sections 2.5.3. Titres of anti-DHBc antibodies are expressed as the reciprocal of the serum dilution required to achieve an OD of 0.47 at 490 nm. The negative cut-off for anti-DHBc-positive samples is set at two standard deviations above the average background obtained by assaying all 6 ducks in this study (337, 338, 339, 342, 343, 350) at 0 dpi (Miller *et al.*, 2004). As the minimum serum dilution was 1/500, the minimum titre is 500 (shown as the dotted line in Figure 8.5B), with values under 500 represented as "1" (Foster *et al.*, 2005).

The levels of anti-DHBs antibodies present in the serum were detected by quantitative ELISA as described in Sections 2.5.4. Titres of anti-DHBs antibodies are expressed as the reciprocal of the serum dilution required to achieve an OD of 0.24 at 490 nm. The negative cut-off for anti-DHBs-positive samples is set at two standard deviations above the average background obtained by assaying all 6 ducks in this study (337, 338, 339, 342, 343, 350) at 0 dpi (Miller *et al.*, 2004). As the minimum serum dilution was 1/100, the minimum titre is 100 (shown as the lower dotted line in Figure 8.5C), with values under 100 represented as "1". As the maximum serum dilution was 1/12,500, the maximum titre is 12,500 (shown as the upper dotted line in Figure 8.5C) (Foster *et al.*, 2005).

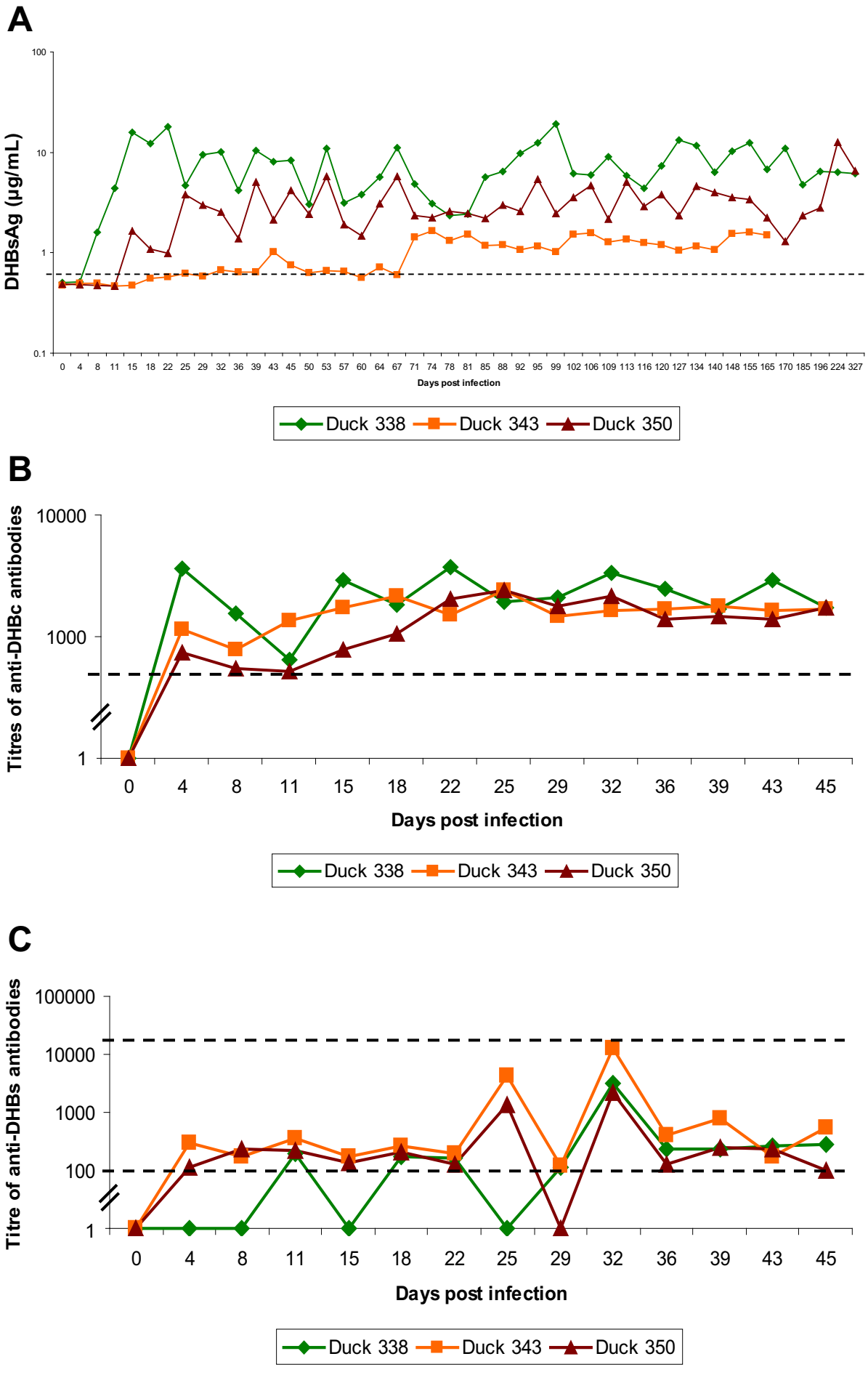

A
DHBsAg (µg/mL)
100
10
1
0.1
0 4 8 11 15 18 22 25 29 32 36 39 43 45 50 53 57 60 64 67 71 74 78 81 85 88 92 95 99 102 106 109 113 116 120 127 134 140 148 155 165 170 185 196 224 327
Days post infection
Duck 338
Duck 343
Duck 350
B
Titres of anti-DHBc antibodies
10000
1000
1
0 4 8 11 15 18 22 25 29 32 36 39 43 45
Days post infection
Duck 338
Duck 343
Duck 350
C
Titre of anti-DHBs antibodies
100000
10000
1000
100
1
0 4 8 11 15 18 22 25 29 32 36 39 43 45
Days post infection
Duck 338
Duck 343
Duck 350

Figure 8.5

Figure 8.6: Levels of DHBV total DNA present in the serum (A), and levels of DHBV total and cccDNA present in the liver (B) of ducks 338, 343 and 350 with chronic DHBV infection as detected by qPCR reactions.

The levels of DHBV total DNA present per mL serum was determined as described in Section 2.8.9.1 using the primer set 423 – 576c (Table 2.2). The limit of detection of the assay shown as the dotted line in Figure 8.6A is determined by the limit of sensitivity of the qPCR machine which does not accurately detect less than 10 copies of DHBV total DNA per 4 μL of serum, or 2500 copies of DHBV total DNA per mL of serum.

The levels of DHBV total and cccDNA in the liver were determined as described in Section 2.8.9.2 using the primer sets 423 – 576c and CC2 – MG1 respectively (Table 2.2). The levels of DHBV DNA per cell were calculated as described in Section 2.8.9.3.2. The limit of detection of the assay shown as the dotted line in Figure 8.6B is determined by the limit of sensitivity of the qPCR machine which does not accurately detect less than 10 copies of DHBV total and cccDNA per 53,571 cells, or 0.00019 copies of DHBV DNA per cell.

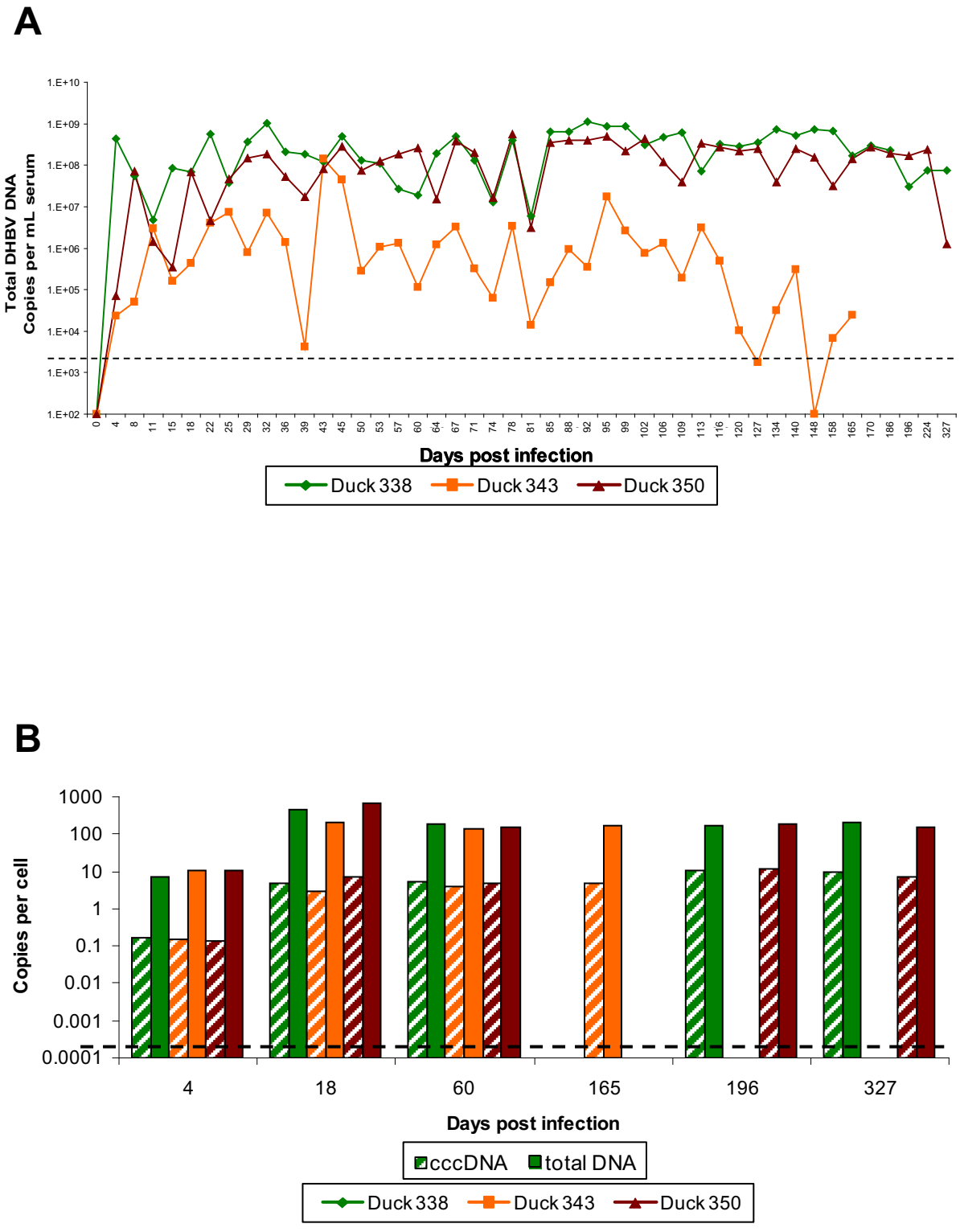

A
Total DHBV DNA Copies per mL serum
1.E+10
1.E+09
1.E+08
1.E+07
1.E+06
1.E+05
1.E+04
1.E+03
1.E+02
0 4 8 11 15 18 22 25 29 32 36 39 43 45 50 53 57 60 64 67 71 74 78 81 85 88 92 95 99 102 106 109 113 116 120 127 134 140 148 158 165 170 186 196 224 327
Days post infection
Duck 338
Duck 343
Duck 350
B
Copies per cell
1000
100
10
1
0.1
0.01
0.001
0.0001
4 18 60 165 196 327
Days post infection
cccDNA
total DNA
Duck 338
Duck 343
Duck 350

Figure 8.6

Figure 8.7: Multiple sequence alignment showing the 639 bp sequenced region of the DHBV genome from ducks 338, 343 and 350 with chronic DHBV infection, aligned with the duck AusDHBV genome (GenBank Accession AJ006350, REGION: 2389 – 3027).

DNA was extracted from duck liver tissues using total DNA extraction method as described in Section 2.6.3, and was used as template for PCR reactions using primer set DRS F2 – R2 (Table 2.2), and sequenced as described in Section 8.4.1. The multiple sequence alignment was performed using ClustalW2 program and output file viewed and arranged by Jalview program as described in Section 2.8.11.

Individual alignment scores of the AusDHBV and the duck DHBV DNA sequence were obtained using the BLAST Align 2 Sequences programme as described in Section 2.8.12. The scores were 100% coverage and 99% sequence similarity for all ducks 338, 343 and 350.

Note:
REGION refers to the specific region of nucleotide sequence that was used for alignment in this multiple sequence alignment, and was based on the nucleotide numbering obtained from the AusDHBV (GenBank Accession AJ006350) sequence. REGION was chosen to match with the range of the amplified and sequenced target gene (DHBV genome). The numbers shown in the multiple sequence alignment output figure refer to the nucleotide numbering of the specified REGIONs.

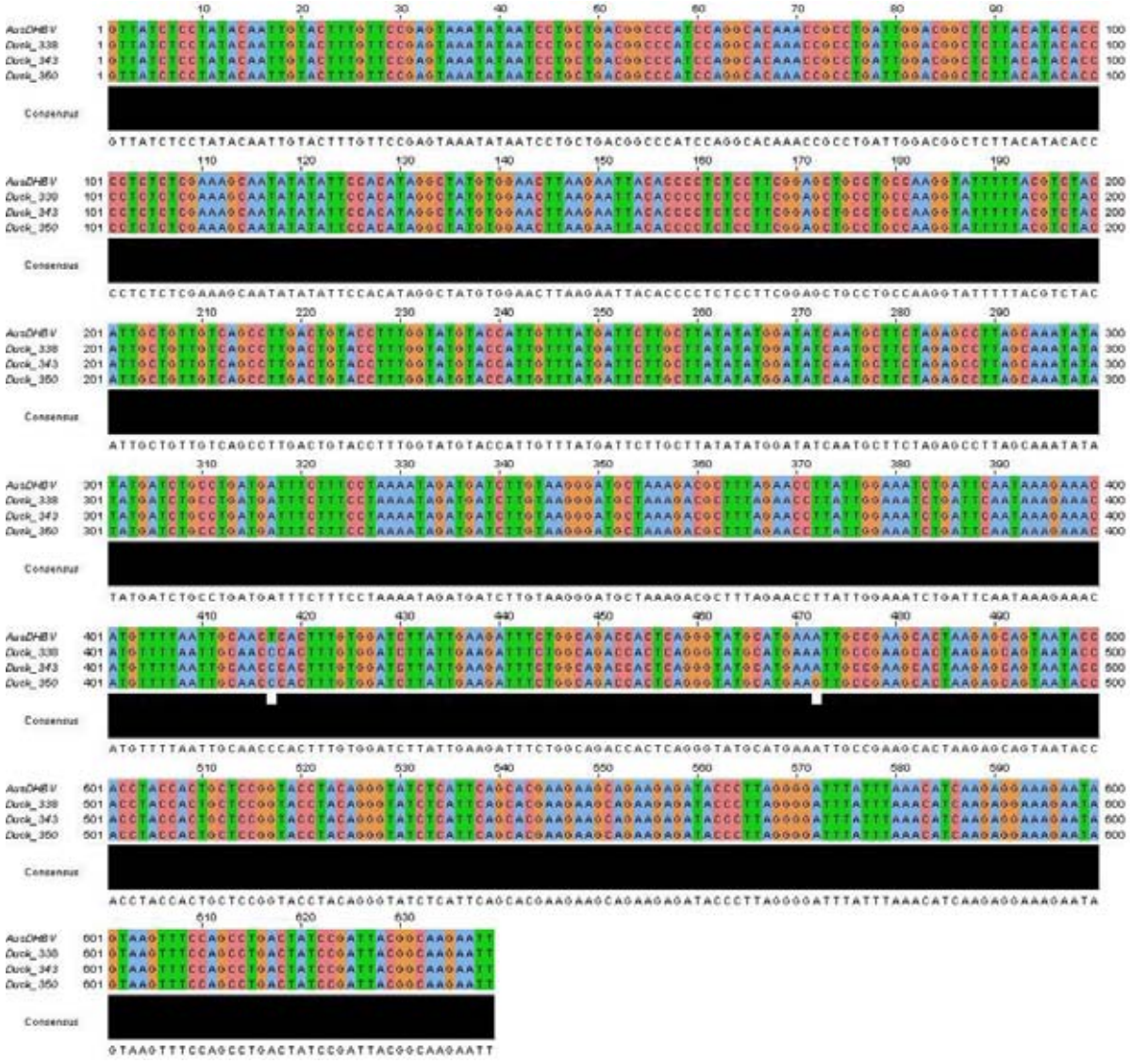


Figure 8.7

Figure 8.8: Examples of invPCR products obtained from the duck invPCR assays.

DNA was extracted from duck liver tissues and inverted as described in Section 8.4.2. The inverted DNA fragments were either 1/3 serially diluted in the 96-well PCR tray as shown in Figure 2.8 (Figure 8.8A), or were distributed evenly to all 96 PCR wells (Figure 8.8B), as DNA templates during nested PCR. Products were visualised using 96-well agarose gel electrophoresis as under 365 nm UV light as described in Section 2.10.5.

The letters A – H refer to the rows of the PCR wells. The DNA marker used (at the lanes labelled "m") was 1 μg of the GeneRuler 1 kbp Plus DNA Ladder (Thermo Fisher Scientific, Canada). Wells H7 – H12 (marked by red box) that did not contain any DNA templates were used as PCR negative controls (-ve).

Based on Figure 8.8A, the optimal amount of inverted DNA fragment that can produce a single invPCR product in most of the PCR wells, was the amount of DNA in Row G.

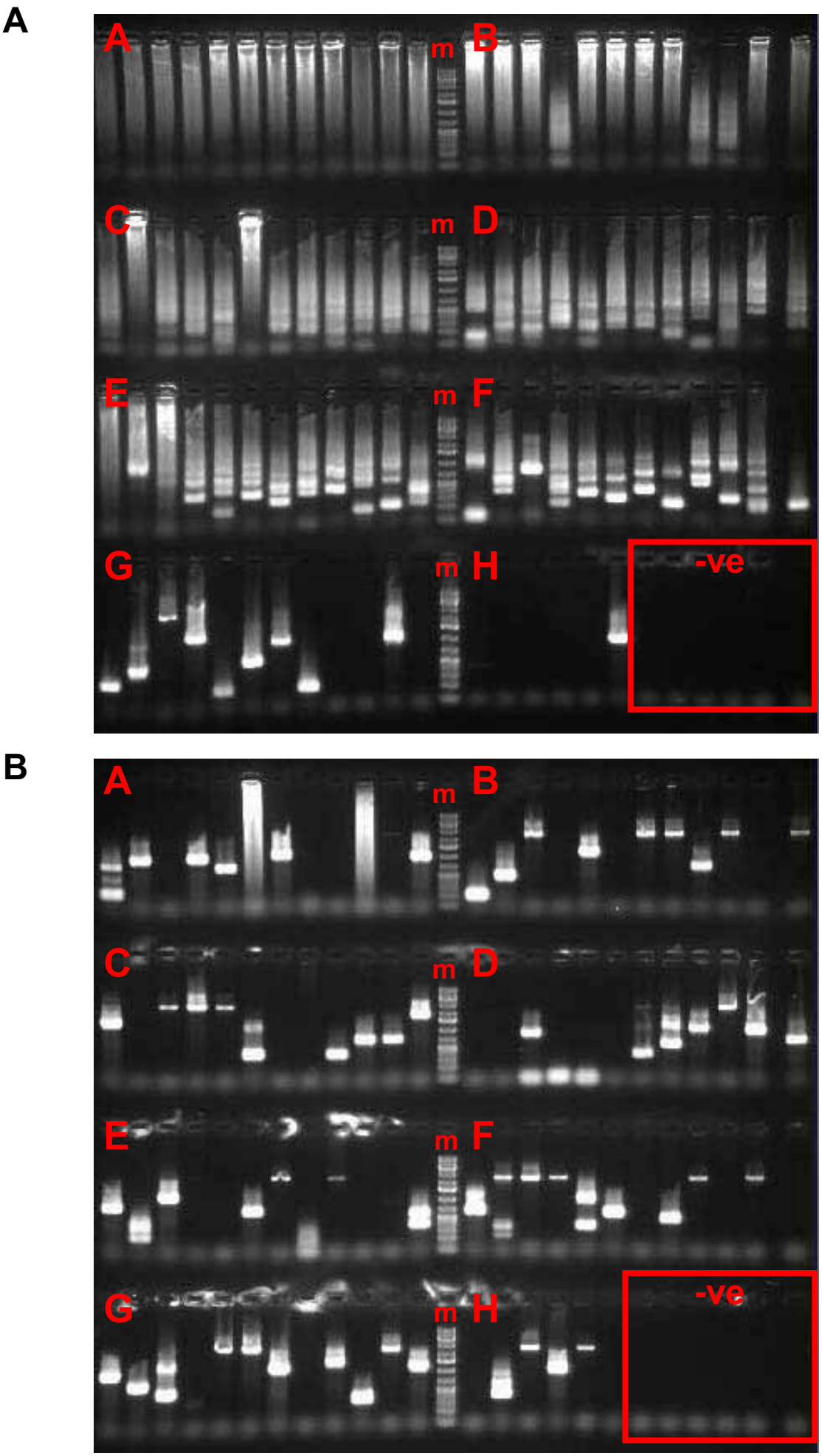


Figure 8.8

Figure 8.9: Integrated virus-cell junctions detected from invPCR assays performed using liver tissues from ducks with chronic DHBV infection.

The duck D3 invPCR assays were performed as described in Section 8.4.2. All the integrated virus-cell junctions detected were consistent with the expected inverted DNA fragment that will be produced by the duck D3 invPCR assay design (refer Figure 6.4).

Figure 8.9A shows the sequences of the integrated virus-cell junction detected in liver DNA extracted from duck 350 at 4 dpi. BLAST analysis showed that the 173 bp sequence consisted of a 18 bp insert DNA (black font) flanked by the DHBV genome (GenBank Accession AJ006350) 2653 – 2535 nt (blue bold font) and 3027 – 3011 nt (red bold font) at the *Eco*RI first cut restriction enzyme site (underlined). Further BLAST analysis showed that the insert DNA shared homology with the *Gallus gallus* (chicken) breed Red Jungle fowl, inbred line UCD001 chromosome 5, Gallus_gallus-4.0 (GenBank Accession NC_006092.3) 35713396 – 35713411 nt.

Figure 8.9B shows the sequences of the integrated virus-cell junction detected in liver DNA extracted from duck 338 at 196 dpi. BLAST analysis showed that the 628 bp sequence consisted of a 338 bp insert DNA (black font) flanked by the DHBV genome (GenBank Accession AJ006350) 2675 – 2538 joined to 126 – 1 nt (blue bold font) and 3027 – 3011 nt (red bold font) at the *Eco*RI first cut restriction enzyme site (underlined). Further BLAST analysis showed that the insert DNA shared homology with the *Gallus gallus* (chicken) chromosome 1 genomic contig (GenBank Accession NW_001471549) 1192104 – 1191798 nt.

Figure 8.9C shows the sequences of the integrated virus-cell junction detected in liver DNA extracted from duck 350 at 327 dpi. BLAST analysis showed that the 302 bp sequence consisted of a 283 bp insert DNA (black font) joined to 3027 – 3011 nt (red bold font) at the *Eco*RI first cut restriction enzyme site (underlined). Further BLAST analysis showed that the insert DNA shared homology with the *Taeniopygia guttata* (Zebra finch) chromosome 20 genomic contig (GenBank Accession NW_002197832.1) 813362 – 813236 nt.

A

GGAATGCCCGCTTGTTCGCCTATATAAGCAAGAATCATAAACAATGGT
AATACCAAAGGGACAGCCAAGGCTCACAACAGCAATGTAGACGTAAAA
ATACCTTCGGAGGCCGCTCCGAAGGAGAGGGGTGTAATTCTTGCTTTT
ATGCGTGCATGAATTCTTGCCGTAATCGA

B

GCTCTAGAGCATTGATATCCATATATAAGCAAGAATCATAAACAATGG
TACATACCAAAGGTACAGTCAAGGCTGACAACAGCAATGTAGACGTAA
AAATACCTTGGCAGGCAGCTCCGAAGGAGAGGGGTGTAATTCTTAAGT
TCCGAGAAATATAATTAGTAACGTTAGCTTCTCCCCACAGTAAACAAT
TGTAATGCCACCAAAGCAATCTCCTAGCCCGATCCAATGATTCCTCAT
TAATCTTTGCATATGCTTTTAGGTGTGCATGAATTCCTACCTGCTTCA
AGCCTGATAGCTGCATTAAGAAAATCAGTACATTTGGAGTTACCTATG
TTGTATATTACAAGCGTATTAGTGAGCTTTGTCTCAATGGTTAATTAT
CACAGCTATTAAAGTGTGTTTTATTTCAAGACTATCTCTTGTCAGCCT
TTCACTTTCATACAGTATTTGAACACTAGACTCAAAATCCCTCTGCTA
TCCATGTCCTCATTAAAATTTCAGCTAAAACAATAAAATTCCAACCTT
AATTTTGCTAGTATTTATTTTATCTCTGGTGCATGCATATTCTCTCCA
ATGCAATAACCCATTCCTCAGGTGTATGAATCTGAATTCTTGCCGTAA
TCGA

C

AAGATGAGGTCTCCTGGGAGCATAATACACATTTCCAGCATCTGAAAG
CTGCAGGAATACCAGCCAAATTTTTTCTGCCTACTCTGGACACTTTGT
GCTTTTCGGAAAGTGCAAAATGATCATGCTTCTGCCACTTGGGGAGGT
CATAAGTGGCACCTTCGCTTCATCTGCCCTGATCACAAGGAAATTGAG
AATGGAAAAAGGGGGAAATGGAAGGGCTGAGGGTAAGGGCTTCTCTGC
AGCAGCTCGCAGCTGGCCTGTTGTCATTTGTAGACACCTTTGTGAATT
CTTGCCGTAATCGA

A

ACCACTGATCGACGTATATAAGCAAGAATCATAAACAATGGTACGTAC
CAAAGGTACAGTCAAGGCTGACAACAGCAATGTAGACGTAAAAATACC
TTGGCAGGCAGCTCCGAAGGAGGGGGGTGTAATTCTGCATTAGGGACG
AG**GAATTCTTGCCGTAATCGAA**

B

TGCTAGCTCTAGAGCATTGATATCCATATATAAGCAAGAATCATAAAC
AATGGTACATACCAAAGGTACAGTCAAGGCTGACAACAGCAATGTAGA
CGTAAAAATAATGGTTGGGGCATCACGGCCTCTGTACTTCTCAGGTGT
TGACAACCAAGTACGGAGCCGAGAAATATAATTAGTAACGTTAGCTTC
TCCCCACAGTAAACAATTGTAATGCCACCAAAGCAATCTCCTAGCCCG
ATCCAATGATTCCTCATTAATCTTTG*CATATG*CTTTTAGGTGTGCATG
AATTCTTGCCGTAATCGA

Figure 8.10: Example of DNA sequencing results obtained from invPCR assays performed using liver tissues from ducks with chronic DHBV infection.

The duck D3 invPCR assays were performed as described in Section 8.4.2.

Figure 8.10A shows an example of the DNA sequencing results for an unknown sequence. BLAST analysis showed that the 166 bp sequence consisted of a 14 bp insert DNA (black font) flanked by the DHBV genome (GenBank Accession AJ006350) 2653 – 2536 nt (blue bold font) and 3027 – 3011 nt (red bold font). The *Eco*RI first cut restriction enzyme site is underlined.

Figure 8.10B shows an example of the DNA sequencing result for a virus-virus sequence, which was a false positive result. BLAST analysis showed that the 306 bp sequence consisted of 2 fragments of the DHBV genome (GenBank Accession AJ006350), 2682 – 2574 nt (blue bold font) and 183 – 3011 nt (black bold font). This shows that the virus-virus false positive sequence was likely to be formed by the ligation of 2 DHBV DNA fragments. The *Eco*RI first cut restriction enzyme digestion site is underlined, while the *Nde*I cccDNA destroying enzyme digestion site is underlined and italicized.

Chapter 9: Final discussion and concluding remarks

9.1. Introduction

During replication of HBV, the transcriptional template for the production of viral pregenomic and mRNA (Summers and Mason, 1982; Tuttleman *et al.*, 1986) exists in a stable cccDNA form at 5 – 50 copies in the nucleus of each infected hepatocyte (Summers *et al.*, 1990; Newbold *et al.*, 1995; Bock *et al.*, 2001; Zhang *et al.*, 2003). During the resolution of acute HBV infection, the majority of infected hepatocytes are cleared by cytolytic or non-cytolytic mechanisms and immune control of infection is established. Trace amounts of cccDNA have been found to persist in the liver after resolution of acute HBV and DHBV infections (Michalak *et al.*, 1999; Le Mire *et al.*, 2005) and to persist despite antiviral treatment, suggesting that residual cccDNA is not being replenished by viral replication (Reaiche *et al.*, 2010). Due to the presence of this residual cccDNA, individuals face the risk of HBV reactivation should they become immunosuppressed (Grewal *et al.*, 2007; Savas *et al.*, 2007; Kusumoto *et al.*, 2011). However, the mechanisms involved in immune clearance of acute and residual hepadnavirus infections are still poorly understood.

As described earlier in this thesis, HBV dslDNA is produced during HBV replication and can integrate into random sites of the liver genome (Tokino and Matsubara, 1991) at a low rate of ~1 integrant in 10^3 – 10^4 cells (Yang and Summers, 1999). Each integration event produces a unique integrated virus-cell junction. These integration junctions can be detected by the invPCR assay (Yang and Summers, 1999) and have been used as genetic markers for individual infected hepatocytes, allowing clonal proliferation of hepatocytes to be monitored in the liver during various stages of both acute and chronic HBV infection.

The integration of DHBV DNA into the chicken hepatocellular carcinoma cell line, LMH, has been characterised by invPCR (Triglia *et al.*, 1988; Gong *et al.*, 1995), Southern blot hybridisation (Petersen *et al.*, 1997; Gong *et al.*, 1999), and by screening genomic DNA cloned into bacteriophage (Gong *et al.*, 1999). These studies showed that full-length DHBV DNA (~3 kbp), that was introduced into LMH cells by stable transfection, was initially integrated in an un-rearranged fashion into the LMH genome (Gong *et al.*, 1995). However, with successive cell generations the integrated DNA was unstable and was lost or rearranged, likely due to the genetic instability of the LMH cells (Gong *et al.*, 1996). It was also found that integrated DHBV DNA may alter expression of proto-oncogenes or tumour suppressor genes (Gong *et al.*, 1996), and that the integration frequencies increased when DNA repair mechanisms are impaired (Petersen *et al.*, 1997).

Apart from the extensive studies of DHBV integration into LMH cell lines, the integration of DHBV DNA has not been extensively studied in other cell lines or in liver tissues. Of the few studies published, Yang and Summers, using the invPCR assay, showed that integration of DHBV DNA can occur as early as 6 dpi in DHBV-infected ducks at a rate of ~1 integrant per 10^3 – 10^4 cells (Yang and Summers, 1999); while Yokosuka *et al*, using Southern blot hybridisation, reported that integrated DHBV DNA was present in liver tumour tissue or HCC of Chinese Pekin ducks from Qi-dong, but not in up to 100 DHBV-infected Chinese and Japanese ducks without liver tumours (Yokosuka *et al.*, 1985).

The studies described in this thesis aimed to explore the mechanisms involved during the clearance of virus-infected hepatocytes during acute DHBV infection, by detecting integrated virus-cell junctions during various stages of acute infection using the invPCR assay. The molecular assays established in this study were also applied to study events occurring during chronic DHBV infection. In particular, the histological and serological changes during different stages of chronic DHBV infection were characterised. Levels of clonal proliferation of hepatocytes that occurred during chronic DHBV infection were also assessed to study the changes in the hepatocyte population during chronic infection.

9.2. Development of methods

Several molecular assays which are routinely used in this study and in the Hepatitis Research Laboratory were established or optimised. DNA sequencing protocols and subsequent purification of DNA sequencing products were optimised for single tube reactions, and established for 96-well reactions (**Chapter 3.1**). These were essential as it allowed DNA sequencing reactions to be performed optimally on a large scale (96-well format) in a time- and cost-efficient manner. qPCR assays for the detection of DHBV total and cccDNA were also optimised (**Chapter 3.2**). Some of the improvements made to the qPCR assays include the linearization of supercoiled plasmids and viral DNA, as PCR amplification of linear DNA was found to be more efficient and accurate compared to supercoiled DNA (Chen *et al.*, 2007; Hou *et al.*, 2010; Lin *et al.*, 2011), and introduction of NDL DNA into the plasmid standard curves, to standardise the amounts of any PCR inhibitors that may be present in the duck liver DNA extracts, for greater accuracy of target DNA amplifications (De Boever *et al.*, 2008).

In addition, internal controls for the qPCR assays were also established using 2 novel duck cellular genes, β actin and GAPDH (**Chapter 4**). Both of these cellular genes are single copy genes in the chicken genome (Cleveland *et al.*, 1980; Stone *et al.*, 1985), and the levels of β actin (Bishop *et al.*, 2000; Ni *et al.*, 2006; De Boever *et al.*, 2008) and GAPDH (Zhang *et al.*,

2008; Zimmerman *et al.*, 2008; Barber *et al.*, 2010) mRNA have been routinely used as internal controls during RT-qPCR.

The cellular genes encoding the mRNA for duck β actin and GAPDH were successfully amplified, sequenced and cloned into plasmid vectors. These plasmids were subsequently used in qPCR assays to normalise the amount of DHBV total and cccDNA detected per cell. Other published duck genes that have been used as internal controls include the IFN-α gene (GenBank Accession X84764) (Dallmeier *et al.*, 2008). However, as up to 10 copies of IFN-α could be present in each haploid duck genome (Nanda *et al.*, 1989), both the β actin and GAPDH genes, as single copy genes, would be advantageous for normalisation during qPCR. None of the other previously identified single copy genes, including the duck heart lactate dehydrogenase B-like protein (Hendriks *et al.*, 1988) and the duck serum amyloid A protein (Guo *et al.*, 1996), have been used as internal controls during qPCR or Southern blot hybridisation. Characterisation of the duck β actin and GAPDH genes showed that both genes had intron sequences that comprised approximately 40% of their total size, and shared ~80% of sequence homology with the chicken β actin and GAPDH genes. Interestingly, the splice sites and the intron-exon DNA fragment lengths of the duck and chicken β actin and GAPDH were the same. Intron positions have been found to be generally conserved, even between fungi-bacteria-plants-animals (up to 30% of conserved intron sites) (Fedorov *et al.*, 2002; Rogozin *et al.*, 2003), and have been suggested to be suitable as phylogenetic markers to determine the evolutionary distance between species (Sahrawy *et al.*, 1996; Venkatesh *et al.*, 1999). Thus, it was not surprising that ducks and chickens, being closely related birds and from the same Aves class, share the same β actin and GAPDH splice sites despite having ~20% nucleotide sequence differences. Further detailed phylogenetic analysis of the duck β actin and GAPDH genes with other mammals or eukaryotes could definitely be performed in future studies, to determine whether these genes are conserved genes throughout eukaryotes, or had specifically diverged in the avian species.

9.3. Development of the invPCR assay

At the outset of the studies described in this thesis, the invPCR assay had not been performed in the Hepatitis Research Laboratory. Thus, extensive optimisations of the methods involved in the invPCR assay were required for their use in the studies reported in this thesis.

Firstly, DNA extraction methods that most efficiently extract high MW liver cellular DNA from small quantities of frozen liver tissues (1 – 10 mg), whilst removing most viral DNA, were assessed (**Chapter 5.1**). This was essential during invPCR assays, as the integrated

virus-cell junctions are present in the high MW cellular DNA in much lower quantities (<1 copy per hepatocyte) compared to the non-integrated viral RI, rcDNA and cccDNA (up to 500 copies per hepatocyte) (Jilbert *et al.*, 1992). These forms of virus DNA can also be detected during invPCR assays as virus-virus false positive sequences. Thus, selectively extracting the high MW cellular DNA while removing most of the low MW non-integrated viral DNA would increase the detection of the integrated virus-cell junctions and reduce the cost of sequencing virus-virus false positive sequences. However, high losses of DNA would be expected using the selective extraction methods (estimated to be ~50% by Dr. William Mason, personal communication), which on top of mostly having only limited liver biopsy tissues available for analysis, may result in the loss of the few integrated virus-cell junctions present in each liver tissue. It was determined that the most suitable extraction method for invPCR assays was the total DNA extraction method, a non-selective method that extracts all DNA (and RNA) present in the liver tissues, which has been commonly used during previously published invPCR assays (Summers *et al.*, 2003; Mason *et al.*, 2009b). Although higher levels of virus-virus false positive sequences would be detected, the use of this extraction method would ensure that there were minimal losses of integrated virus-cell junctions. When the removal of DHBV DNA was essential, it was found that low melting temperature agarose gel electrophoresis and the subsequent purification of high MW cellular DNA could be performed to selectively extract the high MW DNA, but with the compromise of potential losses of integrated virus-cell junctions (Mason *et al.*, 2009a).

Then, to specifically reduce virus-virus false positive sequences detected during the invPCR assay, the use of LNA oligonucleotides was explored (**Chapter 5.2**). LNA oligonucleotides have been shown to have strong hybridisation affinity to the complementary DNA sequence, forming LNA:DNA complexes with high melting temperature (Vester and Wengel, 2004). Although LNA oligonucleotides have been extensively used, for instance, to detect single-nucleotide polymorphisms (Johnson *et al.*, 2004), as probes (Ostergaard *et al.*, 2010) or even as antisense oligonucleotide therapeutic agents (Deng *et al.*, 2009; Zhang *et al.*, 2010), LNA oligonucleotides have not been tested as specific inhibitors during PCR amplification. By designing LNA oligonucleotides specific for the AusDHBV genome, it was found that one of the LNA oligonucleotides successfully blocked the amplification of DHBV DNA when added at the molar ratio of LNA:plasmid DNA of 50,000:1 and higher. This showed that LNA oligonucleotides have the ability to specifically inhibit PCR amplification of a particular sequence, and could potentially be applied in many other areas of research. Despite that, the use of LNA oligonucleotides to prevent false positives during invPCR assays was not further pursued in this study, as it would not be feasible to add up to 50,000-fold molar excess of

LNA oligonucleotides per PCR well, considering that large scale 96-well PCRs were routinely performed during invPCR, and the high cost of LNA oligonucleotides' synthesis.

Besides the invPCR assay, several other molecular assays have been used to detect integrated virus-cell junctions. These include the linker ligation assay (Summers *et al.*, 2003), Southern blot hybridisation (Hino *et al.*, 1985), *in situ* hybridisation using biotinylated probes (Negro *et al.*, 1985), *Alu*-PCR (Kawai *et al.*, 2001), semi-degenerate oligonucleotide-primed (DOP) PCR (Telenius *et al.*, 1992), and cloning and characterisation of restriction enzyme-digested total nuclear DNA into bacteriophage clones (Gong *et al.*, 1999). In this thesis, linker ligation assay was assessed for its ability to detect integrated virus-cell junctions as a possible alternative to the invPCR assay (**Chapter 5.3**). Many variations of linker ligation assay have been widely applied, for instance to screen and sequence neighbouring unknown genome sequences (Balavoine, 1996), for high-throughput of integration sites of *Agrobacterium* transfer DNA in the *Arabidopsis* plant genome (Malley *et al.*, 2010), human papillomavirus integration in cervical carcinoma-derived cell lines (Luft *et al.*, 2001), HIV-1 integration sites in cell cultures (Schroder *et al.*, 2002; Kim *et al.*, 2006), or whole genome Adeno-associated virus integration sites in cell cultures (Drew *et al.*, 2007). For HBV-related studies, a group has also successfully applied linker ligation assay to detect HBV integration in HCC from various patient cohorts, including HBsAg-negative patients with chronic HCV (Tamori *et al.*, 2005), HBsAg-negative and anti-HCV negative patients (Tamori *et al.*, 2003), and chronic HBV patients (Tamori *et al.*, 2005; Shinkawa *et al.*, 2008). In this thesis, the linker ligation assay used by Summers *et al.* (Summers *et al.*, 2003) to characterise integration of WHV DNA was adapted to determine integrated virus-cell junctions in WHV-infected woodchuck and DHBV-infected duck liver tissues. When compared to the integrated virus-cell junctions detected using the invPCR assay, the efficiency of the detection of integrated virus-cell junctions was similar in woodchucks, but much higher in ducks. There were also lower levels of virus-virus false positive sequences detected in both woodchucks and ducks using the linker ligation assay. However, the linker ligation assay was more complicated and complex to perform. The linker ligation assay was advantageous for all the studies described earlier, and a high-throughput of integration sites could be efficiently generated, as there were generally high levels of integration present in, for instance, HCC tumours (Tamori *et al.*, 2003; Tamori *et al.*, 2005; Shinkawa *et al.*, 2008). In the DHBV-infected ducks, only low levels of integration were expected (~1 in 10^3 – 10^4 cells by 6 dpi as described by Yang and Summers) (Yang and Summers, 1999). Therefore, as the simpler invPCR assay should be sufficient to detect the integrated virus-cell junctions in the DHBV-infected duck livers in this study, the linker ligation assay was not further developed.

In addition, to determine the sensitivity and efficiency of the invPCR assays established in this thesis, plasmid DNA constructs were used as a model system, in a series of tests adapted from those performed by Yang and Summers (Yang and Summers, 1999) (**Chapter 5.4**). Similar to the sensitivity and efficiency of invPCR assays reported by Yang and Summers, it was found that invPCR assays in this thesis were sensitive enough to detect down to a single copy of DNA template, and would preferably amplify from the shorter DNA template if DNA templates of different lengths were present in a reaction mix. It was also found that the sensitivity of the invPCR assays were slightly reduced in the presence of cellular DNA, as suggested by De Boever *et al.* (De Boever *et al.*, 2008), possibly due to inhibition, interference, or saturation of the invPCR assay reagents by the large quantities of cellular DNA. In addition to these tests, to further determine the quality of the invPCR assays established in this thesis, invPCR assays were performed in parallel with studies conducted by collaborator Dr. William Mason (**Chapter 5.5**). Using the invPCR assays to detect integrated virus-cell junctions in WHV-infected woodchuck and HBV-infected chimpanzee liver tissues, both studies produced similar numbers of integrated virus-cell junctions per liver DNA analysed, as well as the trends of the unique and repeated integration virus-cell junctions for each liver tissue. All of these finding increased our confidence that the invPCR assays established in this thesis were of equal quality to other well established and published invPCR assays, and that invPCR assays were ready to be applied in this study. The results obtained in Chapter 5.5 were included as a subset of the data published by Mason *et al.* 2009a and 2009b.

Lastly, invPCR assays specific for the AusDHBV strain were established, and preliminary invPCR assays for the detection of integrated virus-cell junctions in ducks with either acute or chronic DHBV infection were performed using duck liver tissues collected from various previous studies (Trahair, 2008; Noordeen, 2009; Reaiche *et al.*, 2010; Teoh, unpublished) (**Chapter 6**). These preliminary studies are novel, as the detection of integrated virus-cell junctions have not been previously reported in ducks with acute DHBV infection, or in ducks with chronic DHBV infection for more than 6 dpi. From these studies, 1 integrated virus-cell junction was detected in the liver of a duck with acute DHBV infection, and 37 integrated virus-cell junctions were detected in the livers of ducks with chronic DHBV infection at 29, 34 and 41 dpi. Among these 37 junctions there were 3 hepatocyte clones at least 2 – 3 cells in size. Further characterisation of the integrated DHBV DNA confirmed that the most probable left and right hand ends of the integrated DHBV dslDNA were at nucleotide positions 2537 nt and ~2485 nt respectively (Yang and Summers, 1999). There were also no significant patterns or apparent preferences of DHBV integration sites in the duck genome, which was consistent with previous analysis of HBV integration sites in humans (Tokino and Matsubara, 1991;

Murakami *et al.*, 2005; Mason *et al.*, 2010) and chimpanzees (Mason *et al.*, 2009a). These findings suggest that integration of DHBV DNA in duck livers had occurred in the same manner as the integration of HBV DNA in humans and chimpanzees and integration of WHV DNA in woodchucks, which is via non homologous end joining of the dslDNA into random sites of the liver genome (Yang and Summers, 1995).

On a separate note, the size of the hepatocyte clones found in the ducks with chronic DHBV infection were much smaller than the size of hepatocyte clones previously reported in humans, chimpanzees and woodchucks with chronic HBV or WHV infections. In chronic WHV-infected woodchucks, at least 2% of the liver consisted of hepatocyte clones 1,000 – 26,000 cells in size (Mason *et al.*, 2005); in chronic HBV-infected chimpanzees, 50 hepatocyte clones ranging from 35 to 10,000 cells in size were found in a sample size of ~3 x 10^7 hepatocytes (Mason *et al.*, 2009a); while in chronic HBV-infected humans, up to 8 hepatocyte clones 100 – 60,000 cells in size were found in 1 – 3 mg of liver tissues (Mason *et al.*, 2010). However, the woodchuck liver tissues were from 22 – 28 months post WHV infection (Mason *et al.*, 2005), and at least 20 years post HBV infection in chimpanzees (Mason *et al.*, 2010) and humans (Mason *et al.*, 2010). Due to the shorter timeframe of chronic DHBV infection in the ducks tested (29 – 41 dpi), the levels of liver turnover and clonal proliferation of hepatocytes that had occurred in the ducks would be quite low. It was therefore expected that smaller hepatocyte clones and at lower abundance would be found in the liver of these ducks.

9.4. The use of invPCR assays to explore the mechanisms involved in clearance of DHBV-infected hepatocytes during acute DHBV infection in ducks

As described in Section 9.1, during the resolution of acute HBV infection and establishment of immune control of infection, the mechanisms involved in immune clearance of HBV infection, specifically cccDNA, are poorly understood. It is hypothesised that clearance of cccDNA occurs cytolytically through CTL attack on infected cells, or non-cytolytically through cytokine "curing" of the infected hepatocytes while leaving the cells intact.

Evidence consistent with cytolytic hepatocyte killing as the main mechanism involved in clearance of hepadnavirus infection has been found in several studies. For instance, in DHBV-infected duck and WHV-infected woodchuck primary hepatocyte cultures, reductions in cccDNA levels occurred during hepatocyte death (Fourel *et al.*, 1994b; Moraleda *et al.*, 1997), while in chronic DHBV-infected ducks and chronic WHV-infected woodchucks, decreases in cccDNA levels were found to coincide with the rate of hepatocyte death in those animals (Fourel *et al.*, 1994b; Zhu *et al.*, 2001). Although hepdnaviruses are considered non-

cytopathic (Baumert *et al.*, 2007), during chronic HBV infection in humans, HBV-infected hepatocytes were found to have a half-life of 10 – 100 days, corresponding to a daily 0.3% – 3.0% loss of HBsAg-positive hepatocytes (Nowak *et al.*, 1996). These findings suggested that constant host-mediated cytolytic hepatocyte killing had occurred in response to infection, consistent with studies of acute WHV-infected woodchucks and acute DHBV-infected ducks, which showed enhanced rates of hepatocyte turnover during resolution of acute infection (Jilbert *et al.*, 1992; Kajino *et al.*, 1994; Summers *et al.*, 2003).

On the other hand, evidence consistent with non-cytolytic hepatocyte curing as the main mechanism involved in clearance of hepadnavirus infection has also been found in several studies. For instance, reduction in cccDNA levels were found to neither coincide with reductions in the percentage of HBcAg-positive hepatocytes in acute HBV-infected chimpanzees (Wieland *et al.*, 2004), nor correlate with changes in ALT, HBcAg- and HBsAg-positive hepatocytes over 48 weeks of follow-up in antiviral-treated patients with chronic HBV infection (Werle-Lapostolle *et al.*, 2004). CD8+ CTL also showed more non-cytopathic functions during early phases of HBV clearance in chimpanzees with acute HBV infection, like the release of cytokine IFN-γ and TNF-α (Guidotti *et al.*, 1996), as the levels of cccDNA were significantly reduced in the presence of cytokines (Murray *et al.*, 2005). Although it has been found in HBV-transgenic mice that cytokines inactivate HBV replication by preventing the formation of and degrading the HBV nucleocapsids containing RI DNA (Guidotti *et al.*, 1996; Wieland *et al.*, 2000; Guidotti *et al.*, 2002; Wieland *et al.*, 2005), HBV-transgenic mice do not produce cccDNA, preventing studies of the effects of cytokines on cccDNA. It was also shown that cytokines could not directly reduce levels of cccDNA in chimeric mice (urokinase-type plasminogen activator/SCID mice transplanted with human hepatocytes) (Lutgehetmann *et al.*, 2011). Therefore the mechanisms involved in the clearance of cccDNA without hepatocyte death are still undetermined, although it has been implied that cytokines may destabilise cccDNA to increase the chances for degradation (Lutgehetmann *et al.*, 2010).

Thus, it seems that on top of the issue of cytolytic hepatocyte killing vs. non-cytolytic hepatocyte curing of infected hepatocytes, another major unresolved issue is the fate of cccDNA present in the hepatocytes. cccDNA, as described in Section 9.1, is present as compact mini-chromosomes at 5 – 50 copies in the nucleus of each infected hepatocyte (Summers *et al.*, 1990; Newbold *et al.*, 1995; Bock *et al.*, 2001; Zhang *et al.*, 2003). Although the half-life of cccDNA has been found to be 2 – 5 days in PDH (Civitico and Locarnini, 1994) and LMH cells (Guo *et al.*, 2003), and 33 – 50 days in WHV-infected woodchucks (Zhu *et al.*, 2001), cccDNA has been found to be stable, and to persist at low levels in the

liver of ducks (Le Mire *et al.*, 2005; Reaiche *et al.*, 2010), woodchucks (Kajino *et al.*, 1994; Michalak *et al.*, 1999) and chimpanzees (Wieland *et al.*, 2004; Murray *et al.*, 2005) for long periods (months to years) after clearance of hepadnavirus during acute infections.

As the hepatocyte undergoes mitosis, there could be several possible fates of the stable cccDNA present in the nucleus: cccDNA could be lost during hepatocyte mitosis, or be distributed to progeny cells, either by equal or non-equal distributions (Zhang *et al.*, 2003). There are few studies that have shown convincing evidences for the fate of cccDNA during hepatocyte mitosis. *In vitro* studies have found that cccDNA could be passed to progeny cells, as similar levels of total cccDNA were found in proliferating primary woodchuck hepatocyte cultures (Dandri *et al.*, 2000), and as the decline in levels of cccDNA were found to correlate to dilutions during passage of LMH cells (Guo *et al.*, 2003); while *in vivo* studies calculating cccDNA levels and hepatocyte proliferation (by PCNA staining) in chronic WHV-infected woodchucks found that the loss of cccDNA was consistent with its distribution to progeny cells (Zhu *et al.*, 2001). However, other *in vivo* studies that also calculated cccDNA levels and hepatocyte turnover (by measuring the complexity of integrated virus-cell junctions) in acute WHV-infected woodchucks found that cccDNA is likely lost during hepatocyte mitosis (Mason *et al.*, 2009b). To complicate things further, other studies have suggested that cccDNA could be both lost and passed to progeny cells during mitosis, as the calculations of cccDNA levels and hepatocyte division/turnover did not convincingly fit either one of the proposed fates of cccDNA during mitosis (Fourel *et al.*, 1994b; Lutgehetmann *et al.*, 2010).

As part of extensive studies in the Hepatitis Research Laboratory, the studies described in this thesis aimed to explore the mechanisms involved in clearance of acute DHBV infection, whether by cytolytic hepatocyte killing or non-cytolytic hepatocyte curing, by measuring the complexity of integrated virus-cell junctions present using the invPCR assay during various stages of acute DHBV infection (**Chapter 7**). Previous i*n vivo* studies of the clearance of virus-infected hepatocytes have been complex, as during early stages of infection, up to 100% of the hepatocytes in the liver could be infected (Summers *et al.*, 2003; Murray *et al.*, 2005). Thus, integrated viral DNA would potentially be present in every hepatocyte in the liver, resulting in no available uninfected hepatocytes to replace the hepatocytes that were killed during the clearance of infection, and making the observation of whether non-cytolytic hepatocyte curing had occurred less straight forward. Therefore, this study experimentally infected <5% of the hepatocyte population of the duck livers during early stages of DHBV infection. It is expected that if cytolytic hepatocyte killing occurs, the DHBV-infected hepatocytes would be destroyed and replaced by neighbouring uninfected hepatocytes, thus

integrated virus-cell junctions would no longer be present in the liver after resolution of acute DHBV infection. Conversely, if non-cytolytic hepatocyte curing occurs, integrated virus-cell junctions would still be present in the liver after resolution of acute DHBV infection, with similar junction complexities expected before and after resolution of infection.

Acute DHBV infection was established in three 6-week-old Pekin-Aylesbury ducks, and the histological and serological changes that occurred in these ducks were characterised. It was found that at 4 dpi, up to ~4.4% of the hepatocytes were DHBsAg-positive, with 159 and 3.6 copies of DHBV total and cccDNA per infected hepatocyte respectively, consistent with previous studies which showed that the resolution of DHBV infection in some ducks but not in others was not due to the failure of establishment of DHBV infection, or the natural resistance of the hepatocytes to DHBV infection (Jilbert *et al.*, 1992). Rather, it was the rapidly activated duck immune responses, both innate and adaptive, that had successfully controlled and cleared the DHBV infection by 45 dpi.

It was likely that no integrated virus-cell junctions were successfully detected in this study due to the low levels of DHBV integration into the duck liver genome, high levels of virus-virus false positive sequences detected, and the large proportion of DNA sequencing reactions that failed to produce any readable DNA sequences. Although the mechanisms involved during the clearance of DHBV-infected hepatocytes during acute DHBV infection could not be conclusively determined in this study, the molecular assays developed in this study could be used as a platform for further studies described in Sections 9.6 and 9.7.

The studies described in this thesis formed part of extensive, ongoing studies in the Hepatitis Research Laboratory that aim to explore the fate of cccDNA during hepatocyte mitosis using various approaches. These studies include: (i) *in vitro* studies observing the reduction of cccDNA levels during mitosis of PDH, ensuring the complete inhibition of viral replication using multiple antiviral drugs or a DHBV polymerase-mutant strain which is infectious but replication incompetent (Zhu, 2010; Trevorrow, 2011; Reaiche, in progress); (ii) *in vivo* studies of the decline of cccDNA levels in 2-day-old ducks infected with ~1 DHBV virion per hepatocyte (Thorpe, 2007), or in 6-week-old ducks for up to 316 dpi after clearance of DHBV infection in ducks treated with single (Reaiche *et al.*, 2010) or multiple antiviral drugs (Reaiche, in progress) to inhibit any DHBV replication that may replenish the cccDNA pool (Zhu *et al.*, 2001). Ultimately, these studies aim to use the results obtained from the DHBV-infected duck model to add onto the wealth of HBV studies in other animal models as well as

in humans, to allow for a more complete understanding of HBV pathogenesis and clearance, and to develop new therapeutic directions for the clearance of HBV infection.

9.5. The use of invPCR assay to assess levels of clonal proliferation of hepatocytes during various stages of chronic DHBV infection in ducks

Persistence of chronic HBV infection has been associated with the development of various liver diseases in humans. For instance, 1 – 37 year follow-up studies of chronic HBV patients showed that the incidence of cirrhosis in asymptomatic HBsAg carriers ranged from 0% – 0.01% (de Franchis *et al.*, 1993; Manno *et al.*, 2004), while it ranged from 1% – 54% during chronic active hepatitis (Fattovich *et al.*, 1988; Liaw *et al.*, 1988; Oka *et al.*, 1990), with annual incidences reported to be 1% – 2.4% (Lin *et al.*, 2005). By contrast, the incidence of HCC ranged from 0.02% – 1% in non-cirrhotic asymptomatic HBsAg carriers (Manno *et al.*, 2004), and from 0.8% – 6.6% in compensated cirrhotic patients (Xu *et al.*, 2003), with annual incidences reported to be 0.02% – 1% and 3% – 6.6% respectively (Lin *et al.*, 2005). There would also be increased risks of disease progression when patients are co-infected for instance with HCV (Liaw *et al.*, 2004) or hepatitis delta virus (Fattovich *et al.*, 1988), infected with certain HBV genotypes that cause more severe clinical outcomes, for example HBV genotype F (Livingston *et al.*, 2007), or lead poor lifestyles with excessive drinking and smoking (Chen *et al.*, 1991; Fattovich *et al.*, 2008). On the other hand, in animal models, at least 60% of WHV-infected woodchucks developed HCC 2 – 4 years post infection with no cirrhosis observed (Summers *et al.*, 1978; Popper *et al.*, 1981; Popper *et al.*, 1987). GSHV-infected ground squirrels also showed higher risk of development of HCC 2.4 years post infection (Marion *et al.*, 1986) with no cirrhosis observed (Cullen and Marion, 1996). However, neither cirrhosis or HCC have been observed in HBV-infected chimpanzees (Shouval *et al.*, 1980; Mason *et al.*, 2009b) or in DHBV-infected ducks (Marion *et al.*, 1984; Yokosuka *et al.*, 1985). Although liver fibrosis and HCC has been reported in DHBV-infected ducks from Qi-dung, China, most of these ducks have been exposed to the liver toxin Aflatoxin (Omata *et al.*, 1984; Duflot *et al.*, 1995), which in the absence of DHBV infection, has been shown to cause HCC in ducks (Cova *et al.*, 1990; Cova *et al.*, 1994).

The development of hepadnavirus-related HCC is still not well understood. Mutations of *p53*, a common marker for most cancerous cells, were not always observed in HCC cells from humans (Oda *et al.*, 1992; Su *et al.*, 2008), woodchucks and ground squirrels (Rivkina *et al.*, 1994). Although hepadnavirus DNA integration has been found in most HCC tumours (Hino *et al.*, 1985; Tamori *et al.*, 2003), there is little evidence of direct oncogenesis via integrated viral DNA, as the integration sites in the host liver genome has been mostly random in HBV-

infected humans (Tokino and Matsubara, 1991; Murakami *et al.*, 2005; Tamori *et al.*, 2005) and chimpanzees (Mason *et al.*, 2009a). The exception is the frequent integration-mediated activation of *N-myc* oncogene in WHV-infected woodchucks (Fourel *et al.*, 1990; Fourel *et al.*, 1994a), while activation of oncogenes described in GSHV-infected ground squirrels (Transy *et al.*, 1992; Transy *et al.*, 1994) and humans (Paterlini-Brechot *et al.*, 2003) may or may not be integration-mediated. However, most HCC and cirrhotic nodules have been found to be clonal in nature (Farber, 1991; Yasui *et al.*, 1992; Ochiai *et al.*, 2000), and it is likely that HCC tumours originated with clonal proliferation of pre-neoplastic hepatocytes, which occurs as the hepatocytes undergo mitosis to replace neighbouring hepatocytes that have died, forming hepatocyte clones in the liver (Summers *et al.*, 2003; Michalopoulos, 2007; Marongiu *et al.*, 2008). In chronic HBV infections, as the host immune response constantly targets and kills infected hepatocytes at low levels throughout the course of infection (Guidotti *et al.*, 1996; Menne and Tennant, 1999), constant clonal proliferation of hepatocytes would be required to replace the dead hepatocytes (Mason *et al.*, 1998). Thus, through selective proliferation of hepatocytes with survival or proliferation advantages, clonal proliferation of hepatocytes may significantly contribute to hepatocarcinogenesis.

Several studies that assessed clonal proliferation of hepatocytes (including a subset of data from **Chapter 5.5**) reported that ~2% of the chronically WHV-infected woodchuck liver consisted of hepatocyte clones 1,000 – 26,000 cells in size (Mason *et al.*, 2005); 50 hepatocyte clones ranging from 35 – 10,000 cells in size were found in a sample size of ~$3x10^7$ of hepatocytes from chronically HBV-infected chimpanzees (Mason *et al.*, 2009a); while hepatocyte clones of 60 – 36,450 cells in size were found in a sample size of 8.95 x 10^6 of hepatocytes from long-term HBV-infected human carriers (Mason *et al.*, 2010). Currently, there have been no long-term studies of changes in the liver population in ducks with chronic DHBV infection. Thus, this study aimed to assess the levels of clonal proliferation of hepatocytes during long-term chronic DHBV-infected in ducks using the invPCR assay (**Chapter 8**). It is expected that as the frequency of the unique integrated virus-cell junctions would increase upon clonal proliferation of the DHBV-infected hepatocytes, the size of hepatocytes clones formed and the rate of hepatocyte clonal proliferation could be determined based on the copy number for each unique integrated virus-cell junction. In addition, the site of DHBV DNA integration in the duck genome could also be determined, to observe whether the integration sites are random as previously found (Tokino and Matsubara, 1991), and whether the integration events had altered the expression of any genes that, for instance, may lead to survival advantages of hepatocytes as precursors to the development of liver tumours.

Chronic DHBV infection was established in three 6-week-old Pekin-Aylesbury ducks, and the histological and serological changes that occurred in these ducks were characterised. This was a novel study, as the immune responses and the liver disease development in adult ducks during long-term (up to 327 dpi) chronic DHBV infection has not been extensively studied and published. It was found that extensive portal and lobular liver inflammation were observed in these ducks compared to levels found in chronic DHBV infections established in younger ducks (congenitally to 4-week-old) (Freiman *et al.*, 1988; Cullen *et al.*, 1989; Vickery *et al.*, 1999; Jilbert and Kotlarski, 2000), which was expected as the older ducks, with a more developed immune system, would elicit stronger immune responses against DHBV infection. Despite higher levels of liver inflammation and hepatocellular injury, the progression of liver diseases, including the development of fibrosis, cirrhosis and HCC, were not observed in these ducks at the last time-point of this study (327 dpi). Besides that, compared to age matched ducks that developed acute DHBV infection (**Chapter 7**) it was found that Kupffer cell infiltration and activation and the production of anti-DHBs antibodies in these ducks were delayed and at produced at lower levels. These suggest that the ability of ducks to rapidly stimulate the activation of Kupffer cells and produce neutralising anti-DHBs antibodies may be essential for the successful control and clearance of DHBV infection (Vickery *et al.*, 1989; Pugh *et al.*, 1995; Tohidi-Esfahani *et al.*, 2010).

Integrated virus-cell junctions were successfully detected in these ducks along chronic DHBV infection. However, no heaptocytes clones were detected. Although the levels of clonal proliferation of hepatocytes during chronic DHBV infection could not be conclusively determined in this study using the invPCR assay, this study could be used as a platform for further studies as described in Sections 9.6 and 9.7.

Ultimately, this study aimed to further understand hepatocarcinogenesis by detecting clonal proliferation of hepatocytes, to add to the wealth of HBV studies in other animal models as well as in humans, in the hope of discovering new therapeutic directions for the early detection, prevention and curing of the currently untreatable HCC. However, as ducks have shorter lifespan (9 – 12 years), significant rates of amyloidosis (Guo *et al.*, 1996), and generally milder liver diseases during chronic hepadnavirus infections compared to humans and other animal models (Duflot *et al.*, 1995), these may result in lower levels of hepatocyte turnover and clonal proliferation the formation of smaller hepatocyte clones, ducks may not be an ideal model for the study of liver disease progression during chronic infections.

9.6. Future studies for characterisation of histological and serological changes occurring during acute and chronic DHBV infection

For future studies, several other characterisations could be performed on these duck samples. For instance, further histological analysis could include specific assays to determine levels of hepatocyte proliferation and apoptosis, to determine the liver turnover during acute DHBV infection. This could be done by the use of PCNA staining, Ki-67 (anti-cell proliferation-associated nuclear antigen) staining or Bromodeoxyuridine (BrdU) incorporation into the genome to determine the levels of hepatocyte proliferation; and terminal deoxynucleotidyl transferase dUTP nick end labelling (TUNEL) assays to determine levels of hepatocyte apoptosis. These methods are more specific because observations of hepatocyte proliferation and apoptosis by histological analysis on H&E stained liver sections (**Sections 7.3.2.3 and 8.3.2.3**) were dependent on individual observations and assessments, and thus may not be indicative of the actual levels of hepatocyte proliferation and apoptosis that are occurring in the liver. Subsequently, by determining the levels of hepatocyte proliferation and apoptosis, liver turnover that had occurred could then be calculated using mathematical modelling. Based on that, it could be calculated as to whether cytolytic hepatocyte killing was enough to clear the DHBV infection, as well as calculating the expected size of hepatocyte clones that can be formed if non-cytolytic hepatocyte curing had occurred during acute DHBV infection. In addition, the hepatocyte clone sizes expected to be formed during chronic DHBV infection could also be estimated using mathematical modelling (Tu, unpublished).

In addition, immunofluorescent co-staining of liver tissue sections for proliferation (PCNA) and DHBV infection (DHBsAg) could be performed to visualise whether DHBsAg-positive or -negative hepatocytes have clonally proliferated to compensate for the loss of hepatocytes, as it is hypothesised that compensatory hepatocyte proliferation, or proliferation of neighbouring hepatocytes to replace the killed hepatocytes and restore liver mass, occurs during the clearance of DHBV infection. It is expected that if cytolytic hepatocyte killing occurs, DHBsAg-positive hepatocytes would gradually be killed and replaced by neighbouring DHBV-negative hepatocytes. However, if non-cytolytic hepatocyte curing occurs, the rate of liver turnover would be much lower, and that both DHBsAg-positive and -negative hepatocytes would proliferate at similar rates. On a similar note, immunofluorescent co-staining of liver tissue sections for apoptosis (TUNEL) and DHBV infection (DHBsAg) could also be performed to further visualise whether the DHBsAg-positive hepatocytes were being selectively killed at a higher rate compared to DHBV-negative hepatocytes during the clearance of DHBV infection, as assumed in this study.

To add to that, the pancreas, spleen and kidney tissues that were collected from each duck during autopsy (45 dpi in **Chapter 7** and 165 or 327 dpi in **Chapter 8**) could also be characterised, to determine whether residual of DHBV DNA could be found in tissues of ducks after clearance of DHBV infection, and also characterise the regions that were DHBV-infected during DHBV infection, as well as any inflammatory infiltration or morphological changes associated with long-term chronic DHBV infection. Previous studies have shown that during chronic DHBV infection, DHBV could be detected in the islet cells and acinar cells of the pancreas, in the splenic red and white pulp and germinal centres in the spleen, in the glomeruli of the kidney in some of the DHBV-infected ducks, with evidence of active replication in those organs (Jilbert *et al.*, 1987; Freiman *et al.*, 1988; Cullen *et al.*, 1989). Some inflammatory cells were also found around the pancreas ducts and islet cells, and no significant morphological changes were observed up to 6 weeks post infection (Freiman *et al.*, 1988; Cullen *et al.*, 1989). However, it is not known if extrahepatic DHBV infection occurs in the early stages of acute infection, particularly in the absence of extended periods of viraemia which have been previously thought to be necessary to seed extrahepatic sites of DHBV replication (Jilbert *et al.*, 1987).

Besides histological characterisations, a range of innate immune responses could also be further characterised in these ducks. These include determining the levels of production of cytokines like TNF-α, IFN-β, IFN-γ, IL-2, IL-8 by reverse transcription PCR (RT-PCR), as these cytokines, as described in Chapter 1.4, are involved in the activation of other immune cells like T cells and NK cells, or could destabilise virus nucleocapsids (TNF-α, IFN-γ) (Schultz *et al.*, 2004; Narayan *et al.*, 2006; Puro and Schneider, 2007). These would be particularly important in exploring the delayed infiltration and activation of Kupffer cells observed in ducks with chronic DHBV infection (**Section 8.3.2.4**), as Kupffer cells have been known to be activated by cytokines and chemokines like TNF-α and IFN-γ (Smedsrod *et al.*, 1994; Kolios *et al.*, 2006). If the early activation of Kupffer cells was indeed a key to the early control and resolution of HBV infection (Tohidi-Esfahani *et al.*, 2010), chemokine or cytokine therapies, or any other therapies to increase the infiltration and activation of Kupffer cells in the liver, may be further explored as potential therapeutic tools to help clear chronic HBV infections in humans. Furthermore, the effects of different cytokine production on the rate of integration of DHBV DNA into the host genome could also be potentially explored.

In addition, levels of activation, expression and roles of toll like receptors (TLRs) during DHBV infection could also be characterised by RT-PCR, especially TLR-2, which recognises triacyl lipoproteins like the viral envelope glycoprotein (Huang *et al.*, 2011), that have been

shown to be upregulated *in vitro* in primary duck hepatocytes (PDH) after DHBV challenge (Reaiche, 2008) and inhibit HBV replication *in vivo* in transgenic mice (Isogawa *et al.*, 2005).

On top of that, the levels of NK cell activation could also be determined by flow cytometry (detecting activation markers like CD69 and NKG2D) or cytotoxicity assays, as NK cells are critical during early phases of viral infections as the "first line of defence", for rapid recognition and destruction of infected cells, and play an essential role in subsequent activation of the adaptive immune system and other immune cells by secretion of a range of cytokines and chemokines like IFN-γ, IL-10, IL-13 (Andoniou *et al.*, 2006; Li *et al.*, 2011). It is expected that the ability of ducks to rapidly activate NK cells during the early stages of DHBV infection would be one of the main keys for the successful clearance of DHBV infection (Li *et al.*, 2011). It would also be interesting to explore whether the failure of the ducks to clear DHBV infection were also due to the low activation of NK cells, or the low secretion of cytokines and chemokines. Lastly, the T lymphocyte activation in the ducks, both CD8+ CTL and Th1 or Th2 CD4+ T cells, could also be determined by RT-PCR, immunohistochemical staining, or by flow cytometry (using anti-CD4 and -CD8 antibodies specific for ducks) (Kothlow *et al.*, 2005) after *in vitro* stimulation of the purified duck T cells with DHBV antigens. However, these assays could only determine the overall T lymphocyte activation occurring, and would not be able to specifically identify DHBV-specific T lymphocyte activation. Previous studies have shown that higher levels of HBV-specific T cells, especially CD8+ CTL, were produced in during acute HBV infection compared to chronic HBV infection in humans and in transgenic mice (Chisari and Ferrari, 1995; Li *et al.*, 2011). Influx of CD3+ T cells were also observed in woodchucks during early stages of acute WHV infection (Guo *et al.*, 2000). All these strongly suggest the importance of CD8+ CTL in both cytolytic and non-cytolytic clearance of viral infection (Thimme *et al.*, 2003). This could also be confirmed if lower levels of CD8+ CTL were found to be produced in ducks with chronic DHBV infection. If true, the activation of CD8+ CTL could also be explored as potential therapeutic tools to help clear chronic HBV infections in humans.

Furthermore, the complement components present in the duck serum could also be characterised. The human complement system is part of the innate immune responses and is a complex system that comprises up to 20 proteins. Complement can be activated by the classical or alternative pathway for instance when antibodies complex with viral antigens, and were shown to play an essential role in enhancing the neutralisation of the virions by antibodies and subsequent opsonization of antibody-virion aggregates by phagocytic cells, in interfering with the binding of virions to cellular receptors by coating the virions, or by

directly causing lysis of the virus-infected cells (Sissons and Oldstone, 1980; Lachmann, 1985). Complement binding has been shown to increase the sensitivity of HBV-infected hepatocytes to complement-dependent cytolysis in transgenic mice models (Qu *et al.*, 2009), but may not be essential for the neutralisation of some viruses like HIV by antibodies (Hessell *et al.*, 2007). The components of duck complement have been characterised, and found to be similar to the mammalian components especially in the classical activation pathway (Wirtz, 1967; Koppenheffer *et al.*, 1999). There are currently no reported studies on the direct characterisation of complement during DHBV infection. However, the complement protein C3d (fused to the F gene of the Newcastle disease virus) had been found to enhance a Th2-biased humoral immune response in infected ducks (Liu *et al.*, 2010), and to enhance complement-dependent antibody cytotoxicity of chicken serum against cells of a Marek's disease lymphoma-derived cell line (Sugimoto *et al.*, 1979).

Lastly, as described in **Section 8.3.2.7**, during chronic DHBV infection, circulating DHBV virions were found to be in the serum in excess of anti-DHBs antibodies. Therefore, it would be interesting to determine the neutralising capabilities of the anti-DHBs antibodies present in the serum, to explore the reasons behind the failure of the antibodies to remove the DHBV virions during chronic DHBV infection. These could be determined by pre-incubation of heat-inactivated duck serum with a standard dose of DHBV virions. Heat-inactivation at 53^{o}C – 56^{o}C was essential to destroy complement present in the serum that may affect the results of the neutralisation assay, without affecting or causing the formation of aggregates of immunoglobulin (Soltis *et al.*, 1979). After that, the levels of DHBV that were not complexed with the anti-DHBs antibodies could be measured by *in vitro* inoculation of PDH to observe the levels of DHBV replication (Jilbert *et al.*, 1992; Zhang and Summers, 2004), or *in vivo* infection of 1-day-old ducks to observe the establishment of DHBV infection, as the 1-day-old ducks are shown to be susceptible to DHBV infection even with 1 DHBV virion (Jilbert *et al.*, 1996; Meier *et al.*, 2003). In addition, the levels of production of anti-DHBs IgM antibodies could also be detected on top of the anti-DHBs IgY antibodies detected in this study, as it had been reported in 3-week-old ducks that developed acute DHBV infection, the production of IgM antibodies at 1 – 2 dpi were essential as the main neutralising antibodies, before the IgY antibodies levels gradually increased after 3 dpi (Zhang and Summers, 2004). Therefore, it would be interesting to determine whether the levels of anti-DHBs IgM antibodies production in the ducks that developed chronic DHBV infection were also delayed and were produced at lower levels, compared to ducks that developed acute DHBV infection.

9.7. Future directions to detect integrated virus-cell junctions using invPCR assay

There are a lot of ways that this study can be further expanded to explore the mechanisms involved during the clearance of DHBV-infected hepatocytes during acute DHBV infection, and to assess the levels of clonal proliferation of hepatocytes during chronic DHBV infection, using the integrated virus-cell junctions as genetic markers of individual infected hepatocytes.

Firstly, after optimising the invPCR assay to reduce the levels of virus-virus false positive sequences detected and to improve the DNA sequencing reactions, more invPCR reactions could be performed on larger liver cell DNA samples to increase the chances of detecting integrated virus-cell junctions. This was because low levels of integration were expected in these ducks with acute DHBV infection (1 – 12 integration in $2.9x10^5$ cells as calculated in **Section 7.4.4**), especially after resolution of infection when only ~0.01 copies of cccDNA were detected per hepatocyte (**Section 7.3.2.9**) with integrated DHBV DNA expected at even lower copy numbers than that. Previous studies had to analyse up to 477 μg of DNA from ducks with chronic DHBV infection to detect 143 integrated virus-cell junctions (frequency of 1 integration in 10^3 – 10^4 cells) (Yang and Summers, 1999). Similarly, to detect 150 integrated virus-cell junctions in this study, up to $4.4x10^7$ cells or DNA extracted from ~64 mg of liver tissue (calculated based on Section 2.8.9.3.2) may need to be analysed.

In addition, to increase the range of integrated virus-cell junctions detected, several different invPCR assay designs could be preformed on the same liver tissues. Each invPCR assay design would have limitations of integrated virus-cell junctions that could be detected, due to the nature of specific recognition/binding sites of the restriction enzymes and PCR primers used in the invPCR assay, in addition to the random site of DHBV integration into the duck genome that generates variable sizes of invPCR products depending on the distance between the integrated virus-cell junction and the first cut restriction enzyme digestion site in the duck genome (refer Figures 2.6 and 2.7). Because of this, integration events that occurred far from a first cut restriction enzyme digestion site (>2 kbp) in the duck genome would generally not be detected. Therefore, to broaden the range of integrated virus-cell junctions detectable, various invPCR assay designs, for instance the duck D1 invPCR assay that detects the right hand end integration junctions, could be performed in addition to the duck D3 and D4 invPCR assays that detect the left hand end integration junction (refer Table 2.3 for invPCR assay designs). It is hoped that by doing this, the compiled invPCR assay results would provide a more accurate representation of the pool of integrated virus-cell junctions present in the liver.

Thirdly, several other assays could also be performed on top of the invPCR assay to detect integrated virus-cell junctions present in the liver tissue. These assays include the linker ligation assay established and explored in **Chapter 5.3**, or the *Alu*-PCR (Kawai *et al.*, 2001). Briefly, *Alu*-PCR involves the amplification of the integrated virus-cell junctions using a viral-specific primer and a *Alu*-primer (Sonza *et al.*, 1996; O'Doherty *et al.*, 2002). As the *Alu* family is a highly repetitive ubiquitous short sequence (~300 bp) of DNA found in 3% – 6% of the human genome (Jelinek and Schmid, 1982), a range of integration junctions would be amplified. The PCR products could subsequently be cloned into plasmid vectors to sequence the integration junctions, or could be inverted similar to the invPCR assays for subsequent nested PCR amplification of the integration junctions. Several variations of *Alu*-PCR have been successfully used to detect and quantitate integrated HIV provirus *in vivo* (Butler *et al.*, 2001) and in human samples (Carr *et al.*, 2007). However, *Alu*-PCR could not be applied for the detection of integrated virus-cell junctions in ducks liver tissues in this study, as the *Alu* family equivalent in the avian genome has so far not been found or reported. In the future, when more studies has been performed to sequence and characterise the duck or avian species genome, *Alu*-PCR would be a promising tool to detect integrated virus-cell junctions in the duck liver. It is hoped that by performing multiple assays, the compiled results would provide a more accurate representation of the integrated virus-cell junctions present in the liver.

When repeated integrated virus-cell junctions were detected in the duck liver tissues, the size of hepatocyte clones present in the liver could further be explored by qPCR assays, using the detected repeated integrated virus-cell junctions in the same liver tissue as PCR primers. By determining the number of repeats of unique integrated virus-cell junctions in a liver tissue, the hepatocyte clone size, the levels of hepatocyte clonal proliferation turnover, as well as the number liver turnover that had occurred could be calculated using mathematical modelling.

In addition, if repeated integrated virus-cell junctions were detected in the duck liver tissues, *in situ* hybridisation could be performed using the repeated integrated virus-cell junction sequences as probes, to histologically observe hepatocyte clones present in that liver tissue. If the assay is not sensitive enough, *in situ* PCR could first be performed using the same repeated integrated virus-cell junction sequences as primers, to amplify the single copy of integrated virus-cell junctions present in each hepatocyte. By identifying hepatocytes that contained the integrated virus-cell junctions histologically, adjacent tissue slides could then be used to determine whether the hepatocytes are DHBsAg-positive or -negative. In addition, any morphological changes to the hepatocytes that contained integrated DHBV could also be identified and observed, especially to determine whether the hepatocyte clones showed any

signs of pre-neoplastic changes, as it was likely that clonal proliferation of hepatocytes may contribute to hepatocarcinogenesis during chronic hepadnavirus infections.

After identifying hepatocyte clones histologically, laser capture technology could also be performed to precisely extract a selected area of the liver tissue section. This precise technology allows DNA to be extracted from, for instance, an isolated hepatocyte clone or a hepatocyte focus of interest. By being able to extract DNA from isolated hepatocyte populations, this opens up a range of potential analysis to better understand the characteristics of these hepatocyte clones. For instance, the epigenetic changes in the hepatocytes could be explored by determining the methylation changes in CpG islands by methylation-specific PCR (Herman *et al.*, 1996) or bisulfite genome sequencing (Hayatsu, 2008). It has been found that abnormal methylation of genes, especially the *p53* and *β-catenin* genes, were often early events during the development of HCC, and up to 30% of HCC tumours contained these mutations (Su *et al.*, 2008). In addition, to determine whether a hepatocyte focus showed specific changes in gene expression, microarray assays could be used as a broad study to determine the increase or decrease of gene expressions (Wieland *et al.*, 2004). Alternatively, the changes in protein expression could also be determined using proteomic mass spectrometry assays could also determine the increase or decrease in protein expression in a cell population. This could be done by MALDI imaging mass spectrometry, which briefly involves using laser beams to measure the ratio of the mass of protein molecules found in a tissue section to the charge of gaseous ions (peptide or protein ions), generating a mass spectrometry spectrum which allows the profiling of proteins present in a tissue section, as well as visualising the distribution of proteins in that tissue section (Gustafsson *et al.*, 2011). Based on all these data, a range of characteristics of hepatocyte clones could be determined, including survival advantages that allowed the hepatocytes to escape from host immune responses, or pre-cancerous growth advantageous mutations present. Some of these studies have been performed and presented by Thomas Tu in his Ph.D. thesis (2012, in preparation).

Specific to the study described in **Chapter 7**, to increase the levels of DHBV integration into the duck genome which would in turn increase the chances of detection by the invPCR assay, the levels of hepatocytes infected with DHBV could be increased from 4.4% in this study (**Section 7.3.2.1**) up to <45% during early stages of acute DHBV infection. This could be achieved as the outcome of DHBV infection, as well as the levels of hepatocytes initially infected in the liver in ducks have been shown to be dependent on the age of ducks upon infection and the dose of virions used (Jilbert *et al.*, 1998). Therefore, the ducks could either be infected with a higher dose of DHBV virions (up to $1x10^{11}$ vge), or younger ducks could

be used for the study. However, one issue is that young ducks that are still growing would not be especially suitable, as the ducks would have normal liver proliferation to increase the liver mass during growth, on top of compensatory proliferation of hepatocytes due to DHBV infection. Therefore, accurate estimation of liver turnover due to DHBV infection could not be determined. In addition, the other issue of using higher dose of DHBV virions and younger ducks is the increased risk of the ducks developing chronic DHBV infection instead (Jilbert *et al.*, 1998), making the ducks no longer suitable for the study.

Lastly, specific to the study described in **Chapter 8**, the design of this study could be improved by reducing the DHBV load present in the ducks prior to liver tissue collection using antiviral drugs like ETV or TFV. As shown in **Chapter 6**, more integrated virus-cell junctions seemed to be detected in ducks that were treated with antiviral drugs (ducks FN1 and FN3). It is expected that by inhibiting the production of new virions, the levels of DHBV RI DNA could be reduced, and thus the virus-virus false positives produced could also be reduced. However, as it was found that some antiviral drugs, like the cytosine nucleoside analogue FTC, may interfer with the Taq polymerases during PCR amplifications (**Chapter 6**), the effects of nucleoside analogue loads present in the tissue samples on downsteam PCR amplifications would also need to be explored before implementing this in future studies.

9.8. Concluding remarks

From studies conducted during this Ph.D., several molecular assays including DNA sequencing reactions and subsequent purification of DNA sequencing products, qPCR assays for the detection of DHBV total and cccDNA and duck cellular genes, and sequencing and characterisation of the duck β actin and GAPDH genes were performed and optimised. The invPCR assay was also extensively developed to detect integrated virus-cell junctions in ducks. Histological and serological changes during various stages of acute and chronic DHBV infections were characterised, and the invPCR assay was used to explore the mechanisms involved in clearance of DHBV-infected hepatocytes during acute DHBV infection, and to assess levels of clonal proliferation of hepatocytes during chronic DHBV infection. Despite not being able to achieve all of the aims of this thesis, the overall findings in this study have contributed significant new information for hepadnavirus research. The methods developed in this thesis are being applied in several other studies, including the detection of integrated virus-cell junctions in HBV-infected human livers and studies of the fate of cccDNA during hepatocyte mitosis. The ultimate aim of our research is to contribute new information to allow development of novel therapies for HBV infections, and to increase understanding of hepatocarcinogenesis during chronic HBV infections.

References

Alevy, M., Tsai, M. and O'Malley, B. (1984). DNase I sensitive domain of the gene coding for the glycolytic enzyme glyceraldehyde-3-phosphate dehydrogenase. Biochemistry. 23(10): 2309-2314.

Anderson, A., Banks, K., Pontoglio, M., Yaniv, M. and McLachlan, A. (2005). Alpha/beta interferon differentially modulates the clearance of cytoplasmic encapsidated replication intermediates and nuclear covalently closed circular hepatitis B virus (HBV) DNA from the livers of hepatocyte nuclear factor 1alpha-null HBV transgenic mice. Journal of Virology. 79(17): 11045-11052.

Andersson, K. and Dienstag, J. (2008). Epidemiology and prevention of hepatitis B. Hepatitis B Virus: Human Virus Guides. Lai, C. and Locarnini, S. London, International Medical Press. 1**:** 9.1-9.19.

Andoniou, C., Andrews, D. and Degli-Esposti, M. (2006). Natural killer cells in viral infection: more than just killers. Immunological Reviews. 214: 239-250.

Applied Biosystems (2002). BigDye Terminator v3.1 Cycle Sequencing Kit: Protocol**:** Protocol summary.

Applied Biosystems (2003). Creating standard curves with genomic DNA or plasmid DNA templates for use in quantititative PCR.

Applied Biosystems (2006). BigDye XTerminator Purification Kit protocol summary**:** Protocol summary.

Applied Biosystems (2009). AmpliTaq 360 DNA polymerase**:** Product bulletin.

Asabe, S., Wieland, S., Chattopadhyay, P., Roederer, M., Engle, R., Purcell, R. and Chisari, F. (2009). The size of the virus inoculum contributes to the outcome of hepatitis B virus infection. Journal of Virology. 83(19): 9652-9662.

Augesse-Germon, S., Liu, S., Chevallier, M., Pichoud, C., Jamard, C., Borel, C., Chu, C., Trepo, C., Cheng, Y. and Zoulim, F. (1998). Inhibitory effect of 2'-fluoro-5-methyl-beta-L-

arabinofuranosyl-uracil on duck hepatitis B virus replication. Antimicrobial Agents and Chemotherapy. 42(2): 369-376.

Balavoine, G. (1996). Identification of members of several homeobox genes in a planarian using a ligation-mediated polymerase chain reaction technique. Nucleic Acids Research. 24(8): 1547-1553.

Ballantyne, K., van Oorshot, R. and Mitchell, R. (2008). Locked nucleic acids in PCR primers increase sensitivity and performance. Genomics. 91: 301-305.

Barber, M., Aldridge, J., Webster, R. and Magor, K. (2010). Association of RIG-I with innate immunity of ducks to influenza. PNAS (PNAS). 107(13): 5913-5918.

Bartholomeusz, A. and Schaefer, S. (2004). Hepatitis B virus genotypes: comparison of genotyping methods. Reviews in Medical Virology. 14: 3-16.

Baumert, T., Thimme, R. and von Weizsacker, F. (2007). Pathogenesis of hepatitis B virus infection. World Journal of Gastroenterology. 13(1): 82-90.

Bayani, J. and Squire, J. (2004). Fluorescence in situ hybridization (FISH). Current protocols in cell biology. USA, John Wiley & Sons Inc. Unit 22.4**:** Chapter 22.

Beasley, R., Hwang, L., Lin, C., Leu, M., Stevens, C., Szmuness, W., Chen, K. (1982). Incidence of hepatitis B virus infections in preschool children in Taiwan. Journal of Infectious Diseases. 146(2): 198-204.

Bedossa, P. and Poynard, T. (1996). An algorithm for the grading of activity in chronic hepatitis C. Hepatology. 24: 289-293.

Belloni, L., Pollicino, T., De Nicola, F., Guerrieri, F., Raffa, G., Fanciulli, M., Raimondo, G. and Levrero, M. (2009). Nuclear HBx binds the HBV minichromosomes and modifies the epigenetic regulation of cccDNA function. PNAS. 106(47): 19975-19979.

Benham, F. and Povey, S. (1989). Members of the human glyceraldehyde-3-phosphate dehydrogenase-related gene family map to dispersed chromosomal locations. Genomics. 5: 209-214.

Bertram, E. (1997). Characterisation of duck lymphoid cell populations and their role in immunity to duck hepatitis B virus. Discipline of Microbiology and Immunology, School of Molecular and Biomedical Science. Adelaide, South Australia, The University of Adelaide**:** 218.

Biesecker, G., Harris, J., Thierry, J., Walker, J. and Wonacott, A. (1977). Sequence and structure of D-glyceraldehyde 3-phosphate dehydrogenase from Bacillus stearothermophilus. Nature. 266: 328-333.

Bill, C. and Summers, J. (2004). Genomic DNA double-strand breaks are targets for hepadnaviral DNA integration. PNAS. 101(30): 11135-11140.

Bio-Rad Laboratories. (2010). Certified agarose powders**:** Product catalogue.

Bishop, C., McCabe, C., Gittoes, N., Butler, P. and Franklyn, J. (2000). Tissue-specific regulation of thyroid hormone receptor mRNA isoforms and target gene proteins in domestic ducks. Journal of Endocrinology. 165(3): 607-615.

Blanchet, M. and Sureau, C. (2007). Infectivity determinants of the hepatitis B virus pre-S domain are confined to the N-terminal 75 amino acid residues. Journal of Virology. 81(11): 5841-5849.

Bloquel, B., Jeulin, H., Burty, C., Letranchant, L., Rabaud, C. and Venard, V. (2010). Occult hepatitis B infection in patients infected with HIV: report of two cases of hepatitis B reactivation and prevalence in a hospital cohort. Journal of Medical Virology. 82: 206-212.

Bock, C., Schwinn, S., Locarnin, S., Fyfe, J., Manns, M., Trautwein, C. and Zentgraf, H. (2001). Structural organization of the hepatitis B virus minichromosome. Journal of Molecular Biology. 307: 183-196.

Boni, C., Penna, A., Bertoletti, A., Lamonaca, V., Rapti, I., Missale, G., Pilli, M., Urbani, S., Cavalli, A., Cerioni, S., Panebianco, R., Jenkins, J. and Ferrari, C. (2003). Transient restoration of anti-viral T cell responses induced by lamivudine therapy in chronic hepatitis B. Journal of Hepatology. 39: 595-605.

Bouwens, L., Baekeland, M., De Zanger, R. and Wisse, E. (1986). Quantitation, tissue distribution and proliferation kinetics of Kupffer cells in normal rat liver. Hepatology. 6(4): 718-722.

Bowden, S. (2008). Laboratory diagnosis of hepatitis B. Hepatitis B virus. Lai, C. and Locarnini, S. London, International Medical Press. 1**:** 11.1-11.16.

Bruni, R., Conti, I., Villano, U., Giuseppetti, R., Palmiter, R. and Rapicetta, M. (2006). Lack of WHV integration nearby N-myc2 and n the downstream b3n and win loci in a considerable fraction of liver tumors with activated N-myc2 from naturally infected wild woodchucks. Virology. 345: 258-269.

Bruni, R., D'Ugo, E., Giuseppetti, R., Argentini, C. and Rapicetta, M. (1999). Activation of the N-myc2 oncogene by woodchuck hepatitis virus integration in the linked downstream b3n locus in woodchuck hepatocellular carcinoma. Virology. 257(2): 483-490.

Bulinski, J. (2006). Actin discrimination. Science. 313: 180-181.

Burrell, C., Gowans, E., Rowland, R., Hall, P., Jilbert, A. and Marmion, B. (1984). Correlation between liver histology and markers of hepatitis B virus replication in infected patients: a study by in situ hybridization. Hepatology. 4(1): 20-24.

Butler, S., Hansen, M. and Bushman, F. (2001). A quantitative assay for HIV DNA integration in vivo. Nature Medicine. 7(5): 631-634.

Carotenuto, P., Artsen, A., Osterhaus, A. and Pontesilli, O. (2011). Reciiprocal changes of naive and effector/memory CD8+ T lymphocytes in chronic hepatitis B virus infection. Viral Immunology. 24(1): 27-33.

Carr, J., Cheney, K., Coolen, C., Davis, A., Shaw, D., Ferguson, W., Chang, G., Higgins, G., Burrell, C. and Li, P. (2007). Development of methods for coordinate measurement of total cell-associated and integrated human immunodeficiency virus type 1 (HIV-1) DNA forms in routine clincal samples: levels are not associated with clinical parameters, but low levels of integrated HIV-1 DNA may be prognostic for continued successful therapy. Journal of Clinical Microbiology. 45(4): 1288-1297.

CDC (2010). Disease Burden from Viral Hepatitis A, B, and C in the United States. Accessed on: 18 June 2011: http://www.cdc.gov/hepatitis/HBV/StatisticsHBV.htm.

CDC (2011). Hepatitis B FAQs for health professionals. Accessed on: 23 June 2011: http://www.cdc.gov/hepatitis/HBV/HBVfaq.htm.

Chang, M., Chen, C., Lai, M., Hsu, H., Wu, T., Kong, M., Liang, D., Shau, W. and Chen, D. (1997). Universal hepatitis B vaccination in Taiwan and the incidence of hepatocellular carcinoma in children. New England Journal of Medicine. 336(26): 1855-1859.

Chang, S., Netter, H., Bruns, M., Schneider, R., Frolich, K. and Will, H. (1999). A new avian hepadnavirus infecting snow geese (Anser caerulescens) produces a significant fraction of virions containing single-stranded DNA. Virology. 262: 39-54.

Chemello, L., Mondelli, M., Bortolotti, F., Schiavon, E., Pontisso, P., Alberti, A., Rondanelli, E. and Realdi, G. (1986). Natural killer activity in patients with acute viral hepatitis. Clinical and Experimental Immunology. 64: 59-64.

Chen, C., Liang, K., Chang, A., Chang, Y., Lu, S., Liaw, Y., Chang, W., Sheen, M. and Lin, T. (1991). Effects of hepatitis B virus, alcohol drinking, cigarette smoking and familial tendency on hepatocellular carcinoma. Hepatology. 13(3): 398-406.

Chen, J., Kadlubar, F. and Chen, J. (2007). DNA supercoiling suppresses real-time PCR: a new approach to the quantification of mitochondrial DNA damage and repair. Nucleic Acids Research. 35(4): 1377-1388.

Chisari, F. and Ferrari, C. (1995). Hepatitis B virus immunopathogenesis. Annual Review of Immunology. 13: 29-60.

Chisari, F., Pinkert, C., Milich, D., Filippi, P., McLachlan, A., Palmiter, R. and Brinster, R. (1985). A transgenic mouse model of the chronic hepatitis B surface antigen carrier state. Science. 230(4730): 1157-1160.

Chu, C. and Lok, A. (2002). Clinical significance of hepatitis B virus genotypes. Hepatology. 35(5): 1274-1276.

Civitico, G. and Locarnini, S. (1994). The half-life of duck hepatits B virus supercoild DNA in congenitally infected primary hepatocyte cultures. Virology. 203: 81-89.

Cleveland, D., Lopata, M., MacDonald, R., Cowan, N., Rutter, W. and Kirschner, M. (1980). Number and evolutionary conservation of a- and b-tubulin and cytoplasmic b- and y-actin genes using specific cloned cDNA probes. Cell. 20: 95-105.

Colell, A., Green, D. and Ricci, J. (2009). Novel roles for GAPDH in cell death and carcinogeneis. Cell Death and Differentiation. 16: 1579-1581.

Commonwealth of Australia (2011). Number of notifications of hepatitis B (newly acquired), Australia, in the period of 1991 to 2010 and year-to-date notifications for 2011. National Notifiable Diseases Surveillance System. 2011.

Cote, P., Korba, B., Miller, R., Jacob, J., Baldwin, B., Hornbuckle, W., Purcell, R., Tennant, B. and Gerin, J. (2000). Effects of age and viral determinants on chronicity as an outcome of experimental woodchuck hepatitis virus infection. Hepatology. 31(1): 190-200.

Cova, L., Mehrotra, R., Wild, C., Chutimataewin, S., Cao, S., Duflot, A., Prave, M., Yu, S., Montesano, R. and Trepo, C. (1994). Duck hepatitis B virus infection, aflatoxin B1 and liver cancer in domestic Chinese ducks. British Journal of Cancer. 69(1): 104-109.

Cova, L., Wild, C., Mehrotra, R., Turusov, V., Shirai, T., Lambert, V., Jacquet, C., Tomatis, L., Trepo, C. and Montesano, R. (1990). Contribution of aflotoxin B1 and hepatitis B virus infection in the induction of liver tumors in ducks. Cancer Research. 50: 2156-2163.

Crawford, J. (2007). Basic mechanisms in hepatopathology. MacSween's Pathology of the Liver. Burt, D., Portmann, B. and Ferrell, L. Philadelphia, PA, USA, Churchill Livingstone Elsevier**:** 75-117.

Cullen, J. and Marion, P. (1996). Non-neoplastic liver disease associated with chronic ground squirrel hepatitis viral infection. Hepatology. 23(6): 1324-1329.

Cullen, J., Marion, P. and Newbold, J. (1989). A sequential histologic and immunohistochemical study of duck hepatitis B virus infection in Pekin ducks. Veterinary Pathology. 26(164-172).

Dallmeier, K., Schultz, U. and Nassal, M. (2008). Heterologous replacement of the supposed host determining region of avihepadnaviruses: high in vivo infectivity despitte low infectivity for hepatocytes. Public Library of Science Pathogens. 4(12): e1000230.

Dandri, M., Burda, M., Will, H. and Petersen, J. (2000). Increased hepatocyte turnover and inhibition of woodchuck hepatitis B virus replication by adefovir in vitro do not lead to reductino of the closed circular DNA. Hepatology. 32: 139-146.

Dandri, M. and Petersen, J. (2005). Hepatitis B virus cccDNA clearance: kililing for curing? Hepatology. 42(6): 1453-1455.

De Boever, S., Vangestel, C., De Backer, P., Croubels, S. and Sys, S. (2008). Identification and validation of housekeeping genes as internal control for gene expression in an intravenous LPS inflammation model in chickens. Veterinary Immunology and Immunopathology. 122(2008): 312-317.

de Franchis, R., Meucci, G., Vecchi, M., Tatarella, M., Colombo, M., Del Ninno, E., Rumi, M., Donato, F. and Ronchi, G. (1993). The natural history of asymptomatic hepatitis surface antigen carriers. Annals of Internal Medicine. 118: 191-194.

de Kok, J., Roelofs, R., Giesendorf, B., Pennings, J., Waas, E., Feuth, T., Swinkels, D. and Span, P. (2005). Normalization of gene expression measurements in tumor tissues: comparison of 13 endogenous control genes. Laboratory Investigation. 85: 154-159.

Deng, Y., Nong, L., Huang, W., Pang, G. and Wang, Y. (2009). Inhibition of hepatitis B virus replication using antisense LNA targeting to both S and C genes in HBV. Zhonghua Gan Zang Bing Za Zhi. 17(12): 900-904.

Desmyter, J., Liu, W., de Somer, P. and Mortelmans, J. (1973). Primates as a model for human viral hepatitis: transmission of infection by human hepatitis B virus. Vox Sanguinis. 24(Supplement s1): 17-26.

Dienstag, J. (2008). Hepatitis B virus infection. New England Journal of Medicine. 359(14): 486-500.

Drew, H., Lockett, L. and Both, G. (2007). Increased complexity of wild-type adeno-associted virus-chromosomal junctions as determined by analysis of unselected cellular genomes. Journal of General Virology. 88: 1722-1732.

Duflot, A., Mehrotra, R., Yu, S., Barraud, L., Trepo, C. and Cova, L. (1995). Spectrum of liver disease and duck hepatitis B virus infection in a large series of Chinese ducks with hepatocellular carcinoma. Hepatology. 21(1493-1491).

Ellegren, H. (2001). Hens, cocks and avian sex determination. The European Molecular Biology Organization reports. 21(3): 192-196.

Ellison, S., Emslie, K. and Kassir, Z. (2011). A standard additions method reduces inhibitor-induced bias in quantitative real-time PCR. Analytical and Bioanalytical Chemistry. 401: 3221-3227.

Fabris, P., Giordani, M., Tositti, G., Rassu, M. and De Lalla, F. (2003). Occult hepatitis B virus infection in HIV/hepatitis C virus co-infected patients. AIDS. 17(10): 1581-1582.

Farber, E. (1991). Hepatocyte proliferation in stepwise development of experimental liver cell cancer. Digestive Diseases and Sciences. 36(7): 973-978.

Fattovich, G., Bortolotti, F. and Donato, F. (2008). Natural history of chronic hepatitis B: speical emphasis on disease progression and prognostic factors. Journal of Hepatology. 48: 335-352.

Fattovich, G., Brollo, L., Alberti, A., Pontisso, P., Giustina, G. and Realdi, G. (1988). Long-term follow-up of anti-HBe-positive chronic active hepatitis B. Hepatology. 8(6): 1651-1654.

Fattovich, G., Stroffolini, T., Zagni, I. and Donato, F. (2004). Hepatocellular carcinoma in cirrhosis: incidence and risk factors. Gastroenterology. 127(5): S35-S50.

Fedorov, A., Merican, A. and Gilbert, W. (2002). Large-scale comparison of intron positions among animal, plant, and fungal genes. PNAS. 99(25): 16128-16133.

Feitelson, M. and Lee, J. (2007). Hepatitis B virus integration, fragile sites, and hepatocarcinogenesis. Cancer Letters. 252(2): 157-170.

Feng, F., Teoh, C., Qiao, Q., Boyle, D. and Jilbert, A. (2010). The development of persistent duck hepatitis B virus infection can be prevented using antiviral therapy combined with DNA or recombinant fowlpoxvirus vaccines. Vaccine. 28: 7436-7443.

Fillon, V., Vignoles, M., Crooijmans, R., Groenen, M., Zoorob, R. and Vignal, A. (2007). FISH mapping of 57 BAC clones reveals strong conservation of synteny between Galliformes and Anseriformes. Animal Genetics. 38: 303-307.

Foster, W., Miller, D., Marion, P., Colonno, R., Kotlarski, I. and Jilbert, A. (2003). Entecavir therapy combined with DNA vaccination for persistent duck hepatitis B virus infection. Antimicrobial Agents and Chemotherapy. 47(8): 2624-2635.

Foster, W., Miller, D., Scougall, C., Kotlarski, I., Colonno, R. and Jilbert, A. (2005). Effect of antiviral treatment with entecavir on age- and dose-related outcomes of duck hepatitis B virus infection. Journal of Virology. 79(9): 5819-5832.

Fourel, G., Couturier, J., Wei, Y., Apiou, F., Tiollais, P. and Buendia, M. (1994a). Evidence for long-range oncovene activation by hepadnavirus insertion. The European Molecular Biology Organization Journal. 13(11): 2526-2534.

Fourel, G., Trepo, C., Bougueleret, L., Henglein, B., Ponzetto, A., Tiollais, P. and Buendia, M. (1990). Frequent activation of N-myc genes by hepadnavirus insertion in woodchuck liver tumours. Nature. 347: 294-298.

Fourel, I., Cullen, J., Saputelli, J., Aldrich, C., Schaffer, P., Averett, D., Pugh, J. and Mason, W. (1994b). Evidence that hepatocyte turnover is required for rapid clearance of duck hepatitis B virus during antiviral therapy of chronically infected ducks. Journal of Virology. 68(12): 8321-8330.

Fourel, I., Saputelli, J., Schaffer, P. and Mason, W. (1994c). The carbocyclic analog of 2'-deoxyguanosine induces a prolonged inhibition of duck hepatitis B virus DNA synthesis in primary hepatocyte cultures and in the liver. Journal of Virology. 68(2): 1059-1065.

Freiman, J., Jilbert, A., Dixon, R., Holmes, M., Gowans, E., Burrel, C., Wills, E. and Cossart, Y. (1988). Experimental duck hepatitis B virus infection: pathology and evolution of hepatic and extrahepatic infection. Hepatology. 8(3): 507-513.

Frieman, J. and Cossart, Y. (1986). Natural duck hepatitis B virus infection in Australia. Australian Journal of Experimental Biology & Medical Science. 64(Part 5): 477-484.

Fu, L., Jia, H., Dong, Q., Wu, J., Zhao, Y., Zhou, H., Ren, N., Ye, Q. and Qin, L. (2009). Suitable reference genes for real-time PCR in human HBV-related haptocellular carcinoma with different clinical prognoses. BioMed Central Cancer. 9: 49-59.

Funk, A., Mhamdi, M., Will, H. and Sirma, H. (2007). Avian hepatitis B viruses: molecular and cellular biology, phylogenesis, and host tropism. World Journal of Gastroenterology. 13(1): 91-103.

Funk, M., Rosenberg, D. and Lok, A. (2002). World-wide epidemiology of HBeAg-negative chronic hepatitis B and associated precore and core promoter variants. Journal of Viral Hepatitis. 9: 52-61.

Galibert, F., Chen, T. and Mandart, E. (1982). Nucleotide sequence of a cloned woodchuck hepatitis virus genome: comparison with the hepatitis B virus sequence. Journal of Virology. 41(1): 51-65.

Geller, S., Pitman, M. and Nicols, W. (2007). Cellular and molecular diagnostic techniques. MacSween's Pathology of the Liver. Burt, D., Portmann, B. and Ferrell, L. PA, USA, Churchill Livingstone Elsevier**:** 119-146.

Ghosh, T., Soni, K., Scaria, V., Halimani, M., Bhattacharjee, C. and Pillai, B. (2008). MicroRNA-mediated up-regulation of an alternatively polyadenylated variant of the mouse cytoplasmic B-actin gene. Nucleic Acids Research. 36(19): 6318-6332.

Gong, S., Jensen, A., Chang, C. and Rogler, C. (1999). Double-stranded linear duck hepatitis B virus (DHBV) stably integrates at a higher frequency than wild-type DHBV in LMH chicken hepatoma cells. Journal of Virology. 73(2): 1492-1502.

Gong, S., Jensen, A. and Rogler, C. (1996). Loss and acquisition of duck hepatitis B virus integrations in lineages of LMH-D2 chicken hepatoma cells. Journal of Virology. 70(3): 2000-2007.

Gong, S., Jensen, A., Wang, H. and Rogler, C. (1995). Duck hepatitis B virus integrations in LMH chicken hepatoma cells: identification and characterization of new episomal derived integrations. Journal of Virology. 69(12): 8102-8108.

Goodman, Z. (2008). Histopathology of infection. Hepatitis B Virus: Human Virus Guides. Lai, C. and Locarnini, S. London, International Medical Press. 1**:** 10.1-10.14.

Gordon, L., Yang, S., Tran-Gyamfi, M., Baggott, D., Christensen, M., Hamilton, A., Crooijmans, R., Groenen, M., Lucas, S., Ovcharenko, I. and Stubbs, L. (2007). Comparative analysis of chicken chromosome 28 provides new clues to the evolutionary fragility of gene-rich vertebrate regions. Genome Research. 17(11): 1603-1613.

Gowans, E., Burrell, C., Jilbert, A. and Marmion, B. (1985). Cytoplasmic (but not nuclear) hepatitis B virus (HBV) core antigen reflects HBV DNA synthesis at the level of the infected hepatocyte. Intervirology. 24(4): 220-225.

Gregory, T., Nicol, J., Tamm, H., Kullman, B., Kullman, K., Leitch, I., Murray, B., Kapraun, D., Greilhuber, J. and Bennett, M. (2007). Eukaryotic genome size databases. Nucleic Acids Research. 35: D332-D338.

Grewal, J., Dellinger, C. and Yung, W. (2007). Fatal reactivation of hepatitis B with temozolomide. New England Journal of Medicine. 356(15): 1591-1592.

Guidotti, L., Ishikawa, T., Hobbs, M., Matzke, B., Schreiber, R. and Chisari, F. (1996). Intracellular inactivation of the hepatitis B virus by cytotoxic T lymphocytes. Immunity. 4: 25-36.

Guidotti, L., Morris, A., Mendez, H., Koch, R., Silverman, R., Williams, B. and Chisari, F. (2002). Interferon-regulated pathways that control hepatitis B virus replication in transgenic mice. Journal of Virology. 76(6): 2617-2621.

Guidotti, L., Rochford, R., Chung, J., Shapiro, M., Purcell, R. and Chisari, F. (1999). Viral clearance without destruction of infected cells during actue HBV infection. Science. 284: 825-829.

Guo, J., Aldrich, C., Mason, W. and Pugh, J. (1996). Characterization of serum amyloid A protein mRNA expression and secondary amyloidosis in the domestic duck. PNAS. 93: 14548-14553.

Guo, J., Pryce, M., Wang, X., Barrasa, M., Hu, J. and Seeger, C. (2003). Conditional replication of duck hepatitis B virus in hepatoma cells. Journal of Virology. 77(3): 1885-1893.

Guo, J., Zhou, H., Liu, C., Aldrich, C., Saputelli, J., Whitaker, T., Barrasa, M., Mason, W. and Seeger, C. (2000). Apoptosis and regeneration of hepatocytes during recovery from transient hepadnavirus infections. Journal of Virology. 74(3): 1495-1505.

Gustafsson, J., Oehler, M., Ruszkiewicz, A., McColl, S. and Hoffmann, P. (2011). MALDI Imaging Mass Spectrometry (MALDI-IMS) - application of spatial proteomics for ovarian cancer classification and diagnosis. International Journal of Molecular Sciences. 12: 773-794.

Hackett, S., Kimball, R., Reddy, S., Bowie, R., Braun, E., Braun, M., Chojnowski, J., Cox, W., Han, K., Harshman, J., Huddleston, C., Marks, B., Miglia, K., Moore, W., Sheldon, F., Steadman, D., Witt, C. and Yuri, T. (2008). A Phylogenomic study of birds reveals their evolutionary history. Science. 320: 1763-1768.

Hanauer, A. and Mandel, J. (1984). The glyceraldehyde 3 phosphate dehydrogenase gene family: structure of a human cDNA adn of an X chromosome linked pseudogene; amazing complexity of the gene family in mouse. The European Molecular Biology Organization Journal. 3(11): 2627-2633.

Hayashi, Y., Kitamura, Y., Nakanishi, M. and Koike, K. (2000). The binding site of transcription factor YY1 is required for intramolecular recombination between terminally repeated sequences of linear replicative hepatitis B virus DNA. Journal of Virology. 74(20): 9471-9478.

Hayatsu, H. (2008). The bisulfite genomic sequencing used in the analysis of epigenetic states, a technique in the emerging environmental genotoxicology research. Mutation Research. 659: 77-82.

Hendriks, W., Mulders, J., Bibby, M., Slingsby, C., Bloemendal, H. and de Jong, W. (1988). Duck lens e-crystallin an dlactate dehydrogenase B4 are identical: a single-copy gene product with two distinct functions. PNAS. 85: 7114-7118.

Herman, J., Graff, J., Myohanen, S., Nelkin, B. and Baylin, S. (1996). Methylation-specifc PCR: a novel PCR assay for methylation status of CpG islands. PNAS. 93: 9821-9826.

Hessell, A., Hangartner, L., Hunter, M., Havenith, C., Beurskens, F., Bakker, J., Lanigan, C., Landucci, G., Forthal, D., Parren, P., Marx, P. and Burton, D. (2007). Fc receptor but not complement binding is important in antibody protection against HIV. Nature. 449: 101-104.

Hino, O., Kitagawa, T. and Sugano, H. (1985). Relationship between serum and histochemical markers for hepatitis B virus and rrate of viral integration in hepatocellular carcinomas in Japan. International Journal of Cancer. 25(1): 5-10.

Hou, Y., Zhang, H., Miranda, L. and Lin, S. (2010). Serious overestimation in quantitative PcR by circular (supercoiled) plasmid standard: microagal pcna as the model gene. PLoS ONE. 5(3): e9545.

Hu, X., Lin, J., Xie, Q., Ren, J., Chang, Y., Wu, W. and Xia, Y. (2010). DNA double-strand breaks, potential targets for HBV integration. Journal of Huazhong University of Science and Technology Medical Sciences. 30(3): 265-270.

Huang, C., Cheng, Y., Rouvier, R., Yang, K., Wu, C., Huang, H. and Huang, M. (2009). Duck (Anas platyrhynchos) linkage mapping by AFLP fingerprinting. Genetics Selective Evolution. 41: 28-35.

Huang, Y., Temperley, N., Ren, L., Smith, J., Li, N. and Burt, D. (2011). Molecular evolution of the vertebrate TLR1 gene family - a complex history of gene duplication, gene conversion, positive selection and co-evolution. BMC Evolutionary Biology. 11: 149-165.

Huggett, J., Dheda, K., Bustin, S. and Zumla, A. (2005). Real-time RT-PCR normalisation; strateies and considerations. Genes and Immunity. 6: 279-284.

International Chicken Genome Sequencing Consortium (2004). Sequence and comparative analysis of the chicken genome provide unique perspectives on vertebrate evolution. Nature. 432: 695-716.

International Chicken Polymorphism Map Consortium (2004). A genetic variation map for chicken with 2.8 million single-nucleotide polymorphisms. Nature. 432: 717-721.

Invitrogen (2010). Isolation of Genomic DNA from Tissue Using ChargeSwitch Technology: Protocols. Accessed on: 17 August 2010: http://www.invitrogen.com/site/us/en/home/References/protocols/nucleic-acid-purification-and-analysis/dna-extraction-protocols/isolation-of-genomic-dna-from-tissue.html

Ioannau, A., Alexiadou, D., Kouidou, S., Voulgaropoulos, A. and Girousi, S. (2010). Electroanalytical study of SYBR Green I and ethidium bromide intercalation in methylated and unmethylated amplicons. Analytica Chimeca Acta. 657: 163-168.

Isogawa, M., Robek, M., Furuichi, Y. and Chisari, F. (2005). Toll-like receptor signalling inhibits hepatitis B virus replciation in vivo. Journal of Virology. 79(11): 7269-7272.

Jelinek, W. and Schmid, C. (1982). Repetitive sequences in eukaryotic DNA and their expression. Annual Review of Biochemistry. 51: 813-844.

Jiang, Y., Ma, Z., Xin, G., Yan, H., Li, W., Xu, H., Hao, C., Niu, J. and Zhao, P. (2010). Th1 and Th2 immune response in chronic hepatitis B patiens during a long-term treatment with adefovir dipivoxil. Mediators of Inflammation. 2010: doi:10.1155/2010/143026.

Jilbert, A. (2000). In situ hybridization protocols for detection of viral DNA using radioactive and nonradioactive DNA probes. In Situ Hybridization Protocols. I. Darby. New Jersey, USA, Humana Press. 123: 177-193.

Jilbert, A. (2005). Recent advances in the duck hepatitis B virus model. Models of Viral Hepatitis. von Weizsacker, F. and Roggendorf, M. Basel, Switzerland, Karger. 25**:** 42-55.

Jilbert, A., Botten, J., Miller, D., Bertram, E., Hall, P., Kotlarski, J. and Burrel, C. (1998). Characterization of age- and dose-related outcomes of duck hepatitis B virus infection. Virology. 244(2): 273-282.

Jilbert, A., Freiman, J., Gowans, E., Holmes, M., Cossart, Y. and Burrel, C. (1987). Duck hepatitis B virus DNA in liver, spleen, and pancreas: analysis by in situ and Southern blot hybridization. Virology. 158(2): 330-338.

Jilbert, A. and Kotlarski, I. (2000). Immune responses to duck hepatitis B virus infection. Developmental and Comparative Immunology. 24: 285-302.

Jilbert, A., Mason, W. and Kann, M. (2008a). Hepatitis B virus replication. Hepatitis B Virus: Human Virus Guides. Lai, C. and Locarnini, S. London, International Medical Press. 1**:** 4.1-4.13.

Jilbert, A., Litwin, S. and Mason, W. (2008b). Pathogenesis of hepatitis B virus infections. Hepatitis B Virus: Human Virus Guides. Lai, C. and Locarnini, S. London, International Medical Press**:** 7.1-7.17.

Jilbert, A., Miller, D., Scougall, C., Turnbull, H. and Burrell, C. (1996). Kinetics of duck hepatitis B virus infetion following low dose virus inoculation: one virus DNA genome is infectious in neonatal ducks. Virology. 226: 338-345.

Jilbert, A., Wu, T., England, J., Hall, P., Carp, N., O'Connell, A. and Mason, W. (1992). Rapid resolution of duck hepatitis B virus infections occurs after massive hepatocellular involvement. Journal of Virology. 66(3): 1377-1388.

Johnson, M., Haupt, L. and Griffiths, L. (2004). Locked nucleic acid (LNA) single nucleotide polymorphism (SNP) genotype analysis and validation using real-time PCR. Nucleic Acids Research. 32(6): e55 (1-9).

Kajino, K., Jilbert, A., Saputelli, J., Aldrich, C., Cullen, J. and Mason, W. (1994). Woodchuck hepatitis virus infections: very rapid recovery after a prolonged viremia and infection of virtually every hepatocyte. Journal of Virology. 68(9): 5792-5803.

Kann, M. (2008). Structural and molecular virology. Hepatitis B Virus: Human Virus Guides. Lai, C. and Locarnini, S. London, International Medical Press. 1**:** 2.1-2.14.

Kao, J., Wu, N., Chen, P., Lai, M. and Chen, D. (2000). Hepatitis B genotypes and the response to interferon therapy. Journal of Hepatology. 33(6): 998-1002.

Kawaguchi, T., Nomura, K., Hirayama, Y. and Kitagawa, T. (1987). Establishment and characterization of a chicken hepatocellular carcinoma cell line, LMH. Cancer Research. 47: 4460-4464.

Kawai, S., Imazeki, F., Yokosuka, O., Ohto, M., Shiina, S., Kato, N. and Omata, M. (1995). Clonality in hepatocellular carcinoma: analysis of methylation pattern of polymorphic X-chromosome-linked phosphoglycerate kinase gene in females. Hepatology. 22: 112-117.

Kawai, S., Yokosuka, O., Imazeki, F., Maru, Y. and Saisho, H. (2001). State of HBV DNA in HBsAg-negative, anti-HCV-positive hepatocellular carcinoma: existence of HBV DNA possibly as nonintegrated form with analysis by Alu-HBV DNA PCR and conventional HBV PCR. Journal of Medical Virology. 64: 410-418.

Kew, M. (2008). Hepatitis B virus and hepatocellular carcinoma. Hepatitis B Virus: Human Virus Guides. Lai, C. and Locarnini, S. London, International Medical Press. 1**:** 14.1-14.12.

Kew, M. (2011). Hepatitis B virus x protein in the pathogeneis of hepatitis B virus-induced hepatocellular carcinoma. Journal of Gastroenterology and Hepatology. 26(Supplement 1): 144-152.

Kidd-Ljunggren, K., Miyakawa, Y. and Kidd, A. (2002). Genetic variability in hepatitis B viruses. Journal of General Virology. 83: 1267-1280.

Kiernan, J. (2008). Fixation. Histological and histochemical methods: theory and practice. United Kingdom, Scion Publishing Limited**:** 12-44.

Kim, S., Kim , Y., Liang, T., Sinsheimer, J. and Chow, S. (2006). A high-throughput method for cloning and sequencing human immunodeficiency virus type 1 integration sites. Journal of Virology. 80(22): 11313-11321.

Kolios, G., Valatas, V. and Kouroumalis, E. (2006). Role of Kupffer cells in the pathogenesis of liver disease. World Journal of Gastroenterology. 12(46): 7413-7420.

Koppenheffer, T., Chan, S. and Higgins, D. (1999). The complemetn system of the duck. Avian Pathology. 28(1): 17-25.

Kothlow, S., Mannes, N., Schaerer, B., Rebeski, D., Kaspers, B. and Schultz, U. (2005). Characterization of duck leucocytes by monoclonal antibodies. Developmental and Comparative Immunology. 29(8): 733-748.

Krastev, Z. (2006). The "return" of hepatitis B. World Journal of Gastroenterology. 12(44): 7081-7086.

Kraus, R., Kerstens, H., Van Hooft, P., Crooijmans, R., Van Der Poel, J., Elmberg, J., Vignal, A., Huang, Y., Li, N., Prins, H. and Groenen, M. (2011). Genome wide SNP discovery, analysis and evaluation in mallard (Anas platyrhynchos). BMC Genomics. 12: 150-160.

Krishan, A., Dandekar, P., Nathan, N., Hamelik, R., Miller, C. and Shaw, J. (2005). DNA index, genome size, and electronic nuclear volume of vertebrates from the Miami Metro Zoo. Cytometry Part A. 65: 26-34.

Kusumoto, S., Tanaka, Y., Ueda, R. and Mizokami, M. (2011). Reactivation of hepatitis B virus following rituximab-plus-steroid combination chemotherapy. Journal of Gastroenterology. 46: 9-16.

Lachmann, P. (1985). Antibody and complement in viral infections. British Medical Bulletin. 41(1): 3-6.

Lai, C. and Yuen, M. (2008). Treatment of chronic hepatitis B. Hepatitis B Virus: Human Virus Guides. Lai, C. and Locarnini, S. London, International Medical Press. 1**:** 15.1-15.41.

Lampertico, P., Vigano, M., Manenti, E., Iavarone, M., Sablon, E. and Colombo, M. (2007). Low resistance to adefovir combined with lamivudine: a 3-year study of 145 lamivudine-resistant hepatitis B patients. Gastroenterology. 133(5): 1445-1451.

Lan, J., Chen, Y., Hsieh, T., Chen, Y., Hsieh, C., Chen, D. and Yang, S. (2011). Kinetics of viral loads and risk of hepatitis B virus reactivation in hepatitis B core antibody-positive rheumatoid arthritis patients undergoing anti-tumour necrosis factor alpha therapy. Annals of the Rheumatic Disease: doi:10.1136/ard.2010.148783.

Lanford, R., Chavez, D., Brasky, K., Burns, R. r. and Rico-Hesse, R. (1998). Isolation of a hepadnavirus from the woolly monkey, a New World primate. PNAS. 95(10): 5757-5761.

Lavanchy, D. (2004). Hepatitis B virus epidemiology, disease burden, treatment, and current and emerging prevention and control measures. Journal of Viral Hepatitis. 11: 97-107.

Le Mire, M. (2003). Detection and analysis of residual duck hepatitis B virus DNA. Department of Microbiology and Immunology, School of Molecular and Biomedical Science. Adelaide, South Australia, The University of Adelaide**:** 189.

Le Mire, M., Miller, D., Foster, W., Burrell, C. and Jilbert, A. (2005). Covalently closed circular DNA is the predominant form of duck hepatitis B virus DNA that persists following transient infection. Journal of Virology. 79(19): 12242-12252.

Lee, C., Gong, Y., Brok, J., Boxall, E. and Gluud, C. (2006). Effect of hepatitis B immunisation in newborn infants of mothers positive for hepatitis B surface antigen: systematic review and meta-analysis. British Medical Journal. 332(7537): 328-336.

Lemon, S. and Thomas, D. (1997). Vaccines to prevent viral hepatitis. The New England Journal of Medicine. 336(3): 196-204.

Lenhoff, R., Luscombe, C. and Summers, J. (1999). Acute liver injury following infection with a cytopathic strain of duck hepatitis B virus. Hepatology. 29: 563-567.

Li, J., Han, Y., Jin, K., Wan, Y., Wang, S., Liu, B., Liu, Y., Lu, S. and Huang, Z. (2011). Dynamic changes of cytotoxic T lymphocytes, natural killer cells, and natural killer T cells in patients with acute hepatitis B infection. Virology Journal. 8: 199-206.

Liaw, Y., Chen, Y., Sheen, I., Chien, R., Yeh, C. and Chu, C. (2004). Impact of acute hepatiits C virus superinfection in patients with chronic hepatitis B virus infection. Gastroenterology. 126(4): 1024-1029.

Liaw, Y., Lin, S., Chen, T., Chien, R., Sheen, I. and Chu, C. (1994). Beneficial effect of prednisolone withdrawal followed by human lymphoblastoid interferon on the treatment of chronic type B hepatitis in Asians: a randomized controlled trial. Journal of Hepatology. 20: 175-180.

Liaw, Y., Tai, D., Chu, C. and Chen, T. (1988). The development of cirrhosis in patients with chronic type B hepatiits: a prospective study. Hepatology. 8(3): 493-496.

Lin, C., Chen, Y. and Pan, T. (2011). Quanification bias caused by plasmid DNA conformation in quantitative real-time PCR assay. PLoS ONE. 6(12): e29101.

Lin, X., Robinson, N., Thursz, M., Rosenberg, D., Weild, A., Pimenta, J. and Hall, A. (2005). Chronic hepatitis B virus infection in the Asia-Pasific region and Africa: review of disease progression. Journal of Gastroenterology and Hepatology. 20: 833-843.

Liu, D., Wang, J. and Niu, Z. (2010). Contribution of Chinese Pekin duck complement component C3d-P29 repeats to enhancement of Th2-biased immune responses against NDV F gene induced by DNA immunization. Immunopharmacology and Immunotoxicology. 32(2): 297-306.

Livingston, S., Simonetti, J., McMahon, B., Bulkow, L., Hurlburt, K., Homan, C., Snowball, M., Cagle, H., Williams, J. and Chulanov, V. (2007). Hepatitis B virus genotypes in Alaska native people with hepatocellular carcinoma: preponderance of genotype F. The Journal of Infections Diseases. 195(1): 5-11.

Lok, A. (2000). Hepatitis B infection: pathogenesis and management. Journal of Hepatology. 32(supplementary 1): 89-97.

Low, H. (2006). Using integrated duck hepatitis B virus-cell DNA junction as a genetic marker for individual infected hepatocytes. Discipline of Microbiology and Immunology, School of Molecular and Biomedical Science. Adelaide, South Australia, The University of Adelaide**:** 93.

Lucifora, J., Arzberger, S., Durantel, D., Belloni, L., Strubin, M., Levrero, M., Zoulim, F., Hantz, O. and Protzer, U. (2011). Hepatitis B virus X protein is essential to initiate and

maintain virus replication after infection. Journal of Hepatology. doi: 10.1016/j.jhep.2011.02.015.

Luft, F., Klaes, R., Nees, M., Durst, M., Heilmann, V., Melsheimer, P. and von Knebel Doeberitz, M. (2001). Detection of integrated papillomavirus sequences by ligation-mediated PCR (DIPS-PCR) and molecular characterization in cervical cancer cells. International Journal of Cancer. 92: 9-17.

Lundqvist, M., Middleton, D., Radford, C., Warr, G. and Magor, K. (2006). Immunoglobulins of the non-galliform birds: antibody expression and repertoire in the duck. Developmental and Comparative Immunology. 30: 93-100.

Lutgehetmann, M., Bornscheuer, T., Volz, T., Allweiss, L., Bockmann, J., Pollok, J., Lohse, A., Petersen, J. and Dandri, M. (2011). Hepatitis B virus limits response of human hepatocytes to interferon-a in chimeric mice. Gastroenterology. 140(7): 2074-2083.

Lutgehetmann, M., Volz, T., Kopke, A., Broja, T., Tigges, E., Lohse, A., Fuchs, E., Murray, J., Petersen, J. and Dandri, M. (2010). In vivo proliferation of hepadnavirus-infected hepatocytes induces loss of covalently closed circular DNA in mice. Hepatology. 52(1): 16-24.

Maini, M., Boni, C., Lee, C., Larrubia, J., Reignat, S., Ogg, G., King, A., Herberg, J., Gilson, R., Alisa, A., Williams, R., Vergani, D., Naoumov, N., Ferrari, C. and Bertoletti, A. (2000). The role of virus-specific CD8+ cells in liver damage and viral control during persistent hepatitis B virus infection. The Journal of Experimental Medicine. 191(8): 1269-1280.

Malley, R., Alonso, J., Kim, C., Leisse, T. and Ecker, J. (2010). An adapter ligation-mediated PCR method for high-throughput mapping of T-DNA inserts in the Arabidopsis genome. Nature Protocols. 2(11): 2910-2917.

Manno, M., Camma, C., Schepis, F., Bassi, F., Gelmini, R., Gianni, F., Miselli, F., Grottola, A., Ferretti, I., Vecchi, C., De Palma, M. and Villa, E. (2004). Natural history of chronic HBV carriers in northern Italy: morbidity and mortality after 30 years. Gastroenterology. 127: 756-763.

Marinone, C. and Mestriner, M. (2011). HBV disease: HBsAg carrier and occult B infection reactivation in haematological setting. Digestive and Liver Disease. 43S: S49-S56.

Marion, P., Knight, S., Ho, B., Guo, Y., Robinson, W. and Popper, H. (1984). Liver disease associated with duck hepatitis B virus infection of domestic ducks. PNAS. 81: 898-902.

Marion, P., Van Develaar, M., Knight, S., Salazar, F., Garcia, G., Popper, H. and Robinson, W. (1986). Hepatocellular carcinoma in ground squirrels persistently infected with ground squirrel hepatitis virus. PNAS. 83(12): 4543-4546.

Marongiu, F., Doratiotto, S., Montisci, S., Pani, P. and Laconi, E. (2008). Liver repopulation and carcinogenesis: two sides of the same coin. The American Journal of Pathology. 172(4): 857-864.

Maruoka, T., Tanabe, H. and Chiba, M. (2005). Chicken CD1 genes are located in the MHC:CD1 and endothelial protein C receptor genes constitute a distinct subfamily of class-I-like genes that predates the emergence or mammals. Immunogenetics. 57: 570-600.

Mason, W., Cullen, J., Moraleda, G., Saputelli, J., Aldrich, C., Miller, D., Tennant, B., Frick, L., Averett, D., Condreay, L. and Jilbert, A. (1998). Lamivudine therapy of WHV-infected woodchucks. Virology. 245: 18-32.

Mason, W., Cullen, J., Saputelli, J., Wu, T., Liu, C., London, W., Lustbader, E., Schaffer, P., O'Connell, A., Fourel, I., Aldrich, C. and Jilbert, A. (1994). Characterization of the antiviral effects of 2'carbodeoxyguanosine in ducks chronically infected with duck hepatitis B virus. Hepatology. 19(2): 398-411.

Mason, W., Jilbert, A. and Summers, J. (2005). Clonal expansion of hepatocytes during chronic woodchuck hepatitis virus infection. PNAS. 102(4): 1139-1144.

Mason, W., Litwin, S. and Jilbert, A. (2008). Immune selection during chronic hepadnavirus infection. Hepatology International. 2: 3-16.

Mason, W., Liu, C., Aldrich, C., Litwin, S. and Yeh, M. (2010). Clonal expansion of normal-appearing human hepatocytes during chronic hepatitis B virus infection. Journal of Virology. 84(16): 8308-8315.

Mason, W., Low, H., Xu, C., Aldrich, C., Scougall, C., Grosse, A., Clouston, A., Chavez, D., Litwin, S., Peri, S., Jilbert, A. and Lanford, R. (2009a). Detection of clonally expanded hepatocytes in chimpanzees with chronic hepatitis B virus infection. Journal of Virology. 83(17): 8396-8408.

Mason, W., Seal, G. and Summers, J. (1980). Virus of Pekin ducks with structural and biological relatedness to human hepatitis B virus. Journal of Virology. 36(3): 829-836.

Mason, W., Xu, C., Low, H., Saputelli, J., Aldrich, C., Scougall, C., Grosse, A., Colonno, R., Litwin, S. and Jilbert, A. (2009b). The amount of hepatocyte turnover that occurred during resolution of transient hepadnavirus infections was lower when virus replication was inhibited with Entecavir. Journal of Virology. 83(4): 1778-1789.

Meier, P., Scougall, C., Burrell, C. and Jilbert, A. (2003). Analysis of infectivity and *in vivo* growth charateristics of a cytopathic DHBV mutant, G133E. 11th International Symposium on Viral Hepatitis & Liver Disease, Sydney, Australia, Australian Centre for Hepatitis Virology.

Meier, P., Scougall, C., Will, H., Burrell, C. and Jilbert, A. (2003). A duck hepatitis B virus strain with a knockout mutation in the putative X ORF shows similar infectivity and in vivo growth characteristics to wild-type virus. Virology. 317: 291-298.

Menne, S. and Cote, P. (2007). The woodchuck as an animal model for pathogenesis and therapy of chronic hepatitis B virus infection. World Journal of Gastroenterology. 13(1): 104-124.

Menne, S. and Tennant, B. (1999). Unraveling hepatitis B virus infection of mice and men (and woodchucks and ducks). Nature Medicine. 5(10): 1125-1126.

Mesa, C., Thulien, K., Moon, D., Veniamin, S. and Magor, K. (2004). The dominant MHC class I gene is adjavent to the polymorphic TAP2 gene in the duck, Anas platyrhynchos. Immunogenetics. 56: 192-203.

Michalak, T., Pardoe, I., Coffin, C., Churchill, N., Freake, D., Smith, P. and Trelegan, C. (1999). Occult lifelong persistence of infectious hepadnavirus and residual liver inflammation in woodchucks convalescent from acute viral hepatitis. Hepatology. 29(3): 928-938.

Michalak, T., Pasquinelli, C., Guilhot, S. and Chisari, F. (1994). Hepatitis B virus persistence after recovery from acute viral hepatitis. Journal of Clinical Investigation. 93(2): 230-239.

Michalopoulos, G. (2007). Liver regeneration. Journal of Cellular Physiology. 213: 286-300.

Milich, D., Chen, M., Hughes, J. and Jones, J. (1998). The secreted hepatitis B precore antigen can modulate the immune response to the nucleocapsid: a mechanism for persistence. The Journal of Immunology. 160: 2013-2021.

Miller, D., Bertram, E., Scougall, C., Kotlarski, I. and Jilbert, A. (2004). Studying host immune responses against duck hepatitis B virus infection. Methods in Molecular Medicine. 96: 3-25.

Miller, D., Boyle, D., Feng, F., Reaiche, G., Kotlarski, I., Colonno, R. and Jilbert, A. (2008). Antiviral therapy with entecavir combined with post-exposure "prime-boost" vaccination eliminates duck hepatitis B virus-infected hepatocytes and prevents the development of persistent infection. Virology. 373: 329-341.

Miller, D., Halpern, M., Kotlarski, I. and Jilbert, A. (2006). Vaccination of ducks with a whole-cell vaccine expressing duck hepatitis B virus core antigen elicits antiviral immune responses that enable rapid resolution of de novo infection. Virology. 348: 297-308.

Moraleda, G., Saputelli, J., Aldrich, C., Averett, D., Condreay, L. and Mason, W. (1997). Lack of effect of antiviral therapy in nondividing hepatocyte cutures on the closed circular DNA of woodchuck hepatitis virus. Journal of Virology. 71(12): 9392-9399.

Murakami, Y., Saigo, K., Takashima, H., Minami, M., Okanoue, T., Brechot, C. and Paterlini-Brechot, P. (2005). Large scaled analysis of hepatitis B virus (HBV) DNA integration in HBV related hepatocellular carcinoma. Gut. 54: 1162-1168.

Murray, J., Wieland, S., Purcell, R. and Chisari, F. (2005). Dynamics of hepatitis B virus clearance in chimpanzees. PNAS. 102(49): 17780-17785.

Nanda, I., Sick, C., Munster, U., Kaspers, B., Schartl, M., Staeheli, P. and Schmid, M. (1989). Sex chromosome linkage of chicken and duck type I interferon genes: further evidence of evolutionary conservation of the Z chromosome in birds. Chromosoma. 107(3): 204-210.

Narayan, R., Buronfosse, T., Schultz, U., Chevallier-Gueyron, P., Guerret, S., Chevallier, M., Saade, F., Ndeboko, B., Trepo, C., Zoulim, F. and Cova, L. (2006). Rise in gamma interferon expression during resolution of duck hepatitis B virus infection. Journal of General Virology. 87: 3225-3232.

Negro, F., Berninger, M., Chiaberge, E., Gugliotta, P., Bussolati, G., Actis, G., Rizzetto, M. and Bonino, F. (1985). Detection of HBV-DNA by in situ hybridization using a biotin-labeled probe. Journal of Medical Virology. 15(4): 373-382.

Nelson, K. and Williams, C. (2007). Molecular epidemiology and infectious diseases. Infectious Disease Epidemiology: Theory and Practice. Francis, J., Harrington, S., Carroll, K. and Bishai, W. Massachusett, USA, Jones and Barlett Publishers**:** 281-316.

Newbold, J., Xin, H., Tencza, M., Sherman, G., Dean, J., Bowden, S. and Locarnini, S. (1995). The covalently closed duplex form of the hepadnavirus genome exists in situ as a heterogenous population of viral minichromosomes. Journal of Virology. 69(6): 3350-3357.

Ng, P. and Higgins, D. (1986). Bile immunoglobulin of the duck (Anas platyrhynchos) I: Preliminary Characterization and Ontogeny. Immunology. 58: 323-327.

Ng, S., Gunning, P., Eddy, R., Ponte, P., Leavitt, J., Shows, T. and Kedes, L. (1985). Evolution of the functional human beta-actin gene and its multi-pseudogene family: conservation of noncoding regions and chromosomal dispersion of pseudogenes. Molecular and Cellular Biology. 5(10): 2720-2732.

Ni, Y., Zhou, Y., Lu, L., Grossmann, R. and Zhao, R. (2006). Developmental changes of FSH-R, LH-R, ER-B and GnRH-I expression in the ovary of prepubertal ducks (Anas platyrhynchos). Animal Reproduction Science. 100(2007): 318-328.

Noordeen, F. (2009). Development of antiviral therapies for chronic hepatitis B virus infection. Discipline of Microbiology and Immunology, School of Molecular and Biomedical Science. Adelaide, South Australia, The University of Adelaide**:** 188.

NorDiag (2010). PCR and Sequencing Cleanup. Accessed on: 12 January 2010: http://www.nordiag.com/index.php?option=com_content&view=article&id=258&Itemid=151

Nowak, M., Bonhoeffer, S., Hill, A., Boehme, R., Thomas, H. and McDade, H. (1996). Viral dynamics in hepatiits B virus infection. PNAS. 93(9): 44398-4402.

Ochiai, T., Urata, Y., Yamano, T., Yamagishi, H. and Ashihara, T. (2000). Clonal expansion in evolution of chronic hepatitis to hepatocellular carcinoma as seen at an X-chromosome locus. Hepatology. 31(3): 615-621.

Oda, T., Tsuda, H., Scarpa, A., Sakamoto, M. and Hirohashi, S. (1992). Mutation pattern of the p53 gene as a diagnostic marker for multiple hepatocellular carcinoma. Cancer Research. 52: 3674-3678.

O'Doherty, U., Swiggard, W., Jeyakumar, D., McGain, D. and Malim, M. (2002). A sensitive, quantitative assay for human immunodeficiency virus type 1 integration. Journal of Virology. 76(21): 10942-10950.

Oka, H., Kurioka, N., Kim, K., Konna, T., Kuroki, T., Mizoguchi, Y. and Kobayashi, K. (1990). Prospective study of early detection of hepatocellular carcinoma in patients with cirrhosis. Hepatology. 12(4): 680-687.

Omata, M., Yokosuka, O., Imazeki, F., Matsuyama, Y., Uchiumi, K., Ito, Y., Mori, J. and Okuda, K. (1984). Transmissionn of duck hepatitis B virus from Chinese carrier ducks to Japanese ducklings: a study of viral DNA in serum and tissue. Hepatology. 4(4): 603-607.

Osborn, M. and Lok, A. (2006). Antiviral options for the treatment of chronic hepatitis B. Journal of Antimicrobial Chemotherapy. 57: 1030-1034.

Ostergaard, M., Maity, J., Babu, B., Wengel, J. and Hrdlicka, P. (2010). Novel insights into the use of Glowign LNA as nucleic acid detection probes- influence of labeling density and nucleobases. Bioorganic & Medicinal Chemistry Letters. 20(24): 7765-7268.

Pan, C. and Zhang, J. (2005). Natural history and clinical consequences of hepatitis B virus infection. International Journal of Medical Sciences. 2(1): 36-40.

Park, I., Baek, K., Cho, E. and Ahn, B. (2011). PKR-dependent mechanisms of interferon-alpha for inhibiting hepatitis B virus replication. Molecules and Cells: DOI/10.1007/s10059-011-1059-6.

Park, I., Sohn, B., Yu, E., Suh, D., Chung, Y., Lee, J., Surzycki, S. and Lee, Y. (2007). Aberrant epigenetic modifications in hepatocarcinogenesis induced by hepatitis B virus X protein. Gastroenterology. 132(4): 1476-1494.

Paterlini-Brechot, P., Saigo, K., Murakami, Y., Chami, M., Gozuacik, D., Mugnier, C., Lagorce, D. and Brechot, C. (2003). Hepatitis B virus-related insertional mutagenesis occurs frequently in human liver cancers and recurrently targets human telomerase gene. Oncogene. 22(25): 3911-3916.

Penna, A., Artini, M., Cavalli, A., Levrero, M., Bertoletti, A., Pilli, M., Chisari, F., Rehermann, B., Del Prete, G., Fiaccadori, F. and Ferrari, C. (1996). Long-lasting memory T cell responses following self-limited acute hepatitis B. Journal of Clinical Investigation. 98(5): 1185-1194.

Penna, A., Del Prete, G., Cavalli, A., Bertoletti, A., D'Elios, M., Sorrentino, R., D'Amato, M., Boni, C., Pilli, M., Fiaccadori, F. and Ferrari, C. (1997). Predominant T-helpter 1 cytokine profine of hepatitis B virus nucleocapsid-specific T cells in acute self-limited hepatitis B. Hepatology. 25(4): 1022-1027.

Petersen, J., Dandri, M., Burkle, A., Zhang, L. and Rogler, C. (1997). Increase in the frequency of hepadnavirus DNA integrations by oxidative DNA damage and inhibition of DNA repair. Journal of Virology. 71(7): 5455-5463.

Petersen, M. and Wengel, J. (2003). LNA: a versatile tool for therapeutics and genomics. Trends in Biotechnollgy. 21(2): 74-81.

Piechaczyk, M., Blanchard, J., Riaad-El, S., Dani, C., Marty, L. and Jeanteur, P. (1984). Unusual abundance of vertebrate 3-phosphate dehydrogenase pseudogenes. Nature. 312(5993): 469-471.

Pigozzi, M. (2007). Localization of single-copy sequences on chicken synaptonemal complex spreads using fluorescence in situ hybridization (FISH). Cytogenetic and Genome Research. 119: 105-112.

Pollicino, T., Belloni, L., Raffa, G., Pediconi, N., Squadrito, G., Raimondo, G. and Levrero, M. (2006). Hepatitis B virus replication is regulated by the acetylation status of hepatitis B virus cccDNA-bound H3 and H4 histones. Gastroenterology. 130(3): 823-837.

Ponte, P., Gunning, P., Blau, H. and Kedes, L. (1983). Human actin genes are single copy for a-skeletal and alpha-cardiac actin but multicopy for beta- and gamma-cytoskeletal genes: 3' untranslated regions are isotype specific but are conserved in evolution. Molecular and Cellular Biology. 3(10): 1783-1791.

Popper, H., Roth, L., Purcell, R., Tennant, B. and Gerin, J. (1987). Hepatocarcinogenicity of the woodchuck hepatitis virus. PNAS. 84(3): 866-870.

Popper, H., Shih, J., Gerin, J., Wong, D., Hoyer, B., London, W., Sly, D. and Purcell, R. (1981). Woodchuck hepatitis and hepatocellular carcinoma: correlation of histologic with virologic observations. Hepatology. 1(2): 91-98.

Prassolov, A., Hohenberg, H., Kalinina, T., Schneider, C., Cova, L., Krone, O., Frolich, K., Will, H. and Sirma, H. (2003). New hepatitis B virus of cranes that has an unexpected broad host range. Journal of Virology. 77(3): 1964-1976.

Price, P., Banerjee, R., Jeffrey, A. and Acs, G. (1992). The mechanism of inhibition of hepatitis B virus replication by the carbocyclic analog of 2'-deoxyguanosine. Hepatology. 16(1): 8-12.

Pugh, J., Di, Q., Mason, W. and Simmons, H. (1995). Susceptibility to duck hepatitis B virus infection is associated with the presence of cell surface receptor sites that efficiently bind viral particles. Journal of Virology. 69(8): 4814-4822.

Pult, I., Abbott, N., Zhang, Y. and Summers, J. (2001). Frequency of spontaneous mutations in an avian hepadnavirus infection. Journal of Virology. 75: 9623-9632.

Pult, I., Netter, H., Bruns, M., Prassolov, A., Sirma, H., Hohenberg, H., Chang, S., Frolich, K., Krone, O., Kaleta, E. and Will, H. (2001). Identification and analysis of a new hepadnavirus in white storks. Virology. 289: 114-128.

Puro, R. and Schneider, R. (2007). Tumor necrosis factor activates a conserved innate antiviral response to hepatitis B virus that destabalizes nucleocapsids and reduces nuclear viral DNA. Journal of Virology. 81(14): 7351-7362.

Qiagen (2010). DNeasy Blood & Tissue Kit**:** Product catalog. Accessed on: 17 August 2010: http://www.qiagen.com/products/genomicdnastabilizationpurification/dneasytissuesystem/dneasybloodtissuekit.aspx#Tabs=t1

Qiao, Q. (2009). Antiviral resistance and hepatitis B virus infection: studies using the duck hepatitis B virus model. Discipline of Microbiology and Immunology, School of Molecular and Biomedical Science. Adelaide, South Australia, The University of Adelaide**:** 48.

Qu, Z., Liang, X., Liu, Y., Du, J., Liu, S. and Sun, W. (2009). Hepatitis B virus sensitizes hepatocytes to complement-dependent cytotoxicity through downregulating CD59. Molecular Immunology. 47: 283-289.

Rabe, B., Delaleau, M., Bischof, A., Foss, M., Sominskaya, I., Pumpens, P., Cazenave, C., Castroviejo, M. and Kann, M. (2009). Nuclear entry of hepatitis B virus capsids involves disintegration to protein dimers followed by nuclear reassociation to capsids. Public Library of Science Pathogens. 5(8): e1000563.

Raimondo, G., Pollicino, T., Cacciola, I. and Squadrito, G. (2007). Occult hepatitis B virus infection. Journal of Hepatology. 46: 160-170.

Reaiche, G. (2003). Events that occur during transient duck hepatitis B virus infection. Discipline of Microbiology and Immunology, School of Molecular and Biomedical Science. Adelaide, South Australia, The University of Adelaide**:** 52.

Reaiche, G. (2008). Characterisation of the events involved in the resolution of acute duck hepatitis B virus infection. Discipline of Microbiology and Immunology, School of Molecular and Biomedical Science. Adelaide, South Australia, The University of Adelaide**:** 193.

Reaiche, G., Le Mire, M., Mason, W. and Jilbert, A. (2010). The persistence in the liver of residual duck hepatitis B virus covalently closed circular DNA is not dependent upon new viral DNA synthesis. Virology. 406: 286-292.

Rehermann, B., Ferrari, C., Pasquinelli, C. and Chisari, F. (1996). The hepatitis B virus persists for decades after patients' recovery from acute viral hepatitis despite active maintenance of a cytotoxic T-lymphocyte response. Nature Medicine. 2(10): 1104-1108.

Rivkina, M., Cullen, J., Robinson, W. and Marion, P. (1994). State of the p53 gene in hepatocellular carcinomas of ground squirrels and woodchucks with past and ongoing infection with hepadnaviruses. Cancer Research. 54(20): 5430-5437.

Rogozin, I., Wolf, Y., Sorokin, A., Mirkin, B. and Koonin, E. (2003). Remarkable interkingdom conservation of intron positions and massive, lineage-specifi intron loss and gain in eukaryotic evolution. Current Biology. 13: 1512-1517.

Roskams, T., Desmet, V. and Verslype, C. (2007). Development, structure and function of the liver. MacSween's Pathology of the Liver. Burt, A., Portmann, B. and Ferrell, L. USA, Churchill Livingstone Elsevier**:** 1-73.

Roux, K. (2009). Optimization and troubleshooting in PCR. Cold Spring Harbor Protocols. doi:10.1101/pdb.ip66(4).

Runger, T., Farahvash, B., Hatvani, Z. and Rees, A. (2011). Comparison of DNA damage responses followign equimutagenic doses of UVA and UVB: a less effective cell cycle arrest with UVA may render UVA-induced pyrimidine dimers more mutagenic than UVB-induced ones. Photochemical and Photobiological Sciences. DOI: 10.1039/c1pp05232b.

Sabath, D., Broome, H. and Prystowsky, M. (1990). Glyceraldehyde-3-phosphate dehydrogenase mRNA is a major interleukin 2-induced transcript in a cloned T-helper lymphocyte. Gene. 91: 185-191.

Sahrawy, M., Hecht, V., Lopez-Jaramillo, J., Chueca, A., Chartier, Y. and Meyer, Y. (1996). Intron position as an evolutionary marker of thioredoxins and thioredoxin domains. Journal of Molecular Evolution. 42: 422-431.

Savas, N., Colak, T., Yilmaz, U., Emiroglu, R. and Haberal, M. (2007). Hepatitis B virus reactivation after renal transplantation: report of two cases. European Society for Organ Transplantation. 20(3): 301-304.

Schaefer, S. (2005). Hepatitis B virus: significance of genotypes. Journal of Viral Hepatitis. 12: 111-124.

Schmid, M., Nanda, I., Guttenbach, M., Steinlein, C., Hoehn, H., Schartl, M., Haaf, T., Weigend, S., Fries, R., Buerstedde, J., Wimmers, K., Burt, D., Smith, J., A'Hara, S., Law, A., Griffin, D., Bumstead, N., Kaufman, J., Thomson, P., Burke, T., Groenen, M., Crooijmans, R., Vignal, A., Fillon, V., Morisson, M., Pitel, F., Tixier-Boichard, M., Ladjali-Mohammedi, K., Hillel, J., Maki-Tanila, A., Cheng, H., Delany, M., Burnside, J. and Mizuno, S. (2000). First report on chicken genes and chromosomes 2000. Cytogenetics and Cell Genetics. 90: 169-218.

Schmittgen, T. and Zakrajsek, B. (2000). Effect of experimental treatment on housekeeping gene expression: validation by real-time, quantitative RT-PCR. Journal of Biochemical and Biophysical Methods. 46: 69-81.

Schroder, A., Shinn, P., Chen, H., Berry, C., Ecker, J. and Bushman, F. (2002). HIV-1 integration in the human genome favors active genes and local hotspots. Cell. 110(4): 521-529.

Schultz, U., Grgacic, E. and Nassal, M. (2004). Duck hepatitis B virus: an invaluable model system for HBV infection. Advances in Virus Research. 63: 1-70.

Seeger, C. and Mason, W. (2000). Hepatitis B virus biology. Microbiology and Molecular Biology Reviews. 64(1): 51-68.

Seigneres, B., Martin, P., Werle, B., Schorr, O., Jamard, C., Rimsky, L., Trepo, C. and Zoulim, F. (2003). Effects of pyrimidine and purine analog combinations in the duck hepatitis B virus infection model. Antimicrobial Agents and Chemotherapy. 47(6): 1842-1852.

Setlow, B. and Setlow, P. (1995). Small, acid-soluble proteins bound to DNA protect Bacillus subtilis spores from killing by dry heat. Applied and Environmental Microbiology. 61(7): 2787-2790.

Shinkawa, H., Nakai, T., Tamori, A., Tanaka, H., Takemura, S., Ohba, K., Uenishi, T., Ogawa, M., Yamamoto, S., Hai, S., Ichikawa, T., Kodai, S., Hirohashi, K., Wakasa, K. and Kubo, S. (2008). Hepatocellular carcinoma (HCC) recurring 10 years after clearance of hepatitis B surface antigen and 20 years after resection of hepatitis B virus-related HCC. international Journal of Clinical Oncology. 13: 562-566.

Shouval, D., Chakraborty, P., Ruiz-Opazo, N., Baum, S., Spigland, I., Muchmore, E., Gerber, M., Thung, S., Popper, H. and Shafritz, D. (1980). Chronic hepatitis in chimpanzee carriers of hepatitis B virus: morphologic, immunologic, and viral DNA studies. PNAS. 77(10): 6147-6151.

Sirover, M. (1999). New insights into an old protein: the functional diversity of mammalian glyceraldehyde-3-phosphate dehydrogenase. Biochimica et Biophysica Acta. 1432: 159-184.

Sissons, J. and Oldstone, M. (1980). Killing of virus-infected cells: the role of antiviral antibody and complement in limiting virus infection. The Journal of Infections Diseases. 142(3): 442-448.

Sitia, G., Iannacone, M., Aiolfi, R., Isogawa, M., van Rooijen, N., Scozzesi, C., Bianchi, M., von Andrian, U., Chisari, F. and Guidotti, L. (2011). Kupffer cells hasten resolution of liver immunopathology in mouse models of viral hepatitis. Public Library of Science Pathogens. 7(6): e1002061.

Skarp, K. and Vartiainen, M. (2010). Actin on DNA- an ancient and dynamic relationship. Cytoskeleton. 67: 487-495.

Skinner, B., Robertson, L., Tempest, H., Langley, E., Ioannou, D., Fowler, K., Crooijmans, R., Hall, A., Griffin, D. and Volker, M. (2009). Comparative genomics in chicken and Pekin duck using FISH mapping and microarray analysis. BMC Genomics. 10: 357-67.

Smedsrod, B., De Bleser, P., Braet, F., Lovisetti, P., Vanderkerken, K., Wisse, E. and Geerts, A. (1994). Cell biology of liver endothelial and Kupffer cells. Gut. 35(11): 1509-1516.

Soltis, R., Hasz, D., Morris, M. and Wilson, I. (1979). The effect of heat inactivation of serum on aggregation of immunoglobulins. Immunology. 36: 37-45.

Sonza, S., Maerz, A., Deacon, N., Meanger, J., Mills, J. and Crowe, S. (1996). Human immunodeficiency virus type 1 replication is blocked prior to reverse transcription and integration in freshly isolated peripheral blood monocytes. Journal of Virology. 70(6): 3863-3869.

Sprengel, R., Kaleta, E. and Will, H. (1988). Isolation and characterization of a hepaitis B virus endemic in herons. Journal of Virology. 62(10): 3832-3839.

Sridhar, G., Valliammai, T., Varalakshmi, S., Udayasankar, K., Panchanadam, M., Ramakrishna, J., Gopal, K., Jayaraman, K. and Thyagarajan, S. (1993). Duck hepatitis B virus infection in Indian domestic ducks: a pilot study. Tropical Animal Health and Production. 25(4): 229-233.

Staprans, S., Loeb, D. and Ganem, D. (1991). Mutations affecting hepadnavirus plus-strand DNA synthesis dissociate primer cleavage from translocation and reveal the origin of linear viral DNA. Journal of Virology. 65(3): 1255-1262.

Stevens, C., Beasley R., Tsui, J., Lee, W. (1975). Vertical transmission of hepatitis B antigen in Taiwan. New England Journal of Medicine. 292: 771-774.

Stone, E., Rothblum, K., Alevy, M., Kuo, T. and Schwartz, R. (1985). Complete sequence of the chicken glyceraldehyde-3-phosphate dehydrogenase gene. PNAS. 82: 1628-1632.

Su, H., Zhao, J., Xiong, Y., Xu, T., Zhou, F., Yuan, Y., Zhang, Y. and Zhuang, S. (2008). Large-scale analysis of the genetic and epigenetic alterations in hepatocellular carcinoma from Southeast China. Mutation Research. 641: 27-35.

Sugimoto, C., Kodama, H. and Mikami, T. (1979). Complement-dependent antibody cytotoxicity test of chicken antibody with duck complement used against cells of a Marek's disease lymphoma-derived cell line (MSB-1). Avian Diseases. 23(1): 229-234.

Summers, J., Jilbert, A., Yang, W., Aldrich, C., Saputelli, J., Litwin, S., Toll, E. and Mason, W. (2003). Hepatocyte turnover during resolution of a transient hepadnaviral infection. PNAS. 100(20): 11652-11659.

Summers, J. and Mason, W. (1982). Replication of the genome of a hepatitis B-like virus by reverse transcription of an RNA intermediate. Cell. 29(2): 403-415.

Summers, J. and Mason, W. (2004). Residual integrated viral DNA after hepadnavirus clearance by nucleoside analog therapy. PNAS. 101(2): 638-640.

Summers, J., Smith, P. and Horwich, A. (1990). Hepadnavirus envelope proteins regulate covalently closed circular DNA amplification. Journal of Virology. 64(6): 2819-2824.

Summers, J., Smolec, J. and Snyder, R. (1978). A virus similar to human hepatitis B virus associated with hepatitis and hepatoma in woodchucks. PNAS. 75(9): 4533-4537.

Tagawa, M., Omata, M., Yokosuka, O., Uchiumi, K., Imazeki, F. and Okuda, K. (1985). Early events in duck hepatitis B virus infection. Sequential appearance of viral deoxyribonucleic acid in the liver, pancrease, kidney, and spleen. Gastroenterology. 89(6): 1224-1229.

Takada, S., Gotoh, Y., Hayashi, S., Yoshida, M. and Koike, K. (1990). Structural rearrangement of integrated hepatitis B virus DNA as well as cellular flanking DNA is present in chronically infected hepatic tissues. Journal of Virology. 64(2): 822-828.

Tamori, A., Nishiguchi, S., Kubo, S., Narimatsu, T., Habu, D., Takeda, T., Hirohashi, K. and Shiomi, S. (2003). HBV DNA integration and HBV-transcript expression in non-B, non-C hepatocellular carcinoma in Japan. Journal of Medical Virology. 71: 492-498.

Tamori, A., Nishiguchi, S., Shiomi, S., Hayashi, T., Kobayashi, S., Habu, D., Takeda, T., Seki, S., Hirohashi, K., Tanaka, H. and Kubo, S. (2005). Hepatitis B virus DNA integration in hepatocellular carcinoma after interferon-induced disappearance of hepatits C virus. American Journal of Gastroenterology. 100: 1748-1753.

Tamori, A., Yamanishi, Y., Kawashima, S., Kanehisa, M., Enomoto, M., Tanaka, H., Kubo, S., Shiomi, S. and Nishiguchi, S. (2005). Alteration of gene expression in human hepatocellular carcinoma with integrated hepatitis B virus DNA. Clinical Cancer Research. 11: 5821-5826.

Telenius, H., Carter, N., Bebb, C., Nordenskjold, M., Ponder, B. and Tunnacliffe, A. (1992). Degenerate oligonucleotide-primed PCR: general amplification of target DNA by a single degenerate primer. Genomics. 13(3): 718-725.

Testut, P., Renard, C., Terradillos, O., Vitvitski-Trepo, L., Tekaia, F., Degott, C., Blake, J., Boyer, B. and Buendia, M. (1996). A new hepadnavirus endemic in artic ground squirrels in Alaska. Journal of Virology. 70(7): 4210-4219.

Theise, N., Bodenheimer Jnr, H. and Ferrell, L. (2007). Acute and chronic viral hepatitis. MacSween's Pathology of the Liver. Burt, D., Portmann, B. and Ferrell, L. Philadelphia, PA, USA, Churchill Livingstone Elsevier**:** 399-441.

Thermo Fisher Scientific (2008). NanoDrop 1000 Spectrophotometer V3.7 User's Manual.22 July 2010 http://www.nanodrop.com/Support.aspx?Type=User Guides&Cat=NanoDrop 1000.

Thimme, R., Wieland, S., Steiger, C., Ghrayeb, J., Reimann, K., Purcell, R. and Chisari, F. (2003). CD8+ T cells mediate viral clearance and disease pathogenesis during acute hepatitis B virus infection. Journal of Virology. 77(1): 68-76.

Thorpe, M. (2007). Studies on the survival of duck hepatitis B virus covalently closed circular DNA through hepatocyte mitosis *in vivo*. Department of Microbiology and Immunology, School of Molecular and Biomedical Science. Adelaide, South Australia, The University of Adelaide**:** 48.

Tiersch, T. and Wachtel, S. (1991). On the evolution of genome size of birds. Journal of Heredity. 82(5): 363-368.

Tohidi-Esfahani, R., Vickery, K. and Cossart, Y. (2010). The early host innate immune responses to duck hepatitis B virus infection. Journal of General Virology. 91: 509-520.

Tokino, T. and Matsubara, K. (1991). Chromosomal sites for hepatitis B virus integration in human hepatocellular carcinoma. Journal of Virology. 65(12): 6761-6764.

Trahair, H. (2008). Understanding and optimising prime-boost vaccination strategies. Discipline of Microbiology and Immunology, School of Molecular and Biomedical Science. Adelaide, South Australia, The University of Adelaide**:** 54.

Transy, C., Fourel, G., Robinson, W., Tiollais, P., Marion, P. and Buendia, M. (1992). Frequent amplification of c-myc in ground squirrel liver tumors associate with past or ongoing infection with a hepadnavirus. PNAS. 89(9): 3874-3878.

Transy, C., Renard, C. and Buendia, M. (1994). Analysis of integrated ground squirrel hepatitis virus and flanking host DNA in two hepatocellular carcinomas. Journal of Virology. 68(8): 5291-5295.

Treichel, U., Meyer zum Buschenfelde, K., Dienes, H. and Gerken, G. (1997). Receptor-mediated entry of hepatitis B virus particles into liver cells. Archives of Virology. 142: 493-498.

Trevorrow, S. (2011). Studies on the mitotic survival of covalently closed circular DNA (cccDNA) using in vitro duck hepatitis B virus models. Discipline of Microbiology and Immunology, School of Molecular and Biomedical Science. Adelaide, South Australia, The University of Adelaide**:** 56.

Triglia, T., Peterson, M. and Kemp, D. (1988). A procedure for in vitro amplification of DNA segments that lie outside the boundaries of known sequences. Nucleic Acids Research. 16(16): 8186.

Triyatni, M. (1998). Studies on the protective and therapeutic efficacy of duck hepatitis B virus vaccines. Department of Microbiology and Immunology, School of Molecular and Biomedical Science. Adelaide, South Australia, The University of Adelaide**:** 187.

Triyatni, M., Ey, P., Tran, T., Le Mire, M., Qiao, M., Burrell, C. and Jilbert, A. (2001). Sequence comparison of an Australian duck hepatitis B virus strain with other avian hepadnaviruses. Journal of General Virology. 82: 373-378.

Tuttleman, J., Pourcel, C. and Summers, J. (1986). Formation of the pool of covalently closed circular viral DNA in hepadnavirus-infected cells. Cell. 47: 451-460.

Vandekerckhove, J. and Weber, K. (1978). At least six different actins are expressed in a higher mammal: an analysis based on the amino acid sequences of the amino-terminal tryptic peptide. Journal of Molecular Biology. 126: 783-802.

Vandesompele, J., De Preter, K., Pattyn, F., Poppe, B., Van Roy, N., De Paepe, A. and Speleman, F. (2002). Accurate normalization of real-time quantitative RT-PCR data by geometric averaging of multiple internal control genes. Genome Biology. 3(7): 1-12.

Venkatesh, B., Ning, Y. and Brenner, S. (1999). Late changes in spliceosomal introns define clades in vertebrate evolution. PNAS. 96: 10267-10271.

Venkatesh, B., Tay, B., Elgar, G. and Brenner, S. (1996). Isolation, characterization and evolution of nine pufferfish (Fugu rubripes) actin genes. Journal of Molecular Biology. 259: 655-665.

Vester, B. and Wengel, J. (2004). LNA (locked nucleic acid): high-affinity targeting of complementary RNA and DNA. Biochemistry. 43(42): 13233-13241.

Vickery, K., Cossart, Y. and Dixon, R. (1999). Cellular immune response of ducks to duck hepatitis B virus infection. Journal of Medical Virology. 58: 19-25.

Vickery, K., Frieman, J., Dixon, R., Kearney, R., Murray, S. and Cossart, Y. (1989). Immunity in Pekin ducks experimentally and naturally infected with duck hepatitis B virus. Journal of Medical Virology. 28(4): 231-236.

Vickery, K., Tohidi-Esfahani, R., Pouliopoulos, J., Welschinger, R., Dixon, R., Deva, A. and Cossart, Y. (2006). The effect of surgical immunomodulation on liver inflammation and clearance of DHBV infection. Journal of Medical Virology. 78(12): 1572-1578.

Visvanathan, K. (2008). Immunopathogenesis of hepatitis B virus infection. Hepatitis B Virus: Human Virus Guides. Lai, C. and Locarnini, S. London, International Medical Press. 1.

Vogelstein, B., Fearon, E., Hamilton, S., Preisinger, A., Willard, H., Michelson, A., Riggs, A. and Orkin, S. (1987). Clonal analysis using recombinant DNA probes from the X-chromosome. Cancer Research. 47: 4806-4813.

Wada, Y., Tsukada, M., Kamiyama, S. and Koizumi, A. (1990). Evidence on clonal proliferation of hepatocytes after carbon-tetrachloride-induced hepatic injury in PGK-1 mosaic mice. Toxicology Letters. 52: 81-90.

Wai, C., Chu, C., Hussain, M. and Lok, A. (2002). HBV genotype B is associated with better response to interferon therapy in HBeAg(+) chronic hepatitis than genotype C. Hepatology. 36(6): 1425-1430.

Wang, C. (2008). Toll-like receptors and early events during duck hepatitis B virus infection. Discipline of Microbiology and Immunology, School of Molecular and Biomedical Science. Adelaide, South Australia, The University of Adelaide**:** 50.

Wang, J., Chenivesse, X., Henglein, B. and Brechot, C. (1990). Hepatitis B virus integration in a cyclin A gene in a hepatocellular carcinoma. Nature. 343(6258): 555-557.

Warrington, J., Nair, A., Mahadevappa, M. and Tsyganskaya, M. (2000). Comparison of human adult and fetal expression and identification of 535 housekeeping/maintenance genes. Physiologial Genomics. 2: 143-147.

Weiskirchen, R., Siemeister, G., Hartl, M. and Bister, K. (1993). Sequence and expression of glyceraldehyde-3-phosphate dehydrogenase-encoding gene from quail embryo fibroblasts. Gene. 128: 269-272.

Werle-Lapostolle, B., Bowden, S., Locarnini, S., Wursthorn, K., Petersen, J., Lau, G., Trepo, C., Marcellin, P., Goodman, Z., Delaney, W. I., Xiong, S., Brosgart, C., Chen, S., Gibbs, C. and Zoulim, F. (2004). Persistence of cccDNA during the natural history of chronic hepatitis B and decline during adefovir dipivoxil therapy. Gastroenterology. 126(7): 1750-1758.

WHO (2008). Hepatitis B.18 June Media fact sheets. 2011:http://www.who.int/mediacentre/factsheets/fs204/en/.

WHO (2010). Hepatitis B.18 June New vaccines and technologies. 2011:http://www.who.int/immunization_delivery/new_vaccines/hepb/en/index.html.

WHO (2011). Cancer.18 June Media fact sheets. 2011:http://www.who.int/mediacentre/factsheets/fs297/en/.

WHO (2011). Hepatitis B.12 July Immunization, Vaccines and Biologicals. 2011:www.who.int/immunization/topics/hepatitis_b/en/index.html.

WHO (2011). Hepatitis B.18 June Global Alert and Response (GAR). 2011:http://www.who.int/csr/disease/hepatitis/whocdscsrlyo20022/en/index1.html.

Wieland, S., Eustaquio, A., Whitten-Bauer, C., Boyd, B. and Chisari, F. (2005). Interferon prevents formation of replication-competent hepatitis B virus RNA-containing nucleocapsids. PNAS. 102(28): 9913-9917.

Wieland, S., Guidotti, L. and Chisari, F. (2000). Intrahepatic induction of alpha/beta interferon eliminates viral RNA-containing capsids in hepatitis B virus transgenic mice. Journal of Virology. 74(9): 4165-4173.

Wieland, S., Spangenberg, H., Thimme, R., Purcell, R. and Chisari, F. (2004). Expansion and contraction of the hepatitis B virus transcriptional template in infected chimpanzees. PNAS. 101(7): 2129-2134.

Wieland, S., Thimme, R., Purcell, R. and Chisari, F. (2004). Genomic analysis of the host response to hepatitis B virus infection. PNAS. 101(17): 6669-6674.

Wirtz, G. (1967). Avian complement; duck complement adn natural hemolysin. Immunochemistry. 4(2): 118-121.

Wirz, T., Brandle, U., Soldati, T., Hossle, J. and Perriard, J. (1990). A unique chicken B-reatine kinase gene gives rise to two B-creatine kinase isoproteins with distinct N termini by alternative splicing. The Journal of Biological Chemistry. 265(10): 11656-11666.

Wu, T., Coates, L., Aldrich, C., Summers, J. and Mason, W. (1990). In hepatocytes infected with duck hepatitis B virus, the template for viral RNA synthesis is amplified by an intracellular pathway. Virology. 175(1): 255-261.

Xu, B., Hu, D., Rosenberg, D., Jiang, Q., Lin, X., Lu, J. and Robinson, N. (2003). Chronic hepatitis B: a long-term retrospective cohort study of disease progression in Shanghai, China. Journal of Gastroenterology and Hepatology. 18: 1345-1352.

Xu, C., Guo, H., Pan, X., Mao, R., Yu, W., Xu, X., Wei, L., Chang, J., Block, T. and Guo, J. (2010). Interferons accelerate decay of replication-competent nucleocapsids of hepatitis B virus. Journal of Virology. 84(18): 9332-9340.

Yang, J., Wang, F., Tian, L., Su, J., Zhu, X., Lin, L., Ding, X., Wang, X. and Wang, S. (2010). Fibronectin and asialoglyprotein receptor mediated hepatitis B surface antigen binding to the cell surface. Archives of Virology. 155(881-888).

Yang, P., Althage, A., Chung, J., Maier, H., Wieland, S., Isogawa, M. and Chisari, F. (2010). Immune effectors required for hepatitis B virus clearance. PNAS. 107(2): 798-802.

Yang, W., Mason, W. and Summers, J. (1996). Covalently closed circular viral DNA formed from two types of linear DNA in woodchuck hepatitis virus-infected liver. Journal of Virology. 70(7): 4567-4575.

Yang, W. and Summers, J. (1995). Illegitimate replication of linear hepadnavirus DNA through nonhomologous recombination. Journal of Virology. 69(7): 4029-4036.

Yang, W. and Summers, J. (1999). Integration of hepadnavirus DNA in infected liver: evidence for a linear precursor. Journal of Virology. 73(12): 9710-9717.

Yasui, H., Hino, O., Ohtake, K., Machinami, R. and Kitagawa, T. (1992). Clonal growth of hepatitis B virus-integrated hepatocytes in cirrhotic liver nodules. Cancer Research. 52: 6810-6814.

Yatsuji, H., Suzuki, F., Sezaki, H., Akuta, N., Suzuki, Y., Kawamura, Y., Hosaka, T., Kobayashi, M., Saitoh, S., Arase, Y., Ikeda, K., Watahiki, S., Iwasaki, S., Kobayashi, M. and Kumada, H. (2008). Low risk of adefovir resistance in lamivudine-resistant chronic hepatitis B patients treated with adefovir plus lamivudine combination therapy: two-year follow-up. Journal of Hepatology. 48(6): 923-931.

Yim, H. and Lok, A. (2006). Natural history of chronic hepatitis B virus infection: what we knew in 1981 and what we know in 2005. Hepatology. 43: S173-A181.

Yokosuka, O., Omata, M., Zhou, Y., Imazeki, F. and Okuda, K. (1985). Duck hepatitis B virus DNA in liver and serum of Chinese ducks: integration of viral DNA in a hepatocellular carcinoma. PNAS. 82(15): 5180-5184.

Yuan, J., Tang, B., Zhang, L. and Li, N. (2005). Comparative FISH mapping suggests poor conservation between chicken and duck genes. Animal Genetics. 36: 435-462.

Yuen, M. and Lai, C. (2008). The natural history of chronic hepatitis B. Hepatitis B Virus: Human Virus Guides. Lai, C. and Locarnini, S. London, International Medical Press. 1**:** 12.1-12.11.

Yuen, M. and Lai, C. (2011). Treatment of chronic hepatitis B: evolution over two decades. Journal of Gastroenterology and Hepatology. 26(Supplementary 1): 138-143.

Zhang, W., Li, H., Cheng, G., Hu, S., Li, Z. and Bi, D. (2008). Avian influenza virus infection induces differential expression of genes in chicken kidney. Research in Veterinary Science. 84(2008): 374-381.

Zhang, Y., Qu, Z., Kim, S., Shi, V., Liao, B., Kraft, P., Bandaru, R., Wu, Y., Greenberger, L. and Horak, I. (2010). Down-modulation of cancer targets using locked nucleic acid (LNA)-based antisense oligonucleotides without transfection. Gene Therapy: 1-8.

Zhang, Y. and Summers, J. (2004). Rapid production of neutralizing antibody leads to transient hepadnavirus infection. Journal of Virology. 78(3): 1195-1201.

Zhang, Y., Zhang, B., Theele, D., Litwin, S., Toll, E. and SUmmers, J. (2003). Single-cell analysis of covalently closed circular DNA copy numbers in a hepadavirus-infected liver. PNAS. 100(21): 12372-12377.

Zhu, W. (2010). Studies on the mitotic survival of covalently closed circular DNA (cccDNA) using in vitro duck hepatitis B virus models. Discipline of Microbiology and Immunology, School of Molecular and Biomedical Science. Adelaide, South Australia, The University of Adelaide**:** 48.

Zhu, Y., Yamamoto, T., Cullen, J., Saputelli, J., Aldrich, C., Miller, D., Litwin, S., Furman, P., Jilbert, A. and Mason, W. (2001). Kinetics of hepadnavirus loss from the liver during inhibition of viral DNA synthesis. Journal of Virology. 75(1): 311-322.

Zimmerman, K., Fischer, K., Joyce, M. and Tyrrell, D. (2008). Zinc finger proteins designed to sepecifically target duck hepatitis B virus covalently closed circular DNA inhibit viral transcription in tissue culture. Journal of Virology. 86(16): 8013-8021.

Zoulim, F. (2011). Hepatitis B virus resistance to antiviral drugs: where are we going? Liver International. 2011: 111-116.

Zoulim, F., Saade, F., Buronfosse, T., Abdul, F. and Cova, L. (2008). Animal models for the study of infection. Hepatitis B Virus: Human Virus Guides. Lai, C. and Locarnini, S. London, International Medical Press. 1**:** 6.1-6.20.

William S. Mason, Huey-Chi Low, Chunxiao Xu, Carol E. Aldrich, Catherine A. Scougall, Arend Grosse, Andrew Clouston, Deborah Chavez, Samuel Litwin, Suraj Peri, Allison R. Jilbert and Robert E. Lanford, (2009) Detection of Clonally Expanded Hepatocytes in Chimpanzees with Chronic Hepatitis B Virus Infection.
Journal of Virology, v. 18 (17), pp. 8396-8408, September 2009

NOTE: This publication is included in the print copy of the thesis held in the University of Adelaide Library.

It is also available online to authorised users at:

http://dx.doi.org/10.1128/JVI.00700-09

William S. Mason, Chunxiao Xu, Huey Chi Low, Jeffry Saputelli, Carol E. Aldrich, Catherine Scougall, Arend Grosse, Richard Colonno, Sam Litwin and Allison R. Jilbert (2009) The Amount of Hepatocyte Turnover That Occurred during Resolution of Transient Hepadnavirus Infections Was Lower When Virus Replication Was Inhibited with Entecavir.
Journal of Virology, v. 18 (4), pp. 1778-1789, February 2009

NOTE: This publication is included in the print copy of the thesis held in the University of Adelaide Library.

It is also available online to authorised users at:

http://dx.doi.org/10.1128/JVI.01587-08